Department of Mechanical Engineering

Structure-function relations of biological hydrogel macromolecules

a thesis
presented by

Benjamin Tillmann Käsdorf

Technical University of Munich

Technische Universität München

Fakultät für Maschinenwesen

Professur für Biomechanik

Structure-function relations of biological hydrogel macromolecules

Benjamin Tillmann Käsdorf

Vollständiger Abdruck der von der Fakultät für Maschinenwesen der Technischen Universität München zur Erlangung des akademischen Grades

eines

Doktor der Naturwissenschaften (Dr. rer. nat.)

genehmigten Dissertation.

Vorsitzender:	Prof. Dr.-Ing. Andreas Kremling
Prüfer der Dissertation:	1. Prof. Dr. rer. nat. Oliver Lieleg
	2. Prof. Dr. Job Boekhoven

Die Dissertation wurde am 12.12.2017 bei der Technischen Universität München eingereicht und durch die Fakultät für Maschinenwesen am 11.03.2018 angenommen.

Summary

Biological hydrogels are complex macromolecular structures which fulfill many crucial tasks in the human body. For example, they provide protection from pathogenic infection, lubricate many tissue surfaces, establish mechanical stability and regulate the uptake of nutrients. However, such hydrogels often also prevent the efficient treatment of diseases, as they constitute a barrier for many pharmaceuticals, which have to pass these networks. In addition, many diseases either develop as a result of defective hydrogel systems or entail alterations of such hydrogels, resulting in dysfunction of these complex structures. Although these polymer networks comprise up to 99 % water, it is the small amount of macromolecules which is mainly responsible for the variety of hydrogel properties, and also those macromolecules are affected when hydrogel-associated diseases occur. Thus, it is not only necessary to understand the crucial processes which are governed by biological hydrogels, but also to identify macromolecular key players of those systems and their specific functions.

In this thesis, the structure and function relations of biological hydrogel components are characterized. The first part of the thesis focuses on the selective permeability of such hydrogels with a strong emphasis on the vitreous humor and mucosal membranes. It is demonstrated that the vitreous humor constitutes a selective barrier towards the diffusion of cationic nanoparticles as well as small cationic molecules as they bind to the vitreous polymer network through electrostatic interactions. Especially for small molecules the amount of charge that these molecules carry is pivotal for their diffusive mobility within the vitreous. This mobility can range from slightly hindered diffusion up to total immobilization within the polymer network. As macromolecular key players which are responsible for those electrostatic binding interactions, the polyanionic glycosaminoglycans hyaluronic acid and heparan sulfate are identified. These insights might prove beneficial for the design of pharmaceuticals for intravitreal treatment of ocular diseases.

Additionally, these insights on how to influence the diffusive mobility of nanoparticles and molecules within a hydrogel network are transferred to a drug delivery system integrated into an artificial wound hydrogel: here, spatio-temporal control over the release of aggregated gold nanoparticles is achieved by combining a sophisticated, multi-cascade release mechanism with the deposition of charge traps into the artificial hydrogel. This strategy allows for a delayed release of those nanoparticles for a period of over two weeks and might help to develop advanced drug delivery strategies, especially for long-term drug release.

Furthermore, the selective barrier properties of biological hydrogels such as mucosal membranes are transferred to an artificial filtration device with a high surface-to-volume ratio. By dissolving embedded sugar fibers from a PDMS matrix, a finely structured capillary system is generated. Subsequent coating of this capillary network with synthetic

or purified biological macromolecules enables the selective removal of nanoparticles or molecules from a solution which is pumped through that capillary system. Here, e.g., physisorption of mucin macromolecules purified from mucosal membranes allows for filtration by means of electrostatic interactions. Depending on the source of those high-molecular-weight glycoproteins (commercial purification vs. manual lab purification), removal of either cationic and/or anionic particles/molecules is possible. This difference in the performance of commercial and native mucins likely results from the harsh conditions during the purification process of the commercially available products where important glycan moieties of the mucin molecules are damaged.

Thus, to obtain mucin glycoproteins in high amounts while preserving their important native properties, a manual mucin purification process from porcine stomachs is optimized regarding efficiency and mucin yield. At the same time, quality control protocols are established. Mucin properties such as establishing a selective hydrogel barrier towards charged molecules, being able to form viscoelastic gels under acidic conditions as well as efficiently lubricating surfaces are preserved throughout this process. This process optimization on the one hand facilitates the application of native mucins in medical applications since this requires larger amounts of those unique glycoproteins. On the other hand, this process enables proper mucin-related research since the characteristic properties of mucin are still well-preserved after the purification process.

An example for such an important property of mucin macromolecules is the ability to protect tissues from pathogenic infection. By forming a dense, viscoelastic network that constitutes a barrier towards most pathogens, mucins prevent these pathogens from reaching and thus infecting the epithelial cell layer. In this thesis, manually purified porcine gastric mucin is used to mimic a mechanism used by the pathogen *Helicobacter pylori*, a bacterium which has found a strategy to overcome this mucin barrier by transiently liquefying the mucin gel. This mechanism is transferred to an artificial micro swimmer, which is then able to efficiently penetrate reconstituted mucin layers. This proof of principle study might provide the tools to engineer a highly efficient drug delivery system which can overcome the gastric mucus layer – thus enabling the administration of smaller doses of pharmaceutical drugs and, consequently, reducing systemic side effects.

The barrier function of gastric mucus towards drug molecules is further investigated by studying the diffusive penetration of reconstituted mucin hydrogels by small molecules. It is demonstrated, that cationic molecules bind to the polyanionic mucin macromolecules which entails a strong accumulation of cationic molecules at the mucin gel interface compared to anionic or neutral molecules. However, these electrostatic binding interactions of cationic molecules indeed not only promote the penetration efficiency of mucin gels but also result in an increased transport of cationic molecules across the mucin gels. However, this increased transport is only efficient over short gel thicknesses and/or

long diffusion times. The design of pharmaceutical drugs and their delivery across the gastrointestinal mucus barrier might benefit from those findings.

In addition to the selective barrier function of biological hydrogels, protecting body tissues from mechanical damage is a second important task these macromolecular systems fulfill. In the second part of this thesis, the mucin-mediated lubrication process is investigated. Here, the lubricating abilities of mucin during ingestion of certain food and beverages is analyzed as the interaction of selected food components with saliva and mucosal membranes in the oral cavity entails a loss in lubrication, called astringency. Using purified human salivary mucins as a model system, it is demonstrated, that it is indeed the mucin molecules which provide such saliva-mediated lubrication. Furthermore, it is shown that the loss of lubrication upon ingestion of astringent substances such as cationic ions, proteins or macromolecules is a result of mucin aggregation caused by ionic crosslinking as induced by the cationic astringent substances. The aggregation of mucins results in a strongly reduced concentration of free mucins in solution which, in turn, reduces lubricity. These investigations might help to study the effect of food components on the experienced mouthfeel and, by employing purified salivary mucins as a model system, can help with the gustatory optimization of food or beverage products.

In a second step, the mucin-mediated lubrication mechanism is analyzed on a molecular level: here, it is demonstrated that the terminal hydrophobic mucin domains are crucial for mucin to adsorb to hydrophobic surfaces such as PDMS and thus to provide lubrication. This knowledge is then transferred to dextran macromolecules: introducing hydrophobic moieties into those highly hydrated polysaccharides provides anchor points which enable those macromolecules to adsorb to a hydrophobic PDMS surface and, consequently, to reduce friction. Here, the density of hydrophobic groups grafted onto the molecules influences their adsorption efficiency and their ability to act as a lubricant – especially in the boundary lubrication regime. These results may pinpoint novel strategies for the rational design of artificial boundary lubricants.

The structure-function analysis conducted in this thesis provides novel insights on the molecular processes that establish the selective permeability of biological hydrogel systems or enable efficient lubrication of body surfaces. The discussed results may help to gain a better understanding of these processes and might prove valuable for developing new approaches in the fight against hydrogel-associated diseases. Furthermore, as demonstrated in this thesis, certain strategies employed by biological macromolecules can indeed be transferred to other synthetic systems, thus, e.g., enabling the design of spatio-temporally controlled drug release/delivery systems and artificial super lubricants or the usage of purified or synthetic mucins in filtration devices. It is very likely, that a plethora of other medical applications could also benefit from the native properties of biological hydrogel macromolecules as well.

Contents

1 Introduction

Biological hydrogels are complex networks of crosslinked proteins or polysaccharides with a high water content of 80 – 99 %. These structures can additionally comprise various other components such as lipids, nucleic acids and salts. Such hydrogel systems cover all wet body epithelia, extend throughout the whole gastrointestinal and respiratory tract, and cover the urogenital tract (**Figure 1**). They surround internal organs, protect epithelial cell layers, enclose single cells, and allow for specific interactions of these cells with their environment.

These virtually ubiquitary biological networks serve as the first line of defense against pathogenic attack, possess antiviral and antibacterial properties, regulate the uptake of nutrients and prevent entrance of unwanted xenobiotics [1-7]. Additionally, they protect the underlying epithelial tissue against mechanical forces and provide lubrication [8, 9].

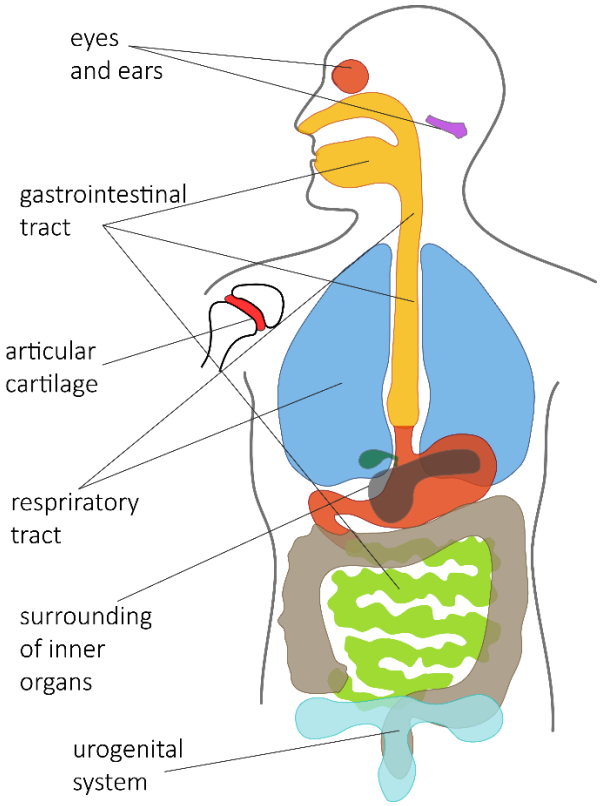

Figure 1: Schematic illustration of the distribution of biological hydrogels in the human body: Biological hydrogels are distributed throughout the entire human body and fulfill various tasks (e.g., protection of tissue against mechanical damage and pathogenic infection or providing lubrication). Examples include mucus (gastrointestinal tract, respiratory system, urogenital tract and inner organs, eyes, ears), vitreous and aqueous humor in the eye as well as cartilage (e.g., in articular joints).

Those processes rely on the viscoelastic properties of those hydrogels and their selective permeability. Hydrogels in the human body comprise high amounts of water and minor amounts of biopolymers. However, it is these polymers which are responsible for the

stability of the gel and which confer specific properties such as their selective permeability. This barrier function can be mediated by two different mechanisms: first, the biopolymers within this gel are crosslinked and therefore establish a three dimensional mesh. If the mesh size is smaller than the diameter of a diffusing object, translocation through the gel is prevented as a consequence of size sieving (**Figure 2a**). The second mechanism can even prevent particles and molecules that are considerably smaller than the gel mesh size from passing that gel via specific binding interactions with hydrogel components (**Figure 2b**) as documented in a variety of studies [10-18]. These barrier functions of biological hydrogels are crucial for the protection against pathogens such as viruses and bacteria: the microorganisms are trapped in the hydrogel barrier and thus are prevented from reaching and thus infecting the underlying epithelial cell layer.

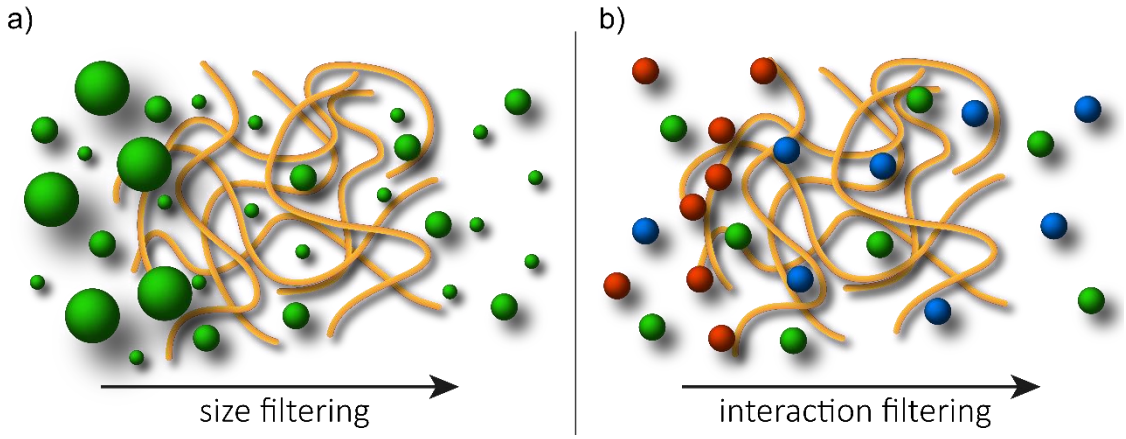

Figure 2: Schematic illustration of the selective permeability of a hydrogel: The surface properties of particles or molecules determine if these objects can diffuse freely through a biological network or if interactions with the hydrogel components retard that process or even completely prevent a transmigration through the gel (b). Yet, this is only true for particles and molecules smaller than the mesh size of that gel: larger objects are prevented from entering the network by steric hindrance (a).

However, those hydrogels do not only pose a barrier for pathogens but are able to prevent molecules from translocating through the gel as well. Whereas the body benefits from this protective function against pathogens and xenobiotics, the efficiency of many therapeutic treatments is also drastically reduced when drug molecules are prevented from penetrating those networks. Thus, efficient treatment of several diseases, up to date, often remains a challenging task. One major example is the treatment of ocular diseases, especially those concerning the retina (e.g., age-related macular degeneration or diabetic retinopathy [19]): as efficient systemic treatment via the bloodstream is prevented by the virtually impermeable blood-ocular barrier [20], topical treatment via eye drops often is employed. However, the drug molecules administered onto the cornea have to penetrate

three different barriers: the cornea itself, the aqueous humor and the vitreous humor – rendering topical drug administration a fairly inefficient form of treatment [21-23]. The only currently remaining alternative of drug administration is via intravitreal injection. This delivery method however, is efficient only, if the injected molecules are able to reach the target site, e.g., the retina, and are not trapped by the vitreous hydrogel along the way. The vitreous consists of up to 98 % water – the remaining 2 % comprise several biopolymers which provide the vitreous humor with the selective permeability. Possessing the right chemical properties thus is crucial for an efficient translocation through the vitreous gel. Yet, the design of such freely diffusing pharmaceuticals requires a profound understanding of the molecular processes involved in the interaction with hydrogels such as the vitreous humor. This issue is addressed in Section 4.1 where the influence of distinct vitreous hydrogel components on the diffusive mobility of particles and molecules is evaluated.

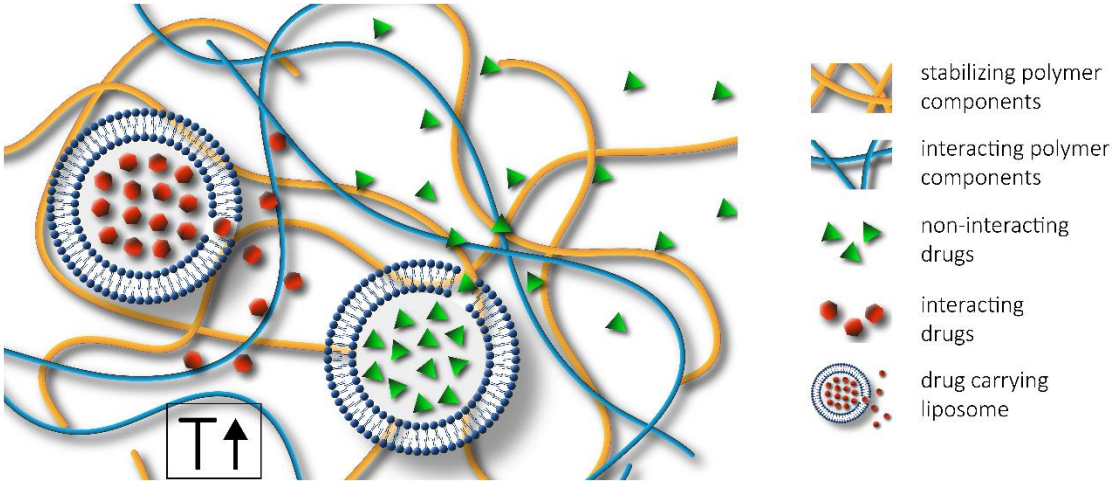

Figure 3: Schematic illustration of a tunable hydrogel drug delivery system: Encapsulated drug molecules can be released from their liposome carrier particle, e.g., by increasing temperature. Depending on the ability to interact with hydrogel components, the diffusive distribution of the drug molecules throughout the hydrogel can be prolonged.

Insights gained from investigating those complex processes might not only pave the way for the rational design of drug molecules which are able to overcome the barrier of biological hydrogels, but also be of valuable use for the development of completely new ways of delivering such pharmaceutical agents. Whereas nature has evolved complex healing cascades that take place during the process of wound healing in the human body [24-26], pharmaceutical treatments that provide a spatio-temporally controlled release cascade are very challenging. A promising method is the drug delivery via customized liposomes as these synthetic vesicles are highly tunable and can be loaded with pharmaceutical drugs [27-31]. Mimicking nature's strategy and utilizing the selective permeability of hydrogels may prove as a powerful tool for the design of a multistage

cascaded drug release (**Figure 3**). In Section 4.2 such an approach is presented and it is demonstrated how the release of test particles from a hydrogel can be controlled by the incorporation of charged entities into the hydrogel.

A different application where insights on the selective permeability of biological hydrogels can be of value, is the field of purification and filtration: transferring the elaborate molecular sieving mechanisms of biological hydrogels to artificial setups may facilitate the removal of unwanted particles or molecules from a solution via binding interactions with biopolymeric compounds. One hydrogel system has gained increasing attention over the last years: mucous membranes, which can be found on every wet surface in the human body, maintain many crucial functions (**Figure 4**): in addition to providing lubrication and mechanical protection of those surfaces [32-37], mucous membranes are responsible for preventing the infection of the underlying epithelial cells with pathogens such as viruses and bacteria [3-5, 38-48] and furthermore play an important role in the prevention of cancer development [49, 50]. Key players involved in those processes are mucins, the main components of mucous hydrogels. Mucins are high-molecular-weight proteins with large amounts of polysaccharide chains attached to their protein backbone [51]. It has repeatedly been demonstrated, that those special, gel-forming biopolymers establish selective permeability towards molecules and particles and are able to immobilize certain viruses and bacteria within the polymer network. A transfer of those properties to artificial filtration setups could prove helpful, e.g., for medical filtration applications such as dialysis or in laboratory research, e.g., when studying the binding interactions of molecules/particles/pathogens with specific biopolymers. A realization of such a highly tunable filtration system based on the employment of biological and synthetic polymers is presented in Section 4.3.

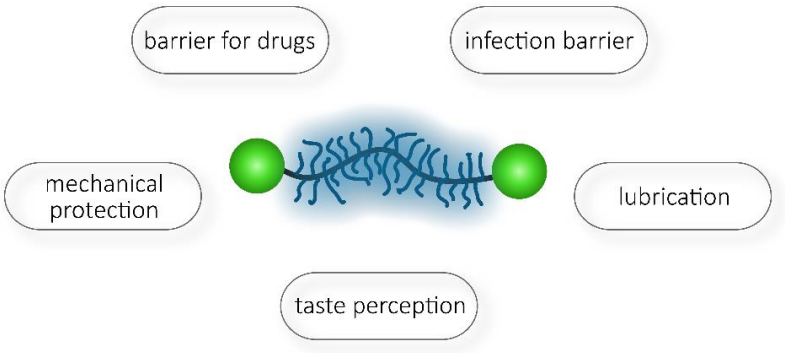

Figure 4: Overview of the versatile physiological functions of mucins: Mucins are involved in several diverse, but essential processes in the human body. They provide protection from mechanical damage and pathogenic infection, lubricate body surfaces and are involved in the perception of taste. However, they also pose a barrier for the uptake of beneficial molecules such as pharmaceuticals.

However, to boost research in this particular field, sufficient amounts of those mucin proteins have to be available. Over the last years, a wide variety of purified mucins was offered by commercial vendors. These products come – despite their complexity – in relatively large amounts and are rather cheap in comparison to other purified proteins. However, numerous studies attested those commercial mucins poor purity and the outstanding qualities of native mucins such as gel-formation under acidic conditions and lubrication of surfaces as well as their barrier function seem to be impaired or even entirely lost after these purification processes [5, 52-56]. It is believed, that harsh conditions during those commercial purification processes are responsible for physical or chemical damage to mucin molecules and that important functional moieties of those macromolecules might be affected. Hence, those commercially available mucins are not suitable for researching the special qualities of native mucins. Thus, establishing an optimized purification process, which preserves the properties of native mucin but still yields large amounts of this special biopolymer, is of great importance. Such a process would enable proper research of those macromolecules and facilitate the implementation of mucins into medical applications. In Section 4.4, the optimization of a mucin purification process is illustrated which, on the one hand yields comparably large amount of that glycoprotein, but on the other hand still preserves its native form and properties.

The availability of larger quantities of fully functional mucins helps to acquire a profound understanding of mucins and the crucial processes they are involved in. This is a necessary step – not only in regard of, e.g., understanding and preventing pathogenic infection but also when it comes to the delivery of pharmaceuticals that have to pass a mucin barrier. Similar to the polymer network in the vitreous humor, also a mucin hydrogel blocks the passage of pathogens and certain molecules and thus eventually prevents them from reaching the underlying epithelial layer [5, 17, 57-61]. Especially in the stomach, the secreted mucins form a thick gel under the prevailing acidic conditions [62, 63]. However, since most pharmaceutical drugs are ingested orally, those molecules must overcome this barrier in the gastrointestinal tract to enter the blood stream and thus to enable an effective systemic treatment. A detailed understanding of the molecular mechanisms involved in the physico-chemical interaction of mucin with particles/molecules is therefore essential.

As orally administered drugs are often encapsulated to protect them from degradation, also the passage of those carriers must be guaranteed for the pharmaceuticals to reach the target site. If these drug carriers are smaller than the prevailing mesh size of the mucin layers, a virtually unhindered passage is possible – if the carrier system is designed in such a way, that its surface chemistry prevents binding interactions with the mucin polymers. In contrast, if the carrier size exceeds the maximal distance between two mucin polymers, steric hindrance cannot be avoided, even if chemically inert carrier particles

are chosen. The size of drug-loaded liposomes, however, often is close to the micrometer range, and native mucosal membranes, e.g., in the gastric system, exhibit mesh sizes in the range of a few hundred nanometers [64-67] thus preventing the translocation of larger liposomes. Some pathogens, however, have developed strategies to overcome this steric barrier and are able to penetrate gastric mucus layers. The flagellated bacterium *Helicobacter pylori* has developed a special mechanism (**Figure 5**): as it is too large to navigate through the finely-meshed mucin gel, it transiently alters the gastric mucosa by locally increasing the pH. This pH alteration induces a liquefaction of the mucin gel (which is only stable under acidic conditions) – rendering the mucin layer permeable for the pathogen [68-71].

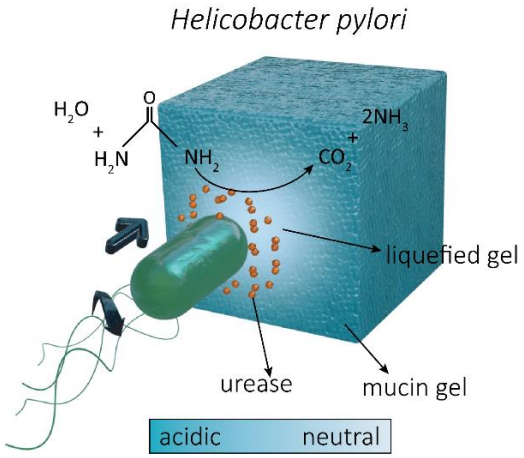

Figure 5: Schematic illustration of the mechanism that enables the pathogen *Helicobacter pylori* to navigate through the gastric mucus layer by transiently altering the mucus properties: By secreting the enzyme urease, the naturally occurring urea in the gastrointestinal tract is hydrolyzed. The resulting ammonia locally increases the pH which induces a transient gel-sol transition of the mucin gel. The lack of a steric barrier now enables the pathogen to navigate through the liquefied mucin gel. Figure adapted from Walker *et al.* [72].

What is particular about that mechanism, is, that it only transiently changes the mucus properties. When the bacterium has passed, acidic conditions are restored by gastric juices and the mucin forms a viscoelastic gel again. Transferring this strategy onto artificial carrier systems, that are additionally chemically designed not to bind to mucin biopolymers, could help to efficiently deliver drugs without causing permanent damage to the protective gastric mucosa. Thus, the natural barrier function of this special hydrogel would be brought back after the drug carrier has penetrated the mucus. In Section 4.5 the transfer of the *Helicobacter pylori* mechanism onto an artificial micro swimmer that can penetrate reconstituted gastric mucin gels is demonstrated.

However, the entire lack of particle-hydrogel interactions might – against intuition – be not the most efficient way to penetrate such a biological barrier. Recent studies on the basal lamina, a hydrogel system which separates the epithelial cell layer from the connective tissue, suggested, that binding interactions with the basal lamina biopolymers might indeed promote the penetration of molecules [73], as the interactions of charged molecules with the basal lamina leads to an increased uptake of those molecules into the hydrogel. Such a behavior might have a strong impact on the design and delivery of

pharmaceuticals, e.g., via the gastro intestinal tract. Thus, it is crucial to fully understand the dynamic mechanisms which are involved in the process of molecule/particle penetration of a mucus layer to develop efficient drug delivery systems. Rational design of specifically adapted pharmaceuticals or drug carriers that deliberately interact with mucins might increase the percentage of drug molecules that eventually reach the blood stream. This would help to minimize systemic side effects as the dosage of drugs could be considerably decreased. In the appendix Section D.1, the uptake kinetics of cationic molecules into reconstituted gastric mucin gels are analyzed.

However, for a more detailed understanding of interactions of drug molecules with mucin, the responsible domains of those large glycoproteins must be identified. The complex structure of mucins comprises not only distinct structural motives and numerous protruding glycan chains, but as well hydrophobic domains and various charged moieties [51]. To identify or eliminate the involvement of such functional structures, a top-down approach might offer a suitable solution: sequential removal of specific elements of the polymer accompanied by experimentally probing the modified mucins, might reveal valuable key players involved in the interaction with molecules such as pharmaceutics. In Section 4.7 and the appendix Section 0, such top-down approaches are presented: here, the role of the hydrophobic termini of mucin as well as the mucin-associated charged glycans is evaluated.

In addition to its protective function towards pathogens and the regulation of molecule passage, mucins also play an essential role in lubrication processes on many wet body surfaces [9, 33, 37, 74-77]. When in- or digesting food, highly hydrated mucosal membranes in the gastro intestinal tract prevent the damage of underlying tissue by sharp-edged food particles and enable a smooth sliding along the digestive tract. Also the perception of food and beverages in the mouth seems to be associated with the lubricating ability of oral mucins: upon ingestion of certain food products, a dry, puckering perception occurs in the mouth, called astringency. This mouthfeel is evoked by interaction of certain foods or beverages with saliva components and the mucosal membrane in the mouth, resulting in a loss of lubricity in the oral cavity [78-83]. However, the detailed mechanisms provoking this mouthfeel are yet to be revealed. The food industry has developed increasing interest in understanding those mechanisms, as this rather particular mouthfeel is essential for the taste of certain products such as red wine, whereas it is undesired in other foods. Unveiling the role mucin lubricity plays in the sensation of astringency might therefore set the stage for the development of food products with an optimized taste experience. In Section 4.6 the loss of saliva lubricity upon ingestion of cationic astringents is investigated and it is demonstrated, that purified salivary mucin solutions constitute a model system to study the influence of food components on salivary lubrication.

Mucin-mediated lubrication, however, is not only limited to the gastrointestinal tract. Other examples include the movement of the eyelid on the cornea [84-86] or vaginal penetration during intercourse [87]. A proper lubrication of those tissues is required to prevent tissue damage so that the body can function smoothly. Accordingly, if those mucin-mediated lubrication processes are impaired, irritation of the affected tissue will occur [88, 89]. Numerous studies have tackled this issue and at least partial compensation of insufficient mucosal lubrication is provided by commercial products such as eye drops or lubes for intercourse. However, those solutions can only be applied temporarily and only fight the symptoms, not the causes. Importantly, the molecular mechanisms involved in the lubricating processes of mucins are not fully understood. This, however, is crucial to efficiently treat mucin-related illnesses that lead to diminished lubrication of body tissues, and provide more effective pharmaceutical solutions.

To accomplish those goals, the basic processes of mucin-mediated lubrication must be investigated. In general, boundary lubrication provided by polymers is achieved by two main mechanisms which involve the adsorption onto and subsequent shearing off of highly hydrated biomolecules from a surface [90-97]. Thus, lubricating polymers such as mucin need to be able to firmly adsorb to those surfaces. However, it remains still unclear which domains of the complex mucin glycoproteins are involved in this process. Gaining new insights in these basic mechanisms and identifying domains on the mucin molecule which are crucial for this process, could motivate new pharmaceutical therapies which provide remedy for people suffering from defective mucins. On the long run these insights may also help with the development of artificial boundary lubricants which could replace defective mucins. In Section 4.7, the importance of distinct mucin domains for the process of mucin-mediated lubricity is evaluated.

In conclusion, this thesis evaluates the structure-function relations of polymeric components of biopolymers. The focus of this evaluation is set on both the molecular mechanisms that render biological hydrogels such special entities, as well as the involvement of single hydrogel components such as proteins and polymers in those molecular mechanisms. By making use of top-down and bottom-up approaches, the importance of specific structural or chemical motives for the execution of these molecular processes is revealed. Additionally, these valuable insights are transferred to other biopolymers and confer them specific functions such as the ability to adsorb to a surface and function as a boundary lubricant. These insights provide a valuable tool for the bio-inspired design of artificial polymers which allow for the combination of several desired functions at once. Such bio-mimetics could be of great use for medical applications, lubrication in the industrial context, or further investigation of the structure-function relations of biopolymers.

2 Materials

2.1 Vitreous humor

The term vitreous humor describes the clear, gel-like structure which fills the inner part of the eye of vertebrates between the lens and the retina (**Figure 6**). It mainly serves as a stabilizer and maintains the shape of the eye. The vitreous is in contact with the retina and prevents it from detaching by pressing it against the choroid. The vitreous gel is free of blood vessels and consists mainly of water (98-99 %). Other components include salts, sugars and a network of biopolymers [98]. Collagen II fibrils are responsible for the mechanical stability [99], whereas polyanionic glycosaminoglycans such as hyaluronic acid or heparan sulfate are able to bind large amounts of water [98, 100-102]. The vitreous is nearly cell free and only contains few hyalocytes which produce hyaluronic acid, and phagocytes which remove debris from the vitreous and therefore maintain a clear visual field [103].

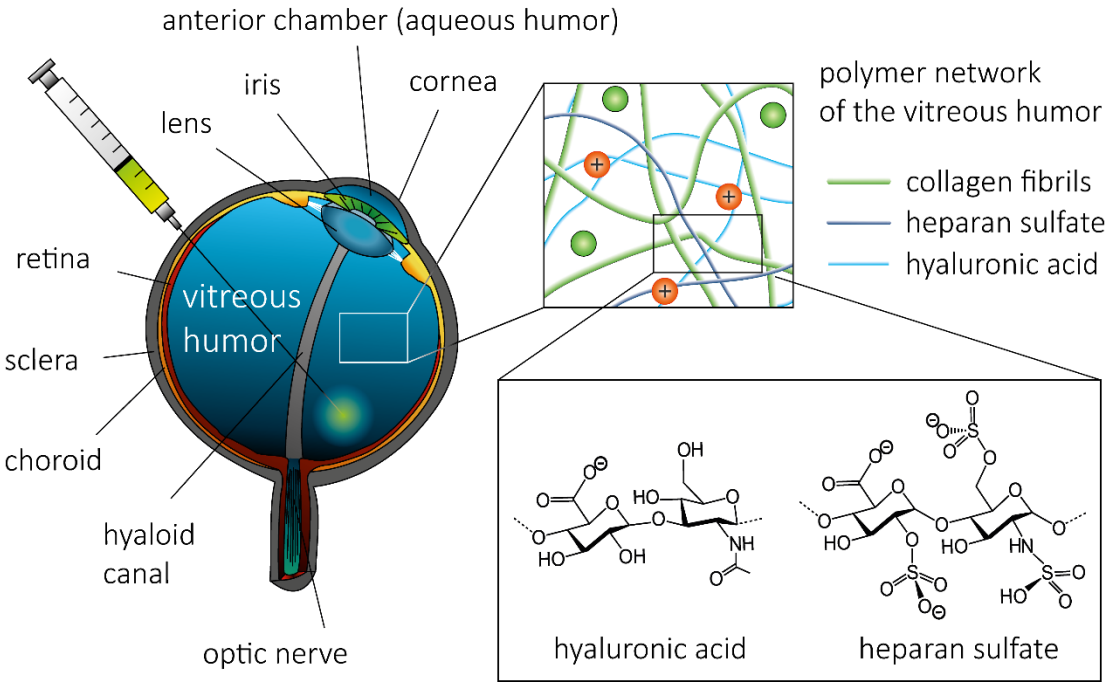

Figure 6: Schematic illustration of a human eye and the polymer network of the vitreous humor: In addition to a network of collagen fibrils, which can impede the diffusive movement of large pharmaceutical drug carriers via steric hindrance, polyanionic hydrogel components such as the glycosaminoglycans hyaluronic acid or heparan sulfate may pose an electrostatic diffusion barrier – even for drug molecules which are considerably smaller than the mesh size of the polymer network.

2.2 Mucin

Mucins are large, extracellular glycoproteins that are distributed throughout the whole human body. They are the main constituent of mucus, the slippery secretion that covers mucous membranes, and are mainly responsible for its characteristic properties.

2.2.1 Structure

Mucins are high-molecular-weight glycoproteins with sizes of up to several MDa, with the polysaccharide chains accounting for up to 80 % of their total mass [42, 51, 104]. These chains, which usually comprise 5-20 glycan units [105, 106], are concentrated in the core region of the mucin peptide, where repeating peptide sequences containing serine and threonine provide numerous anchor points for O-linked glycosylation [107].

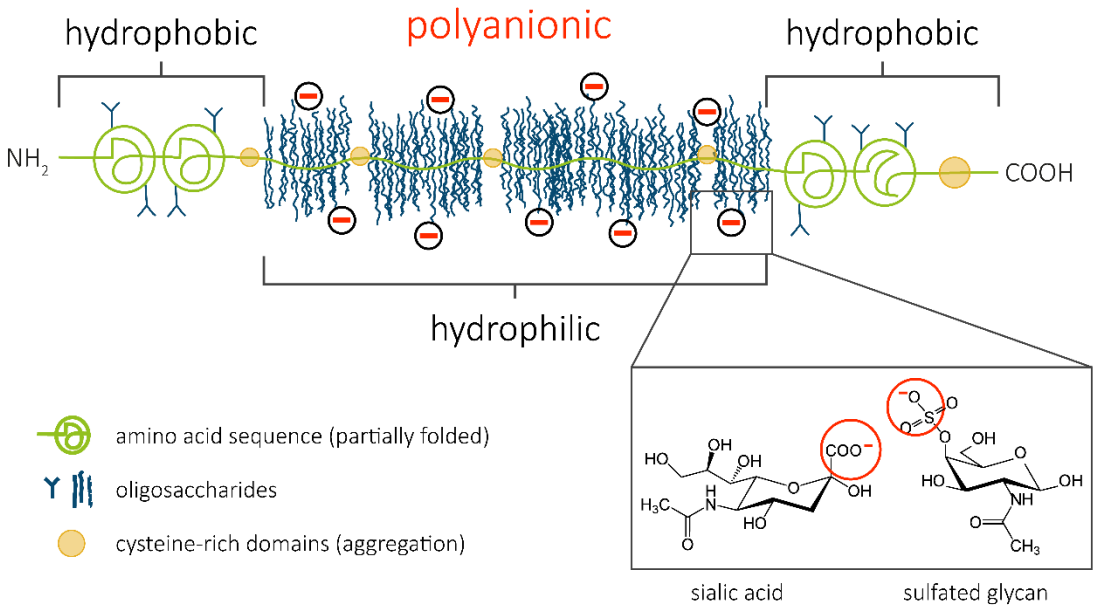

Figure 7: Schematic illustration of the structure of mucin: The hydrophilic, unfolded and glycosylated core region of mucins is flanked by two hydrophobic, partially folded terminal domains. Anionic glycans attached to the core region confer mucins their strong polyanionic character. Intermolecular disulfide bonds formed by cysteine-rich domains are suggested to induce aggregation of mucin molecules, generating ultra-high-molecular-weight agglomerates.

In addition to this particular amino acid sequence, the high density of attached glycans is responsible for the mainly unfolded structure of this central domain. Furthermore, the already hydrophilic character of this domain is enhanced via the attachment of hydrophilic glycans. The majority of glycans attached to the protein core consists of neutral carbohydrates, only a minor fraction comprises sulfated glycans and sialic acid [51, 108-115]. In contrast to the hydrophilic core region, the terminal domains are partially

folded and exhibit a rather hydrophobic character as a result of their amino acid composition and the lack of glycosylation. The elongated form of the mainly unfolded amino acid sequence of mucins, combined with the laterally protruding carbohydrate chains, results in a bottle brush-like structure of those large molecules [105, 116] (**Figure 7**). Cysteine-rich domains, which are located in between the glycosylated domains are suggested to be involved in intermolecular aggregation processes [117, 118], resulting in mucin aggregates that can exceed a molecular weight of 20 MDa – this aggregated form often is referred to as a 'train of brushes' [119-121].

2.2.2 Classification

Mucins are mainly divided into two distinct subfamilies [42]: cell-surface associated mucins and secreted, gel-forming mucins. Mucins attached to the cell-surface are part of the glycocalyx, a thin polysaccharide layer on top of the cell membrane which fulfills important tasks in cell-cell or cell-molecule interactions. Secreted mucins, however, are produced by goblet cells and seromucinous glands and are the main constituent of the mucosal membranes in the human body [122]. Over 20 different mucin variants have been identified so far with five of them being secreted and gel-forming (see **Table 1**). Although different mucins such as MUC2, MUC5AC and MUC5B exhibit a similar size, structure and glycosylation pattern, all three variants can be found, e.g., in the respiratory tract simultaneously. The reason for this redundancy, however, remains unclear.

Table 1: Distribution of the different secreted, gel-forming mucins in the human body. (Table adapted from [42]).

MUC2	Small intestine, colon, respiratory tract, eye, middle ear epithelium
MUC5AC	Respiratory tract, stomach, cervix, eye, middle ear epithelium
MUC5B	Respiratory tract, salivary glands, cervix, gallbladder, seminal fluid, middle ear epithelium
MUC6	Stomach, duodenum, gallbladder, pancreas, seminal fluid, cervix, middle ear epithelium
MUC19	Sublingual gland, submandibular gland, respiratory tract, eye, middle ear epithelium

2.2.3 Selective barrier function

With the exception of MUC7, all secreted mucins are able to reversibly form gels under certain conditions. Mucin gelation has been observed at high mucin concentration, acidic pH [63, 114, 123, 124] or driven by temperature changes [125]. Single mucin molecules form

intermolecular, non-covalent crosslinks and create a viscoelastic network. In recent years, there have been attempts to explain the mucin gelation mechanism via theoretical models. It was suggested that a combination of electrostatic and hydrophobic interactions within the amino acid sequence results in a conformational change of the mucins [51, 55, 125]. Also the interpenetration of carbohydrate side chains during the gelation process was proposed [126, 127]. However, convincing experimental evidence revealing the details of the gelation mechanisms has not been presented yet. Moreover, the particular domains of the complex mucin polymer involved in gelation remain to be identified.

Additional to the reversible pH-induced gelation of MUC5AC and MUC6 under acid conditions in the stomach, where a strong barrier is necessary to prevent the stomach epithelium from being digested by acidic gastric juices [32, 60, 128-130], the gel state of mucin in general is necessary to establish a barrier towards pathogens such as viruses and bacteria. Depending on the mucin concentration, the mesh size of this network varies. Therefore mucin gels can employ a size sieving mechanism, preventing both pathogenic as well as opportunistic commensal microbes from reaching and infecting the underlying epithelial tissue, whereas small molecules such as nutrients from digested food can pass this barrier. However, also many viruses which can be considerably smaller than bacteria and also than the mesh size of such mucus gels, cannot overcome this barrier [5, 131]. This indicates, that the permeability of mucin barriers is also governed by additional mechanisms other than size sieving. Previous studies have discovered that interactions of charged molecules and particles with mucin networks play an important role. This suggests electrostatic interactions as a plausible filtration mechanism – even for objects smaller than the prevailing mesh size of a mucin gel [17, 58, 61, 67, 132, 133].

2.3 Test particles

In this thesis, hydrogels and hydrogel components were probed with different particle and molecule systems, each with distinct characteristics. Different surface properties, shapes and conformations as well as sizes in the range of several nanometers up to the micrometer scale have been tested. In particular, various charge states of each system were evaluated to gain information about electrostatic interactions between the test particles/molecules and the polymer networks. All utilized particle systems were fluorescently labeled to enable a detailed observation via fluorescent light microscopy. **Figure 8** shows a schematic overview of the employed particle sets. Each particle/molecule species has its own distinctive benefit, e.g., specific chemical characteristics, good tunability, or availability in a broad range of sizes (see **Table 2** for details).

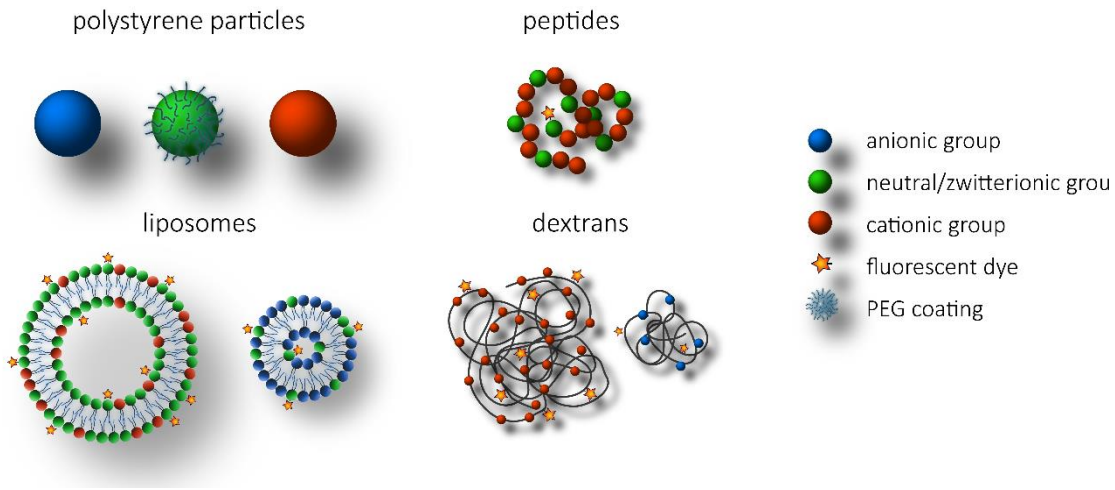

Figure 8: Overview of the fluorescent test particles and molecules utilized in this thesis: Various particle and molecule species were used to analyze interactions of those particle/molecule systems with the polymer network of the analyzed hydrogels. Please note that these schematic illustrations are not in scale.

2.3.1 Polystyrene particles

The synthetic polymer polystyrene can be used to produce quite monodisperse nano- and microparticles with defined diameters. It is a hydrophobic material, thus polystyrene particles tend to aggregate in aqueous solution. Chemical surface modifications can reduce this effect and additionally provide the opportunity to generate particles with different surface charges or chemistry, rendering those particles a helpful tool to study particle-molecule interactions at the nanoscale. Possible modifications include COOH, NH_2 and SO_4^{2-} groups, but also particles conjugated to biological molecules such as biotin are commercially available. However, it has to be noted, that, if the density of charged groups is too low, aggregation might still occur (especially in salt-free environment) and influence the obtained results (e.g., when employing single particle tracking). Thus, a surface potential strong enough to guarantee the presence of individual particles is necessary. In addition to aggregation, weakly charged polystyrene particles might as well engage in unwanted hydrophobic interactions with a polymer network. Especially using electrostatically neutral, unmodified polystyrene particles is challenging. However, coating those particles with low molecular weight polyethylene glycol (PEG) has been proven to efficiently render those particles virtually chemically inert. Another advantage, especially for the use of small polystyrene nanoparticles, is the possibility of incorporating fluorescent dyes into the bulk volume of the particles. This enables observation of those particles with light microscopy, even if their size is below the Abbe diffraction limit. Additionally, volume labelled particles provide a bright fluorescent signal and are hardly susceptible to photobleaching. This makes them a convenient platform for single particle tracking experiments.

2.3.2 Liposomes

In contrast to synthetic polystyrene particles, liposomes are biologically relevant as they serve as transport carriers in various biological systems. They are assembled from amphiphilic lipids that consist of a hydrophobic aliphatic chain and a hydrophilic head group, and they can form a bilayer in aqueous medium that builds the liposome. The lipid composition of a liposome influences several factors such as stability, rigidity or the permeability of the liposome [134-138]. A variety of lipids is available from commercial vendors, enabling the usage of liposomes for numerous experimental setups. Either the aliphatic chain or the head group can be chemically functionalized and/or fluorescently labelled. Furthermore, a mixture of different types of lipids within one liposome is possible, rendering those particle species a highly tunable tool for binding interaction studies or single particle tracking experiments. However, achieving a homogenous mixture of various lipids within one liposome species can be challenging as two criteria must be met: first, the fatty acid tails of different incorporated lipid species must match, otherwise their varying spatial configuration prevents the formation of a stable bilayer. Second, if a lipid bilayer comprising several lipid species forms, the rigidity of that layer must be high enough to prevent the diffusion of single lipids within the bilayer thus, preventing the thermodynamically driven formation of patches of a distinct lipid species. Additionally, liposomes are also sensitive to osmotic pressure effects and temperature changes. High salt conditions can result in an increase of permeability of the bilayer or even total breakdown of the liposome. Also hydrophobic interactions can promote liposome disintegration. Thus, the usage of this particle species in experimental setups makes it necessary to consider if the prevailing conditions could influence the properties of those particles.

In addition to binding interaction studies between liposomes and other molecular objects, those biological particles offer the possibility to incorporate small molecules such as pharmaceutical agents. By choosing a particular lipid composition, the susceptibility of this particle species towards particular experimental conditions (e.g., temperature or osmotic pressure) can be taken advantage of: e.g., the lipid bilayer can be chosen to be leaky and, as a consequence, to be permeable for incorporated molecules. Those molecules can thus be released from the liposome volume in a controlled manner, qualifying this particle system for the usage in drug delivery [27-31].

2.3.3 Dextrans

Dextrans are high-molecular-weight polysaccharide chains consisting of repeating glucose units and are of bacterial origin or can be synthesized from sucrose by bacterial enzymes.

The glucan chains have a molecular weight of a few kDa up to several MDa and can either be linear or branched. Dextrans are widely used in medical procedures [139, 140] and in laboratory use (e.g., in size-exclusion chromatography). However, as dextrans are commercially available in various defined molecular weights and offer the possibility to be chemically modified, they are also frequently used as test molecules in molecular research. Chemical modifications (e.g., via diethylaminoethyl (DEAE), carboxymethyl (CM), or sulfate groups), and the availability of fluorescent labels make dextrans a valuable tool for experimental research such as penetration studies. Additionally, the degree of those chemical modifications can be altered. This allows for tuning the amount of charges present on dextran molecules of a specific molecular weight, i.e. the charge density.

Although dextrans are linear molecules, they adopt the form of a Gaussian coil in aqueous solutions and can be approximated as a colloidal particle. This coiling is driven by entropy as the coil shape represents the most probable conformation a freely jointed chain-like polymer will adopt. Therefore, the Stokes radius of such a dextran molecule is an important parameter to quantify their sphere-approximated size. However, this approximation may not be fully accurate if the polymer carries a high number of charged groups: intramolecular electrostatic repulsion can result in the adoption of a more rod-like polymer structure. This should be kept in mind when performing experiments with dextran molecules with a high charge density as they may show a differing behavior compared to ideal entropic dextran coils.

2.3.4 Peptides

Synthesized peptides also represent an interesting platform for penetration studies. Similar to dextrans, they are linear polymers. Additionally, the amino acid composition can virtually be chosen at will. Both numerous repetitions of a single amino acid (e.g., polylysine) or a custom sequence of different amino acids are possible which renders peptides a highly tunable system. Although customized synthesis is limited by the overall number of consecutive amino acids, the generated peptide is much better defined in comparison to dextrans, as the exact number and position of, e.g., charged moieties can be set. Additionally, a much higher – and also more defined – charge density is possible when synthesizing peptides. Finally, those molecules can be fluorescently labelled with a great variety of dyes.

Table 2: Characteristics of test particles and molecules: The maximal number of charged groups on polystyrene particles, liposomes, dextrans and peptides utilized in this thesis was estimated at physiological pH based on particle/molecule size, molecule structure, pKa of the specific groups and supplier information.

Particle type	Particle size [nm]	estimated max. net charge [e] at neutral pH
polystyrene particles [141]	~ 200 - 1000	~ 10^6 - 10^8
liposomes	~ 200 - 2000	~10^5 - 10^7
dextrans [142]	~ 1 - 10	~10^0 - 10^3
peptides	~ 1.5	~10^0 – 2x10^1

2.4 Polydimethylsiloxane (PDMS)

PDMS is a silicone-based organic polymer which is used in various applications ranging from medicine and cosmetics to food production and industrial applications. It is a transparent material, chemically inert, non-toxic and therefore biocompatible. PDMS can be polymerized and crosslinked, thus forming a solid, elastic material. It exhibits a hydrophobic surface with contact angles towards water around 110° [143]. These surface properties promote the interactions with many proteins, which readily adsorb to an untreated PDMS surface [144]. Chemical modification of this surface is possible via plasma oxidation (e.g., using oxygen plasma), which introduces silanol groups into the surface silicone layers. Also, further functionalization with silanes such as APTES ((3-Aminopropyl)triethoxysilane) is possible by covalently grafting those molecules onto the silanol groups. Plasma treatment renders the PDMS surface hydrophilic [143, 145] and facilitates bonding to glass surfaces [146]. Whereas this covalent bonding is irreversible, the surface properties recover and the PDMS becomes hydrophobic again over time. This recovery process is accelerated at high temperatures. PDMS is impermeable for water; however, gases and water vapor can pass this elastomer. These characteristics make PDMS a suitable platform for many applications in laboratory use such as microfluidics and lab-on-chip setups: here, the hydrophobic nature of PDMS facilitates a controlled flow of aqueous solutions through channels in the micrometer scale. Additionally, its hydrophobic nature and the ability to serve as an adsorption layer for a variety of proteins makes PDMS useful for protein adsorption studies. Finally, PDMS surfaces are also a good platform to study bio lubricity: here, the hydrophobic PDMS surface mimics hydrophobic surfaces in the human body which can be found, e.g., in the corneal epithelium, the tongue, or articular cartilage [34, 84, 90, 147-149].

3 Theoretical background and methods

3.1 Diffusion

The process of diffusion describes the random movement of an object in a liquid or gas induced by thermal energy. This process was first observed by the Scottish botanist Robert Brown in 1827 and later described by Marian Smoluchowski [150] and Albert Einstein [151]. The molecules of a solvent, e.g., H_2O, fluctuate as a consequence of the thermal energy present in a system. These water molecules collide with the particles and transfer part of their momentum onto the particles. At a given time point, numerous molecules simultaneously collide with a given particle in a stochastic process, resulting in a random movement of the particle within the liquid. Although every single particle moves randomly and its detailed trajectory of movement is unpredictable, it is possible to make predictions on the mean squared displacement (MSD) of a single particle: on average, the overall displacement of a particle is zero since the momentum transfer from colliding solvent molecules is equal from each direction; however, the radius of the volume a diffusing particle is traversing, i.e. the MSD, grows with increasing diffusion time. The MSD is related to the diffusion coefficient as follows:

$$< x^2 > = 2nDt \qquad \textbf{(Equation 1)}$$

Depending on the dimension in which a particle movement it observed, the MSD reflects either the distance (n = 1), the area (n = 2) or the volume (n = 3) a particle traverses in a given time. **Equation 1** can be used to derive a diffusion coefficient D from a particle's MSD. This calculated coefficient can be compared to the theoretical diffusion coefficient which is given by the Einstein-Stokes relation (**Equation 2**). Here, k_BT denotes the thermal energy of the diffusing particle at the given temperature, R the particle radius and η the dynamic viscosity of the solvent:

$$D = \frac{k_B T}{6\pi\eta R} \qquad \textbf{(Equation 2)}$$

However, the calculation of a diffusion coefficient with **Equation 1** is only valid, if the observed particles undergo normal diffusion. If active transport of particles occurs via flux of the solvent (superdiffusion) or if the particles are restricted in their movement by any kind of obstacles (subdiffusion), no valid diffusion coefficient can be calculated. In all cases, the MSD is proportional to the time, and the exponent α describes the type of diffusive process:

$$< x^2 > \sim t^{\alpha} \qquad \textbf{(Equation 3)}$$

Here, a value of $\alpha = 1$ indicates free diffusion, whereas values of $\alpha < 1$ indicate subdiffusive and $\alpha > 1$ superdiffusive processes. However, when observing a particle movement in a more complex environment such as a polymer solution or a crosslinked hydrogel, the particle movement will exhibit a mixture of free diffusion (in between polymer strands) and restrained diffusion or even a complete stop of diffusion if the particle engages in binding interactions with the polymers, e.g., via electrostatic interactions. Despite those mixed diffusive states, an apparent diffusion coefficient D_{app} can be calculated via **Equation 1** to obtain comparable values that allow for comparing different scenarios.

3.2 Single particle tracking and microrheology

By observing the diffusive mobility of test particles in a hydrogel and determining the MSD and D_{app} respectively, conclusions regarding particle/polymer interactions can be drawn. Additionally, with test particles where the particle radius is equal or larger than the mesh size ξ, the particle movement can serve as a microrheological probe and provides valuable insights about the viscoelastic properties of said hydrogel system. To obtain such information, the MSD of diffusing particles can be calculated from its trajectory of movement over time as follows:

$$MSD(\tau) = \frac{1}{N}\sum_{i=1}^{N}[\vec{r}\,(i\Delta t + \tau) - \vec{r}(i\Delta t)]^2 \qquad \textbf{(Equation 4)}$$

For two-dimensional movies (e.g., obtained with a conventional light microscope), the trajectory of a particle $\vec{r}(t)$ contains an x and y value for each distinct time point. However, diffusion is a three-dimensional process and the movement of a diffusing object is typically isotropic. Thus, the MSD can as well be calculated from two- or one-dimensional movement information of the particles. For the calculation of the diffusion coefficient D (see **Equation 1**), the dimensionality has to be corrected (e.g., n = 2).

When probing the local viscoelastic properties of a crosslinked hydrogel, test particles bigger than the mesh size ($R > \xi$) are required. Here, the MSD of those particles will reach a plateau value at a certain time point. At short time scales, the particle can diffuse freely but eventually it gets in contact with polymer strands which hinder its diffusive movement. However, the elastic properties of that hydrogel allow stretching of the polymer mesh to a certain degree. As soon as the thermal energy of the fluctuating particle is smaller than the elastic forces, the particle cannot move further in this direction and exhibits a constrained diffusion behavior – resulting in a plateau of the MSD. With the given radius R this plateau value can be directly converted into an elastic modulus (i.e., the plateau modulus G_0):

$$< \Delta x^2(\tau \to \infty) > = \frac{k_B T}{\pi G_0 R} \quad \text{(Equation 5)}$$

In **Equation 5**, the plateau modulus describes a measure of the local mechanical properties of the polymer network. However, the test particles must be selected carefully: if the chosen particle size is too small and far below the mesh size, the diffusion coefficient of the solvent is measured instead of the viscoelasticity of the network. Therefore the approximate mesh size of a hydrogel, as well as the chemical properties of its components are valuable information when conducting microrheological measurements.

3.3 Macrorheology

In addition to microrheological measurements, the viscoelasticity of a polymer system can also be determined via macrorheology. However, in contrast to microrheology, where the mechanical properties are only probed locally, macrorheology techniques determine the material response of the entire hydrogel system. Therefore, values obtained from those two experimental methods can deliver deviating results.

In a macrorheological setup, the hydrogel can be probed by dynamic shear measurements: the hydrogel sample is placed between a stationary and an oscillating plate and the sample is sheared at a certain frequency with a defined amplitude. This two-plate model allows to evaluate the viscoelastic parameters of the hydrogel. The applied shear stress results in a strain response of the probed material. When the applied oscillatory stress σ is within the linear response regime, i.e. Hooke's law applies, the strain response γ follows the same frequency as the applied stress but with a certain phase shift δ:

$$\sigma(t) = \sigma_0 sin(2\pi f t) \quad \text{(Equation 6)}$$

$$\gamma(t) = \gamma_0 sin(2\pi f t + \delta) \quad \text{(Equation 7)}$$

This phase shift, however, depends on the material properties: whereas ideally elastic materials exhibit no shift in the strain response, the response is shifted by 90° when probing purely viscous materials. However, most materials possess viscoelastic properties and exhibit a phase shift of $0° < \delta < 90°$. With those given and measured parameters, the viscoelastic moduli G' and G'' can be calculated, where G' represents the elastic part and therefore the amount of energy stored in a system (storage modulus) and G'' the viscous part, i.e. the loss of energy during deformation (loss modulus):

$$G'(f) = \frac{\sigma_0}{\gamma_0} cos\delta(f) \quad \text{(Equation 8)}$$

$$G''(f) = \frac{\sigma_0}{\gamma_0} sin\delta(f) \quad \text{(Equation 9)}$$

3.3.1 Viscoelasticity of polymer systems

Polymer solutions exhibit a behavior observed for all non-Newtonian fluids, meaning that the viscosity is dependent on the shear strain. Structural changes within the polymer system (e.g., alignment of the single polymer strands) with increasing strain (or strain rate) result in a shear-thinning behavior. Furthermore, such polymer solutions can show a time dependent shear-thinning behavior called thixotropy: some structural changes need a certain amount of time to occur and the effect of the shear stress is delayed.

Another important parameter which influences the viscoelastic behavior is the frequency with which the polymer system is probed. This dependency can be so drastic, that polymer solutions can behave as viscoelastic solids and transiently crosslinked polymer gels as viscoelastic solutions – at least at certain shear frequencies (**Figure 9**). Here, a gel-like behavior is usually observed for a viscoelastic material, where the elastic part dominates the viscous part, i.e. $G' > G''$.

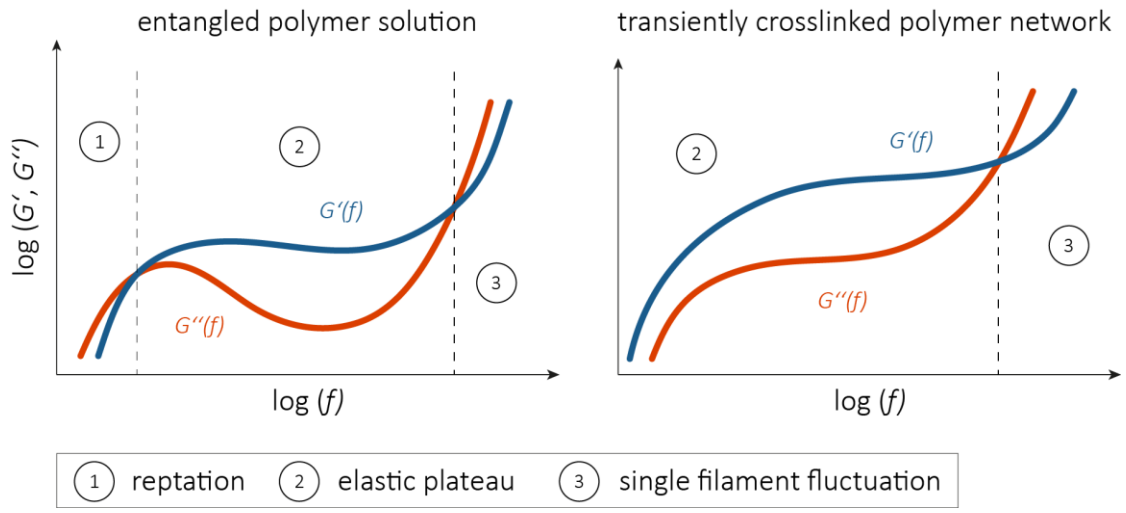

Figure 9: Frequency-dependent viscoelastic behavior of polymer systems: The viscoelastic behavior of entangled polymer solutions (left) and crosslinked polymer networks (right) strongly depends on the frequency with which the system is probed. Molecular reptation processes, entanglements of polymer strands, or single filament fluctuations can influence the viscoelastic response of polymer systems subjected to shear stress.

When applying a shear stress at low frequencies, the polymers in an entangled solution have enough time to slide past each other and thus can relax internal stresses – this process is called reptation. With increasing frequencies, the polymers do not have enough time to disentangle – the polymer consortium starts to act as a single coherent system and exhibits an elastic character, and the viscous modulus G'' has a local minimum. However, when probing an entangled polymer solution at very high frequencies, the wavelength of the oscillation is so short, that this oscillation can also develop in between

contact points with adjacent entangled polymers, thus dissipating energy and behaving like a viscoelastic solution again. For transiently crosslinked polymer gels, the curve progression is quite similar, however here, at low frequencies, no reptation takes place as the polymers are connected to each other. Therefore, *G'* dominates at low and medium frequencies and is approximately constant in this regime.

3.3.2 Gel-formation of polymer systems

Parameters that influence the viscoelastic properties of polymer solutions and can induce gelation processes include temperature, pH, and the addition of, e.g., crosslinker substances. The gelation point of a viscoelastic solution is usually defined as the point where the elastic part *G'* starts to dominate the viscous part *G''*. Polymers such as agarose or methyl cellulose can form viscoelastic solutions or gels, depending on the prevailing temperature. Whereas the polysaccharide agarose behaves as a viscoelastic fluid at high temperatures and is able to form inter- and intramolecular hydrogen bonds that induce gelation when the temperature decreases, methylated cellulose is a viscoelastic liquid at low temperatures and forms gels at high temperatures only. This reverse temperature dependency compared to agarose is based on intramolecular interactions of the hydrophobic methyl groups. In a sol state at low temperatures, these groups are surrounded by structured water molecules. When the temperature is increased, these water clathrates are disrupted and the hydrophobic interaction between the methyl groups is enhanced resulting in the formation of a methyl cellulose gel [152].

A prominent example for a sol-gel transition triggered by pH is observed for the gel-forming variants of the glycoprotein mucin. However, the detailed mechanism behind this gelation process is not fully understood. Recent studies proposed a combination of hydrophobic and electrostatic interactions, but clear experimental evidence is still missing (see Section 2.2.3). However, electrostatic interactions play an important role in various other gelation processes of charged polymers: polyanionic polymers such as alginate can be easily crosslinked by the addition of multivalent cationic ions such as Ca^{2+} which serve as a crosslinker between the single alginate strands thus evoking a sol-gel transition.

Those gelling abilities of biopolymer solutions are used intensively in many industrial applications: agarose is employed for the production of bubble tea or, in laboratory settings, for the separation of proteins and molecules (e.g., in agarose gel electrophoresis). Methyl cellulose is used in the food industry as a thickener or emulsifier. The gelation of gel-forming mucins is not yet used in industrial applications but is of great importance to maintain the fundamental function of mucin as a selective barrier towards pathogens.

3.4 Microfluidics

The analysis of biological hydrogels or their individual components *in vitro*, especially when of human source, is a cost and labor intensive endeavor. Often, the amount of source material is quite limited or the purification processes are time consuming and accompanied by a considerable loss of the desired product throughout the whole process. Hence, it is of great importance to reduce the amount of sample material needed in experimental settings as much as possible. For molecular penetration studies, where the binding interaction of, e.g., nanoparticles or molecules with reconstituted hydrogel components, such as mucins, needs to be evaluated, microfluidic setups offer a convenient solution. Here, the design of setups with microscopic channels allows for the analysis of hydrogel systems with sample volumes in the microliter or even nanoliter range. Additionally, also the amount of test molecules/particles, which often are expensive as well, can be reduced drastically in comparison to other techniques. Another positive aspect is the relatively easy visualization of those setups on a conventional inverse light microscope, which also allows for monitoring and recording the measurement in real time via a digital camera – especially when employing fluorescent test molecules/particles.

3.5 Biotribology

Tribology describes the study of friction, wear and lubrication. These processes occur throughout the whole human body and are crucial to prevent tissue damage to many body surfaces which need to be properly lubricated. This important task is carried out by biopolymers. Prominent representatives of this class are, e.g., hyaluronic acid, lubricin, or mucins. The former are found in the synovial fluid of joints whereas the latter is found on various body surfaces such as the cornea, the inner lining of the gastrointestinal tract, or the urogenital tract of women.

3.5.1 Lubrication regimes: the Stribeck curve

In contrast to industrial lubricants such as oil, biopolymer solutions can lead to friction coefficients even lower than 10^{-2}, and thus can even provide low friction over a broad range of sliding speeds. The Stribeck curve (named after the German engineer Richard Stribeck), describes the different friction regimes which can be observed when sliding two liquid-lubricated surfaces against each other at varying sliding speeds.

In the boundary lubrication regime, i.e., at low sliding speeds, the opposing surfaces are in direct contact with each other and there is no liquid lubrication – the coefficient of friction is at a maximum value (**Figure 10**, black curve). With increasing sliding speeds,

the Stribeck curve enters the mixed lubrication regime, as a thin liquid film starts to build up between the two surfaces, partially separating them and thus reducing the friction. Depending on the surface roughness, this effect occurs at lower sliding speeds for smooth surfaces, whereas rough surfaces require higher speeds to be separated by a liquid film. At even higher sliding speeds, the two surfaces are fully separated by the liquid film. Thus, friction is drastically reduced as only the shear forces between the surfaces and the lubricant itself or internal friction processes within the lubricant generate friction. In this hydrodynamic lubrication regime, the coefficient of friction is now only depending on the viscosity of the lubricating medium, whereas the microscopic properties of the opposing surfaces become irrelevant. Therefore, the subsequent increase in friction with increasing sliding speeds follows a linear function if the lubricant shows the behavior of a Newtonian fluid.

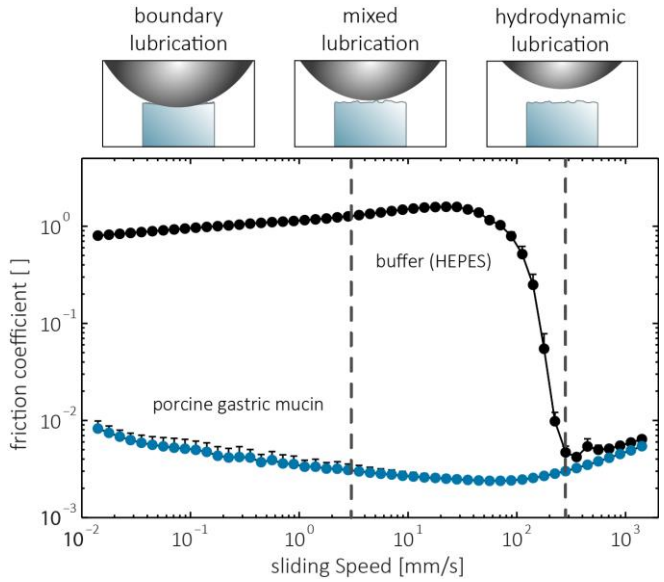

Figure 10: Exemplary Stribeck curve with the characteristic lubrication regimes: When sliding two surfaces against each other, the degree of friction depends on the sliding speed. The buffer curve (black dots) clearly depicts the three different friction regimes as predicted by Stribeck's theory. However, when employing a biopolymeric lubricant, e.g., mucin (blue dots), the coefficient of friction can be very low ($\mu < 10^{-2}$), even in the boundary lubrication regime at low sliding speeds.

This characteristic Stribeck curve is similar for oil and water based lubricants. However, if the lubricant viscosity increases, the curve is shifted to lower sliding speeds as the surfaces are separated earlier. Furthermore, the slope in the hydrodynamic regime is higher for solutions with higher viscosities. However, when biopolymers such as mucins are probed as lubricants, e.g., between a steel and PDMS surface, a completely different curve shape is observed: throughout the whole mixed and boundary lubrication regimes, a very low friction coefficient can be obtained (**Figure 10**, blue curve).

3.5.2 Polymer-mediated boundary lubrication

The outstanding lubricating qualities of biopolymer solutions are based on the synergistic combination of two molecular processes (**Figure 11**). The first mechanism, called sacrificial

layer mechanism, involves the adsorption of polymers to one or both of the opposing surfaces, combined with subsequent shearing off and reattachment of those polymers. This cyclic exchange of polymers leads to the dissipation of friction energy [91, 97]. However, reducing friction forces via this sacrificial layer formation is efficient only, when the second mechanism, hydration lubrication, is active as well: when the adsorbed polymers are highly hydrated, they provide a thin hydrated layer between two surfaces. This surface bound water layer thus prevents those two sliding surfaces from coming into direct contact – even at very low sliding speeds in the boundary lubrication regime [93, 94]. This process enables smooth gliding of the surfaces against each other and reduces friction forces.

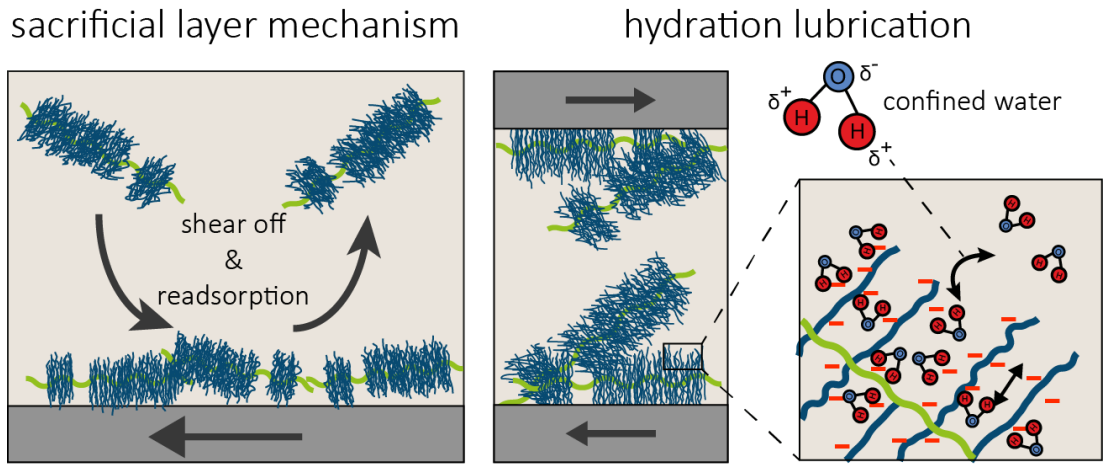

Figure 11: Mechanisms of mucin-mediated boundary lubrication: A combination of two mechanisms (sacrificial layer mechanism, and hydration lubrication) enables efficient lubrication, even in the boundary friction regime. Here, hydrated polymers adsorb to a surface and are sheared off again, thus dissipating energy. Additionally, two opposing surfaces are separated by a thin hydrated layer and therefore high friction forces are prevented.

Additionally, under pressure, the trapped water molecules are exchanged with free water molecules from the solution, thus dissipating even more friction energy. This effect can even be more pronounced for highly charged polymers, as the interactions of charged polymer moieties with the electric dipole of water molecules results in more strongly confined water molecules within the polymer. Thus, larger amounts of energy are dissipated when the bound water is exchanged with free H_2O molecules.

In many physiological friction processes, the sliding speeds are rather low so that boundary lubrication is a necessary requirement. Typically, this task is fulfilled by highly hydrated biopolymers such as mucin, lubricin or hyaluronic acid.

3.6 Quartz crystal microbalance

In addition to being strongly hydrated, lubricating biopolymers must be able to adsorb to at least one of the surfaces, which are supposed to be lubricated. A quartz crystal microbalance (QCM) offers a suitable technique to quantify the adsorption kinetics of proteins or polymers to surfaces. Here, the piezoelectrical potential of a quartz crystal is utilized. An alternating voltage is applied which causes the crystal to oscillate at its resonance frequency (usually several MHz). If additional mass is deposited onto the surface of the crystal (e.g., by adsorption of proteins), the resonance frequency changes linearly with the adsorbed mass. This relation was first described by Günter Sauerbrey in 1959 [153]:

$$\Delta f = -\frac{2f_0^2}{A\sqrt{\rho_Q \mu_Q}}\Delta m \qquad \textbf{(Equation 10)}$$

Here, f_0 denotes the resonance frequency of the quartz crystal, A the piezoelectrically active quartz crystal area and ρ_Q and μ_Q the density and the shear modulus of quartz respectively. Conveniently, when measuring with a defined set of quartz crystals, all these specific coefficients can be summed up by a single constant, C_f, simplifying the equation to:

$$\Delta f = C_f \Delta m \qquad \textbf{(Equation 11)}$$

However, when observing the adsorption kinetics of molecules in liquid environments, the Sauerbrey equation is only valid, when the adsorbed mass forms rigid layers. Thus, quantifying the adsorption of proteins in aqueous environment is more challenging: most proteins interact very well with water and therefore the adsorbed layers exhibit a viscoelastic character. To solve this problem, a second measured variable in addition to the frequency is evaluated: the dissipation. To do so, the quartz crystal is first set into oscillation, then it is separated from the voltage source and the dampening of its oscillation by the surrounding liquid is analyzed. With this additional parameter, it can be determined if the adsorbed layer is rigid and can be treated as an elastic material or if viscoelastic properties need to be considered for evaluating the shift in the measured resonance frequency [154].

4 Summaries of publications

4.1 Diffusion regulation in the vitreous humor

***Benjamin T. Käsdorf**, Fabienna Arends, and Oliver Lieleg* [155]

Efficient treatment of ocular diseases concerning the posterior eye segment, e.g., the retina, is a very challenging task. Topical and systemic administration of pharmaceuticals suffers from low efficiency due to poor drug penetration through the barriers of the human eye, leaving intravitreal injection as the best delivery route of drugs. However, there are major drawbacks for this method as well, such as injection-associated infections, patient noncompliance and poor residence time of drugs in the vitreous humor. This multicomponent hydrogel possesses selective permeability properties which allow for the unhindered passage of certain molecules and particles, whereas others are immobilized within the vitreous polymer network. However, for an efficient treatment it is crucial for pharmaceutical drugs to diffuse freely to the target site.

This study investigated the selective permeability properties of the vitreous humor of three mammalian species. The obtained results identified two macromolecular components of the vitreous as well as physical key principles which establish selectivity in this multi-component hydrogel.

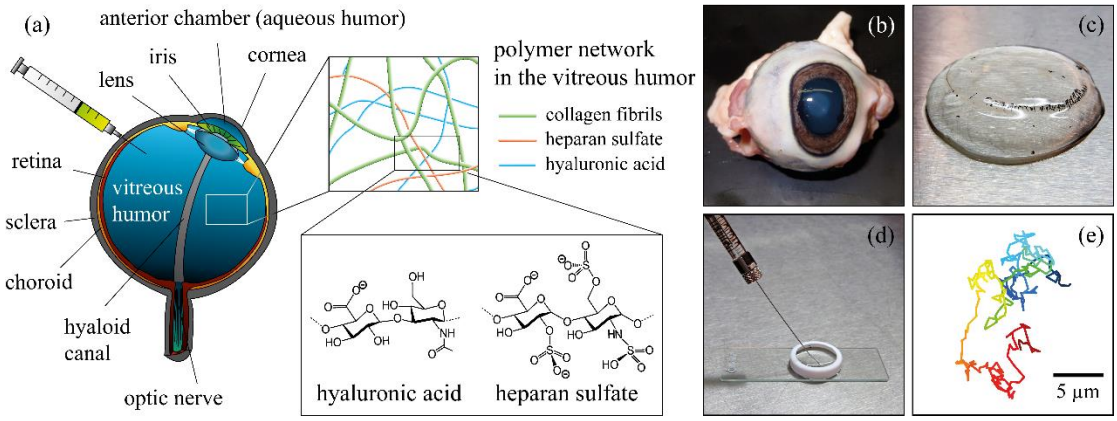

Figure 12: Table of content graphic: Schematic overview of the hydrogel network in the vitreous humor (a) and the procedure of probing the permeability of this hydrogel with single particle tracking of injected nanoparticles (b-e).

Single particle tracking is employed to determine the apparent diffusion coefficient of 200 nm polystyrene particles (net charge anionic, neutral or cationic) in bovine, porcine and ovine eyes. In contrast to anionic and neutral particles, the cationic particles are

partially immobilized within the vitreous polymer network and show a bimodal distribution of normal and sub-diffusing particles in all three species. This suggests binding and unbinding events when interacting with the polymer network of the vitreous humor. Probing this selectivity with a second particle system (liposomes) revealed a virtually identical picture. Additionally, Debye screening with high-concentrated salt solutions prevented cationic particle immobilization, suggesting that this effect is indeed based on electrostatic interactions. Furthermore, enzymatic digestion of hyaluronic acid and heparan sulfate results in a strong increase of the mobility of cationic particles, identifying those two polyanionic glycosaminoglycans as key players for establishing the selective permeability of vitreous humor. In a final step, the penetration efficiency of dextrans and peptides into ovine vitreous humor was investigated and demonstrated, that the selective barrier exists in addition to nanoparticles also for small molecules, given that the overall net charge of those molecules exceeds a threshold of cationic charges.

In conclusion, this study demonstrates, that cationic particles and molecules interact with the polyanionic polymers hyaluronic acid and heparan sulfate, which drastically decreases their overall diffusive mobility. These novel insights could prove useful when developing new pharmaceuticals for treatments of ocular diseases to ensure efficient intravitreal diffusive transport of those molecules or in contrast, design of carrier particles which are immobilized at the injection site on purpose – enabling long-term release of drug molecules in constant proximity to the target site and thus reducing the need of frequent intraocular injections.

Individual contributions of the candidate: I contributed to the conception of this study, designed and conducted the experiments, performed data analysis, and wrote the article.

4.2 Controlled nanoparticle release from a hydrogel by DNA-mediated particle disaggregation

*Constantin Nowald, **Benjamin T. Käsdorf**, and Oliver Lieleg* [156]

Efficient treatment of numerous diseases requires the presents of different pharmaceutical drugs in the human body at the distinct time points. This can be achieved by sequential administration of those pharmaceuticals, however it requires a specific and complex administration schedule to obtain an optimal treatment. A convenient alternative would be a drug delivery system that releases the needed therapeutic agents at the required point of time.

This study demonstrates a drug delivery system with a controlled sequential release of particles from an artificial hydrogel system, allowing for spatio-temporal control over the administration of drugs.

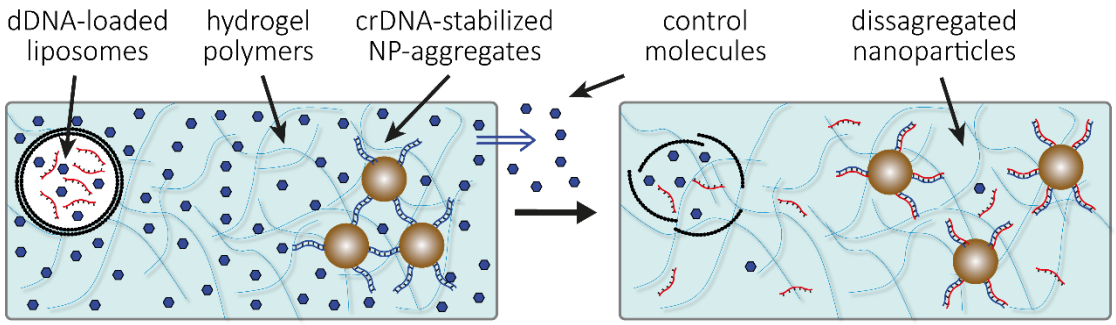

Figure 13: Table of content graphic: Schematic overview of the disaggregation of gold nanoparticles triggered by several subsequent mechanisms, providing spatio-temporal control over the particle release.

For the controlled release, gold nanoparticles, which are extensively investigated in a therapeutic context, are aggregated by linking them with covalently bound, synthetic DNA molecules. These aggregates are embedded into an agarose gel enriched with the control molecule sorbitol where steric interactions prevent those large aggregates from diffusing out of the agarose gel. Additionally, liposomes loaded with a second set of synthetic DNA-molecules and sorbitol are embedded into the hydrogel as well. When incubated in buffer, sorbitol is diffusing out of the gel over time and thus an osmotic pressure is built up in the liposomes where the sorbitol cannot diffuse through the lipid bilayer. This increasing pressure results in swelling of the DNA-loaded liposomes, which subsequently triggers the release of those DNA molecules. A competitive binding of the released DNA strands leads to the displacement of the DNA molecules that aggregate the gold nanoparticles, resulting in the disaggregation of those nanoparticle clusters. Now,

single nanoparticles can diffuse through the hydrogel. Additionally, this disaggregation process can be further prolonged by introducing cationic microparticles into the agarose gel, which slow down the overall diffusive mobility of the released DNA strands by means of electrostatic interactions – delaying the final release of gold nanoparticles even longer. Depending on the concentration of those cationic microparticles, the beginning of the gold nanoparticle release from the hydrogel can be prolonged for over one week.

In conclusion, the system presented in this study enables the controlled release kinetics of nanoparticles, by triggering several cascades. Additionally, the parameters of this system can be further tuned, e.g., the composition of the liposomes in regard to the susceptibility to osmotic pressure or the sequence of the artificial DNA-strands which regulate the disaggregation of the gold nanoparticles. The high tunability of those parameters allows for even more spatio-temporal control when releasing a therapeutic agent and therefore may help facilitating a more efficient pharmaceutical treatment.

Individual contributions of the candidate: I contributed to the design and performance of the experiments, the data analysis, and the writing of the article.

4.3 Macromolecular coating enables tunable selectivity in a porous PDMS matrix

*Benjamin Winkeljann [*], **Benjamin T. Käsdorf** [*], Job Boekhoven, and Oliver Lieleg*
(: equal contribution) (accepted)*

Selective permeability is an essential feature for many biological processes in the human body such as protection against pathogenic attacks or regulation of the uptake of nutrients, whereas denying passage of unwanted xenobiotics at the same time. Many technical filtration applications attempt to mimic those efficient biological filtration mechanisms, however they often are cost-intensive and limited to the filtration according to a defined parameter set and thus lack flexibility.

This study demonstrates a highly tunable PDMS-based filtration system. First, cotton candy was embedded in PDMS. After curing, the sugar fiber were washed out – thus creating a capillary network with a high surface-to-volume ratio within the PDMS. Subsequent functionalization of the inner capillary surface enables this artificial PDMS sponge to selectively filter different particles/molecules from a solution. Depending on the functionalization of those capillaries, various filtration profiles can be created. Coating with biomacromolecules such as mucins allows for selective filtration of liposomes or dextran molecules by means of electrostatic interaction, whereas synthetic molecules such as peptide amphiphiles additionally can sieve by steric hindrance. Capillary functionalization with biotin specifically removes streptavidin coated liposomes from solution. Additionally, the catecholamine dopamine can serve as a basis for numerous secondary coating, enabling the functionalization with a variety of molecules. Also, immobilization of enzymes allows for catalytic assays within this PDMS matrix.

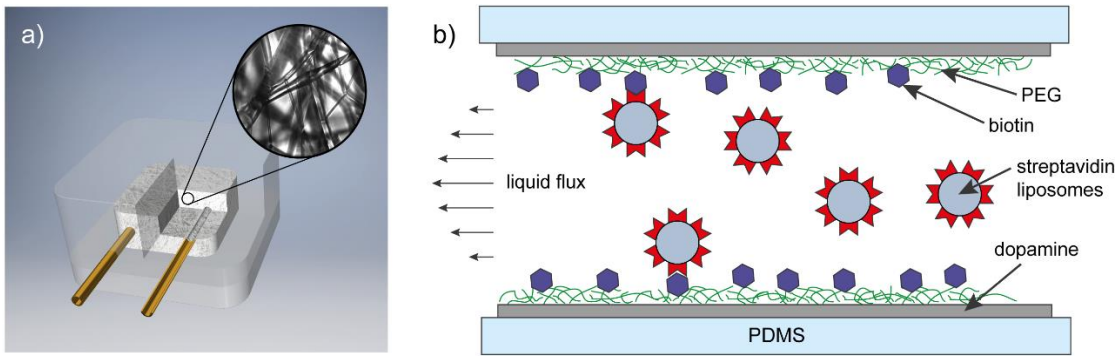

Figure 14: Table of content graphic: Schematic illustration of the PDMS-based capillary system (a) and the filtration of test molecules from solution via specific interaction with functional groups immobilized onto the capillary surface (b).

In conclusion, this highly tunable, artificial, low-cost filtration system allows for multiple different filtration outcomes, depending on the chosen functionalization. Whereas physisorption of several biomolecules is sufficient to provide an efficient filtration outcome, dopamine provides a basis for many additional secondary covalent functionalizations. This renders this defined capillary PDMS-matrix a powerful tool, which can be adapted to the respective need. This facilitates multiple processes in lab-scale purification of solutions or performance of enzymatic digestions with immobilized enzymes – enabling the reuse of those expensive catalysts.

Individual contributions of the candidate: I contributed to the conception of this study, the design and performance of the experiments, the data analysis, and the writing of the article.

4.4 An optimized purification process for porcine gastric mucin with preservation of its native functional properties

*Veronika J. Schömig, **Benjamin T. Käsdorf**, Christoph Scholz, Konstantinia Bidmon, Oliver Lieleg and Sonja Berensmeier* [157]

Mucins are densely glycosylated high-molecular-weight proteins and constitute the major component of mucosal membranes on all wet epithelia in the human body. Those brush-like biopolymers protect underlying tissue from mechanical damage by forming viscoelastic gels under acidic conditions or protect from the infection by bacteria and viruses by constituting a selective barrier. In addition, their highly hydrated nature renders them excellent lubricants. Mucins recently received particular attention and are more and more subject to intensive research as they could prove valuable for biomedical applications. However, characterizing those molecules requires the availability of intact native mucins for research purposes. Although mucins are commercially available, many of their unique properties are lost during the commercial purification processes.

In this study, a purification process for porcine gastric mucins is presented, which, on the one hand delivers high protein yield but on the other hand also preserves the intrinsic properties of native mucin throughout the whole process.

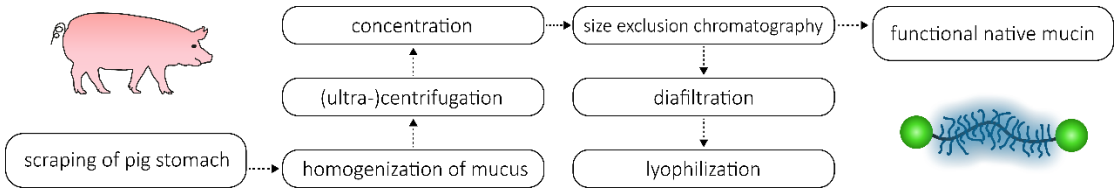

Figure 15: Table of content graphic: Schematic illustration of the purification process of porcine gastric mucin.

Crude mucus is obtained from fresh porcine stomachs, homogenized in buffer and separated from cell debris via several subsequent centrifugation and ultracentrifugation steps. The mucus solution is concentrated and the high-molecular-weight mucins are isolated from other proteins or smaller molecules by size-exclusion chromatography. After a final diafiltration step against ultrapure water, the purified mucins are freeze dried for long-term storage. The overall yield of this process was 66 % and approximately 65 mg mucin could be purified from one porcine stomach. Characterization of the isolated mucin molecules demonstrated, that crucial functions such as the ability to lubricate, gelling at acidic pH, and the selective permeability of those gels is preserved throughout the process.

In conclusion, the demonstrated mucin purification process maintains the native functions of mucin and delivers high yield at the same time. In contrast to commercially available mucins, these mucins isolated here can serve as a model system to characterize mucin/mucus properties or may be of valuable use in biomedical applications where those unique properties of native mucin are essential.

Individual contributions of the candidate: I contributed to the conception of this study, the design and performance of the experiments, and the data analysis.

4.5 Enzymatically active biomimetic micropropellers for the penetration of mucin gels

*Debora Walker, **Benjamin T. Käsdorf**, Hyeon-Ho Jeong, Oliver Lieleg and Peer Fischer* [72]

All wet body epithelia are covered with mucus, a hydrogel which selectively protects them from infection by pathogens. Its main constituent mucin – a high-molecular-weight glycoprotein – is responsible for those selective properties as it forms a dense crosslinked network under acidic conditions (e.g., in the stomach) and interacts with pathogens such as bacteria and viruses and thus preventing them from reaching the underlying epithelial cell layer. However, mucus also constitutes a barrier towards particles or molecules and can therefore interfere with the efficient delivery of drug molecules through those mucus layers, resulting in a diminished effect of the administered pharmaceuticals. The bacterium *Helicobacter pylori* has found a way to overcome this mucus barrier: it secretes the enzyme urease, which hydrolyses naturally occurring urea into carbon dioxide and ammonia, and thus triggers a local increase of the pH value. This alkalization then results in a transient liquefaction of the mucin gel which allows the bacterium to migrate through the mucus layer.

This study demonstrates, that this mechanism of *Helicobacter pylori* can be applied to artificial magnetic micropropellers, enabling them to transmigrate through a barrier of reconstituted pig stomach mucin.

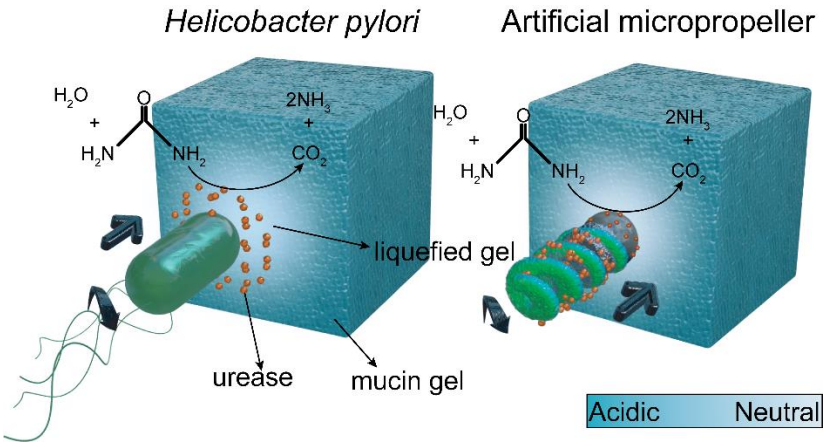

Figure 16: Table of content graphic: Schematic illustration of the mechanism *Helicobacter pylori* utilizes to maneuver through gastric mucin and the mimicry of that mechanism by an artificial magnetic micro swimmer.

Acid-stable magnetic silica micropropellers were fabricated by glancing angle deposition (GLAD) and atomic layer deposition (ALD). Those propellers were functionalized with the enzyme urease. The propellers were embedded in a reconstituted mucin solution (from

porcine stomachs) and a subsequent acidification resulted in a gel-formation of the mucins. By applying a rotating magnetic field, the propellers revolve around their long axis, however they are not able to penetrate the reconstituted mucin gel and only rotate on the spot. However, when embedding those propellers into an acidified mucin gel which additionally contains urea, the substrate of the enzyme urease, a forward propulsion is generated, when applying the magnetic field.

In conclusion, mimicking this molecular strategy of *Helicobacter pylori* could prove as a useful tool when developing novel transport systems for efficient drug delivery in the gastrointestinal tract. Additionally, when considering that the preservation of the integrity of the mucosal membrane is essential for protection against pathogens, this mechanism benefits from the fact that the liquefaction of the mucin gel is only temporary.

Individual contributions of the candidate: I performed the purification of the mucin and the rheological measurement.

4.6 Cationic astringents alter the tribological and rheological properties of human saliva and salivary mucin solutions

*Max Biegler, Judith Delius, **Benjamin T. Käsdorf**, Thomas Hofmann and Oliver Lieleg* [158]

Astringency describes the dry, puckering mouthfeel, upon ingestion of various foods or beverages containing, e.g., metal salts, acids or polyphenolic compounds such as tannins. Although astringency is a well-known taste experience, the molecular mechanisms involved in this process remain to date unclear. However, astringency moved more and more into the focus of the food industry, as this particular taste experience is often unwanted in many food products, but in other cases crucial for the desired taste experience, e.g., when consuming red wine. Therefore, a detailed understanding of the origins of astringency is an important step towards the gustatory optimization of many foods and beverages.

This study investigated the loss of saliva lubricity upon ingestion of cationic astringents which was attributed to the aggregation of mucin-glycoproteins. This behavior could be reproduced with purified salivary mucin solution

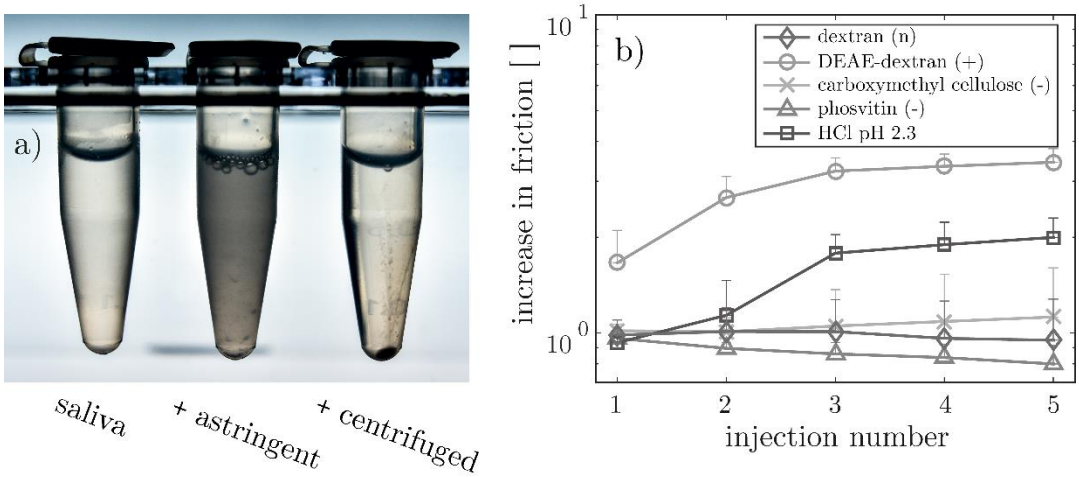

Figure 17: Table of content graphic: Illustration of the effect of astringents on human saliva: human salivary mucin is aggregating when astringent molecules are added (a) which results in a loss of friction (b).

Saliva was collected from volunteers who refrained from eating and drinking (except water) for one hour prior to donation. The saliva was pooled and debris was removed by centrifugation. Human saliva was further purified by ultracentrifugation, size-exclusion chromatography and diafiltration against ultra-pure water. The lubricity of mucin glycoproteins was investigated by probing the molecules as lubricants with a rotational

tribometer at various sliding speeds: here, a steel sphere is rotated on three PDMS pins. Analyzed was the response to the addition of multivalent metal salts, chitosan lysozyme, DEAE-dextran, and several anionic control substances. It was observed that only cationic astringents lead to a loss in lubrication. HPLC-UV analysis and viscoelastic shear measurements with a macrorheometer revealed that those cationic compounds lead to the crosslinking of the polyanionic mucin glycoproteins, which are unable to lubricate in their aggregated form.

In conclusion, it was demonstrated, that the astringent effect of cationic compounds is a consequence of electrostatic interaction with polyanionic mucin glycoproteins present in human saliva. This study not only gives useful insights for the optimization of food products and beverages but also demonstrates, that purified salivary mucins constitute a model system to study the molecular mechanisms of astringency and the influence of food components on salivary lubricity and thus on the perceived mouthfeel when ingesting those foods.

Individual contributions of the candidate: I contributed to the conception of this study, the design and performance of the experiments, the data analysis, and the writing of the article.

4.7 Mucin-inspired lubrication on hydrophobic surfaces

***Benjamin T. Käsdorf**, Florian Weber, Georgia Petrou, Vaibhav Srivastava, Thomas Crouzier and Oliver Lieleg* [159]

In the human body, protection and lubrication of wet epithelial surfaces is mediated by mucins. Those well-hydrated, high-molecular-weight glycoproteins adsorb onto many hydrophilic and hydrophobic surfaces, render the latter hydrophilic and function as exceptional boundary lubricants. However, neither the key features that are responsible for those outstanding lubricating abilities, nor the molecular mechanisms involved in this process are, to date, fully understood.

This study demonstrates the importance of the hydrophobic terminal domains of porcine gastric mucin (MUC5AC) and human salivary mucin (MUC5B) in the process of adsorbing onto and lubricating a hydrophobic PDMS surface. Furthermore, it is shown that chemically modifying hydrated dextrans with hydrophobic groups confer them the ability to lubricate a hydrophobic PDMS surface as well.

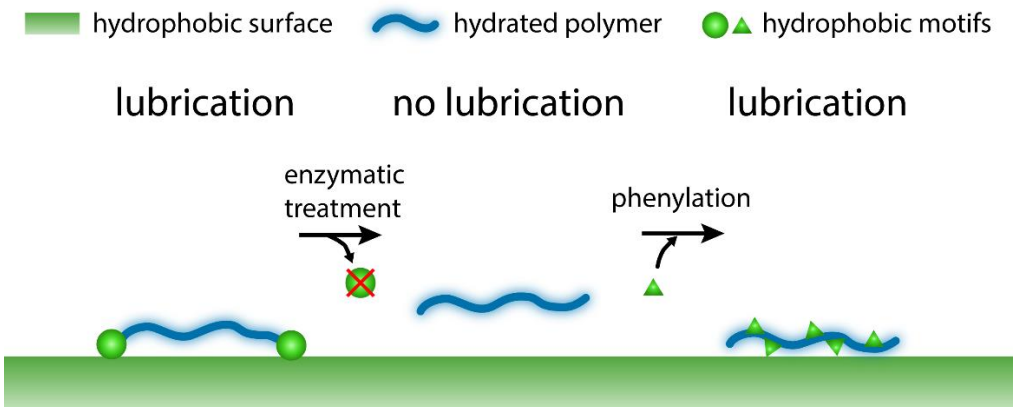

Figure 18: Table of content graphic: Schematic illustration of the lubrication of a hydrophobic surface with a hydrated polymer depending on its ability to adsorb to the surface.

An amino acid sequence analysis of MUC5AC and MUC5B revealed the amphiphilic character of those mucins, with the unfolded core domain being rather hydrophilic and equipped with numerous possible glycosylation sites, whereas the terminal domains being rather hydrophobic. Tryptic treatment of mucin resulted in the digestion of those terminal domains, and only the densely glycosylated core domains remain. However, those impaired mucins lack the ability to adsorb to the hydrophobic PDMS surface and therefore cannot function as a boundary lubricant. In a repair approach of those damaged mucins, hydrophobic phenyl groups were covalently grafted to the remaining glycosylated

domains – partially restoring the ability to adsorb to PDMS and serve as a boundary lubricant. In a final step, this approach was transferred to native dextrans which are highly hydrated but naturally do not adsorb to PDMS and thus lack the ability to lubricate such a hydrophobic surface. It was demonstrated, that modifying dextrans with hydrophobic groups, confers them the ability to adsorb to PDMS and function as a good boundary lubricant – provided that the density of hydrophobic groups is high enough.

In conclusion, it was demonstrated, that the terminal hydrophobic domains of MUC5AC and MUC5B are crucial for the adsorption to and the lubrication of a hydrophobic PDMS surface. Mucins missing those domains and thus lacking the ability to adsorb to and lubricate the hydrophobic PDMS surface, can be partially 'repaired' by attaching hydrophobic phenyl groups to these molecules. As this approach can be transferred to other biopolymer species such as dextrans, these insights could set the stage for the development of artificial macromolecular superlubricants.

Individual contributions of the candidate: I contributed to the conception of this study, the design and performance of the experiments and the data analysis, and the writing of the article.

5 Discussion and Outlook

Biological hydrogels are remarkable physiological structures. These diverse polymer/protein networks carry out various essential functions, ranging from the protection of many body tissues to the regulation of molecule and particle passage. This thesis provides a deeper understanding of the molecular mechanisms involved in these crucial processes. The first part of this work focusses on understanding the molecular interactions of those hydrogel systems with microscopic and macroscopic objects thus exploring the mechanisms regulating the selective transport through such biological networks. The second part aims at improving the understanding of biological lubrication processes mediated by such hydrogels or their components. In a last step, this acquired knowledge is transferred to other simple biomacromolecules such as dextrans and thus conferring them individual qualities that render biological hydrogels so unique (e.g., adsorbing to hydrophobic surfaces and performing as a boundary lubricant). The design of these artificial hybrid macromolecules might prove valuable for a variety of medical applications or can assist in the research of further fundamental molecular processes.

The selective permeability of biological hydrogels is a curse and a blessing at the same time: preventing pathogenic organisms from infecting epithelia cells and avoiding the interference of toxic xenobiotics with the sensitive metabolic processes of those cells is necessary to maintain the healthy state of a biological system. However, it is exactly those protective barrier functions of hydrogels that often prevent efficient pharmaceutical treatment. As described in Section 4.1, the selective permeability of the hydrogels in the eye, especially the vitreous humor, hinders the free passage of distinct particle and molecule species across those polymer networks. Here, the biopolymers hyaluronic acid and heparan sulfate establish this selective permeability towards cationic particles and molecules. In addition to steric hindrance that prevents large particles from diffusing freely through the polymer network, electrostatic interactions between the polyanionic polymers and objects with the opposite surface charge result in a reduced apparent diffusion coefficient or even in complete immobilization of those objects. Unfortunately, various pharmaceutical drugs possess positively charged moieties, which are either essential for the therapeutic function of these drugs, or for a sufficient solubility of these molecules at physiological conditions [160]. Thus, efficient treatment of ocular diseases is still a challenging task. An increase in dosage of those therapeutic drugs seems to be a simple way to overcome this obstacle. However, aside from the usually high prices for most drugs, a treatment with high amounts of drugs is regularly accompanied by severe systemic side effects [161, 162], rendering this approach impractical. Hence, the development

of chemically compatible drugs is necessary. With regard to the vitreous humor, neutral or anionic charge properties should guarantee nearly unhindered diffusion for particle or molecules within the vitreous network. But also cationic molecules might be able to translocate through the vitreous gel – provided the number of charges on such a molecule is below the critical charge threshold described in Section 4.1.

However, the specific binding interaction of drugs with components of a hydrogel such as the vitreous might also be beneficial. A possible scenario involves the long-term treatment of retina-associated illnesses such as age-related macular degeneration or diabetic retinopathy: a normal treatment would involve repetitive intravitreal injections of pharmaceutics to provide a sufficient concentration of drugs over several weeks. Now, taking advantage of the selective permeability properties of the vitreous gel, those pharmaceuticals can be encapsulated in high concentrations in drug carriers such as liposomes – a particle system which has proven valuable for long-term drug release [163, 164]. When these liposomes are equipped with cationic surface moieties (e.g., liposomes comprising phospholipids with cationic head groups such as DOTAP or even multivalent forms such as MVL5), these particles strongly bind to the polyanions hyaluronic acid and heparan sulfate. If these drug carriers are injected in close proximity to the retina, the electrostatic interactions result in their virtually complete immobilization within the polymer network. As liposomes are a highly tunable particle system, those carriers can be designed in such a way that they are slightly permeable for drug molecules incorporated into the liposome. As a consequence, a steady long-term release of pharmaceuticals can be provided in close proximity to the site of infection. This approach could render multiple consecutive intravitreal injections unnecessary and thus minimize the risk of injection-associated infections as well as increase patient compliance.

When such an approach is taken one step further, the selective properties of hydrogels can be taken advantage of once again: as described in Section 4.2, a liposome-based drug release within an artificial hydrogel can be prolonged by several means. In addition to tuning the susceptibility of liposomes towards temperature or osmotic pressure, charged or hydrophobic polymers within a hydrogel could be used to create a well-orchestrated drug release from an artificial wound gel. Traditional wound healing approaches might benefit from such artificial hydrogels as the coordinated release of various drug molecules from such a gel into the wound tissue can be controlled precisely. The usage of multiple polymer species that confer stability as well as the desired selectivity to the hydrogel combined with a set of drug molecules encapsulated in tunable carrier systems could lead to a precise spatio-temporal control over the release process of these pharmaceuticals.

However, a complete lack of binding interactions between drug molecules and hydrogel components might not always be of advantage if fast and efficient drug delivery is desired:

In the appendix Section D.1, it was demonstrated that a certain degree of binding interactions between cationic diffusing objects and a polyanionic mucin network can promote the translocation of those objects across the gel. These binding interactions can probably be attributed to the anionic moieties of mucins (e.g., sialic acid, sulfated glycans and associated DNA) and transient binding of molecules to mucin polymers results in an increased penetration efficiency of cationic molecules in comparison to anionic or neutral molecules. Whereas the charge-dependent diffusion of microscopic objects within mucin gels has been studied intensively [61, 67, 165], the phenomenon that mucin-binding molecules are able to penetrate mucin layers more efficiently than non-interacting molecules is at first surprising. This fact may prove valuable for the formulation of new drugs. Such designed pharmaceuticals could overcome physiological hydrogel barriers such as mucus more efficiently, i.e. in larger quantities, not *although*, but *because* they interact with the hydrogel network. However, the thickness of the barrier which has to be overcome as well as the timespan available for hydrogel translocation are key: interaction-promoted penetration is efficient only over short distances or longer penetration times. As the turnover of the mucosal layer in the gastrointestinal tract is quite rapid (approx. 1 hour [166, 167]), the barrier thickness that can be overcome efficiently is limited. But even within the short turnover time of gastric mucus, the stomach mucus barrier having an average thickness of 100-200 µm [168-170] might be efficiently penetrated by cationic molecules. However, as demonstrated in Section 4.1, the charge density of molecules is crucial as well for their ability to penetrate hydrogels: whereas slightly charged molecules can penetrate the hydrogel network of the vitreous humor, molecules with dense charge clusters accumulate at the gel interface and their penetration efficiency is drastically reduced. A possible explanation for this observation is that the binding interactions between the numerous charges present on the molecules and the anionic moieties of the hydrogel result in a very low k_{off}-rate which prevents efficient penetration of the vitreous gel. Thus, detailed knowledge of a charge threshold is of great importance for each individual hydrogel system to design drug molecules or shuttle systems that can efficiently penetrate these semipermeable networks.

A different approach for penetrating such a hydrogel barrier is described in Section 4.5: here, a reconstituted barrier of stomach mucin is overcome by an artificial micro swimmer which transiently liquefies the mucus gel and thus makes it permeable. Even though this *in vitro* study is to be understood as a proof of principle, the presented mechanism has the potential for an efficient *in vivo* drug delivery system. If further modifications of this silica micropropeller are performed, an uptake of pharmaceutical cargos is possible. This drug-loaded shuttle could then penetrate the mucosal barriers in the gastrointestinal tract without permanently destroying the protective mucus layer and deliver its cargo to the mucosal epithelia nonetheless. Although the presented study in Section 4.5 makes use of

magnetically actuated microswimmers, the functionalization approach with the enzyme urease should also improve the transmigration of passively diffusing drug delivery vehicles. **Figure 19** illustrates such a scenario. Similar to muco-adhesive particles, which are prevented from efficiently penetrating the gastric mucus layer (**Figure 19, I**), also non-adhesive nanoparticles (rendered chemically inert via PEGylation) may not be able to enter the finely-meshed mucus hydrogel due to steric hindrance (**Figure 19, II**). Many studies propose PEGylated nanoparticles as a suitable drug delivery system [171-174] due to their increased diffusive transport within biological hydrogels (such as mucins) compared to nanoparticles which are not coated with PEG [175, 176].

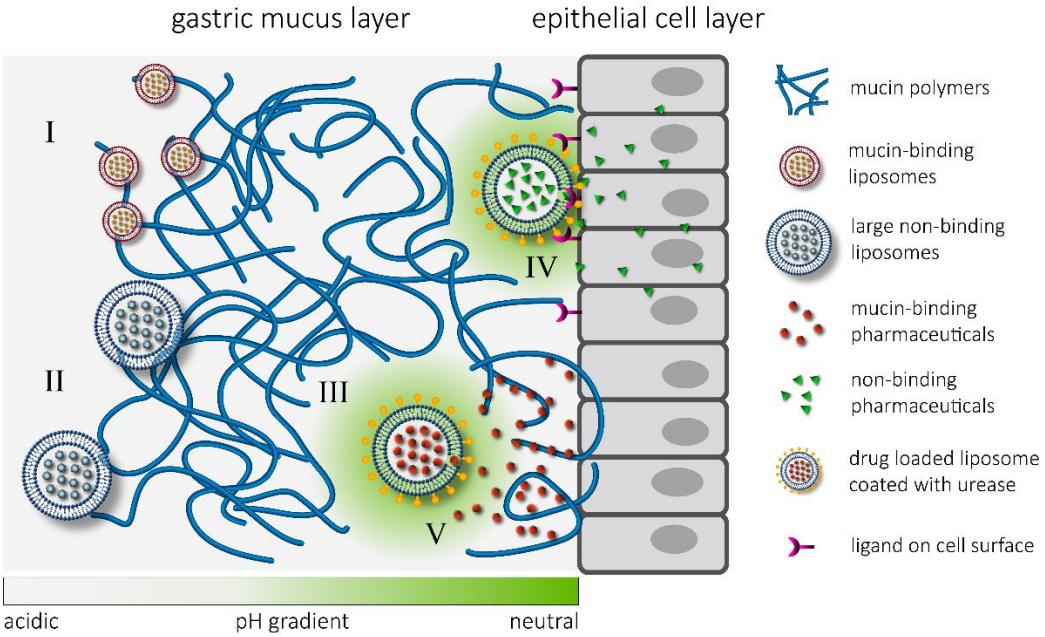

Figure 19: Schematic illustration of drug delivery scenarios through the mucus layer in the gastrointestinal tract: Efficient drug delivery to the gastrointestinal epithelial cell layer requires the penetration of the gastric mucus barrier. When the drug delivery carrier binds to the mucus layer, efficient penetration of those particles is prevented (I). When the particles do not bind, e.g., due to PEGylation, the penetration of the mucus hydrogel is often prevented as well since only small carrier systems can enter the finely-meshed hydrogel (II). A possible scenario to efficiently overcome this mucus barrier might involve the transient modification of the hydrogel (e.g., via urease coating of the carrier systems) which allows for penetration and translocation of the mucus layer (III). Spatio-temporal control over the release of encapsulated pharmaceuticals can be gained by either modifying the surface of the carrier system (e.g., by introducing specific chemical motives which are recognized by the glycocalyx of the epithelial cells and trigger a fusion of the carrier system with the cell membrane and thus initiate an intracellular cargo release (IV)), or by tuning the properties of drug molecules to enable muco-adhesion of drug molecules which can promote a more efficient gel translocation of those molecules (V).

However, the reported diffusion coefficients of PEGylated nanoparticles are still far below values obtained for unhindered free diffusion. Furthermore, the translocation of particles within a hydrogel and the initial penetration of particles into the hydrogel are two

different processes. Thus, the ability of a particle to transmigrate a hydrogel does not necessarily concur with its ability to overcome the gel interface. A urease-coated drug delivery carrier, however, can transiently dissolve the mucin polymer mesh and thus penetrate the mucus barrier and translocate to the epithelial cell layer (**Figure 19, III**). After reaching this cell layer, the loaded cargo can then be released via various mechanisms [177], e.g., via direct fusion of the drug carrier with the cell membrane (**Figure 19, IV**) or by release into the hydrogel network, e.g., through a 'leaky' carrier and subsequent diffusion through the cell membrane. For the latter approach, additional spatio-temporal control can be achieved by taking advantage of the interaction of the drug molecules with mucus components: either a prolonged or accelerated drug delivery is possible – depending on the degree of binding interactions of the pharmaceuticals with the hydrogel (**Figure 19, V**).

However, gaining valuable insights from mucin-related research that can be applied to physiological conditions (e.g., studying the interaction of mucins and pharmaceuticals or pathogens) requires the availability of isolated mucins in their native, i.e. functional form. Yet, commercially available mucins are highly impure and lack essential functions compared to native mucins. Thus, the experiments conducted in this thesis were performed with manually purified mucins. In Section 4.4 an optimization of that purification process is presented, which provides larger quantities of that unique glycoprotein and preserves its properties at the same time. Although the obtained yields are indeed sufficient for mucin-related research in the lab scale, medical applications such as wound gels would require even larger amounts of those functional purified mucins. Thus, a further development of this purification process is necessary. However, although a switch from laboratory to industrial scale might encourage the employment of chemicals to increase the process performance, caution is advised here, as such harsh conditions during the isolation process might impair the crucial functions of mucins such as the lubricating ability [178] – as it is also the case for the commercially available mucins at the moment. Thus, a mechanical approach seems to be most suitable for purifying native mucins from biological tissue. **Figure 20** illustrates such a possible scale-up for harvesting gastric mucins from porcine stomachs.

Since porcine stomachs are mostly a waste product in large slaughterhouses, they are a convenient source material for gastric mucins. To omit the manual scraping of the gastric mucus layer, the stomachs could be cut open along the longitudinal axis and fixated on a plate by applying vacuum. The inner stomach surface is then pressed onto a rotating belt with rubber studs and the gastric mucosa is gently scraped.

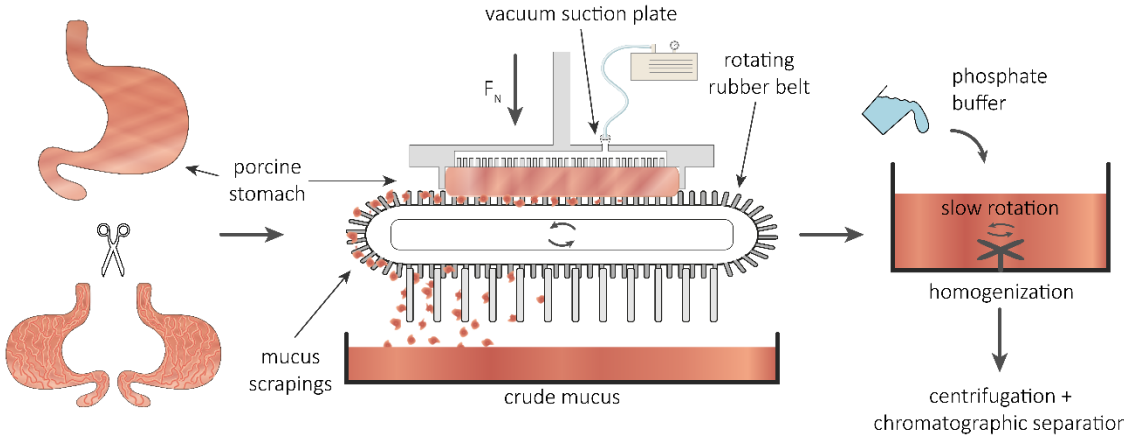

Figure 20: Schematic illustration of the process automatization of scraping porcine gastric mucosa: Fresh porcine stomachs are cut open and the mucosal surfaces is pressed onto a rotating belt. Protruding rubber studs gently harvest the gastric mucosa without damaging the underlying epithelial tissue and thus prevent unwanted contamination. After gentle homogenization, the crude mucus is further purified by centrifugation steps and chromatographic separation.

Here, the geometry and rigidity of the rubber studs as well as the pressure applied on the stomach can be adjusted to obtain a high scraping yield without introducing major contaminations by damaging the underlying tissue. The crude mucus scrapings are collected, mixed with buffer and homogenized. Subsequently, the mucins are purified from the crude mucus solution by centrifugation steps and chromatographic separation.

An alternative approach would be the biotechnological production of recombinant mucins or mucin-like molecules. A recent study has demonstrated, that mucin-like proteins expressed via mammalian cell lines are able to act as a good lubricant on PMMA surfaces [120]. An essential advantage of this approach is the relative broad tunability of those designed molecules, as size, amino acid composition as well as glycosylation pattern can be influenced [119]. Furthermore, as the conditions during protein overexpression can be controlled meticulously, these synthetic bio-products would come in a far more homogenous and defined state compared to native mucins from biological sources. However, it is mandatory to use eukaryotic cell lines for posttranslational protein modifications such as glycosylation, which implies a demanding, elaborate as well as costly cultivation of those cell lines. Thus, in contrast to the purification of native mucins from biological material or the biotechnological production of mucin-like glycoproteins, the design of fully synthetic mucin mimetics may prove to be a promising alternative. Here, abundant polysaccharides, such as cellulose, could be tuned by grafting chemical groups onto the polymers to obtain molecules with mucin-like properties (e.g., synthetic molecules with the ability to form networks that can establish a selective permeability towards molecules or pathogens). Such a mucin-mimicry is discussed in more detail in the second part of this discussion section (see **Figure 22**).

The usage of purified mucins in medical products, however, is not the only possible application of this glycoprotein species. In Section 4.3 an alternative employment of mucins in the field of filtration is presented. Here, the ability of mucins to selectively interact with specific molecules and particles is taken advantage of and the removal of such objects from a solution is enabled by immobilizing mucin molecules on the surface of the porous PDMS-based filtration device. The filtration system presented here is a highly adaptable solution for the purification in lab scale, but this device could also be further developed for the dialysis of human blood: several studies demonstrate that mucins are able to interact and bind several viruses, including influenza A, herpes simplex virus, human papillomavirus, or even HIV type 1 [4, 5, 47, 59, 179, 180]. This ability is an important part of the physiological protection mechanism against infection by those pathogens. Isolated mucin molecules in combination with the capillary filtration system presented here might provide the potential to remove those viruses from human blood, whereas other cellular blood components such as erythrocytes or thrombocytes would remain in the filtered blood. However, in addition to the small capillary diameter, the interaction of blood components such as platelets with PDMS [181], might lead to clogging of these capillaries. Recent developments in the field of anti-fouling surface coatings, however, might help to resolve this issue [182].

In addition to the remarkable selective properties of mucins, the second part of this thesis focuses on a different, but equally fundamental ability of this glycoprotein family: lubrication and therefore protection of body tissues against mechanical stress. As presented in Section 4.6, this property of mucin is also involved in the perception of taste during the consumption of foods and beverages: when ingesting, e.g., cationic molecules, an interaction between those astringents and mucin molecules in the saliva fluid or on the oral mucosa can be observed. These astringents act as crosslinkers and lead to the formation of large mucin aggregates. This aggregated form of mucins is no longer able to function as a proper lubricant and, as a consequence, a particular mouthfeel, called astringency, is perceived in the oral cavity. The gustatory optimization of food or beverage products can benefit from these novel insights, especially from the fact, that reconstituted salivary mucin solutions can serve as a model system to study this effect. Usually, the intensity of the astringent perception of a substance is measured with procedures such as the half-tongue test: here, trained test persons have to determine the intensity of diluted astringent solutions placed on their tongues [183]. However, this rather subjective test method fails to deliver exact numbers for the measured astringent effect. In contrast, the analytical methods described in Section 4.6, enable a quantitative determination of this effect – if reconstituted mucins solutions are employed. As isolated salivary mucins can be reconstituted in a defined concentration and are free of other substances (e.g., residual food particles that can influence the astringency effect), a far

more defined analysis of astringent substances is feasible. Thus, this model system has great potential for the development of optimized food products and illustrates once again the benefits of purified native mucins for both research and industry.

In addition to optimizing the perception of foods, also medical research regarding mucin-mediated lubrication might benefit from this model system. When this essential process in the human body is impaired, a lack of lubrication leads to irritation of the concerned tissue, causing discomfort or pain. This is the case for certain illnesses such as dry mouth [89] or dry eye syndrome [88]. Although there are several commercial products claiming to provide relief for those conditions, they often achieve only little to none alleviation of the symptoms. This failure can be mainly attributed to two reasons: first, the biological or chemical additives in these products are simply not suitable for a proper lubrication of the concerned tissue (e.g., when the lubricant is not able to adsorb to a surface and thus cannot reduce friction), or second, the employed molecules would be suitable in general, but have lost their essential lubricating ability during the process of purification. Eye drops, for example, that should provide auxiliary lubrication of the corneal epithelium, are often based on the glycosaminoglycan hyaluronic acid. This highly hydrated polymer provides remarkable boundary lubrication between body tissues such as articular cartilage. However, it is not ideally suited to lubricate the hydrophobic cornea [184, 185], as hyaluronic acid is not able to adsorb to this hydrophobic tissue and thus cannot reduce friction via sacrificial layer formation and hydration lubrication. In contrast to hyaluronic acid, mucins are very well suited to efficiently lubricate hydrophobic surfaces, and such mucins are indeed widely used as adjuvants in such products. However, impurities, or even the loss of essential domains of these molecules as a consequence of harsh purification conditions often impair the lubricating ability of those commercial mucins. Thus, it is necessary to match the employed biomolecules or chemicals to the target tissue and to ensure, that the intrinsic properties of those molecules are preserved if they are purified from animal tissue.

For example, the top-down approach employed in Section 4.7 revealed the importance of the hydrophobic terminal domains of mucins for the lubrication process of a hydrophobic surface. A subsequent repair strategy based on the introduction of phenyl groups with hydrophobic properties resulted in a partial recovery of the lubricating abilities of mucin – indicating that the presence of hydrophobic moieties is essential rather than specific structural motives or chemical groups.

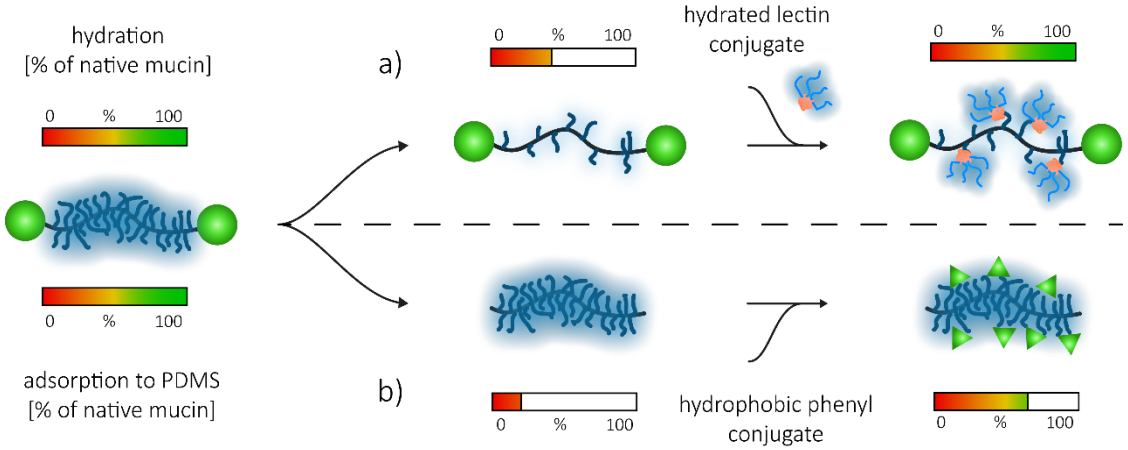

Figure 21: Repair approaches of damaged mucins: Native mucin molecules are highly hydrated and adsorb readily to a hydrophobic PDMS surface. When the mucins are deglycosylated by chemical treatment, the loss of glycans results in a reduction of molecule hydration (a). This hydration however, can be restored, by attaching strongly hydrated PEG conjugates to the damaged mucin. Similarly, when the terminal hydrophobic domains are removed, the adsorption efficiency of the remaining glycosylated core domain to hydrophobic surfaces is drastically reduced (b). Here, the functionalization of the glycan chains with hydrophobic patches partially recovers this adsorption efficiency.

A recent study investigating the importance of mucin hydration for the lubrication process made use of a similar approach [186]: there, the mucins were chemically deglycosylated which entailed a drastic loss in hydration and consequently the ability to lubricate. In a following repair step, polyethylene glycol conjugates were attached to the deglycosylated mucins. These semi-synthetic polymers are highly hydrated [187, 188] and thus were able to replace the removed glycan chains, and could indeed restore the lubricating ability of the 'damaged' mucins. These studies not only identified specific domains of mucin which are involved in the process of lubrication, but also demonstrated, that these properties can be also at least partially established by similar functional motives when replacing the native structures (**Figure 21**).

Therefore, not only a gentle purification of such biological molecules is essential, but a detailed understanding of the molecular mechanisms involved in the lubrication processes is required for each polymeric lubricant as well. Additionally, identifying the specific domains of lubricating molecules such as mucin, that are vital for enabling a proper lubrication, is crucial. In addition to providing further knowledge about how to formulate medical products with biological macromolecules, these insights could lay the foundation for a rational design of artificial macromolecular superlubricants that provide ultra-low friction on a broad range of surfaces. Such tailored hybrid molecules could combine the best of both worlds: inspired by the unique properties of biological lubricants such as mucin, one would, e.g., create a combination of hydrophilic moieties that ensure high hydration of the molecule with hydrophobic patches (which enable the adsorption to

hydrophobic surfaces). Together with the advantages of artificial polymers (i.e. low prices, high purity, availability in large amounts, no need for animal tissue sources as well as being well defined in contrast to biological molecules), such a strategy would enable the design of such super-lubricants.

Those findings could, e.g., be transferred to simple polysaccharides such as cellulose or bacterial dextrans since these polymers are abundant, comparably cheap, and offer the possibility to perform of a variety of chemical modifications.

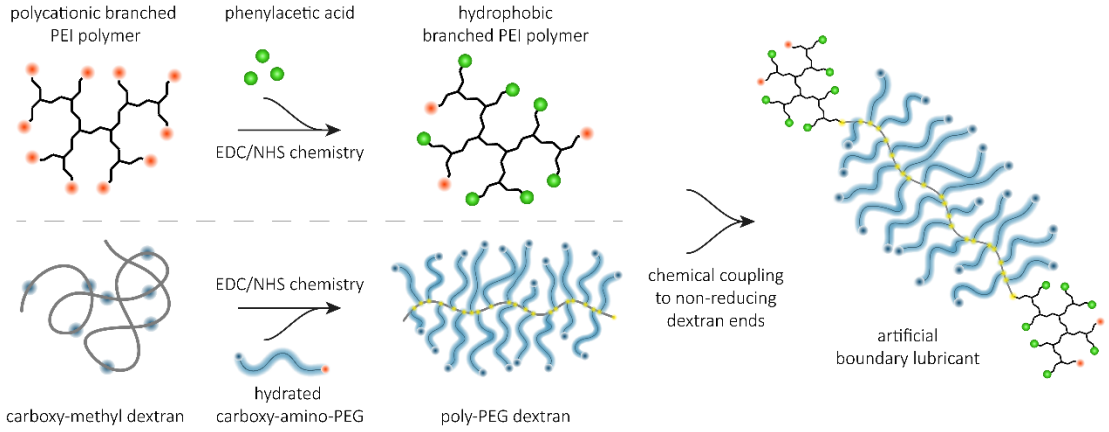

Figure 22: Examples of possible artificial hybrid polymer designs: A combination of the well-established EDC chemistry and other bioconjugate techniques offers a variety of possibilities to create artificial hybrid polymers, e.g., mucin-like boundary lubricants with hydrophobic terminal domains and a highly hydrated brush-like core domain.

Several promising products such as methyl cellulose, which possesses slight hydrophobic properties, or variants of dextrans with different functional groups (e.g., CM, sulfate, DEAE, or phenyl groups) are already commercially available for research purposes. Further, novel modifications of those polymers could turn them into outstanding boundary lubricants: tuning the amount of hydrophobic moieties and attaching additional hydrated polymer chains to a dextran molecule could approximate a mucin-like bottle-brush structure. Such a construct would then also be likely to have lubricating abilities similar to native mucins (**Figure 22**).

However, the design of artificial super-lubricants is not the end of the story. In addition to polymeric lubricants, a variety of artificial polymers can be designed which mimic the remarkable properties of biological hydrogel components, e.g., the selective permeability or the ability to form gels. Numerous techniques for the chemical modification of polymers [189] have been investigated in the last years; they also include enzymatic modifications [190], thus offering a broad range of possibilities: hybrid polymers which are equipped with charged groups combined with intrinsic crosslinking nodes could function as artificial selective hydrogels and could be employed in wound healing applications.

This would allow for an even higher degree of spatio-temporal control over the drug release as the components of the artificial hydrogel now could be tuned as well. Structured polymers such as branched polyethylene imine (PEI) or multivalent sialic-acid constructs even provide the ability to introduce large charge clusters into these artificial polymers thus rendering them highly reactive, e.g., by enabling binding of anionic molecules or particles such as many viruses [191].

Other possible fields of application of such artificial polymer systems include industrial settings. Here, the principles of aqueous boundary lubrication might be transferred to oil-based systems. Recent studies [192, 193] demonstrated the remarkable lubricating abilities of covalently grafted polymer brushes, as they can reach friction coefficients of $\mu < 0.01$ which is far below pure oil-based lubrication. However, such a surface functionalization is too complex to be applied in most industrial settings. Therefore, designing lipophilic polymers that can adsorb to metallic surfaces could be key to enable ultra-low oil based friction between metallic sliding partners.

In Section 4.7, loss-of-function experiments demonstrated the importance of the terminal hydrophobic domains of mucin to lubricate hydrophobic surfaces such as PDMS. In the appendix Section 0 of this thesis, a similar top-down approach was employed but the focus was set on the charged moieties of mucin molecules: sialic acid, sulfated glycans as well as associated DNA. It was demonstrated, that enzymatic removal of both anionic glycans and the DNA drastically influences the lubricating abilities of porcine gastric MUC5AC and human salivary MUC5B. Furthermore, the gel-forming ability of mucins at acidic pH is lost if the majority of the anionic charges are removed. The strong effect of the removal of anionic glycans from mucin on its lubricating ability or gel formation, however, is not obvious. The microscopic principles governing the gel formation of mucins are not fully understood. A combination of electrostatic and hydrophobic interactions was proposed [51, 55, 125], but also the involvement of attached glycan chains was suggested [126, 127]. In contrast, lubrication of hydrophobic surfaces should only require a highly hydrated molecule with suitable anchors to adsorb to the surface. Both requirements should still be met after enzymatic removal of charged glycans or associated DNA molecules.

This may suggest a possible indirect impairment of those processes by the enzymatic removal of charged groups, e.g., DNA. This impairment might be attributed to intramolecular structural changes. Native mucin molecules are often approximated as a bottle brush-like rod with an elongated peptide backbone and laterally protruding sugar chains. It has been stated, that this is based on steric hindrance established by the numerous glycans. This however seems unlikely when estimating the spatial dimensions of a single mucin molecule: the amino acid sequence of gastric MUC5AC comprises over

5600 amino acids. Taking into account, that each amino acid has the size of approximately 3.5 Å, this results in a contour length of nearly 2 µm. The diameter of a mucin molecule can be estimated as the length of the laterally protruding glycan chains. Assuming a length of 5 Å per glycan unit and estimating 5 – 20 glycans per chain [51, 105] (on each side) results in a mucin diameter of approximately 5 – 20 nm. Therefore, this rather thin bottle-brush with an aspect ratio of 100 is likely to adopt some random coil conformation. This hypothesis is also supported by the measured persistence length of mucins which is in the range of 12 – 36 nm [106, 194] which attributes mucin a rather flexible character given its contour length of approximately 2 µm.

However, this estimation does not take into account the presence of specific moieties such as charged groups. The highly polyanionic glycosylated core region might confer mucins a much stiffer character as intramolecular electrostatic repulsions could enforce a rather elongated configuration. Enzymatic removal of these motifs might indeed lead to a collapse of these molecule and entail masking of the hydrophobic terminal domains (**Figure 23**).

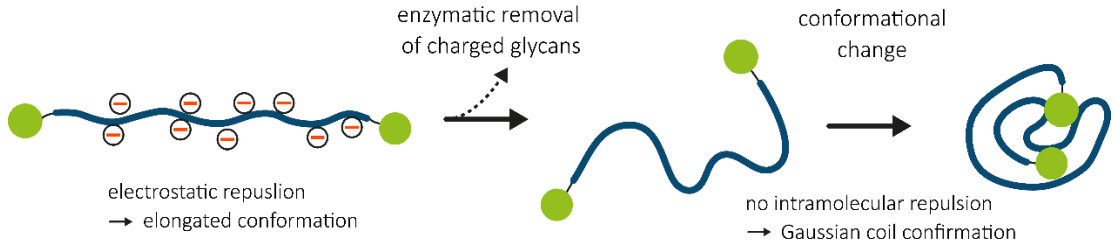

Figure 23: Hypothetical model of the conformational change of mucins induced by the removal of charged moieties: Intramolecular electrostatic repulsion prevents the mucin macromolecule from adapting a Gaussian coil conformation. Partial enzymatic removal of charged glycans or mucin-associated DNA molecules diminishes these intramolecular repulsions and could result in a thermodynamically driven conformational change of the polymer into a Gaussian coil. This structural change could mask the terminal hydrophobic domains (green circles) and thus prevent, e.g., adsorption to hydrophobic surfaces and, consequently, their lubrication.

Accordingly, this would prevent mucin adsorption to hydrophobic surfaces and thus reduce or even abolish the ability to lubricate them. This hypothesis is supported by the findings that desialated ovine salivary mucins exhibit a reduced persistence length in comparison to the native form (6 nm compared to 15 nm) [195]. Similarly, the removal of associated DNA could lead to a comparable effect and result in a coiled protein conformation. An analysis of human airway mucus revealed, that DNAse treatment leads to a decrease in viscosity of the mucus [196] which is in agreement with the theory of a conformational change of the mucin molecules subsequent to DNA removal. A structural analysis of these chemically modified mucins might therefore provide valuable insights into their spatial conformation and how different molecule motifs influence this

parameter. Dynamic/static light scattering (DLS/SLS) or imaging techniques such as transmission electronic microscopy (TEM) or atomic force microscopy (AFM) could help to provide such structural information on native and modified mucins.

Similar to Section 4.7, a repair approach of these 'damaged' mucins might be suitable to confirm this hypothesis. The attachment of negatively charged moieties to the residual glycans in the core domain of, e.g., desialated mucins might restore the native mucin conformation and, as a consequence, its outstanding lubricating abilities. Additionally, a similar bottom-up approach as presented in **Figure 22** could support this hypothesis: comparing the lubricating abilities and spatial conformations of an artificial hybrid polymer as a function of the amount of anionic charges present in the core domain (e.g., coupling of methoxy-amino PEG instead of carboxy-amino PEG to a dextran backbone) could shed light on this matter and help to evaluate the influence of charged mucin moieties on the structural conformation of the glycoprotein.

However, not only sialic acid and sulfated glycans are important for mucin-mediated tasks. In addition to maintaining the mucin barrier function as well as its structure and hydration, the complex glycosylation pattern of mucins is involved in many other physiological processes: the attached glycans protect against autolysis or proteolytic degradation [197] and they can be associated with cancer (when the enzymatic glycosylation activity is altered [198]) or a variety of other diseases [199]. Also the interaction of mucins with bacteria is physiologically important, and this mucin property is linked to the presence of the glycan moieties as well [45, 46]. This interaction is mediated by bacterial adhesins (often lectins) which bind to specific mucin-attached glycans [42]. A change in the complex mucin glycosylation pattern can have severe effects on the mucin barrier function: even minor changes, e.g., of the N-glycosylation pattern of mucin, can entail a complete loss of this function [200]. This distinct glycan composition can also be affected by food-induced stimuli [201] which demonstrates once again the sensitivity of the complex mucin structure towards the various functions these molecules fulfill. These examples show, that recent studies revealed a great number of important facts about the structure-function relationship of molecules from the diverse mucin-family. Yet, they make also clear, that a lot of effort is still necessary to fully understand the complex molecular architecture found in a highly versatile biopolymer such as mucin.

In conclusion, this thesis on the one hand presents valuable insight into the structure-function relations of biological hydrogel components from the vitreous humor or mucus layers with emphasis on their selective permeability as well as their lubricating function. On the other hand, the discussed data also shows, that considerably more research on these systems and the physiological processes they are involved in is mandatory to obtain a fundamental understanding of these particular macromolecular networks. The principles shown in this thesis, however, can be of valuable use in various fields of medical applications such as wound healing or biolubrication. Additionally, the design of artificial polymer species, that mimic the outstanding qualities of biological hydrogel components, might be of valuable use for medical applications, lubrication in the industrial context or further research of the structure-function relations of biopolymers.

Appendix

This appendix contains the following items:

A. Full-text of publications presented in this thesis

B. Licenses for publications

C. Full list of publications

D. Supplemental information

A. Publications

A.1 Diffusion regulation in the vitreous humor

Biophysical Journal Volume 109 November 2015 2171–2181

Article

Diffusion Regulation in the Vitreous Humor

Benjamin Tillmann Käsdorf,[1,2] Fabienna Arends,[1,2] and Oliver Lieleg[1,2,*]
[1]Institute of Medical Engineering (IMETUM) and [2]Department of Mechanical Engineering, Technische Universität München, Garching, Germany

ABSTRACT The efficient treatment of many ocular diseases depends on the rapid diffusive distribution of solutes such as drugs or drug delivery vehicles through the vitreous humor. However, this multicomponent hydrogel possesses selective permeability properties, which allow for the diffusion of certain molecules and particles, whereas others are immobilized. In this study, we perform an interspecies comparison showing that the selective permeability properties of the vitreous are conserved across several mammalian species. We identify the polyanionic glycosaminoglycans hyaluronic acid and heparan sulfate as two key macromolecules that establish this selective permeability. We show that electrostatic interactions between the polyanionic macromolecules and diffusing solutes can be weakened by charge screening or enzymatic glycosaminoglycan digestion. Furthermore, molecule penetration into the vitreous is also charge-dependent and only efficient as long as the net charge of the molecule does not exceed a certain threshold.

INTRODUCTION

Numerous ocular diseases, such as cataract, glaucoma, diabetic retinopathy, or age-related macular degeneration affect the quality of life of millions of people worldwide. Diseases concerning the anterior part of the eye, such as the lens, cornea, ciliary body, etc., allow an effective treatment via topical administration. However, therapy of diseases occurring in the posterior eye segment (except the choroid, which is densely perfused with blood vessels) is very challenging but necessary when the retina is concerned, as it is in cases of age-related macular degeneration, the third leading cause of blindness (1). Topical administration of drugs suffers from low efficiency due to poor drug penetration through barriers of the human eye such as the corneal epithelium, the tear film, or conjunctival absorption (2,3). Treatment of ocular diseases via systemic drug administration is mainly restricted by the blood-retinal barrier, which prevents free passage of xenobiotics from the choroid into the retina and the vitreous humor (4). Diffusion studies of various drugs have confirmed that penetration into the vitreous is much more restricted than into the aqueous humor (5). Macha et al. (6) studied the penetration of systemically applied fluorescein into the vitreous humor of rabbits and found that only 1–2% of the plasma levels of fluorescein can be detected in the vitreous. To achieve intraocular drug levels within the therapeutic range, the drug concentration in the blood stream would lead to severe systemic side effects (7,8).

Therefore, intravitreal injection is an attractive alternative delivery route of drugs to the posterior segment of the eye that does not cause systemic side effects. Yet there are still major drawbacks related to intraocular injection, including patient noncompliance, the need for repeated injections, and injection-associated infections. In addition, the risks of complications increase with the frequency of injections (4). Another major issue is the residence time of drug molecules in the vitreous humor. For prolonged drug release, drug-loaded nanoparticles such as liposomes are used, which provide a long-lasting supply of intravitreal drug molecules while preventing them from degradation (9–12). When therapeutic drug molecules are deposited into the vitreous humor, whether alone or encapsulated in nanoparticles, a detailed knowledge about their intravitreal mobility is crucial for devising an optimal treatment strategy. However, depending on their size and surface properties, the diffusion of these objects can be strongly hindered in the vitreous (13,14).

The mammalian vitreous consists of a strongly hydrated extracellular matrix with a water content of >98%. The gel structure is mainly maintained by collagen fibrils (15). In addition to collagen II, glycosaminoglycans (GAGs) such as hyaluronic acid (HA), heparan sulfate (HS), and chondroitin sulfate are present in the vitreous gel (Fig. 1 *a*), yet in lower concentrations than collagen. The highly hydrated HA serves as a space-filling network between the collagen fibrils (16,17). Due to its heterogeneous distribution of macromolecules throughout the vitreous (18,19), as well as age-related changes in the molecular composition of the vitreous (20), the reported concentration of HA ranges from 65 to 400 μg/mL for human and from 50 to 570 μg/mL for bovine vitreous (19,21,22).

Xu et al. (13) estimated the mesh size of bovine vitreous to be ~550 nm and observed that 200 nm polystyrene

Submitted April 14, 2015, and accepted for publication October 1, 2015.

*Correspondence: oliver.lieleg@tum.de

Editor: Alan Grodzinsky.

0006-3495/15/11/2171/11

http://dx.doi.org/10.1016/j.bpj.2015.10.002

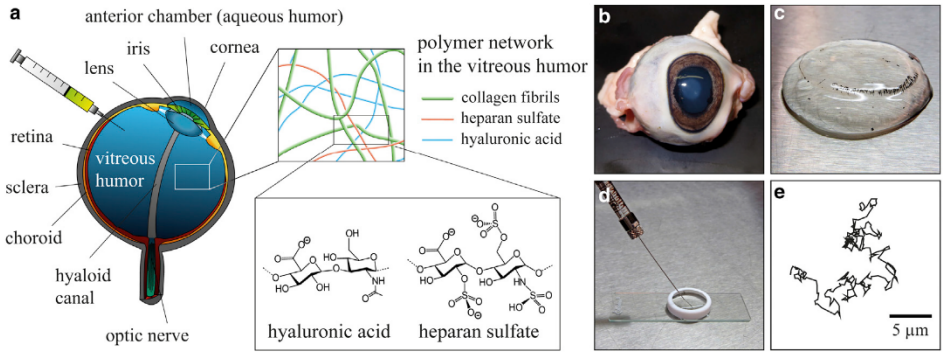

FIGURE 1 Schematic overview of a mammalian eye (*a*) and vitreous preparation process for SPT (*b–e*). (*a*) The vitreous humor of the mammalian eye mainly consists of collagen fibrils, as well as the GAGs HA and HS, both of which carry several negative charges. From fresh ovine eyes (*b*), the vitreous humor is carefully removed (*c*), and nanoparticles are injected into the vitreous (*d*). Trajectories characterizing the thermal motion of the nanoparticles in the vitreous humor (*e*) are obtained by optical microscopy. To see this figure in color, go online.

particles with negative COOH surface groups showed nearly free diffusion in the vitreous, whereas particles of the same size but with positive NH_2-functionalized surfaces were immobilized. A similar charge-dependent suppression of particle diffusion has also been observed in other biological hydrogel systems (23–27), which suggests that this might be a more generic filtering mechanism in biology (28). Hindered mobility for cationic particles in the vitreous, as well as improved mobility of particles coated with polyethylene glycol (PEG), has been reported by several other groups (13,14,29–31), indicating that the vitreous humor gel constitutes a selective diffusion barrier for particles. As a physical mechanism for this selective suppression of particle diffusion, a combination of electrostatic and hydrophobic interactions has been proposed (13,14,29,31). However, clear experimental evidence is still missing, and the detailed molecular components of the vitreous that establish those interactions still need to be identified.

One strategy to achieve this goal is comparing the diffusive mobility of well-defined model molecules or model nanoparticles in the vitreous. Polystyrene particles and liposomes are a well-suited particle platform for such an endeavor, since they can be obtained at comparable sizes but with different surface qualities. Especially tuning the net charge of liposomes is easily possible, e.g., by adjusting the lipid composition used for liposome generation. Similarly, when studying molecule diffusion in the vitreous, dextrans and oligopeptides offer the possibility of tuning two molecule properties, size and charge, independently. Dextrans are available at different molecular masses and can be obtained with different chemical modifications. Thus, they have a well-defined charge/molecular mass ratio, but this cannot easily be tuned. Synthetic oligopeptides, on the other hand, are a very versatile system, as one can create specific charge patterns or charge densities by linking up amino acids (almost) at will during synthesis. Therefore, with those test particles and molecules, a broad range of solute sizes and solute net charges can be modeled, which allows for a systematic analysis of the permeability properties of the vitreous.

Here, we show that the selective permeability of the vitreous humor is largely based on electrostatic interactions between the biopolymer network and diffusing particles or molecules. This charge-selective suppression of diffusion seems to be a conserved mechanism across different mammalian species, as we observe identical behavior in the vitreous humor obtained from bovine, porcine, and ovine eyes. By enzymatic treatment of the vitreous, we identify the polyanionic GAGs HA and HS as two molecular key components that establish selective particle trapping. Removal of those macromolecules, as well as charge screening by high salt concentrations, entails mobilization of trapped particles. The charge-selective trapping ability of the vitreous also extends to molecules such as dextrans and peptides if their net charge is high enough.

MATERIALS AND METHODS

Test particles and molecules

Since the mesh size of bovine vitreous was estimated to be ~550 nm (13), a size of 200 nm for the particles and liposomes employed in this study was chosen to minimize steric hindrance effects.

Fluorescent polystyrene particles (carboxyl-terminated or amine-terminated) 200 nm in diameter were obtained from Invitrogen (Carlsbad, CA). Polyethylene glycol (PEG, molecular mass 750 Da, Rapp Polymere, Tübingen, Germany) coating of carboxyl-terminated beads was performed using a modified carbodiimide-coupling procedure based on the protocol described in Nance et al. (31). In brief, 100 μL of 200 nm carboxyl-terminated polystyrene particles was washed in ultrapure water and diluted fourfold to a final concentration of 0.5% solids. Next, 50 mM α-methoxy-ω-amino-PEG was added to the particle solution and mixed thoroughly, and 100 mM N-hydroxysulfosuccinimide sodium salt (sulfo-NHS, Sigma-Aldrich, St. Louis, MO) was mixed with the suspension. Then, 60 mM *N*-(3-dimethylaminopropyl)-*N'*-ethylcarbodiimide hydrochloride (EDAC, Sigma-Aldrich) was suspended in 600 μL borate buffer (pH 8.5) and mixed with the particle

suspension. Particles were incubated for 4 h at room temperature and then centrifuged and washed with ultrapure water.

Lipids were obtained from Avanti Polar Lipids (Alabaster, AL) in chloroform. Liposomes were prepared from 1,2-dioleoyl-*sn*-glycero-3-phosphocholine (DOPC), 1,2-dioleoyl-3-trimethylammonium-propane (DOTAP), 1,2-dioleoyl-*sn*-glycero-3-(phospho-rac-(1-glycerol)) (DOPG), and fluorescently labeled with 1,2-dioleoyl-*sn*-glycero-3-phosphoethanolamine-N-(lissamine rhodamine B sulfonyl) (Rh-DOPE). Lipids were mixed to a total amount of 0.5 μmol with 5 mol % Rh-DOPE. For preparation of zwitterionic DOPC liposomes 90 mol % of DOPC and an additional 5 mol % DOTAP were mixed to compensate the negative charge of 5 mol % Rh-DOPE. For simplicity, those DOPC/DOTAP/Rh-DOPE liposomes are referred to as DOPC liposomes in this article. Solvent evaporation was conducted overnight to generate a thin lipid film. This lipid film was resuspended in 500 μL 10 mM phosphate buffer (pH 7.3, 154 mM NaCl) and mixed thoroughly. The suspension was then sonicated in an ultrasonic bath for 10 min to produce small unilamellar vesicles. These were extruded through a 0.2 μm polycarbonate membrane with a miniextruder (Avanti Polar Lipids) and stored at 4°C until further use.

Fluorescein-isothiocyanate labeled dextrans (4 kDa or 150 kDa) were obtained from Sigma-Aldrich. We used three dextran variants here: dextrans without modification (FITC-dextrans) and dextrans that have been modified with either carboxymethyl (FITC-CM-dextrans) or diethylaminoethyl groups (FITC-DEAE-dextrans). Stokes radii for the dextrans used here are 1.4 nm for the 4 kDa dextrans and 8.5 nm for the 150 kDa dextrans (according to the supplier's information).

Customized oligopeptides (total length, 24 amino acids, labeled at the N-terminus with 5-carboxytetramethylrhodamine (TAMRA)) were obtained from PEPperPRINT (Heidelberg, Germany). Anionic peptides had the sequences $(QQE)_8$ and $(EEE)_8$, and cationic peptides had the sequences $(QQK)_8$, $(QK)_{16}$, $(QKK)_8$, $(QKKKKK)_4$, and $(KKK)_8$. Here, Q denotes glutamine (neutral at pH 7), E glutamic acid (negatively charged at pH 7), and K lysine (positively charged at pH 7). In the main text, those peptides are referred to as P1–P7, respectively, and details are given in Table S1 in the Supporting Material.

Size and ζ-potentials of polystyrene particles and liposomes were determined with dynamic light scattering using a Zetasizer Nano ZS (Malvern Instruments, Herrenberg, Germany) in 20 mM TRIS/HCl buffer (pH 7.3, 10 mM NaCl). To avoid osmotic pressure, lipids were resuspended in this buffer for size and ζ-potential measurements.

Furthermore, Table S1 gives an overview of the estimated number of net charges of particles and molecules used in this study.

Preparation of fresh vitreous samples

Due to the limited availability of fresh human vitreous humor from patients of similar age, samples from animal sources are much better suited for a systematic study where different experimental conditions are supposed to be probed. Here, fresh ovine, bovine, and porcine eyes (Fig. 1 *b*) were obtained from a local slaughterhouse and immediately placed on ice. Extraocular material was removed and the sclera was carefully incised without cutting into the vitreous humor. The intact vitreous humor (Fig. 1 *c*) was detached from the sclera and immediately used for further experiments.

Single-particle tracking

For single-particle tracking (SPT), either 200 nm fluorescent polystyrene particles or 200 nm liposomes were diluted in phosphate buffer (pH 7.3, 154 mM NaCl) to allow SPT. Of this solution, 2 μL was carefully injected (~0.3 μL/s) into the vitreous humor using a 10 μL Hamilton syringe (gauge 26s, point style 2), as depicted in Fig. 1 *d*. The samples were incubated for ~0.5 h on ice before particle-tracking measurements were initiated.

Fluorescence microscopy was conducted on an Axioskop 2 MAT mot microscope (Zeiss, Oberkochen, Germany) equipped with an LD Plan-Neofluar 40× objective (Zeiss). Images were acquired with a digital camera (Orca-R2 C10600, Hamamatsu, Shizuoka, Japan) at 16 fps using the software HCImageLive provided by Hamamatsu. Particle trajectories were obtained from those movies using the image analysis software OpenBox developed at the Technical University of Munich (32). To quantify the microscopic mobility of the test particles, the mean-squared displacement (MSD) was determined from the trajectory of motion of the particles as described before (23). In brief, the MSD can be determined from the trajectory, $\vec{r}(t)$, of a particle by $\mathrm{MSD}(\tau) = (1/N)\sum_{i=1}^{N}\left[\vec{r}(i\Delta t+\tau) - \vec{r}(i\Delta t)\right]^2$ and is related to the diffusion coefficient via $\mathrm{MSD}(\tau) = 2nD\tau$, where $n = 2$ is used for the quasi-two-dimensional trajectories, $\vec{r}(t) = \langle x(t), y(t)\rangle$ of the analyzed particles. With this procedure, apparent diffusion coefficients are obtained as we explicitly assume a linear dependence of the MSD on τ. Only the first 10% of the MSD(τ) data are used to determine this apparent diffusion coefficient to avoid artifacts arising from statistical limitations (33, 34). However, calculation of the MSD(τ) data includes the entire video length of 20 s.

Charge-screening experiments

For charge-screening experiments, fluorescent amine-terminated polystyrene particles (200 nm in diameter) were diluted in high-salt solution (1 M NaCl, 1 M KCl, 4 M NaCl, and 4 M KCl, pH 7). Of this solution, 10 μL was carefully injected (~0.3 μL/s) into ovine vitreous humor using a 10 μL Hamilton syringe (gauge 26s, point style 2). A higher injection volume compared to the previous SPT experiments was used to achieve a high local concentration of ions in the vitreous. The samples were incubated for 5–15 min on ice before particle-tracking measurements were initiated. The time window between injection and SPT was shortened to ensure that the first measurement was conducted before the concentration of injected ions could equilibrate throughout the vitreous. For each sample, a second measurement was conducted at the same site in the vitreous humor 2 h after the first measurement. We verified that this shortened waiting time, as well as the increased injection volume, did not affect the mobility of the injected particles compared to the experimental conditions chosen for the rest of the SPT experiments (see Fig. S3). Furthermore, additional control experiments confirmed that injecting high-salt solutions into the vitreous did not disrupt the mechanical integrity of the vitreous (see Figs. S4 and S5).

Enzymatic digestion of ovine vitreous humor

For enzymatic digestion, the wet weights of ovine vitreous were determined, and afterward, the whole vitreous was submerged in an equal volume of digestion buffer. For HA digestion, 100 units of hyaluronidase from *Streptomyces hyalurolyticus* (H1136, Sigma-Aldrich) was dissolved in 100 mM sodium acetate buffer (pH 5.7, 77 mM NaCl, 0.01% BSA) for each vitreous humor. For HS digestion, 10 units of a blend of heparinase I and III from *Flavobacterium heparinum* (H3917, Sigma-Aldrich, St. Louis, MO, USA) were dissolved in 20 mM Tris/HCl buffer (pH 7.5, 50 mM NaCl, 0.01% BSA, 4 mM $CaCl_2$) for each vitreous humor. The following protease inhibitors were added to each buffer: 2 mM phenylmethanesulfonylfluoride (Carl Roth, Karlsruhe, Germany) and 5 mM benzamidine hydrochloride (Carl Roth). All enzymatic digestions were performed at 37°C for 72 h in 50 mL centrifuge tubes. Control samples were incubated in the same buffers but without enzymes. After digestion, wet weights of the vitreous samples were determined again to analyze the loss in water content due to enzymatic treatment. Afterward, vitreous samples were washed in phosphate buffer (pH 7.3, 154 mM NaCl) to get rid of residual HA/HS fragments. Particle-tracking measurements were performed in the vitreous to determine the apparent diffusion coefficients, as described above.

To verify the successful removal of HA and HS from fresh vitreous samples, HA and HS concentrations were determined by competitive enzyme-linked immunosorbent assay (ELISA) using commercial kits (Sheep HA

Elisa Kit and Sheep HS Elisa Kit, BlueGene, Shanghai, China). Therefore, treated and untreated vitreous samples were homogenized with a pipette and centrifuged at 1000 rcf for 15 min. Then, the supernatant was used for quantifying the concentrations of HA and HS with the ELISA kits using purifed HA and HS samples as calibration standards.

FITC-dextran and peptide penetration into the vitreous humor

Whole ovine vitreous humor samples or vitreous fragments were placed into FITC-dextran solutions in a 50 mL centrifuge tube so that the samples were fully submerged. Per gram of vitreous sample, 0.2 mL of dextran solution was used. Dextrans were dissolved at a concentration of 10 mg/mL in 10 mM phosphate buffer (pH 7.3, 154 mM NaCl). After incubation at 4°C overnight in the dark, the samples were washed in 10 mM phosphate buffer (pH 7.3, 154 mM NaCl) to remove remaining FITC-dextrans from the surface. The samples were homogenized with a pipette, and three samples of 100 μL each were taken for quantification. Fluorescence intensities were measured with a plate reader (VICTOR X3 Multilabel Plate Reader, Perkin-Elmer, Waltham, MA) at an excitation wavelength of 485 nm and emission wavelength of 535 nm. The same procedure was used for studying oligopeptide penetration into the vitreous humor. There, the peptide concentration was 1 mg/mL and again 0.2 mL of this solution was used per gram of vitreous sample tested. The wavelengths used for fluorescence measurements with peptides were 570 nm for excitation and 642 nm for emission.

Statistical analysis

To determine whether the differences between the examined groups are significant, one-way analyses of variance (ANOVAs) and Tukey post hoc tests were carried out. The Shapiro-Wilk test of normality and the Levene's test for homogeneity of variances were used to verify the assumptions of normal distribution and homogeneity of variances. Differences were considered to be statistically significant for $p < 0.01$. All statistical analyses were performed using R (Foundation for Statistical Computing, Vienna, Austria).

RESULTS AND DISCUSSION

Vitreous humor selectively traps charged polystyrene particles

Similar to previous studies on vitreous permeability (13,14,29), bovine vitreous was chosen for the initial experiments. First, we compare the diffusion coefficients of different polystyrene particles, i.e., amine- and carboxyl-terminated particles, as well as PEGylated particles, all with a diameter of 200 nm in fresh bovine vitreous humor. As illustrated in Fig. 2 *a*, the MSD curves calculated from the trajectories of amine-terminated particles can be divided into two groups: a small fraction of the MSD curves depend linearly on τ, which indicates free diffusion. However, the larger fraction exhibits subdiffusive behavior, with MSD curves that only weakly increase with τ, demonstrating that the motion of the corresponding particles is strongly hindered. Apparent diffusion coefficients (D_{app}) calculated from those MSD curves (Fig. 2 *b*) underscore this impression: the small, mobile fraction of the particles exhibit an apparent diffusion coefficient, which amounts to 25% of the theoretical value of free diffusion in water (D_{free}). In contrast, for the larger fraction of particles with subdiffusive MSD curves, we obtain apparent diffusion coefficients with $D_{app} < 10\%$ of D_{free}, which indicates that the vitreous humor hydrogel constitutes a significant diffusion barrier for these amine-terminated particles. At the same experimental conditions, carboxyl-terminated particles can also be subdivided into nearly freely diffusing and strongly subdiffusive particles (Fig. 2 *b*); however, the subdiffusive part of the population is significantly smaller than for the amine-terminated particles. In contrast, PEGylated particles show a nearly Gaussian distribution of apparent diffusion coefficients centered at a value of 50% of D_{free} (Fig. 2 *b*), and the immobile fraction is missing for this particle variant. These findings confirm previous results showing that the diffusive mobility of polystyrene particles in bovine vitreous humor strongly depends on the surface properties of the particles, and that the charge of the particle surface is a key parameter as cationic surface groups reduce the particle mobility.

Such a bimodal distribution of D_{app} has already been observed for polystyrene particles and polyplexes in bovine vitreous (14) which demonstrates that our results can be directly compared to previous studies on vitreous permeability. There, however, ensemble-averaged diffusion coefficients were calculated from those bimodal distributions, which is different from our categorization approach into

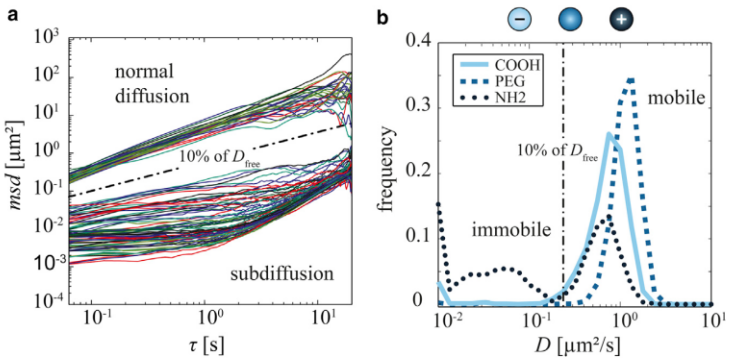

FIGURE 2 Diffusive mobility of 200 nm polystyrene particles in bovine vitreous humor. (*a*) MSD curves calculated from the individual trajectories of amine-terminated 200 nm polystyrene particles in bovine vitreous humor. (*b*) The distribution curves contain data from >1000 apparent diffusion coefficients from carboxyl-terminated (COOH), PEGylated (PEG), and amine-terminated (NH_2) 200 nm polystyrene particles in bovine vitreous humor. The dash-dotted line in both graphs is located at 10% of the diffusion coefficient of 200 nm particles in water (D_{free}). Using this line as a threshold, the particle ensemble can be divided into a mobile and an immobile fraction. To see this figure in color, go online.

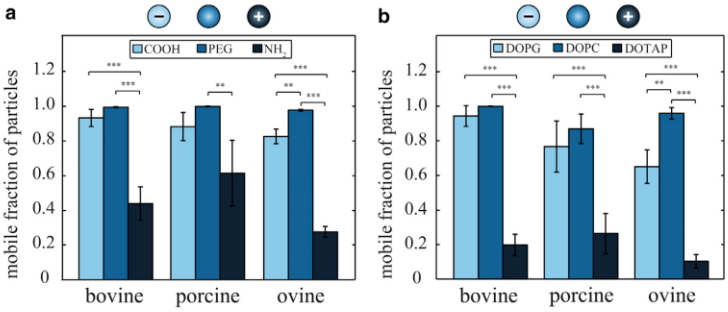

FIGURE 3 Interspecies comparison of the diffusive mobility of polystyrene and liposome particles in vitreous. (*a*) Comparison of the mobile fraction ($D_{app} > 10\%$ of D_{free}) of carboxyl-terminated (COOH), PEGylated (PEG), and amine-terminated (NH_2) 200 nm polystyrene particles in bovine, porcine, and ovine vitreous humor. (*b*) Comparison of the mobile fractions ($D_{app} > 10\%$ of D_{free}) of DOPG, DOPC, and DOTAP 200 nm liposomes in bovine, porcine, and ovine vitreous humor. Several hundred particle trajectories were acquired per sample and then categorized into mobile and immobile fractions. The error bars denote the standard deviation for those fractions as obtained from at least three vitreous samples. Asterisks denote statistically significant differences ($^{**}p < 0.01$; $^{***}p < 0.001$). To see this figure in color, go online.

mobile and immobile particle fractions. Here, the bimodal distribution was most pronounced for amine-terminated particles. This could arise from transient particle trapping and escape events, as previously observed in basal lamina hydrogels (35). In the vitreous, weak or strong particle trapping could, e.g., originate from an inhomogeneous distribution of biopolymers (18,19). Areas with a higher density of macromolecules could result in more tightly trapped particles than areas with fewer macromolecules.

Interspecies comparison of the mobility of polystyrene particles and liposomes

Previous in vitro experiments on vitreous permeability have mostly been conducted using bovine vitreous (13,14). To test whether the observed charge-dependent nanoparticle mobility is conserved across species, we next compare the diffusive mobility of polystyrene particles in bovine, porcine, and ovine vitreous humor. In all vitreous variants, we observe a bimodal distribution of apparent diffusion coefficients for charged polystyrene particles, similar to what we discussed for bovine vitreous (see Fig. S1). Thus, in all cases, we can subdivide the analyzed particle ensembles into an immobile (<10% of D_{free}) and a mobile (>10% of D_{free}) fraction. Fig. 3 *a* displays this fraction of mobile particles in an interspecies comparison. This comparison returns a similar picture for porcine, bovine, and ovine vitreous humor: almost 100% of the PEGylated particles, as well as 80% of the carboxyl-terminated particles, are mobile in all vitreous samples. However, the trapping of amine-terminated particles seems to be somewhat stronger in ovine vitreous than in the other two vitreous variants, as we find only 25% mobile particles here compared to ~45–50% in porcine and bovine vitreous.

Having confirmed that the diffusive mobility of polystyrene particles in the vitreous humor of various species depends on the surface properties of the particles, we next ask whether the chemical origin of the particle charge is relevant for the suppression of particle diffusion. In other words, we aim to test whether unspecific electrostatic interactions or specific binding between the amino groups of polystyrene particles and vitreous components are responsible for particle trapping. To tackle this question, we next investigate the diffusive mobility of a second particle system in addition to polystyrene particles. Liposomes constitute a suitable platform for this purpose for two reasons: on the one hand, the overall net charge of liposomes can be easily tuned by mixing lipids with different headgroups, and the size of the liposomes can be controlled by extrusion. On the other hand, liposomes are medically highly relevant particles, as they are widely used as a carrier system for therapeutic drug delivery.

To allow for a direct comparison to the data obtained with polystyrene particles, we chose 200 nm as an average size for the liposome particles (see Materials and Methods). As shown in Fig. 3 *b*, the diffusive mobility of such 200 nm liposomes in vitreous humor is very similar to that of polystyrene particles of similar ζ-potential (see Table 1). The majority of zwitterionic (DOPC) and anionic (DOPG) liposomes remain mobile in the vitreous, whereas the diffusion of cationic (DOTAP) liposomes is largely suppressed. Again, a bimodal distribution of apparent diffusion coefficients for these cationic liposomes is observed (see Fig. S2), and these results are obtained in all three vitreous variants. These findings demonstrate that indeed a positive particle surface charge is responsible for the reduction in particle mobility and that no specific chemical motif is

TABLE 1 Particle characterization

	Particle Type	Particle Size (nm)	PDI	ζ pH 7,3 (mV)
Polystyrene particles	carboxyl	222	0.033	−34.7 ± 1.0
	PEG	231	0.024	−11.4 ± 1.6
	amine	253	0.087	+7.5 ± 1.7
Liposomes	DOPG	185	0.24	−50.2 ± 1.7
	DOPC	194	0.26	+1.3 ± 0.3
	DOTAP	171	0.19	+41.0 ± 0.8

Particle size, polydispersity index (PDI), and particle ζ-potential are determined from dynamic light scattering for polystyrene particles and liposomes.

required to induce particle immobilization. Of course, liposomes differ from polystyrene beads in terms of surface charge mobility and mechanical deformability. Yet, as we observe identical charge-dependent immobilization behavior of those two particle species in vitreous, these differences in the particle properties seem not to be crucial for what we describe here.

Our finding that the selective permeability properties of the vitreous seem to be conserved across several mammalian species suggests that the results gained here can, to a certain degree, be extrapolated to other mammalian vitreous variants, including human vitreous. For all vitreous variants tested here, we detect a weak trapping of negatively charged particles, which is most prominent for ovine vitreous samples. This finding is in agreement with previous studies on nanoparticle diffusion in bovine vitreous, where it was suggested to arise from hydrophobic interactions between the polystyrene particles and collagen II fibers (13,14,29). However, we observe a similar low fraction of trapped negatively charged DOPG liposomes, and those liposomes should not be able to engage in hydrophobic interactions. In any case, the trapping efficiency of negatively charged particles is clearly less dominant compared to the trapping of positively charged particles.

For the remainder of the article, we aim at identifying the molecular mechanism and the vitreous components that give rise to this trapping of positively charged particles. We approach this goal by employing different strategies to remobilize trapped particles and drawing conclusions from the change in experimental conditions that are required for such a remobilization. As we found ovine vitreous to possess the strongest trapping efficiency for amine-terminated particles, all following experiments were conducted with ovine vitreous. Furthermore, since high-salt injections into the vitreous gel might compromise the stability of liposomes (due to osmotic pressure effects), polystyrene particles were used for the remobilization experiments.

High salt concentrations prevent particle immobilization

If electrostatic interactions between the polymer network of the vitreous humor and particles are mainly responsible for the observed suppression of particle diffusion, these interactions (and therefore the microscopic mobility of charged particles) should depend on the ion content of the vitreous. At higher ionic strength of the vitreous, exposed surface charges of particles or vitreous biopolymers will be partially shielded by a layer of counterions (Fig. 4 *a*), resulting in a reduction of the electrostatic interaction potential. The strength of this charge screening will increase with rising ion concentrations. Therefore, in a next set of experiments, we injected amine-terminated polystyrene particles together with a high-salt buffer to locally increase the ion concentration in ovine vitreous humor and then determine the mobility of the particles.

Fig. 4 *b* shows the results of such a charge screening experiment. When 10 μL of 1 M KCl are injected together with the amine-terminated particles into ovine vitreous humor, the mobile fraction of particles is increased from ~25% (physiological salt conditions of 154 mM) to ~45%. Consistently, a stronger increase of the local salt concentration, as achieved by injecting 10 μL of 4 M KCl, results in an even higher mobile particle fraction of ~70%. This effect has been observed before in another hydrogel system (35) and confirms our notion that the mobility of trapped particles in the vitreous can be restored by inducing electrostatic screening, and that the strength of this effect can be

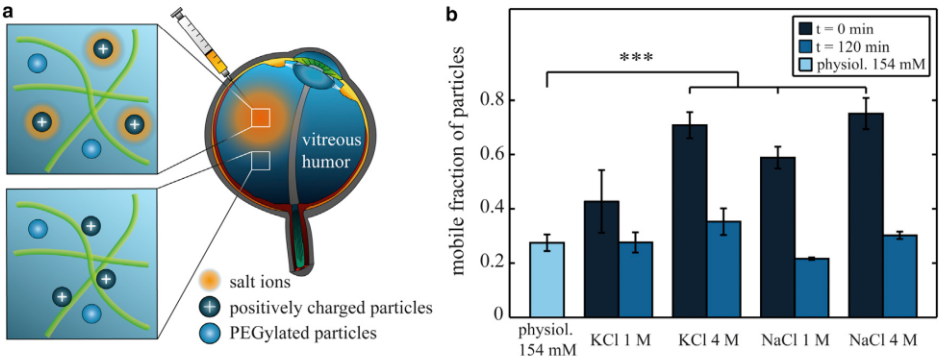

FIGURE 4 The mobility of trapped particles can be restored via charge screening. (*a*) Schematic illustration of charge screening as induced by ions (*orange cloud*) that are added to the vitreous. Charged particles (or polymers of the vitreous) concentrate counterions around their surface and thus avoid electrostatic trapping. (*b*) When KCl or NaCl is injected together with the particles, the mobile fraction of amine-terminated (NH_2) 200 nm polystyrene particles in ovine vitreous humor is increased compared to physiological salt concentrations (154 mM). At 2 h after injection, this remobilization effect is not present any more. More than 1000 particle trajectories were analyzed per experimental condition and categorized into mobile and immobile particle fractions. The error bars denote the standard deviation for those fractions as obtained from at least three vitreous samples. Asterisks denote statistically significant differences compared to physiological salt conditions (***$p < 0.001$). To see this figure in color, go online.

modulated by the amount of ions added to the vitreous. However, according to the Debye-Hückel theory (36), the strength of this screening process should only depend on the valency and concentration of the added ions, and not on the particular ion species. To test this prediction, we repeat the screening experiments with NaCl solutions. Indeed, we find that the injection of 10 μL of either 1 M or 4 M NaCl results in an increase of the mobile particle fraction similar to that observed for KCl injection, which suggests that this remobilization effect is not ion specific.

Since the increase in ion concentration in the vitreous gel is only induced locally, diffusive spreading of the injected ions through the vitreous should lead to a drop in the local ion concentration over time. We estimate the volume of each ovine vitreous sample by weighing and approximating the density of the gel by that of water. With the low injection volume of 10 μL used here, we then can calculate that the salt concentration in the vitreous should equilibrate at ~160 mM after a few hours. Consequently, the charge shielding effect will probably not be measurable any more when the salt concentration has equilibrated. Indeed, such a behavior is observed when the mobility of amine-terminated particles is determined again 2 h after injection (Fig. 4 *b*). For all salt-injection experiments, the fraction of mobile amine-terminated particles returns to ~20–30%, which matches the amount of mobile particles at physiological ion concentrations. These data underline our previous notion that particles can be trapped in the vitreous via electrostatic forces, and that this electrostatic trapping can be countered by charge screening.

However, full mobilization of the particle ensemble could not be achieved at our experimental conditions. A second physical mechanism that could counteract particle mobilization at high salt concentrations could be a gain in entropy due to the replacement of a layer of condensed counterions by charged macromolecules or polystyrene particles. This could occur as a consequence of particle binding to the hydrogel macromolecules and thus might support particle trapping. However, for HA, the Manning criteria for counterion condensation (37) are not fulfilled: the ratio of Bjerrum length and line charge of HA gives a value of 0.7, which corresponds to full ionization. HS carries three to four times the line charge of HA, so the ratio of Bjerrum length and line charge results in a value of 2.1–2.8. Thus, Manning's criterion seems to be fulfilled for HS. However, counterion condensation is dominant only as long as the Debye length is larger than the distance between two charges on the macromolecule (38). At physiological conditions as they apply to our vitreous samples, the Debye length is <1 nm, which corresponds to the distance between two charges on HA. At ion concentrations as high as 1 M (4 M), the Debye length is only ~0.3 nm (0.15 nm), which is even lower than the distance between two charged groups on HS. Finally, we observe that the mobilization of particles depends on the salt concentration. Yet, if Manning condensation were to play a crucial role for immobilizing particles in the vitreous humor, the fraction of trapped particles should be independent of the ion concentration.

As mentioned before, even with injection of 4 M NaCl or KCl, full particle mobilization could not be achieved. We speculate that the residual fraction of trapped particles at high ionic strength could be related to the trapping of negatively charged particles at physiological salt and arise from hydrophobic interactions between the polystyrene particles and vitreous components. As an alternative, even during the short waiting time between salt injection and measurement initiation, the injected ions could have partially been equilibrated—at least at the edge of the injection bolus—thus leading to incomplete particle mobilization.

Enzymatic digestion of polyanionic GAGs increases the fraction of mobile particles

Having shown that electrostatic forces are responsible for the immobilization of positively charged particles, we now set out to identify the key components of the vitreous humor that are involved in this trapping process. The vitreous humor comprises different polymers such as collagen type II and several GAGs, some of which carry polyanionic charges. Several carboxyl, as well as sulfate, groups introduce multiple negative charges into the network (Fig. 1 *a*). As shown in Fig. 4, electrostatic interactions between particles with positive surface charges and the vitreous humor network are responsible for a reduction of particle mobility. To identify the involved polymers we performed a separate enzymatic removal of the negatively charged HA and HS from ovine vitreous humor (Fig. 5). Digestion of collagen II from bovine and chick vitreous results in a loss of structural integrity of the vitreous gel (39,40), and we observe the same behavior for ovine vitreous (see Fig. S6). In contrast, the digestion of HS and HA leads to a decrease in the wet weight of the vitreous (see Table S2) but with its structural integrity maintained (see Figs. S7 and S8).

Enzymatic degradation of HA results in an increase of the mobile fraction of positively charged polystyrene particles to ~45% compared to ~25% in fresh, untreated vitreous and 15% in control samples that were stored in digestion buffer but in the absence of enzymes (Fig. 5). This result clearly indicates that this GAG is involved in the trapping of positively charged particles. Similarly, when the polyanionic GAG HS is digested, the mobile particle fraction is increased to ~40%. In the control groups, we observe a slight decrease of the mobile polystyrene particle fraction compared to fresh, untreated samples. We speculate that this reduction in particle movement could be due to loss of water of the vitreous gels over time, which even occurs to a certain degree when no vitreous components are removed by enzymatic treatment (see Table S2). Such a partial loss of water would entail a decreased gel mesh size and thus a reduced diffusive mobility of the polystyrene particles compared to fresh vitreous.

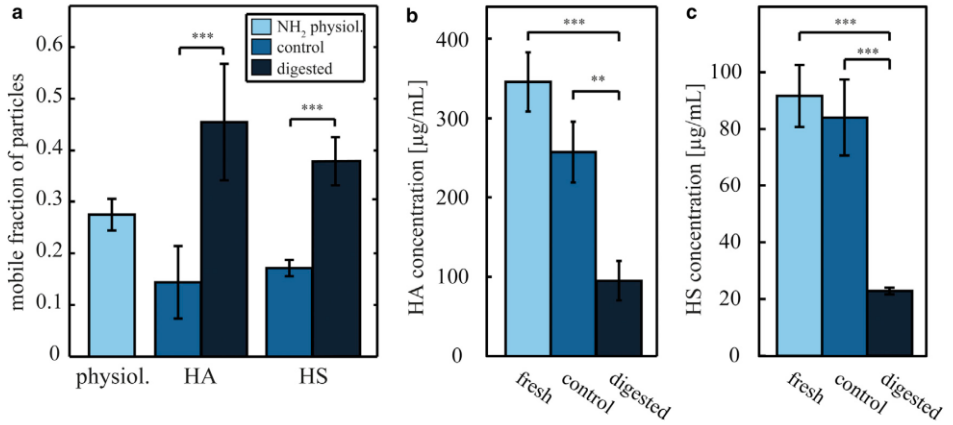

FIGURE 5 Enzymatic degradation of the polyanionic GAGs HA and HS in ovine vitreous increases particle mobility. (*a*) The mobile fraction ($D_{app} > 10\%$ of D_{free}) of amine-terminated (NH_2) 200 nm polystyrene particles after 72 h GAG digestion in ovine vitreous humor is compared to the mobile fraction of those particles in undigested vitreous. The control samples have been incubated in digestion buffer without enzymes. More than 1000 particle trajectories were analyzed per experimental condition and categorized into mobile and immobile particle fractions. The error bars denote the standard deviation for those fractions as obtained from at least three vitreous samples. (*b* and *c*) The concentration of HA and HS in fresh, untreated vitreous, as well as digested samples and control samples, was determined via competitive ELISA. Please note the different *y*-axis scaling for HA and HS. Asterisks denote statistically significant differences (**$p < 0.01$; ***$p < 0.001$). To see this figure in color, go online.

Therefore, statistical differences were only determined between digested and control vitreous samples, and we did not compare data from treated samples to physiological conditions. Fig. 5, *b* and *c*, depicts the measured concentrations of HA (Fig. 5 *b*) and HS (Fig. 5 *c*) in fresh, untreated vitreous compared to digested and control samples. The HA concentration in fresh ovine vitreous is ~350 μg/mL and thus in a range similar what has been measured in human and bovine vitreous (19,21,22). After enzymatic treatment of ovine vitreous, a strong decrease of HA and HS concentrations is observed, which suggests a direct link between HA/HS concentration in the vitreous and the diffusive mobility of amine-terminated polystyrene particles. HA and HS differ in terms of both their charge density and their concentration in the vitreous: HS carries three to four times as many negatively charged groups per length unit as HA, but HA is present at approximately fourfold the concentration of HS in ovine vitreous. In conclusion, both enzymatic treatments should have removed a similar amount of charged groups from the vitreous, and we find that both treatment strategies entail a similar outcome in terms of particle mobilization. This result may indicate that the total (local) amount of charge rather than the local charge density may be the relevant parameter that sets the trapping efficiency of solutes in the vitreous biopolymer network.

The vitreous can selectively prevent penetration of molecules

So far, we have analyzed the selective trapping mechanism of the vitreous using test particles as permeability probes. Particle mobility in the vitreous is medically relevant, as injection of nanoparticles is used for the treatment of certain eye diseases (12,41–47). However, a much more regular treatment strategy employs the delivery of antibiotics through the vitreous to the posterior part of the eye. Such antibiotics are considerably smaller than the nanoparticles studied so far. Thus, in a last step, we test whether the selective permeability properties of the vitreous are also efficient on a molecular scale. As test molecules, we choose dextrans. They are available with various chemical modifications and, at the same time, with different well-defined molecular masses. In detail, we compare fluorescently labeled 4 kDa and 150 kDa dextrans with DEAE or CM groups to unmodified dextrans. Thus, we can explore the difference in diffusion behavior between positively charged, negatively charged, and neutral molecules.

However, SPT is not feasible with those molecules. Accordingly, we switch to macroscopic penetration tests for these experiments (see Materials and Methods). Fig. 6 *a* gives an overview of the penetration efficiency of different FITC-dextran molecules in ovine vitreous humor. Similar to the diffusion of nanoparticles studied before, we observe a different behavior for the 150 kDa dextran variants as a function of their charge: whereas unmodified (i.e., neutral), as well as polyanionic, CM-dextrans efficiently penetrate the vitreous and reach similarly high concentrations on the order of 1 mg/mL, the polycationic DEAE-dextrans show a much lower penetration efficiency and accumulate at the surface of the vitreous (Fig. S10). This demonstrates that the charge-selective permeability of the vitreous is similarly efficient on a molecular scale, at least

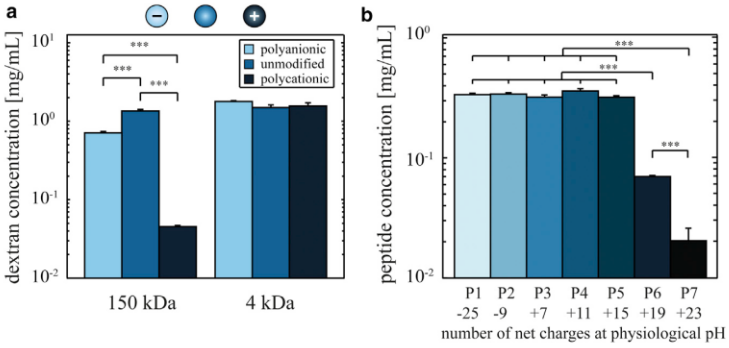

FIGURE 6 Penetration efficiency of different dextran molecules and oligopeptides into ovine vitreous humor. The concentrations of dextrans (*a*) and peptides (*b*) in ovine vitreous humor are shown after incubation of the vitreous samples overnight in different dextran/peptide solutions. DEAE (polycationic), unmodified (neutral), and CM (polyanionic) dextrans are compared at two different molecular masses (*a*). The sequence of the peptides P1–P7 (*b*) is described in Materials and Methods and in the Supporting Material. The error bars denote the standard deviation as obtained from three vitreous samples. Asterisks denote statistically significant differences (***$p < 0.001$). To see this figure in color, go online.

for those 150 kDa dextran molecules. However, when smaller dextrans (4 kDa) are used in those penetration experiments, we do not detect any significant differences between the three dextran variants (Fig. 6 *a*).

Very similar results are obtained when the vitreous samples are divided into three to four fragments before the penetration experiments are conducted (Fig. S11), which demonstrates that our penetration tests indeed probe the bulk permeability of the vitreous. It is important to realize that the 4 kDa dextran molecules carry only about three to five positive charges per molecule, which is very low compared to the number carried by larger 150 kDa variants, i.e., 160–200 charges per molecule. Considering that both dextran variants are significantly smaller than the mesh size of the vitreous and have similar charge densities (i.e., a similar net charge per molecular mass), this indicates the existence of a charge threshold above which the diffusion of solutes is suppressed by the vitreous.

To better characterize this charge threshold, we switch to another molecule model system, which allows for better tuning the molecular net charge at a fixed molecular mass. Synthetic oligopeptides can be generated with specific charge patterns, and therefore, varying the net charge on those molecules is easily possible. We here compare anionic peptides (carrying either −25 or −9 charges) to several cationic peptides (carrying either +7, +11, +15, +19, or +23 charges). Fig. 6 *b* depicts the penetration efficiency of these different oligopeptide species into ovine vitreous. All peptides possess a molecular mass of ~4 kDa. The anionic peptides, as well as some cationic species (P1–P5), efficiently penetrate the vitreous (Fig. S12 a). However, the strongly cationic species with 19 positive charges (P6) exhibits a strongly reduced penetration efficiency into the vitreous, and the polylysine oligopeptide (P7, +23 charges) is virtually unable to penetrate the vitreous but accumulates on the surface (Fig. S12 b). These findings are in good agreement with the results from the dextran penetration experiments and support the idea that a charge threshold exists above which the diffusion of molecules in the vitreous polymer network is strongly suppressed. Whereas polycationic peptides with up to 15 positive charges per molecule are able to penetrate the vitreous with a high efficiency, the vitreous constitutes an efficient barrier for highly cationic peptides. This results either in a strongly reduced penetration efficiency of such molecules (P6, +19 charges) or even an almost complete blocking of penetration (P7, +23 charges).

Whereas nanoparticles (13,14) may easily exceed this charge threshold, antibiotics are typically only weakly charged, similar to the 4 kDa dextrans and peptides studied here. This suggests that if nanoparticles with suitable surface charges are used as drug carriers for intravitreal injection, diffusive spreading of antibiotics through the vitreous will probably not be strongly hindered. This offers the possibility to combine drug-delivery carriers (such as nanoparticles) and drug molecules with different immobilization efficiencies in the vitreous to tailor the distribution/retention times of nanoparticles and the enclosed drugs independently. One could imagine a scenario where injected drug-loaded nanoparticles are supposed to remain strongly localized, e.g., when they are deposited close to the retina to treat a retinal disease. This would then guarantee an efficient delivery of the embedded drugs to the target site and still allow for tuning the drug mobility/retention in the vitreous. The latter can be affected by various factors, e.g., the structure or charge state of the drug molecules. Typical half-life values of antibiotics are usually in the range of only several hours (48). Conversely, for a more global treatment of ocular diseases, nanoparticles with a high mobility in the vitreous could be advantageous. Particles with neutral or negative net charges should be equally suitable for this second scenario.

CONCLUSION

Here, we have shown that the ability of the vitreous humor to suppress diffusion of solutes is largely based on electrostatic interactions, which are mediated by the polyanionic GAGs HA and HS. Together with previous results from other

studies, our findings indicate that the biopolymers comprising the vitreous fulfill very different tasks: collagen II is mainly responsible for providing the vitreous with its mechanical properties and maintaining the structural integrity of the hydrogel. In contrast, the GAGs bind water and regulate the diffusion of particles and molecules within the hydrogel. Such a complementary function of biomacromolecules is also observed in other collagen/GAG hybrid systems such as the basal lamina and articular cartilage. This highlights the generic role polyanionic GAGs assume in setting up the complex material properties of tissues.

SUPPORTING MATERIAL

Supporting Materials and Methods, twelve figures and two tables are available at http://www.biophysj.org/biophysj/supplemental/S0006-3495(15)00112-4.

AUTHOR CONTRIBUTIONS

B.T.K., F.A., and O.L. proposed the experiments. The experiments were performed by B.T.K. Data analysis was performed by B.T.K. and F.A. The article was written by B.T.K., F.A., and O.L.

ACKNOWLEDGMENTS

The authors thank Kathrin Boettcher for assistance with the statistical analysis.

This project was supported by the Deutsche Forschungsgemeinschaft (DFG) through grant LI 1902/3-1.

REFERENCES

1. Resnikoff, S., D. Pascolini, …, S. P. Mariotti. 2004. Global data on visual impairment in the year 2002. *Bull. World Health Organ.* 82:844–851.
2. Bochot, A., B. Mashhour, …, E. Fattal. 1998. Comparison of the ocular distribution of a model oligonucleotide after topical instillation in rabbits of conventional and new dosage forms. *J. Drug Target.* 6:309–313.
3. Hughes, P. M., O. Olejnik, …, C. G. Wilson. 2005. Topical and systemic drug delivery to the posterior segments. *Adv. Drug Deliv. Rev.* 57:2010–2032.
4. Duvvuri, S., S. Majumdar, and A. K. Mitra. 2003. Drug delivery to the retina: challenges and opportunities. *Expert Opin. Biol. Ther.* 3:45–56.
5. Cunha-Vaz, J. G. 1976. The blood-retinal barriers. *Doc. Ophthalmol.* 41:287–327.
6. Macha, S., and A. K. Mitra. 2001. Ocular pharmacokinetics in rabbits using a novel dual probe microdialysis technique. *Exp. Eye Res.* 72:289–299.
7. Henderly, D. E., W. R. Freeman, …, N. A. Rao. 1987. Cytomegalovirus retinitis and response to therapy with ganciclovir. *Ophthalmology.* 94:425–434.
8. Jabs, D. A., C. Newman, …, B. F. Polk. 1987. Treatment of cytomegalovirus retinitis with ganciclovir. *Ophthalmology.* 94:824–830.
9. Meisner, D., J. Pringle, and M. Mezei. 1989. Liposomal ophthalmic drug delivery. III. Pharmacodynamic and biodisposition studies of atropine. *Int. J. Pharm.* 55:105–113.
10. Kurz, D., and T. A. Ciulla. 2002. Novel approaches for retinal drug delivery. *Ophthalmol. Clin. North Am.* 15:405–410.
11. Bochot, A., P. Couvreur, and E. Fattal. 2000. Intravitreal administration of antisense oligonucleotides: potential of liposomal delivery. *Prog. Retin. Eye Res.* 19:131–147.
12. Kaur, I. P., A. Garg, …, D. Aggarwal. 2004. Vesicular systems in ocular drug delivery: an overview. *Int. J. Pharm.* 269:1–14.
13. Xu, Q., N. J. Boylan, …, J. Hanes. 2013. Nanoparticle diffusion in, and microrheology of, the bovine vitreous ex vivo. *J. Control Release.* 167:76–84.
14. Martens, T. F., D. Vercauteren, …, K. Braeckmans. 2013. Measuring the intravitreal mobility of nanomedicines with single-particle tracking microscopy. *Nanomedicine (Lond.).* 8:1955–1968.
15. Bishop, P. 1996. The biochemical structure of mammalian vitreous. *Eye (Lond.).* 10:664–670.
16. Scott, J. E. 1992. The chemical morphology of the vitreous. *Eye (Lond.).* 6:553–555.
17. Bishop, P. N. 2000. Structural macromolecules and supramolecular organisation of the vitreous gel. *Prog. Retin. Eye Res.* 19:323–344.
18. Balazs, E. A., T. C. Laurent, and U. B. Laurent. 1959. Studies on the structure of the vitreous body. VI. Biochemical changes during development. *J. Biol. Chem.* 234:422–430.
19. Lee, B., M. Litt, and G. Buchsbaum. 1994. Rheology of the vitreous body: part 3. Concentration of electrolytes, collagen and hyaluronic acid. *Biorheology.* 31:339–351.
20. Denlinger, J. L., G. Eisner, and E. A. Balazs. 1980. Age-related changes in the vitreus and lens of rhesus monkeys (*Macaca mulatta*). *Exp. Eye Res.* 31:67–79.
21. Grimshaw, J., A. Kane, …, D. Archer. 1994. Quantitative analysis of hyaluronan in vitreous humor using capillary electrophoresis. *Electrophoresis.* 15:936–940.
22. Reardon, A., D. Heinegård, …, P. N. Bishop. 1998. The large chondroitin sulphate proteoglycan versican in mammalian vitreous. *Matrix Biol.* 17:325–333.
23. Lieleg, O., R. M. Baumgärtel, and A. R. Bausch. 2009. Selective filtering of particles by the extracellular matrix: an electrostatic bandpass. *Biophys. J.* 97:1569–1577.
24. Lieleg, O., I. Vladescu, and K. Ribbeck. 2010. Characterization of particle translocation through mucin hydrogels. *Biophys. J.* 98:1782–1789.
25. Lai, S. K., D. E. O'Hanlon, …, J. Hanes. 2007. Rapid transport of large polymeric nanoparticles in fresh undiluted human mucus. *Proc. Natl. Acad. Sci. USA.* 104:1482–1487.
26. Lai, S. K., Y. Y. Wang, …, J. Hanes. 2010. Nanoparticles reveal that human cervicovaginal mucus is riddled with pores larger than viruses. *Proc. Natl. Acad. Sci. USA.* 107:598–603.
27. Cu, Y., and W. M. Saltzman. 2009. Controlled surface modification with poly(ethylene)glycol enhances diffusion of PLGA nanoparticles in human cervical mucus. *Mol. Pharm.* 6:173–181.
28. Lieleg, O., and K. Ribbeck. 2011. Biological hydrogels as selective diffusion barriers. *Trends Cell Biol.* 21:543–551.
29. Peeters, L., N. N. Sanders, …, J. Demeester. 2005. Vitreous: a barrier to nonviral ocular gene therapy. *Invest. Ophthalmol. Vis. Sci.* 46:3553–3561.
30. Kim, H., S. B. Robinson, and K. G. Csaky. 2009. Investigating the movement of intravitreal human serum albumin nanoparticles in the vitreous and retina. *Pharm. Res.* 26:329–337.
31. Nance, E. A., G. F. Woodworth, …, J. Hanes. 2012. A dense poly(ethylene glycol) coating improves penetration of large polymeric nanoparticles within brain tissue. *Sci. Transl. Med.* 4:149ra119.
32. Schilling, J., E. Sackmann, and A. R. Bausch. 2004. Digital imaging processing for biophysical applications. *Rev. Sci. Instrum.* 75:2822–2827.
33. Dunderdale, G., S. Ebbens, …, J. Howse. 2012. Importance of particle tracking and calculating the mean-squared displacement in distinguishing nanopropulsion from other processes. *Langmuir.* 28:10997–11006.

34. Qian, H., M. P. Sheetz, and E. L. Elson. 1991. Single particle tracking. Analysis of diffusion and flow in two-dimensional systems. *Biophys. J.* 60:910–921.

35. Arends, F., R. Baumgärtel, and O. Lieleg. 2013. Ion-specific effects modulate the diffusive mobility of colloids in an extracellular matrix gel. *Langmuir.* 29:15965–15973.

36. Hiemenz, P. C., and R. Rajagopalan. 1997. Principles of Colloid and Surface Chemistry, 3rd ed. CRC Press, Boca Raton, FL.

37. Manning, G. S. 1969. Limiting laws and counterion condensation in polyelectrolyte solutions. I. Colligative properties. *J. Chem. Phys.* 51:924–933.

38. Rant, U., K. Arinaga, …, G. Abstreiter. 2003. Excessive counterion condensation on immobilized ssDNA in solutions of high ionic strength. *Biophys. J.* 85:3858–3864.

39. Pirie, A., G. Schmidt, and J. W. Waters. 1948. Ox vitreous humour. 1.—the residual protein. *Br. J. Ophthalmol.* 32:321–339.

40. Halfter, W., U. Winzen, …, A. Eller. 2006. Regulation of eye size by the retinal basement membrane and vitreous body. *Invest. Ophthalmol. Vis. Sci.* 47:3586–3594.

41. de Kozak, Y., K. Andrieux, …, P. Couvreur. 2004. Intraocular injection of tamoxifen-loaded nanoparticles: a new treatment of experimental autoimmune uveoretinitis. *Eur. J. Immunol.* 34:3702–3712.

42. Díaz-Llopis, M., M. J. Martos, …, F. J. Romero. 1992. Liposomally-entrapped ganciclovir for the treatment of cytomegalovirus retinitis in AIDS patients. Eperimental toxicity and pharmacokinetics, and clinical trial. *Doc. Ophthalmol.* 82:297–305.

43. Herrero-Vanrell, R., and M. F. Refojo. 2001. Biodegradable microspheres for vitreoretinal drug delivery. *Adv. Drug Deliv. Rev.* 52:5–16.

44. Peyman, G. A., B. Khoobehi, …, R. Fiscella. 1987. Intravitreal injection of liposome-encapsulated ganciclovir in a rabbit model. *Retina.* 7:227–229.

45. Shelke, N. B., R. Kadam, …, U. B. Kompella. 2011. Intravitreal poly(L-lactide) microparticles sustain retinal and choroidal delivery of TG-0054, a hydrophilic drug intended for neovascular diseases. *Drug Deliv. Transl. Res.* 1:76–90.

46. Bejjani, R. A., D. BenEzra, …, F. F. Behar-Cohen. 2005. Nanoparticles for gene delivery to retinal pigment epithelial cells. *Mol. Vis.* 11: 124–132.

47. Bourges, J. L., S. E. Gautier, …, F. F. Behar-Cohen. 2003. Ocular drug delivery targeting the retina and retinal pigment epithelium using polylactide nanoparticles. *Invest. Ophthalmol. Vis. Sci.* 44:3562–3569.

48. Radhika, M., K. Mithal, …, H. W. Flynn. 2014. Pharmacokinetics of intravitreal antibiotics in endophthalmitis. *J. Ophthalmic Inflamm. Infect.* 4:22.

Supplemental information for Käsdorf et al.

Table T1: Estimated charge state of particles and molecules used. The maximal number of charged groups on polystyrene particles, liposomes, FITC-dextrans and TAMRA-peptides at physiological pH was estimated based on particle/molecule size, molecule structure, pK_a of the specific groups and supplier information.

	Particle type	Particle size [nm]	estimated max. net charge [e] at pH 7.3
polystyrene particles	carboxyl	~ 200	~ 10^6 (-)
	PEG		~ 0 (assuming full PEGylation)
	amine		~ 10^6 (+)
liposomes	DOPG/Rh	~ 200	~ 10^5 (-)
	DOPC/DOTAP/Rh		~ 0
	DOTAP/Rh		~ 10^5 (-)
4 kDa *FITC-dextrans* 150 kDa	CM	~ 1.4	~ 5 (-)
	unmod.		~ 1 (-)
	DEAE		~ 5 (+)
	CM	~ 8.5	~ 160 (-)
	unmod.		~ 4 (-)
	DEAE		~ 200 (+)
TAMRA-peptides (~ 4 kDa)	P1 – $(EEE)_8$	~ 1.5	25 (-)
	P2 – $(QQE)_8$		9 (-)
	P3 – $(QQK)_8$		7 (+)
	P4 – $(QK)_{12}$		11 (+)
	P5 – $(QKK)_8$		15 (+)
	P6 – $(QKKKK)_4$		19 (+)
	P7 – $(KKK)_8$		23 (+)

Distribution of apparent diffusion coefficients for polystyrene particles and liposomes in mammalian vitreous humor.

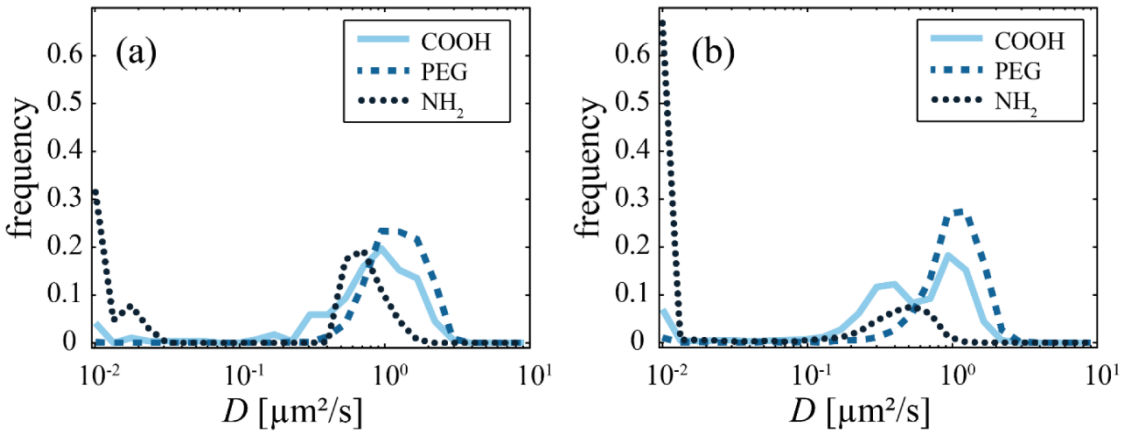

Fig. S1: Diffusive mobility of 200 nm polystyrene particles in (*a*) porcine and (*b*) ovine vitreous humor. The distribution curves contain data from > 1000 carboxyl-terminated (COOH), PEGylated (PEG) and amine-terminated (NH_2) 200 nm polystyrene particles. For the calculation of these distributions, data from at least three different vitreous samples have been pooled.

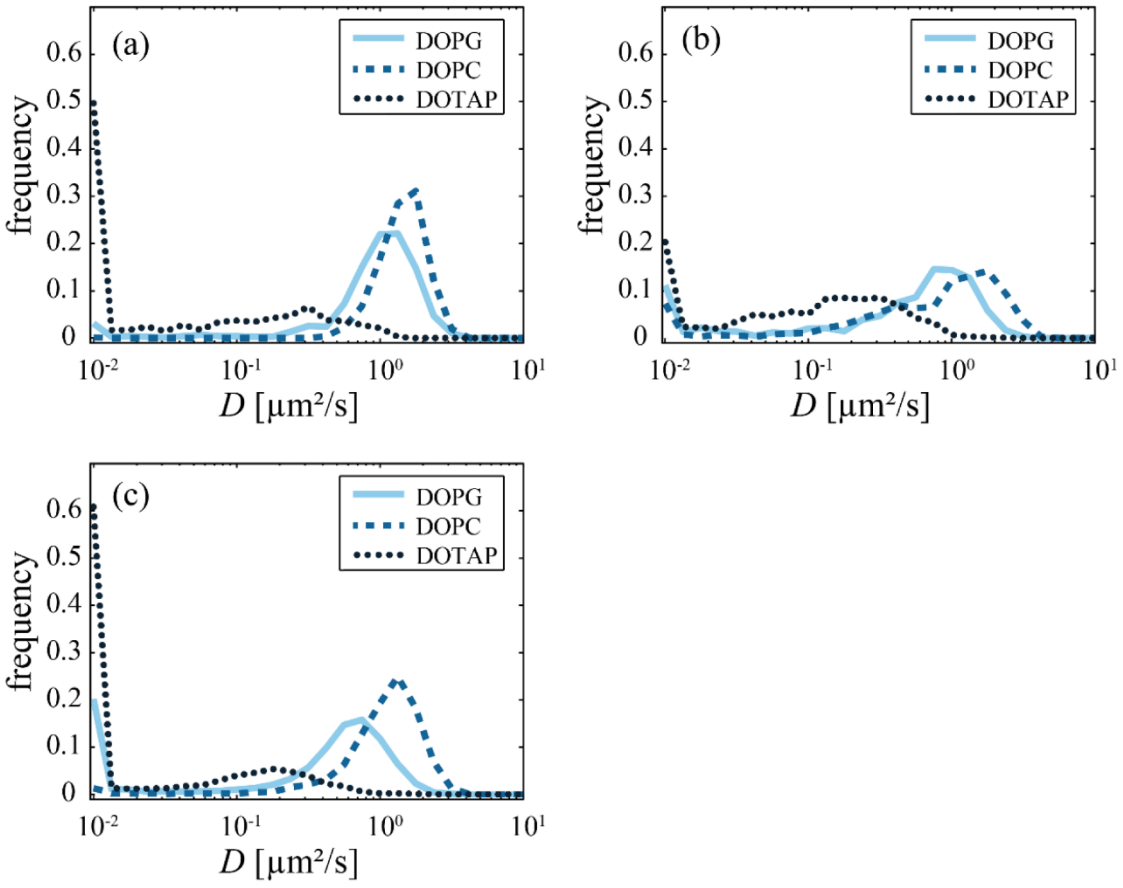

Fig. S2: Diffusive mobility of 200 nm liposomes in (*a*) bovine, (*b*) porcine and (*c*) ovine vitreous humor. The distribution curves contain data from > 1000 apparent diffusion coefficients is determined for DOPG, DOPC and DOTAP 200 nm liposomes in vitreous humor. For the calculation of these distributions, data from at least three different vitreous samples have been pooled.

Distribution of apparent diffusion coefficients for polystyrene particles in ovine vitreous humor at different injection volumes and different salt concentrations.

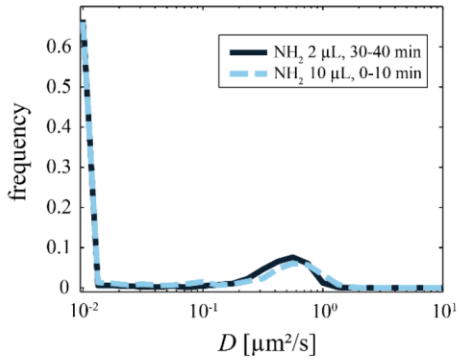

Fig. S3: Diffusive mobility of 200 nm polystyrene particles in ovine vitreous humor at different injection volumes and incubation times before SPT. Comparison of the diffusive mobility of amine-terminated polystyrene particles for injections of 10 µL particle solution into the vitreous (SPT was started 0-10 min after injection) and injection of 2 µL (SPT was started 30-40 min after injection). The distribution curves contain data from > 1000 apparent diffusion coefficients of amine-terminated (NH_2) 200 nm polystyrene particles. For the calculation of these distributions, data from at least three different vitreous samples have been pooled.

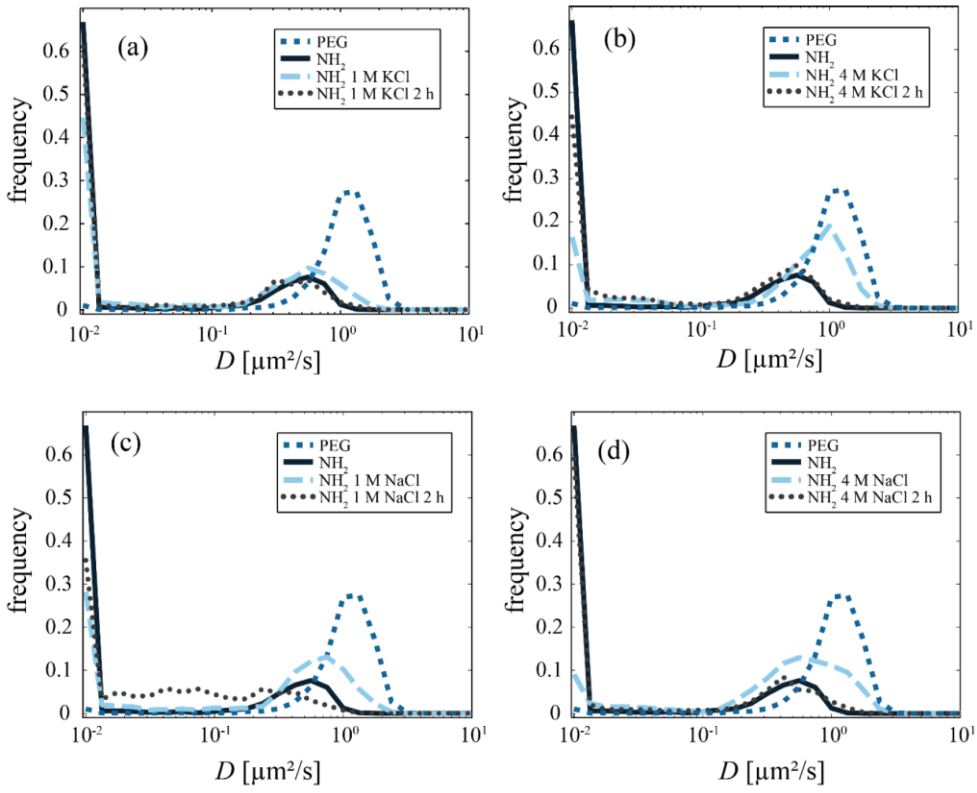

Fig. S4: Diffusive mobility of 200 nm polystyrene particles in ovine vitreous humor at various salt concentrations. Comparison of the diffusive mobility of amine-terminated polystyrene particles at different KCl (*a, b*) and NaCl (*c, d*) concentrations shortly after injection of a salt-particle solution and after 2 additional hours. PEGylated particles at physiological salt concentrations are shown as a reference for nearly free moving particles. The distribution curves contain data from > 1000 amine-terminated (NH_2) as well as PEGylated (PEG) 200 nm polystyrene particles. The peak of the mobile fraction of NH_2 particles is only increased in height but not shifted towards faster diffusion coefficients. Therefore, the NH_2 particles became more mobile but did not exhibit faster diffusion. For the calculation of these distributions, data from at least three different vitreous samples have been pooled.

Unconfined compression tests of ovine vitreous after incubation in high-salt solution

Compression experiments were performed on a rheometer (MCR 302, Anton Paar, Graz, Austria) using a plate-plate 25 mm measuring geometry (PP25, Anton Paar, Graz, Austria) with an indentation speed of 10 µm/s until a normal force of 0.5 N was reached. For measurements, the vitreous samples were placed in a 50 mm glass petri dish which was positioned in the middle of the measuring plate of the rheometer. Each vitreous humor sample was compressed three times to verify that the compression of the vitreous itself does not influence its mechanical integrity. Samples were compressed first in the fresh state and then again after a 5 h incubation in salt solution. The Young's moduli were calculated by fitting the stress/strain data for strains above 5 %.

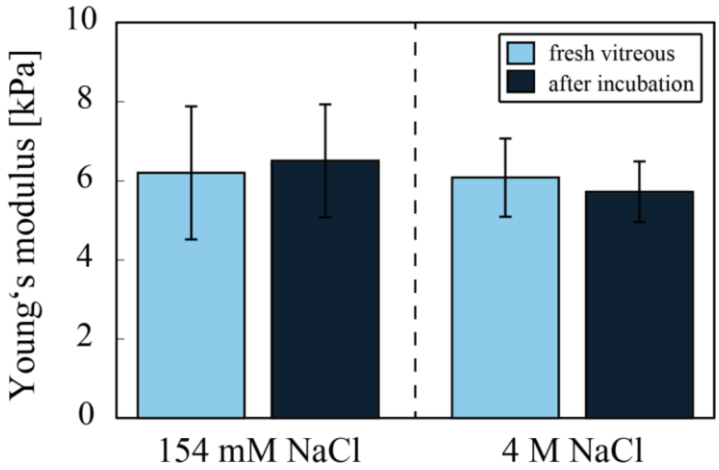

Fig. S5: Young's moduli of ovine vitreous humor after incubation in salt solutions. Unconfined compression tests were performed on ovine vitreous samples both in the fresh state and after those samples have been incubated for 5 hours either in a physiological (154 mM) NaCl solution or a high-salt (4 M) NaCl solution (pH 7). The error bars denote the standard deviation as obtained from three different vitreous samples.

Enzymatic removal of ovine vitreous humor components

Digestion of collagen II was performed by incubating fresh vitreous samples each in 7.5 mL 50 mM TRIS/HCl buffer (pH 7.4, 4 mM $CaCl_2$) containing 1 mg/mL of collagenase type II from *Clostridium histolyticum* at 37 °C overnight. Control samples were incubated at the same conditions but without the enzyme. Incubation of vitreous samples with collagenase type II resulted in total liquefaction of the vitreous (Fig. S6*a*) whereas the control samples maintained their structural integrity (Fig. S6*b*).

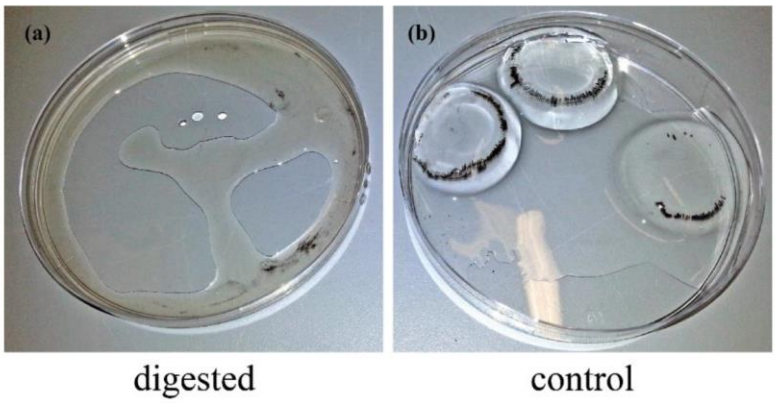

Fig. S6: Ovine vitreous humor after digestion with collagenase type II. Ovine vitreous humor samples are shown after 24 hour digestion with collagenase type II from *Clostridium histolyticum* (*a*). Control samples which were stored in digestion buffer but in the absence of enzymes are shown in (*b*).

Digestion of vitreous samples with heparinase and hyaluronidase was performed as described in the methods section of the main paper. Fig. S7 and S8 show that the treated vitreous samples maintained their structural integrity although the samples lost some water and slightly decreased in size as a consequence of the enzymatic treatment.

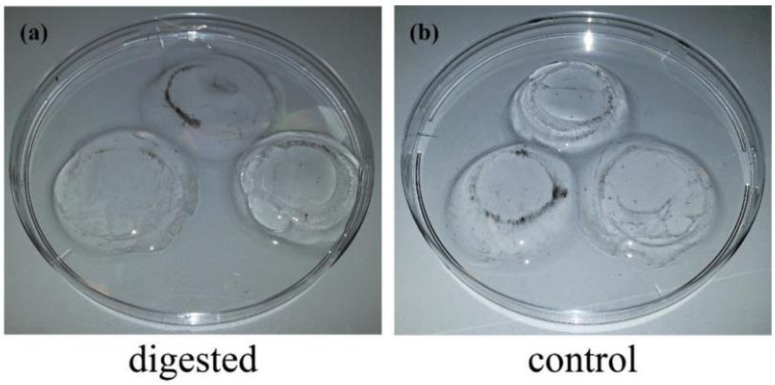

Fig. S7: Ovine vitreous humor after digestion with heparinase I and III. Ovine vitreous humor samples are shown after 72 hour digestion with heparinase I and III from *Flavobacterium heparinum* (*a*). Control samples which were stored in digestion buffer but in the absence of enzymes are shown in (*b*).

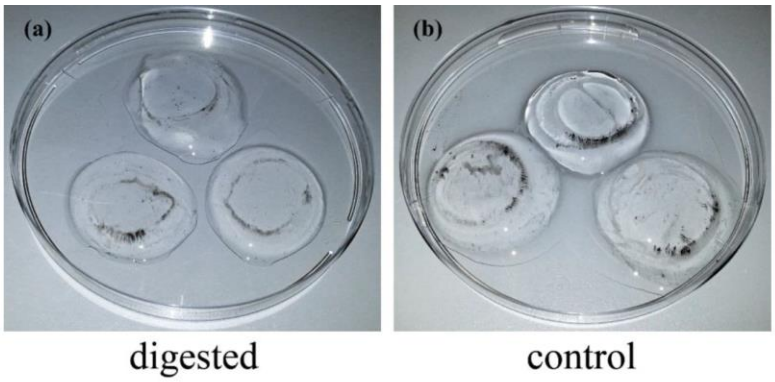

Fig. S8: Ovine vitreous humor after digestion with hyaluronidase. Ovine vitreous humor samples are shown after 72 hour digestion with hyaluronidase from *Streptomyces hyalurolyticus* (*a*). Control samples which were stored in digestion buffer but in the absence of enzymes are shown in (*b*).

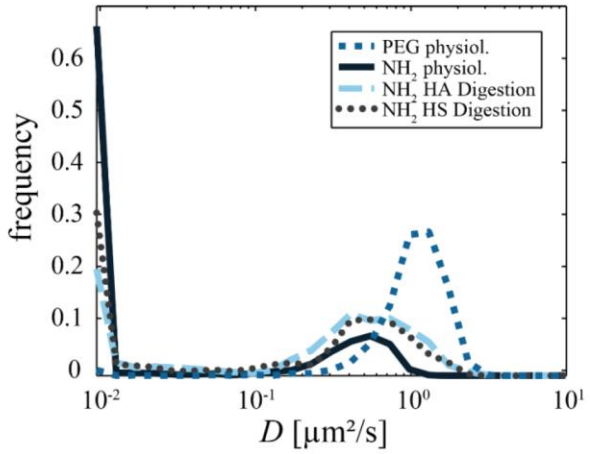

Fig. S9: Diffusive mobility of 200 nm polystyrene particles in ovine vitreous humor after digestion of HA or HS. Comparison of the diffusive mobility of amine-terminated polystyrene particles in vitreous humor at physiological conditions and after enzymatic removal of HA and HS. PEGylated particles at physiological salt concentrations are shown as a reference and represent nearly free moving particles. The distribution curves contain data from > 1000 apparent diffusion coefficients of amine-terminated (NH_2) 200 nm polystyrene particles. For the calculation of these distributions, data from at least three different vitreous samples have been pooled.

Table T2: Percentage of wet weight of ovine vitreous after enzymatic digestion of HA or HS. The percentage of wet weight was determined by weighing the vitreous samples before and after enzymatic treatment. The depicted percent values refer to the wet weight of fresh vitreous samples before the treatment (= 100 %). The errors denote the standard deviation as obtained from at least three vitreous samples.

wet weight compared to untreated state [%]	control (buffer only)	digested
treatment with hyaluronidase	80 ± 8.5	47 ± 7.2
treatment with heparinase	88 ± 3.5	75 ± 7.3

Penetration of molecules into ovine vitreous humor

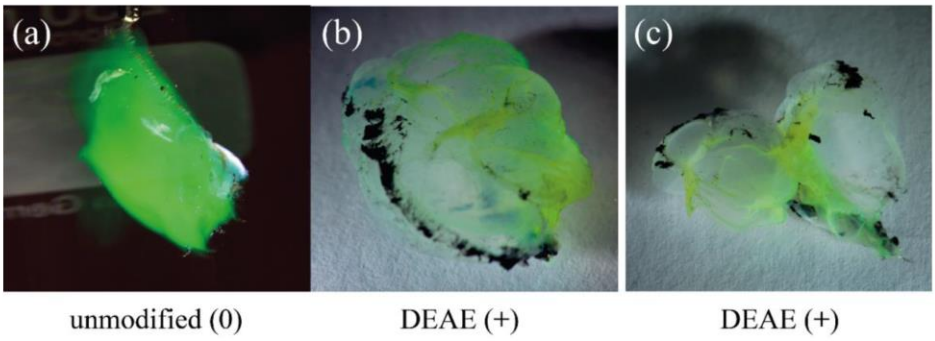

Fig. S10: Penetration of FITC-labeled 150 kDa dextrans into ovine vitreous humor. Ovine vitreous humor samples are shown after overnight incubation in unmodified (*a*) and cationic DEAE-modified (*b, c*) dextran solutions (dextran concentration in the incubation buffer was 10 mg/mL). Whereas the neutral dextrans are able to penetrate the whole vitreous humor (*a*), the cationic DEAE-dextrans accumulate at the outside of the vitreous (*b*) and are not able to penetrate into the bulk volume of the vitreous (*c*).

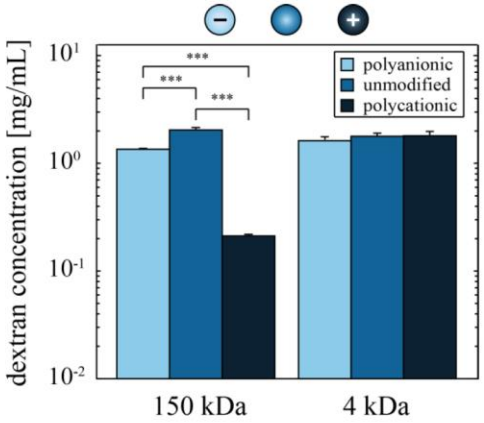

Fig S11: Penetration efficiency of different dextran molecules into ovine vitreous humor fragments. The concentration of dextrans in ovine vitreous humor is shown after incubation of the vitreous fragments overnight in different dextran solutions (dextran concentration in the incubation buffer was 10 mg/mL). DEAE (polycationic), unmodified (neutral) and CM (polyanionic) dextrans are compared at two different molecular weights. The error bars denote the standard deviation as obtained from three vitreous samples. Asterisks denote statistically significant differences (*** := $p < 0.001$).

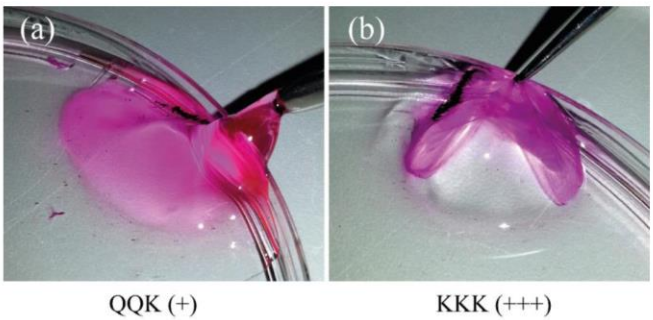

Fig. S12: Penetration of TAMRA-labeled oligopeptides into ovine vitreous humor. Ovine vitreous humor samples are shown after overnight incubation in $(QQK)_8$ (*a*) and $(KKK)_8$ (*b*) peptide solutions prepared at 1 mg/ml. Whereas the slightly positive oligopeptide $(QQK)_8$ is able to penetrate the whole vitreous humor (*a*), the strongly cationic $(KKK)_8$ accumulates at the outside of the vitreous (*b*) and is not able to penetrate the bulk volume of the vitreous.

A.2 Controlled nanoparticle release from a hydrogel by DNA-mediated particle disaggregation

Journal of Controlled Release 246 (2017) 71–78

Contents lists available at ScienceDirect

Journal of Controlled Release

journal homepage: www.elsevier.com/locate/jconrel

Controlled nanoparticle release from a hydrogel by DNA-mediated particle disaggregation

C. Nowald, B.T. Käsdorf, O. Lieleg *

Department of Mechanical Engineering and Institute of Medical Engineering, Technical University of Munich, Boltzmannstrasse 11, 85748 Garching, Germany

ARTICLE INFO

Article history:
Received 22 September 2016
Accepted 9 December 2016
Available online 23 December 2016

Keywords:
Drug delivery
DNA linker
Nanoparticles
Liposomes
Osmotic pressure

ABSTRACT

For many pharmaceutical applications, it is important that different drugs are present in the human body at distinct time points. Typically, this is achieved by a sequential administration of different therapeutic agents. A much easier alternative would be to develop a drug delivery system containing a whole set of medically active compounds which are liberated in an orchestrated and controlled manner. Yet, such a controlled, sequential release of drugs from a carrier system that can be used in a physiological situation is difficult to achieve. Here, we combine two molecular mechanisms, i.e. a build-up of osmotic pressure by the depletion of a control molecule and triggered disaggregation of nanoparticle clusters by synthetic DNA sequences. With this approach, we gain spatio-temporal control over the release of molecules and nanoparticles from a gel environment. The strategy presented here has strong implications for developing complex drug delivery systems for wound healing applications or for the sustained release of pharmaceuticals from a drug-loaded gel and will lower the need for multiple drug administrations.

1. Introduction

To function smoothly, the human body relies on the spatio-temporal interplay of countless molecules. One example of a complex biological process requiring the orchestrated action of multiple molecules is wound healing: Here, the regeneration of lost tissue is more successful if growth factors are released sequentially within narrow time windows [1]. After an injury, a finely tuned and well-timed healing cascade takes place: Different kinds of cytokines are needed at certain points in time, including the platelet-derived growth factor (PDGF), transforming growth factor-beta (TGF-β) and vascular endothelial cell growth factor (VEGF). PDGF initiates the chemotaxis of a variety of cell types such as neutrophils, macrophages, smooth muscle cells and fibroblasts – a process that is critically needed to initiate wound healing. TGF-β is also required during the early stage of a healing cascade, as it attracts macrophages and stimulates them to secrete additional cytokines [2–4]. VEGF, in contrast, is the most important cytokine of the angiogenic cascade, which takes place at a later stage of wound healing [5,6]. This example involving only three different cytokines already illustrates the complexity of the wound healing process. It also shows that these three molecules need to be available at different time points to ensure that the process correctly runs its course.

To support the natural wound healing abilities of the human body after injuries or to compensate for a pathological defect in the wound healing cascade of certain patients, medical products loaded with a set of therapeutic agents can be used. Typically, a gel enriched with molecules beneficial for the wound healing process is applied to the damaged tissue area [7–10]. In many cases, it is necessary to replace such wound gels several times during the healing process or to apply different liquids or gel formulations – each containing another set of bioactive molecules [11,12]. Even though certain medical treatments are more efficient when drugs are administered sequentially [13], this is not easily possible when repetitive access to the tissue area is restricted, e.g. for internal wounds after surgery. Here, all relevant molecules and pharmaceuticals are typically applied at the same time [14,15] – although their individual function is required at different time points. In addition to wound healing, also pharmaceutical applications in cancer therapy could benefit from a precisely controlled release of multiple drugs from a gel. Here, e.g. pre-treatment with a first drug can be used to sensitize the tumor environment to a second chemotherapeutic agent, thus enhancing the delivery efficiency of this second drug into the tumor [16,17]. Such a sequential combination therapy can also reduce the potential risk of toxicity or unwanted pharmacological interaction – phenomena that need to be considered when a combination of drugs is simultaneously applied during a cancer treatment even though the individual therapeutic agents are only needed at distinct time points of the therapy [18].

One existing strategy for establishing control over the release kinetics of therapeutic agents from gels targets the chemical composition of these gels to tune their pore size [19,20], or the binding affinity of the drug to the gel constituents [20]. However, this strategy requires a

* Corresponding author.
E-mail address: oliver.lieleg@tum.de (O. Lieleg).

http://dx.doi.org/10.1016/j.jconrel.2016.12.015
0168-3659/

Appendix A.2 Controlled nanoparticle release from a hydrogel by DNA-mediated particle disaggregation

tailored gel matrix for each drug. Examples for such a tailored drug/gel release system include the release of lidocaine from poloxamer 407 or sodiumcarboxymethyl cellulose gels [21], or the release of doxorubicin from acrylate-based hydrogels [22]. Another approach makes use of the liberation of molecules from nanoparticles (NPs); here, the type and architecture of the NP determines the release kinetics of the encapsulated drug [23]. When liposomes are used as drug carriers, variations in the lipid composition result in different release kinetics [24]. Inorganic NPs, on the other hand, such as mesoporous silica nanoparticles (MSNs) and titanium dioxide (TiO_2) particles can be generated with a uniform porous structure, a high surface area, tunable pore sizes and well-defined surface properties [25–29]. When such porous NPs are loaded with drugs, they release their cargo by diffusion. Surface modifications of porous NPs such as amination make use of electrostatic interactions to achieve high loading rates and sustained release of (negatively) charged drugs like Ibuprofen and Aspirin [30,31]. A different drug release mechanism requires polymeric NPs and combines the diffusive release of cargo molecules from the NPs with NP degradation [32]. Examples for polymers used for such polymeric NPs include chitosan [33,34], dextran [35,36] and poly(methyl methacrylate) [37].

For medical applications such as wound treatment, NPs are typically incorporated into hydrogels. This makes it possible to retard the release of the incorporated drugs by two mechanisms: release from the NP and subsequent release from the gel [38,39]. Yet, whereas this combined strategy is sufficient to achieve prolonged drug release, always the same molecule is liberated. Therefore, drug co-delivery systems have been developed which make use of encapsulating multiple therapeutic agents into NPs or embedding multiple NP species into a hydrogels [40,41].

As complex as those release approaches already are, they still share a key disadvantage: drug release can be prolonged but is immediately initiated for all molecules at the same time, i.e. after the gel sample is prepared. Yet, there is a clear need for devising a control mechanism which allows for coordinating the release of the different incorporated drugs, e.g. liberating a second drug only when a another one has already left the gel. The key idea pursued here is to achieve such control by making use of artificial DNA-sequences to trap drug carriers in a gel and liberate the very same drug carriers from the gel in a controlled way. When their length is short, synthetic DNA sequences are easy to generate, programmable, allow for tuning the interaction strength between two DNA strands by varying the sequences of the constructs [42], and they can serve as a tool to control nanoparticle aggregate formation [43,44].

The DNA-based strategy introduced here enables the controlled release of NPs from a hydrogel and is based on a NP disaggregation process, which separates individual NPs from a NP cluster. As this NP cluster is stabilized by DNA-mediated cross-links, NP disaggregation can be achieved by binding of complementary DNA strands. Those complementary DNA sequences, in turn, are liberated from liposome particles, which have been embedded into the gel as well. DNA release is triggered by a build-up of osmotic pressure inside the gel after diffusive depletion of a small control molecule from the gel. Furthermore, control over the kinetics of the release process is achieved by retarding the diffusive spreading of the disaggregation-inducing DNA strands through the gel.

2. Materials and methods

2.1. Polynucleotide design

We designed cross-linker DNA (crDNA) sequences with self-complementary regions such that the constructs can form cross-links between gold nanoparticles (Au-NPs, 5 nm in diameter, PDI ≤ 0.2, stock solution of $5.5 * 10^{13}$ Au-NP/mL stabilized in a citrate buffer, Sigma-Aldrich) onto which they are bound (Fig. 1a). For simplicity, only a single crDNA cross-link is depicted in Fig. 1a. In the experiments discussed in our manuscript, each gold NP is likely to carry several crDNA sequences on its surface and thus can form multiple cross-links with other gold NPs. As a consequence of this cross-linking process, the Au-NPs are supposed to build large aggregates (Fig. 2a) which are then trapped in the gel due to geometric constraints. Au-NP disaggregation is supposed to occur only in the presence of a suitable displacement DNA (dDNA) with a higher affinity to the crDNA.

To enable covalent binding of the crDNA to the surface of Au-NPs, we integrated a thiol-C6 capped poly(A)-tail at the 5′-end of the sequence. The self-complementary region of the crDNA was chosen such that it had a melting temperature T_m above 37 °C so that the construct allows for the formation of stable cross-linked Au-NP aggregates at temperatures ≤ T_m. In contrast, the dDNA sequence was designed to exhibit a higher affinity to the crDNA than two crDNA molecules have to each other. Thus, the crDNA/dDNA complex had a much higher (predicted) melting temperature than the crDNA/crDNA complex. As a control molecule, a polynucleotide sequence (coDNA) with the same number of nucleotides as the dDNA was chosen but designed such that it had only a negligible binding affinity to the crDNA sequence.

Two sets of polynucleotides pairs (crDNA and dDNA) with different T_m values and different sequences were designed as described, tested with the software OligoAnalyzer 3.1 [45] (parameters: target type, DNA; oligo concentration: 0.25 μM; Na^+ concentration: 150 mM; Mg^{2+} concentration: 5 mM; deoxynucleoside triphosphate (dNTPs) concentration: 0 mM) to ensure that they fit the above mentioned requirements and then obtained from Integrated DNA Technologies (IDT, München, Germany). The detailed sequences and calculated melting temperatures of those constructs are listed in Table 1.

Here, the self-complementary regions of the respective crDNA sequences responsible for establishing cross-links are highlighted in red, and the melting temperatures given in the figure describe the stability of the formed crDNA/crDNA or dDNA/crDNA complex. The NUPACK web application was used to calculate the minimum free energy (MFE) structures of the designed DNA sequences. The free energy of a secondary structure was calculated using nearest-neighbor empirical parameters as outlined in ref. [46] for DNA at 37 °C in the presence of 150 mM Na^+ and 5 mM Mg^{2+}.

2.2. PAGE analysis of DNA-hybridization efficiency

To verify that our designed polynucleotide constructs only efficiently hybridize when DNA constructs with complementary sequences are mixed, we performed an analysis by polyacrylamide gel electrophoresis (PAGE). In our constructs, a high degree of complementarity is only expected for sequence combinations with a high calculated T_m (i.e. only for matching crDNA/dDNA sequences). As a control, synthetic DNA sequences (coDNA) with a length identical to the crDNA molecules but with a different sequence (and thus very low calculated T_m) was used. DNA sequences were mixed in 1:1 ratios at a concentration of 1 nmol each and were incubated at room temperature (RT) for 2 h in presence of 500 mM dithiothreitol (DTT) and 0.5 mM tris-(2-carboxyethyl)-phosphin hydrochlorid (TCEP, Carl Roth, Karlsruhe, Germany) to prevent the formation of S-S-bonds. Subsequently, 6× sample loading buffer (Sigma-Aldrich, Schnelldorf, Germany) was added, and the samples were loaded into Mini-PROTEAN TBE Precast Gels (BIO-RAD, Munich, Germany). Electrophoresis was performed at 100 V in 0.5× Tris-Borat-EDTA (TBE) buffer (pH 8.0) containing 5 mM DTT, and pictures were recorded on a Molecular Imager Gel Doc XR System (BIO-RAD) after the gels were stained at RT for 1 h with SYBR Green I solution (Sigma-Aldrich) in 0.5× TBE buffer.

2.3. Gold nanoparticle functionalization and aggregate formation

Polyvalent DNA-functionalized gold nanoparticles were generated by coating colloidal gold with a monolayer of DNA. This coating approach makes use of the strong interaction between gold and thiols, the latter of which have been integrated at the terminus of the synthetic

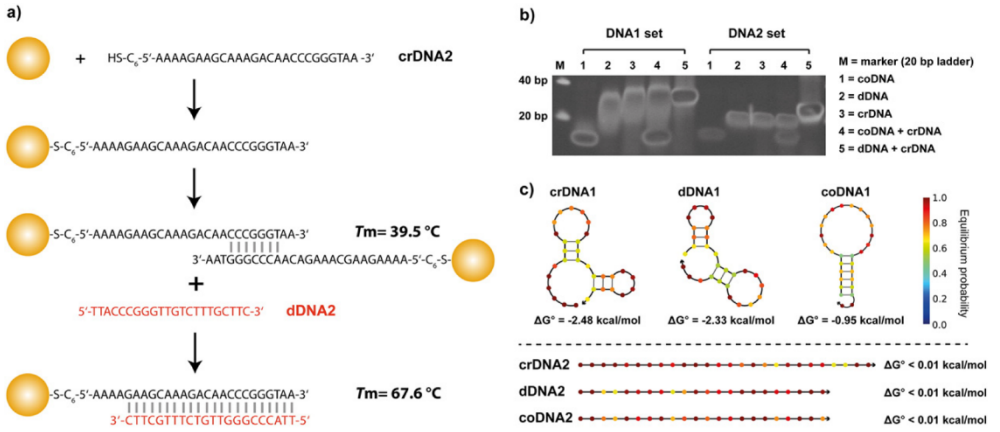

Fig. 1. Molecular design of the DNA sequences. (a) Two gold NPs are connected via an 8 bp crDNA cross-link (see main text for details). Displacement (dDNA) DNA molecules are designed to hybridize with a larger part of the crDNA molecule (22 bps) thus forming an energetically more favorable double strand. b) Electrophoretic separation of SYBR Green I stained DNA mixtures, indicating hybridization efficiency of the different DNA mixtures. c) Estimated minimum free energy secondary structures for the designed polynucleotide sequences at 37 °C. Each base is colored according to the probability at which it will assume the depicted paired or unpaired state at equilibrium.

polynucleotides via a 5′-Thio-Modifier C6 S-S linker. Such thiol-modified crDNA sequences were obtained from IDT in their oxidized form, i.e. with the sulfur atoms protected by a S-S-bond. Thus, to enable thiol-gold interactions, those disulfide bridges had to be reduced. Lyophilized crDNA was therefore dissolved in 180 mM phosphate buffer (pH 8.0) containing 100 mM DTT and incubated at RT for 1 h. Deprotected crDNA was separated from the protection groups by means of SEC using a NAP-25 Sephadex G-25 column (GE Healthcare, Freiburg, Germany); in this step, also a buffer exchange was performed to 180 mM phosphate buffer (pH 8.0) without DTT. The crDNA concentration was then measured with a NanoDrop-1000 spectral photometer (Thermo Fischer Scientific, Ulm, Germany) and adjusted to 100 μM. To obtain a sufficiently high coating density of Au-NPs with crDNA while minimizing the required amount of crDNA, the following estimation [47] was used to determine the number of crDNA molecules needed:

$$Mol\,(crDNA) = A_{NP} * c_{NP} * D_{crDNA} * V_{NP} \quad (1)$$

Here, A_{NP} denotes the surface area of the Au-NP, c_{NP} the concentration of the Au-NP solution (in units of Au-NPs/L), D_{crDNA} the crDNA density on each Au-NP (estimated to be ~35 pmol crDNA/cm^2 according to ref. [48]) and V_{NP} the volume of Au-NP solution used (in L). For our Au-NPs, this estimation gave a value of ~1.5 nmol crDNA for 1 mL of Au-NP solution. A corresponding volume of crDNA was then incubated in the presence of 100 μM of the reducing agent TCEP at RT for 1 h before commercial Au-NPs (5 nm in diameter, stock solution of $5.5 * 10^{13}$ Au-

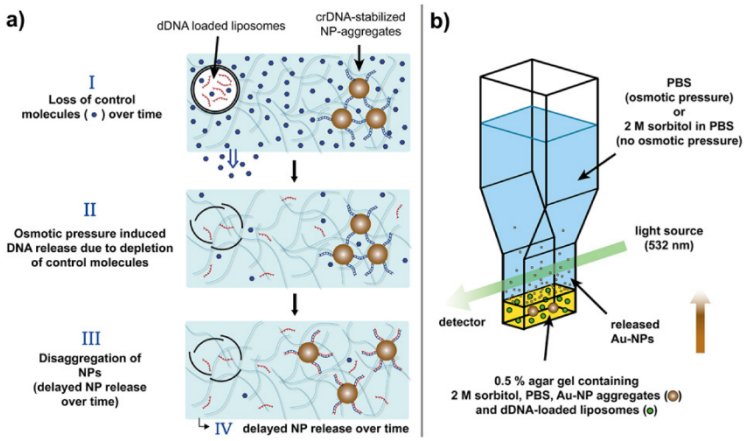

Fig. 2. Schematic illustration of the triggered NP release mechanism from a gel. (a) Two different types of NPs are imbedded into the gel environment: DNA-loaded liposomes and gold NP aggregates, the latter of which are stabilized by DNA cross-links (crDNA). A depletion of control molecules from the gel entails a build-up of osmotic pressure, which triggers the bursting of liposomes and thus a release of displacement DNA (dDNA) into the gel. These dDNA molecules can then diffuse through the gel, bind complementarily to the crDNA sequences and thus dissolve the crDNA-mediated cross-links. As a consequence, individual gold NPs are removed from the aggregate, become mobile, and can leave the gel by diffusion. (b) Schematic representation of the light absorption assay used for quantifying NP release from the gel. Individual Au-NPs (or small Au-NP complexes) are released from the agar gel and can be detected in the buffer supernatant spectroscopically.

Appendix A.2 Controlled nanoparticle release from a hydrogel by DNA-mediated particle disaggregation

Table 1
Nucleotide sequence and melting temperature of both DNA sets (DNA1 and DNA2).

Abbreviation	Sequence from 5′ to 3′	T_m [°C]	Secondary structure at 37 °C
crDNA1	AAAAAAGCGACGCTGACGCAACAGGCCTGTT	50.5	Yes
dDNA1	AACAGGCCTGTTGCGTCAGCGTCGCTTT	76.8	Yes
coDNA1	ATCCGCCGTGACCCGTCTGTGTGGATAT	N/A	Yes
crDNA2	AAAAGAAGCAAAGACAACCCGGGTAA	39.5	No
dDNA2	TTACCCGGGTTGTCTTTGCTTC	67.6	No
crDNA2	AATGAGCACAACAGAAACGAAG	N/A	No

NP/mL stabilized in a citrate buffer, Sigma-Aldrich) were added. After 12 h of incubation, the NaCl concentration of the Au-NP/crDNA mixture was increased by 50 mM, followed by a 10 s sonication step and 20 min of incubation at RT. This process was repeated until a final NaCl concentration of 1 M was reached, a process that promotes aggregate formation. At this high ionic strength, the Au-NP/crDNA solution was then incubated at RT for 48 h and subsequently stored at 4 °C. For each experiment, equal volumes of this Au-NP solution were centrifuged at 10000 ×*g* for 20 min to separate the crDNA cross-linked Au-NP aggregates from unreacted reagents, and three washing steps with the desired final buffer were added for the same purpose.

2.4. Calcein- and DNA-loaded liposomes

Liposomes loaded with calcein were generated by means of lipid film hydration as follows. First, 0.5 μmol of 1,2-dioleoyl-sn-glycero-3-phospho-(1'rac-glycerol) (DOPG) (Avanti Polar Lipids, Alabaster, USA) dissolved in chloroform was transferred into a glass vial. The chloroform was then evaporated overnight and the remaining lipid film was hydrated with 120 μL PBS containing 2 M sorbitol (PBS-2MS) and 1.5 mM calcein, before the lipid/calcein solution was thoroughly vortexed and sonicated. Free calcein (= calcein which was not enclosed into liposomes) was removed by SEC using a PCR Kleen Spin Column (BIO-RAD) following the manufacturer's instructions.

Liposomes loaded with dDNA were produced in the same way, but using 0.5 μmol of a lipid mixture consisting of L-α-phosphatidylcholine from egg yolk (Egg-PC), 1,2-dioleoyl-3-trimethylammonium-propane (DOTAP) and cholesterol in a molar ratio of 3:1:1. All lipids were obtained from Avanti Polar Lipids, (Alabaster, USA). After rehydration in 120 μL PBS containing 2 M sorbitol (PBS-2MS) and 600 μM dDNA, the solution subjected to five freeze/thaw cycles (freezing in liquid nitrogen/thawing at 37 °C) to increase the DNA loading efficiency, before free DNA was removed. For testing the efficiency of dDNA release by osmotic pressure, 30 μL of liposomes were added either to 270 μL of PBS (thus inducing a strong osmotic pressure) or PBS-2MS (= osmotically balanced buffer, serving as a control). For DNA detection, SYTOX green (a membrane impermeable nucleic acid stain, Thermo Fischer Scientific, Ulm, Germany) was used as this dye shows very low autofluorescence (i.e. more than a 500× fluorescence enhancement upon binding to nucleic acids). For DNA staining, SYTOX green was added to a final concentration of 1 μM and incubated at 37 °C for 30 min. dDNA release was then quantified spectroscopically using a Victor3 plate reader (Perkin Elmer, Rodgaum, Germany) at $\lambda_{ex} = 485$ nm and $\lambda_{em} = 535$ nm.

2.5. Formulation of NP-loaded agar gels

A 2% (*w*/*v*) agarose solution (Type IX-A, ultra-low gelling temperature agarose, Sigma-Aldrich) was prepared in 2MS-PBS and was allowed to cool down from 80 °C to RT. Au-NP aggregates (obtained from 0.5 mL of a crDNA cross-linked Au-NP solution by centrifugation) were incorporated into 100 μL of this RT agarose solution, supplemented with buffer containing either 0.33 μM dDNA or coDNA to a final agarose concentration of 0.5% (*w*/*v*) and incubated at 4 °C for 20 min to form a gel. At this agar concentration, the gels should have mesh sizes on the order of 100 nm [49] which is much larger than the size of individual gold nanoparticles used here.

Both gel preparations, the one containing dDNA and the control (containing coDNA), were then incubated at 37 °C. At Au-NP disaggregation could visually be followed by the development of a red color in the gel which originates from released single Au-NPs. Pictures of this NP-loaded agar gels were acquired over a time period of 24 h using a Canon SX240 HS camera (Canon, Krefeld, Germany). All the agar gels used in this study had comparable viscoelastic properties with elastic moduli in the range of 100–300 Pa. These values were determined on a commercial shear rheometer (MCR 302, Anton Paar, Graz, Austria) using a plate/plate geometry (PP25 measuring head, Anton Paar, Graz, Austria) and a plate separation of 200 μm. Small torques in the range of 1 μNm were applied to ensure linear material response.

2.6. Quantification of Au-NP disaggregation

To quantify the observed Au-NP disaggregation process and the subsequent release of individual Au-NPs (or small Au-NPs complexes) from the agar gels, NP-loaded gels were prepared as described above. However, this time a larger amount of Au-NP aggregates (i.e. the amount obtained from 1 mL of a crDNA cross-linked Au-NP solution) was used. Also, instead of free DNA, now 20 μL of a DNA-loaded liposome solution was incorporated. The prepared mixtures were then transferred to cuvettes (UV-Cuvette semi-micro, Brand, Wertheim, Germany) which had already been filled with 75 μL of the respective liposome-loaded agar gel (but lacking Au-NP aggregates). This procedure allowed to prevent sedimentation of the relatively large Au-NP aggregates and to trap them on top of the pre-filled liposome loaded ager gel layer, i.e. in the middle of an agar gel with a total volume of 150 μL (Fig. 2b). Another benefit of this filling procedure was that the Au-NPs were surrounded by dDNA-containing liposomes from above and from below.

After gel formation had been concluded, the experiment was initiated by adding either 1350 μL of PBS (thus inducing a strong osmotic pressure) or PBS-2MS (= osmotically balanced buffer serving as a control). The cuvettes were sealed with PARAFILM M (Wagner & Munz, Munich, Germany) to prevent dehydration and were incubated at 37 °C. Release of single Au-NPs was monitored spectroscopically at 532 nm (see Fig. 2b) over a time period of several days using a specord 210 spectral photometer (Analytikjena, Jena, Germany). Samples were inverted carefully before each measurement to achieve homogeneous distribution of the released Au-NPs throughout the buffer phase of the cuvette to ensure accurate measurement signals. To retard the triggered liberation of Au-NPs, positively charged polystyrene microparticles (amine-terminated, size 1 μm, fluorescent yellow green, stock solution with $5 * 10^{10}$ particles/mL, Sigma-Aldrich, Schnelldorf, Germany) serving as charge traps for the negatively charged dDNA were added to the gel matrix. Therefore, polystyrene beads in dilutions ranging from 1:100 up to 1:10 were incorporated into the agar/Au-NP solution together with the DNA-loaded liposomes prior to gelation.

A similar setup was used to quantify the release of calcein from liposomes embedded into agar gels. Here, cuvettes were filled with 150 μL of agar containing calcein loaded liposomes, and the gel was layered either with 1350 μL PBS or PBS-2MS to initiate the experiment. Samples of 200 μL each were taken from the supernatant, measured and returned to the cuvettes afterwards. The calcein concentration in the supernatant samples was quantified spectroscopically using a Victor3 plate reader (Perkin Elmer, Rodgaum, Germany) at $\lambda_{ex} = 485$ nm and $\lambda_{em} = 535$ nm.

3. Results and discussion

The goal of this study is to achieve a controlled release of nanoparticles (NPs) from a gel by triggering NP disaggregation (see Fig. 2a). To enable this goal, it is necessary to use NPs, which are small enough so they can leave the gel by diffusion, but to generate relatively large NP-

aggregates, which are trapped in the gel matrix according to their increased size.

We aim at releasing NPs from the gel as those NPs can serve as potential drug carriers. For our study, we selected Au-NPs due to their unique physical, chemical, optical and electronic properties [50]. As a strategy for NP-aggregation, we employ cross-linking by complementary DNA sequences: such DNA-mediated NP-aggregates can be disassembled by adding complementary DNA sequences to the gel, which open the NP-cross-links through competitive binding.

For the formation of DNA-mediated Au-NP-aggregates, we designed two sets of DNA sequences (DNA1 and DNA2) consisting of a cross-linking DNA sequence (crDNA), the corresponding displacement DNA (dDNA) and a non-complimentary sequence serving as a control (coDNA). After attaching the crDNA molecules to the surface of 5 nm Au-NPs by a thiol linker present at the 5′-end of the polynucleotide, the crDNA molecules are supposed to form cross-links between Au-NPs by hybridizing with complementary parts of other crDNA molecules. To ensure sufficient stability of this hybridized DNA strands, the sequences were designed such that they had a calculated melting temperature $T_m > 37$ °C (Table 1). Indeed, when we load those crDNA sequences onto a PAGE gel, we detect a band at higher molecular weight (indicating successful hybridization) – but not for coDNA (Fig. 1b).

To meet the second requirement for our DNA-mediated (de)aggregation process, the dDNA sequences are designed to possess a considerably higher affinity to crDNA than the crDNA molecule to itself – which is indicated by the higher T_m values for the dDNA/crDNA complex (see Table 1). If this requirement is met, then the dDNA molecules should be able to displace one crDNA molecule from the crDNA/crDNA cross-link established between Au-NPs thus inducing NP disaggregation. Consistently, also for dDNA, we find a band at higher molecular weight in our PAGE gel, which reflects both the ability of this polynucleotide sequence to hybridize with itself and the successful formation of a dDNA/crDNA complex. In contrast, the coDNA constructs have only negligible affinity to our crDNA molecules and thus should be unable to hybridize, neither with themselves nor with the other polynucleotide sequences. Indeed, for the coDNA constructs, bands at higher molecular weight are absent.

In a next step, we test whether our dDNA sequences can indeed dissolve crDNA-cross-linked Au-NP-aggregates when they are incorporated into agarose gels. Successful NP disaggregation can be followed visually as single Au-NPs released from the aggregate introduce red color into the gel (Fig. 3) – similar to individual Au-NPs in solution before aggregation is induced.

Surprisingly, even though both crDNA sequences induce efficient Au-NP-aggregation and both sets of DNA sequences should be able to form dDNA/crDNA complexes as suggested from gel electrophoresis, only crDNA2-cross-linked Au-NP-aggregates could be dissolved in presence of the corresponding displacement DNA (dDNA2). To demonstrate that crDNA1 cross-linked Au-NP aggregates can in principle be disaggregated as well, Au-NP aggregates incorporated into agarose gels were heated up to 80 °C for 1 h. As this temperature is clearly above the T_m of crDNA1, thermal energy should suffice to induce disaggregation. As shown in Fig. 3, this is indeed the case.

One possible explanation for the failure of dDNA1 molecules to induce such a disaggregation could be that this polynucleotide sequence might be able to form secondary structures at 37 °C, which are too stable to allow for efficient hybridization with the crDNA1 sequences. Indeed, a calculation of free energy secondary structures for the different DNA sequences suggests that dDNA1 tends to from looped regions, which first need to unfold to enable binding to the crDNA1 (Fig. 1c). This unfolding process may drastically slow down the kinetics of the disaggregation process and might also be responsible for the observation that the bands involving dDNA1 molecules are broader than those involving dDNA2. In this context, it is important to realize that the Au-NPs are probably stabilized via multiple crDNA/crDNA cross-links between each pair of neighboring NPs. Thus, efficient dDNA/crDNA hybridization is required for triggering NP-aggregate disassembly. In contrast, such a secondary structure formation is very unlikely for the dDNA2 construct, which agrees with the high efficiency of this displacement DNA. Thus, for the remainder of this article, the second set of polynucleotides is used (crDNA2, dDNA2, coDNA2).

Having identified a suitable set of polynucleotide constructs for the aggregation and disaggregation of Au-NPs, we next aim at triggering this NP-disaggregation process by inducing a controlled release of dDNA molecules into the gel. As a depot for those dDNA molecules, we chose liposome particles as they can easily be embedded into hydrogels [51] and can be loaded with a broad range of (macro)molecules including proteins, peptides, DNA/RNA, and hydrophilic as well as hydrophobic drugs [52,53]. When searching for a simple external trigger for inducing the release of incorporated molecules from liposomes, there are in principle several options. When a NP-loaded gel is brought in contact with the human body, external parameters such as the temperature or the pH can immediately change – provided that the gel is produced at non-physiological conditions. If the ambient temperature is increased upon contact with the warm body surface, the liposome membrane can become permeable if the ambient temperature matches the transition temperature of the lipid composition [54]. Although temperature sensitive liposomes are able to release molecules with a molecular weight of 70 kDa and above [55], such a temperature based release is more efficient for small molecules - but also here some time is needed until the whole liposome content is set free [56]. As the dDNA sequences used here are already quite large and we prefer full and immediate dDNA release to initiate our disaggregation mechanism, we decided against such a simple temperature trigger. Employing differences in pH as a trigger for inducing molecule release from liposomes is difficult: a significant deviation of gel pH from physiological levels will lead to discomfort or even tissue damage. In turn, designing a release mechanism based on minor changes in pH would be highly challenging. Instead, it is important to recall that molecules embedded into the gel will be able to leave the gel by diffusion when the gel is applied to a different environment. If the gel is loaded with a control molecule whose depletion from the gel can trigger liposome disassembly, then applying the gel onto a body surface may induce the desired dDNA release.

Based on this idea, we enriched our gel with such a control molecule, i.e. the small monosaccharide sorbitol, which is harmless when applied to body surfaces but absent from human tissue. As a consequence, when a sorbitol-enriched gel is applied to human tissue, the sorbitol molecules can leave the gel over time by diffusion. Of course, instead of sorbitol, also a pharmaceutical compound could be used for initiating the osmotic trigger. To achieve osmotic balance as long as the agar gel is not exposed to another water-based environment, we also enriched the loaded liposomes with an identical concentration of sorbitol. When the sorbitol molecules are depleted from the gel, an osmotic pressure will build up. Once a critical pressure is reached, the liposomes should burst and their incorporated cargo be released into the agar gel. First, we loaded DOPG liposomes with 1.5 mM of the fluorescent dye calcein and embedded the liposomes into the gel. As shown in Fig. 4a, after 72 h, we detect a ~ 3fold higher calcein release from the agar gel when an osmotic pressure is present compared to when osmatic balance is maintained, i.e. when the gel is layered with sorbitol-enriched PBS. This demonstrates that the build-up of an osmotic pressure by the depletion of a control molecule from the gel can indeed be a suitable trigger for the aim pursued here.

To verify that such a build-up of an osmotic pressure is also sufficient to release dDNA from liposomes, dDNA2-loaded liposomes were diluted 1:10 with PBS, and dDNA release was quantified in this liquid environment at 37 °C. However, even at osmotic balance we detect a small amount of released dDNA. Liposomes are known to release their cargo if the lipid membrane spreads on a suitable surface; such a behavior is e.g. observed for DOTAP liposomes on silica [57] and might also occur on the inner surface of the cuvettes used in our assays. In addition, embedding the liposomes into the hydrogel matrix may induce mechanical

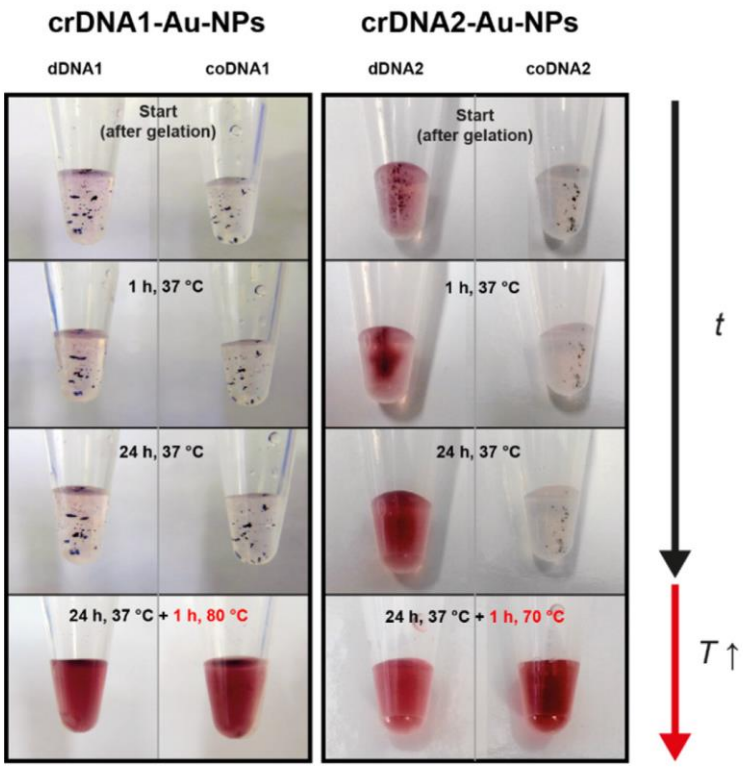

Fig. 3. DNA-mediated disaggregation of DNA-crosslinked Au-NP-aggregates in a gel. When incorporated into agarose gels, crDNA2-crosslinked Au-NP-aggregates can successfully be dissolved by dDNA2 at 37 °C. Released Au-NPs introduce a red color into the gel, which makes it possible to visually follow the disaggregation process over time. Such a disaggregation process, however, is not observed when control DNA (coDNA) or the crDNA1/dDNA1 constructs are used. In all cases, heating the samples for 1 h to temperatures above the T_m of the corresponding crDNA induced full disaggregation.

pressure onto the lipid shell thus reducing the life time of the liposomes compared to when they are stored in a fluid. A liposome spreading mechanism could also explain the low amount of dDNA release from liposome solutions in the absence of osmotic pressure. In contrast, when osmotic pressure is present, we observe a 4–5 times higher dDNA2 release (inset of Fig. 4b). The amount of liberated dDNA is >20 μM which should be sufficient to trigger NP disaggregation. Indeed, when we enrich an agar gel with both cDNA-cross-linked Au-NP aggregates and dDNA-loaded liposomes and then follow the amount of released Au-NPs over a time period of several days, the amount of released Au-NPs is considerably higher in the presence of osmotic pressure (Fig. 4c). In the control sample, i.e. without the build-up of an osmotic release trigger, there is virtually no NP release detectable for the first 10 h. The occurring NP-release at later time points reflects the intrinsic life time of liposomes which are subjected to chemical and physical degradation [58]. Moreover, if the liposomes are loaded with coDNA instead of dDNA, we detect only minor amounts of Au-NP release (Fig. 4c). Conversely, if the Au-NPs are added to the gel without inducing DNA-mediated aggregates, their release is much faster and saturates after ~24 h – independent from whether osmotic pressure is applied or not (Fig. 4b).

In a last step, we ask whether the onset of triggered NP-release can be delayed by implementing an additional control mechanism into the gel. As the dDNA molecules released from the liposomes need to reach the cross-linked NP-aggregates by diffusion, retarding the diffusion of the DNA constructs through the gel could provide such a control mechanism. DNA molecules are highly negatively charged. Thus, distributing local 'charge traps' throughout the gel should give rise to a 'sticky diffusion' process of the DNA molecules as already observed for NPs in complex biological gels [59]. Experimentally, such local charge traps can be generated in the agar gel by adding positively charged polystyrene microparticles to the gel matrix. If the size of those particles is large enough, they will be trapped in the gel. Then, the particles should engage in transient binding interactions with the diffusing DNA molecules thus retarding their diffusive spreading. As depicted in Fig. 4d, such a behavior is indeed observed: the onset of Au-NP particle release is delayed compared to the gel formulation without polystyrene particles, and the strength of this effect depends on the concentration of particles added. Of course, if the binding affinity between the polystyrene particles and the DNA molecules were too strong, the charge traps could permanently reduce the total amount of free DNA molecules by competing with the Au-NP aggregates for dDNA. However, we find that, at longer time points, the amount of liberated NPs approaches the quantity released from the sample lacking charge traps – at least for moderate concentrations of charge traps. This suggests that, indeed, the dDNA molecules released from the liposomes are only retarded by the installed charge traps, and the amount of permanently trapped dDNA molecules is negligible.

4. Conclusion

We here have introduced a mechanism, which combines a triggered build-up of osmotic pressure and subsequent liberation of synthetic DNA constructs to evoke NP disaggregation and thus NP release from a hydrogel. We have chosen gold NPs as one possible NP species that

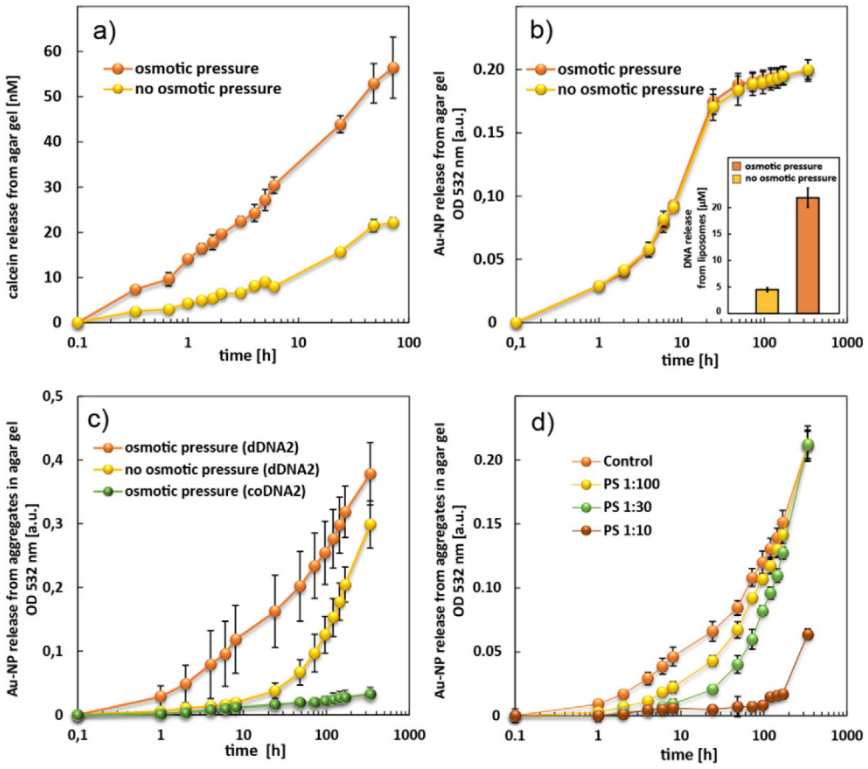

Fig. 4. Release of molecules and NPs from gels can be triggered by a build-up of osmotic pressure. a) Calcein-loaded DOPG liposomes embedded into an agar gel release more cargo in the presence of osmotic pressure than under osmotic balance. The experiment was conducted at 37 °C. b) At 37 °C, osmotic pressure can also efficiently induce the release of larger molecules such as DNA from liposomes. The amount of released DNA was determined 30 min after the depletion of the control molecule sorbitol was initiated. c) A release of dDNA triggered by a build-up of osmotic pressure leads to liberation of individual Au-NPs (or small Au-NP complexes) from the agar gel over time. d) By supplementing the gel with positively charged polystyrene beads (PS) acting as charge traps, the triggered liberation of Au-NPs can be retarded. The amount of PS beads added is given by the dilution factor (1:10, 1:30, 1:100) with respect to the PS bead stock solution ($5 \cdot 10^{10}$ particles/ml.). In all subfigures, the error bars denote the standard deviation as obtained from at least three independent experiments.

can be released from a gel by a disaggregation process. One reason for this choice is that those Au-NPs have been extensively studied in a biological and therapeutic context, and there are already several approaches, which make use of Au-NPs for the selective delivery of therapeutic agents [60–63]. Of course, the methodology introduced here can also be transferred to other suitable drug carrier systems – provided that they can be functionalized with DNA sequences.

Our system of liposomes and cross-linked NPs already offers the possibility to release two types of molecules/particles at different time points. By depositing charge traps in the gel, we are able to modulate the time interval between DNA release into the gel and NP release from the gel. However, the strategy presented here may also allow for installing even more complex control mechanisms into hydrogels thus enabling the orchestrated release of different molecules/particles from the gel at well-defined but separated time points. One possibility for such further adjustment of the process could make use of the tunability of liposomes: Depending on their lipid composition, the sensitivity of liposomes towards osmotic pressure changes [64]. Furthermore, the sequences of the cross-linking and displacing DNA molecules can be varied. This offers additional opportunities to control the dynamics of the process, e.g. by tuning the binding affinity between the DNA sequences or between the DNA sequences, adding competitive constructs or by introducing another step in the release cascade which is triggered by displaced cross-linker DNA.

A hydrogel system with a controlled and orchestrated drug release mechanism as we demonstrate it here would greatly benefit wound healing approaches since it allows for the release of different therapeutic agents at distinct time points but only requires a single gel application. Moreover, from a pharmacokinetic point of view, it would also be advantageous to utilize the methodology presented here to achieve a prolonged release of one and the same molecule, e.g. by loading both the liposomes and the NPs with the identical drug.

Acknowledgements

The authors thank Jan Lang for conducting pilot experiments and for assisting with the production of crDNA-Au-NP aggregates and Fritz Simmel for helpful discussions.

References

[1] B. De la Riva, E. Sanchez, A. Hernandez, R. Reyes, F. Tamimi, E. Lopez-Cabarcos, et al., Local controlled release of VEGF and PDGF from a combined brushite-chitosan system enhances bone regeneration, J. Control. Release 143 (1) (2010) 45–52.
[2] R.F. Diegelmann, M.C. Evans, Wound healing: an overview of acute, fibrotic and delayed healing, Front. Biosci. 9 (2004) 283–289.
[3] A. Hameedaldeen, J. Liu, A. Batres, G.S. Graves, D.T. Graves, FOXO1, TGF-beta regulation and wound healing, Int. J. Mol. Sci. 15 (9) (2014) 16257–16269.
[4] J. Massague, TGF[beta] signalling in context, Nat. Rev. Mol. Cell Biol. 13 (10) (2012) 616–630.

Appendix A.2 Controlled nanoparticle release from a hydrogel by DNA-mediated particle disaggregation

[5] P. Bao, A. Kodra, M. Tomic-Canic, M.S. Golinko, H.P. Ehrlich, H. Brem, The role of vascular endothelial growth factor in wound healing, J. Surg. Res. 153 (2) (2009) 347–358.
[6] N. Ferrara, H.P. Gerber, J. LeCouter, The biology of VEGF and its receptors, Nat. Med. 9 (6) (2003) 669–676.
[7] J.H. Sung, M.R. Hwang, J.O. Kim, J.H. Lee, Y.I. Kim, J.H. Kim, et al., Gel characterisation and in vivo evaluation of minocycline-loaded wound dressing with enhanced wound healing using polyvinyl alcohol and chitosan, Int. J. Pharm. 392 (1–2) (2010) 232–240.
[8] E. Caló, V.V. Khutoryanskiy, Biomedical applications of hydrogels: a review of patents and commercial products, Eur. Polym. J. 65 (2015) 252–267.
[9] H.K. Lau, K.L. Kiick, Opportunities for multicomponent hybrid hydrogels in biomedical applications, Biomacromolecules 16 (1) (2015) 28–42.
[10] B. Singh, S. Sharma, A. Dhiman, Design of antibiotic containing hydrogel wound dressings: biomedical properties and histological study of wound healing, Int. J. Pharm. 457 (1) (2013) 82–91.
[11] S. Enoch, J.E. Grey, K.G. Harding, ABC of wound healing. Non-surgical and drug treatments, BMJ 332 (7546) (2006) 900–903.
[12] C.T. Hess, R.S. Kirsner, Orchestrating wound healing: assessing and preparing the wound bed, Adv. Skin Wound Care 16 (5) (2003) 246–257 (quiz 58-9).
[13] J. Song, X. Yang, O. Jacobson, L. Lin, P. Huang, G. Niu, et al., Sequential drug release and enhanced photothermal and photoacoustic effect of hybrid reduced graphene oxide-loaded ultrasmall gold nanorod vesicles for cancer therapy, ACS Nano 9 (9) (2015) 9199–9209.
[14] S.P. Hudson, R. Langer, G.R. Fink, D.S. Kohane, Injectable in situ cross-linking hydrogels for local antifungal therapy, Biomaterials 31 (6) (2010) 1444–1452.
[15] A. Hasan, A. Khattab, M.A. Islam, K.A. Hweij, J. Zeitouny, R. Waters, et al., Injectable hydrogels for cardiac tissue repair after myocardial infarction, Adv. Sci. 2 (11) (2015) (n/a-n/a).
[16] V.P. Chauhan, J.D. Martin, H. Liu, D.A. Lacorre, S.R. Jain, S.V. Kozin, et al., Angiotensin inhibition enhances drug delivery and potentiates chemotherapy by decompressing tumour blood vessels, Nat. Commun. 4 (2013) 2516.
[17] W. Xu, R. Thapa, D. Liu, T. Nissinen, S. Granroth, A. Narvanen, et al., Smart porous silicon nanoparticles with polymeric coatings for sequential combination therapy, Mol. Pharm. 12 (11) (2015) 4038–4047.
[18] D. Miles, G. von Minckwitz, A.D. Seidman, Combination versus sequential single-agent therapy in metastatic breast cancer, Oncologist 7 (Suppl. 6) (2002) 13–19.
[19] H. Kamata, X. Li, U.I. Chung, T. Sakai, Design of Hydrogels for biomedical applications, Adv. Healthc. Mater. 4 (16) (2015) 2360–2374.
[20] T.R. Hoare, D.S. Kohane, Hydrogels in drug delivery: progress and challenges, Polymer 49 (8) (2008) 1993–2007.
[21] A. Paavola, J. Yliruusi, Y. Kajimoto, E. Kalso, T. Wahlstrom, P. Rosenberg, Controlled release of lidocaine from injectable gels and efficacy in rat sciatic nerve block, Pharm. Res. 12 (12) (1995) 1997–2002.
[22] G. Bayramoglu, D. Gozen, G. Ersoy, V.C. Ozalp, K.C. Akcali, M.Y. Arica, Examination of fabrication conditions of acrylate-based hydrogel formulations for doxorubicin release and efficacy test for hepatocellular carcinoma cell, J. Biomater. Sci. Polym. Ed. 25 (7) (2014) 657–678.
[23] M. Barzegar-Jalali, K. Adibkia, H. Valizadeh, M.R. Shadbad, A. Nokhodchi, Y. Omidi, et al., Kinetic analysis of drug release from nanoparticles, J. Pharm. Pharm. Sci. 11 (1) (2008) 167–177.
[24] A.R. Mohammed, N. Weston, A.G. Coombes, M. Fitzgerald, Y. Perrie, Liposome formulation of poorly water soluble drugs: optimisation of drug loading and ESEM analysis of stability, Int. J. Pharm. 285 (1–2) (2004) 23–34.
[25] G. Ahuja, K. Pathak, Porous carriers for controlled/modulated drug delivery, Indian J. Pharm. Sci. 71 (6) (2009) 599–607.
[26] M. Kawashita, Y. Tanaka, S. Ueno, G. Liu, Z. Li, T. Miyazaki, In vitro apatite formation and drug loading/release of porous TiO2 microspheres prepared by sol-gel processing with different SiO2 nanoparticle contents, Mater. Sci. Eng. C Mater. Biol. Appl. 50 (2015) 317–323.
[27] T. Wang, H. Jiang, L. Wan, Q. Zhao, T. Jiang, B. Wang, et al., Potential application of functional porous TiO2 nanoparticles in light-controlled drug release and targeted drug delivery, Acta Biomater. 13 (2015) 354–363.
[28] C. Bharti, U. Nagaich, A.K. Pal, N. Gulati, Mesoporous silica nanoparticles in target drug delivery system: a review, Int. J. Pharm. Investig. 5 (3) (2015) 124–133.
[29] Z. Yufang, Mesoporous silica nanoparticles with a core-shell structure for drug delivery, J. Bioanal. Biomed. 5 (3) (2013).
[30] E. Ahmadi, N. Dehghannejad, S. Hashemikia, M. Ghasemnejad, H. Tabebordbar, Synthesis and surface modification of mesoporous silica nanoparticles and its application as carriers for sustained drug delivery, Drug Deliv. 21 (3) (2014) 164–172.
[31] S.K. Natarajan, S. Selvaraj, Mesoporous silica nanoparticles: importance of surface modifications and its role in drug delivery, RSC Adv. 4 (28) (2014) 14328–14334.
[32] M. Caldorera-Moore, N. Guimard, L. Shi, K. Roy, Designer nanoparticles: incorporating size, shape and triggered release into nanoscale drug carriers, Expert Opin. Drug Deliv. 7 (4) (2010) 479–495.
[33] J.J. Wang, Z.W. Zeng, R.Z. Xiao, T. Xie, G.L. Zhou, X.R. Zhan, et al., Recent advances of chitosan nanoparticles as drug carriers, Int. J. Nanomedicine 6 (2011) 765–774.
[34] M. Prabaharan, Chitosan-based nanoparticles for tumor-targeted drug delivery, Int. J. Biol. Macromol. 72 (2015) 1313–1322.
[35] I. Wasiak, A. Kulikowska, M. Janczewska, M. Michalak, I.A. Cymerman, A. Nagalski, et al., Dextran nanoparticle synthesis and properties, PLoS One 11 (1) (2016), e0146237.
[36] T. Thambi, D.G. You, H.S. Han, V.G. Deepagan, S.M. Jeon, Y.D. Suh, et al., Bioreducible carboxymethyl dextran nanoparticles for tumor-targeted drug delivery, Adv. Healthc. Mater. 3 (11) (2014) 1829–1838.
[37] J. Ge, E. Neofytou, J. Lei, R.E. Beygui, R.N. Zare, Protein-polymer hybrid nanoparticles for drug delivery, Small 8 (23) (2012) 3573–3578.
[38] M. Rafat, D. Mondal, M. Islam, B. Liedberg, M. Griffith, Nanoparticles incorporated collagen hydrogels for sustained release of EGF, Acta Ophthalmol. 91 (2013) 0.
[39] J. Zhu, R.E. Marchant, Design properties of hydrogel tissue-engineering scaffolds, Expert Rev. Med. Devices 8 (5) (2011) 607–626.
[40] H. Zou, W. Guo, W.Z. Yuan, Supramolecular hydrogels from inclusion complexation of alpha-cyclodextrin with densely grafted chains in micelles for controlled drug and protein release, J. Mater. Chem. B 1 (45) (2013) 6235–6244.
[41] Z.J. Liu, P. Yao, Versatile injectable supramolecular hydrogels containing drug loaded micelles for delivery of various drugs, Polym. Chem. 5 (3) (2014) 1072–1081.
[42] I. Saaem, T.H. LaBean, Overview of DNA origami for molecular self-assembly, Wiley Interdiscip. Rev. Nanomed. Nanobiotechnol. 5 (2) (2013) 150–162.
[43] L.Y. Chou, K. Zagorovsky, W.C. Chan, DNA assembly of nanoparticle superstructures for controlled biological delivery and elimination, Nat. Nanotechnol. 9 (2) (2014) 148–155.
[44] S. Ohta, D. Glancy, W.C. Chan, DNA-controlled dynamic colloidal nanoparticle systems for mediating cellular interaction, Science 351 (6275) (2016) 841–845.
[45] R. Owczarzy, A.V. Tataurov, Y. Wu, J.A. Manthey, K.A. McQuisten, H.G. Almabrazi, et al., IDT SciTools: a suite for analysis and design of nucleic acid oligomers, Nucleic Acids Res. 36 (2008) (W163-W9).
[46] J.N. Zadeh, C.D. Steenberg, J.S. Bois, B.R. Wolfe, M.B. Pierce, A.R. Khan, et al., NUPACK: analysis and design of nucleic acid systems, J. Comput. Chem. 32 (1) (2011) 170–173.
[47] T.A. Taton, Preparation of gold nanoparticle-DNA conjugates, Curr. Protoc. Nucleic Acid Chem. (2002) (Chapter 12:Unit 12 2).
[48] L.M. Demers, C.A. Mirkin, R.C. Mucic, R.A. Reynolds 3rd, R.L. Letsinger, R. Elghanian, et al., A fluorescence-based method for determining the surface coverage and hybridization efficiency of thiol-capped oligonucleotides bound to gold thin films and nanoparticles, Anal. Chem. 72 (22) (2000) 5535–5541.
[49] N. Janaky, X. Jun-Ying, L. Xiang-Yang, Determination of agarose gel pore size: absorbance measurements vis a vis other techniques, J. Phys. Conf. Ser. 28 (1) (2006) 83.
[50] E.C. Dreaden, L.A. Austin, M.A. Mackey, M.A. El-Sayed, Size matters: gold nanoparticles in targeted cancer drug delivery, Ther. Deliv. 3 (4) (2012) 457–478.
[51] C. Nowald, A. Penk, H.Y. Chiu, T. Bein, D. Huster, O. Lieleg, A selective mucin/methylcellulose hybrid gel with tailored mechanical properties, Macromol. Biosci. (2016).
[52] A. Akbarzadeh, R. Rezaei-Sadabady, S. Davaran, S.W. Joo, N. Zarghami, Y. Hanifehpour, et al., Liposome: classification, preparation, and applications, Nanoscale Res. Lett. 8 (1) (2013) 102.
[53] J.O. Eloy, M. Claro de Souza, R. Petrilli, J.P. Barcellos, R.J. Lee, J.M. Marchetti, Liposomes as carriers of hydrophilic small molecule drugs: strategies to enhance encapsulation and delivery, Colloids Surf. B: Biointerfaces 123 (2014) 345–363.
[54] O.G. Mouritsen, K. Jorgensen, Micro-, nano- and meso-scale heterogeneity of lipid bilayers and its influence on macroscopic membrane properties, Mol. Membr. Biol. 12 (1) (1995) 15–20.
[55] V. Saxena, C. Gacchina Johnson, A.H. Negussie, K.V. Sharma, M.R. Dreher, B.J. Wood, Temperature-sensitive liposome-mediated delivery of thrombolytic agents, Int. J. Hyperth. 31 (1) (2015) 67–73.
[56] M. Ueno, S. Yoshida, I. Horikoshi, Characteristics of the membrane permeability of temperature-sensitive liposome, Bull. Chem. Soc. Jpn. 64 (5) (1991) 1588–1593.
[57] R.P. Richter, J.L.K. Him, A. Brisson, Supported lipid membranes, Mater. Today 6 (11) (2003) 32–37.
[58] M.-R. Toh, G.N.C. Chiu, Liposomes as sterile preparations and limitations of sterilisation techniques in liposomal manufacturing, Asian J. Pharm. Sci. 8 (2) (2013) 88–95.
[59] F. Arends, R. Baumgartel, O. Lieleg, Ion-specific effects modulate the diffusive mobility of colloids in an extracellular matrix gel, Langmuir 29 (51) (2013) 15965–15973.
[60] C.L. Zavaleta, B.R. Smith, I. Walton, W. Doering, G. Davis, B. Shojaei, et al., Multiplexed imaging of surface enhanced Raman scattering nanotags in living mice using noninvasive Raman spectroscopy, Proc. Natl. Acad. Sci. U. S. A. 106 (32) (2009) 13511–13516.
[61] E.C. Dreaden, S.C. Mwakwari, Q.H. Sodji, A.K. Oyelere, M.A. El-Sayed, Tamoxifen-poly(ethylene glycol)-thiol gold nanoparticle conjugates: enhanced potency and selective delivery for breast cancer treatment, Bioconjug. Chem. 20 (12) (2009) 2247–2253.
[62] S. Dhar, W.L. Daniel, D.A. Giljohann, C.A. Mirkin, S.J. Lippard, Polyvalent oligonucleotide gold nanoparticle conjugates as delivery vehicles for platinum(IV) warheads, J. Am. Chem. Soc. 131 (2009) 14652 (2010;132(48):17335).
[63] D.A. Giljohann, D.S. Seferos, A.E. Prigodich, P.C. Patel, C.A. Mirkin, Gene regulation with polyvalent siRNA-nanoparticle conjugates, J. Am. Chem. Soc. 131 (6) (2009) 2072.
[64] E. Nagamachi, Y. Hirai, K. Tomochika, Y. Kanemasa, Studies on osmotic stability of liposomes prepared with bacterial membrane lipids by carboxyfluorescein release, Microbiol. Immunol. 36 (3) (1992) 231–234.

A.3 Macromolecular coating enables tunable selectivity in a porous PDMS matrix

Macromolecular Bioscience (accepted version, accepted on 2017/11/17)

DOI: 10.1002/mabi.201700311

Macromolecular coating enables tunable selectivity in a porous PDMS matrix

Benjamin Winkeljann [1*], *Benjamin T. Käsdorf* [1*], *Job Boekhoven* [2], *and Oliver Lieleg* [1#]

[1]Department of Mechanical Engineering and Munich School of Bioengineering,
Technical University of Munich,
Boltzmannstraße 11, 85748 Garching, Germany

[2]Department of Chemistry and Institute for Advanced Study, Technical University of Munich, Lichtenbergstraße 4, 85748, Garching, Germany

[*] Both authors contributed equally to the work

[#] Corresponding author:

Prof. Dr. Oliver Lieleg
Department of Mechanical Engineering and Munich School of Bioengineering,
Technical University of Munich,
Boltzmannstraße 11, 85748 Garching, Germany
e-mail: oliver.lieleg@TUM.de

Keywords

Biomacromolecules, Separation, PDMS, Mucin

Abstract

Whether for laboratory use or clinical practice, many fields in Life Sciences require selective filtering. However, most existing filter systems lack the ability to easily tune their filtration behavior. Two key elements for efficient filtering are a high surface-to-volume ratio and the presence of suitable chemical groups which establish selectivity. We here present an artificial PDMS-based capillary system with highly tunable selectivity properties. The high surface-to-volume ratio of this filter system is generated by first embedding sugar fibers into a synthetic polymer matrix and then dissolving these fibers from the cured polymer. To functionalize this filter, the inner surface of the capillaries is coated with purified or synthetic macromolecules. Depending on the type of macromolecule used for filter functionalization, we observe selective sieving based on steric hindrance, electrostatic binding, electrostatic repulsion, or specific binding interactions. Furthermore, we demonstrate that enzymes can be immobilized in the capillary system which allows for performing multiple cycles of enzymatic reactions with the same batch of enzymes and without the need to separate the enzymes from their reaction products. In addition to lab-scale filtration and enzyme immobilization applications demonstrated here, the functionalized porous PDMS matrix may also be used to test binding interactions between different molecules.

Appendix A.3 Macromolecular coating enables tunable selectivity in a porous PDMS matrix

1. Introduction

Selective permeability and filtration is an essential feature of many biological processes, and technical filtration applications often make use of procedures which imitate biological strategies. For instance, the renal filtration mechanism of the human kidney is mimicked in cross-flow filtration and in purification processes for drinking water (1).

Although there are several technical solutions for achieving selective filtration, these methods are often designed to sieve according to a certain parameter set and thus lack flexibility. Chromatographic methods, for example, provide the basis for a broad variety of filtration approaches (2). However, a chromatography column designed for size exclusion filtration cannot filter molecules by means of affinity (which is implemented in, e.g., ion exchange chromatography) as those techniques are based on different filtration mechanisms. Moreover, chromatographic filtration approaches typically require specific resins and thus can be cost-intensive (3). Especially in lab-scale settings, where the need for versatile filtration and purification methods arises as research progresses, classical filtration options may not always be sufficient. Novel approaches to selectively sieve proteins (by shape or size) based on mesoporous structures (4-6) or to remove heavy metal ions from aqueous solutions (7, 8) have been introduced in the last years; however, the flexibility of those novel methods is limited.

Over the last years, several studies have analyzed the selective filtration properties of biological hydrogels (9-14). Many of these protein/polymer based structures have a protective function in the human body as they pose a barrier towards a variety of pathogens but allow for the passage of nutrients or other beneficial molecules (15). However, owing to the high water content of these biological filters, they are very soft. Thus, harnessing the natural and versatile filtration abilities of such hydrogel macromolecules for technical applications is difficult and, e.g., requires the immobilization of macromolecules on a solid surface.

A porous PDMS matrix offers a suitable platform for such an adaptable solid immobilization system, as it can be functionalized with a high number of molecules (16-19) which then can provide the desired selectivity properties. Additionally, a porous PDMS-based filtration system can be fabricated at low cost and can serve as a matrix providing a high surface-to-volume ratio, a feature which is essential for an efficient small-scale filtration process. However, commonly used porogens such as sugar, salt or air bubbles tend to give rise to insufficiently interconnected pores – unless they are added in very high concentrations (20). As a consequence, the major part of the generated pores often constitute dead ends, and unleached porogens remain in the structure (21) which decreases the filtration efficiency. A comparably easy way of fabricating a well-interconnected porous PDMS system was presented by Bellan *et al.* (22) which is based on washing out embedded sugar fibers from a PDMS cube thus generating a PDMS structure containing a well-connected capillary system.

Here, we introduce an optimization of this fabrication process and produce reproducible low-cost filtration devices with well-defined capillary diameters, total filtration volume and flow resistance. By coating the inner surface of the capillaries with either bio(macro)molecules such as mucins or polylysine, synthetic molecules (6-aminohexanoic acid and polyethylenimine), or fibers self-assembled from artificial peptide amphiphiles, we are able to achieve various filtration profiles with the identical porous PDMS matrix. Depending on the macromolecule used for coating, we obtain a filtration device that selectively removes either positively or negatively charged liposome particles from a test solution – or both. Further variation of the macromolecules used for filter coating enables filtration not only according to charge, but also size-dependent sieving and filtering by means of specific binding to chemical motifs. In addition to the selective removal of particles, our highly versatile system can also be used to immobilize enzymes and to study the binding of test molecules to immobilized (bio)macromolecules.

2. Experimental section

Production of the filter

The capillary system was created by modifying a protocol described in Bellan et al. (22). PDMS (Sylgard 184 Silicone Elastomer, Dow Corning, Midland MI, USA) prepolymer and cross-linker were mixed in a 10:1 ratio. Air bubbles were removed from the mixture by applying a vacuum for a minimum of 30 min. An aluminum cavity with dimensions of 35 mm x 35 mm was filled with 4 g of mixed PDMS to generate a continuous bottom layer and cured at 80 °C for 60 min. Sacrificial sugar structures were produced using a modified cotton candy machine (ZVM 3478, Clatronic International GmbH, Kempen, Germany), and 600 mg of these fibers were added into a second aluminum mold with smaller dimensions (i.e. 20 mm x 20 mm) to a height of ~8 mm and covered with 4 g of mixed PDMS. Again, vacuum was applied to remove air bubbles before curing this PDMS/cotton candy composite.

The cured PDMS/sugar block was then placed into the center of the larger aluminum mold, i.e. on top of the previously generated PDMS layer and, fixed with two copper wires (d = 1.5 mm) with a length of 10 mm each. The cavity around this PDMS/sugar block was filled with PDMS and cured once more. The copper wires were removed, and the remaining two channels were extended to reach all the way through the PDSM/sugar block by using a 1.3 mm HSS spiral drill to create an in- and an outlet. The whole PDMS/sugar block was then placed into hot water (70 °C) for several days to dissolve the sugar fibers.

Finally, two brass tubes with an outer diameter of 2 mm were placed into the drilled in- and outlet to enable a connection of the porous PDMS structure to tubings (cross-linked silicone peroxide, inner diameter = 1 mm, outer diameter = 3 mm, VWR, Darmstadt, Germany).

The amount of cotton candy used in our protocol represents a compromise between obtaining a high surface area, good capillary interconnectivity and maintaining an easy handling during the filter production process.

Filter characterization

The total volume of the filters was calculated by measuring the difference in weight between water filled and dried filters. The average diameter and the density of the capillaries were determined from profilometric images of sliced filters acquired on a µsurf light profilometer (Nanofokus

AG, Oberhausen, Germany) using a lens with 50x magnification and a NA = 0.8 (UMPlanFl 50x/0.80, Olympus Deutschland GmbH, Hamburg, Germany). To characterize the flow resistance of the filters, the pressure right before the inlet was measured at a constant flowrate of 1 mL/min. The measured pressure loss is directly linked to the flow resistance of the capillary system. For more detailed information see Supplemental Information.

Filter functionalization

Three different biological polymers were used to coat the inner surface of the filter: manually purified porcine gastric mucin (MUC5AC, the purification process of these mucins was conducted as described in Schömig et al. (23)), commercially purified porcine gastric mucin (M2378, Sigma-Aldrich, Schnelldorf, Germany) and poly-L-lysine (P8920, Sigma-Aldrich). Each macromolecule was dissolved in PBS (pH 7.3, DPBS, Lonza, Verviers, Belgium) at a concentration of 0.1 % (w/v). The filter was then filled with one of those solutions and incubated at room temperature for 90 min (in case of mucins) or for 180 min (in case of poly-L-lysine), respectively. After this incubation step, the capillaries were rinsed with 2 mL of PBS.

Peptide synthesis and purification was performed as described in Tantakitti et al. (24). To generate peptide amphiphile fibers, purified peptides were diluted in ultrapure water. Depending on the concentration used, the generated fibers are shorter (l ~200 nm, c = 0.01 % (w/v)) or longer (l >1 µm, c = 0.5 % (w/v)), respectively. The solution was heated to 80 °C and kept at this temperature for 20 min. For the generation of short fibers, the solution was sonicated during this incubation step in an ultrasonic bath, for longer fibers, sonication was omitted. Afterwards, the solution was cooled down to room temperature at a cooling rate of ~1 °C/min. To functionalize the filter, the solution containing long PA fibers was further diluted 1:8 in distilled water to avoid clogging of the filtration device during incubation. For the short fibers, no further dilution was necessary. The filter was filled with the PA fiber solution and incubated at room temperature for 90 min and then rinsed with PBS. To block uncoated areas on the PDMS surface, the filter was incubated afterwards with a BSA solution (0.5 % (w/v) in PBS) for 20 min and finally rinsed with PBS again.

To functionalize the filter with artificial molecules, the capillaries were coated with dopamine first. 4 mL of dopamine solution (0.2 % (w/v) in 10 mM TRIS buffer, pH 8.5) were pumped through the filter at a flow rate of 1 mL/min to generate a dopamine surface coating and flushed afterwards with 2 mL TRIS buffer. The pre-coated filter was then filled with either 6-aminohexanionicacid or polyethylenimine (0.1 % (w/v) or 10.0 % (w/v), respectively, both in TRIS buffer) and for probing specific filtering with streptavidin/biotin with amine-PEG-biotin (2.3 kDa) or bis-amine-PEG (1.5 kDa) (both dissolved 0.2 % (w/v) in TRIS buffer). The incubation period was 90 min and afterwards the filter was rinsed with 2 mL of PBS. All substances mentioned above were obtained from Sigma Aldrich.

Liposome preparation

For the filtration tests, liposomes were produced by lipid film hydration from five different lipids: 1,2-dioleoyl-sn-glycero-3-phosphocholine (DOPC), 1,2-dioleoyl-3-trimethyl-ammonium-propane (DOTAP), 1,2-dioleoyl-sn-glycero-3-(phospho-rac-(1-glycerol)) (DOPG) or 1,2-dioeloyl-sn-glycero-3-Phosphoethanolamine-N-(biotinyl) (Biotin-PE), and fluorescently labeled with 1,2-dioleoyl-sn-glycero-3-phosphoethanolamine-N-(lissamine rhodamine B sulfonyl) (Rh-DOPE). All lipids were obtained from Avanti Polar Lipids (Alabaster, AL, USA) and dissolved in chloroform. Lipids were mixed to a concentration of 0.5 mM (~$1.2*10^{12}$ liposomes/mL) and each mixture contained 5 mol% Rh-DOPE as a fluorescence label. For preparing zwitterionic ("neutral") DOPC liposomes, 90 mol% of DOPC and 5 mol% DOTAP were mixed to compensate for the negative charge introduced by the 5 mol% Rh-DOPE. For simplicity, those DOPC/DOTAP/Rh-DOPE liposomes are referred to as DOPC liposomes in the main article. For the preparation of biotinylated liposomes, the composition of the DOPC liposomes was modified by replacing 1 mol% of DOPC by Biotin-PE. Solvent evaporation was conducted overnight to generate a thin lipid film. This lipid film was resuspended in 500 µL PBS and mixed thoroughly. The suspension was then sonicated in an ultrasonic bath for 10 min to produce small unilamellar vesicles followed by extrusion through a 0.2, 0.4 or 1.0 µm polycarbonate membrane using a mini extruder (Avanti Polar Lipids) and stored at 4 °C until further use.

To coat liposomes with streptavidin, the biotinylated liposomes were diluted to a concentration of ~0.09 mM in PBS containing 2.5 mg/mL streptavidin (S4762, Sigma-Aldrich). The mixture was incubated at 4 °C on a shaker for 60 minutes. Afterwards, unbound streptavidin was removed from the liposome solution using size exclusion chromatography (PCR Kleen Purification Spin Columns, Bio-Rad). Prior to their use in filtration experiments, the streptavidin coated liposomes were extruded again to break up aggregates that might have formed during the functionalization process.

Characterizing the filtration behavior of functionalized filters

For testing the selective properties of the filters with liposomes, the liposome stock solutions were diluted to a concentration of ~$1.2*10^{9}$ liposomes/mL in PBS and 4 mL were flushed through the filter at a flow rate of 1 mL/min using a syringe pump. The first mL of a solution, which had passed the filter, was discarded. Then, three drops of filtrate were collected at three time intervals of 1 min each. The difference in liposome quantity before and after flushing through the filter was determined by counting using the 'Find Maxima' command implemented into the analysis tool ImageJ (version 1.49v). For this counting procedure, 1.5 µL of each sample were filled into a Thoma Cell Counting Chamber (Poly-Optik GmbH, Bad Blankenburg, Germany). Fluorescence images were acquired on a Axioskop 2 Mat mot microscopic (Zeiss, Oberkochen, Germany) using a 50x lens (EC Epiplan-Neofluar 50x/0.8 HD DIC M27, Zeiss, Oberkochen, Germany). Each filter was tested with three sets of liposome solutions: DOPG, DOPC and DOTAP. In between each filtration test, the capillary system was rinsed with 2 mL PBS. Control experiments showed that the filtration efficiency did not depend on the order in which the liposomes were flushed through the filter (**Figure S5e**).

For testing the selective properties of the filters with fluorescently labeled dextrans, either unmodified FITC-dextrans (Mw = 150 kDa, ordered from Sigma Aldrich) or chemically modified FITC-dextrans with carboxymethyl (CM) groups or diethylaminoethyl (DEAE) groups were diluted at a concentration of 10 µg/mL in PBS buffer. 4 mL of this solution were flushed through the filter at a flow rate of 1 mL/min, and filtered solution was collected as described above for liposomes. The fluorescence intensity of the collected solutions was measured using a plate reader (VICTOR X3 Multilabel Plate Reader, Perkin-Elmer, Waltham, MA, USA) at an excitation wavelength of $\lambda_{485\,nm}$ and emission wavelength of $\lambda_{535\,nm}$.

Enzymatic catalysis by immobilized horseradish peroxidase (HRP)

Horseradish peroxidase (HRP) was obtained from Sigma Aldrich. For coating the inner capillary surface, 100 µg HRP were dissolved in 1 mL ultrapure water. The enzyme solution was injected into the filter and incubated for 30 minutes. Afterwards, the filter was rinsed with 5 mL ultrapure water to remove excess HRP. To measure enzymatic activity, the substrate ADHP (10-acetyl-3,7-dihydroxyphenoxazine) from a commercial kit (QuantaRed™ Enhanced Chemifluorescent HRP Substrate Kit, Thermo Fisher, MA, USA) was used. The substrate solution was freshly prepared by adding ADHP to a mix of buffer and enhancer solution as provided by the commercial kit and pumped through the filter at a flow rate of 1 mL/min. Successful conversion of the substrate was indicated by the solution acquiring a pink color. The converted substrate solution was collected at the filter outlet and the change in color was quantified spectrophotometrically in a 96-well plate with a Victor^3 plate reader (PerkinElmer, MA, USA) at an excitation wavelength of $\lambda_{570\,nm}$ and an emission wavelength of $\lambda_{642\,nm}$.

For assessing the stability of the physisorbed HRP, the coated capillary system was rinsed with up to 500 mL of ultrapure water. At distinct time points of this rinsing procedure, 1 mL of substrate was injected to test for enzymatic activity. For testing the influence of filter storage, HRP coated filter systems were either filled with PBS, covered in Parafilm and incubated at room temperature for 48 hours or dried and incubated at room temperature for 72 h. Afterwards, the enzyme activity was determined as described above.

3. Results and Discussion

For a quantitative comparison of the filtering efficiency of different macromolecular coatings, it is crucial to fabricate filtration units with consistent characteristics. To evaluate the filtration performance of uncoated porous PDMS constructs, we measure a set of structural parameters for a minimum of three independent filter realizations. Indeed, we are able to generate capillary PDMS structures with which we obtain reproducible structural characteristics such as average capillary diameter or density, and total volume of the capillary system (**Figure 1**). We also measure the net flow resistance of the capillary system and find that this value agrees well with a corresponding estimate based on the structural parameters (see Supplemental Information).

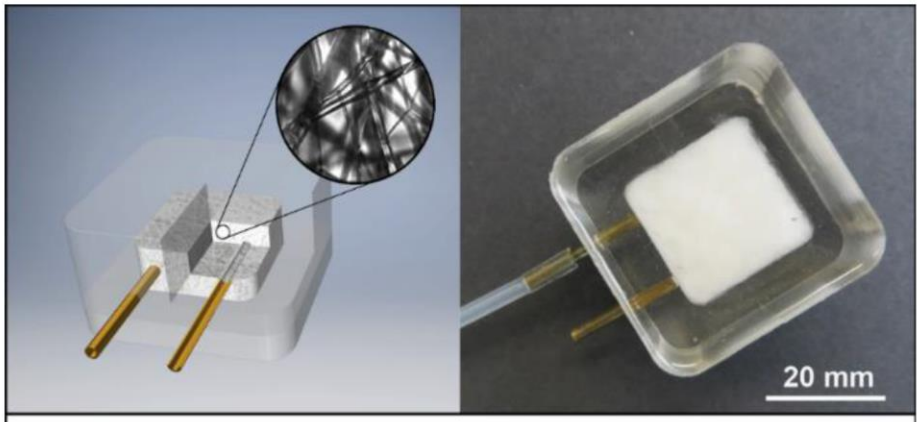

Average capillary diameter	d	=	8.26 µm (± 3.84 µm)
Capillary density	n	=	595 mm^{-2} (± 58 mm^{-2})
Volume	V	=	133 mm^3 (± 24 mm^3)
Flow velocity in capillaries	v	=	5.2 mms^{-1} *
Reynolds Number	Re	=	0.04*
Flow resistance	Δp	=	365 mbar (± 52 mbar)*

*Flow rate Q = 1.0 mLmin^{-1}

Figure 1: **Schematic representation (left) and photograph (right) of the capillary filtration system.** Brass tubes serve as in- and outlets into the capillary system, which was generated by leaching out sacrificial sugar structures from the PDMS cube. The production process established here allows for generating filtration devices with reproducible properties as depicted in the table below the pictures.

To provide this capillary structure with selective filtering abilities, we coat the capillary surfaces with suitable macromolecules. Several studies have already demonstrated the selective permeability properties of mucus, a biopolymer layer which constitutes the first line of defense against pathogens in the human body (14, 25-27). As mucin glycoproteins are the key molecules responsible for the selectivity of those mucus gels, we first test a coating with purified porcine gastric mucins (PGM). Mucins strongly adhere to hydrophobic materials such as PDMS (28-30); thus, performing a mucin coating by physisorption should be sufficient. In the central part of the molecule, the mucin glycoprotein comprises densely glycosylated regions, and several carbohydrates found in this region (such as sialic acid or sulfated sugar residues) possess a strongly anionic character (31). Consistently, mucins have been previously reported to bind cationic particles and molecules (32-36), and we expect that a mucin coating will allow our filter to selectively remove cationic particles or molecules by electrostatic forces.

Liposomes are a suitable platform for probing various filter functionalizations as the size and net charge of these particles can be easily and independently tuned, i.e. via extrusion and adjusting the lipid composition. Another advantage of this particle system is that fluorescently labeled lipids (for visualization) as well as lipids carrying specific binding motifs can be incorporated at tunable concentrations. Moreover, liposomes are highly relevant particles in the field of drug delivery. Thus, characterizing the binding interaction of liposomes with immobilized mucins or other biomacromolecules present in physiological diffusion barriers (15, 37) might provide helpful insights for the development of efficient drug carriers.

To test the interaction of immobilized mucins with such liposome test particles we pump equal amounts of different liposome solutions (i.e. negatively charged, zwitterionic/neutral, and positively charged liposomes - see Method section) through the mucin-functionalized filter and determine the percentage of particles that were able to successfully pass the filter. As depicted in **Figure 2a,** the mucin-coated capillary system allows anionic as well as zwitterionic liposomes to pass with high efficiency but retains a high fraction of the cationic particles: only ~15 % of DOTAP liposomes reach the outlet. The virtually identical result is obtained when three variants of fluorescent dextrans are used to determine the filtration profile (**Figure S2**): Although those macromolecules have hydrodynamic radii in the range of 8-9 nm and are thus ~20x smaller than the liposome particles, also here only the positively charged species (i.e. DEAE-functionalized dextrans) is removed. This result, an 'electrostatic low pass', is consistent with our expectation and demonstrates that physisorption of the mucins to the PDMS is indeed a sufficient functionalization method. Moreover, it shows that the glycan-motifs on the mucin glycoprotein are indeed major players in establishing selective permeability. This selectivity of the mucin coated filter is maintained for up to ~200 filtration cycles which corresponds to a total number of ~10^{11} filtered DOTAP liposomes (**Figure S3a**). This shows that indeed a large amount of mucin molecules is immobilized on the capillary surface. However, such a saturated mucin-coated filtration device can be regenerated by flushing the capillaries with a concentrated salt solution. After such a rinsing step, the filtration device performs equally well as a freshly produced filter (**Figure S3b**). Furthermore, the capillary coating via mucin physisorption is stable enough to maintain a constant filtration behavior of liposomes even after a volume of 50 mL PBS is flushed through the filtration device (**Figure S8a**). This agrees with our observation that mucin leeching only occurs during the initial phase of this rinsing step – indicating that only weakly adsorbed mucins are removed by this rinsing (**Figure S8b**).

Of course, liposomes are fragile particles, thus they might also be removed from the filtration solution by mechanical shear forces. However, this seems not to be the case: when we inspect the capillary system after a filtration test with cationic liposomes, we find mostly intact liposome particles, which decorate the inner surface of the PDMS filter (**Figure S4**).

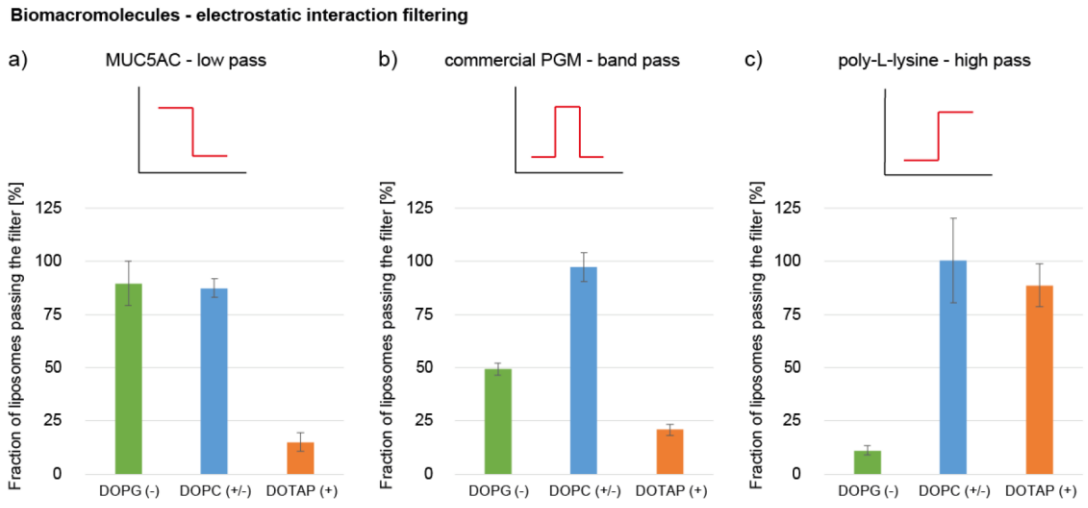

Figure 2: **Different macromolecular coatings of the PDMS-based capillary system lead to different selectivity profiles.** Depending on the molecule used for coating, the filter removes either (a) positively charged particles (electrostatic "low pass"), (b) particles of either charge (electrostatic "band pass") or (c) negatively charged particles (electrostatic "high pass"). Error bars denote the standard error of the mean as obtained from 3 different filter realizations.

Appendix A.3 Macromolecular coating enables tunable selectivity in a porous PDMS matrix

Instead of coating the inner surface of the PDMS capillaries with manually purified mucins, it would be easier to use commercial porcine gastric mucins, which are available in larger amounts. However, those commercial mucins have been reported to possess altered properties compared to their native counterparts (23, 38, 39). It was suggested, that this difference is due to damages in the glycosylation pattern which result from the commercial purification process. If this glycosylation pattern were to be incomplete, then the protein backbone of the commercial mucin glycoprotein would be exposed – and this backbone carries many amino acids, which can be positively (lysine, histidine, and arginine) or negatively (glutamic acid, aspartic acid) charged at neutral pH. Thus, it would be reasonable to expect that coatings performed with those commercial mucins entail a filtration outcome different from that obtained with native mucins. Indeed, as depicted in **Figure 2b,** the PDMS filter system exhibits a 'bandpass'-like filtration behavior when coated with commercial PGM: only the zwitterionic (= neutral, see **Table S1**) liposomes can pass at high efficiency. However, now at least 50 % of cationic liposomes and ~70 % of anionic liposomes are removed. We hypothesize that the incomplete glycosylation of commercial PGMs mentioned before is responsible for this result: in commercial PGMs, the cationic amino acid residues can contribute to the selective trapping of charged particles. As a consequence, anionic liposomes are filtered out – a process that is absent when native mucins are used. To support this idea, a coating with the polycationic polypeptide poly-L-lysine is tested. Based on the results obtained so far, we expect a 'high pass' filter behavior, i.e. the system should selectively filter out anionic particles only. In agreement with this expectation, a poly-L-lysine coated filter removes up to 90 % of the anionic liposomes whereas positive and neutral liposomes can pass the capillary system (**Figure 2c**).

The three biopolymer coatings presented so far gave rise to three different filtration profiles: an electrostatic low pass, band pass and high pass. In a next step, we aim at exploring similar filtration strategies with synthetic macromolecules. Peptide amphiphiles constitute an interesting and versatile system as they can be designed to carry a variety of chemical head groups. Furthermore, they can engage in hydrogen-bonded β-sheets and form self-assembled fibers (24). We here employ C_{16}-$V_3A_3K_3$ peptide amphiphiles (PA) assembled into short fibers (length ~200 nm) as coatings of our capillary system. These PA molecules possess a positively charged head group with three repetitions of the amino acid lysine (**Figure 3a**). Therefore, we expect a similar result as obtained for the poly-L-lysine filter coating. However, now all three liposome species are filtered by the capillary system (**Figure S5a**). As liposomes are labile particles stabilized by hydrophobic interactions, competing hydrophobic interactions with the aliphatic part of the peptide amphiphiles or with partially exposed, uncoated PDMS areas could be responsible for this effect. Such hydrophobic interactions can indeed either lead to adsorption of liposomes to a hydrophobic surface (40, 41) or to disintegration of liposomes and the formation of lipid films (42). This idea agrees with our finding that uncoated PDMS constructs remove all liposome variants with similar efficiency (**Figure S5b**) and that liposomes tend to disintegrate on uncoated PDMS (**Figure S6**). To avoid these competing hydrophobic interactions, we introduce a secondary coating with BSA, a protein which is often employed to prevent unspecific binding events. However, since the isoelectric point of BSA is with 4.7 in the acidic range (43), the overall net charge of the protein is negative at neutral pH. As a consequence, both anionic and cationic liposomes are filtered out with a high efficiency of ~80 % whereas the zwitterionic species passes the filter virtually unhindered (**Figure 3b**).

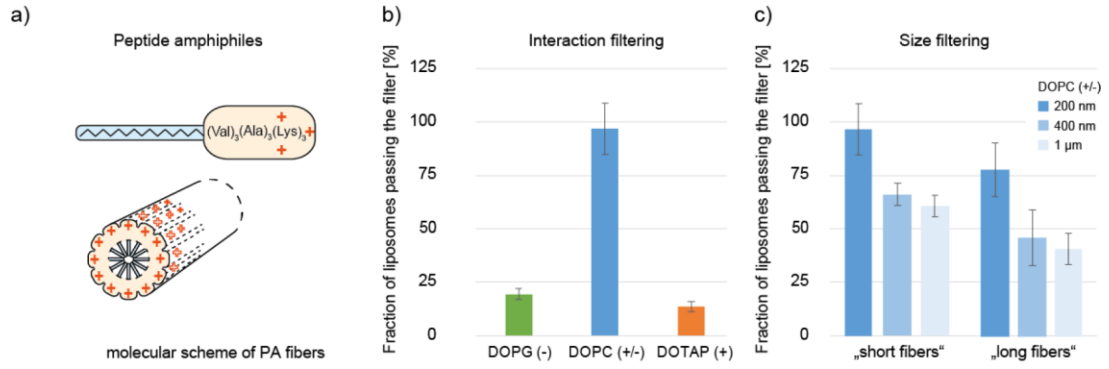

Figure 3: **Surface coating with synthetic peptide amphiphile fibers enables selective filtration.** Synthetic fibers comprising peptide amphiphiles (a) enables the removal of charged liposomes (b) or filtration according to particle size (c). Error bars denote the standard error of the mean as obtained from 3 different filter realizations.

So far, we have demonstrated different approaches of how to enable selective filtration based on binding interactions. In a next step, we ask if we can also achieve size dependent sieving with our system, i.e. if we can find a coating that discriminates between different liposomes smaller than the average capillary diameter. One advantage of the PA system is that, even with a single PA species, different fiber realizations can be created. Depending on the assembly conditions (24), not only short fibers (~200 nm) but also longer fibers with a typical length of several µm can be generated. Since filtration by size does not occur when coating the capillaries with purified mucins (**Figure S5d**), we now utilize short and long PA fibers to install obstacles in the capillaries, and those obstacles should retain larger liposomes by means of steric hindrance. As depicted in **Figure 3c,** such size-dependent sieving can be achieved with either fiber variant. However, different from when the short fibers are used, coating the PDMS capillaries with long PA-fibers also constitutes a slight barrier for zwitterionic 200 nm liposomes. This agrees with the notion that, due to their high length, those fibers can form a network within the capillaries. For the short PA fibers, it is less obvious why

they can affect the passage of zwitterionic liposomes (400 nm and 1 µm). Although these shorter fibers can also generate networks, their average length (200 nm) is rather small in comparison to the capillary diameter (~8 µm). However, since their size distribution is expected to be very broad (24), they might still create networks - albeit with lower densities than the large PA fibers. In either case, i.e., for both short and long PA fibers, hydrophobic interactions between the fiber core and the PDMS surface of the filter microchannels are expected to be responsible for the stability of the PA fiber coating. Such hydrophobic interactions are probably made possible through defects in the fiber structure or by uncovered fiber endcaps – both of which will render the hydrophobic core of the fibers accessible.

In addition to passive physisorption by hydrophobic interactions, PDMS also offers the possibility to covalently link molecules through different coupling reactions (16-19). Yet, the required chemical reactions to generate covalent surface coatings on PDMS can be challenging and involve several consecutive steps. As an alternative, we choose the catecholamine dopamine for PDMS functionalization, a molecule which can form strongly adherent polymer films via self-polymerization on a wide variety of materials including PDMS surfaces (44) (**Figure 4a).** Since dopamine reacts with thiols or amines via Michael addition or Schiff base reaction (45-47), a dopamine coating can serve as a versatile platform for multiple secondary reactions. As a reaction partner to dopamine, we first choose 6-aminohexanoic acid, of which the amine reacts with dopamine; then, the carboxylic group would extend into the volume of a capillary presenting a negative charge. With this macromolecular coating, we are able to remove cationic liposomes from a filtration solution with similar efficiency as with the mucin coating (**Figure 4b**). However, zwitterionic liposomes are filtered out as well. We attribute this result to unspecific interactions between the liposomes and the underlying dopamine layer, which might be accessible for the liposomes – at least in part. This notion is supported by the observation that applying a dopamine coating only (i.e. without performing a secondary coating step) generates a filtration system which removes all three liposome variants with similarly high efficiency (**Figure S5c**). When we combine a dopamine coating with polyethylenimine, a molecule carrying cationic terminal groups, a similar picture emerges (**Figure 4c**): now, both the anionic DOPG liposomes as well as the zwitterionic DOPC liposomes are removed with high efficiency. Together, these results suggest that our dopamine coated filter allows selective passage of particles based on electrostatic repulsion: in both dopamine-based scenarios, only those particles can pass which have the identical net charge as the chemical groups extending into the capillaries. In contrast to the coatings shown in **Figure 2a-c**, zwitterionic liposomes (having a neutral net charge thus lacking electrostatic repulsion forces) seem to be removed by unspecific binding as they get in contact with the underlying dopamine layer. This repulsion-based strategy selectively permits one charged particle species to pass whereas the other two particle types are removed.

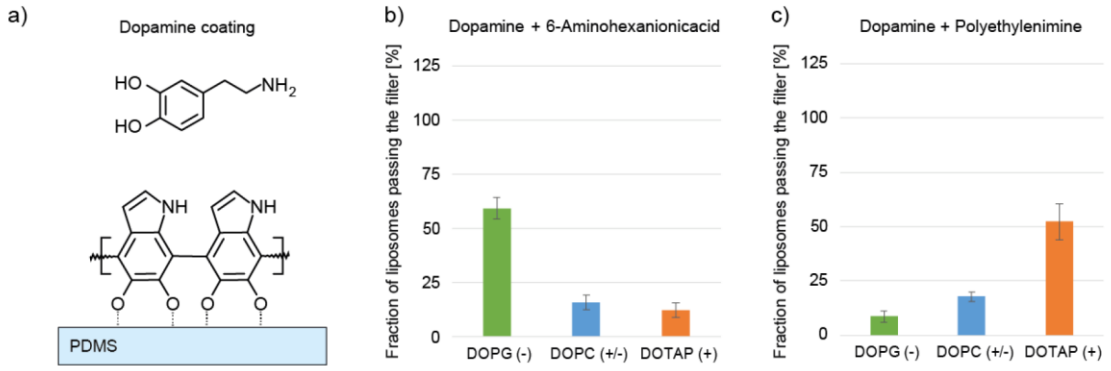

Figure 4: **Dopamine-based secondary coatings allow filtration based on repulsion.** Coating the capillary surface with the catecholamine dopamine (a) creates a basis for secondary reaction partners. Secondary coatings with 6-aminohexanoic acid or polyethylenimine enables repulsion based filtration such that only anionic (b) or cationic liposomes (c), respectively, can pass the filter. Error bars denote the standard error of the mean as obtained from 3 different filter realizations.

So far, we have described how electrostatic and hydrophobic interactions as well as steric hindrance effects can be used to provide the capillary PDMS filter with different selectivity properties. However, all interactions employed so far are rather nonspecific and can occur with numerous chemical motifs. Thus, we next aim at achieving a more precise filtration process by employing specific binding interactions. A well-known and thoroughly investigated specific binding interaction occurs between the vitamin biotin and the protein streptavidin (48). To allow our capillary PDMS construct to selectively filter particles by means of biotin-streptavidin binding, we use streptavidin-coated biotinylated liposomes in combination with a biotin-PEG coating of dopamine pre-coated capillaries (**Figure 5a**, for details see methods). Indeed, when these streptavidin liposomes are pumped through the functionalized filter, we observe a liposome removal efficiency of ~85 %. In contrast, biotinylated liposomes lacking streptavidin can pass this filter (**Figure 5b**). To rule out unspecific binding, we coat the filter with simple PEG (lacking the biotin-terminus). As expected, both liposome species can pass the filter nearly unhindered (**Figure 5c**).

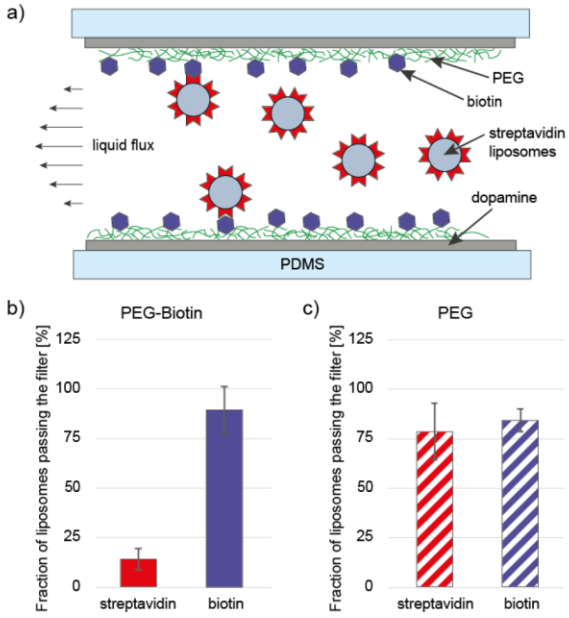

Figure 5: **Specific removal of liposomes by means of biotin-streptavidin binding.** (a) Schematic illustration of a functionalized capillary modified to achieve specific filtering. The capillary is coated in two steps: first, a dopamine pre-coating is applied and afterwards a functionalization with biotinylated PEG is performed. Streptavidin coated biotinylated DOPC-liposomes are filtered out since they can bind to the biotin groups on the functionalized capillary surface (a, b). Biotinylated DOPC-liposomes lacking a streptavidin coat, however, can pass the filter unhindered (b). Both types of liposomes can pass a dopamine-PEG coated system when the biotin functionalization is omitted (c). Error bars denote the standard error of the mean as obtained from 3 different filter realizations.

Up to now, we utilized the porous PDMS system to remove particles/molecules from a solution via specific and unspecific interactions with immobilized macromolecules. In a final step, we aim at utilizing the selective interaction of an immobilized enzyme and its corresponding substrate to enable enzymatic catalysis inside the capillary system.

Performing enzymatic assays can be quite cost-intensive, especially when the enzymes cannot be recovered after the catalysis has been performed. However, immobilizing enzymes on surfaces, e.g. on magnetic or silica nanoparticles (49), offers the possibility to reuse these expensive catalysts several times. PDMS as well can be utilized as a basis for protein and enzyme immobilization via unspecific binding of proteins and molecules to the hydrophobic material (16, 50-52). Here, we employ this immobilization strategy and use our porous PDMS matrix as an immobilization platform. As a model enzyme, we choose horseradish peroxidase (HRP). Using H2O2 as an oxidizing agent, this protein can catalyze an oxidization reaction for several substrates. Whereas the substrate itself does not return a fluorescent signal, the converted substrates then can be detected via spectrophotometric methods. When we coat the inner PDMS surface of our capillary system with HRP via physisorption and pump the substrate ADHP (10-acetyl-3,7-dihydroxyphenoxazine) through the enzyme-coated filter (Figure 6a), we indeed observe efficient substrate conversion (Figure 6b). This indicates that a significant fraction of the immobilized HRPs remained in an active conformation after adsorbing to the PDMS surface, and that enough active sites of the adsorbed enzyme population (HRP possesses only one active site per protein) are accessible for the substrate.

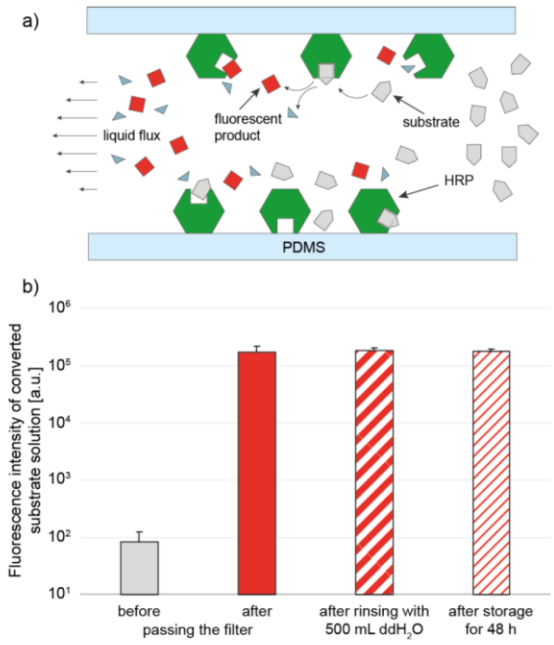

Figure 6: **Immobilization of enzymes onto the PDMS surface of the capillary system allows performing catalytic reactions with the filtration system.** Physisorption of the enzyme HRP leads to the conversion of a substrate which is pumped through the filter (a). The fluorescent intensity of the substrate solution is measured spectrophotometrically before and after passing the filter and indicates enzymatic activity (b). After rinsing the capillary system with 500 mL of ultrapure water, no decrease in the enzymatic activity is observed. Similarly high enzymatic activity is obtained when the HRP coated filter is stored at room temperature for 48 hours prior to use. Error bars denote the standard deviation as obtained from 3 different filter realizations.

Since the enzymes are immobilized onto the PDMS surface by simple physisorption only, it is possible that the enzyme is washed out over time when the substrate solution is pumped through the filter. This might limit the usability of the device and might require a covalent attachment of the enzyme to the capillary surface. However, control experiments indicate otherwise: even when the filter is flushed with a high volume of water, a subsequent injection of a substrate containing solution still returns a constantly high fluorescent signal after passing the filter. After a total rinsing volume of 500 mL (which corresponds to more than 3000 filter volumes), the substrate conversion efficiency is equal to right after enzyme immobilization (**Figure 6b and S7**). Furthermore, storage of a HRP coated filtration system at room temperature for 2 days returns similar catalytic activity: even though continuous rinsing water might induce a loss of enzymes from the porous PDMS sponge, the enzymatic activity of the functionalized PDMS matrix is not perceivably decreased **(Figure 6b)**. Even after drying a HRP-coated filtration system (which was achieved by incubating it at room temperature for 72 h) and subsequently rehydrating it, we did not detect a measurably reduced enzymatic activity (**Figure S7b**). Together, those experiments show that simple physisorption is efficient enough so that the HRP coated filter can be used multiple times suggesting an additional application for this porous PDMS device in addition to the removal of particles from solution. In contrast to the preparation of microfluidic systems for performing or studying enzymatic reactions, the fabrication of our porous PDMS matrix does not require any expensive equipment but only standard devices and a cotton candy machine (**Table S2**).

Conclusions

We here presented a low-cost PDMS-based capillary filtration device with a high surface/volume ratio and well-defined characteristics. The selective properties of this filtration device can be easily tuned by introducing different macromolecular coatings. The large area of the capillary surface allows for filtration of a considerable number of particles before saturation occurs. Depending on the molecules chosen for coating of the capillary surface, filtration by electrostatic binding, electrostatic repulsion, steric hindrance and selective filtering based on specific interactions is possible. As synthetic peptide amphiphiles are highly tunable, i.e. they allow for chemically varying both the head group and the hydrophobic tail, a broad range of filtering strategies may be feasible with this self-assembled fiber system when used as functionalization layer in combination with the capillary filtration device presented here.

Tailored filtration outcomes can also be achieved by pre-coating the capillaries with dopamine, a molecule which allows for a high number of secondary reaction partners. Such a two-step coating process should enable a broad range of filter functionalizations with a variety of molecular species. Furthermore, as described and illustrated above, purified mucins are promising molecular tools for creating a selective barrier (25, 27, 33). Since manually purified PGMs can selectively trap several viruses (14), a specific removal of such viruses from aqueous solutions such as human blood might also be feasible with the presented filtration device. However, in addition to the small capillary diameter, interaction of blood components such as platelets with exposed PDMS (53) may cause clogging of the capillaries. Recent developments of anti-fouling coatings (also dopamine-based) could help circumventing this issue as these coatings drastically reduce the interactions of blood platelets and fibrinogen and PDMS (54).

Alternative applications of this multifunctional device could involve studying the binding interactions of immobilized bio-macromolecules such as mucins with a set of smaller test molecules as well as the immobilization of enzymes, thus providing a low-cost stationary phase for performing enzymatic reactions in a laboratory scale without the need of separating the enzymes from the substrates afterwards.

In conclusion, the numerous surface coatings possible with this PDMS-based capillary filter system in combination with the easy and inexpensive production process should make this device an interesting, self-made alternative to existing lab methods: it allows not only for the selective removal of particles/molecules from solutions but also for performing small-scale enzymatic reactions and determining the binding interaction profiles of macromolecules with test particles/molecules.

Statement of ethics approval

Approval of ethics is not required for the experiments conducted in this manuscript.

Supplementary Material

The supplementary material contains additional information on the properties of the filtration system, characteristics of the liposomes and fluorescence micrographs of a sliced device. Furthermore, different control measurements as well as a brief cost estimation are presented.

Author Contributions

OL, JB, BW and BK planned the experiments. BW and BK performed the experiments and analyzed data. The manuscript was written by BK, OL and BW.

Acknowledgements

This work was supported by the Deutsche Forschungsgemeinschaft through the project B11 in the framework of SFB 863.

References

1. Wah, T. Y. 2016. Nature-inspired membrane set to reduce purification costs. Membrane Technology 2016:7.
2. Issaq, H. J. 2001. A century of separation science. CRC Press.
3. Lundanes, E. 2013. Chromatography : Basic Principles, Sample Preparations and Related Methods.
4. El-Safty, S., and M. A. Shenashen. 2011. Size-selective separations of biological macromolecules on mesocylinder silica arrays. Analytica Chimica Acta 694:151-161.
5. El-Safty, S. A., M. A. Shenashen, M. Ismael, and M. Khairy. 2012. Mesocylindrical Aluminosilica Monolith Biocaptors for Size-Selective Macromolecule Cargos. Advanced Functional Materials 22:3013-3021.
6. Yiu, H. H. P., C. H. Botting, N. P. Botting, and P. A. Wright. 2001. Size selective protein adsorption on thiol-functionalised SBA-15 mesoporous molecular sieve. Physical Chemistry Chemical Physics 3:2983-2985.
7. Hu, J., G. Chen, and I. M. C. Lo. 2006. Selective Removal of Heavy Metals from Industrial Wastewater Using Maghemite Nanoparticle: Performance and Mechanisms. Journal of Environmental Engineering 132:709-715.
8. Sdiri, A., M. Khairy, S. Bouaziz, and S. El-Safty. 2016. A natural clayey adsorbent for selective removal of lead from aqueous solutions. Applied Clay Science 126:89-97.
9. Tsang, K. Y., M. C. H. Cheung, D. Chan, and K. S. E. Cheah. 2009. The developmental roles of the extracellular matrix: beyond structure to regulation. Cell and Tissue Research 339:93.
10. Leong, Y.-Y., and L. Tong. 2015. Barrier Function in the Ocular Surface: From Conventional Paradigms to New Opportunities. The Ocular Surface 13:103-109.
11. Colwell, L. J., M. P. Brenner, and K. Ribbeck. 2010. Charge as a selection criterion for translocation through the nuclear pore complex. PLoS Comput Biol 6:e1000747.
12. Witten, J., and K. Ribbeck. 2017. The particle in the spider's web: transport through biological hydrogels. Nanoscale 9:8080-8095.
13. Lieleg, O., R. M. Baumgartel, and A. R. Bausch. 2009. Selective filtering of particles by the extracellular matrix: an electrostatic bandpass. Biophysical journal 97:1569-1577.
14. Lieleg, O., C. Lieleg, J. Bloom, C. B. Buck, and K. Ribbeck. 2012. Mucin biopolymers as broad-spectrum antiviral agents. Biomacromolecules 13:1724-1732.
15. Lieleg, O., and K. Ribbeck. 2011. Biological hydrogels as selective diffusion barriers. Trends in cell biology 21:543-551.
16. Zhou, J., A. V. Ellis, and N. H. Voelcker. 2010. Recent developments in PDMS surface modification for microfluidic devices. ELECTROPHORESIS 31:2-16.
17. Muck, A., and A. Svatoš. 2007. Chemical modification of polymeric microchip devices. Talanta 74:333-341.
18. Kuddannaya, S., Y. J. Chuah, M. H. Lee, N. V. Menon, Y. Kang, and Y. Zhang. 2013. Surface chemical modification of poly(dimethylsiloxane) for the enhanced adhesion and proliferation of mesenchymal stem cells. ACS applied materials & interfaces 5:9777-9784.
19. Diaz-Quijada, G. A., and D. D. M. Wayner. 2004. A Simple Approach to Micropatterning and Surface Modification of Poly(dimethylsiloxane). Langmuir 20:9607-9611.
20. Mikos, A. G., A. J. Thorsen, L. A. Czerwonka, Y. Bao, R. Langer, D. N. Winslow, and J. P. Vacanti. 1994. Preparation and characterization of poly(l-lactic acid) foams. Polymer 35:1068-1077.
21. Thomson, R. C., M. J. Yaszemski, J. M. Powers, and A. G. Mikos. 1996. Fabrication of biodegradable polymer scaffolds to engineer trabecular bone. Journal of Biomaterials Science, Polymer Edition 7:23-38.
22. Bellan, L. M., S. P. Singh, P. W. Henderson, T. J. Porri, H. G. Craighead, and J. A. Spector. 2009. Fabrication of an artificial 3-dimensional vascular network using sacrificial sugar structures. Soft Matter 5:1354-1357.
23. Schömig, V. J., B. T. Käsdorf, C. Scholz, K. Bidmon, O. Lieleg, and S. Berensmeier. 2016. An optimized purification process for porcine gastric mucin with preservation of its native functional properties. RSC Adv. 6:44932-44943.
24. Tantakitti, F., J. Boekhoven, X. Wang, R. V. Kazantsev, T. Yu, J. Li, E. Zhuang, R. Zandi, J. H. Ortony, C. J. Newcomb, L. C. Palmer, G. S. Shekhawat, M. O. de la Cruz, G. C. Schatz, and S. I. Stupp. 2016. Energy landscapes and functions of supramolecular systems. Nat Mater 15:469-476.
25. Linden, S. K., P. Sutton, N. G. Karlsson, V. Korolik, and M. A. McGuckin. 2008. Mucins in the mucosal barrier to infection. Mucosal immunology 1:183-197.
26. McGuckin, M. A., S. K. Linden, P. Sutton, and T. H. Florin. 2011. Mucin dynamics and enteric pathogens. Nat Rev Microbiol 9:265-278.
27. Cone, R. A. 2009. Barrier properties of mucus. Adv Drug Deliv Rev 61:75-85.
28. Shi, L., and K. D. Caldwell. 2000. Mucin Adsorption to Hydrophobic Surfaces. Journal of Colloid and Interface Science 224:372-381.

29. Coles, J. M., D. P. Chang, and S. Zauscher. 2010. Molecular mechanisms of aqueous boundary lubrication by mucinous glycoproteins. Curr Opin Colloid In 15:406-416.

30. Lee, S., M. Muller, K. Rezwan, and N. D. Spencer. 2005. Porcine gastric mucin (PGM) at the water/poly(dimethylsiloxane) (PDMS) interface: influence of pH and ionic strength on its conformation, adsorption, and aqueous lubrication properties. Langmuir 21:8344-8353.

31. Bansil, R., and B. S. Turner. 2006. Mucin structure, aggregation, physiological functions and biomedical applications. Curr Opin Colloid In 11:164-170.

32. Lieleg, O., I. Vladescu, and K. Ribbeck. 2010. Characterization of particle translocation through mucin hydrogels. Biophysical journal 98:1782-1789.

33. Olmsted, S. S., J. L. Padgett, A. I. Yudin, K. J. Whaley, T. R. Moench, and R. A. Cone. 2001. Diffusion of macromolecules and virus-like particles in human cervical mucus. Biophysical journal 81:1930-1937.

34. Nowald, C., A. Penk, H. Y. Chiu, T. Bein, D. Huster, and O. Lieleg. 2016. A Selective Mucin/Methylcellulose Hybrid Gel with Tailored Mechanical Properties. Macromol Biosci.

35. Lai, S. K., D. E. O'Hanlon, S. Harrold, S. T. Man, Y. Y. Wang, R. Cone, and J. Hanes. 2007. Rapid transport of large polymeric nanoparticles in fresh undiluted human mucus. Proceedings of the National Academy of Sciences of the United States of America 104:1482-1487.

36. Norris, D. A., and P. J. Sinko. 1997. Effect of size, surface charge, and hydrophobicity on the translocation of polystyrene microspheres through gastrointestinal mucin. Journal of Applied Polymer Science 63:1481-1492.

37. Kasdorf, B. T., F. Arends, and O. Lieleg. 2015. Diffusion Regulation in the Vitreous Humor. Biophysical journal 109:2171-2181.

38. Kočevar-Nared, J., J. Kristl, and J. Šmid-Korbar. 1997. Comparative rheological investigation of crude gastric mucin and natural gastric mucus. Biomaterials 18:677-681.

39. Svensson, O., and T. Arnebrant. 2010. Mucin layers and multilayers - Physicochemical properties and applications. Curr Opin Colloid In 15:395-405.

40. Zheng, R., J. Arora, B. Boonkaew, S. R. Raghavan, D. L. Kaplan, J. He, N. S. Pesika, and V. T. John. 2014. Liposomes tethered to a biopolymer film through the hydrophobic effect create a highly effective lubricating surface. Soft Matter 10:9226-9229.

41. Dowling, M. B., V. Javvaji, G. F. Payne, and S. R. Raghavan. 2011. Vesicle capture on patterned surfaces coated with amphiphilic biopolymers. Soft Matter 7:1219-1226.

42. Jass, J., T. Tjarnhage, and G. Puu. 2000. From liposomes to supported, planar bilayer structures on hydrophilic and hydrophobic surfaces: an atomic force microscopy study. Biophysical journal 79:3153-3163.

43. Li, R., Z. Wu, Y. Wangb, L. Ding, and Y. Wang. 2016. Role of pH-induced structural change in protein aggregation in foam fractionation of bovine serum albumin. Biotechnology Reports 9:46-52.

44. Lee, H., S. M. Dellatore, W. M. Miller, and P. B. Messersmith. 2007. Mussel-inspired surface chemistry for multifunctional coatings. Science 318:426-430.

45. Burzio, L. A., and J. H. Waite. 2000. Cross-Linking in Adhesive Quinoproteins: Studies with Model Decapeptides. Biochemistry 39:11147-11153.

46. LaVoie, M. J., B. L. Ostaszewski, A. Weihofen, M. G. Schlossmacher, and D. J. Selkoe. 2005. Dopamine covalently modifies and functionally inactivates parkin. Nat Med 11:1214-1221.

47. Sugumaran, M., H. Dali, and V. Semensi. 1989. Chemical- and cuticular phenoloxidase- mediated synthesis of cysteinyl–catechol adducts. Archives of Insect Biochemistry and Physiology 11:127-137.

48. Green, N. M. 1975. Avidin. Adv Protein Chem 29:85-133.

49. Datta, S., L. R. Christena, and Y. R. S. Rajaram. 2013. Enzyme immobilization: an overview on techniques and support materials. 3 Biotech 3:1-9.

50. Kim, D., and A. E. Herr. 2013. Protein immobilization techniques for microfluidic assays. Biomicrofluidics 7:041501.

51. Mao, H., T. Yang, and P. S. Cremer. 2002. Design and Characterization of Immobilized Enzymes in Microfluidic Systems. Analytical Chemistry 74:379-385.

52. Toepke, M. W., and D. J. Beebe. 2006. PDMS absorption of small molecules and consequences in microfluidic applications. Lab on a Chip 6:1484-1486.

53. Keough, E. M., W. C. Mackey, R. Connolly, T. Foxall, K. Ramberg-Laskaris, J. L. McCullough, T. F. O'Donnell, and A. D. Callow. 1985. The interaction of blood components with PDMS(polydimethylsiloxane) and LDPE (low-density polyethylene) in a baboon ex vivo arteriovenous shunt model. Journal of Biomedical Materials Research 19:577-587.

54. Amoako, K. A., H. S. Sundaram, A. Suhaib, S. Jiang, and K. E. Cook. 2016. Multimodal, Biomaterial-Focused Anticoagulation via Superlow Fouling Zwitterionic Functional Groups Coupled with Anti-Platelet Nitric Oxide Release. Advanced Materials Interfaces 3:1500646.

Appendix A.3 Macromolecular coating enables tunable selectivity in a porous PDMS matrix

Table of contents

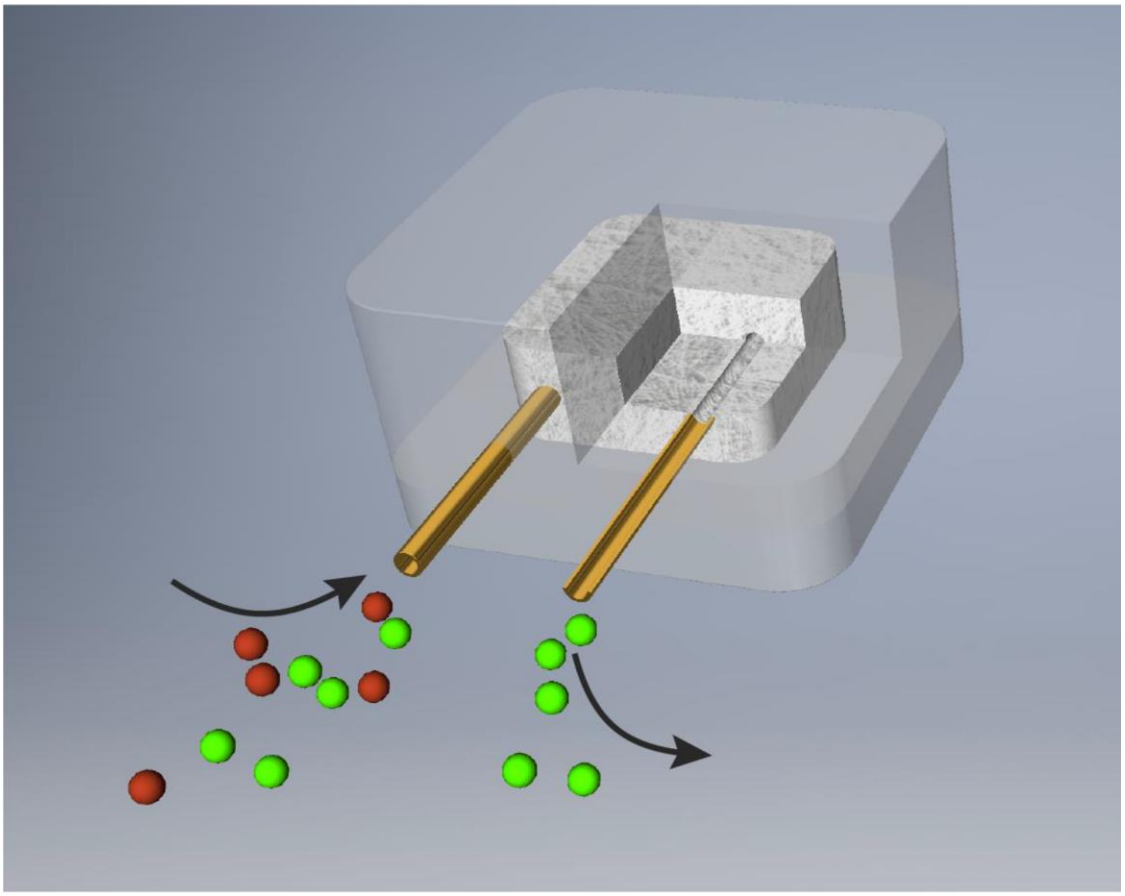

Dissolving embedded sugar fibers from a PDMS matrix generates a capillary system that allows for functionalization with a wide range of macromolecules. These surface coatings enable highly tunable selectivity and allow for sieving of particles and molecules based on steric hindrance, electrostatic binding, electrostatic repulsion, or specific binding interactions.

Macromolecular coating enables tunable selectivity in a porous PDMS matrix

Benjamin Winkeljann [1*], *Benjamin T. Käsdorf* [1*], *Job Boekhoven* [2], *and Oliver Lieleg* [1#]

[1]Department of Mechanical Engineering and Munich School of Bioengineering,
Technical University of Munich,

Boltzmannstraße 11, 85748 Garching, Germany

[2]Department of Chemistry and Institute for Advanced Study, Technical University of Munich, Lichtenbergstraße 4, 85748, Garching, Germany

[*] Both authors contributed equally to the work

[#] Corresponding author:

Prof. Dr. Oliver Lieleg

Department of Mechanical Engineering and Munich School of Bioengineering,
Technical University of Munich,

Boltzmannstraße 11, 85748 Garching, Germany

e-mail: oliver.lieleg@TUM.de

Characterization of the filtration system

The capillary density of c = 596 (± 58) mm^{-2} was determined by counting capillaries on profilometric images obtained from three different filters. To calculate the total number of capillaries, we estimated the area A perfused with capillaries (highlighted in red, **Figure S1**) to be $l_{drilled}$ = 20 mm in width (which is the length of the drilled inlet) and h = 5 mm in height (which is the height of the cured fiber/PDMS composite). With this estimated area, the calculated total number of capillaries n is:

$$n = c \times l_{drilled} \times h = 59560 \qquad \textbf{(Equation S1)}$$

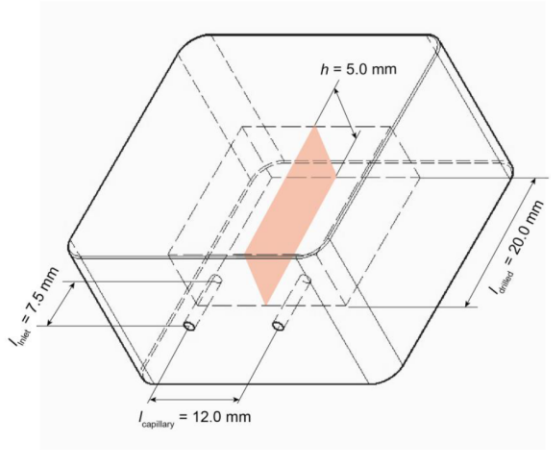

***Figure S1*: Geometry of the filter system.** The schematic shows an illustration of the filter cube together with the relevant measures required for calculating the flow resistance.

Using the law of Hagen-Poiseuille, the flow resistance of a single capillary (approximated as a cylindrical tube) can be calculated as

$$R_{\text{capillary}} = \frac{8\eta \times l_{\text{capillary}}}{\pi {r_{\text{capillary}}}^4} = 105\ \text{Ns/mm}^5 \qquad \textbf{(Equation S2)}$$

where $R_{capillary}$ denotes the flow resistance of a single capillary [Ns/mm^5], η the viscosity of water [Pa*s], $l_{capillary}$ the length of the capillary [mm] and $r_{capillary}$ = 4.13 µm the average radius of a capillary.
To simplify the calculation, we make the approximation that all capillaries are oriented in parallel, reaching directly from the inlet to the outlet. Then, in analogy to Ohm´s law, the overall flow resistance of a parallel circuit can be calculated:

$$\frac{1}{R_{\text{total}}} = \sum_{i=1}^{n} \frac{1}{R_{\text{i}}} \qquad \textbf{(Equation S3)}$$

Here, R_{total} represents the total flow resistance of the parallel circuit consisting of individual capillaries with flow resistances R_i [Ns/m^5]. For similar R_i = $R_{capillary}$, this equation is reduced to:

$$R_{\text{total}} = \frac{R_{\text{capillary}}}{n} = 1.76 * 10^{-3}\ \text{Ns/mm}^5 \qquad \textbf{(Equation S4)}$$

For a defined flow rate of Q = 1.0 mL/min, we can now calculate the pressure drop across the filter Δp as:

$$\Delta p = R_{\text{total}} \times Q = 300\ \text{mbar} \qquad \textbf{(Equation S5)}$$

To determine the flow resistance of the filter, the pressure right before the inlet was measured. Therefore, a syringe was connected to a T-connector of which one end was linked to a manometer and the other end to the filter inlet. A constant flow of 1.0 mL/min was set using a syringe pump (LA 100, Landgraf Laborsysteme HLL GmbH, Langenhagen, Germany). In this configuration, the pressure loss indicated by the manometer represents the flow resistance of the capillary system. This estimated pressure drop is only ~18 % lower and therefore in good agreement with the measured value of 365 mbar considering the approximations made and keeping in mind that some capillaries in the filter might constitute `dead ends` (and thus will not contribute to the flow resistance).

Liposome characterization

Size and ζ -potential of liposomes were determined with dynamic light scattering using a Zetasizer Nano ZS (Malvern Instruments, Herrenberg, Germany). For size and ζ -potential measurements, lipids were resuspended in 20 mM TRIS buffer (pH 7.3, 10 mM NaCl).

Table S1: Diameter and ζ-potential of all liposome species was determined in 20 mM TRIS buffer at pH 7.3 and 10 mM NaCl. The error values represent the standard deviation as obtained from three different measurements.

liposome species	diameter [nm]	PDI [ ]	ζ-potential at pH 7.3 [mV]
DOPG	199 ± 35	0.16 ± 0.03	-55.8 ± 1.3
DOPC 200	235 ± 31	0.17 ± 0.04	+5.4 ± 0.3
DOPC 400	529 ± 39	0.38 ± 0.03	+1.4 ± 0.1
DOPC 1000	836 ± 43	0.41 ± 0.03	+5.4 ± 0.3
DOTAP	230 ± 46	0.17 ± 0.04	+48.6 ± 0.9
DOPC-biotin	203 ± 2	0.26 ± 0.02	-4.7 ± 0.4

Filtration efficiency of a mucin-coated capillary system towards dextran molecules

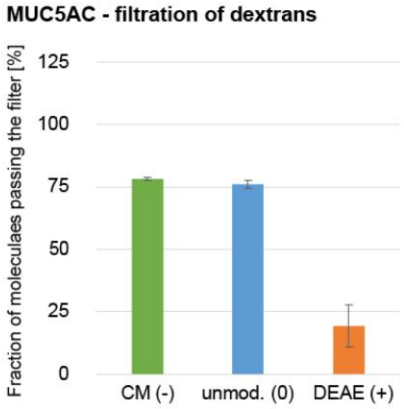

***Figure S2*: Filtration of a mucin-coated PDMS-filter when flushed with different dextran variants.** FITC-labeled dextrans (M_w = 150 kDa) – modified with either carboxymethyl (CM) groups, diethylaminoethyl (DEAE) groups or unmodified – were pumped through the capillary system. The fluorescence intensity of the dextran solution prior and after passing the filter was measured to determine the fraction of molecules that has passed the filter. The error bars denote the standard deviation as obtained from three independent filter realizations.

Saturation behavior of a mucin-coated filtration device and filter regeneration

Using the total number of capillaries we determined before, we are also able to estimate the surface and volume of the filtration device. With l_{inlet} = 7.5 mm, r_{inlet} = 0.75 mm, $l_{drilled}$ = 20 mm, $r_{drilled}$ = 0.65 mm, $l_{capillary}$ = 12.0 mm and $r_{capillary}$ = 4.13 µm, the surface and the volume can be calculated as follows:

$$A = 2 \times (l_{\mathrm{inlet}} \times 2r_{\mathrm{inlet}} \times \pi + l_{\mathrm{drilled}} \times 2r_{\mathrm{drilled}} \times \pi) + n \times l_{\mathrm{capillary}} \times 2r_{\mathrm{capillary}} \times \pi = 18781\ mm^2 \quad \textbf{(Equation S6)}$$

$$V = 2 \times (l_{\mathrm{inlet}} \times r_{\mathrm{inlet}}^2 \times \pi + l_{\mathrm{drilled}} \times r_{\mathrm{drilled}}^2 \times \pi) + n \times l_{\mathrm{capillary}} \times r_{\mathrm{capillary}}^2 \times \pi = 118\ mm^3 \quad \textbf{(Equation S7)}$$

This estimate agrees very well with the actual volume (V = 133 µm ± 24 µm) we determined for our device (see main paper). Assuming that each liposome can cover an area of ~ 200 nm x 200 nm, the device allows for a maximum number of ~$4.7*10^{11}$ liposomes to bind to its surface. Normalized to the volume of the filter, ~$4.0*10^{12}$ liposomes can be bound per mL. And indeed, control measurements (**Figure S2**) indicate that saturation effects set in after a comparable number of liposomes (i.e. ~$3.0*10^{11}$) have passed the filter.

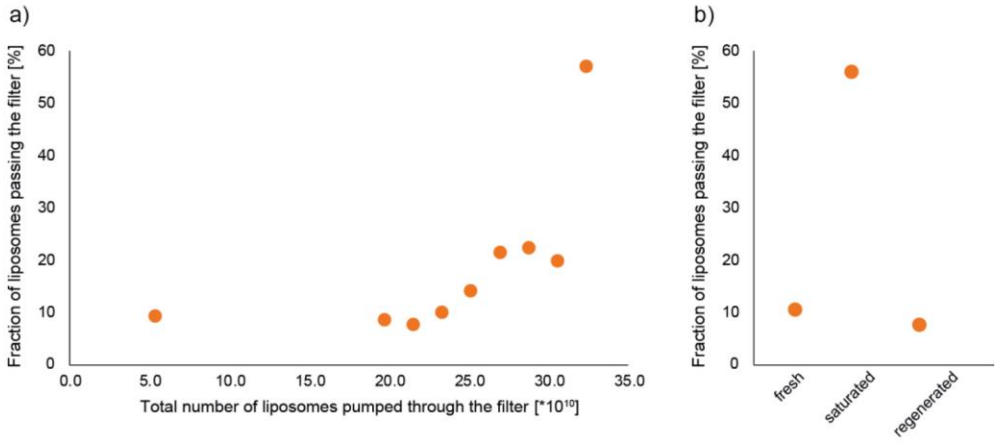

Figure S3: **Saturation behavior of a PDMS capillary system coated with native porcine gastric mucins.** a) The filter system does not show any sign of a saturation effect up to a total number of ~2.5*10[11] liposomes (here shown for a MUC5AC functionalized system). This is equivalent to almost 200 standard filtration cycles as they were performed in the measurements shown in the manuscript. b) A saturated filter can be regenerated by flushing it with a 3 M NaCl solution. This rinsing step removes bound liposomes – probably by a combination of two effects: first, by weakening electrostatic binding interactions (Debye screening) and, second, by inducing osmotic liposome bursting.

Immobilized liposomes in the capillaries of a mucin-coated filtration device

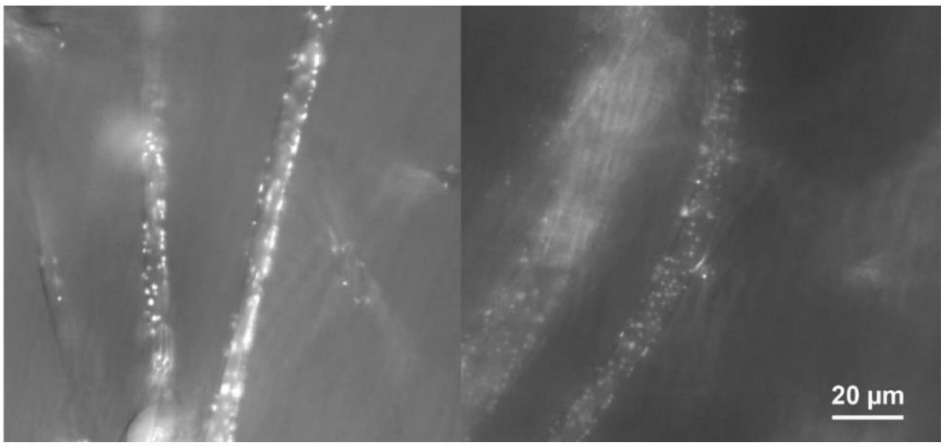

Figure S4: **Fluorescence micrographs of a mucin-coated PDMS capillary system after a filtration test with cationic (DOTAP) liposomes.** Many intact liposome particles are observed which decorate the surface of the capillaries. The scale bar represents 20 µm.

Control measurements with various filter coatings

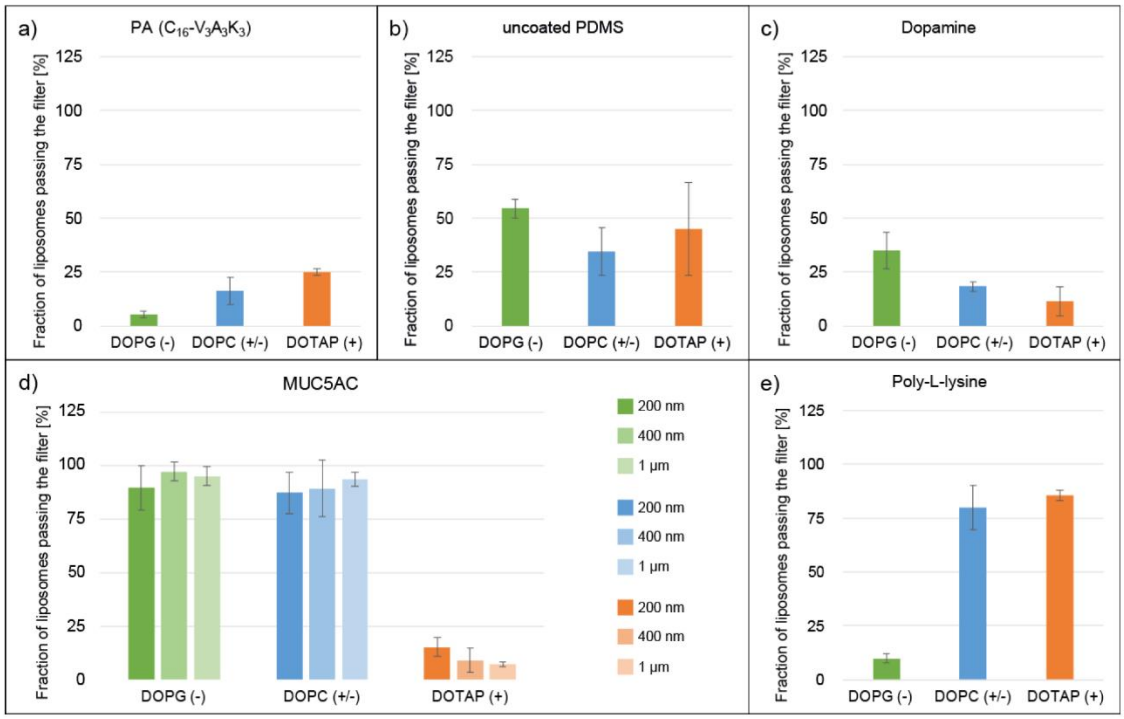

Figure S5: **Control filtration measurements performed with different coatings.** A functionalization of the capillaries with short peptide amphiphile fibers without additional BSA passivation removes all three liposome species from the solution, with a slightly decreasing efficiency the more positive the liposomes become (a). In the absence of a molecular coating layer, all three liposome variants (DOPG, DOPC and DOTAP) are removed from a filtration solution at similar efficiencies (b). When dopamine is absorbed to the PDMS capillaries and no secondary coating is performed, all three liposome variants are filtered out (c). The filtration outcome of a MUC5AC coated filter is independent of the liposome size used here (200 nm, 400 nm, 1 µm) (d). Filtration of the three liposome species in a changed order (DOTAP, DOPC and DOPG) does not influence the filtration outcome (here shown for a poly-L-lysine coated filter) (e). The error bars denote the standard error of the mean as obtained from three independent filter realizations (b, c, d and e) or two independent filter systems (a), respectively.

Disintegration of liposomes on a PDMS surface

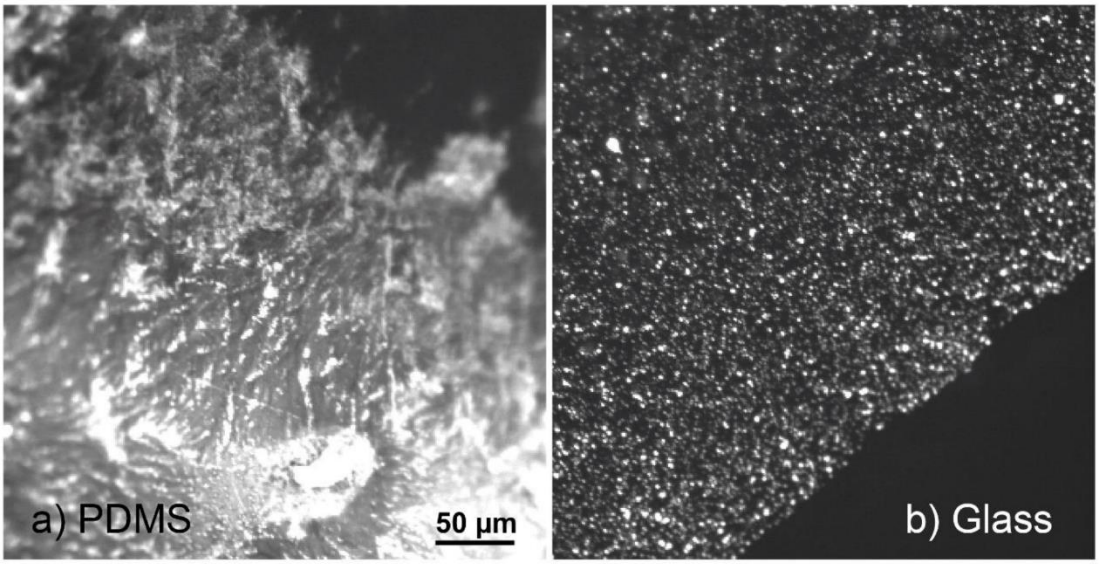

Figure S6: **Fluorescence micrograph of DOPC liposomes on a PDMS and a glass surface.** Whereas liposomes seem to disintegrate on a hydrophobic PDMS surface (a) they remain intact on a hydrophilic glass plate (b). The scale bar represents 50 µm and applies to both images.

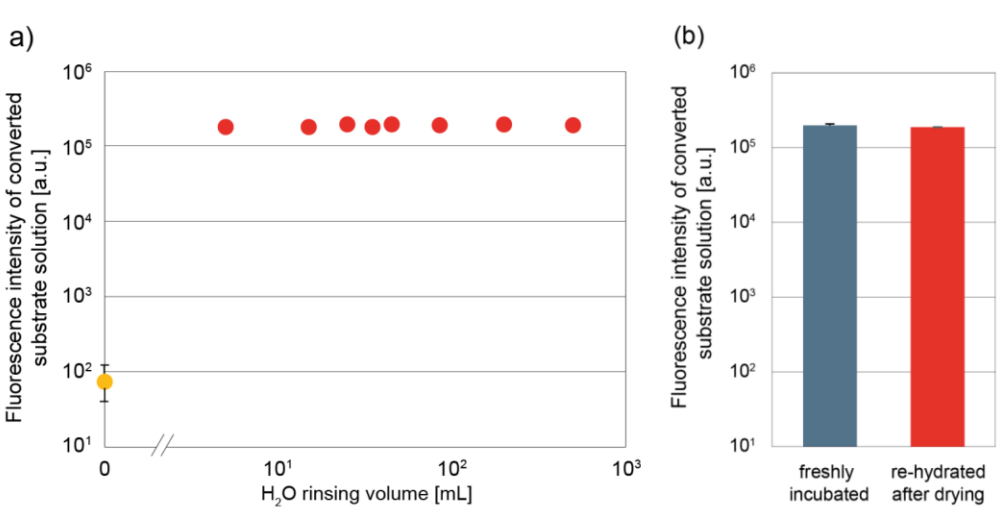

Figure S7: **Spectrophotometric analysis of converted ADHP substrate by HRP.** (a) To test the stability of HRP physisorption to the PDMS channels, the fluorescent signal of ADHP substrate converted by immobilized HRP on the capillary surface is measured after flushing the filter system with different amounts of ultrapure water. The yellow data point represents the fluorescent signal obtained for an unconverted substrate solution. Standard deviations were determined from three independent filter realizations and are shown as error bars for the unconverted substrate solution; for the other data points, the error bars are smaller than the symbol size. (b) The enzymatic stability of HRP was investigated by drying a HRP-coated filtration system and measuring the enzymatic activity of the very same filter after rehydration. The error bars represent the standard error as determined from three measurements obtained with a given rehydrated filter.

Stability Analysis of a physisorbed mucin coating of the PDMS capillaries

To quantify if and how much mucin is washed out from the capillaries during flushing the filter, the rinsing solution was analyzed via ELISA. 250 µL of the rinsing solution was collected from the outlet of a MUC5AC functionalized filter at distinct volume intervals, i.e. between 1 to 50 mL of rinsing volume. From each sample, two wells of a standard 96-well plate were filled with 100 µL each. The solutions were incubated in the well plate at room temperature for 60 min to allow for mucin adsorption to the polystyrene surface of the wells. Afterwards, the solutions were removed and the wells were washed with PBS-Tween (pH 7.4): the well was first filled with 200 µL of PBS-Tween and then placed onto a shaker (Promax 1020, Heidolph Instruments GmbH & Co. KG, Schwabach, Germany) at 120 rpm for 1 min. Afterwards, the washing buffer was removed. This step was repeated four times. Finally, all samples were incubated in 300 µL of blocking buffer (5 % milk powder dissolved in PBS-Tween) on the shaker at room temperature for 120 min.

After another washing step, the samples were incubated in a primary antibody (200 µL per well) for 60 min while sitting on the plate shaker. For this step, specific antibodies for MUC5AC (ABIN966608, antibodies-online GmbH, Aachen, Germany) detection were used. The mucin antibody was diluted 1:400 in blocking buffer. After incubating the samples, they were washed again with PBS-Tween. A second antibody staining was then performed using a goat anti-mouse (murine) IgG antibody (ABIN237501, antibodies-online GmbH, Aachen, Germany). This secondary antibody was diluted 1:5000 in blocking buffer. Incubation was performed on the plate shaker at room temperature for 60 min.

Next, the samples were washed in pure PBS (since Tween tends to interfere with the solutions used for following steps). After washing the samples, 100 µL of QuantaRed Working Solution were added to each well. QuantaRed Working Solution consists of 50 parts QuantaRed Enhancer Solution, 50 parts QuantaRed Stable Peroxide and 1 part of QuantaRed ADHP Concentrate (QuantaRed Enhanced Chemifluorescent HRP Substrate Kit 15159, Thermo Fisher Scientific, Waltham, Massachusetts, USA). Since the Working Solution is light sensitive, direct light contact was avoided and the solution was used within 30 min.

After 2 min of incubation at room temperature, the peroxidase activity was stopped by adding 10 µL of QuantaRed Stop Solution to each well. The plate was incubated on the shaker again for 30 s before samples were removed from the wells and fluorescence of the converted substrate was measured with a multi-label plate reader (Viktor3, PerkinElmer, Inc., Massachusetts, USA). The whole plate was measured three times with a 10 s break in between each measurement run. Fluorescence was measured at an excitation wavelength of $\lambda_{570\,nm}$ and an emission wavelength of $\lambda_{642\,nm}$ using a data acquisition time of 0.1 s. Every fluorescence value was corrected by subtracting the value obtained for a control sample containing no mucin. For each sample, the two measured values were averaged and normalized to the first collected sample.

To test if the mucin layer on the capillary surface is still intact, a standard filtration cycle with liposomes (see main paper for details) was performed after the rinsing procedure. The whole experiment was conducted for three independent filter realizations.

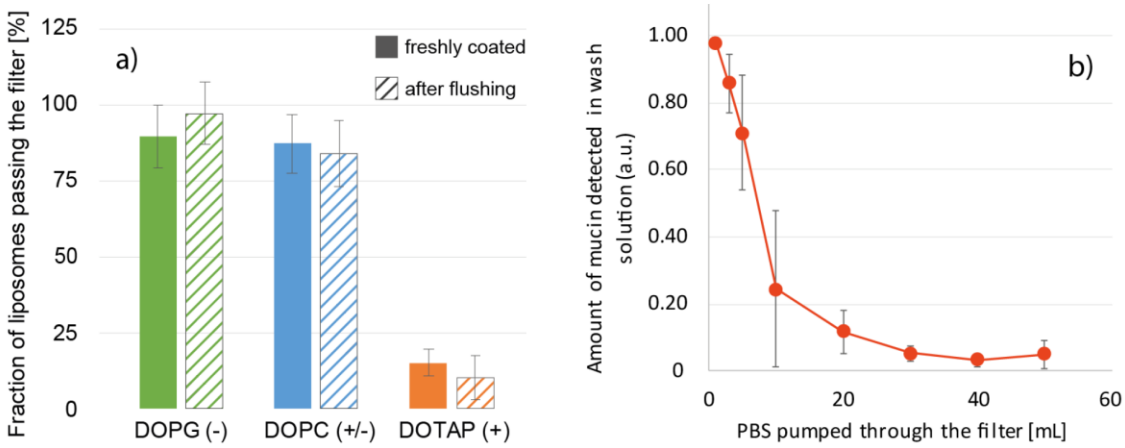

Figure S8: **Stability test of a physisorbed mucin coating.** The filtration behavior obtained by a mucin coated filter is compared to the filtration behavior of a mucin coated filter which was flushed with 50 mL PBS (a). Amount of mucin washed out the filter as determined via ELISA (b). The error bars denote the standard deviations determined from three independent filter realizations.

Table S2: Cost estimate for the production of a single PDMS-based filtration device. Listed are the consumables required for the production of a PDMS capillary system coated with the enzyme HRP.

consumable	amount	cost [€]
PDMS	25 g	5
sugar	~3 g	0.01
functionalization (e.g. enzyme)	~100 µg	0.18 (HRP)
		total = 5.19 €

Required equipment

cotton candy machine (30 €)

Additional (standard lab) equipment

vacuum pump, oven, syringe pump (for controlled flow rates)

A.4 An optimized purification process for porcine gastric mucin with preservation of its native functional properties

RSC Advances

PAPER

View Article Online
View Journal | View Issue

Cite this: *RSC Adv.*, 2016, **6**, 44932

An optimized purification process for porcine gastric mucin with preservation of its native functional properties†

Veronika J. Schömig,[a] Benjamin T. Käsdorf,[b] Christoph Scholz,[a] Konstantinia Bidmon,[b] Oliver Lieleg[b] and Sonja Berensmeier*[a]

Purified gastric mucins are currently used for a wide range of applications *e.g.* as a model system for native mucus, as lubricants or antiviral/antibacterial supplements. However, commercially available porcine gastric mucins (PGM) do not exhibit gel-forming properties and show only greatly reduced anti-viral/anti-bacterial activity. Thus, we established a robust purification process for PGM, maintaining its desired properties such as lubricity, gel formation and the selective binding of molecules. We optimized the process in terms of yield and productivity and evaluated the influence of different buffer conditions on mucin quality. Cross-flow filtration using 100 kDa membranes was introduced and optimized to pre-concentrate the mucin solution prior to size exclusion chromatography. A conductivity of less than 100 μS cm^{-1} after diafiltration was found to be crucial for gel formation. The mucin yield of the optimized process was 66%. The scale-up resulted in a productivity of 0.15 mg purified mucin per mL crude mucus an hour. In total, approx. 65 mg mucin could be purified from one pig stomach. Tribological studies, rheological measurements and co-localization experiments confirmed the retained functionality of purified mucin in terms of lubricity, gel formation and binding interactions with charged molecules, respectively.

Received 21st March 2016
Accepted 23rd April 2016

DOI: 10.1039/c6ra07424c

www.rsc.org/advances

1. Introduction

Mucins, highly glycosylated proteins, are found in the mucous membranes of animals and humans. Mucus covers the inner surface of the body such as in the abdomen, stomach, nose, eye or female genital tract. In addition to mucins, native mucus contains water (~95%), lipids, salts, growth factors and enzymes[1] and serves as a barrier towards pathogens such as bacteria and viruses and thus protects the underlying tissue from infection.[2,3] This is partly due to its physical properties, as mucin gelation is induced at acidic pH values by gel forming mucins such as Muc5AC (mainly found in the stomach) and Muc5B (present in the oral cavity). Moreover, the polyanionic nature of mucins at neutral pH[4–6] can lead to electrostatic interactions with cationic groups, as they are present on the surface of many bacteria and viruses.

In monomeric form, mucin has a molecular weight of about 640 kDa[7] where the carbohydrates amount up to 80% of the whole mass, whereas the protein backbone only contributes 20% of the weight.[8] These mainly O-linked glycans such as *N*-acetylgalactosamine, *N*-acetylglucosamine, fucose, galactose and sialic acid (*N*-acetylneuraminic acid) are attached to the hydroxyl side chains of threonine and serine. Mucins are rich in cysteines, which form inter- and intramolecular disulfide bonds resulting in oligomers and polymers of up to 40 MDa.[8–10] Once the disulfide interactions are chemically reduced, mucin gel formation is disturbed.[10] Additionally, the pH and ionic strength determine the conformation of native mucin.[11] The mechanism of the gel formation of mucins like Muc5AC has been investigated in various studies but is not fully understood.[5,11–15] It seems, in addition to the disulfide bonds, a complex interplay between hydrophobic and electrostatic interactions is responsible for the crosslinking of gel-forming mucins[16] that is observed at acidic pH.

Native mucin has shown promising properties regarding the adsorption onto[4] and lubrication of surfaces[17–19] which could be very interesting for biomedical applications. Moreover, by investigating the bulk and surface properties of mucin layers and gels, a better understanding of native mucus and its

[a]*Bioseparation Engineering Group, Department of Mechanical Engineering, Technical University of Munich, Boltzmannstr. 15, D-85748 Garching, Germany. E-mail: s.berensmeier@tum.de*

[b]*Institute of Medical Engineering and Department of Mechanical Engineering, Technical University of Munich, Boltzmannstr. 11, D-85748 Garching, Germany*

† Electronic supplementary information (ESI) available: Rheological measurements of different mucin concentrations (Fig. S1) and the influence of buffer and protease inhibitors on viscoelasticity (Fig. S2a and b, respectively); SDS-PAGE of enzymatically digested PGM (Fig. S3); temperature dependence before and after purification (Fig. S4); preliminary studies of cross-flow filtration with commercially available mucin type III (Sigma Aldrich) (Fig. S5a and b); calculations of the flow conditions within filtration modules (eqn (S1) and (S2) and Table S1); PAS assay analyses of purification processes using different filter modules (Tables S2–S4). See DOI: 10.1039/c6ra07424c

permeability towards molecules,[20,21] nanoparticles[22] and pathogens[2] can be achieved. Although porcine gastric mucins are commercially available *e.g.* from Sigma Aldrich, most commercial mucins do not form a hydrogel, are only partially purified and are inferior in inhibiting virus infection compared to natively purified mucins obtained in the lab.[2] In cell culture experiments[2] even cell toxic effects were observed when epithelial cells were treated with reconstituted solutions of commercial mucin. Commercial mucins are often further purified with anion exchange chromatography, size exclusion chromatography (SEC)[21] or centrifugation and filtered through a dead end filter to remove aggregates and undesired proteins.[23] Nevertheless, in our hands, gel formation of commercially obtained PGMs could not be reconstructed even after further purification (unpublished data). Also Kočevar-Nared and coworkers[16] found that commercial mucins cannot reproduce the properties of native gastric mucus, which limits the usefulness of commercial mucins *e.g.* for experiments mimicking the barrier properties of native mucus towards pathogens. The origin of the missing gel formation abilities of commercial mucin is not completely understood, but the purification process itself or fragmentation with proteases are possible explanations.[24]

Several studies have been performed to purify enzymatically digested or chemically reduced mucins using SEC or CsCl density centrifugation.[8,25–27] Also, the addition of protease inhibitors and stabilizers is widely used in the purification of mucins[13,28,29] but can complicate the purification process. The purification of native mucin from pig colonic mucosa has been published.[26] However, so far most purification attempts have been carried out with the aim to further process the glycoproteins or to characterize the purified mucins. To our knowledge, optimizing the yield and productivity of a mucin purification from pig stomachs has not been addressed yet. Such an optimization of the purification process is, however, crucial to meet the growing demand for functional PGM, be it for further academic studies or for biomedical applications.

Therefore, our aim was to establish a robust downstream process to purify native porcine gastric mucin while maintaining its unique properties. We addressed the following aspects that are crucial in downstream processing: (1) the requirement for additives, temperature and buffering conditions during purification, (2) volume reduction for increased product concentration and less process streams, (3) functionality of the protein, (4) improvement of the total yield and (5) higher productivity. First, we established a reproducible protocol in small scale before implementing the changes to an upscaled system. We introduced and optimized cross-flow filtration as a new process unit to achieve a reduction of the initial volume and depletion of small molecules before size exclusion chromatography. To our knowledge, this process unit has so far not been published as a concentration step of mucins, but has high potential in enhancing the protein yield. After further purification by subsequent SEC and diafiltration, functionality tests of PGM solutions and gels were used to verify the success of our optimized process.

2. Experimental

2.1. Materials

Commercial porcine gastric mucins (PGM) type II and III were obtained from Sigma Aldrich (St. Louis, United States), Schiff's stain and periodic acid 1% were purchased from Carl Roth (Karlsruhe, Germany), antibodies against Muc5AC (ABIN966608) and horse radish peroxidase HRP conjugated antibodies (ABIN237501) were obtained from antibodies-online.de (Aachen, Germany). Filter cassettes with a membrane area of 200 cm^2 and MWCO of 100 kDa (Hydrosart®) and 300 kDa MWCO (polyethersulphone, PESU) were obtained from Sartorius Stedim (Goettingen, Germany), Xampler™ laboratory-scale hollow fiber cartridge with a length of 31.7 cm, an inner diameter of 0.1 mm and membrane area of 110 cm^2 and 100 kDa MWCO (polysulfone) was from GE Healthcare Life Sciences (Freiburg, Germany).

2.2. Methods

Sample collection. In general it must be noted, that the mucus samples used for purification are of animal origin and from different stomach batches. Therefore, different yields and variations in the viscoelastic properties of the purified material are likely to occur. However, we pooled the mucus of 20 to 60 stomachs per batch to minimize these variances. We do not focus on variations between different batches, but discuss the properties of our purified mucin in general. Absolute values are to be taken with care and do not indicate significant differences in gel formation abilities of the purified mucins but are the result of natural variances. Sample collection was based on the protocol described by Libao-Mercado and coworkers.[8] In detail, fresh pig stomachs were obtained from a local slaughterhouse and stored on ice. The stomachs were cut along their longitudinal axis and the remaining food and debris was gently rinsed with tap water. The mucosal surface of the stomach was manually scraped with spoons and the mucus was collected in a beaker placed on ice. A mean volume of 40 mL mucus was obtained from one stomach. The mucus was diluted 1 to 5 in 10 mM phosphate buffer pH 7.0 with 170 mM NaCl containing 0.04% (w/v) NaN_3. pH was adjusted to 7.4 and 5 mM benzamidine HCl (Carl Roth, Karlsruhe, Germany), 1 mM 2,4′-dibromoacetophenone (Sigma Aldrich, St. Louis, United States), 1 mM phenylmethylsulfonyl-fluoride (Carl Roth, Karlsruhe, Germany) and 5 mM EDTA (Carl Roth, Karlsruhe, Germany) pH 7.4 were added and gently stirred over night at 4 °C.

Centrifugation. The solubilized mucus was centrifuged at 8300 × *g* (Sorvall Evolution RC, SLC-4000 rotor, Thermo Scientific, Waltham, MA, USA) for 30 minutes at 4 °C. Afterwards, the supernatant was again centrifuged at 15 000 × *g* for 45 minutes at 4 °C. The supernatant was stored either at −20 °C, −80 °C or in liquid nitrogen. For further processing, the supernatant was thawed or used directly after the centrifugation steps. An ultracentrifugation step at 150 000 × *g* (Beckman LE-70 Optima, rotor 70-Ti, Beckman Coulter, Krefeld, Germany) for 1 h at 4 °C was conducted before filtration. For the upscaled process, the centrifugation steps were identical.

Concentration. After the processing of porcine mucus, a concentration step (4–5 fold) was conducted at room temperature using cross-flow filtration (SARTOFLOW® Slice 200 benchtop crossflow system, Sartorius AG, Goettingen, Germany, for hollow fiber module: UFP – 100-E-3MA QuixStand GE Healthcare, Freiburg, Germany). The MWCO was 100 or 300 kDa depending on the experiment with a membrane area of 200 cm^2 or 110 cm^2 for the hollow fiber membrane. Constant pressure mode was applied with Δp_{TM} between 0.5 and 1.5 bar to achieve the optimized filtration mode with the lowest loss of product. The washing of the membrane was performed in 50 mL of 10 mM phosphate buffer (pH 7.0, supplemented with 170 mM NaCl) for 5 min in circular flow and analyzed for protein content. Samples of retentate, permeate and washing fraction were taken for protein analysis. The washing fraction was added to the retentate. For the upscaled process, a hollow fiber membrane with 100 kDa MWCO and a membrane area of 110 cm^2 was used.

Parameter calculation during cross-flow filtration. The filtration performances of various setups were examined using mass transfer relations with the Reynolds (Re) number, the Schmidt (Sc) number and Sherwood (Sh) number.[30] In laminar flow, the following relation holds:

$$\mathrm{Sh} = \frac{k d_h}{D} = \frac{d_h}{\delta_{BL}} = 1.62\left(\mathrm{ReSc}\frac{d_h}{L}\right)^{1/3} \quad (1)$$

with k being the mass-transfer coefficient (m s^{-1}), D the diffusion coefficient of the protein (m^2 s^{-1}), d_h the hydrodynamic diameter (m), and δ_{BL} the thickness of the boundary layer (m). In turbulent flow, Sh is approximated with:

$$\mathrm{Sh} = 0.04\mathrm{Re}^{3/4}\mathrm{Sc}^{1/3} \quad (2)$$

Detailed information is provided in the ESI (Table S1†). Also, the permeate flux and fouling resistances during concentration were calculated as follows. *Darcy's law* (eqn (3)) describes the flow rate of a fluid phase through a porous medium:[31]

$$J = \frac{\dot{V}}{A} = \frac{\Delta p_{TM}}{\eta_{perm} R_{tot}} \quad (3)$$

with J being the flux (kg m^{-2} h^{-1}); η_{perm} the viscosity of the permeate (Pa s); R_{tot} the total resistance of the membrane (m^{-1}); Δp_{TM} the transmembrane pressure (bar).

The fouling resistance $R_{fouling}$ is determined by combining eqn (3) and (4), with R_m being the membrane resistance of water:[32]

$$R_{tot} = R_m + R_{fouling} \quad (4)$$

Size exclusion chromatography. Size exclusion chromatography to receive fractions according to the molecular weight was conducted using Äkta Explorer (GE Healthcare, Amersham Biosciences, Freiburg, Germany). Sepharose 6 *Fast Flow* was used as column material (GE Healthcare, UK) with a bed volume of 176 mL and 1650 mL, respectively. 10 mM phosphate buffer (pH 7.0, supplemented with 170 mM sodium chloride) was used as equilibration buffer and running buffer to elute the target protein. Approx. 0.11 column volumes (CV) (20 mL and 180 mL, of the concentrated mucus) were loaded onto the column. The flow rate was 30 cm h^{-1}. Absorbance at 280 nm and 215 nm were recorded online. Fractions of either 5 or 11 mL were collected (depending on the column size) and analyzed with ELISA and periodic acid/Schiff's stain (PAS) assay. Glycoprotein containing fractions were pooled and a sample was taken for further analysis.

Diafiltration. In the optimized filtration protocol, pooled fractions were diafiltrated against ddH_2O with a 100 kDa membrane of 200 cm^2/110 cm^2 for the hollow fiber membrane and 1 bar transmembrane pressure until a conductivity of <100 μS cm^{-1} was obtained. Washing was performed as described for the concentration step. The protein solution was aliquoted, a sample taken and lyophilized over night at −60 °C and 0.06 mbar (Alpha 1-2 LD, Christ, Osterode am Harz, Germany). For the upscaled process, a hollow fiber membrane with 100 kDa MWCO and a membrane area of 110 cm^2 was used. Where applicable, the retentate was further concentrated until the dead volume of the module was reached.

2.3. Analytical methods

Quantitative PAS-assay. Quantitative periodic acid/Schiff's stain (PAS) assay was used for the detection of carbohydrates. Based on Kilcoyne and coworkers,[33] the analysis was conducted in microtiter plates (Nunc® MicroWell™ F bottom Sigma Aldrich, Crailsheim, Germany) for high throughput determination. In brief, 25 μL of sample was pipetted into a well and incubated with 120 μL of 0.06% (v/v) periodic acid diluted in 7% (v/v) acetic acid for 90 min at room temperature. 100 μL Schiff's stain (Carl Roth GmbH & Co. KG, Karlsruhe, Germany) was added and incubated for another 60 min at room temperature to allow complete staining of carbohydrates. Absorption was measured at 550 nm after 5 s of shaking (Infinite M 200 PRO Series, Software: Magellan V 7.0, Tecan Deutschland GmbH, Crailsheim, Germany). Self-purified mucin was used as standard in the range of 0.125 mg mL^{-1} to 1 mg mL^{-1}.

ELISA. An indirect ELISA was performed to investigate the gel forming Muc5AC containing samples. 100 mL samples were pipetted into microtiter plates (Nunc® MicroWell™ F bottom Sigma Aldrich, Crailsheim, Germany), incubated with a monoclonal anti-Muc5AC antibody (antibodies-online.de, ABIN966608) and visualized by a secondary antibody labelled with HRP (antibodies-online.de, ABIN237501). Between all incubations, the wells were extensively washed with blocking buffer (5% (w/v) milk powder in PBS with 0.1% (w/v) Tween 80). The substrate *o*-phenylenediamine (oPD) (AppliChem GmbH, Darmstadt, Germany) was added and the enzymatic reaction was stopped with 1 M H_2SO_4 after 6–8 min of incubation. Absorption was measured at 490 nm in a photometer (Infinite M 200 PRO Series, Software: Magellan V 7.0, Tecan Deutschland GmbH, Crailsheim, Germany). Purified Muc5AC was used as standard in the range of 1.25 μg mL^{-1} to 80 μg mL^{-1}. 50 mM carbonate buffer (pH 9.6) was used as blank and for the dilution of samples and standard, respectively.

2.4. Characterization

Rheology. Rheological measurements were conducted with either 2% (w/v) or 1% (w/v) purified mucin. The change in viscoelasticity and the gelation behavior of reconstituted mucin solutions were analyzed as a function of pH. Lyophilized mucin was weighed and hydrated in 90% ddH_2O and filled with 10% of 10× phosphate buffer (pH 2 or pH 6) 2 h prior to analysis. Rheological evaluation of mucin solutions and gels was performed on a stress-controlled shear rheometer (MCR 302, Anton Paar, Graz, Austria) using a plate/plate measuring setup (PP25, Anton Paar, Graz, Austria) and 125 μm plate separation. When determining frequency dependent viscoelastic moduli, small torques in the range of 0.5 μNm were applied to ensure linear material response. 100 μL of samples were used for the analysis for full loading of the gap between plate and measuring head. The storage modulus G' and loss modulus G'' were recorded within frequencies of 0.1–10 Hz. The temperature during measurements was set to 21 °C.

Tribology. The friction measurements were conducted with a rotational tribology setup assembled on a shear rheometer (MCR 302, Anton Paar). The rheometer was equipped with a tribology unit (T-PTD 200, Anton Paar), and the measurements were performed in a sphere-on-cylinder geometry as described in Boettcher *et. al.*, 2014.[34] Steel spheres with a diameter of 12.7 mm were purchased at Kugel Pompel (Vienna, Austria). The cylinders were prepared by mixing PDMS (SYLGARD 184, Dow Corning) in a 10 : 1 ratio with the curing agent. Air bubbles were removed under vacuum and the PDMS was cured at 80 °C for 1 h. For each measurement, fresh cylinders were used that were cleaned with 80% (v/v) EtOH before usage. 600 μL of a 0.1% (w/v) mucin solution dissolved in 20 mM HEPES (pH 7.4) were added and the steel sphere was rotated on the PDMS cylinders at a normal force of 6 N. The friction behavior was evaluated by performing a speed ramp from 1000 to 0.01 mm s^{-1}. The measurements were conducted at 21 °C, and three individual measurements with fresh PDMS cylinders were performed for each condition.

Co-localization experiments. For determining the charge-selective permeability of mucin gels, mucin was rehydrated in ddH_2O and incubated with 10 μg mL^{-1} lectin (fluorescently labeled with rhodamine, Sigma-Aldrich, St. Louis, USA) for 1 h during shaking at 4 °C. 0.1 mg mL^{-1} of either negatively charged 150 kDa carboxymethyl (CM) dextrans or positively charged diethylaminoethyl (DEAE) dextrans (both obtained from Sigma-Aldrich, St. Louis, USA) fluorescently labeled with fluorescein isothiocyanate (FITC) were added to the mucin–lectin solution and incubated for another hour during shaking at 4 °C. To induce gelation of the mucin solution, 10% 10× phosphate buffer (pH 2) was added and the solution incubated for 1 h during shaking at 4 °C. The final mucin concentration was 1% (w/v). Fluorescence microscopy images were obtained on an Axioskop 2 MAT mot microscope (Zeiss, Oberkochen, Germany) equipped with a 20× objective (Zeiss) using a digital camera (Orca-R2 C10600, Hamamatsu, Japan) and the image acquisition software HCImageLive (Hamamatsu).

3. Results & discussion

A schematic overview of the optimized process is shown in Fig. 1. Dashed lines qualitatively indicate the mucin concentration and dilution during downstream steps. After harvesting the mucus from pig stomachs by manual scraping, the mucus was homogenized in buffer in the ratio 1 : 5, and cells, cell debris and finally lipids were removed in centrifugation steps. After the centrifugation steps, the pellets accounting for 33% and 10% of the total volume, were discarded, and we assumed that no mucin was lost within these steps. Next, a concentration step using cross-flow ultrafiltration was introduced. To our knowledge, this novel process step has not yet been published regarding mucin purification. It not only led to depletion of smaller proteins but also entailed an important volume reduction and concentration of the target protein. An increase in productivity was expected because a highly concentrated protein solution was further processed and thereby more protein was loaded onto the SEC while keeping the volume constant. Process parameters such as membrane pore size and

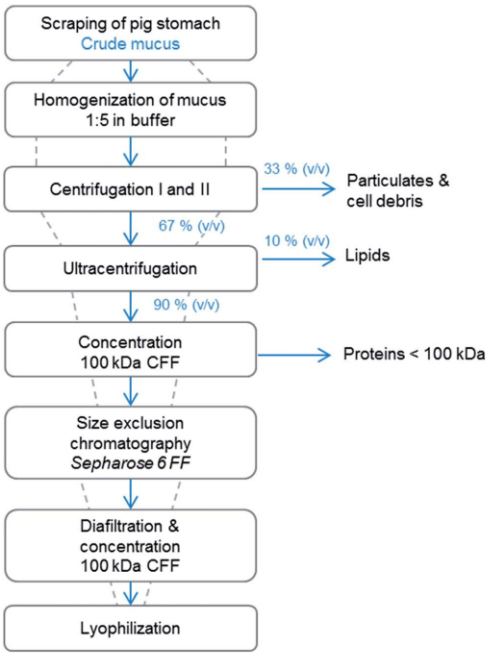

Fig. 1 Schematic illustration of the purification process of mucin from porcine stomachs. The dashed lines indicate the volume reduction or increase after each process step. After centrifugation II, the pellet, accounting for 33% of the volume, was discarded. After ultracentrifugation, the pellet, consisting of 10% of the total volume, was removed, before the supernatant was further concentrated with cross-flow filtration (CFF). Size exclusion chromatography was performed and finally salts were removed by CFF before the protein solution was lyophilized.

membrane system were investigated during cross-flow filtration and the yields of mucin compared. The following step, size exclusion chromatography, has already been used for the purification of mucins from animal or human sources.[26,27,35] Because of the high molecular weight of mucin in its native form, SEC is suitable for the separation of glycoproteins, and the fractions can be analyzed to detect carbohydrates and mucins. Thereafter, removal of salts (and further concentration in the upscaled process) was conducted by the same cross-flow ultrafiltration system, and the target protein was lyophilized. Samples were taken after each step of the purification process and analyzed both for glycoprotein content in general and Muc5AC content in particular. We did not determine the exact purity of the purified mucin with conventional protein assays such as UV absorption, BCA or Bradford reagent since – due to the high glycosylation density of mucin – the mucin concentration would be underestimated and thereby falsified results would be obtained when referring to a standard curve of a model protein such as BSA.

3.1. Influence of buffer composition and storage temperature

As a first step for optimizing the purification process and improving the yield of functional mucin, the influence of buffer additives such as salts and protease inhibitors as well as the influence of different storage temperatures on mucin quality were evaluated.

Influence of buffer. In former studies native mucins were mostly purified using 200 mM NaCl either as a hydration solution or running solvent during gel filtration.[6,8,26,36] However, the use of a buffered system for protein solubilization and gel filtration has only been described few times[25,36,37] where either a Tris–HCl buffer, or a sodium phosphate buffer was used for chromatography. For a robust downstream process buffered systems are especially important for biological systems to retain a reproducible process performance. Due to its pH-induced gelation behavior, the viscosity of mucin solutions is highly sensitive to pH, thus (partial) pH-induced mucin gelation during the purification process may lead to difficulties during chromatography by blocking the column material. We therefore chose a 10 mM sodium phosphate buffer at pH 7.0 for mucin dilution and chromatography to avoid mucin gelation. We added 170 mM NaCl to this buffer to mimic the total ionic strength used in former purifications. The functionality of mucin purified with this 10 mM sodium phosphate buffer (pH 7.0 supplemented with 170 mM NaCl) was determined with rheological measurements. No differences in the pH-induced gelation behavior of the mucin solutions were observed compared to mucin purified in 200 mM NaCl (ESI Fig. S2a†). Additionally, blocking of the column did not occur and stripping of the column could be set to a minimum. Hence, all further purification steps were conducted in a buffered system at pH 7.0.

Protease inhibitors. Next, process optimization was conducted by testing the necessity of additives like protease inhibitors and stabilizing agents. In small biochemical preparations of proteins from animal tissue, protease inhibitors such as benzamidine HCl and phenylmethylsulfonylfluoride are traditionally added at the beginning of the purification to protect the proteins from enzymatic cleavage by trypsin or serine proteases.[8,10] However, the use of additives should – if possible – be avoided: on the one hand, such protease inhibitors are typically toxic and, on the other hand, they constitute further contaminants that need to be removed again in later steps of the purification process. Glycoproteins are in general known for their resistance against proteolytic activity.[38–40] Also mucins are relatively insensitive to proteolytic digestion, which is due to their high density of carbohydrate side chains.[12] However, the highly glycosylated regions of mucin are intersected by non-glycosylated sequences that are protease-sensitive.[10] In our experiments we could not observe enzymatic proteolysis of PGM at pH 7. This might be explained by the fact that pepsin, the most abundant protease in the stomach, is inactive at neutral pH.[41] Thus, we tested a purification protocol at pH 7 and compared mucin functionality after purification in either the presence or the absence of a mix of sodium azide, benzamidine HCl, phenylmethylsulfonylfluoride, 2,4′-dibromoacetophenone, DMSO and EDTA, respectively. Again, we tested the gel-forming ability of the purified mucin and found that the absence of the above named components did not have any influence on mucin gel formation (ESI Fig. S2b†). This finding allowed us to omit those additives.

Storage temperature. The influence of the freezing and storage temperature of crude mucus (after centrifugation steps I and II) and purified mucin was evaluated by testing the gelation behavior of the corresponding solutions of reconstituted mucins. As freezing conditions for crude mucus and partially purified mucin, we compared snap freezing in liquid nitrogen, freezing in a −80 °C freezer and freezing in a −20 °C freezer. Our findings indicated that freezing of mucus samples at −80 °C was sufficient and no shock-freezing in liquid nitrogen was necessary. Furthermore, we found that, once lyophilized, the purified mucin is still able to form gels in the range of several pascal, even after long-term storage at room temperature (ESI Fig. S4†).

3.2. Process optimization of mucin purification

In general, the purification of proteins includes several steps until the desired purity is reached. In addition to obtaining a pure product, maintaining functionality of the molecule is a key goal. With every step, target protein is lost. Thus, the purification is usually a cost-intensive process making a high recovery of proteins and productivity essential. Early volume reduction is one step to increase the efficiency of the process. Thus, we first introduced cross-flow filtration as an essential measure during the purification process of mucins to achieve a concentration of mucin and, at the same time, depletion of undesired smaller proteins. Using the cross-flow configuration, the protein solution circulates tangentially to the membrane. By applying pressure, the solution permeates through the pores. With this process, less cake formation is observed on the membrane compared to dead-end filtration.[42] In the following,

the optimization of this cross-flow filtration is discussed in detail and subsequent size exclusion chromatography is presented.

Cross-flow filtration. For the concentration of centrifuged, partially purified mucin we examined two different systems, *i.e.* membrane cassettes and a hollow fiber membrane. Also, we varied membrane pore sizes and evaluated the permeate flux and fouling resistances as well as the recovery of the target protein. Δp_{TM} was varied between 0.5 and 1.5 bar, and we found that a Δp_{TM} of 1 bar resulted in the highest recovery of mucin in the retentate (ESI Fig. S5†). Thus, all following results were obtained using a Δp_{TM} of 1 bar. Two membrane cassettes (100 kDa Hydrosart®, 300 kDa PESU) and one hollow fiber membrane (100 kDa polysulfone) were compared with respect to flux and fouling resistance calculated according to eqn (3) and (4) (see Experimental). The volume concentration factor (VCF) was kept constant at 4.9 for all filtrations.

As presented in Fig. 2, the flux through the hollow fiber system decreased only weakly with time and reached a nearly constant value of 60 kg m^{-2} h^{-1} after 9 min. In contrast the flux through the membrane cassettes decreased much more strongly and reached final values of only 40 kg m^{-2} h^{-1} (300 kDa membrane) and 35 kg m^{-2} h^{-1} (100 kDa membrane) respectively, after the same time. For both membrane systems, the fouling resistance reached 4×10^{12} m^{-1} after 9 min, and there seemed to be a tendency towards even higher values. Conversely, the hollow fiber system reached a nearly constant fouling resistance just below 4×10^{12} m^{-1}.

The three membrane systems were also characterized in terms of their capability to retain glycoproteins in general and our target protein Muc5AC in particular. Fig. 3 displays the recovery of glycoproteins and Muc5AC in the retentate and permeate, respectively, after 4.9 fold volume concentration. The amount of protein collected in the washing steps of the membrane was included in the retentate.

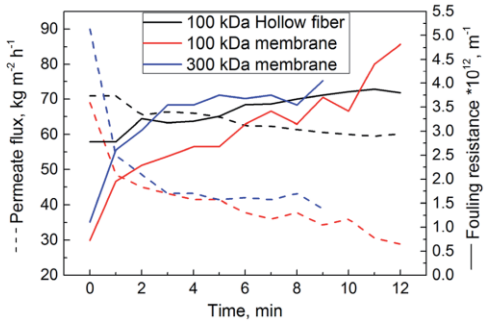

Fig. 2 Permeate flux (dashed lines) and fouling resistance (solid lines) determined for a 100 kDa hollow fiber system and membrane cassettes (100 kDa and 300 kDa, respectively) at $\Delta p_{TM} = 1$ bar. In each setup, 200 mL of mucin solution (containing 0.27 mg mL^{-1} Muc5AC) as obtained after the centrifugation steps were used for concentration. In all three systems, mucin concentration was performed until a volume concentration factor of 4.9 was reached.

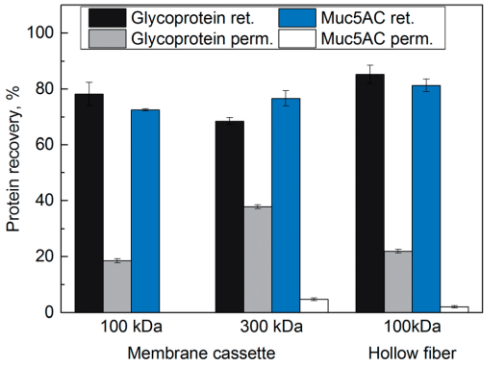

Fig. 3 Recovery of Muc5AC and total glycoprotein measured in the retentate (ret.) and permeate (perm.) after 4.9 fold volume concentration with 100 kDa (Hydrosart®) and 300 kDa (PESU) membrane cassettes and 100 kDa hollow fiber membrane (PSU) at $\Delta p_{TM} = 1$ bar. Protein recovered from the washing steps was included in the retentate values. Glycoprotein concentration was determined with quantitative PAS assay, Muc5AC concentration was determined with ELISA. Error bars represent the ±s.d. of analytical triplicates.

For the 100 kDa membrane cassette, 78% of the glycoproteins were retrieved in the retentate, whereas 19% glycoproteins were found in the permeate. The Muc5AC content in the retentate was 73%, the permeate was free of Muc5AC. Similar results were obtained with the hollow fiber module: with this cross-flow system, the recovery of glycoproteins in the retentate and permeate was 85% and 22% respectively. 81% of Muc5AC were retrieved in the retentate, and only 2% in the permeate. For the 300 kDa membrane, the glycoprotein content in the permeate was twice as high as for the 100 kDa membrane cassette, and 5% of Muc5AC was found in the permeate.

Glycoproteins as well as glycosylated peptides smaller than the nominal MWCO can pass the membranes. Typically, it is suggested to use a pore size three to six times smaller than the molecular weight of the target protein for successful retention. As Muc5AC has a monomer size of approximately 640 kDa,[7] the MWCO of 300 kDa may not be ideal. Indeed, the highest mucin concentration was detected in the permeate of this cross-flow variant. Both 100 kDa membranes showed a better retention of the target protein Muc5AC in contrast to the 300 kDa membrane as is shown in Fig. 3.

Despite the MWCO, the differences in filtration- and retention behavior might also be explained by the different geometries of the filtration setups. For the ultrafiltration systems used here, diffusion dominates over hydrodynamic effects.[30] Filtration through a membrane creates a concentration polarization of the protein solution towards the surface which can, in laminar flow conditions, lead to irreversible gel layer formation. To decide which flow conditions apply in our three setups, we estimated the flow within the different modules by calculating the Reynolds number (ESI Table S1†). For these calculations, we approximated the mucin solution with the viscosity and density of water (0.89 mPa s and 1000 kg m^{-3}, respectively) and

assumed a mean diffusion coefficient for mucins of 4×10^{-8} cm^2 s^{-1}.[43] For all configurations, the boundary layer was calculated using the Sherwood and Schmidt number (see Experimental). The calculated boundary layer thickness was 0.01 μm for the hollow fiber system and 19 to 20 μm for the membrane cassettes (Table S1†). For the hollow fiber, the calculated Reynolds number suggested a turbulent flow through the filtration area ($Re > 4 \times 10^4$). Shear forces created by the turbulent flow drag the molecules away from the concentration polarization zone and membrane surface, creating a thinner and mostly reversible boundary layer. A steady state of flux and fouling resistance is reached after a certain time. In contrast, the flow through both membrane cassettes was laminar ($Re < 10^4$). Because laminar flow promotes the deposition of molecules on the membrane surface and thereby leads to a continuous decrease in flux and increase in fouling resistance, as was indeed observed for both membrane cassettes (Fig. 2), we concluded that an irreversible gel layer must have formed on the membranes. The layers built on the membrane cassettes might also explain a loss of product of up to 28%. For the hollow fiber the loss of protein was lower at 17%.

In addition, a difference in the adsorption behavior of mucin on the different membrane materials may have to be considered when it comes to protein loss. Mucins adsorb especially well on hydrophobic surfaces.[4,44,45] However, regenerated cellulose as well as polyethersulfone are both hydrophilic materials and are supposed to exhibit only minimal protein binding (as claimed by the manufacturer Sartorius). Together with our observations above and the fact that the hollow fiber system reached a flux twice as high as the membrane cassettes although having a surface area of nearly half the membrane area of the membrane cassettes, we concluded that a hollow fiber system is advantageous, especially for upscaling of the process: our hollow fiber module can handle larger sample volumes at a constant flux and therefore was chosen as the cross-flow system in the up-scaled process we describe later. However, on a smaller scale, the membrane cassettes may be preferable since the minimal volume needed for the cassette system is at 20 mL significantly smaller than the approx. 80 mL that are required for running the hollow fiber system. For better comparability and because no target protein was lost in the permeate, the small purification process was conducted with the 100 kDa membrane cassette. The optimized parameters of $\Delta p_{TM} = 1$ bar and a pore size of 100 kDa were also transferred to the diafiltration step after chromatography. The results are discussed in the summary of the purification process.

Size exclusion chromatography. After the concentration of mucus by cross-flow filtration, 20 mL (0.11 CV) of concentrated mucus (0.42 mg mL^{-1} Muc5AC) were injected onto a Sepharose 6 *Fast Flow* column. The obtained chromatogram showed two major peaks at a wavelength of 280 nm (Fig. 4). The first peak eluted after 52 mL (0.29 CV), whereas the major peak, containing proteins of smaller sizes appeared between 100 and 250 mL (0.57–1.4 CV). Fractions were analyzed for glycoproteins by qualitative PAS assay. Glycoproteins were mostly found in the first peak. Since the purity of mucin was of high importance to obtain a gelation behavior at acidic pH, the fractions that overlapped with the major peak containing contaminating proteins were omitted. The fractions (gray in Fig. 4) were finally pooled, analyzed for protein content and prepared for diafiltration. The Muc5AC concentration obtained was 0.38 mg mL^{-1}. Muc5AC was completely recovered (see also Table 1), whereas the recovery of general glycoprotein in the pooled fractions was only 83% (ESI Table S3†). This indicated that the SEC step was successful in further decreasing the content of non-mucin glycoproteins.

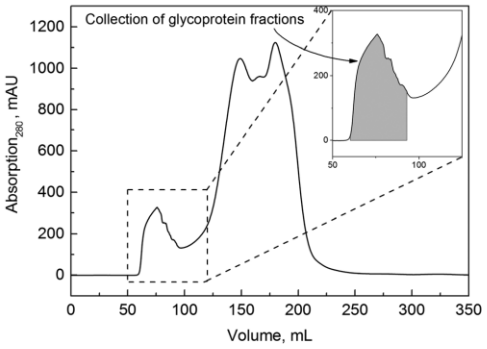

Fig. 4 Size exclusion chromatogram of concentrated mucus at 280 nm. Flowrate: 30 cm h^{-1}, column volume: 176 mL, column diameter: 16 mm, running buffer: 10 mM phosphate buffer with 170 mM NaCl, pH 7. The grey area indicates the fractions that were pooled after screening for glycoproteins with PAS assay.

Diafiltration. For the diafiltration step, the optimized parameters of the concentration step ($\Delta p_{TM} = 1$ bar and a pore size of 100 kDa) were used again. Since the process volume after SEC was small compared to the cassette volume, no further volume reduction of the target solution was possible. We performed diafiltration until the conductivity of the mucin solution was less than 100 μS cm^{-1} in the retentate. The reason for this choice was twofold: first, low ionic strength was required to successfully induce gelation of a 1% (w/v) solution of purified mucin at pH 2.[15] Second, the diafiltrated mucin solution was, in a last step, lyophilized to receive a stable product that could be stored at room temperature. A low concentration of remaining ions in the lyophilized mucin allowed for reconstituting mucin solutions with arbitrary buffer conditions, *i.e.* both at high and low ionic strength.

Yield and productivity of the purification process. Maximum Muc5AC yields of 66% were achieved with the illustrated process referring to the concentration after centrifugation (see Fig. 1). The yields per purification step are summarized in Table 1. As already mentioned, purity was not determined quantitatively due to the possible underestimation of glycoproteins. Instead, SDS-PAGE (Fig. S3b†) showed that our purified mucin did not contain visible amounts of contaminating proteins with molecular weights smaller than 212 kDa. However, no statement can be made about the presence of other high molecular weight proteins such as similar glycoproteins. A 4.9 fold volume

Appendix A.4 An optimized purification process for porcine gastric mucin with preservation of its native functional properties

Table 1 Summary and yield of the overall Muc5AC purification process following the optimized protocol (*i.e.* mucus concentration with the 100 kDa membrane cassette system, Sepharose 6 *Fast Flow* size exclusion chromatography (CV = 176 mL), 100 kDa diafiltration). Mucin yield, concentrations, process volumes and mass before and after each purification step, volume concentration factor VCF and concentration factor CF are given for each step. Determination of Muc5AC concentration was conducted with ELISA. Results shown represent the mean ± s.d. of analytical triplicates

Downstream process step	Yield, %	c_{before}, mg mL^{-1}	c_{after}, mg mL^{-1}	V_{before}, L	V_{after}, L	m_{before}, mg	m_{after}, mg	VCF	CF
Concentration	73 ± 7	0.27 ± 0.02	0.42 ± 0.01	0.196	0.09	52.4 ± 3.4	38.1 ± 0.2	4.9[b]	3.5[b]
Chromatography	113 ± 6	0.42 ± 0.01	0.38 ± 0.03	0.02	0.025	8.5 ± 0.1	9.5 ± 0.6	—	—
Diafiltration	80 ± 7	0.38 ± 0.03	0.18 ± 0.01	0.025	0.042	9.5 ± 0.6	7.6 ± 0.3	—	—
Lyophilization	—			0.042			13.1[a]	—	—
Total	66%						13.1[a]		

[a] Weighed after lyophilization; purified mucin after purification of 20 mL concentrated mucus. [b] Before washing of membrane.

concentration with cross-flow filtration resulted in 40 mL retentate. The washing volume of 50 mL was also analyzed for Muc5AC content and pooled with the retentate, finally yielding a 90 mL retentate solution. A yield of 73% with the optimized concentration protocol was achieved. 20 mL (according to 0.11 CV) of 90 mL retentate were loaded onto our gel filtration system. The purification using size exclusion chromatography resulted in a complete recovery of Muc5AC. In diafiltration, a yield of 80% was achieved. Due to different analysis methods there was a discrepancy in the calculated amount of Muc5AC after diafiltration (7.6 ± 0.3 mg) and the weight obtained after lyophilization (13.1 mg). The increase by 5.5 mg might be explained by the presence of other high molecular weight mucins such as Muc6 present in porcine stomach mucus[46,47] or residual DNA indicating that the purity of Muc5AC was around 60%. For yield and productivity calculations and further experiments the lyophilized mucin was used. In total, 13.1 mg mucin from 20 mL concentrated mucus before chromatography was purified. Assuming that no mucin was lost during the first process units until concentration the overall recovery was 1.0 mg mucin per mL crude mucus after stomach scraping. The productivity was 0.08 mg mL$_{crude\ mucus}^{-1}$ h^{-1} referring to the process time from the concentration of mucus, over SEC to diafiltration, not accounting lyophilization.

Scale-up of mucin purification. As mentioned earlier, the amount of scraped mucus and mucin concentration differed for each stomach. Although 20 to 60 stomachs were pooled before purification experiments, variances in initial mucin concentrations and scraping procedure were observed between the batches and might account for the 8.7 fold higher Muc5AC initial concentration of 2.34 mg mL^{-1}.

To satisfy the demand of purified native mucin a scale-up to the 10 fold column volume of size exclusion chromatography was aimed for. Optimized parameters were transferred to the large scale and the scale-up was analytically analyzed in terms of concentration and concentration factors, yield and productivity. Its results are summarized in Table 2. A total Muc5AC yield of 33% was achieved. During concentration with the hollow fiber membrane the volume was reduced by a factor of 4. Due to the high initial filtration volume, the washing volume has less impact compared to the small scale. The Muc5AC concentration was increased from 2.34 to 3.34 mg mL^{-1} resulting in a yield of 36%. During SEC, again a total recovery of the target protein was obtained, while diluting the protein by a factor of 0.6. During subsequent diafiltration with the 100 kDa hollow fiber membrane salts were removed and the sample further concentrated by a factor of two in terms of volume and a factor of 1.7 with regard to Muc5AC. 85% were yielded in the diafiltration step.

In total, 482 mg mucin was purified from 180 mL concentrated mucus before SEC, accounting for 236 mL crude scraped mucus. The upscaled purification process was reproduced four times with a mean mucin amount of 382 mg, resulting in 1.63

Table 2 Summary and yield of the overall upscaled Muc5AC purification process following the optimized protocol (*i.e.* mucus concentration with the 100 kDa hollow fiber system, Sepharose 6 *Fast Flow* size exclusion chromatography (CV = 1650 mL), 100 kDa hollow fiber diafiltration). Mucin yield, concentrations, process volumes and mass before and after each purification step, volume concentration factor VCF and concentration factor CF are given for each step. Determination of Muc5AC concentration was conducted with ELISA. Results shown represent the mean ± s.d. of analytical triplicates

Downstream process step	Yield, %	c_{before}, mg mL^{-1}	c_{after}, mg mL^{-1}	V_{before}, L	V_{after}, L	m_{before}, mg	m_{after}, mg	VCF	CF
Concentration	36 ± 32	2.34 ± 0.45	3.34 ± 0.86	0.72	0.18	1685 ± 324	601 ± 154	4.0	3.2[b]
Chromatography	109 ± 27	3.34 ± 0.86	2.18 ± 0.22	0.18	0.3	601 ± 154	655 ± 66	—	—
Diafiltration	85 ± 23	2.18 ± 0.22	3.71 ± 0.79	0.3	0.15	655 ± 66	556 ± 118	—	—
Lyophilization		0.32					482[a]	—	—
Total	33%						382[c]		

[a] Weighed after lyophilization; purified mucin after purification of 180 mL concentrated mucus. [b] Before washing of membrane. [c] Mean of $n = 5$ purifications.

mg of purified mucin per mL crude mucus. We were able to purify 65 mg mucin per stomach with 40 mL mucus in one stomach (mean of 60 stomachs). During one purification process the content of up to six stomachs could be processed and their containing mucin purified. The productivity of the optimized upscaled process was 0.15 mg $mL_{crude\ mucus}^{-1}\ h^{-1}$.

The yields are in accordance to the yields achieved in the small scale and only differ in the concentration step (36 ± 32% compared to 73 ± 7% in the small scale). The initial concentration of the target protein was 2.34 mg mL^{-1} and thus by factor 8.7 higher than the initial concentration of the small scale process (0.27 mg mL^{-1}). These differences are most likely based on different batches, where mucin concentrations in the stomachs are not predictable. The tangential flow filtration of a highly concentrated solution, containing not only proteins but also rests of DNA, phospholipids and solutes causes a high concentration on the membrane surface, possibly triggering the buildup of a gel layer.[48,49] Even after the washing of the membrane and collection of the washing solution, the recovery of Muc5AC did not increase. In our previous studies performed with initially 0.2–0.3 mg mL^{-1} concentrated mucin solutions, no such loss of Muc5AC occurred (see also Fig. 2). The Muc5AC concentrations during the concentration and diafiltration step are nearly the same at 2.34 and 2.18 mg mL^{-1}, respectively. However, in the concentration process many contaminating proteins were present while in the protein solution to be diafiltered an already purified solution was applied. Thus, fewer solutes accumulate on the membrane interface leading to a lower decrease in flux and higher recovery.[50] Additionally, the standard deviation of 32% might be the result of varieties in ELISA signal. It has been stated that high concentrations of contaminating proteins or lipids might lead to cross reactivity with the target protein.[51] This phenomenon is apparent with the high amount of contaminations from crude mucus like phospholipids and (glyco-) proteins and variances in biological material in general. Considering that the diafiltration step which was performed under the same conditions as the concentration step resulted in a yield of 85%, underestimation of the Muc5AC concentration in the first filtration step is probable due to shielding of the antibody binding region. We observed that ELISA provided the most reliable results after the concentration step of mucus.

Although the time needed for filtration increased with the processed volume and the recovery of the concentration process was lower in the upscaled process, productivity was 2 fold compared to the small scale process due to the high load onto the size exclusion chromatography, being 0.15 mg $mL_{crude\ mucus}^{-1}\ h^{-1}$.

3.3. Quality control of purified mucin

As described above, the optimized and upscaled process of PGM purification resulted in a considerable improvement of the overall mucin amount as well as in a 2 fold increase in productivity (*i.e.* purified mucin per mL crude mucus and time). The quality of the purified mucin obtained from the optimized process was assessed by testing if its unique properties were preserved. Only then would the purified mucin be suitable for academic or biomedical applications. We first analyzed the gel-forming abilities of mucin at pH 2 and then investigated the lubricity of mucin solutions. As a high density of sugar molecules is required for the superior lubricity of mucin solutions,[4,18,19] such friction force measurement can indirectly demonstrate the intactness of mucin glycosylation. Additionally, we probed the selective binding properties of mucins with co-localization experiments.[2]

Gelation of mucin solutions. For verifying the gel-forming abilities of purified mucin, rheological measurements were conducted. Fig. 5 depicts the frequency-dependent viscoelastic moduli G' and G'' as determined at a shear frequency of 1 Hz for 1% (w/v) mucin solutions at pH 2 and 6. At acidic conditions, the purified mucin formed a clear gel with a shear stiffness in the range of $\sim 10^1$ Pa whereas at pH 6 the viscous properties of the mucin solution dominated. This observation was the expected behavior for solutions of functional porcine gastric mucin[5,11,13–15] and showed that this important mucin property was preserved after process optimization and upscaling. In contrast, solutions reconstituted from commercial porcine gastric mucin (Sigma Aldrich type II and III) lacked the ability to form a gel at acidic pH. This suggested that the mucin was somehow damaged during the commercial purification process, potentially by breaking the molecule into subunits or affecting important chemical moieties of the glycoprotein due to harsh conditions during the purification procedure.[16,24]

Lubricity of mucin solutions. Solutions of porcine gastric mucins are excellent lubricants, especially in the boundary lubrication and mixed lubrication regime.[4,18,19] Friction values measured in a steel/PDMS tribology pairing at low sliding speeds can be as low as 0.01.[19] These low friction values were suggested to originate from hydration lubrication: mucins adsorb very well on hydrophobic surfaces such as PDMS and form thin surface layers.[4] In these mucin layers, the oligosaccharide side-chains on the mucin backbone bind water. During the application of shear forces, energy is dissipated by moving the water molecules in this mucin layer, and this leads

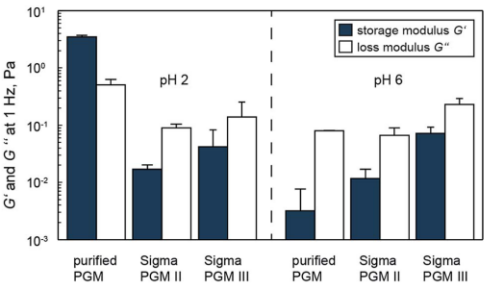

Fig. 5 Comparison of the storage modulus G' and loss modulus G'' of 1% (w/v) mucin solution at acidic (pH 2) and nearly neutral (pH 6) conditions. Solutions of manually purified and commercial PGMs are compared. Only the manually purified mucin solutions show pH-induced gelation. Error bars represent the ± s.d. of analytical triplicates.

to strongly reduced friction. In a tribological setup (see Experimental), we compared the friction between PDMS and steel when lubricated with 0.1% (w/v) mucin solutions and compared this scenario to lubrication with 20 mM HEPES buffer (pH 7). As displayed in Fig. 6, mucin solutions obtained from the optimized and upscaled purification process do indeed reach very low friction values around 0.01 and showed a good lubricity. In contrast, the commercial PGMs type II and III from Sigma Aldrich were poor lubricants, especially in the boundary lubrication regime, where their lubricity was virtually indistinguishable from buffer without mucin. We speculated that, for the commercial mucins, either the formation of a mucin surface layer is disturbed or mucin hydration is low.[19]

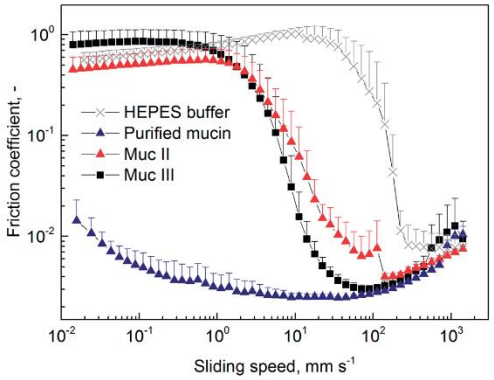

Fig. 6 Lubrication of a PDMS/steel setup with 20 mM HEPES buffer (pH 7) or 0.1% mucin solutions (self-purified PGM or commercial PGM type II and III, dissolved in 20 mM HEPES, pH 7). The friction coefficient was determined over a broad range of sliding speeds. Error bars represent the s.d. obtained from analytical triplicates.

Selective permeability of mucin gels. In the body of mammalians, mucin gels constitute a barrier towards pathogens and bacteria.[2,3] Previous studies showed that PGM convey selective permeability to mucin gels: depending on their surface charge, particles and molecules show different mobility in mucus and reconstituted mucin gels. Mucin glycoproteins carry several negative charges, especially through sialic acid or sulfate groups.[11] As a consequence, mucins have been described to bind cationic molecules with much higher efficiency than anionic molecules.[20,52] Therefore, we compared the behavior of two different fluorescently labelled dextran variants in mucin gels: anionic carboxymethyl dextran (CM-dextran) and cationic diethylaminoethyl dextrans (DEAE-dextran) in mucin gels at pH 2. Fig. 7 depicts the outcome of a co-localization experiment. Whereas anionic dextrans homogeneously distributed in the mucin gel, the cationic dextrans colocalized with the mucins. This verified that gels reconstituted from purified mucin exhibit selective permeability. Since the commercial PGMs do not form gels at acidic pH, the selective binding properties of these mucins could not be assessed here.

4. Conclusions

Mucins from porcine stomachs intended for lubrication studies or virus–mucin interaction studies[19,53] have recently gained much attention. However, most commercially available PGMs lack crucial properties, in particular the ability to form gels at acidic pH and possessing sufficient lubricity. We have described a successful purification process for native mucin from pig stomachs that satisfies the demands of functional PGM for biomedical applications. Furthermore, we evaluated and improved important aspects of protein purification including buffer composition, volume reduction, efficiency, yield and functionality of the purified mucin. We were able to purify 65

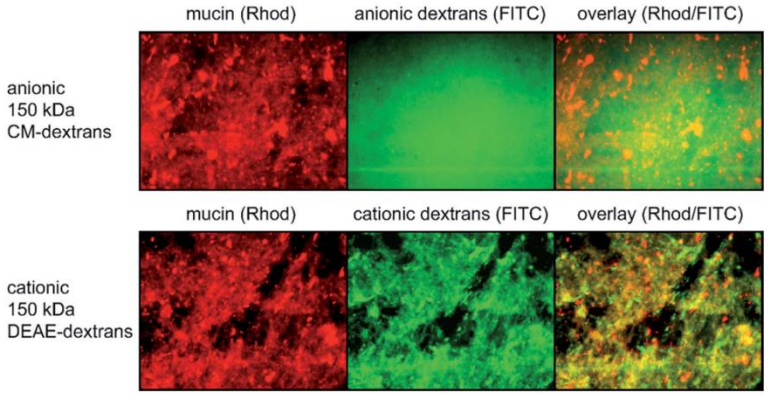

Fig. 7 Selective permeability of mucin gels reconstituted at pH 2: fluorescence microscopy images of rhodamine labeled mucin mixed with FITC-labeled 150 kDa charged dextran molecules. The rhodamine channel depicts the spatial distribution of mucin, the FITC channel the distribution of dextran molecules. The two channels are merged into one picture, displayed in the overlay image and show the co-localization of cationic dextrans and mucin.

mg mucin per pig stomach at a productivity of 0.15 mg mucin per mL crude mucus and hour. The process was successfully upscaled with the purified mucin retaining the desired key properties of gel formation at acidic pH, lubricity and preservation of binding interactions with charged molecules.

The purification method discussed here can be applied to a wide range of diverse high molecular weight glycoproteins including mucins obtained from various sources such as those from human saliva. Because synthetic mucins with the identical properties of PGM are not available yet, efficient purification of endogenous mucins remains the only viable strategy for large-scale production of these glycoproteins. In future studies, we intend to introduce alternative capture steps such as liquid–liquid extraction to further optimize productivity to meet the increasing demand for these glycoproteins in research and biomedical applications.

Abbreviations

BSA	Bovine serum albumin
CF	Concentration factor
CV	Column volume
FITC	Fluorescein isothiocyanate
GI	Gastrointestinal tract
Muc5AC	Mucin 5AC
MWCO	Molecular weight cut off
PDMS	Polydimethylsiloxane
PGM	Porcine gastric mucin
s.d.	Standard deviation
SEC	Size exclusion chromatography
VCF	Volume concentration factor

Acknowledgements

We thank Franziska Hirschmann and Eda Isik for conducting pilot experiments and Sabine Günzkofer for technical assistance. The project has been funded by the Dean's Innovation Fond of the TUM Department of Mechanical Engineering of the Technical University of Munich. OL and BTK gratefully acknowledge the financial support of the Deutsche Forschungsgemeinschaft (DFG) through grant LI 1902/3-1.

Notes and references

1 A. Allen, The structure and function of gastrointestinal mucus, in *Basic Mechanisms of Gastrointestinal Mucosal Cell Injury and Protection*, Baltimore, 1981.
2 O. Lieleg, C. Lieleg, J. Bloom, C. B. Buck and K. Ribbeck, *Biomacromolecules*, 2012, **13**, 1724–1732.
3 M. A. McGuckin, S. K. Lindén, P. Sutton and T. H. Florin, *Nat. Rev. Microbiol.*, 2011, **9**, 265–278.
4 S. Lee, M. Müller, K. Rezwan and N. D. Spencer, *Langmuir*, 2005, **21**, 8344–8353.
5 X. Cao, R. Bansil, K. R. Bhaskar, B. S. Turner, J. T. LaMont, N. Niu and N. H. Afdhal, *Biophys. J.*, 1999, **76**, 1250–1258.
6 L. A. Sellers, A. Allen, E. R. Morris and S. B. Ross-Murphy, *Carbohydr. Res.*, 1988, **178**, 93–110.
7 R. Mejías-Luque, L. Cobler and C. de Bolós, Atlas of Genetics and Cytogenetics in Oncology and Haematology, 2011, vol. 14, pp. 566–569.
8 A. J. Libao-Mercado and C. F. M. de Lange, *Livest. Sci.*, 2007, **109**, 141–144.
9 B. Jan-Willem Van Klinken, A. W. C. Einerhand, H. A. Büller and J. Dekker, *Anal. Biochem.*, 1998, **265**, 103–116.
10 G. J. Strous and J. Dekker, *Crit. Rev. Biochem. Mol. Biol.*, 1992, **27**(1/2), 57–92.
11 R. Bansil and B. S. Turner, *Curr. Opin. Colloid Interface Sci.*, 2006, **11**, 164–170.
12 K. Jumel, I. Fiebrig and S. E. Harding, *Int. J. Biol. Macromol.*, 1996, **18**, 133–139.
13 A. Maleki, G. Lafitte, A. L. Kjoniksen, K. Thuresson and B. Nystrom, *Carbohydr. Res.*, 2008, **343**, 328–340.
14 K. R. Bhaskar, D. H. Gong, R. Bansil, S. Pajevic, J. A. Hamilton, B. S. Turner and J. T. LaMont, *Am. J. Physiol.*, 1991, **261**, G827–G832.
15 J. P. Celli, B. S. Turner, N. H. Afdhal, R. H. Ewoldt, G. H. McKinley, R. Bansil and S. Erramilli, *Biomacromolecules*, 2007, **8**, 1580–1586.
16 J. Kočevar-Nared, J. Kristl and J. Šmid-Korbar, *Biomaterials*, 1997, **18**, 677–681.
17 I. C. Hahn Berg, L. Lindh and T. Arnebrant, *Biofouling*, 2004, **20**, 65–70.
18 J. M. Coles, D. P. Chang and S. Zauscher, *Curr. Opin. Colloid Interface Sci.*, 2010, **15**, 406–416.
19 T. Crouzier, K. Boettcher, A. R. Geonnotti, N. L. Kavanaugh, J. B. Hirsch, K. Ribbeck and O. Lieleg, *Adv. Mater. Interfaces*, 2015, **2**, 1500308.
20 L. D. Li, T. Crouzier, A. Sarkar, L. Dunphy, J. Han and K. Ribbeck, *Biophys. J.*, 2013, **105**, 1357–1365.
21 A. A. Feiler, A. Sahlholm, T. Sandberg and K. D. Caldwell, *J. Colloid Interface Sci.*, 2007, **315**, 475–481.
22 O. Lieleg, I. Vladescu and K. Ribbeck, *Biophys. J.*, 2010, **98**, 1782–1789.
23 N. V. Efremova, Y. Huang, N. A. Peppas and D. E. Leckband, *Langmuir*, 2002, **18**, 836–845.
24 O. Svensson and T. Arnebrant, *Curr. Opin. Colloid Interface Sci.*, 2010, **15**, 395–405.
25 M. Faure, D. Moënnoz, F. Montigon, L. B. Fay, D. Breuillé, P. A. Finot, O. Ballèvre and J. Boza, *Anal. Biochem.*, 2002, **307**, 244–251.
26 M. Mantle and A. Allen, *Biochem. J.*, 1981, **195**, 267–275.
27 T. Marshall and A. Allen, *Biochem. J.*, 1978, **173**, 569–578.
28 R. Gupta, N. Jentoft, A. M. Jamieson and J. Blackwell, *Biopolymers*, 1990, **29**, 347–355.
29 J. Dekker, W. Van Beurden-Lamers, A. Oprins and G. J. Strous, *Biochem. J.*, 1989, **260**, 717–723.
30 T. Melin and R. Rautenbach, *Membranverfahren – Grundlagen der Modul- und Anlagenauslegung*, Springer Verlag, 2007.
31 B. Espinasse, P. Bacchin and P. Aimar, *Desalination*, 2002, **146**, 91–96.
32 S. Ripperger and T. Grein, *Chem. Ing. Tech.*, 2007, **79**, 1765–1776.

33 M. Kilcoyne, J. Q. Gerlach, M. P. Farrell, V. P. Bhavanandan and L. Joshi, *Anal. Biochem.*, 2011, **416**, 18–26.
34 K. Boettcher, S. Grumbein, U. Winkler, J. Nachtsheim and O. Lieleg, *Rev. Sci. Instrum.*, 2014, **85**, 093903.
35 I. Carlstedt, H. Lindgren, J. K. Sheehan, U. Ulmsten and L. Wingerup, *Biochem. J.*, 1983, **211**, 13–22.
36 J. P. Pearson, A. Allen and S. Parry, *Biochem. J.*, 1981, **197**, 155–162.
37 Z. Kučerová, H. Muselová, E. Miarková and M. Tichá, *Prague Med. Rep.*, 2010, **111**, 200–206.
38 M. Scawen and A. Allen, *Biochem. J.*, 1977, **163**, 363–368.
39 N. Jentoft, *Trends Biochem. Sci.*, 1990, **15**, 291–294.
40 A. Allen and A. Garner, *Gut*, 1980, **21**, 249–262.
41 D. W. Piper and B. H. Fenton, *Gut*, 1965, **6**, 506–508.
42 A. Saxena, B. P. Tripathi, M. Kumar and V. K. Shahi, *Adv. Colloid Interface Sci.*, 2009, **145**, 1–22.
43 R. Bansil, E. Stanley and J. T. Lamont, *Annu. Rev. Physiol.*, 1995, **57**, 635–657.
44 M. Malmsten, E. Blomberg, P. Claesson, I. Carlstedt and I. Ljusegren, *J. Colloid Interface Sci.*, 1992, **151**, 579–590.
45 L. Shi and K. D. Caldwell, *J. Colloid Interface Sci.*, 2000, **224**, 372–381.
46 H. Nordman, J. R. Davis, A. Herrmann, N. G. Karlsson, G. C. Hansson and I. Carlstedt, *Biochem. J.*, 1997, **326**, 903–910.
47 S. K. Linden, P. Sutton, N. G. Karlsson, V. Korolik and M. A. McGuckin, *Mucosal Immunol.*, 2008, **1**, 183–197.
48 L. G. Peeva, E. Gibbins, S. S. Luthra, L. S. White, R. P. Stateva and A. G. Livingston, *J. Membr. Sci.*, 2004, **236**, 121–136.
49 L. Song and M. Eiimelech, *J. Chem. Soc., Faraday Trans.*, 1995, **91**, 3389–3398.
50 G. B. van den Berg and C. A. Smolders, *Desalination*, 1990, **77**, 101–133.
51 J. Schiettecatte, E. Anckaert, J. Smitz, *Adv. Immunoassay Technol.*, ed. N. H. Chiu, InTech, Croatia, 2012, ch. 3, pp. 45–62.
52 C. Nowald, A. Penk, H.-Y. Chiu, T. Bein, D. Huster and O. Lieleg, *Macromol. Biosci.*, 2016, **16**, 567–579.
53 B. A. Dancho, H. Chen and D. H. Kingsley, *Int. J. Food Microbiol.*, 2012, **155**, 222–226.

ESI - Electronic Supplementary Information

An optimized purification process for porcine gastric mucin with preservation of its native functional properties

Veronika J. Schömig[a], Benjamin T. Käsdorf[b], Christoph Scholz[a], Konstantinia Bidmon[b], Oliver Lieleg[b], Sonja Berensmeier[a*]

a Bioseparation Engineering Group, Department of Mechanical Engineering, Technical University of Munich, Boltzmannstr. 15, D-85748 Garching, Germany

b Institute of Medical Engineering and Department of Mechanical Engineering, Technical University of Munich, Boltzmannstr. 11, D-85748 Garching, Germany

* Corresponding author, s.berensmeier@tum.de

Gel formation of 1 % or 2 % (w/v) self-purified mucin only differs in strength of the gel:

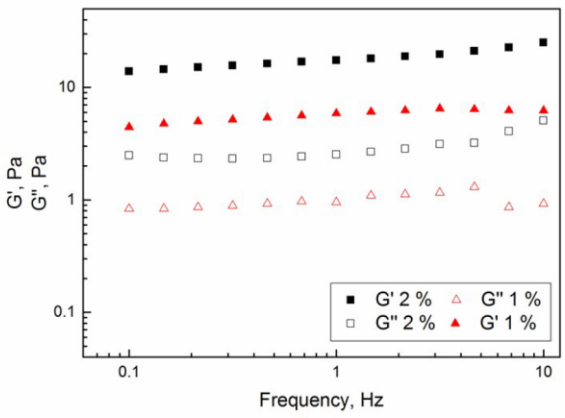

Figure S1. Frequency dependent storage (G') and loss modulus (G'') between 0.1 and 10 Hz for 1 % and 2 % (w/v) purified mucin at pH 2. No qualitative difference is observed in gel-forming behavior; only the strength of the gel is reduced with lower concentration.

Rheological measurement to determine the influence of 10 mM phosphate buffer containing 170 mM NaCl compared to the unbuffered system (200 mM NaCl) (a), and rheological measurements to determine the influence of protease inhibitors during the purification process (b):

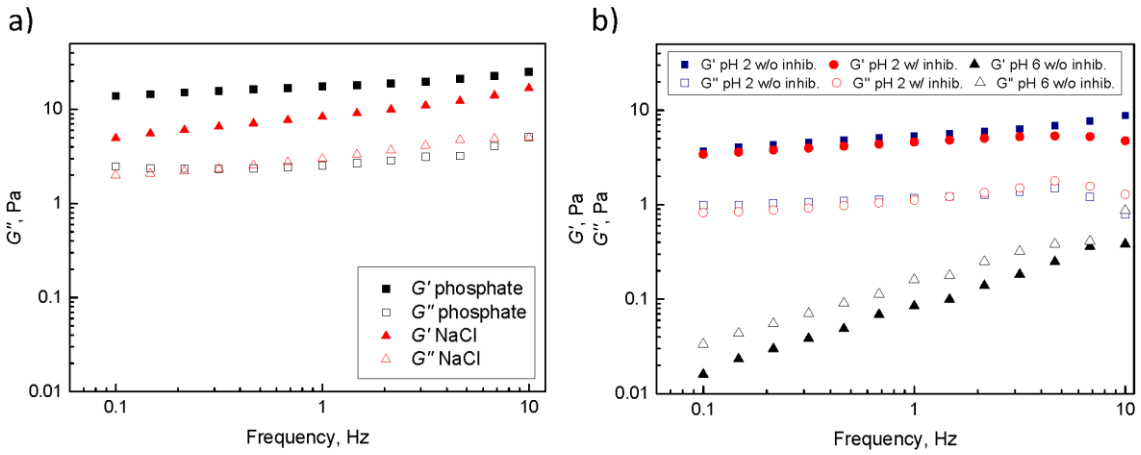

Figure S2. Frequency dependent storage (*G'*) and loss modulus (*G''*) between 0.1 and 10 Hz. a) Rheological measurements of 2 % (w/v) mucin purified in either 200 mM NaCl (NaCl) or 10 mM phosphate buffer containing 170 mM NaCl (phosphate) at pH 2. b) Rheological measurements of 1 % (w/v) mucin purified in 10 mM phosphate buffer and 170 mM NaCl with and without protease inhibitors at pH 2.

Enzymatic digestion of mucin with pepsin in 10 mM phosphate buffer pH 2/ 5/ 7/ 9: SDS-PAGE was used as qualitative analysis of digested and undigested mucins.

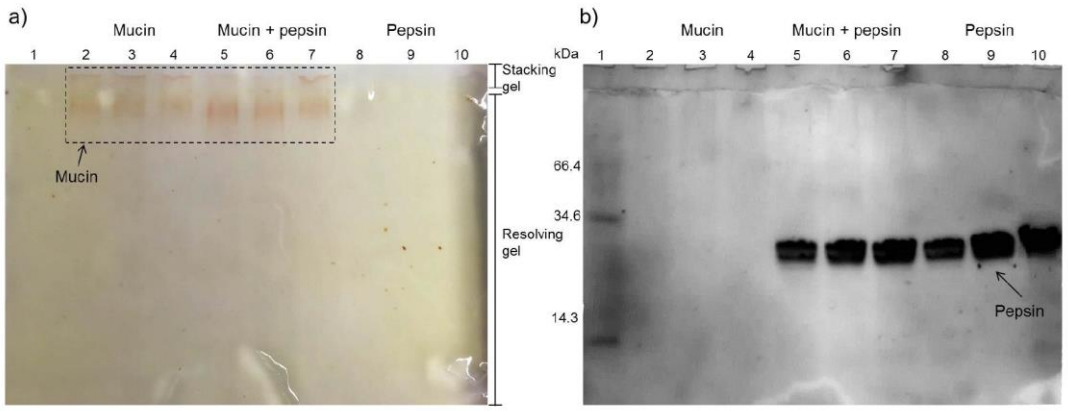

Figure S3. SDS-PAGE of undigested and digested mucin, and pure pepsin at pH 2, 5, and 7. a) Staining of glycoproteins with thymol staining. b) Staining of the same gel with Coomassie Brilliant G250 for detection of all proteins. Lane 1 Marker, Lanes 2-4: pure mucin (13 µg) at pH 2, 5, 7. Lanes 5-7: digested mucin with pepsin (13 µg mucin with 500 µg pepsin) at pH 2, 5, 7. Lanes 8-10: pepsin (500 µg) at pH 2, 5, 7. The stacking and resolving gel are displayed.

Influence of temperature before and after purification:

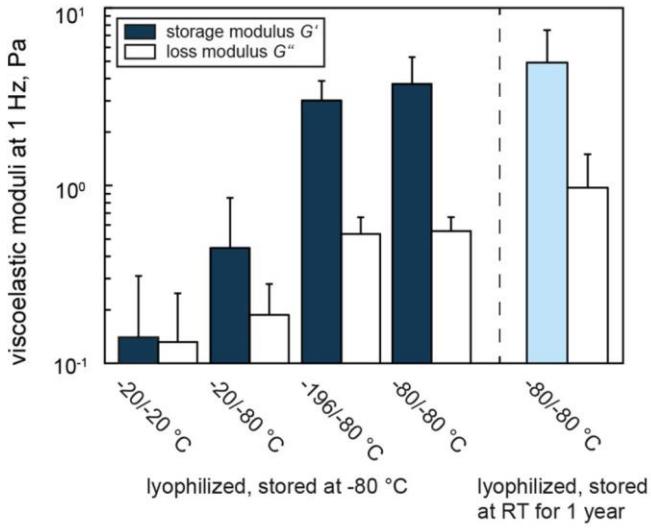

Figure S4. Viscoelastic moduli *G'* and *G''* of 1 % (w/v) mucin solution at pH 2 and 1 Hz for different storage temperatures of mucus/mucin. Column sets 1-4: Unpurified mucus was frozen at either -20 °C, -80 °C or in liquid nitrogen and long-term stored afterwards at -20 °C or -80 °C. Purified and lyophilized mucin was stored at -80 °C. Column set 5: Unpurified mucus

was frozen and stored at -80 °C, purified, lyophilized and stored at room temperature afterwards for 1 year in an Eppendorf tube. The -20/-20 °C freeze/storage condition did not always form a gel. The error bars denote the s.d. of at least three measurements.

Preliminary studies of crossflow filtration using membrane cassettes with commercially available Mucin type III (Sigma Aldrich):

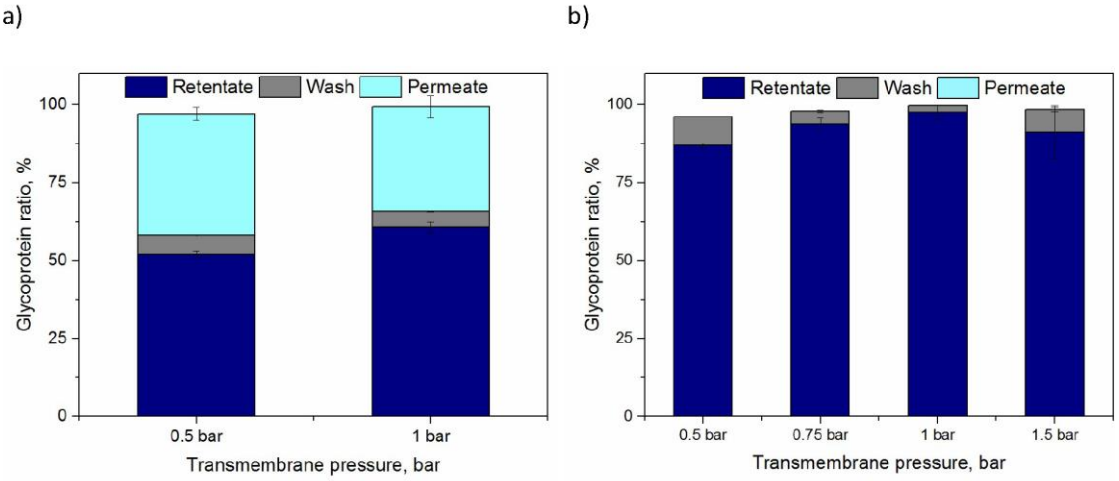

Figure S5. a) Glycoprotein ratio of commercially available Muc type III at different transmembrane pressures 0.5 bar and 1 bar using 300 kDa PESU filtration membrane. b) Glycoprotein ratio of Muc III at different transmembrane pressures 0.5 / 0.75 / 1 / 1.5 bar using 100 kDa regenerated cellulose filtration membrane. The buffer was 10 mM phosphate buffer pH 7 with 170 mM NaCl. Glycoprotein content in the retentate, permeate and washing step were analyzed with PAS Assay. Error bars represent ± s.d. of analytical triplicates.

Comparison of filtration modules regarding their fluid flow:

$$Re = \frac{v \rho d_h}{\eta}$$ Equation S1

$$Sc = \frac{\eta}{\rho D}$$ Equation S2

With v being the velocity in m s^{-1}, ρ the density of fluid (assumption of water: 1000 kg m^{-3}), η the

viscosity of fluid (assumption of water: 0.89 mPa s) and *D* the diffusion coefficient (mean diffusion coefficient of mucins taken from the literature [43]: $4*10^{-8}$ cm^2 s^{-1}).

Table S1. Comparison of feed stream, hydrodynamic diameter and cross sectional area for calculation of the Reynolds (*Re*), Sherwood (*Sh*) and Peclet (*Pe*) number. The boundary layer was theoretically calculated depending on laminar or turbulent flow.

	Membrane cassettes		Hollow fiber
	100 kDa	**300 kDa**	**100 kDa**
Feed stream, mL min^{-1}	200	240	200
Hydrodynamic diameter, d_h, m	0.002[a)]	0.002[a)]	0.0001
Cross-sectional area, m^2	$6.7*10^{-5}$	$6.7*10^{-5}$	$7.9*10^{-9}$
Re	112	134	47687
Sh	102	108	7822
Pe	83	100	8
Boundary layer δ_{BL}, µm	19.6	18.5	0.012

[a)] Estimated gap between the membranes of cassettes: 1 mm. With $b >> d$: $d_{hyd} = 2\,d$

Summary of glycoprotein purification processes (PAS Assay):

- 300 kDa membrane - small scale process:

Table S2. Summary of the overall purification process with the optimized protocol with 300 kDa concentration (membrane cassette), Sepharose 6 *Fast Flow* size exclusion chromatography, 300 kDa diafiltration in terms of yield, concentrations, volumes and mass before and after process units. Determination of glycoprotein concentration was conducted with the PAS Assay. Results are the mean ± s.d. of analytical triplicates.

Downstream process step	Yield	C_{before}, g L^{-1}	C_{after}, g L^{-1}	V_{before}, L	V_{after}, L	m_{before}, mg	m_{after}, mg
Concentration	69%	0.45	0.65	0.2	0.096	90.4	61.9
SEC	82%	0.65	0.42	0.02	0.025	12.9	10.5
Diafiltration	72%	0.42	0.17	0.025	0.044	10.5	7.6
Lyophilization		0.32		0.042			**9.0**
Total	40.3%						

- 100 kDa membrane - small scale process:

Table S3. Summary of the overall purification process with the optimized protocol with 100 kDa concentration (membrane cassette), Sepharose 6 *Fast Flow* size exclusion chromatography, 100 kDa diafiltration in terms of yield, concentrations, volumes and mass before and after process units. Determination of glycoprotein concentration was conducted with the PAS Assay. Results are the mean ± s.d. of analytical triplicates.

Downstream process step	Yield	C_{before}, g L^{-1}	C_{after}, g L^{-1}	V_{before}, L	V_{after}, L	m_{before}, mg	m_{after}, mg
Concentration	78%	0.45	0.77	0.196	0.09	88.2	69.0
SEC	83%	0.77	0.51	0.02	0.025	15.3	12.7
Diafiltration	87%	0.51	0.27	0.025	0.042	12.7	11.0
Lyophilization		0.32		0.042			**13.1**
Total	56.3%						

- 100 kDa hollow fiber module – upscaled process:

Table S4. Summary of the overall purification process with the optimized and upscaled protocol with 100 kDa concentration (hollow fiber module), Sepharose 6 *Fast Flow* size exclusion chromatography, 100 kDa diafiltration via hollow fiber module in terms of yield, concentrations, volumes and mass before and after process units. Determination of glycoprotein concentration was conducted with the PAS Assay. Results are the mean ± s.d. of analytical triplicates.

Downstream process step	Yield	C_{before}, g L^{-1}	C_{after}, g L^{-1}	V_{before}, L	V_{after}, L	m_{before}, mg	m_{after}, mg
Concentration	79%	1.16	3.58	0.7	0.18	812.0	644.2
SEC	68%	3.58	1.21	0.15	0.3	536.8	363.2
Diafiltration	80%	1.21	1.94	0.3	0.150	363.2	290.3
Lyophilization		0.32					**415.0**
Total	42.9%						

A.5 Enzymatically active biomimetic micropropellers for the penetration of mucin gels

RESEARCH ARTICLE

BIOMOLECULES

10.1126/sciadv.1500501

Enzymatically active biomimetic micropropellers for the penetration of mucin gels

Debora Walker,[1,2] Benjamin T. Käsdorf,[3] Hyeon-Ho Jeong,[1] Oliver Lieleg,[3] Peer Fischer[1,2]*

In the body, mucus provides an important defense mechanism by limiting the penetration of pathogens. It is therefore also a major obstacle for the efficient delivery of particle-based drug carriers. The acidic stomach lining in particular is difficult to overcome because mucin glycoproteins form viscoelastic gels under acidic conditions. The bacterium *Helicobacter pylori* has developed a strategy to overcome the mucus barrier by producing the enzyme urease, which locally raises the pH and consequently liquefies the mucus. This allows the bacteria to swim through mucus and to reach the epithelial surface. We present an artificial system of reactive magnetic micropropellers that mimic this strategy to move through gastric mucin gels by making use of surface-immobilized urease. The results demonstrate the validity of this biomimetic approach to penetrate biological gels, and show that externally propelled microstructures can actively and reversibly manipulate the physical state of their surroundings, suggesting that such particles could potentially penetrate native mucus.

INTRODUCTION

The human body has numerous mechanisms that protect it against the invasion of pathogens. These defenses include mucosal layers that line all wet epithelial surfaces, including the airway system and lungs, the gastrointestinal tract, and the urogenital tract. Mucus barriers not only make it difficult for microorganisms to reach and penetrate the host's tissues but also hinder the delivery of other substances such as potential pharmaceutical carriers, while allowing nutrients and other beneficial substances to pass freely (*1*–*3*). The stomach poses a particular challenge in this context, because here the combination of the mucus layer and the very low pH presents a major obstacle for various drug delivery applications (*4*, *5*). At the same time, most pharmaceuticals on the market are designed for oral administration (*5*); hence, efficient approaches for drug uptake in the gastrointestinal tract are of significant medical importance.

The glycoprotein mucin, a major component of mucus, is primarily responsible for the medium's mechanical properties. Mucin forms a highly viscoelastic interconnected network that regulates transport at the gastric epithelial surface. The complex filtering behavior can be traced back to two main effects, namely, the structure and pore size of the polymeric network, as well as mucin-particle interactions (*1*, *3*, *5*–*7*). Previous studies have verified that penetration of mucin gels may be enhanced by the addition of mucolytic agents (*8*–*11*), and it has been shown that the presence of degrading enzymes in the medium can enhance the transport of particles in other hydrogels as well (*12*). However, complete degradation of the mucus is generally not desirable because of the gel's important protective function and the resulting need to preserve the integrity of the mucosa (*5*). Many pathogens have developed strategies to overcome the mucus barrier, which include specific surface interactions, a modulation of mucin production, and the use of mucolytic enzymes; these approaches have been suggested to be potentially transferrable to artificial particulate delivery systems (*13*–*16*). *Helicobacter pylori*, a flagellated bacterium that inhabits the stomach and is associated with peptic ulcer disease and gastritis (*17*, *18*), uses a simple approach to locally and reversibly manipulate the gastric mucus. It has recently been demonstrated that *H. pylori* secretes large amounts of the enzyme urease not only as a defense against the harsh acidic environment of the stomach but also to actively change mucus viscosity and facilitate propulsion, as shown schematically in Fig. 1 (*19*). Urease catalyzes the hydrolysis of urea, which results in the release of ammonia. The subsequent local rise in pH induces a gel-sol transition of the mucus and thus reduces its viscosity by liquefying it (*4*, *20*). It could be shown that *H. pylori* bacteria are capable of moving freely through mucin solutions at neutral pH, whereas they are immobile in acidic mucin gels if the solution does not contain urea, even though they can be observed to move their flagella under these conditions (*19*). If urea is added to the solution under acidic conditions, the bacteria again move almost freely.

Here, we demonstrate an artificial system of magnetic micropropellers that mimic *H. pylori* in their strategy to propel through gastric mucus (see Fig. 1). Thus far, drug carriers and other particles have been treated mostly with substances that modulate mucus-surface interactions, such as polyethylene glycol, various polymers, adsorbed bile salts, lectins, and microbial ligands (*7*, *16*, *21*–*24*). The present study shows that it is possible to significantly enhance the mobility of microparticles in mucin gels by urease immobilization on their surface. This avoids both a systemic treatment and the use of enzymes that irreversibly degrade the protective mucus lining. To implement *H. pylori*'s strategy for active mucin penetration described above, we developed magnetic micropropellers that are stable under acidic conditions, are capable of efficient propulsion in mucin solutions at neutral pH, and have a high enough activity of immobilized urease on the surface to allow for propulsion in slightly acidified mucin gels that contain urea. The results demonstrate the validity of using this catalytic approach to penetrate viscoelastic biological media. To our knowledge, this is the first example of an externally propelled microstructure that actively manipulates the physical state of its surroundings by changing the rheological properties of the medium.

Several kinds of artificial micro- and nanostructures that can be wirelessly moved at low Reynolds number have been developed in recent years (*25*–*33*). It has been shown that magnetic helical (screw-like) structures can be actuated precisely, even over larger distances, when they are subjected to a homogeneous rotating magnetic field (*25*, *26*, *33*–*35*). Most studies have shown propulsion in low-viscosity model fluids, such

[1]Max Planck Institute for Intelligent Systems, Heisenbergstrasse 3, 70569 Stuttgart, Germany. [2]Institute for Physical Chemistry, University of Stuttgart, Pfaffenwaldring 55, 70569 Stuttgart, Germany. [3]Institute for Medical Engineering and Department of Mechanical Engineering, Technische Universität München, Boltzmannstrasse 11, 85748 Garching, Germany.
*Corresponding author. E-mail: fischer@is.mpg.de

as water, simple buffer solutions, serum, or blood (*25*, *26*, *31*, *34*). Recently, the retention of Zn-powered micromotors in the stomach was demonstrated to be higher than that of passive particles (*36*). It was furthermore shown that the ability of helical propellers to move through macromolecular networks of hyaluronic acid depends strongly on the size of the penetrating particle, and that particles with diameters on the order of the medium's pore size can penetrate these biological gels much more effectively than larger particles (*33*). A different strategy to overcome viscous tissues or penetrate a protective mucous lining is to render these particles reactive. Here, we borrow such a mechanism of active micropropulsion from nature and mimic the mucus penetration strategy of *H. pylori*.

RESULTS

Fabrication of acid-stable micropropellers

The micropropellers used in this study are produced via a highly parallel physical vapor deposition (PVD) process, known as glancing angle deposition (GLAD) (*37*, *38*). We generated glass (SiO_2) helices into which a thin magnetic section was incorporated. The entire fabrication process of the enzyme-functionalized magnetic propellers is depicted in Fig. 2. Details of the fabrication process have been reported previously (*39*). However, here, the magnetic Ni section was deposited on the structures at the very end of the PVD process, and the GLAD step was then followed by atomic layer deposition (ALD) where the helices were coated with an 8-nm shell of alumina (Al_2O_3) to render the magnetic section resistant to oxidation in acidic solution (this was verified by propulsion experiments after dispersing the particles in pH 4.6 phosphate buffer for 24 hours). The micropropellers are shaped like small screw-like drills that are magnetized orthogonal to the helix axis; thus, when a rotating magnetic field is applied, the propellers rotate about their long axis and thus translate by virtue of their chiral shape (*25*, *39*, *40*).

Urease immobilization

We found that the ALD-stabilized micropropellers could be readily functionalized with urease, using published protocols (*41*, *42*). For this, the propellers were first treated with 3-aminopropyltriethoxysilane (APTES) and activated with glutaraldehyde (GA), which then allowed the enzyme to be coupled to the surface. A visual control of the pH increasing ability of urease-functionalized control particles is shown in Fig. 3 to ensure that this coupling procedure maintains the enzymatic activity of the urease. Silica beads with a diameter of ~50 μm were functionalized in the same manner as the micropropellers and were added into a solution of urea together with a small amount of the pH indicator bromothymol blue. The color change over the course of several minutes clearly visualizes the local increase in pH. The enzyme activity (maximum rate at high urea concentrations) of urease immobilized on silica particles (diameter, 1.5 μm) was furthermore quantified using an established method (*43*). The results were generally on the order of ~1 μmol s^{-1} urea hydrolysis per gram of silica particles. Stöber particles are smooth and have a specific surface area not much higher than their geometric surface area (*44*, *45*); thus, this value translates very roughly to an ammonia release rate on the order of ~1 μmol s^{-1} m^{-2}. Using Fick's first law and an ion diffusion coefficient of ~5×10^{-11} m^2 s^{-1} in mucus (*46*), one can estimate that the Stöber particles would be able to maintain a concentration difference on their surface relative to the medium on the order of ~20 μM. Taking into account that silica GLAD structures are rough/porous with specific surface areas on the order of hundreds of square meters per gram (*47*), this yields a concentration difference on the order of ~1 mM on the surface of the micropropellers. This value is in agreement with the observation that propulsion experiments were only successful at HCl concentrations less than 1 mM above the minimum amount needed for gelation (see below).

After functionalization with urease, the micropropellers (Fig. 2) were magnetized on the wafer. Dispersion in the desired solution by sonication allowed individual structures to be propelled by a weak rotating homogeneous magnetic field of about 10 mT (100 G).

Mucin gel characterization

In the stomach, *H. pylori* encounters a viscoelastic mucus gel at acidic pH. Here, we used a reconstituted system of purified porcine gastric mucins (PGMs). The addition of 5.5 mM HCl to 2% PGM was chosen for subsequent propulsion experiments, because this concentration

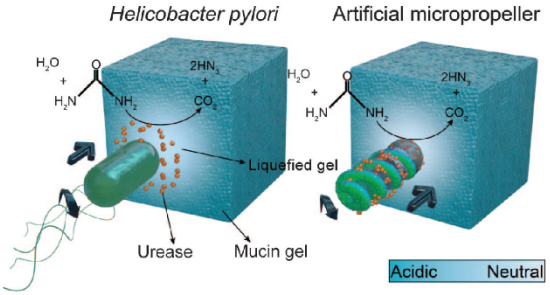

Fig. 1. Mechanism for mucin penetration. Schematic illustration of the propulsion strategy of *H. pylori* through mucin gels and the catalytically active magnetic micropropellers presented here. The enzyme on the helices' surface hydrolyzes urea and liquefies the environment via the resulting local rise in pH.

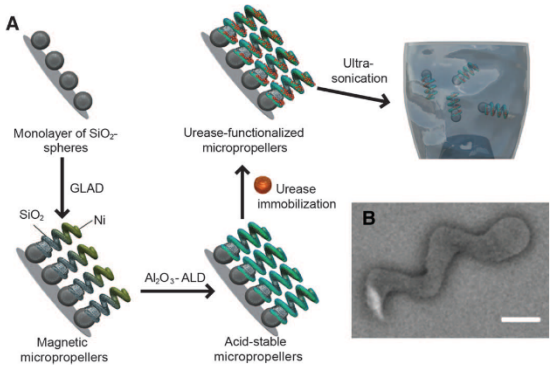

Fig. 2. Acid-stable enzyme-functionalized micropropellers. (**A**) Fabrication process of acid-stable enzyme-functionalized magnetic micropropellers consisting of GLAD on top of a monolayer of silica beads, atomic layer deposition (ALD) to protect the resulting magnetic helices, enzyme immobilization, and ultrasonication in solution to remove the particles from the wafer. (**B**) ESB-SEM (energy-selective backscatter–scanning electron microscopy) image of a magnetic micropropeller, with the Ni section clearly visible. Scale bar, 500 nm.

supplied the necessary acidity for gelation. Such an HCl concentration usually led to the formation of gels with a pH between 4 and 5. The rheological measurements presented in Fig. 4A demonstrate that a 2% solution of PGMs exhibits a sol-gel transition somewhere between pH 4.5 and pH 7; that is, it behaves as a viscoelastic fluid under neutral conditions and as a viscoelastic gel at pH 4.5 [the storage modulus $G'(f)$ exceeds the loss modulus $G''(f)$ at low pH for all frequencies tested, and vice versa at neutral pH]. However, the detailed gelation transition depends on both the mucin concentration and the ionic strength of the mucin reconstitution buffer (*4*). We verified, therefore, that neither the use of HCl, instead of the reconstitution buffer used for the characterization of the gelation behavior, nor the addition of bile salts and urea suppressed gel formation. In addition, by sonicating a gel sample for 5 min before rheological characterization, we confirmed that ultrasonication did not have any long-term influence on the gel properties. Results of the above tests are shown in Fig. 4B.

Propulsion in mucin gels

In the following, we describe in detail how the urease-covered microparticles are able to effectively move through a mucin gel. In brief, this is achieved by two steps: First, the presence of naturally occurring bile salts prevents adhesion of the mucin to the particles' surface. Second, urea, which is also present in the stomach at concentrations of a few millimolar (*48*–*50*), is converted by the urease to ammonia, which raises the pH and thus induces the gel-sol transition, thereby lowering the viscosity around the micropropellers.

When placed in pure PGM solution at neutral pH (corresponding to a low viscosity), most of the time, the magnetic propellers appear to rotate when a rotating magnetic field is applied but do not exhibit any forward propulsion, even at very low concentrations of only 0.25% PGM. We postulate that this is due to mucoadhesion (*1*, *22*, *23*), that is, the adsorption of mucin to the surface of the particles. One explanation for the low motility is that adsorbed mucin reduces the rotation rate by immobilizing the particles in the polymeric matrix. However, our evidence seems to suggest that rather than exhibiting diminished rotation, the propellers become entangled in the polymer chains during rotation, which reduces their effective geometric helicity and thus their rotation-translation coupling, preventing directional movement. This explanation is supported by the tendency of the propellers to form linear chains in the direction of propulsion along which individual particles are not in direct contact but still seem rigidly connected. A video of micropropellers being actuated at a frequency of 30 Hz and a magnetic field strength of 10 mT in 0.5% neutral mucin solution, together with a video of a chain of the kind mentioned above (in 0.25% mucin), can be found in the Supplementary Materials (movie S1).

Various coatings and surface passivation techniques have been designed to reduce mucoadhesion (*7*, *21*–*23*). The one that proved most effective in our case, partly because it does not require any covalent surface functionalization and is thus compatible with enzyme immobilization on the surface of the micropropellers, was the addition of bile salts to the mucin solutions (*22*). We stress that bile salts are in any case present in naturally occurring mucus of the stomach at low concentrations (*51*). For all experiments, we used the same combination of bile salts (that is, sodium glycodeoxycholate and sodium taurocholate) that Macierzanka *et al.* found to be optimal for preventing mucoadhesion on both latex microparticles and model food emulsion droplets (*22*). We found that a bile salt concentration of 1 mM was sufficient to suppress adsorption, while not interfering with the gelation ability of

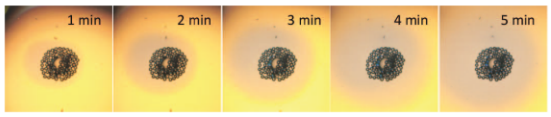

Fig. 3. Urease activity. SiO_2 beads (~50 μm in diameter) functionalized with urease using GA coupling, in a solution of 100 mM urea colored with the pH indicator bromothymol blue. The beads were dried on a coverslip and micrographs were recorded 1, 2, 3, 4, and 5 min after the addition of urea solution. The blue coloring clearly demonstrates the increase in pH due to catalytic urea hydrolysis.

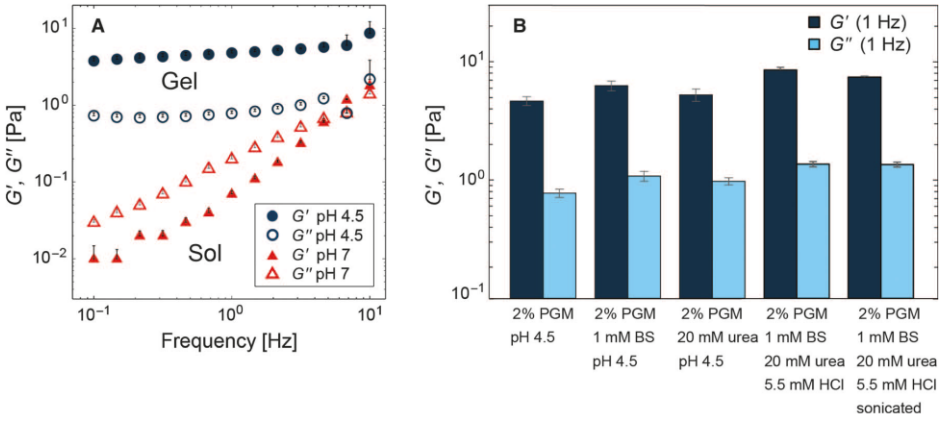

Fig. 4. Mucin rheology. (**A**) Viscoelastic properties of reconstituted PGMs at different pH conditions. A 2% solution of PGMs exhibits a clear sol-gel transition between pH 4.5 and pH 7. Closed symbols denote the storage modulus $G'(f)$, and open symbols denote the loss modulus $G''(f)$. (**B**) Gelation of the PGM solution is neither suppressed by the addition of 1 mM bile salts (BS; sodium glycodeoxycholate and sodium taurocholate) nor suppressed by the addition of 20 mM urea, the use of 5.5 mM HCl instead of a pH 4.5 reconstitution buffer, or ultrasonication.

the mucin solution (see Fig. 3). In neutral mucin solutions with concentrations up to 2% containing 1 mM bile salts, the micropropellers were then indeed able to propel, although both the dimensionless velocity (the velocity normalized by the helix's pitch and the frequency of the magnetic field, about 0.11 ± 0.03 at a frequency of 30 Hz and a mucin concentration of 2%) and the step-out frequency (<60 Hz at 10 mT and 2%) were lower than what can generally be observed in water or other low-viscosity Newtonian fluids (*33*, *39*). The lower step-out frequency is plausible because of the higher viscosity of mucin relative to water, whereas the lower dimensionless velocity is potentially more surprising because some studies in other complex viscous and viscoelastic environments have found propulsion enhancement relative to low-viscosity Newtonian fluids (*33*, *52*–*54*). However, theoretically, both enhancement and reduction of propulsion velocities in viscoelastic media compared to Newtonian liquids have been predicted, depending on the exact conditions, particle geometry, and fluid model (*55*–*60*).

Next, we verified that the micropropellers are unable to move at acidic pH where the mucins form a viscoelastic gel. In solutions of 2% mucin, 1 mM bile salts, and small amounts of hydrochloric acid (for our samples, this value was typically slightly more than 5 mM, but it can vary between different mucin batches), no propulsion could be observed at a magnetic field strength of 10 mT. The gel state of the mucin was obvious in that it not only prevented propulsion of the magnetic helices but also reduced Brownian motion of any passive particles in the sample. Adding 20 mM urea to the solution did not change this observation in the case of unfunctionalized propellers, which is consistent with our finding that this amount of urea does not interfere with the gelation properties of a 2% solution of PGMs (see Fig. 3).

Finally, we tested whether micropropellers functionalized with urease are indeed able to navigate through a mucin gel by actively changing the rheological properties of its surroundings. We observed effective propulsion of urease-functionalized micropropellers in urea-containing mucin solutions containing 5.5 mM HCl. Figure 5B shows tracks of helices with immobilized urease in such slightly acidified mucin solutions, and the propellers' average velocity obtained under these conditions is shown in Fig. 5E. In the absence of urease, these micropropellers do not move (see Fig. 5A), as expected. The corresponding videos can be found in the Supplementary Materials. It should be noted that the velocity observed for the micropropellers that induce a gel-sol transition is lower than what can be observed for micropropellers moving in low-viscosity mucin control solutions (that is, at neutral pH). At a frequency of 30 Hz and a magnetic field strength of 10 mT, the propellers in the neutral control mucin solution moved at an average speed of 2.6 ± 0.8 μm s^{-1}, whereas the catalytic propellers in the acidified mucin were observed to move at an average speed of 1.4 ± 0.5 μm s^{-1}. Our experiments clearly demonstrate that only the urease-functionalized micropropellers can actively penetrate the mucin gel and that this active motion is only enabled in the presence of the enzyme substrate urea.

DISCUSSION

The concentrations used in our mucus model differ only in a few respects from those found in the actual mucosal stomach lining. The mucin content, which is one of the most crucial parameters that determine the viscoelasticity of the material, is on the lower end of the range typically encountered in the gastric mucus layer, where one typically finds concentrations of 2 to 5% mucin by weight (*2*, *6*). Typical urea concentrations in the human stomach are on the order of several millimolar in healthy subjects and can be higher for a number of pathological conditions (*48*–*50*, *61*); therefore, the concentration used in this study is biomedically relevant. The same holds true for the concentration of bile salts used here (1 mM), because the bile acid content in the gastric juice can reach hundreds of micromolar in healthy subjects (*51*). However, the HCl content can exceed 100 mM in the stomach (*62*), which is significantly more than the amount that was used in this study. One of the reasons for this is that the commercially available urease (isolated from jack bean) is not optimized for and thus not very active at low pH. So-called acid ureases (*63*) could potentially provide significantly higher enzyme activity under conditions found in the stomach and should be used in potential applications; however, these enzymes were not available to the authors for this study. Furthermore, future

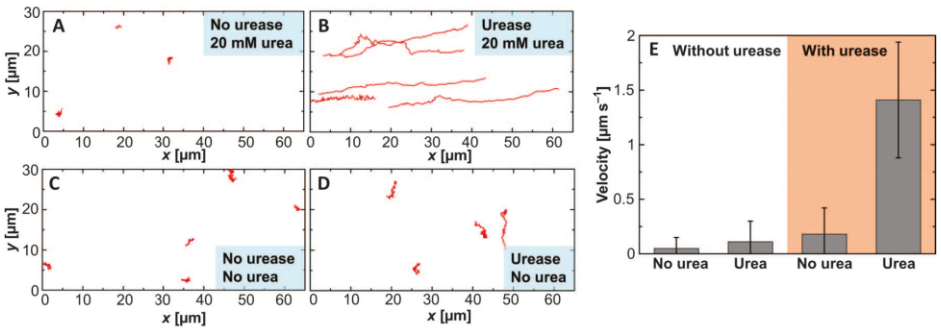

Fig. 5. Propulsion in mucin gels. (**A** to **D**) Tracks of micropropellers with (B and D) and without (A and C) urease immobilized on the surface, in an acidified 2% mucin gel with (A and B) and without (C and D) 20 mM urea over a time frame of 25 s. The particles were propelled in the *x* direction at a frequency of 30 Hz and a magnetic field strength of 10 mT. Each graph shows the tracks from one video recording. (**E**) The average velocity under these conditions is shown and represents an average of a minimum of 50 particles tracked over at least 10 s. Only the *x* component of the velocity was taken into account; the small drift in the *y* direction that can sometimes be observed when the particles are close to the glass surface [as in (D)], or "kinks" in the *y* direction due to hydrodynamic interactions with another propeller in proximity [as in the topmost trajectory in (B)], was neglected. The corresponding videos can be found in the Supplementary Materials.

reactive microparticle systems could be even more effective if the overall enzyme loading is increased; that is, urease is not immobilized on the surface but instead carried in larger amounts in the bulk volume of the particle, so that the enzymes can more quickly neutralize higher amounts of acid, thus allowing for more efficient forward propulsion. This could be achieved if, for instance, porous materials are used for the basis of the microparticles or by immobilizing larger amounts of enzyme onto the particle surface, for example, via branched polymer linkers or enzyme cross-linking.

In summary, our experiments demonstrate that it is possible to engineer microparticles in such a way that they actively manipulate their environment and thus become mobile. We verified that strategies for the penetration of complex biological hydrogel barriers, which are specifically designed to hinder the transport of micrometer-sized structures (that is, certain pathogens), can be borrowed from microorganisms. Magnetically actuated micropropellers can successfully navigate through mucin gels when functionalized with urease, which allows them to induce a gel-sol transition in the surrounding biopolymer network. This mimics the molecular strategy by which the bacterium *H. pylori* achieves motility in the mucus lining of the stomach. In addition to being of interest for the further development of remotely steerable "microbots," our results are also relevant for the generation of more efficient drug and/or particle delivery systems. In particular, our study suggests that uptake and delivery across mucosal barriers, for instance, in the gastrointestinal tract, can potentially be improved even for passively diffusing drug carriers, if they are functionalized to reversibly reduce the viscoelastic properties of the mucosa.

MATERIALS AND METHODS

Micropropeller fabrication

The magnetic micropropellers were produced using a previously described method (*39*), with the magnetic section at one end of the helix. A Langmuir-Blodgett monolayer of 500-nm silica beads was used as a seed layer. After the GLAD step, a thin alumina (Al_2O_3) layer was grown to cover the helices' surface using ALD (Savannah 100, Cambridge NanoTech) at $T = 100°C$ with a growth rate of 0.1 nm per cycle by repeatedly injecting trimethylaluminum for 0.15 s and deionized water for 0.15 s. The stabilized micropropellers were magnetized in plane (that is, transversally relative to the individual helix) at 1.8 T in an electromagnet.

Enzyme immobilization

For the urease immobilization, the wafer with micropropellers (or a few milligrams of silica beads for the control experiments) was first immersed in a 2 volume % solution of APTES (Sigma-Aldrich) and ~0.2 M ammonium hydroxide in ethanol at room temperature for 1.5 hours. After rinsing with ethanol and water, the sample was then immersed in an aqueous solution of 2.5% glutaraldehyde in 50 mM phosphate buffer (pH 7) containing sodium cyanoborohydride (~1 mg/ml) at room temperature for 3 hours. After thoroughly rinsing with water, the wafer was then suspended in 50 mM phosphate buffer (pH 7) again containing sodium cyanoborohydride (~1 mg/ml) and urease (~2 mg/ml; type IX from jack bean, Sigma-Aldrich) at 4°C overnight. The sample was then washed with 25 mM phosphate buffer (pH 7) and stored on the wafer at 4°C. Enzyme-functionalized samples were generally used in the experiments for about 2 weeks before a fresh sample was prepared. The enzyme activity of functionalized silica beads was confirmed quantitatively according to the following procedure: 0.5 mg of functionalized silica particles (1.5 μm) was incubated at room temperature in 250 μl of a solution of 50 mM urea and 40 mM NaCl for 5 to 30 min. The reaction was quenched by the addition of 550 μl of a solution of 60 mM sodium salicylate (Sigma-Aldrich) and 5 mM sodium nitroprusside (Sigma-Aldrich) and 400 μl of 10 mM sodium hypochlorite in 400 mM sodium hydroxide solution. After centrifugation and incubation at room temperature for roughly 30 min, the absorbance of the solution at 690 nm was determined with a Cary 4000 UV-Vis Spectrometer. Calibration was performed using solutions containing appropriate amounts of ammonium sulfate. The supernatant of the functionalized particles after washing was verified to exhibit negligible enzyme activity. Washing of the particles involved multiple redispersion steps using ultrasonication, which did not result in a measurable change in enzyme activity of the particles or of the supernatant.

Mucin preparation and characterization

Porcine gastric mucins were purified from scrapings of fresh pig stomachs essentially as described previously (*64*), with the exception that the cesium chloride density gradient ultracentrifugation was omitted. In brief, mucus was collected from the surface of pig stomachs by gentle scraping and dissolved in phosphate-buffered saline (10 mM, 170 mM NaCl adjusted to pH 7.4). The mucins were then purified by a series of centrifugation and size-exclusion chromatography steps and then concentrated and desalted by cross-flow dialysis until a conductance of less than 50 μS was reached. Then, the obtained mucin MUC5AC was stored in lyophilized form at −80°C until further use. Such lyophilized mucins can be reconstituted at a given pH and ionic strength by rehydration at 4°C overnight. Reconstituted mucin solutions exhibit a pH-dependent sol-gel transition as described previously, provided that the ionic strength of the rehydration buffer is kept low (*64*).

Rheological characterization of mucin solutions and gels was performed on a stress-controlled shear rheometer (MCR 302, Anton Paar) using a plate/plate measuring setup (PP25, Anton Paar) and 150-μm plate separation. When determining frequency-dependent viscoelastic moduli, small torques in the range of 0.5 μNm were applied to ensure a linear material response. Phosphate-buffered saline (10 mM, pH 7.0) and acetate buffer (10 mM, pH 4.5) were used as reconstitution buffers.

Propulsion experiments

For the propulsion experiments, solutions of 4% mucin containing 1 mM sodium taurocholate and 1 mM sodium glycodeoxycholate (Sigma-Aldrich) were prepared at 4°C overnight. As-prepared solutions were used in experiments within 24 hours of reconstitution. This solution was then mixed thoroughly 1:1 with a solution containing the appropriate amount of hydrochloric acid (11 mM for the acidified gels and 0 mM for the control experiments) and urea (0 or 40 mM). Right before the propulsion experiments, the micropropellers were dispersed in the solution by ultrasonication. The mixture was then transferred to a 25-μl gene frame (Thermo Scientific) and positioned in a water-cooled three-axis Helmholtz coil setup described previously (*39*). Propulsion experiments were performed at room temperature within 5 to 20 min of propeller dispersion at a magnetic field strength of 10 mT. Videos were recorded with a minimum pixel resolution of 5 pixels/μm. For the velocity measurements, the particles were tracked for a minimum of 10 s and the average velocity over that time frame only in the direction of propulsion

was determined. The reported results therefore do not reflect the amount of Brownian motion present in the sample or any motion perpendicular to the axis of rotation, which can arise from interactions with the surface of the coverslip (that is, rolling). For each reported value, at least 50 particles were averaged. The propulsion experiments with enzymatically active and plain propellers in urea-containing mucin gels were repeated and reproduced from scratch four times (one of which was performed using a different batch of lyophilized mucin and therefore needed a different acid concentration for the experiment to succeed). The control experiments without urea were each performed at least twice. Propulsion in mucin concentrations other than 2% was tested only under neutral pH. Even in the sol state, 4% mucin solutions were too viscous to allow for propulsion at the magnetic field strengths used in this study. For very low mucin concentrations, that is, below 0.5%, rheological measurements indicate that gelation does not occur any longer; hence, accordingly, an experiment involving an induced gel-sol transition would not be possible anymore.

SUPPLEMENTARY MATERIALS

Supplementary material for this article is available at http://advances.sciencemag.org/cgi/content/full/1/11/e1500501/DC1

Movie S1. Magnetic microhelices in neutral PGM solutions (0.5% mucin in the left panel and 0.25% in the right panel) being propelled in the *x* direction at a frequency of 30 Hz and a magnetic field strength of 10 mT.

Movie S2. Magnetic microhelices with and without urease immobilized on the surface in an acidified 2% mucin gel containing 1 mM bile salts, with and without 20 mM urea over a time frame of 40 s.

REFERENCES AND NOTES

1. O. Lieleg, I. Vladescu, K. Ribbeck, Characterization of particle translocation through mucin hydrogels. *Biophys. J.* **98**, 1782–1789 (2010).
2. S. K. Lai, Y.-Y. Wang, D. Wirtz, J. Hanes, Micro- and macrorheology of mucus. *Adv. Drug Deliv. Rev.* **61**, 86–100 (2009).
3. R. A. Cone, Barrier properties of mucus. *Adv. Drug Deliv. Rev.* **61**, 75–85 (2009).
4. J. P. Celli, B. S. Turner, N. H. Afdhal, R. H. Ewoldt, G. H. McKinley, R. Bansil, S. Erramilli, Rheology of gastric mucin exhibits a pH-dependent sol–gel transition. *Biomacromolecules* **8**, 1580–1586 (2007).
5. L. M. Ensign, R. Cone, J. Hanes, Oral drug delivery with polymeric nanoparticles: The gastrointestinal mucus barriers. *Adv. Drug Deliv. Rev.* **64**, 557–570 (2012).
6. R. Bansil, B. S. Turner, Mucin structure, aggregation, physiological functions and biomedical applications. *Curr. Opin. Colloid Interface Sci.* **11**, 164–170 (2006).
7. J. Kirch, A. Schneider, B. Abou, A. Hopf, U. F. Schaefer, M. Schneider, C. Schall, C. Wagner, C.-M. Lehr, Optical tweezers reveal relationship between microstructure and nanoparticle penetration of pulmonary mucus. *Proc. Natl. Acad. Sci. U.S.A.* **109**, 18355–18360 (2012).
8. J. S. Suk, S. K. Lai, N. J. Boylan, M. R. Dawson, M. P. Boyle, J. Hanes, Rapid transport of muco-inert nanoparticles in cystic fibrosis sputum treated with *N*-acetyl cysteine. *Nanomedicine* **6**, 365–375 (2011).
9. N. N. Sanders, S. C. De Smedt, E. Van Rompaey, P. Simoens, F. De Baets, J. Demeester, Cystic fibrosis sputum: A barrier to the transport of nanospheres. *Am. J. Respir. Crit. Care Med.* **162**, 1905–1911 (2000).
10. S. Ferrari, C. Kitson, R. Farley, R. Steel, C. Marriott, D. A. Parkins, M. Scarpa, B. Wainwright, M. J. Evans, W. H. Colledge, D. M. Geddes, E. W. F. W. Alton, Mucus altering agents as adjuncts for nonviral gene transfer to airway epithelium. *Gene Ther.* **8**, 1380–1386 (2001).
11. I. Vladescu, O. Lieleg, S. Jang, K. Ribbeck, An adsorption chromatography assay to probe bulk particle transport through hydrogels. *J. Pharm. Sci.* **101**, 436–442 (2012).
12. J. H. Hou, A. E. Cohen, Motion induced by asymmetric enzymatic degradation of hydrogels. *Soft Matter* **8**, 4616–4624 (2012).
13. A.-R. Colina, F. Aumont, N. Deslauriers, P. Belhumeur, L. de Repentigny, Evidence for degradation of gastrointestinal mucin by *Candida albicans* secretory aspartyl proteinase. *Infect. Immun.* **64**, 4514–4519 (1996).
14. S. Z. Hasnain, M. A. McGuckin, R. K. Grencis, D. J. Thornton, Serine protease(s) secreted by the nematode *Trichuris muris* degrade the mucus barrier. *PLOS Negl. Trop. Dis.* **6**, e1856 (2012).
15. A. J. Silva, K. Pham, J. A. Benitez, Haemagglutinin/protease expression and mucin gel penetration in El Tor biotype *Vibrio cholerae*. *Microbiology* **149**, 1883–1891 (2003).
16. C. Gamazo, N. Martín-Arbella, A. Brotons, A. I. Camacho, J. M. Irache, Mimicking microbial strategies for the design of mucus-permeating nanoparticles for oral immunization. *Eur. J. Pharm. Biopharm.* **96**, 454–463 (2015).
17. G. Sachs, D. L. Weeks, K. Melchers, D. R. Scott, The gastric biology of *Helicobacter pylori*. *Annu. Rev. Physiol.* **65**, 349–369 (2003).
18. B. J. Marshall, J. R. Warren, G. J. Francis, S. R. Langton, C. S. Goodwin, E. D. Blincow, Rapid urease test in the management of *Campylobacter pyloridis*-associated gastritis. *Am. J. Gastroenterol.* **82**, 200–210 (1987).
19. J. P. Celli, B. S. Turner, N. H. Afdhal, S. Keates, I. Ghiran, C. P. Kelly, R. H. Ewoldt, G. H. McKinley, P. So, S. Erramilli, R. Bansil, *Helicobacter pylori* moves through mucus by reducing mucin viscoelasticity. *Proc. Natl. Acad. Sci. U.S.A.* **106**, 14321–14326 (2009).
20. X. Cao, R. Bansil, K. R. Bhaskar, B. S. Turner, J. T. LaMont, N. Niu, N. H. Afdhal, pH-dependent conformational change of gastric mucin leads to sol-gel transition. *Biophys. J.* **76**, 1250–1258 (1999).
21. S. K. Lai, D. E. O'Hanlon, S. Harrold, S. T. Man, Y.-Y. Wang, R. Cone, J. Hanes, Rapid transport of large polymeric nanoparticles in fresh undiluted human mucus. *Proc. Natl. Acad. Sci. U.S.A.* **104**, 1482–1487 (2007).
22. A. Macierzanka, N. M. Rigby, A. P. Corfield, N. Wellner, F. Böttger, E. N. C. Mills, A. R. Mackie, Adsorption of bile salts to particles allows penetration of intestinal mucus. *Soft Matter* **7**, 8077–8084 (2011).
23. M. Gu, H. Yildiz, R. Carrier, G. Belfort, Discovery of low mucus adhesion surfaces. *Acta Biomater.* **9**, 5201–5207 (2013).
24. Y. Cu, W. M. Saltzman, Controlled surface modification with poly(ethylene)glycol enhances diffusion of PLGA nanoparticles in human cervical mucus. *Mol. Pharm.* **6**, 173–181 (2009).
25. A. Ghosh, P. Fischer, Controlled propulsion of artificial magnetic nanostructured propellers. *Nano Lett.* **9**, 2243–2245 (2009).
26. P. L. Venugopalan, R. Sai, Y. Chandorkar, B. Basu, S. Shivashankar, A. Ghosh, Conformal cytocompatible ferrite coatings facilitate the realization of a nanovoyager in human blood. *Nano Lett.* **14**, 1968–1975 (2014).
27. W. Gao, M. D'Agostino, V. Garcia-Gradilla, J. Orozco, J. Wang, Multi-fuel driven Janus micromotors. *Small* **9**, 467–471 (2013).
28. W. Gao, A. Uygun, J. Wang, Hydrogen-bubble-propelled zinc-based microrockets in strongly acidic media. *J. Am. Chem. Soc.* **134**, 897–900 (2012).
29. V. Garcia-Gradilla, J. Orozco, S. Sattayasamitsathit, F. Soto, F. Kuralay, A. Pourazary, A. Katzenberg, W. Gao, Y. Shen, J. Wang, Functionalized ultrasound-propelled magnetically guided nanomotors: Toward practical biomedical applications. *ACS Nano* **7**, 9232–9240 (2013).
30. K. E. Peyer, L. Zhang, B. J. Nelson, Bio-inspired magnetic swimming microrobots for biomedical applications. *Nanoscale* **5**, 1259–1272 (2013).
31. F. Qiu, L. Zhang, K. E. Peyer, M. Casarosa, A. Franco-Obregón, H. Choi, B. J. Nelson, Non-cytotoxic artificial bacterial flagella fabricated from biocompatible ORMOCOMP and iron coating. *J. Mater. Chem.* **2**, 357–362 (2014).
32. V. Magdanz, S. Sanchez, O. G. Schmidt, Development of a sperm-flagella driven micro-bio-robot. *Adv. Mater.* **25**, 6581–6588 (2013).
33. D. Schamel, A. G. Mark, J. G. Gibbs, C. Miksch, K. I. Morozov, A. M. Leshansky, P. Fischer, Nanopropellers and their actuation in complex viscoelastic media. *ACS Nano* **8**, 8794–8801 (2014).
34. W. Gao, X. Feng, A. Pei, C. R. Kane, R. Tam, C. Hennessy, J. Wang, Bioinspired helical microswimmers based on vascular plants. *Nano Lett.* **14**, 305–310 (2014).
35. K. Ishiyama, M. Sendoh, K. I. Arai, Magnetic micromachines for medical applications. *J. Magn. Magn. Mater.* **242–245**, 41–46 (2002).
36. W. Gao, R. Dong, S. Thamphiwatana, J. Li, W. Gao, L. Zhang, J. Wang, Artificial micromotors in the mouse's stomach: A step toward in vivo use of synthetic motors. *ACS Nano* **9**, 117–123 (2015).
37. M. M. Hawkeye, M. J. Brett, Glancing angle deposition: Fabrication, properties, and applications of micro- and nanostructured thin films. *J. Vac. Sci. Technol. A* **25**, 1317–1335 (2007).
38. J. G. Gibbs, A. G. Mark, T.-C. Lee, S. Eslami, D. Schamel, P. Fischer, Nanohelices by shadow growth. *Nanoscale* **6**, 9457–9466 (2014).
39. D. Schamel, M. Pfeifer, J. G. Gibbs, B. Miksch, A. G. Mark, P. Fischer, Chiral colloidal molecules and observation of the propeller effect. *J. Am. Chem. Soc.* **135**, 12353–12359 (2013).
40. K. I. Morozov, A. M. Leshansky, The chiral magnetic nanomotors. *Nanoscale* **6**, 1580–1588 (2014).
41. B. Krajewska Ureases. II. Properties and their customizing by enzyme immobilizations: A review. *J. Mol. Catal. B Enzym.* **59**, 22–40 (2009).
42. K. R. C. Reddy, A. M. Kayastha, Improved stability of urease upon coupling to alkylamine and arylamine glass and its analytical use. *J. Mol. Catal. B Enzym.* **38**, 104–112 (2006).

43. H. Verdouw, C. J. A. Van Echteld, E. M. J. Dekkers, Ammonia determination based on indophenol formation with sodium salicylate. *Water Res.* **12**, 399–402 (1978).
44. A. G. Howard, N. H. Khdary, Spray synthesis of monodisperse sub-micron spherical silica particles. *Mater. Lett.* **61**, 1951–1954 (2007).
45. M. Szekeres, J. Tóth, I. Dékány, Specific surface area of Stoeber silica determined by various experimental methods. *Langmuir* **18**, 2678–2685 (2002).
46. C. V. Nicholas, M. Desai, P. Vadgama, M. B. McDonnell, S. Lucas, pH dependence of hydrochloric acid diffusion through gastric mucus: Correlation with diffusion through a water layer using a membrane-mounted glass pH electrode. *Analyst* **116**, 463–467 (1991).
47. K. M. Krause, M. T. Taschuk, K. D. Harris, D. A. Rider, N. G. Wakefield, J. C. Sit, J. M. Buriak, M. Thommes, M. J. Brett, Surface area characterization of obliquely deposited metal oxide nanostructured thin films. *Langmuir* **26**, 4368–4376 (2010).
48. C. S. Lieber, A. Lefèvre, Ammonia as a source of gastric hypoacidity in patients with uremia. *J. Clin. Invest.* **38**, 1271–1277 (1959).
49. W. D. Neithercut, A. M. El Nujumi, K. E. L. McColl, Measurement of urea and ammonium concentrations in gastric juice. *J. Clin. Pathol.* **46**, 462–464 (1993).
50. K. Blusiewicz, G. Rydzewska, A. Rydzewski, Gastric juice ammonia and urea concentrations and their relation to gastric mucosa injury in patients maintained on chronic hemodialysis. *Rocz. Akad. Med. Bialymst.* **50**, 188–192 (2005).
51. B. J. Collins, P. C. H. Watt, T. O'Reilly, R. J. McFarland, A. H. G. Love, Measurement of total bile acids in gastric juice. *J. Clin. Pathol.* **37**, 313–316 (1984).
52. R. B. Kimsey, A. Spielman, Motility of Lyme disease spirochetes in fluids as viscous as the extracellular matrix. *J. Infect. Dis.* **162**, 1205–1208 (1990).
53. W. R. Schneider, R. N. Doetsch, Effect of viscosity on bacterial motility. *J. Bacteriol.* **117**, 696–701 (1974).
54. B. Liu, T. R. Powers, K. S. Breuer, Force-free swimming of a model helical flagellum in viscoelastic fluids. *Proc. Natl. Acad. Sci. U.S.A.* **108**, 19516–19520 (2011).
55. S. E. Spagnolie, B. Liu, T. R. Powers, Locomotion of helical bodies in viscoelastic fluids: Enhanced swimming at large helical amplitudes. *Phys. Rev. Lett.* **111**, 068101 (2013).
56. T. D. Montenegro-Johnson, D. J. Smith, D. Loghin, Physics of rheologically enhanced propulsion: Different strokes in generalized stokes. *Phys. Fluids* **25**, 081903 (2013).
57. H. C. Fu, V. B. Shenoy, T. R. Powers, Low-Reynolds-number swimming in gels. *Europhys. Lett.* **91**, 24002 (2010).
58. H. C. Fu, C. W. Wolgemuth, T. R. Powers, Swimming speeds of filaments in nonlinearly viscoelastic fluids. *Phys. Fluids* **21**, 033102 (2009).
59. A. M. Leshansky, Enhanced low-Reynolds-number propulsion in heterogeneous viscous environments. *Phys. Rev.* **80**, 051911 (2009).
60. V. A. Martinez, J. Schwarz-Linek, M. Reufer, L. G. Wilson, A. N. Morozov, W. C. K. Poon, Flagellated bacterial motility in polymer solutions. *Proc. Natl. Acad. Sci. U.S.A.* **111**, 17771–17776 (2014).
61. W. D. Neithercut, P. A. Rowe, A. M. El Nujumi, S. Dahill, K. E. L. McColl, Effect of *Helicobacter pylori* infection on intragastric urea and ammonium concentrations in patients with chronic renal failure. *J. Clin. Pathol.* **46**, 544–547 (1993).
62. F. Hollander, The composition and mechanism of formation of gastric acid secretion. *Science* **110**, 57–63 (1949).
63. S. Kakimoto, H. Miyashita, Y. Sumino, S.-i. Akiyama, Properties of acid ureases from *Lactobacillus* and *Streptococcus* strains. *Agric. Biol. Chem.* **54**, 381–386 (1990).
64. J. Celli, B. Gregor, B. Turner, N. H. Afdhal, R. Bansil, S. Erramilli, Viscoelastic properties and dynamics of porcine gastric mucin. *Biomacromolecules* **6**, 1329–1333 (2005).

Acknowledgments: We thank the Department Spatz, Max Planck Institute for Intelligent Systems, for scanning electron microscopy access; the Nanostructuring Laboratory, Max Planck Institute for Solid State Research, for ALD access; and A. Posada for help with designing the figures. **Funding:** We thank the Max Planck Society for financial support. This work was in part supported by the European Research Council under the ERC Grant agreement 278213, the Deutsche Forschungsgemeinschaft (DFG) as part of the project SPP 1726 (microswimmers, FI 1966/1-1), and the Baden Württemberg Stiftung as part of the project BioMatS-10. O.L. and B.T.K. acknowledge support from the DFG through project B7 "Nanoagents in 3-dimensional biopolymer hydrogels" in the framework of SFB1032. **Author contributions:** D.W., P.F., and O.L. proposed the experiments. D.W. fabricated the micropropellers (with the exception of the ALD step), performed enzyme immobilization, verified urease activity, and conducted the propulsion experiments. B.T.K. isolated the mucin and measured its rheological properties, and H.-H.J. performed ALD. The report was written by D.W., B.T.K., O.L., and P.F. **Competing interests:** The authors declare that they have no competing interests. **Data and materials availability:** All data needed to evaluate the conclusions in the paper are present in the paper and/or the Supplementary Materials. Additional data related to this paper may be requested from the authors.

Submitted 21 April 2015
Accepted 25 September 2015
Published 11 December 2015
10.1126/sciadv.1500501

Citation: D. Walker, B. T. Käsdorf, H.-H. Jeong, O. Lieleg, P. Fischer, Enzymatically active biomimetic micropropellers for the penetration of mucin gels. *Sci. Adv.* **1**, e1500501 (2015).

A.6 Cationic astringents alter the tribological and rheological properties of human saliva and salivary mucin solutions

Biotribology 6 (2016) 12–20

Contents lists available at ScienceDirect

Biotribology

journal homepage: http://www.elsevier.com/locate/biotri

Cationic astringents alter the tribological and rheological properties of human saliva and salivary mucin solutions

Max Biegler [a,1], Judith Delius [b,1], Benjamin T. Käsdorf [a], Thomas Hofmann [b], Oliver Lieleg [a,*]

[a] Institute of Medical Engineering IMETUM and Department of Mechanical Engineering, Technical University of Munich, Boltzmannstraße 11, 85748 Garching, Germany
[b] Chair of Food Chemistry and Molecular Sensory Science, Technical University of Munich, Lise-Meitner-Straße 34, 85354 Freising, Germany

ARTICLE INFO

Article history:
Received 25 November 2015
Received in revised form 8 March 2016
Accepted 14 March 2016
Available online 16 March 2016

Keywords:
Friction
Lubrication
Glycoprotein
Astringency
Viscoelasticity

ABSTRACT

Oral astringency, typically described as a dry, puckering perception, arises upon ingestion of cationic or polyphenolic compounds. Although understanding the origin of this astringency sensation would be important for the gustatory optimization of food and beverages, the molecular mechanism remains to date unclear. This is in part due to the limited amount of experimental data on the interaction of cationic astringents with salivary proteins.

We here demonstrate that different cationic astringents entail a loss in saliva lubricity which we quantify with rotational tribology. Since saliva lubricity is governed by mucin glycoproteins, purified salivary mucin solutions reproduce this behavior very well. We show that the loss of lubricity of salivary mucin solutions results from mucin aggregation which we quantify by HPLC-UV.

Our results demonstrate that purified salivary mucins constitute a suitable model system for studying the molecular mechanisms governing alterations in the lubricity of native saliva as e.g. induced by astringents.

1. Introduction

Astringency is a roughening and puckering sensation elicited by the consumption of alimentary products with high polyphenol content such as unripe fruit, seeds, tea, cacao, and red wine [1–4]. In addition to polyphenols, multivalent cations [5,6], proteins exhibiting a high isoelectric point [7–9], and amino functionalized polymers [10], which carry positive charges at physiological pH, are reported to evoke an astringent mouthfeel. However, there is yet no conclusive model explaining the loss of oral lubrication which is suggested to be involved in the mechanism of astringency [11,12].

Although several salivary protein families including proline-rich proteins have been discussed over the past decades to play a potential role for astringency [13–15], mucoproteins have been largely underestimated mainly due to the lacking availability of purified human salivary mucins. Mucins are high molecular weight proteins which carry a high density of oligosaccharide side chains. Those glycans are attached to the protein backbone and constitute 50–90% of the molecular weight of mucins [16]. The two major families of salivary mucins, secreted by the submandibular and sublingual glands, are encoded by the MUC7 and MUC5B genes. MUC5B mucins can form oligomeric chains with molecular weights between 2 and 40 MDa [17] and contribute significantly to the viscoelastic properties of saliva [18]. Owing to their amphiphilic nature, mucins are able to attach to various materials and, due to steric repulsion, the surface-anchored oligosaccharide side chains stretch away from the protein core to form a "bottlebrush"-like superstructure [16]. At physiological pH, salivary mucins carry negative charges, which are surrounded by hydration shells. The lubricity of mucins is based on two mechanisms: First, hydration lubrication is established by forming a hydrated mucin layer on the surface and by exchanging of the bound water molecules with free water under shear [19,20]. Second, continuous de- and readsorption of mucins onto the surfaces dissipates energy as well and contributes to the low friction coefficients measured in mucin lubrication [20,21]. In addition, mucin coatings on surfaces may also lead to electrostatic and/or steric repulsion between the two surfaces thus further decreasing friction [21]. By combining those mechanisms, salivary mucins maintain lubricity of oral surfaces, protect them from irritation and abrasion during speaking and chewing, and facilitate swallowing [22].

Upon exposure to astringent substances, a decrease in salivary lubricity has been attributed to the formation of sensible precipitates of aggregated salivary proteins [30]. An alternative, recent concept suggests the disruption of lubricious mucin coatings on the oral mucosa by astringents, thereby inducing friction and possibly exposing oral receptors [31]. Previous research investigated changes in lubricating properties of fresh saliva induced by polyphenolic astringents [23–26], β-lactoglobulin [26], and alum [26,27], while neglecting other polycationic astringents like the amino functionalized polymer chitosan. Inconsistencies between in vitro saliva-astringent friction

* Corresponding author at: Zentralinstitut für Medizintechnik der Technischen Universität München, Boltzmannstraße 11, 85748 Garching, Germany.
E-mail address: oliver.lieleg@TUM.de (O. Lieleg).
[1] Both authors contributed equally to the work.

http://dx.doi.org/10.1016/j.biotri.2016.03.002
2352-5738/

Appendix A.6 Cationic astringents alter the tribological and rheological properties of human saliva and salivary mucin solutions

measurements and the perception of astringency have been observed and discussed [25–27].

The study presented here aims at further investigating tribological and rheological changes occurring in saliva, and especially in salivary mucin solutions, upon exposure to astringents. The main hypothesis we test here is that different classes of astringents compromise the lubricating properties of salivary mucins, a mechanism which may contribute to the sensation of astringency. We focus on cationic astringents rather than polyphenols, and test the compounds for their astringency thresholds as well as their interactions with saliva and two salivary in vitro model systems. We compare the influence of selected representative astringents, namely the two metal salts iron(III) sulfate and aluminum(III) chloride, the basic protein lysozyme and chitosan, on the tribology and rheology of native human saliva and reconstituted solutions of salivary mucins. As control substances we test substances which are either neutral (high molecular weight dextran), negatively (sodium carboxymethyl cellulose and phosvitin) or positively charged (DEAE-dextran).

All analyzed astringents, when applied at concentrations above their sensory threshold of astringency, reduce the lubricating potential of native human saliva. This effect occurs in a dose-dependent manner and leads to a permanent loss of lubrication at high astringent concentrations. We demonstrate that this loss of salivary lubrication is reproduced by model lubricants comprising either purified bovine or human salivary mucins. In those model lubricants as in saliva, the addition of the cationic astringents induces a weak gelation of the mucin solution which we attribute to polyelectrolyte complexation of the negatively charged mucins by the positively charged astringents through ionic cross linking [7,28]. Finally, we show that this astringent induced gelation reduces the concentration of solubilized and thus lubricating mucins, a mechanism which may contribute to the sensation of astringency perceived in the oral cavity.

2. Experimental

2.1. Saliva collection, mucin purification and chemicals used

Saliva was freshly collected in ice-cooled tubes from up to 12 healthy volunteers (age range: 25–35 years) who have refrained from eating and drinking anything except water for one hour prior to donating saliva. Individual donations were pooled and centrifuged for 30 min at 25,000 RCF and 4 °C to remove larger particles and cell debris. Afterwards, the pellet was discarded, and the clear supernatant (from now on referred to as saliva) was stored at 4 °C and used on the same day. For purification of human salivary mucin (HSM), saliva was diluted 1:1 with ice-cold phosphate buffer (10 mM sodium phosphate, 170 mM NaCl, pH 7) and ultracentrifuged at ~160,000 RCF for 1 h. Further purification of the supernatant was performed by size exclusion chromatography using an Äkta purifier system (GE Healthcare, Chalfont St Giles, UK) equipped with a XK50/100 column filled with sepharose 6FF (GE Healthcare) at a flow rate of 9.5 mL/min. The fractions containing mucin were then pooled, concentrated and desalted by cross-flow dialysis using a hollow fiber cartridge (UFP-100-E-3MA, GE Healthcare) with 100 kDa molecular weight cut off and 110 cm^2 surface area until a conductance of less than 50 μS/cm was reached. The presence of human salivary mucin MUC5B was verified via indirect ELISA. 0.3% (w/v) purified protein was reconstituted in HEPES (20 mM, 154 mM NaCl, pH 7), incubated with a mouse monoclonal anti-MUC5B antibody (abcam, Cambridge, UK) and visualized with a secondary goat anti-mouse antibody (antibodies-online, Atlanta, GA, USA) labeled with horseradish peroxidase. O-phenylenediamine (Sigma-Aldrich, St. Louis, MO, USA) added to this mix was then converted by horseradish peroxidase, and the reaction product was determined spectrophotometrically. Purified MUC5B was lyophilized and stored at −80 °C until further use, where it was solubilized in TRIS buffer at pH 7. Bovine submaxillary mucin (BSM, lot# D00160765) was obtained from Calbiochem (San Diego, USA) and dissolved in TRIS buffer at pH 7.

Astringents were used for tribological and rheological experiments at concentrations where they evoke a comparable supra-threshold orosensory response. (−)-Epigallocatechin gallate (EGCG) and iron(III)sulfate (Sigma-Aldrich, St. Louis, MO, USA) were dissolved at 5 mM in ultrapure H_2O. Aluminum chloride hexahydrate was obtained from Carl Roth (Karlsruhe, Germany) and used either as a 5 mM solution (to mimic the concentration in the commercial mouth rinse Mallebrin®) or 10 mM aqueous solution (to match the molarity of cations to those in the $Fe_2(SO_4)_3$ solution). Lysozyme from chicken egg white (UniProt: P00698) was obtained from Amresco (Solon, USA) and used at a concentration of 0.25 mM. At pH 7, lysozyme carries a net positive charge (17 positive charges and 9 negative charges per molecule, as determined by its amino acid sequence). Highly deacetylated chitosan with a molecular weight of 523 ± 24 kDa (Chitosan 95/3000, batch 212-200415-02) was obtained from Heppe Medical Chitosan GmbH (Halle/Saale, Germany). According to the manufacturer, the degree of deacetylation is larger than 92.6%. Chitosan flakes were dissolved in 0.1 M hydrochloric acid and then diluted with ddH_2O to a final concentration of 2 μM with a pH of 5. At this pH, chitosan is strongly positively charged as it carries ~3200 positive charges per molecule [29]. Phosvitin, sodium carboxymethyl cellulose (CMC, molecular weight ~250 kDa), and diethylaminoethyl dextran (DEAE-dextran, ~500 kDa) were purchased from Sigma-Aldrich and dissolved at 0.25 mM for Phosvitin, 4 μM for CMC and 2 μM for DEAE-dextran. Unmodified dextran (~500 kDa) was obtained from Carl Roth and also dissolved at 2 μM in accordance with the concentration of chitosan.

2.2. Human sensory studies

Psychophysical analyses were performed in a sensory laboratory at 20–22 °C by a trained panel of up to 12 volunteers of the Chair of Food Chemistry and Molecular Sensory Science. To avoid interference by sample color, ambient light in the sensory cabins was adjusted to the color of the samples. Test substances were freshly dissolved in Evian® mineral water, which was also used as a taste neutral rinsing solution.

Taste recognition thresholds of the astringents were determined in the format of an ascending triangle test. Serial aqueous dilutions (1:2) of the substances were presented to the panelists in the order of rising concentrations. pH was adjusted with 0.1 M $HCl_{(aq)}$. Panelists were asked to localize the astringent solution within a set of three samples at any one time. The geometric mean of the first concentration recognized correctly (c_r) and the prior concentration misjudged (c_{r-1}), gave the individual's taste recognition threshold (R_i): $R_i = \sqrt{(c_r)(c_{r-1})}$.

The corresponding taste recognition threshold for the whole panel (R_p) with n subjects was determined by calculating the geometric mean of the individual taste thresholds:

$$R_p = \sqrt[n]{\prod_{i=1}^{n} R_i}$$

2.3. Rotational tribology

Tribology experiments were conducted on an MCR302 shear-rheometer (Anton Paar, Graz, Austria) equipped with a tribology cell (P-PTD200/56/AIR, Anton Paar) and a customized sample holder. The setup is described in detail in Boettcher et al. [30]. In brief, a rotating steel sphere with a diameter of 12.6 mm (Kugel Pompel, Vienna, Austria) is put in contact with three cylindrical pins and lubricated with a fluid (see Fig. 1). As a second partner in this tribology pairing, PDMS (polydimethylsiloxane, Sylgard 184, Dow Corning, Midland,

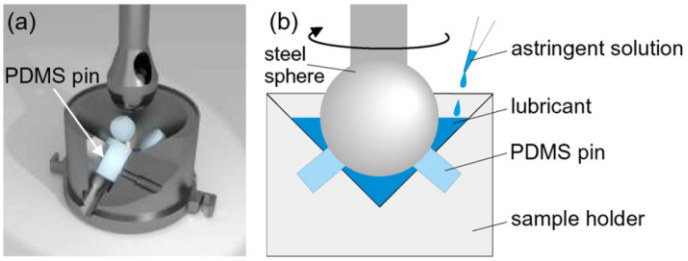

Fig. 1. Schematic representation of the rotational tribology setup used to study saliva lubricity. (a) 3-dimensional rendering of the sample holder. The PDMS pins are inserted into the sample holder until only ~1 mm of each cylinder reaches into the conical lubricant chamber. The pins are laterally fixed with screws, and the steel sphere rotates on those pins at a normal force of 6 N. (b) Schematic cross-section of the sample holder. The sample chamber is filled with lubricant, and astringent solution is added every 6 min.

USA) was chosen to mimic the mechanical and wetting properties of the tongue/palate system: Steel approximates the hard palate and PDMS the elastic properties of the tongue. The Young's modulus of the tongue ranges between 15 and 250 kPa [31] which is approximated by PDMS prepared at a cross-linker/oil ratio of 1:10 resulting in a Young's modulus of ~1.4 MPa [32].

In approximation of the mouth, this tribology pairing leads to a greater contact area under normal load as the soft PDMS deforms to follow the shape of the rigid steel sphere. Additionally, the uncoated tongue tissue has a hydrophobic tendency with a contact angle of ~80° that is lowered through adsorption of saliva and salivary mucins [33]. PDMS approximates this behavior as it is hydrophobic in its untreated state with a contact angle of 109° [34] but becomes hydrophilic by adsorption of saliva with a reduced contact angle of (72 ± 4)°.

For friction measurements, 600 μL of lubricant was added to the sample chamber and the steel sphere was lowered onto the samples until a normal force of 6 N was reached, corresponding to a normal pressure of 0.2 MPa on the PDMS pins. The friction coefficient was evaluated from speed ramps with rotational sliding speeds from 10^{-2} mm/s to 10^{3} mm/s. To assess the influence of astringents on a lubricant, the sliding speed was kept constant at an intermediate speed level of 1 mm/s for a time period of 60 min. In the first minute of the test, the recorded friction coefficient rapidly decreased to a steady state value, which we refer to as μ_0 or initial friction coefficient. This behavior can be attributed to mucin binding to the steel and PDMS surfaces until a steady state between binding and mechanical desorption is reached [26,35]. After 6 min, 150 μL of an astringent solution was added to the lubricant, and the friction coefficient was recorded for 6 min. Then, additional 150 μL of astringent solution was injected, and this procedure was repeated 5 times in total. Afterwards, the friction coefficient was monitored for additional 30 min before the experiment was terminated. Three independent measurements were conducted with freshly prepared solutions for each lubricant/astringent combination.

2.4. Shear rheology

Shear rheology experiments were performed on the shear-rheometer (MCR302, Anton Paar) to assess the viscoelastic properties of sample solutions. A parallel plate setup consisting of a stationary bottom plate and an oscillating measuring head with a diameter of 50 mm (PP50, Anton Paar) was used at a plate separation distance of 450 μm. In preliminary experiments, a time-dependent increase in the viscoelastic behavior was observed after the astringents were added to the lubricants. Thus, all samples were premixed and incubated for 45 min (30 min in a reaction tube and 15 min in the rheometer) before measurements were initiated. To compare pure saliva/mucin solutions with saliva and salivary mucin solutions to which astringents had been added, the pure solutions were diluted in the same 1:1 ratio with ddH_2O to match the mucin concentration in the other samples.

1 mL of test solution was pipetted onto the center of the bottom plate, and the fluid fully filled the space between the plates when the measuring head was lowered. When exposed to air, saliva forms a stiffening interfacial layer [24,36] which introduces an error into the measuring result. To prevent the contact with air during the measurement, PDMS oil (AB112152, ABCR, Karlsruhe, Germany) was applied to the outside of the measuring head where it formed a thin oil film. Frequency sweeps were carried out in a range from 10 Hz to 0.1 Hz. Several tests with varying strains were conducted to characterize the region of linear response for all samples. To perform measurements with a single protocol that ensures linear viscoelastic response for all samples, a small torque that leads to linear response for the softest and the stiffest sample was used in all tests. This torque was set to 0.5 μNm and the rheometer then adjusted the strain for each sample to maintain the set torque.

2.5. Viscosimetry

Viscosity measurements were conducted on a shear-rheometer (MCR302, Anton Paar) with a cone-against-plate setup (Anton Paar, CP50-1 measuring head). 570 μL sample solution was pipetted onto the bottom plate following the standard procedure provided by the manufacturer. A shear-ramp was measured with shear rates between 10^{3} and 10^{-1} s^{-1}. As the measurement progressed from high to low shear rates, potential stiffening-inducing interfacial layers were broken up and the formation of new layers was inhibited by the continuous rotation [18]. Hence, a protective oil film was not necessary in the viscosity measurements.

2.6. Analysis of whole saliva and mucin aggregation

Saliva was mixed with aqueous astringent solutions at a 4:1 ratio and ultrapure H_2O was used as a control. After 30 min samples were centrifuged for 30 min at 16,000 RCF. The supernatants were separated from the precipitates and prepared for sodium dodecyl sulfate polyacrylamide gel electrophoresis (SDS-PAGE) to analyze proteins remaining in solution. 250 μL aliquots of the respective supernatant salivary samples were mixed with a fivefold excess of acetone and stored at −20 °C for 24 h to fully precipitate the remaining proteins. Samples were centrifuged (16,000 RCF, 15 min, 4 °C) and freed from acetone under a stream of nitrogen. To reduce disulfide bonds, proteins were taken up with 70 μL of a 1:1 mixture of 100 mM aqueous dithiothreitol (Amresco, Solon, USA) and NuPAGE sample buffer (Invitrogen, Carlsbad, USA). Samples were heated up to 95 °C, kept shaking at this temperature for 10 min and were then stored at −20 °C for gel electrophoresis. Aliquots of the processed sample material were loaded on a 4–12% NuPAGE®-Novex® protein gel (Invitrogen, Darmstadt, Germany) in an XCell Sure Lock™ electrophoresis cell and run at 200 V for 45 min to separate into distinct protein bands. Precision Plus Protein™ (Bio Rad, München, Germany)

Appendix A.6 Cationic astringents alter the tribological and rheological properties of human saliva and salivary mucin solutions

unstained standard was used as a molecular-weight size marker. Proteins were fixed with 2% acetic acid in 40% methanol while gently shaking the solution for 1 h. Gels were stained for 90 min with an aqueous solution containing 20% colloidal Coomassie blue (Carl Roth, Karlsruhe, Germany) and 20% methanol. For partial destaining, gels were washed with 5% acetic acid in 25% methanol followed by treating with 25% ethanol.

Analogous experiments were carried out with the salivary mucin MUC5B. MUC5B was taken up in TRIS buffer (0.1%, w/v) to reconstitute the mucin content of human saliva. This mucin solution was mixed with astringents at a 1:1 ratio and incubated at room temperature. After centrifugation the supernatants were separated and the mucin content remaining in solution was quantified by HPLC-UV (see Section 2.6). Samples were generated as such in triplicates. Analytical size exclusion chromatography was used to quantify mucin which remains in solution after treating the reconstituted mucin solution with astringents. Isocratic chromatography was conducted on a Jasco HPLC System (Jasco, Groß-Umstadt, Germany) with a Yarra™ gel filtration column SEC-3000, exhibiting a pore size of 290 Å and a dimension of 300 × 7.8 mm (Phenomenex, Aschaffenburg, Germany). As a mobile phase, a buffer composed of 100 mM sodium phosphate (Sigma-Aldrich, St. Louis, MO, USA), pH adjusted with o-phosphoric acid to 6.8, was used at a flow rate of 1.0 mL/min. Ultrapure water was prepared with a Milli-Q Gradient A10 system (Millipore, Schwalbach, Germany). Chromatograms were recorded with a diode array detector. Mucin was quantified by external calibration at a wavelength of 210 nm.

2.7. Statistical analysis

Statistical significance was assessed by one-way ANOVA and Tukey post-hoc tests. To verify the assumptions of normal distribution and homogeneity of variances, the Shapiro–Wilk test of normality and the Levene's test for homogeneity of variances were used. Differences between the examined groups were considered to be statistically significant for $p < 0.05$. All statistical analyses were performed using the software R (R Foundation for Statistical Computing).

3. Results and discussion

Astringents belong to very diverse compound classes such as polyphenols, metal salts, polysaccharides, and proteins. In this study, we aim at comparing different astringents in terms of their influence on the lubricating ability of human saliva and salivary mucin solutions. In detail, we have selected the two metal salts $Fe_2(SO_4)_3$ and $AlCl_3$, the basic protein lysozyme isolated from hen egg white and the cationic polymer poly-(β-(1-4)-D-glucosamine), also referred to as chitosan. This polysaccharide is a highly deacetylated derivative of chitin. In addition, we test the polyphenol (−)-EGCG, a low-molecular weight phenolic belonging to the condensed tannin group [14] for its capacity to precipitate mucins. First, we determine the sensory recognition thresholds of the mouth-puckering compounds EGCG, $Fe_2(SO_4)_3$, chitosan, and lysozyme for the attribute astringency (Table 1). The taste thresholds of the individual compounds appear to cover a broad concentration range (i.e. 0.04–225 μmol/L). The differences in concentrations expressed as g/L are less distinct, considering the huge variation in molecular weights (399–500,000 Da). In the subsequent experiments we use these compounds at concentrations where they evoke a comparable supra-threshold psychophysical response.

Table 1
Sensory recognition thresholds for the test compounds used. The errors denote the standard deviation of two independent sensory trials.

	Test compound	Molecular weight [g/mol]	Astringency threshold [μmol/kg H_2O]	Astringency threshold [% w/w]
Astringents	(−)-EGCG	458	225 ± 50	0.010 ± 0.003
	$Fe_2(SO_4)_3$	399	189 ± 69	0.008 ± 0.003
	Chitosan	~500000	0.04 ± 0.01	0.002 ± 0.001
	Lysozyme	14300	11 ± 1.6	0.016 ± 0.003
Non-astringents	Phosvitin	34000	n.d.[#]	n.d.[#]
	Sodium carboxymethyl cellulose	250000	n.d.[#]	n.d.[#]
	Dextran	~500000	n.d.[#]	n.d.[#]

[#] n.d.: not detectable until highest test conc. of 10 mg/mL

When we analyze the salivary proteins which remain in solution after saliva has been incubated with this set of astringents and centrifuged, we consistently detect a pronounced depletion of proteins in the high molecular weight region by SDS-PAGE (dashed rectangle, Fig. 2). These proteins belong to the mucin family [37] and contribute to the lubricating and viscoelastic properties of saliva [18]. However, not all astringents tested seem to bind these high molecular weight proteins to the same degree. Whereas chitosan eliminates mucins virtually completely and the other cationic compounds remove most of the mucins, the polyphenol EGCG does not deplete these bands in the gel. This indicates that EGCG interacts with salivary proteins in a substantially different manner than the cationic astringents. Binding of EGCG to hydrophobic regions of the mucin molecules, rather than ionic polyelectrolyte complexation, has to be considered here [38,39]. Therefore, the mechanisms underlying EGCG-saliva interactions will not be further investigated here.

Next, we conduct tribological experiments to test whether the astringent compounds reduce the lubricity of human saliva, and if mucins are the governing salivary component for such a mechanism. In comparison to TRIS buffer, the Stribeck curve obtained with human saliva does not exhibit a pronounced plateau in the boundary lubrication regime but shows a continuous decrease in the friction coefficient μ with increasing sliding speeds (Fig. 3a). At a sliding speed of ~100 mm/s, the hydrodynamic regime is reached for both lubricants, and the friction coefficient increases. The lubricity of saliva is significantly lower than that of TRIS buffer for sliding speeds below 7 mm/s ($p < 0.05$). In this study, the influence of astringents on the lubricating abilities of saliva and salivary mucin solutions is evaluated at a constant sliding speed of 1 mm/s. This speed was chosen as mucins are good lubricants in the boundary and mixed lubrication regime and, in the utilized tribology setup, the boundary lubrication regime is entered at this sliding speed. Thus, we can sensitively monitor a loss of lubricity of saliva after astringent addition.

$AlCl_3$ is the astringent component in the commercial mouth rinse Mallebrin®. The addition of a dose of 0.75 mmol $AlCl_3$ to a sample of 600 μL human saliva increases the friction coefficient, and the lubricity of saliva is progressively reduced the more astringent is added (Fig. 4a). After five injections of the astringent, i.e. 3.75 mmol $AlCl_3$, the lubricity does not change any further with continuing astringent addition, and a residual lubrication $\mu_{final} - 10\mu_{initial}$ is observed (Fig. 4d).

The relative increase in the friction coefficient after n astringent injections, i.e. the friction coefficient before the $(n + 1)$th injection normalized by the friction coefficient obtained without any astringent addition, averaged over 20 s, is shown in Fig. 4d–f (see methods for details). Data obtained with native saliva show large sample-to-sample variability. We attribute this to the biological variations in saliva composition, which can be influenced among others by diet, stress level, and physical activity [22,36]. We next ask to what degree salivary mucins can reproduce the tribological and rheological properties of saliva as well as the alterations evoked by astringents. We compare reconstituted solutions of in-house purified human salivary mucin (HSM) at a concentration of 0.02% (w/v), which correspond to the average mucin concentration of human saliva [40]. We confirmed the isolated HSM to be MUC5B by successful application of mouse monoclonal anti-MUC5B antibody (data not shown). Also,

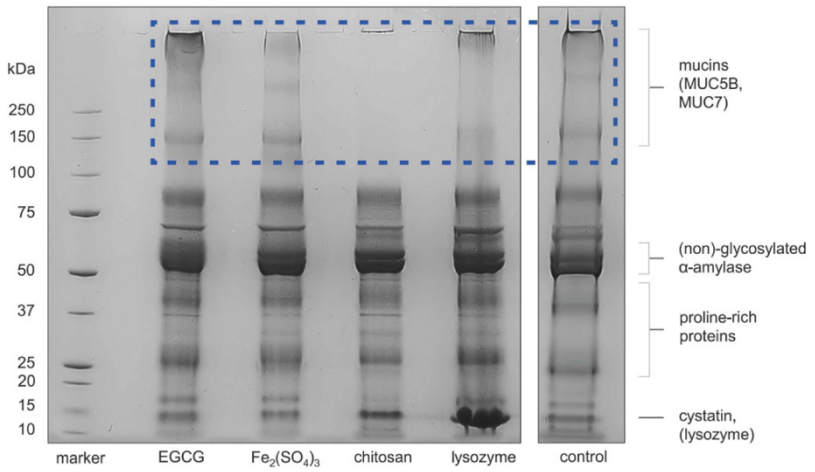

Fig. 2. SDS-PAGE of salivary proteins which remain in solution after treatment with astringents. Whole saliva was mixed in a 4:1 ratio with astringents (EGCG, $Fe_2(SO_4)_3$, chitosan, and lysozyme) and then centrifuged; H_2O was used as a control. Molecular weight markers appear in lane 1. The band region of mucins is accentuated in the gel by a dashed rectangle.

we find that the isolated mucin co-elutes in size exclusion chromatography with the highest molecular protein fraction of a fresh saliva sample (Fig. 3b). When a HSM solution is reconstituted at 0.02% (w/v) in 20 mM TRIS (pH 7) to mimic the typical pH range of human saliva (pH 6.2 to pH 7.4), its buffering capacity [36] and the average mucin concentration [40], the Stribeck curve matches that of native saliva (Fig. 3a). In detail, at a sliding speed of 1 mm/s, we measure an identical friction coefficient $\mu = 0.004 \pm 0.002$ for saliva and 0.02% (w/v) HSM ($n = 3$). Increasing the HSM concentration to 0.1% (w/v) does not significantly change this value as we still measure $\mu = 0.004 \pm 0.002$. However, at these elevated mucin levels, we can determine the friction coefficient with a better signal-to-noise ratio. In contrast, when prepared at matching concentrations of 0.1% (w/v), the BSM solutions result in significantly higher friction coefficients for speed levels <2 mm/s ($p < 0.05$), e.g. an average value of $\mu = 0.017 \pm 0.009$ at 1 mm/s.

To test whether reconstituted mucin solutions can reproduce the dose-dependent loss of lubricity observed for native saliva upon $AlCl_3$ addition, five doses of 0.75 mmol $AlCl_3$ were added to 0.1% HSM and BSM solutions — analogous to the experiments with native saliva. For HSM solutions, a small spike in the friction coefficient is observed after each injection. The friction coefficient approaches a plateau which is higher than the initial value. Whereas the BSM solutions exhibit a similar behavior, i.e. a spike in the friction coefficient upon $AlCl_3$ addition followed by a higher plateau value, the signal-to-noise ratio and sample-to-sample variations are larger for BSM samples. When comparing the normalized increase in friction (Fig. 4d–e), the continuous loss of saliva lubricity described before is approximated by the HSM solutions very well. In addition, the friction curves determined with HSM show a better signal-to-noise ratio than those acquired with native saliva. The BSM solutions lose their lubricity earlier than the two other lubricants, typically after only two astringent injections. We note that, for BSM solutions, the sample-to-sample variations are considerably larger than for HSM solutions, which could reflect impurities in the commercial BSM [41,42].

Together, these initial experiments indicate that, qualitatively, both mucin solutions can approximate the behavior of native human saliva reasonably well. However, HSM solutions appear to be the superior model system as they reproduce the absolute value of the friction coefficient measured for saliva as well as the dose-dependent increase of this friction coefficient with $AlCl_3$ addition more closely than BSM solutions. Similar results are obtained, when the trivalent metal salt $Fe_2(SO_4)_3$ is added to saliva or mucin solutions at identical concentrations as $AlCl_3$, i.e. at 0.75 mmol/injection (see Fig. 4d–f). A total increase in friction by a factor of ~13 is observed for saliva after five injections of $Fe_2(SO_4)_3$. The rise in friction is dose-dependent for all saliva samples challenged with this salt; however, for some samples two doses of $Fe_2(SO_4)_3$ are necessary to induce a measurable loss of

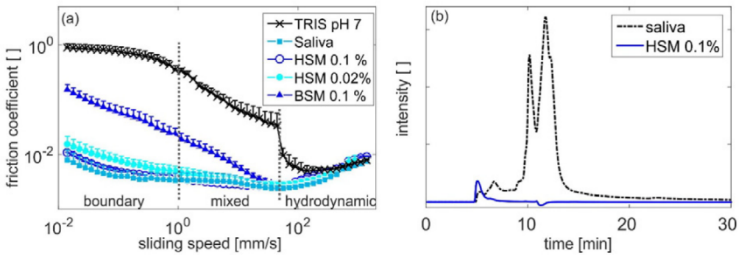

Fig. 3. Lubricating properties and size exclusion chromatogram of human saliva and purified mucins. (a) Stribeck curves for a steel/PDMS tribology pairing are depicted for five lubricants: human saliva (squares), reconstituted HSM (human salivary mucin) solutions (open and closed circles), a BSM (bovine submaxillary mucin) solution (triangles) and TRIS buffer (crosses). The error bars denote the standard deviation as obtained from three independent experiments. (b) UV chromatogram of human whole saliva (dashed line). Mucins elute after 5 min as shown by the overlaid chromatogram of purified human salivary mucin (HSM, solid blue line).

Appendix A.6 Cationic astringents alter the tribological and rheological properties of human saliva and salivary mucin solutions

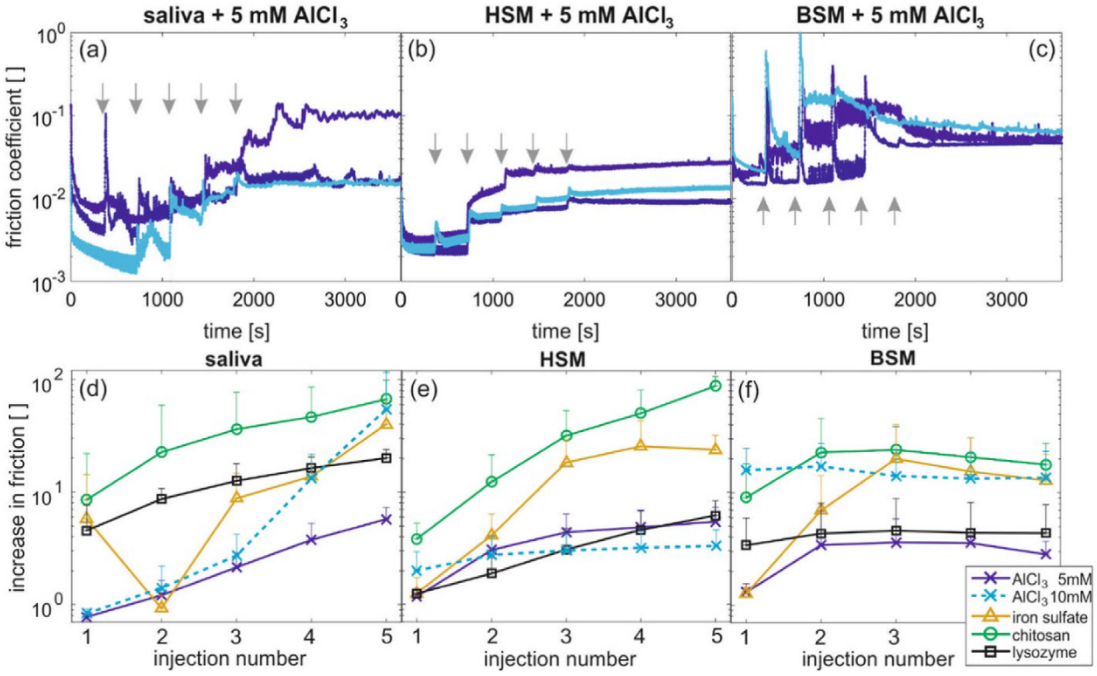

Fig. 4. Astringent-induced changes in the lubricity of human saliva and reconstituted solutions of salivary mucins. (a–c) 150 μL of a 5 mM $AlCl_3$ solution is added to 600 μL of the respective lubricant at distinct time points (indicated by gray arrows) and conducted in triplicate for each lubricant. Human salivary mucin (HSM) solutions are compared to human saliva and bovine submaxillary mucin (BSM) solutions. With added amounts of astringent, the lubricating properties of each solution are reduced until a plateau is reached. (d–f) shows the normalized increase in friction observed for saliva, HSM, and BSM, respectively, after addition of different astringents (see experimental section for details). The error bars denote the standard deviation as determined from three independent experiments.

lubricity — which causes the discontinuity in Fig. 4d. In contrast, for HSM and BSM solutions, the increase in friction is continuous and well-reproducible, and for both mucin variants the decrease in lubricity saturates after three $Fe_2(SO_4)_3$ injections. When we use a 10 mM $AlCl_3$ stock solution with 1.5 mmol/injection (dashed lines in Fig. 4d–f) to compare both metal salts at equal cation concentration, the maximum loss of lubricity is higher and is already reached after fewer astringent injections, which underscores the concentration dependence of the observed effects.

Also the addition of the astringent protein lysozyme to either saliva or HSM solutions evokes a continuous increase in the normalized friction coefficient. The friction coefficient μ_{final} reached after five injections of lysozyme is ~$10\mu_{initial}$ for saliva and ~$6\mu_{initial}$ for HSM, respectively (Fig. 4d and e). In contrast, the lubricating properties of BSM are already lost after the first injection of lysozyme, and the friction factor does not increase any more with further astringent addition. Upon chitosan addition, we find the strongest loss of lubricity among the four astringents tested so far. Chitosan is injected in doses of 0.3 μmol each and we measure a 70-fold increase in the friction coefficient after five chitosan injections both for saliva and HSM solutions. Again, the BSM solution fails to reproduce the continuous loss of lubrication as the friction coefficient remains constant after only two injections at $\mu_{final} \sim 20\mu_{initial}$.

We conclude that all four astringents investigated induce a dose-dependent loss of lubrication in saliva as well as in both mucin model systems. Moreover, in all cases, HSM solutions reproduce the behavior of saliva more precisely. Such a loss of saliva lubricity, as well as a persisting residual lubrication has also been shown before for EGCG [25,26] and the cationic compounds alum and beta-lactoglobulin [26] using a mini-traction machine. In both setups, it was only possible to add 50 mL of aqueous astringent solution to 100 μL of pre-adsorbed saliva, which caused the saliva to lose its lubricity after a single injection. With our setup, we can demonstrate that with progressive addition of small amounts of an astringent solution a dose-dependent loss of lubricity occurs both for saliva and salivary mucin solutions.

We next set out to identify the molecular reason that induces this loss of lubricity. Both $AlCl_3$ and $Fe_2(SO_4)_3$ contain multivalent cations, and both lysozyme and chitosan carry multiple positively charged groups. Due to the presence of sialic acid groups and sulfated glycans [43,44] salivary mucins possess a negative net charge at neutral pH and thus are able to interact with the positively charged astringents through electrostatic binding. Such electrostatic interactions could occur via ionic cross-linking in a network of long polymer chains, which in turn should lead to an increased shear stiffness of the polymer solution.

If such electrostatic interactions are indeed responsible for the effects described so far, then neutral or negatively charged molecules should return different results. To test this hypothesis, we sensorially evaluate three polysaccharides, which are neutral (unmodified dextran), positively (DEAE-dextran) or negatively charged (carboxymethyl cellulose). Additionally, we test the acidic protein phosvitin, one of the major proteins of egg yolk, which is highly phosphorylated and therefore carries multiple negative charges at physiological pH conditions [45]. Panelists do not perceive any roughening feeling in the oral cavity for any of the neutral or negatively charged macromolecules until the highest concentration tested (see Table 1 for details), whereas they sense positively charged DEAE as astringent at equivalent concentrations (data not shown). In full agreement with the sensorial evaluations of those control substances, we also find a

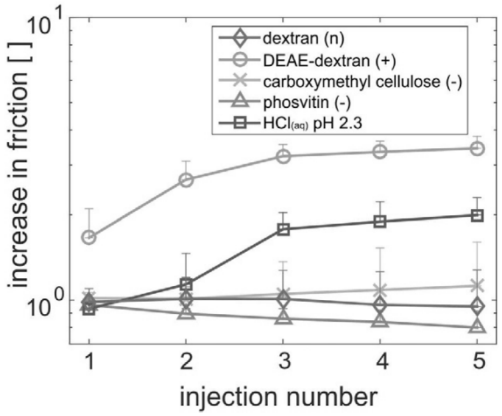

Fig. 5. Friction increase in human salivary mucin solutions after the addition of control substances. The normalized increase in friction is shown for repeating injections of macromolecules carrying different net charges and $HCl_{(aq)}$ as a pH control. The error bars denote the standard deviation as obtained from three independent experiments.

loss of lubricity in HSM solutions solely for the positively charged DEAE-dextran, but not for the other substances. The normalized friction increase for the control substances is shown in Fig. 5.

If the cationic astringents interact with salivary proteins through electrostatic forces, the addition of positively charged astringents to a solution of salivary mucins should also lead to an alteration of the viscoelastic properties of the biopolymer solution as the mucins become cross-linked. A qualitative indication for such a cross-linking reaction mediated by the astringents is an increase in saliva turbidity and pellet formation after centrifugation (Fig. 6a). Quantitatively, a change of the viscoelastic properties – i.e. an alteration of the storage modulus (representing the elastic properties) and of loss modulus (representing the viscous properties) of the material – can be determined by macrorheology as shown in Fig. 6b. Without addition of astringent, both saliva and salivary mucin solutions (0.05% w/v) are clearly dominated by viscous properties, and we hardly measure any elastic response of the biopolymer solutions at all. Also, all three biopolymer fluids show viscosities η close to that of water, and we measure $\eta_{saliva} = 2.7 \pm 0.3$ mPas, $\eta_{BSM} = 1.4 \pm 0.3$ mPas, and $\eta_{HSM} = 1.1 \pm 0.1$ mPas at a shear rate of 100 s^{-1} (Fig. 6c). However, upon addition of any of the four cationic astringents compared here, we observe a clear sol–gel transition for saliva (Fig. 6d), and the elastic properties of the system become not only measurable but even dominate the viscous properties over a broad range of frequencies. In Fig. 6b, the frequency spectrum is shown for saliva before and after addition of chitosan. After chitosan addition, the viscoelastic properties are almost constant over the measured frequency range, thus we quantify the effect of different astringents by comparing the viscoelastic moduli at an intermediate frequency of 1 Hz (Fig. 6d–f). We measure the strongest increase in the elastic properties for chitosan/saliva mixtures, i.e. a storage modulus of ~8 Pa. A slightly weaker increase in the storage modulus is observed for HSM and BSM solutions upon chitosan addition. Also the other cationic astringents evoke a qualitatively comparable alteration of the viscoelastic properties of both saliva and salivary mucin solutions, i.e. a sol–gel transition. Overall, the absolute increase in the shear stiffness is largest for the BSM solutions and lowest for the HSM solutions.

Comparable to MUC5AC [46] and MUC2 [47] solutions, also saliva and solutions of salivary MUC5B exhibit a sol–gel transition when the

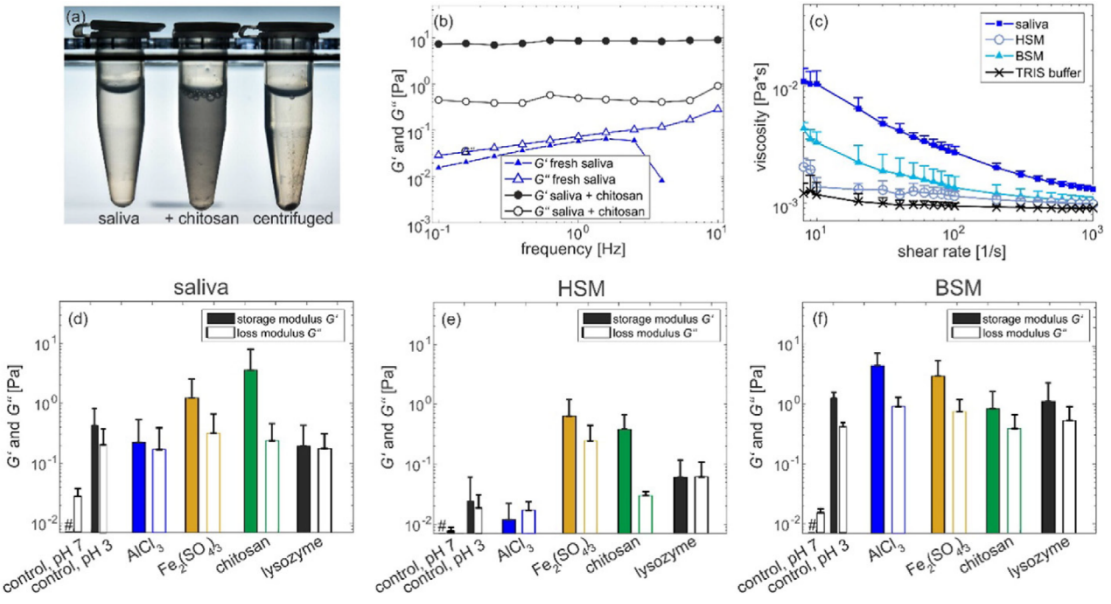

Fig. 6. Influence of astringents on the viscoelastic properties of saliva and salivary mucin solutions. (a) The turbidity of saliva increases after chitosan addition but is diminished after centrifugation, which is accompanied by pellet formation. (b) The addition of e.g. chitosan triggers a sol–gel transition in saliva: different from unmodified saliva, the storage modulus dominates the loss modulus over a broad range of frequencies. (c) The shear-rate dependent viscosity of saliva is compared to that of BSM and HSM solutions. As typical for biopolymer solutions, all samples show shear thinning behavior. (d–f) Comparison of the viscoelastic moduli for the different astringent/lubricant combinations at a probing frequency of 1 Hz. After addition of astringents to saliva, the storage moduli (filled bars) are larger than the respective loss moduli (empty bars). This behavior is approximated by BSM and HSM solutions. The storage moduli of control saliva and mucin solutions, i.e. without astringent addition, are so low that we could not successfully measure them with the rheometer (denoted by #). The error bars in (c)–(f) denote the standard deviation as determined from three independent experiments.

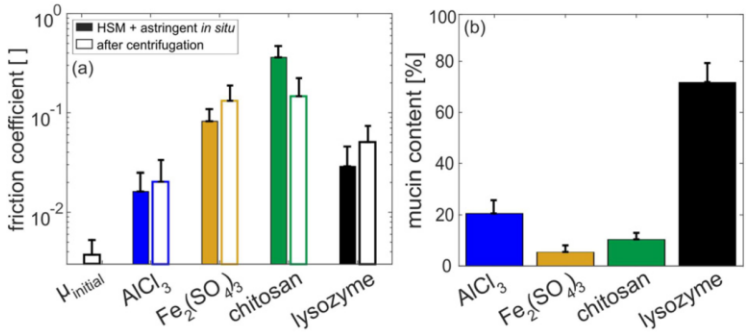

Fig. 7. Lubricity and mucin content of HSM solutions after astringent treatment. (a) Friction coefficients at the end of HSM experiments with in situ astringent addition are compared to the friction coefficient obtained for the supernatant of centrifuged HSM solutions. (b) Depletion of HSM after astringent addition and subsequent centrifugation. Mucin concentrations are referenced to the control (equivalent mixture with H_2O) and expressed as percentage values (w/v). Error bars denote the standard deviation as obtained from three independent experiments.

pH is lowered to acidic conditions (Fig. 6d–f). As the aqueous solutions of $AlCl_3$ and $Fe_2(SO_4)_3$ are acidic (pH 4.4 and 2.4 respectively), pH dependent and astringent-induced gelation can compete in the rheology experiments. However, tribological control experiments with $HCl_{(aq)}$ at equivalent pH as the metal salt solutions showed negligible influence on the lubricity of HSM solutions (Fig. 5). This demonstrates that the observed loss of lubricity we report for $AlCl_3$ and $Fe_2(SO_4)_3$ is indeed due to the cations and their interaction with the salivary mucins.

How can alterations of the viscoelastic properties lead to a loss of lubricity of saliva and salivary mucin solutions? One possible explanation could be that, as a consequence of the sol–gel transition, the increased viscous properties of the biopolymer solutions (as represented by the increased loss moduli) result in an altered Stribeck number ($St = \frac{\eta \cdot v}{P_n}$), thus changing the measured friction coefficient. However, as the normal pressure P_n and the sliding speed v are kept constant during the measurements, the observed sol–gel transition and the ensuing increased viscosity entail a larger Stribeck number. As a consequence, the friction response would be shifted towards the hydrodynamic lubrication regime and thus lower friction coefficients – which is inconsistent with our findings.

An alternative explanation could be that astringent-induced crosslinking of mucins reduces the lubricating potential of mucins by inducing mucin aggregation [48,49]. As the lubricity of mucins is based on their ability to bind to surfaces and to be sheared off again under load [21], this mechanism could be less efficient for mucin aggregates. We observe an increase in turbidity for both saliva and salivary mucin solutions after astringent addition (Fig. 6a) which agrees with the concept of protein aggregation. Also, pellet formation visible after centrifugation of saliva/astringent and mucin/astringent mixtures, agrees with a possible crosslinking of mucins to form higher density networks, at least on a mesoscopic scale. We thus hypothesize that this mucin aggregation reduces the concentration of solubilized and therefore lubricating glycoproteins. Such an astringent-induced depletion of solubilized mucins has already been observed by gel-electrophoresis for chitosan [10] and β-lactoferrin [8], a protein with a high isoelectric point similar to lysozyme. Indeed, when the astringent-treated samples are centrifuged and the supernatant is used as a lubricant, we measure similar friction coefficients as when astringents are added to saliva or salivary mucin solutions during a tribological experiment (Fig. 7a). This demonstrates that the mucin aggregates generated by the astringent addition do not contribute to the lubricity of the solution any more as the friction coefficient does not change when precipitates are removed.

To quantitatively link this depletion of solubilized mucins to the observed loss of lubrication, we measure the concentration of HSM remaining solubilized after astringent addition and subsequent centrifugation (see methods and Fig. 7b). For HSM solutions treated with lysozyme, the highest HSM content in the supernatant is observed, i.e. 73%. In contrast, incubating $AlCl_3$, $Fe_2(SO_4)_3$ or chitosan with HSM causes a strong mucin depletion as we only measure 21% and 6% respective residual mucin for the metal salts and 11% for chitosan. When directly comparing the two metals salts, we measure both a stronger degree of mucin depletion as well as a stronger loss of lubricity for $Fe_2(SO_4)_3$ than for $AlCl_3$, suggesting that those two parameters are directly linked. For these compounds, a correlation between the residual lubricity after aggregation and the amount of aggregated mucins exist. Yet, chitosan is less efficient in precipitating mucin but entails a stronger loss of lubricity than $AlCl_3$. Lysozyme shows by far the lowest tendency to precipitate mucins, but still induces a strong loss of lubrication.

Çelebioğlu and colleagues [50] recently demonstrated that the reduced lubricating properties of a mucin/β-lactoglobulin solution are not solely caused by aggregation between both proteins. Instead, β-lactoglobulin competes with mucins with respect to adsorption onto PDMS and thus reduces mucin lubricity. This process is especially pronounced under tribological stress which reinforces continuous mucin desorption and readsorption. As lysozyme, which has a similar charge as β-lactoglobulin at pH 7 [51], readily adsorbs to PDMS as well [52] and since small globular proteins are generally known for blocking mucin adsorption as discussed for bovine serum albumin [41], it is reasonable to assume that a similar competition mechanism between lysozyme and mucin contributes to the loss of lubricity observed here. We speculate that also the macromolecular astringent chitosan may be able to compete with mucin binding to PDMS which could explain its stronger impact on mucin lubricity compared to the metal ions.

4. Conclusions

Here, we have demonstrated that the addition of cationic astringents to saliva in concentrations above the in vivo sensory threshold of astringency also induces a loss of lubricity in vitro. This effect can be reproduced with model solutions comprising either human or bovine salivary mucin. We have identified binding interactions between mucins and cationic astringents and subsequent mucin gelation/aggregation as one main source for the loss of saliva lubricity. In addition, our results suggest that competitive binding of astringents to surfaces may further reduce the efficiency of mucin lubrication. The observed loss of mucin lubricity may, at least in part, contribute to the astringent sensation in the oral cavity. However, interactions between astringent compounds and smaller salivary proteins as well as mucins bound to the oral mucosa are also likely to play an important role for the sensation of astringency.

Acknowledgments

This work was supported by the International Graduate School of Science and Engineering (IGSSE) in the framework of the focus area "Biomaterials" and by the Deutsche Forschungsgemeinschaft through project B11 in the framework of SFB863.

References

[1] J.C. Hufnagel, T. Hofmann, Orosensory-directed identification of astringent mouthfeel and bitter-tasting compounds in red wine, J. Agric. Food Chem. 56 (2008) 1376–1386.
[2] A. Glabasnia, T. Hofmann, Sensory-directed identification of taste-active ellagitannins in American (*Quercus alba* L.) and European oak wood (*Quercus robur* L.) and quantitative analysis in bourbon whiskey and oak-matured red wines, J. Agric. Food Chem. 54 (2006) 3380–3390.
[3] S. Scharbert, N. Holzmann, T. Hofmann, Identification of the astringent taste compounds in black tea infusions by combining instrumental analysis and human bioresponse, J. Agric. Food Chem. 52 (2004) 3498–3508.
[4] T. Stark, S. Bareuther, T. Hofmann, Sensory-guided decomposition of roasted cocoa nibs (*Theobroma cacao*) and structure determination of taste-active polyphenols, J. Agric. Food Chem. 53 (2005) 5407–5418.
[5] J. Lim, H.T. Lawless, Oral sensations from iron and copper sulfate, Physiol. Behav. 85 (2005) 308–313.
[6] P. Breslin, M.M. Gilmore, G.K. Beauchamp, B.G. Green, Psychophysical evidence that oral astringency is a tactile sensation, Chem. Senses 18 (1993) 405–417.
[7] E. Silletti, M.H. Vingerhoeds, W. Norde, George A. van Aken, Complex formation in mixtures of lysozyme-stabilized emulsions and human saliva, J. Colloid Interface Sci. 313 (2007) 485–493.
[8] B. Vardhanabhuti, M.A. Kelly, P.J. Luck, M.A. Drake, E.A. Foegeding, Roles of charge interactions on astringency of whey proteins at low pH, J. Dairy Sci. 93 (2010) 1890–1899.
[9] P. Andrewes, M. Kelly, B. Vardhanabhuti, E.A. Foegeding, Dynamic modelling of whey protein–saliva interactions in the mouth and relation to astringency in acidic beverages, Int. Dairy J. 21 (2011) 523–530.
[10] P. Luck, K.M. Vårum, E.A. Foegeding, Charge related astringency of chitosans, Food Hydrocoll. 48 (2015) 174–178.
[11] M.R. Bajec, G.J. Pickering, Astringency: mechanisms and perception, Crit. Rev. Food Sci. Nutr. 48 (2008) 858–875.
[12] B. Schwarz, T. Hofmann, Is there a direct relationship between oral astringency and human salivary protein binding? Eur. Food Res. Technol. 227 (2008) 1693–1698.
[13] N.J. Baxter, T.H. Lilley, E. Haslam, M.P. Williamson, Multiple interactions between polyphenols and a salivary proline-rich protein repeat result in complexation and precipitation, Biochemistry 36 (1997) 5566–5577.
[14] A. Bennick, Interaction of plant polyphenols with salivary proteins, Crit. Rev. Oral. Biol. Med. 13 (2002) 184–196.
[15] S. Soares, R. Vitorino, H. Osório, A. Fernandes, A. Venâncio, N. Mateus, et al., Reactivity of human salivary proteins families toward food polyphenols, J. Agric. Food Chem. 59 (2011) 5535–5547.
[16] R. Bansil, B.S. Turner, Mucin structure, aggregation, physiological functions and biomedical applications, Curr. Opin. Colloid Interface Sci. 11 (2006) 164–170.
[17] D.J. Thornton, N. Khan, R. Mehrotra, M. Howard, E. Veerman, N.H. Packer, et al., Salivary mucin MG1 is comprised almost entirely of different glycosylated forms of the MUC5B gene product, Glycobiology 9 (1999) 293–302.
[18] J.R. Stokes, G.A. Davies, Viscoelasticity of human whole saliva collected after acid and mechanical stimulation, Biorheology 44 (3) (2007) 141–160.
[19] L. Ma, A. Gaisinskaya-Kipnis, N. Kampf, J. Klein, Origins of hydration lubrication, Nat. Commun. 6 (2015) 6060.
[20] T. Crouzier, K. Boettcher, A.R. Geonnotti, N.L. Kavanaugh, J.B. Hirsch, K. Ribbeck, et al., Modulating mucin hydration and lubrication by deglycosylation and polyethylene glycol binding, Adv. Mater. Interfaces (2015) (n/a).
[21] G.E. Yakubov, J. McColl, Jeroen H.H. Bongaerts, J.J. Ramsden, Viscous boundary lubrication of hydrophobic surfaces by mucin, Langmuir 25 (2009) 2313–2321.
[22] J.H.H. Bongaerts, D. Rossetti, Stokes JR., The lubricating properties of human whole saliva, Tribol. Lett. 27 (2007) 277–287.
[23] J.F. Prinz, P.W. Lucas, Saliva tannin interactions, J. Oral Rehabil. 27 (2000) 991–994.
[24] D. Rossetti, G.E. Yakubov, J.R. Stokes, A. Williamson, G.G. Fuller, Interaction of human whole saliva and astringent dietary compounds investigated by interfacial shear rheology, Food Hydrocoll. 22 (2008) 1068–1078.
[25] D. Rossetti, J. Bongaerts, E. Wantling, J.R. Stokes, A. Williamson, Astringency of tea catechins: more than an oral lubrication tactile percept, Food Hydrocoll. 23 (2009) 1984–1992.
[26] B. Vardhanabhuti, P.W. Cox, I.T. Norton, E.A. Foegeding, Lubricating properties of human whole saliva as affected by beta-lactoglobulin, Food Hydrocoll. 25 (2011) 1499–1506.
[27] C.A. Lee, Z.M. Vickers, Astringency of foods may not be directly related to salivary lubricity, J. Food Sci. 77 (2012) S302–S306.
[28] B. Bolto, J. Gregory, Organic polyelectrolytes in water treatment, Water Res. 41 (2007) 2301–2324.
[29] P.M. Claesson, B.W. Ninham, pH-dependent interactions between adsorbed chitosan layers, Langmuir 8 (1992) 1406–1412.
[30] K. Boettcher, S. Grumbein, U. Winkler, J. Nachtsheim, O. Lieleg, Adapting a commercial shear rheometer for applications in cartilage research, Rev. Sci. Instrum. 85 (2014) 093903.
[31] H. Ranc, C. Servais, P. Chauvy, S. Debaud, S. Mischler, Effect of surface structure on frictional behaviour of a tongue/palate tribological system, Tribol. Int. 39 (2006) 1518–1526.
[32] I.D. Johnston, D.K. McCluskey, C.K.L. Tan, M.C. Tracey, Mechanical characterization of bulk Sylgard 184 for microfluidics and microengineering, J. Micromech. Microeng. 24 (2014) 035017.
[33] H. Ranc, A. Elkhyat, C. Servais, S. Mac-Mary, B. Launay, P. Humbert, Friction coefficient and wettability of oral mucosal tissue: changes induced by a salivary layer, Colloids Surf. A Physicochem. Eng. Asp. 276 (2006) 155–161.
[34] A. Mata, A.J. Fleischman, S. Roy, Characterization of polydimethylsiloxane (PDMS) properties for biomedical micro/nanosystems, Biomed. Microdevices 7 (2005) 281–293.
[35] L. Macakova, G.E. Yakubov, M.A. Plunkett, J.R. Stokes, Influence of ionic strength changes on the structure of pre-adsorbed salivary films. A response of a natural multi-component layer, Colloids Surf., B 77 (1) (2010) 31–39.
[36] R.G. Schipper, E. Silletti, M.H. Vingerhoeds, Saliva as research material: biochemical, physicochemical and practical aspects, Arch. Oral Biol. 52 (2007) 1114–1135.
[37] L. Becerra, R.V. Soares, L.S. Bruno, C.C. Siqueira, F.G. Oppenheim, G.D. Offner, et al., Patterns of secretion of mucins and non-mucin glycoproteins in human submandibular/sublingual secretion, Arch. Oral Biol. 48 (2003) 147–154.
[38] P. Georgiades, Paul D.A. Pudney, S. Rogers, Thornton DJ, Waigh TA, Tea derived galloylated polyphenols cross-link purified gastrointestinal mucins, PLoS One 9 (2014) e105302.
[39] P. Georgiades, E. Di Cola, R.K. Heenan, Paul D.A. Pudney, D.J. Thornton, T.A. Waigh, A combined small-angle X-ray and neutron scattering study of the structure of purified soluble gastrointestinal mucins, Biopolymers 101 (2014) 1154–1164.
[40] S.A. Rayment, B. Liu, G.D. Offner, F.G. Oppenheim, R.F. Troxler, Immunoquantification of human salivary mucins MG1 and MG2 in stimulated whole saliva: factors influencing mucin levels, J. Dent. Res. 79 (2000) 1765–1772.
[41] N. Nikogeorgos, J.B. Madsen, S. Lee, Influence of impurities and contact scale on the lubricating properties of bovine submaxillary mucin (BSM) films on a hydrophobic surface, Colloids Surf. B Biointerfaces 122 (2014) 760–766.
[42] M. Lundin, T. Sandberg, K.D. Caldwell, E. Blomberg, Comparison of the adsorption kinetics and surface arrangement of "as received" and purified bovine submaxillary gland mucin (BSM) on hydrophilic surfaces, J. Colloid Interface Sci. 336 (2009) 30–39.
[43] S.K. Linden, P. Sutton, N.G. Karlsson, V. Korolik, M.A. McGuckin, Mucins in the mucosal barrier to infection, Mucosal Immunol. 1 (2008) 183–197.
[44] G.J. Strous, J. Dekker, Mucin-type glycoproteins, Crit. Rev. Biochem. Mol. Biol. 27 (1992) 57–92.
[45] S.E. Allerton, G.E. Perlmann, Chemical characterization of the phosphoprotein phosvitin, J. Biol. Chem. 240 (1965) 3892–3898.
[46] J.P. Celli, B.S. Turner, N.H. Afdhal, R.H. Ewoldt, G.H. McKinley, R. Bansil, et al., Rheology of gastric mucin exhibits a pH-dependent sol–gel transition, Biomacromolecules 8 (2007) 1580–1586.
[47] P. Georgiades, Paul D.A. Pudney, D.J. Thornton, T.A. Waigh, Particle tracking microrheology of purified gastrointestinal mucins, Biopolymers 101 (2014) 366–377.
[48] H.L. Gibbins, G.H. Carpenter, Alternative mechanisms of astringency — what is the role of saliva? J. Texture Stud. 44 (2013) 364–375.
[49] H.S. Davies, Paul D.A. Pudney, P. Georgiades, Waigh TA, Hodson NW, Ridley CE, et al., Reorganisation of the salivary mucin network by dietary components: insights from green tea polyphenols, PloS One 9 (2014) e108372.
[50] H.Y. Çelebioğlu, M. Gudjónsdóttir, Chronakis IS, S. Lee, Investigation of the interaction between mucins and beta-lactoglobulin under tribological stress, Food Hydrocoll. (2015).
[51] D.G. Cornell, D.L. Patterson, Interaction of phospholipids in monolayers with beta-lactoglobulin adsorbed from solution, J. Agric. Food Chem. 37 (1989) 1455–1459.
[52] J. Kim, G.A. Somorjai, Molecular packing of lysozyme, fibrinogen, and bovine serum albumin on hydrophilic and hydrophobic surfaces studied by infrared-visible sum frequency generation and fluorescence microscopy, J. Am. Chem. Soc. 125 (2003) 3150–3158.

A.7 Mucin-inspired lubrication on hydrophobic surfaces

BioMACROMOLECULES

Article

pubs.acs.org/Biomac

Mucin-Inspired Lubrication on Hydrophobic Surfaces

Benjamin T. Käsdorf,[†] Florian Weber,[†] Georgia Petrou,[‡] Vaibhav Srivastava,[‡] Thomas Crouzier,[‡] and Oliver Lieleg*[,†]

[†]Department of Mechanical Engineering and Munich School of Bioengineering, Technical University of Munich, Boltzmannstrasse 11, 85748, Garching, Germany

[‡]Division of Glycoscience, School of Biotechnology, Royal Institute of Technology, Albanova University Center, 10691 Stockholm, Sweden

Supporting Information

ABSTRACT: In the human body, high-molecular-weight glycoproteins called mucins play a key role in protecting epithelial surfaces against pathogenic attack, controlling the passage of molecules toward the tissue and enabling boundary lubrication with very low friction coefficients. However, neither the molecular mechanisms nor the chemical motifs of those biomacromolecules involved in these fundamental processes are fully understood. Thus, identifying the key features that render biomacromolecules such as mucins outstanding boundary lubricants could set the stage for creating versatile artificial superlubricants. We here demonstrate the importance of the hydrophobic terminal peptide domains of porcine gastric mucin (MUC5AC) and human salivary mucin (MUC5B) in the processes of adsorbing to and lubricating a hydrophobic PDMS surface. Tryptic digestion of those mucins results in removal of those terminal domains, which is accompanied by a loss of lubricity as well as surface adsorption. We show that this loss can in part be compensated by attaching hydrophobic phenyl groups to the glycosylated central part of the mucin macromolecule. Furthermore, we demonstrate that the simple biopolysaccharide dextran can be functionalized with hydrophobic groups which confers efficient surface adsorption and good lubricity on PDMS to the polysaccharide.

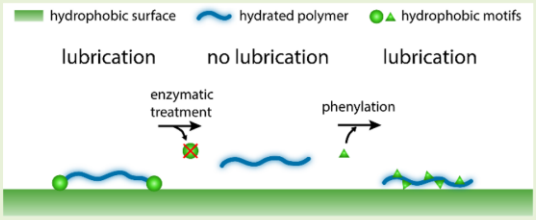

INTRODUCTION

In the human body, all wet epithelia are covered with mucus, a transparent viscoelastic[1] hydrogel, which has two important functions: first, mucus shields the underlying tissue from pathogenic attack,[2,3] and second, it provides mechanical protection for the tissues when they are exposed to shear forces. The macromolecular key component of mucus is mucin, a complex glycoprotein that can have molecular weights up to several MDa.[4] Those densely glycosylated proteins can be divided in three distinct groups: membrane-bound epithelial mucins, secreted nongel-forming mucins, and secreted gel-forming mucins with the latter being the major constituent of mucus.[3,5] Reconstituted solutions of manually purified mucins reproduce key properties of native mucus, that is, they reduce viral activity,[6] limit biofilm formation,[7] and (when used as coatings) reduce cell[8] and bacterial[9] adhesion to surfaces. Moreover, similar to native mucus systems such as saliva[10] and tear fluid,[11] mucin solutions reduce friction both on artificial and biological surfaces:[12−16] in the boundary lubrication regime, the friction coefficient μ measured with mucin-based lubricants can be as small as $\mu = 0.01$ or even less.

In this boundary regime, hydrodynamic effects are negligible and two opposing surfaces come into direct contact.[17] The very low friction coefficients observed with mucin-based lubricants are therefore critically related to the ability of the highly glycosylated mucin molecules to strongly adsorb to a broad range of surfaces.[18−21] Both on hydrophilic and hydrophobic surfaces, mucins assemble into well-hydrated macromolecular layers,[9,22,23] which prevent two opposing surfaces from getting into direct contact with each other. This process enables mucin or mucin-like molecules to lubricate numerous tissues in the human body: those tissues often comprise a mixture of hydrophilic and hydrophobic parts (e.g., the corneal epithelium, the tongue or the surface of articular cartilage) with the latter being rendered hydrophilic by adsorption of, for example, mucins.[24−28]

In part, this separation of two counter surfaces during shear is achieved by the macromolecule itself which is adsorbing to the surfaces and forms a hydrated layer. Friction is reduced by shearing off this polymer layer ("sacrificial layer mechanism").[29,30] The second mechanism that is involved in reducing friction between opposing surfaces is based on surface-bound water molecules ("hydration lubrication") trapped by the various hydrophilic moieties on the mucin molecule[31,32] (Figure 1a). To be efficient, the first mechanism requires the mucin molecule to quickly reattach to a surface after it was

Received: April 27, 2017
Revised: June 13, 2017
Published: June 21, 2017

DOI: 10.1021/acs.biomac.7b00605
Biomacromolecules 2017, 18, 2454−2462

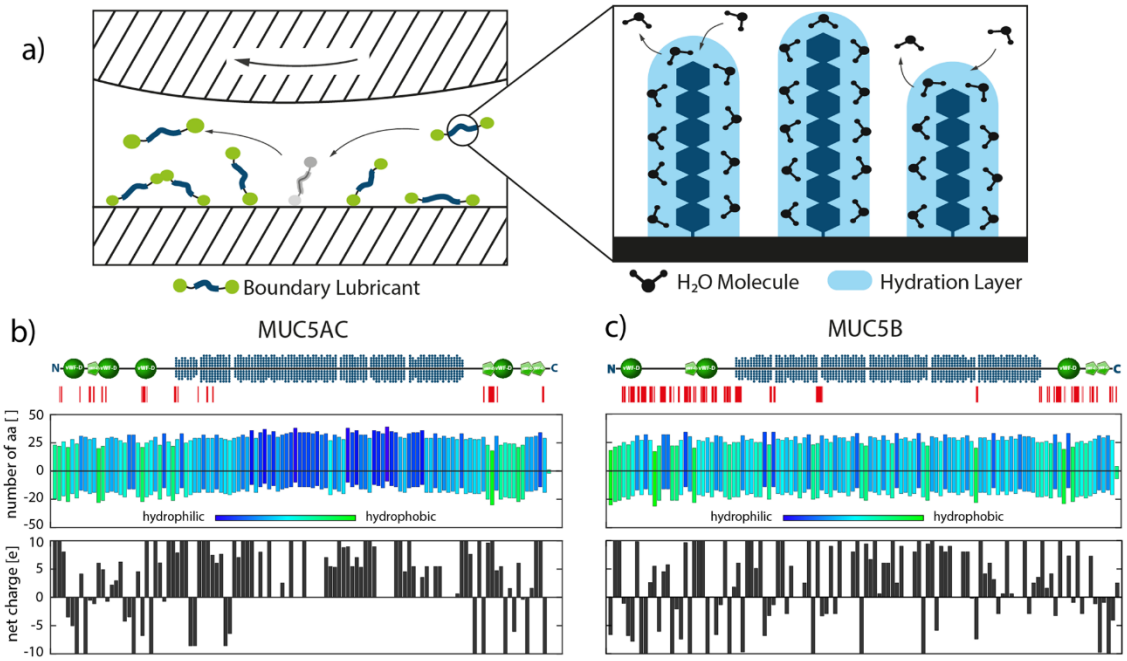

Figure 1. Schematic overview of the molecular mechanisms responsible for the lubricity of mucin based lubricants and mucin structure. (a) Both the formation of a sacrificial surface layer and hydration lubrication contribute to the lubricity of mucin solutions (see main text for details). The amino acid sequence of human MUC5AC (b) and human MUC5B (c) is analyzed in terms of polar/nonpolar side chains and net charge (see Materials and Methods for details). The red marks indicate the fragments of the mucin polypeptide, which were detected by mass spectrometry after tryptic digestion (see Tables S1 and S2 in the Supporting Information).

detached by shear forces during a friction process. The second mechanism involves the exchange of free water molecules from the lubricant solution with water molecules in the hydration layer of surface-adsorbed mucin molecules. This exchange takes place as a consequence of the shear occurring during the friction process and provides a surface-bound water layer that reduces friction.

Together, sacrificial layer formation and hydration lubrication enable mucin-based lubricants to decrease friction by up to 2 orders of magnitude compared to lubrication with simple buffer.[12,33] Mucins carry both charged and polar moieties as well as hydrophobic residues.[4] Thus, mucin physisorption to surfaces can be mediated by two different types of physical forces: electrostatic interactions between charged moieties of the glycoprotein and oppositely charged groups on the surface of the material on the one hand, and hydrophobic interactions between the glycoprotein and the surface on the other hand. A mathematical analysis of the amino acid sequence of human MUC5B (salivary mucin) and human MUC5AC (gastric mucin) reveals that both types of interactions are indeed possible for either mucin variant studied here. Both mucins exhibit a mixed distribution of charged amino acids throughout the whole sequence, and the terminal domains of both MUC5AC and MUC5B feature an increased density of hydrophobic amino acids compared to the central (glycosylated) region of the glycoprotein (Figure 1b,c). In this central part of the molecule, the high amount of serine and threonine (both hydrophilic amino acids to which glycans are typically attached to via O-glycosidic bonds) is responsible for the comparably strong hydrophilic character of the peptide sequence. Together, this unfolded central hydrophilic part and the globular hydrophobic termini result in a daisy-chain-like configuration with amphiphilic character.[34,35] It was already shown that the high glycosylation density on the mucin glycoprotein is crucial for mucin hydration, and that both the hydration state of mucin[22] and the detailed glycosylation pattern[36] are directly related to the lubricity of mucins. This particular molecular architecture suggests that the hydrophilic amino acids in the central region of the polypeptide serve as anchor points for the glycosylation of the protein promoting mucin hydration. In contrast, the hydrophobic terminal regions may be responsible for mediating the attachment of the glycoprotein to hydrophobic surfaces.

We here show that the hydrophobic terminal peptide sequences of both human salivary mucin and porcine gastric mucin are crucial for the lubricating abilities of these glycoproteins on hydrophobic surfaces. Enzymatic removal of those peptide sequences not only eliminates mucin lubricity but also reduces the adsorption efficiency of the glycoproteins to PDMS. Vice versa, we demonstrate that the addition of hydrophobic groups to synthetic dextran molecules promotes the dextran adsorption to PDMS and conveys lubricity to the dextran solution if a hydrophobic surface is part of the tribological material pairing. Finally, we present a molecular repair approach that partially restores the lubricating potential of enzymatically treated mucins on hydrophobic surfaces by grafting artificial hydrophobic groups onto the damaged mucins.

DOI: 10.1021/acs.biomac.7b00605
Biomacromolecules 2017, 18, 2454−2462

MATERIALS AND METHODS

Mucin Purification. The purification process of mucins was described in detail previously.[33] In short, mucus was obtained by manual scraping pig stomachs after rinsing them gently with tap water. The mucus was diluted 5-fold in 10 mM sodium phosphate buffer (pH 7.0) containing 170 mM NaCl and stirred overnight at 4 °C. Cellular debris was removed via several centrifugation steps and a final ultracentrifugation step (150000*g* for 1 h at 4 °C). Afterward, the mucins were separated by size exclusion chromatography using an ÄKTA purifier system (GE Healthcare) and a XK50/100 column packed with Sepharose 6FF. The obtained mucin fractions were pooled, dialyzed against ultrapure water and concentrated by cross-flow dialysis. The concentrate was then lyophilized and stored at −80 °C. For purification of human salivary mucin (MUC5B), unstimulated human whole saliva was collected from healthy, nonsmoking, 20−30 year old donors, which refrained from consuming food or beverages other than water for 1 h prior to saliva donation. Saliva samples were stored on ice during collection and purified using the same protocol as used for MUC5AC. Monomeric MUC5AC and MUC5B has a molecular weight of ∼3 MDa including the glycan motifs attached to the protein backbone. As the formation of oligomers is possible for both mucin types, the molecular weight range for oligomeric MUC5AC and MUC5B is expected to be heterogeneous.

Dextrans. Dextrans with a MW of 150 kDa were obtained from TdB Consultancy (Uppsala, Sweden). The polysaccharides were either unmodified or modified with carboxymethyl (CM), diethylaminoethyl (DEAE), or phenyl groups, the latter of which were present on the dextrans at densities of either 0.15 phenyl groups/glucose or 0.40 phenyl groups/glucose, respectively. The 40 kDa dextran with a phenylation degree of 0.32−0.40 phenyl groups/glucose was obtained from Sigma-Aldrich (St. Louis, MO).

Enzymatic Digestion of Mucin. Enzymatic treatment of mucins with trypsin was performed, as described in Madsen et al.[37] In brief, mucin was dissolved at 10 mg/mL in a 50 mM ammonium bicarbonate solution, and disulfide bonds were reduced by adding 5 vol % 200 mM DTT (dissolved in 100 mM ammonium bicarbonate) at room temperature for 1 h. A total of 4 vol % of 1 M iodoacetamide dissolved in a 100 mM ammonium bicarbonate solution was added to alkylate the mucin again at room temperature for 1 h. The reaction was quenched by adding 20 vol % of DTT. For proteolytic degradation, 40 vol % of 1 mg/mL trypsin (from bovine pancreas, Sigma-Aldrich, St. Louis, MO) dissolved in a 100 mM ammonium bicarbonate solution was added to the mucin solution and incubated at 30 °C for 18 h. Afterward, the trypsinated mucin was purified and desalted via size exclusion chromatography and cross-flow filtration as described above for native mucin.

Mucin Sequence Analysis. The mucin peptide sequences used for analysis in this work were obtained from the UniProt protein database (MUC5AC, P98088; MUC5B, Q9HC84). Up to now, no peptide sequence for porcine gastric mucin is available yet. Thus, for our analysis, we used the sequence of human MUC5AC instead. Both the sequences of MUC5B and MUC5AC were first divided into sections of 50 amino acids each. To characterize the hydrophobic character of these sections, the number of amino acids with nonpolar side chains (i.e., Gly, Ala, Val, Met, Leu, Ile, Pro, Trp, Phe) and polar side chains (i.e., Arg, Lys, Asn, Asp, Gln, Glu, His, Tyr, Ser, Thr, Cys) was counted. To analyze the charge distribution along the amino acid backbone, the number of charged amino acids at neutral pH (negatively charged amino acids: Asp, pK_a = 3.9; Glu, pK_a = 4.1; positively charged amino acids: Arg, pK_a = 12.5; Lys, pK_a = 10.5) was counted. Each charged amino acid was assigned one elementary charge, and the net charge of each section of 50 consecutive amino acids is displayed as a bar in Figure 1. The glycosylation pattern was estimated based on the distribution of the amino acids serine and threonine. They serve as an anchor for O-linked glycans[38] with each O-linked oligosaccharide side chain comprising up to 20 sugar units.[3,15] Each displayed glycan molecule in Figure 1 represents 10 monosaccharides. Cleavage sites of trypsin in the sequences of MUC5AC and MUC5B were analyzed with the tool PeptideCutter from ExPASy Bioformatics Resources Portal.

Adsorption Measurements. Adsorption measurements were performed with an eCell-T quartz crystal microbalance (3T-analytik, Tuttlingen, Germany) and a Gamry eQCM 10 M data acquisition device (Warminster, Pennsylvania, U.S.A.). The quartz crystals used for this study have a gold surface, which was spin-coated with a thin layer of polydimethylsiloxane (PDMS, Sylgard 184, DowCorning, Wiesbaden, Germany). Therefore, PDMS was mixed in a prepolymer/cross-linker ratio of 10:1 and diluted to 1 vol % in *n*-hexane. A total of 100 μL of this solution was applied to the center of the quartz crystal distributed by operating the spin-coater at 3000 rpm for 60 s. Afterward, the PDMS was cured at 80 °C for 4 h. A profilometric analysis of the coated crystals showed that the thickness of the PDMS layer was ∼3 μm (see Supporting Information, Figure S1). The concentration of biomolecules used for adsorption measurements was 100 μg/mL, and each biomolecule type was diluted in filtered 20 mM HEPES buffer (filter threshold: 0.22 μm). For each measurement, a quartz crystal with a fresh PDMS coating was used. Prior to each measurement, the setup was equilibrated with 20 mM HEPES buffer until a stable frequency signal was reached. This procedure ensured that the coated PDMS layer (which can absorb small amounts of water[39]) has reached an equilibrated state so that water uptake into this PDMS layer does not affect the measurement. At the beginning of each measurement, 2 min of HEPES buffer signal was recorded as a baseline. Afterward, the biomolecules were injected at 100 μL/min for 2 min, and the flow rate was set to 10 μL/min.

Tribology. Friction measurements were conducted on a commercial shear rheometer (MCR 302, Anton Paar, Graz, Austria) equipped with a tribology unit (T-PTD 200, Anton Paar). The measurements were performed as described previously.[40] In brief, the setup used was a ball-on-cylinder geometry. As opposing friction partners, PDMS cylinders (Ø 5.5 mm) and steel spheres (Ø 12.7 mm, Kugel Pompel, Wien, Austria) were used. The PDMS cylinders were prepared by mixing PDMS prepolymer and cross-linker in a 10:1 ratio (Sylgard 184, DowCorning), exposing the mixture to 1 h vacuum and performing a final curing step at 80 °C for 4 h. Before a measurement, three pins were inserted into the sample holder and cleaned with 80% EtOH and ultrapure H_2O. The measurements were performed at room temperature and the PDMS cylinders were fully covered with lubricant. To be consistent with our previous study on the lubricity of mucin solutions,[22] a normal force of F_N = 6 N was applied (leading to a contact area of ∼8.1 mm^2 (Figure S2) and, thus, a contact pressure of ≈0.35 MPa), and the friction coefficient was recorded for sliding speeds from 1000 to 0.01 mm/s (logarithmic speed ramp, 10 measuring points per decade) using a measuring time of 10 s per data point. The PDMS surface topology was analyzed (Figure S3) after lubricating with unmodified dextrans (0.1% in 20 mM HEPES) to rule out any artifacts generated by wear while sliding a steel sphere over the PDMS surface. All lubricants were used at a concentration of 1 mg/mL diluted in 20 mM HEPES, pH 7.4.

Hydration Measurements. The hydration of the mucin and dextran coatings was measured by combining two complementary techniques. First, the hydrated mass of mucin and dextran coatings was assessed using quartz crystal microbalance with dissipation monitoring (QCM-D, E4 system, Q-Sense) using gold-coated crystals (QSX 301, Q-sense) that were cleaned prior to use with a mixture of 20% hydrogen peroxide and 80% ammonium heated at 80 °C for 10 min. The mucin and dextran solutions were prepared at 1 mg/mL in 20 mM HEPES pH 7 buffer and injected into the instrument at a rate of 200 μL/min. In QCM-D, the changes in dissipation reflect the viscoelastic properties of the adsorbed coating. The frequency and dissipation shifts were fed into a Voigt-based model which was used to accurately estimate the hydrated mass (Q-tools software).[41] The density of the mucin coating was fixed at 1050 kg/m^3, which is between that of pure water (1000 kg/m^3) and pure protein (1350 kg/m^3).[42]

Second, the dry mass was measured using a surface plasmon resonance technique (SPR, Biacore 2000, GE Healthcare). Mucins or dextrans were injected at a concentration of 1 mg/mL, dissolved in

DOI: 10.1021/acs.biomac.7b00605
Biomacromolecules 2017, 18, 2454−2462

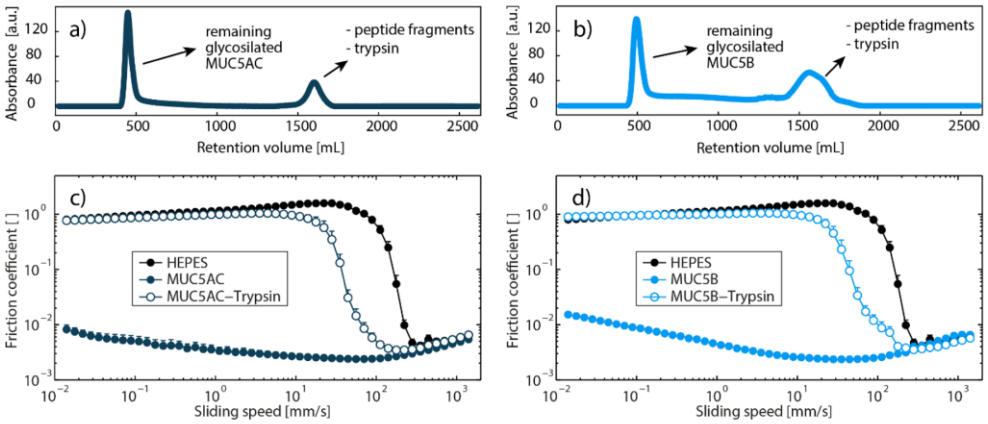

Figure 2. Lubricity of native and enzymatically treated mucins. Chromatograms of size exclusion chromatography of MUC5AC and MUC5B after tryptic digestion are shown in (a) and (b), respectively. Tribological measurements were performed with a steel/PDMS pairing using 0.1 mg/mL mucin dissolved in HEPES buffer. The measurements show the lubricating abilities of either native or tryptic digested MUC5AC (c) or MUC5B (d), respectively. HEPES buffer is included as a reference. The error bars denote the standard deviation as obtained from three independent measurements.

20 mM HEPES, pH 7. The adsorbed mass density was estimated assuming one converting response units corresponded to 0.1 ng/mm^2.[43] The hydration level of the coatings was deduced from the dry and hydrated mass using the relationship described in eq 1.

$$\text{hydration}(\%) = \frac{\text{hydrated mass} - \text{dry mass}}{\text{hydrated mass}} \times 100 \quad (1)$$

Repair of Trypsinated Mucin. Since chemical modification of the termini of trypsin treated mucins is very challenging, phenylation of trypsin treated MUC5B was performed by carbodiimide coupling of phenylethylamine (Sigma-Aldrich) to the carboxylic groups of sialic acid motifs along the central part of the trypsin-treated mucin molecules. Trypsin treated MUC5B was dissolved in a 20 mM MES buffer solution (pH 5.5) together with 58 mM EDC (1-ethyl-3-(3-(dimethylamino)propyl)carbodiimide hydrochloride, ThermoFisher) and 27 mM NHS (*N*-hydroxysulfosuccinimide, Sigma-Aldrich). After complete dissolution, 173 mM phenylethylamine dissolved in 20 mM MES buffer solution (pH 5.5) were added to the mixture, and the pH was adjusted to pH 5.5 by addition of HCl. The solution was left to react at room temperature for 2 h. The mucin was then desalted and purified by chromatography (PD-10 column, GE Healthcare) and lyophilized before further use. The addition of the phenyl functionalities was verified by UV spectra measurement using 1 mg/mL solutions of the mucin variants.

■ RESULTS AND DISCUSSION

Previous studies revealed that commercially available mucins (e.g., porcine gastric mucin from Sigma-Aldrich) lack key properties observed for native mucin systems.[6,44] Prominent examples are that solutions of industrial gastric mucins lack the ability to form oligomers, they do not exhibit a sol−gel transition at acidic pH, and they are not able to reduce friction in the boundary lubrication regime at neutral pH.[13,19,33] As a consequence, we here manually purify porcine gastric mucin following a previously described protocol,[33] which preserves its native functional properties. To investigate the contribution of the terminal hydrophobic peptide domains of mucins to the lubrication potential of mucin solutions, we performed an enzymatic digestion of both MUC5AC and MUC5B using trypsin. This enzyme usually cleaves a broad range of peptide sequences. For this enzyme, an analysis of the sequences of human MUC5AC and MUC5B predicts ∼300 cutting sites for either mucin (see Materials and Methods), and those cutting sites are distributed equally throughout the peptide sequence. However, both mucins are densely glycosylated, and protein glycosylation is generally known to protect the polypeptide against proteolytic activity.[38,45,46] Indeed, it has been demonstrated that porcine gastric mucin is partially resistant to peptidases,[47] and accordingly, we expect only partial degradation of MUC5AC and MUC5B by trypsin. A chromatographic separation after enzymatic treatment of either mucin (Figure 2a,b) indicated that the treated mucins in fact retained a very large molecular weight and that the cleaved groups were much smaller than the remaining glycoprotein.

Mass spectrometry confirmed that the peptide fragments obtained after trypsin treatment of human MUC5B indeed originate from the terminal region of the glycoprotein (Figure 1c and Table S2). We interpret this result such that the central part of human MUC5B, which is densely glycosylated, is shielded against proteolytic degradation. The unprotected terminal parts, however, are accessible for the enzyme and seem to be broken down into small fragments of similar size. For porcine MUC5AC, a detailed peptide sequence is not available yet in the literature. However, the chromatographic profiles obtained for both trypsin treated mucins are very similar and only exhibit one second peak at later fractions in addition to the mucin main peak, which occurs at similar fractions as untreated mucin. Additionally, the analysis of the peptide fragments of trypsinated porcine MUC5AC via mass spectroscopy show a coverage with the human MUC5AC sequence (Table S2). The overall coverage is lower than for MUC5B but the pattern is similar, as fragments only of the terminal mucin domains can be identified. This suggests that also, for the porcine MUC5AC used here, trypsin treatment did mostly generate small peptide fragments, which are likely to originate from the terminal, unglycosylated region of the glycoprotein. After separating them from the proteolytic fragments, the remaining mucin glycoproteins were tested for their lubricity. When the treated mucins were used as a

DOI: 10.1021/acs.biomac.7b00605
Biomacromolecules 2017, 18, 2454−2462

0.1% (w/v) lubricant in a steel/PDMS tribology setup, we observed an almost complete loss of their lubricating abilities, especially in the boundary lubrication regime (Figure 2c,d).

To efficiently reduce friction by enabling hydration lubrication, macromolecular lubricants such as mucins have to form well-hydrated surface coatings. Thus, the inability of trypsin-digested mucins to lubricate in a hydrophobic PDMS/steel pairing could be due to a reduced hydration of such glycoprotein coatings compared to untreated mucins. Since the strong hydration of mucins is established by the high density of hydrophilic glycans in the central region of the protein, the amount of mucin-bound water should not be strongly influenced by our proteolytic degradation procedure. Indeed, hydration measurements of trypsin-digested MUC5AC and MUC5B showed no significant reduction in the amount of mucin-bound water (Figure 3, for detailed information, see Table S3 in the Supporting Information).

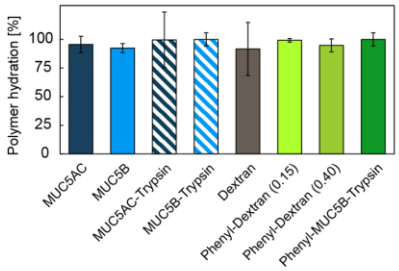

Figure 3. Hydration measurements of surface adsorbed layers of different macromolecules. The hydration is calculated for surface coatings of native MUC5AC and MUC5B, trypsin-treated MUC5AC and MUC5B, unmodified dextrans and phenylated dextrans (phenylation degree 0.15 and 0.40, respectively), as well as trypsin-treated MUC5B with attached phenyl groups. The error bars denote the standard deviation as obtained from three independent measurements.

An alternative explanation for the almost complete loss of mucin lubricity in the boundary lubrication regime could be that the adsorption efficiency of enzymatically treated mucins to surfaces is weakened compared to native mucins. It has been put forward that the terminal (hydrophobic) regions of mucins are involved in the adsorption process of the glycoproteins to hydrophobic surfaces, whereas the glycosylated (hydrophilic) central region of mucins are relevant for mucin adsorption to hydrophilic surfaces.[18] This model suggests that the hydrophobic moieties of the mucin glycoprotein might also be necessary for conveying lubricity on apolar surfaces. Thus, in a next step, we analyzed the adsorption behavior of native and trypsin treated mucins to a hydrophobic PDMS surface. Indeed, in contrast to native MUC5AC and MUC5B, the trypsin-treated mucins showed a strongly reduced adsorption to the hydrophobic PDMS, as indicated by the drastically reduced shift in resonance frequency reported by QCM (Figure 4a,b).

This result motivates that, whereas mucin hydration is still high after trypsin treatment, the efficiency of hydration lubrication will be drastically reduced as this mechanism requires surface adsorbed mucin molecules to take effect. Also, the formation of a sacrificial layer, that is, a dynamic shear-off and readsorption cycle, will be hampered if mucin adsorption is reduced. Together, these findings explain the observed loss in mucin lubricity very well and suggest that the hydrophobic terminal domains of MUC5AC and MUC5B are crucial for promoting mucin adsorption to PDMS as required for a good boundary lubricant on hydrophobic surfaces.

To verify our hypothesis that hydrophobic groups are required for the adsorption and subsequent lubricity of well-hydrated macromolecules on hydrophobic surfaces, we make use of a bottom-up approach. The idea is to test whether a macromolecule that is not an efficient lubricant on hydrophobic PDMS can be turned into a good lubricant when its adsorption to PDMS is improved. Of course, the trypsin treatment performed on the two mucin variants did not only remove

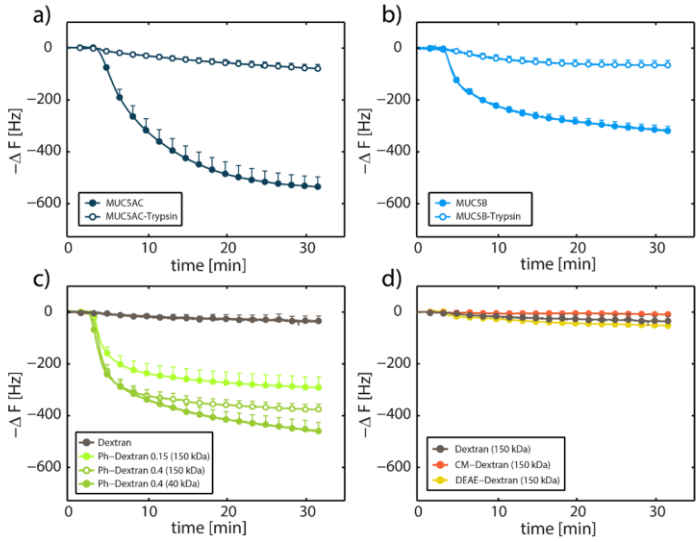

Figure 4. Adsorption kinetics of different mucin and dextran variants onto PDMS. The adsorption of native and trypsin treated mucins (MUC5AC (a) and MUC5B (b), respectively) and different dextran variants (phenylated (c) and charged (d)) to PDMS-coated QCM sensors is shown. The error bars denote the standard deviation as obtained from three independent measurements.

DOI: 10.1021/acs.biomac.7b00605
Biomacromolecules 2017, 18, 2454−2462

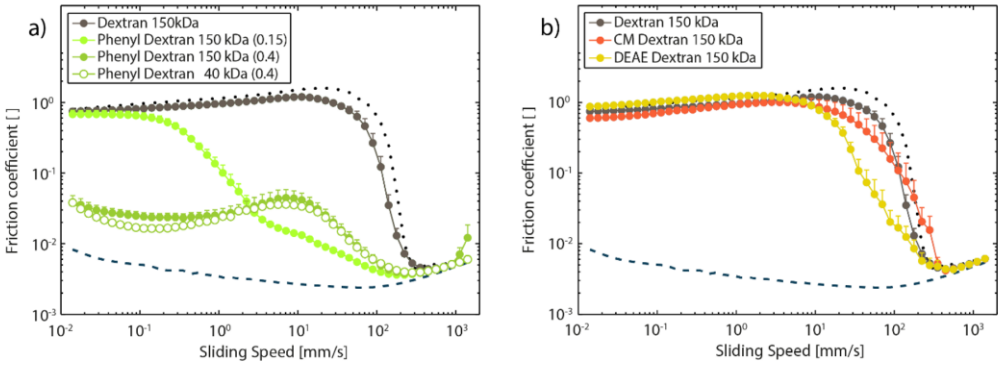

Figure 5. Rotational tribology with dextran solutions as lubricants. Tribological measurements between a steel/PDMS pairing with 0.1 mg/mL dextrans solution. Measured were the lubricating abilities of either hydrophobic (phenyl) dextrans (a) or charged dextrans (b). The dotted line represent the Stribeck curve for HEPES buffer as a reference, the dashed line the Stribeck curve of native MUCSAC. The error bars denote the standard deviation as obtained from three independent measurements.

hydrophobic amino acids from the terminal region of the polypeptide but also cleaved positively and negatively charged amino acids. As a molecular platform to systematically probe the influence of charged and hydrophobic modifications on the adsorption efficiency and lubricity of the molecule, we chose dextrans. Dextrans are strongly hydrated molecules,[48] and their good hydration is due to the high density of hydrophilic hydroxyl groups along the polysaccharide.[49] However, solutions containing unmodified dextrans hardly adsorb to PDMS surfaces at all (Figure 4c). Consistently, the Stribeck curves obtained with solutions containing such dextrans are very similar to those obtained with buffer lacking any macromolecules (Figure 5a).

In a next step, we test a dextran variant which was modified to carry hydrophobic moieties. The idea is that the addition of hydrophobic groups to dextrans should improve the adsorption of the molecules to hydrophobic PDMS and thus provide lubricity to the dextran solution. Indeed, phenylated dextrans with a phenyl content of 0.15 phenyl substituents per glucose molecule adsorb to a hydrophobic PDMS surface, although the recorded shift in crystal resonance frequency is smaller than that observed for adsorption of either MUCSAC or MUCSB (Figure 4c). A possible explanation for the comparably lower adsorption efficiency of phenyl-dextran might be that the amount of hydrophobic groups present on the dextran molecule is smaller than the corresponding number of hydrophobic moieties on the mucin glycoprotein. This idea would be consistent with the biochemical structure of the mucins that comprises large areas with numerous hydrophobic amino acids. To test this hypothesis, we repeated the adsorption measurements with dextrans carrying an increased density of phenyl groups (0.40 phenyl groups per glucose molecule), that is, a higher number of hydrophobic groups per dextran molecule. Indeed, for this dextran variant, we observe a stronger shift in the crystal resonance frequency corresponding to more efficient adsorption than for the 0.15 phenyl-dextran variant. For the 0.40 phenyl-dextran, this frequency shift is now also similar in magnitude as that observed for the adsorption of native mucins (Figure 4c). These findings suggest that the increased degree of dextran phenylation leads to stronger interactions with the hydrophobic PDMS surface and therefore should aid in maintaining a hydrated polymer film on the surface, provided that the phenylation procedure did not interfere with dextran hydration. QCM measurements, however, show that the high degree of hydration observed for native dextrans is maintained after introducing phenyl groups to these polymers (Figure 3). As a consequence, we expect that both phenylated dextrans should show improved lubricity on PDMS compared to unmodified dextrans, but the dextran variant with the higher phenylation degree should exhibit better lubricating abilities than the 0.15 phenyl-dextran.

Tribiological measurements with the two phenylated dextran variants on hydrophobic PDMS indeed agree with this expectation: both phenyl-dextran variants significantly reduce the friction coefficient by up to two decades, especially in the mixed lubrication regime, that is, for sliding speeds between 1 and 100 mm/s (Figure 5a). In the boundary lubrication regime, that is, at low sliding speeds below 1 mm/s, the 0.40 phenyl-dextran is more efficient: we here measure constantly low friction coefficients on the order of $\mu \sim 0.03$, which is a bit higher than the value obtained for mucins but more than an order of magnitude lower than the friction coefficient measured for the 0.15 phenyl-dextran in this regime. This observation is consistent with our notion that a stronger adsorption of hydrated molecules, that is, a more stable hydrated polymer film on the PDMS surface, will lead to better lubrication.

At this point, it is important to recall that the enzymatic treatment of the mucin glycoproteins has not only removed hydrophobic groups from the macromolecule, but also positively and negatively charged amino acids. However, we do not expect that those charged groups contribute significantly to the adsorption of mucins to hydrophobic PDMS surfaces. To verify this, we next test two dextran variants which were modified with anionic carboxymethyl (CM) and cationic diethylaminoethyl (DEAE) groups, respectively. For those two charged dextran variants, we observe similarly low adsorption to PDMS surfaces as for the unmodified dextrans (Figure 4d). This underscores our notion that there are no strong binding interactions between the charged CM or DEAE groups and hydrophobic PDMS, and it suggests that solutions containing those macromolecules should be poor boundary lubricants. Indeed, the lubricity of those macromolecular solutions on PDMS is low: the Stribeck curves measured in lubrication tests performed with these charged dextran variants resemble the results obtained with either simple buffer or unmodified dextrans (Figure 5b). Together, these findings are

DOI: 10.1021/acs.biomac.7b00605
Biomacromolecules 2017, 18, 2454−2462

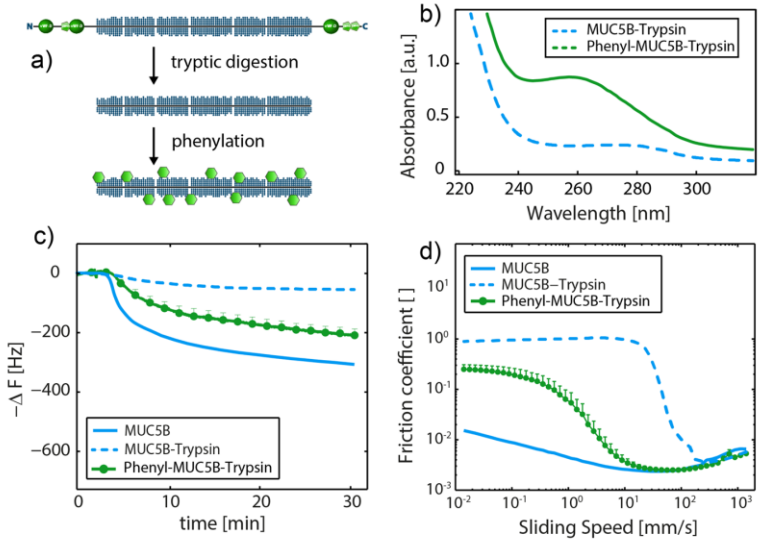

Figure 6. Adsorption properties and lubricity of phenylated trypsin-treated MUC5B. A schematic representation of the "repair approach" (= phenylation) of trypsin-treated MUC5B is depicted in (a). (b) Spectroscopic comparison of MUC5B-trypsin and MUC5B-trypsin with covalently attached phenyl groups. (c) Adsorption kinetics of native, trypsin treated and "repaired" MUC5B onto PDMS. (d) Lubricity of solutions of phenylated MUC5B as probed on a steel/PDMS pairing. The Stribeck curves obtained for native MUC5B (solid line) and trypsin-treated MUC5B (dashed line) are shown for comparison. The error bars denote the standard deviation as obtained from three independent measurements.

in agreement with our hypothesis that it is the hydrophobic character of the terminal peptide sequences of mucins and not the charged groups in this region of the glycoproteins that confers adsorption and lubricity on hydrophobic surfaces such as PDMS to mucins.

The results presented so far highlight the importance of hydrophobic moieties for the lubrication process on hydrophobic surfaces. Furthermore, the extent of these hydrophobic modifications on dextran molecules seems to be linked to the lubricating potential of those polymers. However, a higher phenylation degree not only increases the number of phenyl groups on the dextran molecule but also the density of those hydrophobic groups. Thus, we now ask, whether the overall number of hydrophobic groups on dextrans is important for conveying lubricity or if a certain density of hydrophobic motifs, that is, spatial proximity of phenyl groups, is required for dextran molecules to act as an effective boundary lubricant. To tackle this question, we probe the lubricating abilities of another dextran variant having a lower molecular weight (i.e., 40 kDa) than the dextrans tested so far (150 kDa) but a similar phenylation degree of ∼0.40 phenyl groups/glucose. Interestingly, for the small dextran molecules, we obtain Stribeck curves which are virtually identical to those obtained with the larger dextrans (Figure 5a). Since the phenylation degree is 0.40 in both cases, this may indicate that it is indeed the density of hydrophobic groups on a hydrated macromolecule rather than the total number of hydrophobic motifs, which is relevant for providing low friction in the boundary lubrication regime.

Together, these results demonstrate that the presence of hydrophobic moieties is crucial for biopolymers such as mucin or dextran to act as a boundary lubricant on hydrophobic surfaces. Since the trypsin treatment of mucins entailed a nearly complete loss of mucin lubricity on hydrophobic surfaces, we now, in a last step, try to "repair" the enzymatically treated mucin by grafting artificial hydrophobic groups to the "damaged" mucins. For this approach, we choose to covalently add phenyl groups to the carboxylic groups of trypsin treated mucin (Figure 6a).

Since the terminal peptide domains of the degraded mucin are no longer present and the central part of the polypeptide sequence is shielded by glycans, we aim to graft those phenyl groups to the carboxyl group of sialic acid, a charged monosaccharide, present among the mucin glycans.[50,51] For optimal efficiency of this grafting process, we perform these experiments with MUC5B which has a higher sialic acid content than MUC5AC.[52−54] Since UV-absorbance measurements indicated a successful phenylation of "damaged" (= trypsin-treated) MUC5B (Figure 6b), we next analyze if the addition of those hydrophobic groups would promote the adsorption of the "repaired" mucin onto a hydrophobic PDMS surface. Indeed, we observe a significant increase of adsorbed mucin molecules on a PDMS-coated quartz crystal (Figure 6c). However, the amount of adsorbed molecules seems not to be as high as for native MUC5B. Thus, in a next step, we ask if the "repaired" molecule can achieve similarly good lubricity as native mucin.

When performing friction tests with the "repaired" mucins (Figure 6d), we observe a strong decrease of friction coefficient in the mixed lubrication regime (i.e., for sliding speeds between 1 and 100 mm/s) compared to trypsin treated MUC5B. This decrease in the friction coefficient is, however, less pronounced in the boundary lubrication regime where we measure a friction coefficient of ∼0.2−0.3. This value is still ∼3-fold lower than the corresponding value obtained for "damaged" mucin, but more than an order of magnitude larger than the friction coefficient obtained for native mucins in this regime. It is likely that the incomplete recovery of both the adsorption kinetics as well as the lubricating abilities of this phenylated mucin compared to native mucin can be attributed to the limited amount of phenyl groups grafted onto the damaged mucin

DOI: 10.1021/acs.biomac.7b00605
Biomacromolecules 2017, 18, 2454−2462

molecules. As discussed before (Figure 5a), the density of phenyl groups on dextrans seems to be directly linked to both the adsorption kinetics of the macromolecule and its lubricating ability. Therefore, the amount of sialic acid groups which can be targeted with our phenylation procedure might be too low to achieve a phenylation density that is high enough to achieve adsorption kinetics and lubricity on a level comparable to that of native mucin. This assumption is in good agreement with previous work where it was shown that the adsorption strength and lubricating potential of boundary lubricants are linked.[55,56] However, those findings indicate that MUC5B digested with trypsin can indeed be "repaired": covalently attaching phenyl groups seems to compensate for the lost hydrophobic peptide termini, at least to a certain degree.

CONCLUSION

We here demonstrated that the hydrophobic domains of mucins are crucial to adsorb and further lubricate hydrophobic surfaces such as PDMS. Since several tissue surfaces in the human body exhibit a hydrophobic character,[25−28] the interaction of mucins with these surfaces by means of hydrophobic interactions is essential to provide boundary lubrication in vivo. When the mucin molecules are deprived of their hydrophobic domains, this lubrication on hydrophobic surfaces cannot take place anymore. However, we were able to compensate for the loss of these hydrophobic domains by grafting phenyl groups onto the damaged mucins, which in part recovered their ability to adsorb and lubricate hydrophobic surfaces. This approach can also be transferred to other biomolecules: Dextrans, highly hydrophilic molecules, can function as good boundary lubricants on hydrophobic PDMS when equipped with phenyl groups. The density of attached hydrophobic groups during this bottom-up approach determines the adsorption kinetics and lubricity of this mucin-inspired macromolecule. Of course, we here study macromolecular lubricity on simple PDMS surfaces which are hydrophobic but uncharged. On more complex surfaces that combine hydrophobic and charged characteristics, a phenyl-modified polyelectrolytic dextran variant might provide even better lubricity than the uncharged phenylated dextran molecules presented here.

The results presented here may pave the way toward the rational design of macromolecular superlubricants that provide ultralow friction on a broad range of biological and technical surfaces. A suitable polymer for such an artificial lubricant could be polyethylene glycol (PEG), which is nontoxic, water-soluble, and available with different molecular weights. PEG is already used in numerous fields ranging from industrial to pharmaceutical applications. PEG is highly hydrated and a good lubricant when utilized as surface attached polymer brushes.[57] Moreover, it has been demonstrated that linking PEG polymer chains to deglycosylated mucin can serve as a replacement for the hydrated glycans and restore lubricity.[22] Combining those existing strategies with the results shown here could lead to an artificial brush-like macromolecule with great potential for providing ultralow friction on various surfaces.

ASSOCIATED CONTENT

Supporting Information

The Supporting Information is available free of charge on the ACS Publications website at DOI: 10.1021/acs.biomac.7b00605.

Analysis of PDMS-layer thickness on QCM-chips; Detailed information on the mass spectrometry analysis of trypsin digested MUC5AC and MUC5B; Detailed information on the hydration measurements; and Surface topology analysis of the PDMS pin surface (PDF).

AUTHOR INFORMATION

Corresponding Author

*E-mail: oliver.lieleg@tum.de. Phone: +49 89 289 10952. Fax: + 49 89 289 10801.

ORCID

Oliver Lieleg: 0000-0002-6874-7456

Author Contributions

B.T.K., O.L., and T.C. proposed the experiments. B.T.K., F.W., G.P., and V.S. performed the experiments and analyzed the data. The manuscript was written by B.T.K. and O.L.

Notes

The authors declare no competing financial interest.

ACKNOWLEDGMENTS

The authors thank Christine Braig for assistance with the mucin preparation.

REFERENCES

(1) Lai, S. K.; Wang, Y. Y.; Wirtz, D.; Hanes, J. Micro- and macrorheology of mucus. *Adv. Drug Delivery Rev.* **2009**, *61* (2), 86−100.

(2) McGuckin, M. A.; Linden, S. K.; Sutton, P.; Florin, T. H. Mucin dynamics and enteric pathogens. *Nat. Rev. Microbiol.* **2011**, *9* (4), 265−78.

(3) Linden, S. K.; Sutton, P.; Karlsson, N. G.; Korolik, V.; McGuckin, M. A. Mucins in the mucosal barrier to infection. *Mucosal Immunol.* **2008**, *1* (3), 183−97.

(4) Bansil, R.; Turner, B. S. Mucin structure, aggregation, physiological functions and biomedical applications. *Curr. Opin. Colloid Interface Sci.* **2006**, *11* (2−3), 164−170.

(5) Dekker, J.; Rossen, J. W.; Buller, H. A.; Einerhand, A. W. The MUC family: an obituary. *Trends Biochem. Sci.* **2002**, *27* (3), 126−31.

(6) Lieleg, O.; Lieleg, C.; Bloom, J.; Buck, C. B.; Ribbeck, K. Mucin biopolymers as broad-spectrum antiviral agents. *Biomacromolecules* **2012**, *13* (6), 1724−32.

(7) Caldara, M.; Friedlander, R. S.; Kavanaugh, N. L.; Aizenberg, J.; Foster, K. R.; Ribbeck, K. Mucin biopolymers prevent bacterial aggregation by retaining cells in the free-swimming state. *Curr. Biol.* **2012**, *22* (24), 2325−30.

(8) Crouzier, T.; Jang, H.; Ahn, J.; Stocker, R.; Ribbeck, K. Cell Patterning with Mucin Biopolymers. *Biomacromolecules* **2013**, *14* (9), 3010−3016.

(9) Co, J. Y.; Crouzier, T.; Ribbeck, K. Probing the Role of Mucin-Bound Glycans in Bacterial Repulsion by Mucin Coatings. *Adv. Mater. Interfaces* **2015**, *2* (17), 1500179.

(10) Bongaerts, J. H. H.; Rossetti, D.; Stokes, J. R. The Lubricating Properties of Human Whole Saliva. *Tribol. Lett.* **2007**, *27* (3), 277−287.

(11) Ablamowicz, A. F.; Nichols, J. J. Ocular Surface Membrane-Associated Mucins. *Ocul. Surf.* **2016**, *14* (3), 331−41.

(12) Biegler, M.; Delius, J.; Käsdorf, B. T.; Hofmann, T.; Lieleg, O. Cationic astringents alter the tribological and rheological properties of human saliva and salivary mucin solutions. *Biotribology* **2016**, *6*, 12−20.

(13) Lee, S. Characterization of Lubricity of Mucins at Polymeric Surfaces for Biomedical Applications. *Int. J. Med., Health, Biomed., Bioeng. and Pharm. Eng.* **2013**, *7* (3), 145−150.

(14) Mystkowska, J.; Karalus, W.; Sidorenko, J.; Dąbrowski, J. R.; Kalska-Szostko, B. Biotribological properties of dentures lubricated

DOI: 10.1021/acs.biomac.7b00605
Biomacromolecules 2017, 18, 2454−2462

with artificial saliva. *Journal of Friction and Wear* **2016**, *37* (6), 544–551.
(15) Wang, X.; Du, M.; Han, H.; Song, Y.; Zheng, Q. Boundary lubrication by associative mucin. *Langmuir* **2015**, *31* (16), 4733–40.
(16) Yakubov, G. E.; McColl, J.; Bongaerts, J. H.; Ramsden, J. J. Viscous boundary lubrication of hydrophobic surfaces by mucin. *Langmuir* **2009**, *25* (4), 2313–21.
(17) Hamrock, B. J.; Schmid, S. R.; Jacobson, B. O. *Fundamentals of Fluid Film Lubrication*; CRC Press, 2004.
(18) Coles, J. M.; Chang, D. P.; Zauscher, S. Molecular mechanisms of aqueous boundary lubrication by mucinous glycoproteins. *Curr. Opin. Colloid Interface Sci.* **2010**, *15* (6), 406–416.
(19) Lee, S.; Muller, M.; Rezwan, K.; Spencer, N. D. Porcine gastric mucin (PGM) at the water/poly(dimethylsiloxane) (PDMS) interface: influence of pH and ionic strength on its conformation, adsorption, and aqueous lubrication properties. *Langmuir* **2005**, *21* (18), 8344–53.
(20) Berry, M.; McMaster, T. J.; Corfield, A. P.; Miles, M. J. Exploring the Molecular Adhesion of Ocular Mucins. *Biomacromolecules* **2001**, *2* (2), 498–503.
(21) An, J.; Dedinaite, A.; Nilsson, A.; Holgersson, J.; Claesson, P. M. Comparison of a brush-with-anchor and a train-of-brushes mucin on poly(methyl methacrylate) surfaces: adsorption, surface forces, and friction. *Biomacromolecules* **2014**, *15* (4), 1515–25.
(22) Crouzier, T.; Boettcher, K.; Geonnotti, A. R.; Kavanaugh, N. L.; Hirsch, J. B.; Ribbeck, K.; Lieleg, O. Modulating Mucin Hydration and Lubrication by Deglycosylation and Polyethylene Glycol Binding. *Adv. Mater. Interfaces* **2015**, *2* (18), 1500308–1500315.
(23) Feiler, A. A.; Sahlholm, A.; Sandberg, T.; Caldwell, K. D. Adsorption and viscoelastic properties of fractionated mucin (BSM) and bovine serum albumin (BSA) studied with quartz crystal microbalance (QCM-D). *J. Colloid Interface Sci.* **2007**, *315* (2), 475–481.
(24) Shi, L.; Caldwell, K. D. Mucin Adsorption to Hydrophobic Surfaces. *J. Colloid Interface Sci.* **2000**, *224* (2), 372–381.
(25) Hills, B. A. Boundary lubrication in vivo. *Proc. Inst. Mech. Eng., Part H* **2000**, *214* (1), 83–94.
(26) Ranc, H.; Elkhyat, A.; Servais, C.; Mac-Mary, S.; Launay, B.; Humbert, P. Friction coefficient and wettability of oral mucosal tissue: Changes induced by a salivary layer. *Colloids Surf., A* **2006**, *276* (1–3), 155–161.
(27) Hills, B. A. Lubrication of visceral movement and gastric motility by peritoneal surfactant. *J. Gastroenterol. Hepatol.* **1996**, *11* (9), 797–803.
(28) Davidson, H. J.; Kuonen, V. J. The tear film and ocular mucins. *Vet. Ophthalmol.* **2004**, *7* (2), 71–77.
(29) Hsu, S. M. Boundary lubrication: current understanding. *Tribol. Lett.* **1997**, *3* (1), 1–11.
(30) Chan, S. M. T.; Neu, C. P.; DuRaine, G.; Komvopoulos, K.; Reddi, A. H. Tribological altruism: A sacrificial layer mechanism of synovial joint lubrication in articular cartilage. *J. Biomech.* **2012**, *45* (14), 2426–2431.
(31) Ma, L.; Gaisinskaya-Kipnis, A.; Kampf, N.; Klein, J. Origins of hydration lubrication. *Nat. Commun.* **2015**, *6*, 6060.
(32) Jahn, S.; Klein, J. Hydration Lubrication: The Macromolecular Domain. *Macromolecules* **2015**, *48* (15), 5059–5075.
(33) Schömig, V. J.; Käsdorf, B. T.; Scholz, C.; Bidmon, K.; Lieleg, O.; Berensmeier, S. An optimized purification process for porcine gastric mucin with preservation of its native functional properties. *RSC Adv.* **2016**, *6* (50), 44932–44943.
(34) Yakubov, G. E.; Papagiannopoulos, A.; Rat, E.; Easton, R. L.; Waigh, T. A. Molecular Structure and Rheological Properties of Short-Side-Chain Heavily Glycosylated Porcine Stomach Mucin. *Biomacromolecules* **2007**, *8* (11), 3467–3477.
(35) Yakubov, G. E.; Papagiannopoulos, A.; Rat, E.; Waigh, T. A. Charge and interfacial behavior of short side-chain heavily glycosylated porcine stomach mucin. *Biomacromolecules* **2007**, *8* (12), 3791–9.
(36) An, J.; Jin, C.; Dedinaite, A.; Holgersson, J.; Karlsson, N. G.; Claesson, P. M. Influence of Glycosylation on Interfacial Properties of Recombinant Mucins: Adsorption, Surface Forces, and Friction. *Langmuir* **2017**, *33* (18), 4386–4395.
(37) Madsen, J. B.; Svensson, B.; Abou Hachem, M.; Lee, S. Proteolytic Degradation of Bovine Submaxillary Mucin (BSM) and Its Impact on Adsorption and Lubrication at a Hydrophobic Surface. *Langmuir* **2015**, *31* (30), 8303–8309.
(38) Jentoft, N. Why Are Proteins O-Glycosylated. *Trends Biochem. Sci.* **1990**, *15* (8), 291–294.
(39) Verneuil, E.; Buguin, A.; Silberzan, P. Permeation-induced flows: Consequences for silicone-based microfluidics. *Europhys. Lett.* **2004**, *68* (3), 412–418.
(40) Boettcher, K.; Grumbein, S.; Winkler, U.; Nachtsheim, J.; Lieleg, O. Adapting a commercial shear rheometer for applications in cartilage research. *Rev. Sci. Instrum.* **2014**, *85* (9), 093903.
(41) Voinova, M. V.; Rodahl, M.; Jonson, M.; Kasemo, B. Viscoelastic Acoustic Response of Layered Polymer Films at Fluid-Solid Interfaces: Continuum Mechanics Approach. *Phys. Scr.* **1999**, *59* (5), 391.
(42) Weber, N.; Wendel, H. P.; Kohn, J. Formation of viscoelastic protein layers on polymeric surfaces relevant to platelet adhesion. *J. Biomed. Mater. Res., Part A* **2005**, *72A* (4), 420–427.
(43) Stenberg, E.; Persson, B.; Roos, H.; Urbaniczky, C. Quantitative determination of surface concentration of protein with surface plasmon resonance using radiolabeled proteins. *J. Colloid Interface Sci.* **1991**, *143* (2), 513–526.
(44) Kočevar-Nared, J.; Kristl, J.; Šmid-Korbar, J. Comparative rheological investigation of crude gastric mucin and natural gastric mucus. *Biomaterials* **1997**, *18* (9), 677–681.
(45) Jensen, P. H.; Kolarich, D.; Packer, N. H. Mucin-type O-glycosylation – putting the pieces together. *FEBS J.* **2010**, *277* (1), 81–94.
(46) Russell, D.; Oldham, N. J.; Davis, B. G. Site-selective chemical protein glycosylation protects from autolysis and proteolytic degradation. *Carbohydr. Res.* **2009**, *344* (12), 1508–1514.
(47) Scawen, M.; Allen, A. Action of Proteolytic-Enzymes on Glycoprotein from Pig Gastric Mucus. *Biochem. J.* **1977**, *163* (2), 363–368.
(48) Balasubramanian, D.; Raman, B.; Sundari, C. S. Polysaccharides as amphiphiles. *J. Am. Chem. Soc.* **1993**, *115* (1), 74–77.
(49) Hunger, J.; Bernecker, A.; Bakker, H. J.; Bonn, M.; Richter, R. P. Hydration Dynamics of Hyaluronan and Dextran. *Biophys. J.* **2012**, *103* (1), L10–L12.
(50) Perez-Vilar, J.; Hill, R. L. The structure and assembly of secreted mucins. *J. Biol. Chem.* **1999**, *274* (45), 31751–31754.
(51) Authimoolam, S.; Dziubla, T. Biopolymeric Mucin and Synthetic Polymer Analogs: Their Structure, Function and Role in Biomedical Applications. *Polymers* **2016**, *8* (3), 71.
(52) Bhaskar, K. R.; Gong, D.; Bansil, R.; Pajevic, S.; Hamilton, J. A.; Turner, B. S.; Lamont, J. T. Profound Increase in Viscosity and Aggregation of Pig Gastric Mucin at Low pH. *Am. J. Physiol.* **1991**, *261* (5), G827–G833.
(53) Snary, D.; Allen, A. Studies on gastric mucoproteins. The isolation and characterization of the mucoprotein of the water-soluble mucus from pig cardiac gastric mucosa. *Biochem. J.* **1971**, *123* (5), 845–53.
(54) Thomsson, K. A.; Prakobphol, A.; Leffler, H.; Reddy, M. S.; Levine, M. J.; Fisher, S. J.; Hansson, G. C. The salivary mucin MG1 (MUC5B) carries a repertoire of unique oligosaccharides that is large and diverse. *Glycobiology* **2002**, *12* (1), 1–14.
(55) Zappone, B.; Ruths, M.; Greene, G. W.; Jay, G. D.; Israelachvili, J. N. Adsorption, Lubrication, and Wear of Lubricin on Model Surfaces: Polymer Brush-Like Behavior of a Glycoprotein. *Biophys. J.* **2007**, *92* (5), 1693–1708.
(56) Jahanmir, S.; Beltzer, M. An Adsorption Model for Friction in Boundary Lubrication. *ASLE Trans.* **1986**, *29* (3), 423–430.
(57) Spencer, N. D. Aqueous Lubrication with Poly(Ethylene Glycol) Brushes. *Tribology Online* **2014**, *9* (4), 143–153.

DOI: 10.1021/acs.biomac.7b00605
Biomacromolecules 2017, 18, 2454–2462

Supporting Information

for

Mucin-inspired lubrication on hydrophobic surfaces

Benjamin T. Käsdorf[1], Florian Weber[1], Georgia Petrou[2], Vaibhav Srivastava[2], Thomas Crouzier[2], and Oliver Lieleg[1,]*

[1] Department of Mechanical Engineering and Munich School of Bioengineering, Technical University of Munich, Boltzmannstrasse 11, 85748, Garching, Germany

[2] Division of Glycoscience School of Biotechnology
Royal Institute of Technology, 106 91 Stockholm, Sweden

Measuring the thickness of spin coated PDMS layers

PDMS (Sylgard 184, DowCorning, Wiesbaden, Germany) was mixed in a prepolymer/cross-linker ratio of 10:1 and was diluted to 1 vol% in n-hexane and spin coated (see Methods section in the main text) to a glass slide. After curing the PDMS at 80 °C for 4 h, the glass slide was scratched with a pipet tip. The thickness of the PDMS layer was determined with a µSurf Profilometer (NanoFocus, Oberhausen, Germany). Images were taken with a 20x objective and processed with µSoft analysis software.

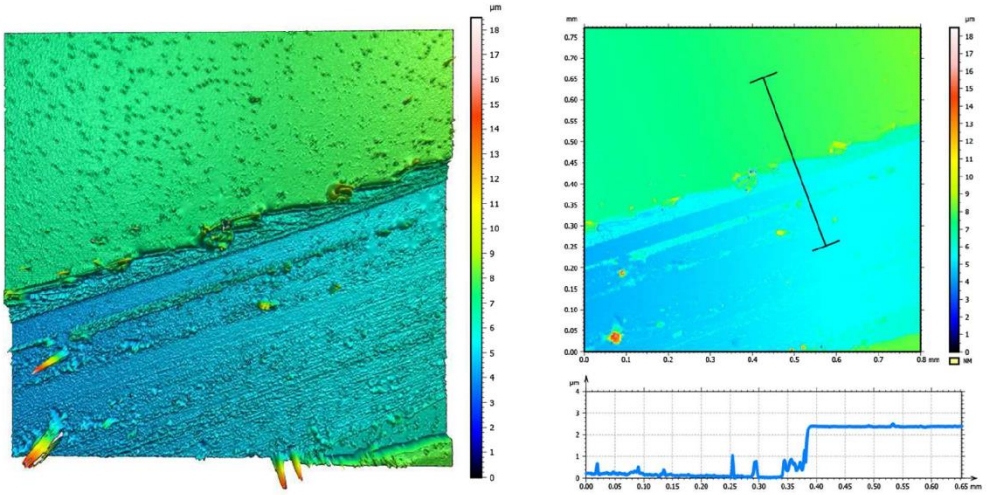

Figure S1: Layer thickness of spin coated PDMS on glass. 3D-profile of the layer thickness of spin coated PDMS on glass (a). A 2D-profile is generated by analyzing a cross section of the scratch and the PDMS layer to illustrate the layer thickness (b). Images were obtained with white light profilometry.

Mass spectrometry of trypsin digested mucins

After trypsination, mucin digestion mixture was filtered through centrifugal concentrators (Vivaspin 20, MWCO 300kDa, Sigma Aldrich, St. Louis, MO). The resulting flow through containing peptides was dried and resuspended in 0.1% formic acid for mass spectrometric analysis. Peptide analysis was completed using a nanoACQUITY Ultra Performance Liquid Chromatography system coupled to a Q-TOF mass spectrometer (Xevo Q-TOF, Waters, Milford, MA, USA) as previously described[1]. Briefly, peptides were loaded on a C18 trap column (Symmetry 180 μm x 20 mm, 5 μm; Waters, Milford, MA) followed by washing with 1% (v/v) acetonitrile, 0.1% (v/v) formic acid at 15 µl/min for 10 min. The samples eluted from the trap column were separated on a C18 analytical column (75 μm x 100 mm, 1.7 μm; Waters, Milford, MA) at 225 nl/min using 0.1% formic acid as solvent A and 0.1% formic acid in acetonitrile as solvent B in a stepwise gradient: 0.1%–10% B (0–5 min), 10%–30% B (5–32 min), 30%–40% B (32-35 min), 40%–85% B (36-38 min), 85% B (38-40 min), 85%–0.1% B (40-42 min), and 0.1% B (42-60 min). The eluting peptides were sprayed in the mass spectrometer (capillary and cone voltages set to 2.3 kV and 35 V, respectively), and MS/MS spectra were acquired using automated data-directed switching between the MS and MS/MS modes using the instrument software (MassLynx V4.0 SP4). Each sample was analyzed four times at different predefined mass ranges (400-600, 600-800, 800-1000, and 1000-1600 m/z). In each analysis, three most abundant signals of a survey scan (different mass ranges, 1 s scan time) were selected by charge state, and collision energy was applied accordingly for sequential MS/MS fragmentation scanning (50-1800 m/z range, 1s scan time).

The MS raw data files were processed using Mascot Distiller (version 2.4.3.2, Matrix Science, London, UK) and the resulting files were submitted to a local Mascot (Matrix Science, version 2.3.1) server using the human sequence library (91,464 sequences) in the International Protein Index (IPI) database. The following settings were used for the database search: trypsin-specific digestion with two missed cleavage allowed, carbamidomethylated cysteine and oxidized methionine as variable modifications, peptide tolerance of 100 ppm and fragment tolerance of 0.4 Da. Peptides with Mascot ion scores exceeding the threshold for statistical significance ($p<0.05$) were selected.

Table S1: Mass spectrometric analysis of trypsin digested human salivary mucin MUC5B. Peptides identified by mass spectrometry are highlighted in red. The protein sequence coverage is 25 %.

```
   1 MGAPSACRTL VLALAAMLVV PQAETQGPVE PSWENAGHTM DGGAPTSSPT
  51 RRVSFVPPVT VFPSLSPLNP AHNGRVCSTW GDFHYKTFDG DVFRFPGLCN
 101 YVFSEHCRAA YEDFNVQLRR GLVGSRPVVT RVVIKAQGLV LEASNGSVLI
 151 NGQREELPYS RTGLLVEQSG DYIKVSIRLV LTFLWNGEDS ALLELDPKYA
 201 NQTCGLCGDF NGLPAFNEFY AHNARLTPLQ FGNLQKLDGP TEQCPDPLPL
 251 PAGNCTDEEG ICHRTLLGPA FAECHALVDS TAYLAACAQD LCRCPTCPCA
 301 TFVEYSRQCA HAGGQPRNWR CPELCPRTCP LNMQHQECGS PCTDTCSNPQ
 351 RAQLCEDHCV DGCFCPPGRS CTVLDDITHS GCLPLGQCPC THGGRTYSPG
 401 TSFNTTCSSC TCSGGLWQCQ DLPCPGTCSV QGGAHISTYD EKLYDLHGDC
 451 SYVLSKKCAD SSFTVLAELR KCGLTDNENC LKAVTLSLDG GDTAIRVQAD
 501 GGVFLNSIYT QLPLSAANIT LFTPSSFFIV VQTGLGLQLL VQLVPLMQVF
 551 VRLDPAHQGQ MCGLCGNFNQ NQADDFTALS GVVEATGAAF ANTWKAQAAC
 601 ANARNSFEDP CSLSVENENY ARHWCSRLTD PNSAFSRCHS IINPKPFHSN
 651 CMFDTCNCER SEDCLCAALS SYVHACAAKG VQLSDWRDGV CTKYMQNCPK
 701 SQRYAYVVDA CQPTCRGLSE ADVTCSVSFV PVDGCTCPAG TFLNDAGACV
 751 PAQECPCYAH GTVLAPGEVV HDEGAVCSCT GGKLSCLGAS LQKSTGCAAP
 801 MVYLDCSNSS AGTPGAECLR SCHTLDVGCF STHCVSGCVC PPGLVSDGSG
 851 GCIAEEDCPC VHNEATYKPG ETIRVDCNTC TCRNRRWECS HRLCLGTCVA
 901 YGDGHFITFD GDRYSFEGSC EYILAQDYCG DNTTHGTFRI VTENIPCGTT
 951 GTTCSKAIKL FVESYELILQ EGTFKAVARG PGGDPPYKIR YMGIFLVIET
1001 HGMAVSWDRK TSVFIRLHQD YKGRVCGLCG NFDDNAINDF ATRSRSVVGD
1051 ALEFGNSWKL SPSCPDALAP KDPCTANPFR KSWAQKQCSI LHGPTFAACR
1101 SQVDSTKYYE ACVNDACACD SGGDCECFCT AVAAYAQACH DAGLCVSWRT
1151 PDTCPLFCDF YNPHGGCEWH YQPCGAPCLK TCRNPSGHCL VDLPGLEGCY
1201 PKCPPSQPFF NEDQMKCVAQ CGCYDKDGNY YDVGARVPTA ENCQSCNCTP
1251 SGIQCAHSLE ACTCTYEDRT YSYQDVIYNT TDGLGACLIA ICGSNGTIIR
1301 KAVACPGTPA TTPFTFTTAW VPHSTTSPAL PVSTVCVREV CRWSSWYNGH
1351 RPEPGLGGGD FETFENLRQR GYQVCPVLAD IECRAAQLPD MPLEELGQQV
1401 DCDRMRGLMC ANSQQSPPLC HDYELRVLCC EYVPCGPSPA PGTSPQPSLS
1451 ASTEPAVPTP TQTTATEKTT LWVTPSIRST AALTSQTGSS SGPVTVTPSA
1501 PGTTTCQPRC QWTEWFDEDY PKSEQLGGDV ESYDKIRAAG GHLCQQPKDI
1551 ECQAESFPNW TLAQVGQKVH CDVHFGLVCR NWEQEGVFKM CYNYRIRVLC
1601 CSDDHCRGRA TTPPPTTELE TATTTTTQAL FSTPQPTSSP GLTRAPPAST
1651 TAVPTLSEGL TSPRYTSTLG TATTGGPTTP AGSTEPTVPG VATSTLPTRS
1701 ALPGTTGSLG TWRPSQPPTL APTTMATSRA RPTGTASTAS KEPLTTSLAP
1751 TLTSELSTSQ AETSTPRTET TMSPLTNTTT SQGTTRCQPK CEWTEWFDVD
1801 FPTSGVAGGD METFENIRAA GGKMCWAPKS IECRAENYPE VSIDQVGQVL
1851 TCSLETGLTC KNEDQTGRFN MCFNYNVRVL CCDDYSHCPS TPATSSTATP
1901 SSTPGTTWIL TKPTTTATTT ASTGSTATPT STLRTAPPPK VLTTTATTPT
1951 VTSSKATPSS SPGTATALPA LRSTATTPTA TSVTPIPSSS LGTTWTRLSQ
2001 TTTPTATMST ATPSSTPETA HTSTVLTATA TTTGATGSVA TPSSTPGTAH
2051 TTKVPTTTTT GFTATPSSSP GTALTPPVWI STTTTPTTRG STVTPSSIPG
2101 TTHTATVLTT TTTTVATGSM ATPSSSTQTS GTPPSLTTTA TTITATGSTT
2151 NPSSTPGTTP IPPVLTTTAT TPAATSNTVT PSSALGTTHT PPVPNTMATT
2201 HGRSLPPSSP HTVRTAWTSA TSGILGTTHI TEPSTVTSHT LAATTGTTQH
2251 STPALSSPHP SSRTTESPPS PGTTTPGHTT ATSRTTATAT PSKTRTSTLL
2301 PSSPTSAPIT TVVTMGCEPQ CAWSEWLDYS YPMPGPSGGD FDTYSNIRAA
2351 GGAVCEQPLG LECRAQAQPG VPLRELGQVV ECSLDFGLVC RNREQVGKFK
2401 MCFNYEIRVF CCNYGHCPST PATSSTAMPS STPGTTWILT ELTTTATTTE
2451 STGSTATPSS TPGTTWILTE PSTTATVTVP TGSTATASST QATAGTPHVS
2501 TTATTPTVTS SKATPFSSPG TATALPALRS TATTPTATSF TAIPSSSLGT
2551 TWTRLSQTTT PTATMSTATP SSTPETVHTS TVLTTTATTT GATGSVATPS
2601 STPGTAHTTK VLTTTTTGFT ATPSSSPGTA RTLPVWISTT TTPTTRGSTV
2651 TPSSIPGTTH TPTVLTTTTT TVATGSMATP SSSTQTSGTP PSLTTTATTI
2701 TATGSTTNPS STPGTTPIPP VLTTTATTPA ATSSTVTPSS ALGTTHTPPV
2751  PNTTATTHGR  SLSPSSPHTV  RTAWTSATSG  TLGTTHITEP  STGTSHTPAA
2801  TTGTTQHSTP  ALSSPHPSSR  TTESPPSPGT  TTPGHTRATS  RTTATATPSK
2851 TRTSTLLPSS PTSAPITTVV TMGCEPQCAW SEWLDYSYPM PGPSGGDFDT
2901 YSNIRAAGGA VCEQPLGLEC RAQAQPGVPL RELGQVVECS LDFGLVCRNR
2951 EQVGKFKMCF NYEIRVFCCN YGHCPSTPAT SSTATPSSTP GTTWILTEQT
3001 TAATTTATTG STAIPSSTPG TAPPPKVLTS TATTPTATSS KATSSSSPRT
3051 ATTLPVLTST ATKSTATSFT PIPSFTLGTT GTLPEQTTTP MATMSTIHPS
3101 STPETTHTST VLTTKATTTR ATSSMSTPSS TPGTTWILTE LTTAATTTAA
3151 TGPTATPSST PGTTWILTEP STTATVTVPT GSTATASSTR ATAGTLKVLT
3201 STATTPTVIS SRATPSSSPG TATALPALRS TATTPTATSV TAIPSSSLGT
3251 AWTRLSQTTT PTATMSTATP SSTPETVHTS TVLTTTTTTT RATGSVATPS
3301 STPGTAHTTK VPTTTTTGFT ATPSSSPGTA LTPPVWISTT TTPTTRGSTV
3351 TPSSIPGTTH TATVLTTTTT TVATGSMATP SSSTQTSGTP PSLTTTATTI
3401 TATGSTTNPS STPGTTPIPP VLTTTATTPA ATSSTVTPSS ALGTTHTPPV
3451 PNTTATTHGR SLPPSSPHTV RTAWTSATSG ILGTTHITEP STVTSHTPAA
3501 TTSTTQHSTP ALSSPHPSSR TTESPPSPGT TTPGHTRGTS RTTATATPSK
3551 TRTSTLLPSS PTSAPITTVV TTGCEPQCAW SEWLDYSYPM PGPSGGDFDT
3601 YSNIRAAGGA VCEQPLGLEC RAQAQPGVPL RELGQVVECS LDFGLVCRNR
3651 EQVGKFKMCF NYEIRVFCCN YGHCPSTPAT SSTATPSSTP GTTWILTKLT
3701 TTATTTESTG STATPSSTPG TTWILTEPST TATVTVPTGS TATASSTQAT
3751 AGTPHVSTTA TTPTVTSSKA TPFSSPGTAT ALPALRSTAT TPTATSFTAI
3801 PSSSLGTTWT RLSQTTTPTA TMSTATPSST PETAHTSTVL TTTATTTRAT
3851 GSVATPSSTP GTAHTTKVPT TTTTGFTVTP SSSPGTARTP PVWISTTTTP
3901 TTSGSTVTPS SVPGTTHTPT VLTTTTTTVA TGSMATPSSS TQTSGTPPSL
3951 ITTATTITAT GSTTNPSSTP GTTPIPPVLT TTATTPAATS STVTPSSALG
4001 TTHTPPVPNT TATTHGRSLS PSSPHTVRTA WTSATSGTLG TTHITEPSTG
4051 TSHTPAATTG TTQHSTPALS SPHPSSRTTE SPPSPGTTTP GHTTATSRTT
4101 ATATPSKTRT STLLPSSPTS APITTVVTTG CEPQCAWSEW LDYSYPMPGP
4151 SGGDFDTYSN IRAAGGAVCE QPLGLECRAQ AQPGVPLGEL GQVVECSLDF
4201 GLVCRNREQV GKFKMCFNYE IRVFCCNYGH CPSTPATSST AMPSSTPGTT
4251 WILTELTTTA TTTASTGSTA TPSSTPGTAP PPKVLTSPAT TPTATSSKAT
4301 SSSSPRTATT LPVLTSTATK STATSVTPIP SSTLGTTGTL PEQTTTPVAT
4351 MSTIHPSSTP ETTHTSTVLT TKATTTRATS STSTPSSTPG TTWILTELTT
4401 AATTTAATGP TATPSSTPGT TWILTELTTT ATTTASTGST ATPSSTPGTT
4451 WILTEPSTTA TVTVPTGSTA TASSTQATAG TPHVSTTATT PTVTSSKATP
4501 SSSPGTATAL PALRSTATTP TATSFTAIPS SSLGTTWTRL SQTTTPTATM
4551 STATPSSTPE TVHTSTVLTA TATTTGATGS VATPSSTPGT AHTTKVPTTT
4601 TTGFTATPSS SPGTALTPPV WISTTTTPTT TTPTTSGSTV TPSSIPGTTH
4651 TARVLTTTTT TVATGSMATP SSSTQTSGTP PSLTTTATTI TATGSTTNPS
4701 STPGTTPITP VLTSTATTPA ATSSKATSSS SPRTATTLPV LTSTATKSTA
4751 TSFTPIPSST LWTTWTVPAQ TTTPMSTMST IHTSSTPETT HTSTVLTTTA
4801 TMTRATNSTA TPSSTLGTTR ILTELTTTAT TTAATGSTAT LSSTPGTTWI
4851 LTEPSTIATV MVPTGSTATA SSTLGTAHTP KVVTTMATMP TATASTVPSS
4901 STVGTTRTPA VLPSSLPTFS VSTVSSSVLT TLRPTGFPSS HFSTPCFCRA
4951 FGQFFSPGEV IYNKTDRAGC HFYAVCNQHC DIDRFQGACP TSPPPVSSAP
5001 LSSPSPAPGC DNAIPLRQVN ETWTLENCTV ARCVGDNRVV LLDPKPVANV
5051 TCVNKHLPIK VSDPSQPCDF HYECECICSM WGGSHYSTFD GTSYTFRGNC
5101 TYVLMREIHA RFGNLSLYLD NHYCTASATA AAARCPRALS IHYKSMDIVL
5151 TVTMVHGKEE GLILFDQIPV SSGFSKNGVL VSVLGTTTMR VDIPALGVSV
5201 TFNGQVFQAR LPYSLFHNNT EGQCGTCTNN QRDDCLQRDG TTAASCKDMA
5251 KTWLVPDSRK DGCWAPTGTP PTASPAAPVS STPTPTPCPP QPLCDLMLSQ
5301 VFAECHNLVP PGPFFNACIS DHCRGRLEVP CQSLEAYAEL CRARGVCSDW
5351 RGATGGLCDL TCPPTKVYKP CGPIQPATCN SRNQSPQLEG MAEGCFCPED
5401 QILFNAHMGI CVQACPCVGP DGFPKFPGER WVSNCQSCVC DEGSVSVQCK
5451 PLPCDAQGQP PPCNRPGFVT VTRPRAENPC CPETVCVCNT TTCPQSLPVC
5501 PPGQESICTQ EEGDCCPTFR CRPQLCSYNG TFYGVGATFP GALPCHMCTC
5551 LSGDTQDPTV QCQEDACNNT TCPQGFEYKR VAGQCCGECV QTACLTPDGQ
5601 PVQLNETWVN SHVDNCTVYL CEAEGGVHLL TPQPASCPDV SSCRGSLRKT
5651 GCCYSCEEDS CQVRINTTIL WHQGCETEVN ITFCEGSCPG ASKYSAEAQA
5701 MQHQCTCCQE RRVHEETVPL HCPNGSAILH TYTHVDECGC TPFCVPAPMA
5751 PPHTRGFPAQ EATAV
```

Table S2: Mass spectrometric analysis of trypsin digested porcine gastric mucin MUC5AC. Peptide identified by mass spectrometry are highlighted in red. The protein sequence coverage of the fragments o digested porcine 5AC with the human 5AC sequence is 7 %.

```
   1 MSVGRRKLAL LWALALALAC TRHTGHAQDG SSESSYKHHP ALSPIARGPS
  51 GVPLRGATVF PSLRTIPVVR ASNPAHNGRV CSTWGSFHYK TFDGDVFRFP
 101 GLCNYVFSEH CGAAYEDFNI QLRRSQESAA PTLSRVLMKV DGVVIQLTKG
 151 SVLVNGHPVL LPFSQSGVLI QQSSSYTKVE ARLGLVLMWN HDDSLLLELD
 201 TKYANKTCGL CGDFNGMPVV SELLSHNTKL TPMEFGNLQK MDDPTDQCQD
 251 PVPEPPRNCS TGFGICEELL HGQLFSGCVA LVDVGSYLEA CRQDLCFCED
 301 TDLLSCVCHT LAEYSRQCTH AGGLPQDWRG PDFCPQKCPN NMQYHECRSP
 351 CADTCSNQEH SRACEDHCVA GCFCPEGTVL DDIGQTGCVP VSKCACVYNG
 401 AAYAPGATYS TDCTNCTCSG GRWSCQEVPC PGTCSVLGGA HFSTFDGKQY
 451 TVHGDCSYVL TKPCDSSAFT VLAELRRCGL TDSETCLKSV TLSLDGAQTV
 501 VVIKASGEVF LNQIYTQLPI SAANVTIFRP STFFIIAQTS LGLQLNLQLV
 551 PTMQLFMQLA PKLRGQTCGL CGNFNSIQAD DFRTLSGVVE ATAAAFFNTF
 601 KTQAACPNIR NSFEDPCSLS VENEKYAQHW CSQLTDADGP FGRCHAAVKP
 651 GTYYSNCMFD TCNCERSEDC LCAALSSYVH ACAAKGVQLG GWRDGVCTKP
 701 MTTCPKSMTY HYHVSTCQPT CRSLSEGDIT CSVGFIPVDG CICPKGTFLD
 751 DTGKCVQASN CPCYHRGSMI PNGESVHDSG AICTCTHGKL SCIGGQAPAP
 801 VCAAPMVFFD CRNATPGDTG AGCQKSCHTL DMTCYSPQCV PGCVCPDGLV
 851 ADGEGGCITA EDCPCVHNEA SYRAGQTIRV GCNTCTCDSR MWRCTDDPCL
 901 ATCAVYGDGH YLTFDGQSYS FNGDCEYTLV QNHCGGKDST QDSFRVVTEN
 951 VPCGTTGTTC SKAIKIFLGG FELKLSHGKV EVIGTDESQE VPYTIRQMGI
1001 YLVVDTDIGL VLLWDKKTSI FINLSPEFKG RVCGLCGNFD DIAVNDFATR
1051 SRSVVGDVLE FGNSWKLSPS CPDALAPKDP CTANPFRKSW AQKQCSILHG
1101 PTFAACHAHV EPARYYEACV NDACACDSGG DCECFCTAVA AYAQACHEVG
1151 LCVSWRTPSI CPLFCDYYNP EGQCEWHYQP CGVPCLRTCR NPRGDCLRDV
1201 RGLEGCYPKC PPEAPIFDED KMQCVATCPT PPLPPRCHVH GKSYRPGAVV
1251 PSDKNCQSCL CTERGVECTY KAEACVCTYN GQRFHPGDVI YHTTDGTGGC
1301 ISARCGANGT IERRVYPCSP TTPVPPTTFS FSTPPLVVSS THTPSNGPSS
1351 AHTGPPSSAW PTTAGTSPRT RLPTASASLP PVCGEKCLWS PWMDVSRPGR
1401 GTDSGDFDTL ENLRAHGYRV CESPRSVECR AEDAPGVPLR ALGQRVQCSP
1451 DVGLTCRNRE QASGLCYNYQ IRVQCCTPLP CSTSSSPAQT TPPTTSKTTE
1501 TRASGSSAPS STPGTVSLST ARTTPAPGTA TSVKKTFSTP SPPPVPATST
1551 SSMSTTAPGT SVVSSKPTPT EPSTSSCLQE LCTWTEWIDG SYPAPGINGG
1601 DFDTFQNLRD EGYTFCESPR SVQCRAESFP NTPLADLGQD VICSHTEGLI
1651 CLNKNQLPPI CYNYEIRIQC CETVNVCRDI TRLPKTVATT RPTPHPTGAQ
1701 TQTTFTTHMP SASTEQPTAT SRGGPTATSV TQGTHTTLVT RNCHPRCTWT
1751 KWFDVDFPSP GPHGGDKETY NNIIRSGEKI CRRPEEITRL QCRAKSHPEV
1801 SIEHLGQVVQ CSREEGLVCR NQDQQGPFKM CLNYEVRVLC CETPRGCHMT
1851 STPGSTSSSP AQTTPSTTSK TTETQASGSS APSSTPGTVS LSTARTTPAP
1901 GTATSVKKTF STPSPPPVPA TSTSSMSTTA PGTSVVSSKP TPTEPSTSSC
1951 LQELCTWTEW IDGSYPAPGI NGGDFDTFQN LRDEGYTFCE SPRSVQCRAE
2001 SFPNTPLADL GQDVICSHTE GLICLNKNQL PPICYNYEIR IQCCETVNVC
2051 RDITRPPKTV ATTRPTPHPT GAQTQTTFTT HMPSASTEQP TATSRGGPTA
2101 TSVTQGTHTT PVTRNCHPRC TWTTWFDVDF PSPGPHGGDK ETYNNIIRSG
2151 EKICRRPEEI TRLQCRAKSH PEVSIEHLGQ VVQCSREEGL VCRNQDQQGP
2201 FKMCLNYEVR VLCCETPKGC PVTSTPVTAP STPSGRATSP TQSTSSWQKS
2251 RTTTLVTTST TSTPQTSTTY AHTTSTTSAP TARTTSAPTT RTTSASPAST
2301 TSGPGNTPSP VPTTSTISAP TTSITSAPTT STTSAPTSST TSGPGTTPSP
2351 VPTTSITSAP TTSTTSAPTT STTSARTSST TSATTTSRIS GPETTPSPVP
2401 TTSTTSATTT STTSAPTTST TSAPTSSTTS SPQTSTTSAP TTSTTSGPGT
2451 TPSPVPTTST TSAPTTRTTS APKSSTTSAA TTSTTSGPET TPRPVPTTST
2501 TSSPTTSTTS APTTSTTSAS TTSTTSGAGT TPSPVPTTST TSAPTTSTTS
2551 APISSTTSAT TTSTTSGPGT TPSPVPTTST TSAPTTSTTS GPGTTPSAVP
2601 TTSITSAPTT STNSAPISST TSATTTSRIS GPETTPSPVP TASTTSASTT
2651 STTSGPGTTP SPVPTTSTIS VPTTSTTSAS TTSTTSASTT STTSGPGTTP
2701 SPVPTTSTTS APTTSTTSAP TTSTISAPTT STTSATTTST TSAPTPRRTS
2751 APTTSTISAS TTSTTSATTT STTSATTTST ISAPTTSTTL SPTTSTTSTT
2801 ITSTTSAPIS STTSTPQTST TSAPTTSTTS GPGTTSSPVP TTSTTSAPTT
2851 STTSAPTTRT TSVPTSSTTS TATTSTTSGP GTTPSPVPTT STTSAPTTRT
2901 TSAPTTSTTS APTTSTTSAP TSSTTSATTT STISVPTTST TSVPGTTPSP
2951 VPTTSTISVP TTSTTSASTT STTSGPGTTP SPVPTTSTTS APTTSTTSAP
3001 TTSTISAPTT STPSAPTTST TLAPTTSTTS APTTSTTSTP TSSTTSSPQT
3051 STTSASTTSI TSGPGTTPSP VPTTSTTSAP TTSTTSAATT STISAPTTST
3101 TSAPTTSTTS ASTASKTSGL GTTPSPIPTT STTSPPTTST TSASTASKTS
3151 GPGTTPSPVP TTSTIFAPRT STTSASTTST TPGPGTTPSP VPTTSTASVS
3201 KTSTSHVSIS KTTHSQPVTR DCHLRCTWTK WFDIDFPSPG PHGGDKETYN
3251 NIIRSGEKIC RRPEEITRLQ CRAESHPEVS IEHLGQVVQC SREEGLVCRN
3301 QDQQGPFKMC LNYEVRVLCC ETPKGCPVTS TPVTAPSTPS GRATSPTQST
3351 SSWQKSRTTT LVTTSTTSTP QTSTTSAPTT STTSAPTTST TSAPTTSTTS
3401 TPQTSISSAP TSSTTSAPTS STISARTTSI ISAPTTSTTS SPTTSTTSAT
3451 TTSTTSAPTS STTSTPQTSK TSAATSSTTS GSGTTPSPVT TTSTASVSKT
3501 STSHVSVSKT THSQPVTRDC HPRCTWTKWF DVDFPSPGPH GGDKETYNNI
3551 IRSGEKICRR PEEITRLQCR AKSHPEVSIE HLGQVVQCSR EEGLVCRNQD
3601 QQGPFKMCLN YEVRVLCCET PKGCPVTSTS VTAPSTPSGR ATSPTQSTSS
3651 WQKSRTTTLV TSSITSTTQT STTSAPTTST TPASIPSTTS APTTSTTSAP
3701 TTSTTSAPTT STTSTPQTTT SSAPTSSTTS APTTSTISAP TTSTISAPTT
3751 STTSAPTAST TSAPTSTSSA PTTNTTSAPT TSTTSAPITS TISAPTTSTT
3801 STPQTSTISS PTTSTTSTPQ TSTTSSPTTS TTSAPTTSTT SAPTTSTTST
3851 PQTSISSAPT SSTTSAPTAS TISAPTTSTT SFHTTSTTSP PTSSTSSTPQ
3901 TSKTSAATSS TTSGSGTTPS PVPTTSTASV SKTSTSHVSV SKTTHSQPVT
3951 RDCHPRCTWT KWFDVDFPSP GPHGGDKETY NNIIRSGEKI CRRPEEITRL
4001 QCRAESHPEV SIEHLGQVVQ CSREEGLVCR NQDQQGPFKM CLNYEVRVLC
4051 CETPKGCPVT STPVTAPSTP SGRATSPTQS TSSWQKSRTT TLVTTSTTST
4101 PQTSTTSAPT TSTIPASTPS TTSAPTTSTT SAPTTSTTSA PTHRTTSGPT
4151 TSTTLAPTTS TTSAPTTSTN SAPTTSTISA STTSTISAPT TSTISSPTSS
4201 TTSTPQTSKT SAATSSTTSG SGTTPSPVPT TSTTSASTTS TTSAPTTSTT
4251 SGPGTTPSPV PSTSTTSAAT TSTTSAPTTR TTSAPTSSMT SGPGTTPSPV
4301 PTTSTTSAPT TSTTSGPGTT PSPVPTTSTT SAPITSTTSG PGSTPSPVPT
4351 TSTTSAPTTS TTSASTASTT SGPGTTPSPV PTTSTTSAPT TRTTSASTAS
4401 TTSGPGSTPS PVPTTSTTSA PTTRTTPAST ASTTSGPGTT PSPVPTTSTT
4451 SASTTSTISL PTTSTTSAPI TSMTSGPGTT PSPVPTTSTT SAPTTSTTSA
4501 STASTTSGPG TTPSPVPTTS TTSAPTTSTT SASTASTTSG PGTSLSPVPT
4551 TSTTSAPTTS TTSGPGTTPS PVPTTSTTSA PTTSTTSGPG TTPSPVPTTS
4601 TTPVSKTSTS HLSVSKTTHS QPVTSDCHPL CAWTKWFDVD FPSPGPHGGD
4651 KETYNNIIRS GEKICRRPEE ITRLQCRAES HPEVNIEHLG QVVQCSREEG
4701 LVCRNQDQQG PFKMCLNYEV RVLCCETPRG CPVTSVTPYG TSPTNALYPS
4751 LSTSMVSASV ASTSVASSSV ASSSVAYSTQ TCFCNVADRL YPAGSTIYRH
4801 RDLAGHCYYA LCSQDCQVVR GVDSDCPSTT LPPAPATSPS ISTSEPVTEL
4851 GCPNAVPPRK KGETWATPNC SEATCEGNNV ISLRPRTCPR VEKPTCANGY
4901 PAVKVADQDG CCHHYQCQCV CSGWGDPHYI TFDGTYYTFL DNCTYVLVQQ
4951 IVPVYGHFRV LVDNYFCGAE DGLSCPRSII LEYHQDRVVL TRKPVHGVMT
5001 NEIIFNNKVV SPGFRKNGIV VSRIGVKMYA TIPELGVQVM FSGLIFSVEV
5051 PFSKFANNTE GQCGTCTNDR KDECRTPRGT VVASCSEMSG LWNVSIPDQP
5101 ACHRPHPTPT TVGPTTVGST TVGPTTVGST TVGPTTPPAP CLPSPICQLI
5151 LSKVFEPCHT VIPPLLFYEG CVFDRCHMTD LDVVCSSLEL YAALCASHDI
5201 CIDWRGRTGH MCPFTCPADK VYQPCGPSNP SYCYGNDSAS LGALPEAGPI
5251 TEGCFCPEGM TLFSTSAQVC VPTGCPRCLG PHGEPVKVGH TVGMDCQECT
5301 CEAATWTLTC RPKLCPLPPA CPLPGFVPVP AAPQAGQCCP QYSCACNTSR
5351 CPAPVGCPEG ARAIPTYQEG ACCPVQNCSW TVCSINGTLY QPGAVVSSSL
5401 CETCRCELPG GPPSDAFVVS CETQICNTHC PVGFEYQEQS GQCCGTCVQV
5451 ACVTNTSKSP AHLFYPGETW SDAGNHCVTH QCEKHQDGLV VVTTKKACPP
5501 LSCSLDEARM SKDGCCRFCP PPPPPYQNQS TCAVYHRSLI IQQQGCSSSE
5551 PVRLAYCRGN CGDSSSMYSL EGNTVEHRCQ CCQELRTSLR NVTLHCTDGS
5601 SRAFSYTEVE ECGCMGRRCP APGDTQHSEE AEPEPSQEAE SGSWERGVPV
5651 SPMH
```

Hydration measurements

Table S*3*: Hydration measurements of mucin and dextran coatings. Hydration was determined by measuring the adsorbed dry mass on a gold surface via SPR and the hydrated mass of this adsorbed coating via QCM-D and calculating the water mass and the hydration, respectively. Please note that the indicated water mass/dry mass ratios are difficult to interpret since distinguishing the hydration level of well-hydrated coatings as we study them here is challenging given the sensitivity and resolution of our QCM-D method.

Sample	dry mass [ng/mm²]	hydrated mass [ng/mm²]	water mass [ng/mm²]	water mass/dry mass ratio [ ]
MUC5AC	1.04 (±0.01)	22.68 (±1.18)	21.64 (±1.18)	21
MUC5B	1.24 (±0.20)	16.11 (±0.35)	14.86 (±0.55)	12
MUC5AC-Trypsin	0.18 (±0.01)	31.75 (±5.46)	31.58 (±5.47)	175
MUC5B-Trypsin	0.71 (±0.19)	25.48 (±0.55)	24.77 (±0.75)	35
Dextran	0.09 (±0.01)	1.01 (±0.17)	0.93 (±0.18)	10
Phenyl-Dextran (0.15)	0.36 (±0.03)	39.77 (±0.42)	39.40 (±0.45)	109
Phenyl-Dextran (0.40)	1.43 (±0.18)	26.67 (±1.01)	25.24 (±1.18)	18
Phenyl-MUC5B-Trypsin	0.16 (±0.03)	104.97 (±4.24)	104.81(±4.27)	655

6

Surface topology analysis of the PDMS pin surface

The topology of PDMS pins was investigated using an optical white light profilometer (µsurf custom, NanoFocus AG, Oberhausen, Germany) equipped with a 20x lens (UMPlanFl 800S NA = 0.46, Olympus Deutschland GmbH, Hamburg, Germany). Images were acquired from a PDMS pin after a tribological measurement with unmodified dextrans (0.1 % in 20 mM HEPES, pH 7). For determining the contact area between the steel sphere and the PDMS pin, images were acquired at low resolution, and a composite image of 25 single images was generated by stitching (**Figure S2**):

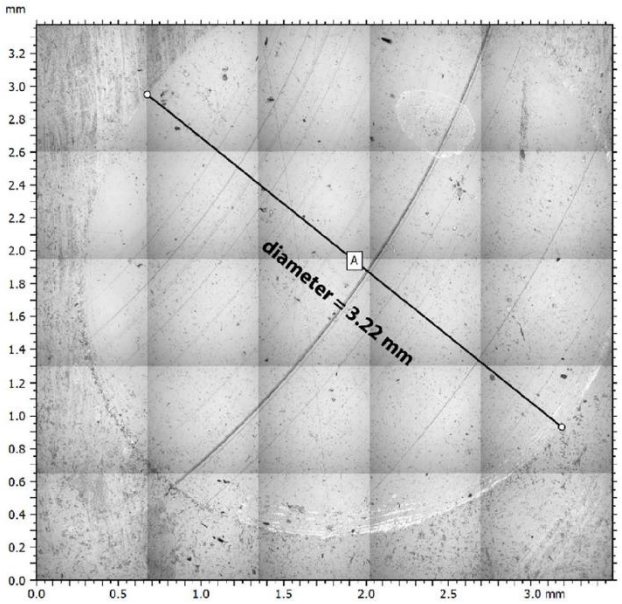

Figure S2: **Surface image of a PDMS pin after tribological treatment with a steel sphere at a normal force of 6 N.** A stitched image (consisting of 25 individual images) shows the size of the contact area between the steel sphere and the pin surface.

For analyzing the roughness of the PDMS pin surface, the resolution of the image was 1.56 µm in lateral direction and the step size in z-direction was set to 0.02 µm. Image analysis was performed using the software µsoft analysis extended V7 (NanoFokus AG, Oberhausen, Germany). To quantify the surface features of both untreated and treated sample regions, the sample tilt was mathematically removed by applying a linear polynomial correction to the

image. From such a topographical image (**Figure S3**), the root mean squared roughness *Sq* was then calculated following ISO 25178-2:

$$S_q = \sqrt{\frac{1}{A}\iint_A (z(x,y))^2 \, dx dy} \qquad \text{(Equation 1)}$$

With this procedure, we find comparable surface roughness values both in the area treated with the steel sphere ($Sq \sim 0.06$) and in the untreated PDMS region ($Sq \sim 0.05$). This shows that, even for the "poor" lubricant containing only unmodified dextran, the surface roughness of the PDMS pins is not altered by the tribological treatment and wear formation does not occur.

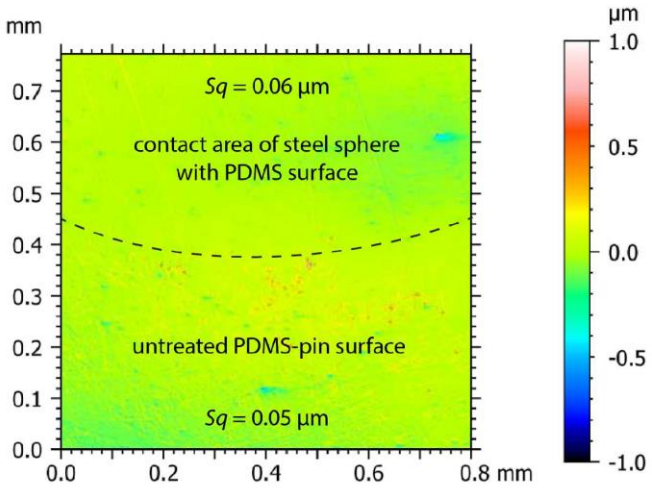

Figure S3: Topographical analysis a PDMS pin surface after tribological measurement. The upper region displays the area where the steel sphere was in contact with the PDMS pin surface. The area below the dashed line shows an untreated PDMS surface which was not in contact with the steel sphere. The *Sq* value for both areas is denoted in each section.

REFERENCES

1. Srivastava, V.; Weber, J. R.; Malm, E.; Fouke, B. W.; Bulone, V., Proteomic Analysis of a Poplar Cell Suspension Culture Suggests a Major Role of Protein S-Acylation in Diverse Cellular Processes. *Frontiers in Plant Science* **2016,** 7, 477.

B. Licenses for publications

B.1 Diffusion regulation in the vitreous humor

ELSEVIER LICENSE
TERMS AND CONDITIONS

Oct 12, 2017

This Agreement between Technical University of Munich -- Benjamin Käsdorf ("You") and Elsevier ("Elsevier") consists of your license details and the terms and conditions provided by Elsevier and Copyright Clearance Center.

License Number	4206470044357
License date	Oct 12, 2017
Licensed Content Publisher	Elsevier
Licensed Content Publication	Biophysical Journal
Licensed Content Title	Diffusion Regulation in the Vitreous Humor
Licensed Content Author	Benjamin Tillmann Käsdorf,Fabienna Arends,Oliver Lieleg
Licensed Content Date	Nov 17, 2015
Licensed Content Volume	109
Licensed Content Issue	10
Licensed Content Pages	11
Start Page	2171
End Page	2181
Type of Use	reuse in a thesis/dissertation
Portion	full article
Format	both print and electronic
Are you the author of this Elsevier article?	Yes
Will you be translating?	No
Order reference number	BK17091302
Title of your thesis/dissertation	Structure-function relations of biological hydrogel macromolecules
Expected completion date	Dec 2017
Estimated size (number of pages)	100
Requestor Location	Technical University of Munich Boltzmannstraße 11 Garching, 85748 Germany Attn: Technical University of Munich
Publisher Tax ID	GB 494 6272 12
Billing Type	Invoice
Billing Address	Technical University of Munich Boltzmannstraße 11 Garching, Germany 85748 Attn: Technical University of Munich
Total	0.00 EUR
Terms and Conditions	

INTRODUCTION

1. The publisher for this copyrighted material is Elsevier. By clicking "accept" in connection with completing this licensing transaction, you agree that the following terms and conditions apply to this transaction (along with the Billing and Payment terms and conditions established by Copyright Clearance Center, Inc. ("CCC"), at the time that you opened your Rightslink account and that are available at any time at http://myaccount.copyright.com).

GENERAL TERMS

2. Elsevier hereby grants you permission to reproduce the aforementioned material subject to the terms and conditions indicated.
3. Acknowledgement: If any part of the material to be used (for example, figures) has appeared in our publication with credit or acknowledgement to another source, permission must also be sought from that source. If such permission is not obtained then that material may not be included in your publication/copies. Suitable acknowledgement to the source must be made, either as a footnote or in a reference list at the end of your publication, as follows:
"Reprinted from Publication title, Vol /edition number, Author(s), Title of article / title of chapter, Pages No., Copyright (Year), with permission from Elsevier [OR APPLICABLE SOCIETY COPYRIGHT OWNER]." Also Lancet special credit - "Reprinted from The Lancet, Vol. number, Author(s), Title of article, Pages No., Copyright (Year), with permission from Elsevier."
4. Reproduction of this material is confined to the purpose and/or media for which permission is hereby given.
5. Altering/Modifying Material: Not Permitted. However figures and illustrations may be altered/adapted minimally to serve your work. Any other abbreviations, additions, deletions and/or any other alterations shall be made only with prior written authorization of Elsevier Ltd. (Please contact Elsevier at permissions@elsevier.com). No modifications can be made to any Lancet figures/tables and they must be reproduced in full.
6. If the permission fee for the requested use of our material is waived in this instance, please be advised that your future requests for Elsevier materials may attract a fee.
7. Reservation of Rights: Publisher reserves all rights not specifically granted in the combination of (i) the license details provided by you and accepted in the course of this licensing transaction, (ii) these terms and conditions and (iii) CCC's Billing and Payment terms and conditions.
8. License Contingent Upon Payment: While you may exercise the rights licensed immediately upon issuance of the license at the end of the licensing process for the transaction, provided that you have disclosed complete and accurate details of your proposed use, no license is finally effective unless and until full payment is received from you (either by publisher or by CCC) as provided in CCC's Billing and Payment terms and conditions. If full payment is not received on a timely basis, then any license preliminarily granted shall be deemed automatically revoked and shall be void as if never granted. Further, in the event that you breach any of these terms and conditions or any of CCC's Billing and Payment terms and conditions, the license is automatically revoked and shall be void as if never granted. Use of materials as described in a revoked license, as well as any use of the materials beyond the scope of an unrevoked license, may constitute copyright infringement and publisher reserves the right to take any and all action to protect its copyright in the materials.
9. Warranties: Publisher makes no representations or warranties with respect to the licensed material.
10. Indemnity: You hereby indemnify and agree to hold harmless publisher and CCC, and their respective officers, directors, employees and agents, from and against any and all claims arising out of your use of the licensed material other than as specifically authorized pursuant to this license.
11. No Transfer of License: This license is personal to you and may not be sublicensed, assigned, or transferred by you to any other person without publisher's written permission.
12. No Amendment Except in Writing: This license may not be amended except in a writing signed by both parties (or, in the case of publisher, by CCC on publisher's behalf).
13. Objection to Contrary Terms: Publisher hereby objects to any terms contained in any purchase order, acknowledgment, check endorsement or other writing prepared by you, which terms are inconsistent with these terms and conditions or CCC's Billing and Payment terms and conditions. These terms and conditions, together with CCC's Billing and Payment terms and conditions (which are incorporated herein), comprise the entire agreement between you and publisher (and CCC) concerning this licensing transaction. In the event of any conflict between your obligations established by these terms and conditions and those established by CCC's Billing and Payment terms and conditions, these terms and conditions shall control.
14. Revocation: Elsevier or Copyright Clearance Center may deny the permissions described in this License at their sole discretion, for any reason or no reason, with a full refund payable to you. Notice of such denial will be made using the contact information provided by you. Failure to receive such notice will not alter or invalidate the denial. In no event will Elsevier or Copyright Clearance Center be responsible or liable for any costs, expenses or damage incurred by you as a result of a denial of your permission request, other than a refund of the amount(s) paid by you to Elsevier and/or Copyright Clearance Center for denied permissions.

LIMITED LICENSE

The following terms and conditions apply only to specific license types:
15. **Translation**: This permission is granted for non-exclusive world **English** rights only unless your license was granted for translation rights. If you licensed translation rights you may only translate this content into the languages you requested. A professional translator must perform all translations and reproduce the content word for word preserving the integrity of the article.
16. **Posting licensed content on any Website**: The following terms and conditions apply as follows: Licensing material from an Elsevier journal: All content posted to the web site must maintain the copyright information line on the bottom of each image; A hyper-text must be included to the Homepage of the journal from which you are licensing at http://www.sciencedirect.com/science/journal/xxxxx or the Elsevier homepage for books at http://www.elsevier.com; Central Storage: This license does not include permission for a scanned version of the material to be stored in a central repository such as that provided by Heron/XanEdu.
Licensing material from an Elsevier book: A hyper-text link must be included to the Elsevier homepage at http://www.elsevier.com . All content posted to the web site must maintain the copyright information line on the bottom of each image.

Posting licensed content on Electronic reserve: In addition to the above the following clauses are applicable: The web site must be password-protected and made available only to bona fide students registered on a relevant course. This permission is granted for 1 year only. You may obtain a new license for future website posting.
17. **For journal authors:** the following clauses are applicable in addition to the above:
Preprints:
A preprint is an author's own write-up of research results and analysis, it has not been peer-reviewed, nor has it had any other value added to it by a publisher (such as formatting, copyright, technical enhancement etc.).
Authors can share their preprints anywhere at any time. Preprints should not be added to or enhanced in any way in order to appear more like, or to substitute for, the final versions of articles however authors can update their preprints on arXiv or RePEc with their Accepted Author Manuscript (see below).
If accepted for publication, we encourage authors to link from the preprint to their formal publication via its DOI. Millions of researchers have access to the formal publications on ScienceDirect, and so links will help users to find, access, cite and use the best available version. Please note that Cell Press, The Lancet and some society-owned have different preprint policies. Information on these policies is available on the journal homepage.
Accepted Author Manuscripts: An accepted author manuscript is the manuscript of an article that has been accepted for publication and which typically includes author-incorporated changes suggested during submission, peer review and editor-author communications.
Authors can share their accepted author manuscript:

- immediately
  - via their non-commercial person homepage or blog
  - by updating a preprint in arXiv or RePEc with the accepted manuscript
  - via their research institute or institutional repository for internal institutional uses or as part of an invitation-only research collaboration work-group
  - directly by providing copies to their students or to research collaborators for their personal use
  - for private scholarly sharing as part of an invitation-only work group on commercial sites with which Elsevier has an agreement
- After the embargo period
  - via non-commercial hosting platforms such as their institutional repository
  - via commercial sites with which Elsevier has an agreement

In all cases accepted manuscripts should:

- link to the formal publication via its DOI
- bear a CC-BY-NC-ND license - this is easy to do
- if aggregated with other manuscripts, for example in a repository or other site, be shared in alignment with our hosting policy not be added to or enhanced in any way to appear more like, or to substitute for, the published journal article.

Published journal article (JPA): A published journal article (PJA) is the definitive final record of published research that appears or will appear in the journal and embodies all value-adding publishing activities including peer review co-ordination, copy-editing, formatting, (if relevant) pagination and online enrichment.
Policies for sharing publishing journal articles differ for subscription and gold open access articles:
Subscription Articles: If you are an author, please share a link to your article rather than the full-text. Millions of researchers have access to the formal publications on ScienceDirect, and so links will help your users to find, access, cite, and use the best available version.
Theses and dissertations which contain embedded PJAs as part of the formal submission can be posted publicly by the awarding institution with DOI links back to the formal publications on ScienceDirect.
If you are affiliated with a library that subscribes to ScienceDirect you have additional

B.2 Controlled nanoparticle release from a hydrogel by DNA-mediated particle disaggregation

ELSEVIER LICENSE
TERMS AND CONDITIONS

Sep 13, 2017

This Agreement between Technical University of Munich -- Benjamin Käsdorf ("You") and Elsevier ("Elsevier") consists of your license details and the terms and conditions provided by Elsevier and Copyright Clearance Center.

License Number	4187010084806
License date	Sep 13, 2017
Licensed Content Publisher	Elsevier
Licensed Content Publication	Journal of Controlled Release
Licensed Content Title	Controlled nanoparticle release from a hydrogel by DNA-mediated particle disaggregation
Licensed Content Author	C. Nowald,B.T. Käsdorf,O. Lieleg
Licensed Content Date	Jan 28, 2017
Licensed Content Volume	246
Licensed Content Issue	n/a
Licensed Content Pages	8
Start Page	71
End Page	78
Type of Use	reuse in a thesis/dissertation
Intended publisher of new work	other
Portion	full article
Format	both print and electronic
Are you the author of this Elsevier article?	Yes
Will you be translating?	No
Order reference number	BK17091301
Title of your thesis/dissertation	Structure-function relations of biological hydrogel macromolecules
Expected completion date	Dec 2017
Estimated size (number of pages)	100
Requestor Location	Technical University of Munich Boltzmannstraße 11 Garching, 85748 Germany Attn: Technical University of Munich
Publisher Tax ID	GB 494 6272 12
Total	0.00 EUR
Terms and Conditions	

INTRODUCTION

1. The publisher for this copyrighted material is Elsevier. By clicking "accept" in connection with completing this licensing transaction, you agree that the following terms and conditions apply to this transaction (along with the Billing and Payment terms and conditions established by Copyright Clearance Center, Inc. ("CCC"), at the time that you opened your Rightslink account and that are available at any time at http://myaccount.copyright.com).

GENERAL TERMS

2. Elsevier hereby grants you permission to reproduce the aforementioned material subject to the terms and conditions indicated.
3. Acknowledgement: If any part of the material to be used (for example, figures) has appeared in our publication with credit or acknowledgement to another source, permission must also be sought from that source. If such permission is not obtained then that material may not be included in your publication/copies. Suitable acknowledgement to the source must be made, either as a footnote or in a reference list at the end of your publication, as follows:
"Reprinted from Publication title, Vol /edition number, Author(s), Title of article / title of chapter, Pages No., Copyright (Year), with permission from Elsevier [OR APPLICABLE SOCIETY COPYRIGHT OWNER]." Also Lancet special credit - "Reprinted from The Lancet, Vol. number, Author(s), Title of article, Pages No., Copyright (Year), with permission from Elsevier."
4. Reproduction of this material is confined to the purpose and/or media for which permission is hereby given.
5. Altering/Modifying Material: Not Permitted. However figures and illustrations may be altered/adapted minimally to serve your work. Any other abbreviations, additions, deletions and/or any other alterations shall be made only with prior written authorization of Elsevier Ltd. (Please contact Elsevier at permissions@elsevier.com). No modifications can be made to any Lancet figures/tables and they must be reproduced in full.
6. If the permission fee for the requested use of our material is waived in this instance, please be advised that your future requests for Elsevier materials may attract a fee.
7. Reservation of Rights: Publisher reserves all rights not specifically granted in the combination of (i) the license details provided by you and accepted in the course of this licensing transaction, (ii) these terms and conditions and (iii) CCC's Billing and Payment terms and conditions.
8. License Contingent Upon Payment: While you may exercise the rights licensed immediately upon issuance of the license at the end of the licensing process for the transaction, provided that you have disclosed complete and accurate details of your proposed use, no license is finally effective unless and until full payment is received from you (either by publisher or by CCC) as provided in CCC's Billing and Payment terms and conditions. If full payment is not received on a timely basis, then any license preliminarily granted shall be deemed automatically revoked and shall be void as if never granted. Further, in the event that you breach any of these terms and conditions or any of CCC's Billing and Payment terms and conditions, the license is automatically revoked and shall be void as if never granted. Use of materials as described in a revoked license, as well as any use of the materials beyond the scope of an unrevoked license, may constitute copyright infringement and publisher reserves the right to take any and all action to protect its copyright in the materials.
9. Warranties: Publisher makes no representations or warranties with respect to the licensed material.
10. Indemnity: You hereby indemnify and agree to hold harmless publisher and CCC, and their respective officers, directors, employees and agents, from and against any and all claims arising out of your use of the licensed material other than as specifically authorized pursuant to this license.
11. No Transfer of License: This license is personal to you and may not be sublicensed, assigned, or transferred by you to any other person without publisher's written permission.
12. No Amendment Except in Writing: This license may not be amended except in a writing signed by both parties (or, in the case of publisher, by CCC on publisher's behalf).
13. Objection to Contrary Terms: Publisher hereby objects to any terms contained in any purchase order, acknowledgment, check endorsement or other writing prepared by you, which terms are inconsistent with these terms and conditions or CCC's Billing and Payment terms and conditions. These terms and conditions, together with CCC's Billing and Payment terms and conditions (which are incorporated herein), comprise the entire agreement between you and publisher (and CCC) concerning this licensing transaction. In the event of any conflict between your obligations established by these terms and conditions and those established by CCC's Billing and Payment terms and conditions, these terms and conditions shall control.
14. Revocation: Elsevier or Copyright Clearance Center may deny the permissions described in this License at their sole discretion, for any reason or no reason, with a full refund payable to you. Notice of such denial will be made using the contact information provided by you. Failure to receive such notice will not alter or invalidate the denial. In no event will Elsevier or Copyright Clearance Center be responsible or liable for any costs, expenses or damage incurred by you as a result of a denial of your permission request, other than a refund of the amount(s) paid by you to Elsevier and/or Copyright Clearance Center for denied permissions.

LIMITED LICENSE

The following terms and conditions apply only to specific license types:
15. **Translation**: This permission is granted for non-exclusive world **English** rights only unless your license was granted for translation rights. If you licensed translation rights you may only translate this content into the languages you requested. A professional translator must perform all translations and reproduce the content word for word preserving the integrity of the article.
16. **Posting licensed content on any Website**: The following terms and conditions apply as follows: Licensing material from an Elsevier journal: All content posted to the web site must maintain the copyright information line on the bottom of each image; A hyper-text must be included to the Homepage of the journal from which you are licensing at http://www.sciencedirect.com/science/journal/xxxxx or the Elsevier homepage for books at http://www.elsevier.com; Central Storage: This license does not include permission for a scanned version of the material to be stored in a central repository such as that provided by Heron/XanEdu.
Licensing material from an Elsevier book: A hyper-text link must be included to the Elsevier homepage at http://www.elsevier.com . All content posted to the web site must maintain the copyright information line on the bottom of each image.

Posting licensed content on Electronic reserve: In addition to the above the following clauses are applicable: The web site must be password-protected and made available only to bona fide students registered on a relevant course. This permission is granted for 1 year only. You may obtain a new license for future website posting.
17. **For journal authors:** the following clauses are applicable in addition to the above:
Preprints:
A preprint is an author's own write-up of research results and analysis, it has not been peer-reviewed, nor has it had any other value added to it by a publisher (such as formatting, copyright, technical enhancement etc.).
Authors can share their preprints anywhere at any time. Preprints should not be added to or enhanced in any way in order to appear more like, or to substitute for, the final versions of articles however authors can update their preprints on arXiv or RePEc with their Accepted Author Manuscript (see below).
If accepted for publication, we encourage authors to link from the preprint to their formal publication via its DOI. Millions of researchers have access to the formal publications on ScienceDirect, and so links will help users to find, access, cite and use the best available version. Please note that Cell Press, The Lancet and some society-owned have different preprint policies. Information on these policies is available on the journal homepage.
Accepted Author Manuscripts: An accepted author manuscript is the manuscript of an article that has been accepted for publication and which typically includes author-incorporated changes suggested during submission, peer review and editor-author communications.
Authors can share their accepted author manuscript:

- immediately
  - via their non-commercial person homepage or blog
  - by updating a preprint in arXiv or RePEc with the accepted manuscript
  - via their research institute or institutional repository for internal institutional uses or as part of an invitation-only research collaboration work-group
  - directly by providing copies to their students or to research collaborators for their personal use
  - for private scholarly sharing as part of an invitation-only work group on commercial sites with which Elsevier has an agreement
- After the embargo period
  - via non-commercial hosting platforms such as their institutional repository
  - via commercial sites with which Elsevier has an agreement

In all cases accepted manuscripts should:

- link to the formal publication via its DOI
- bear a CC-BY-NC-ND license - this is easy to do
- if aggregated with other manuscripts, for example in a repository or other site, be shared in alignment with our hosting policy not be added to or enhanced in any way to appear more like, or to substitute for, the published journal article.

Published journal article (JPA): A published journal article (PJA) is the definitive final record of published research that appears or will appear in the journal and embodies all value-adding publishing activities including peer review co-ordination, copy-editing, formatting, (if relevant) pagination and online enrichment.
Policies for sharing publishing journal articles differ for subscription and gold open access articles:
Subscription Articles: If you are an author, please share a link to your article rather than the full-text. Millions of researchers have access to the formal publications on ScienceDirect, and so links will help your users to find, access, cite, and use the best available version.
Theses and dissertations which contain embedded PJAs as part of the formal submission can be posted publicly by the awarding institution with DOI links back to the formal publications on ScienceDirect.
If you are affiliated with a library that subscribes to ScienceDirect you have additional private sharing rights for others' research accessed under that agreement. This includes use for classroom teaching and internal training at the institution (including use in course packs and courseware programs), and inclusion of the article for grant funding purposes.

Appendix B.2 Controlled nanoparticle release from a hydrogel by DNA-mediated particle disaggregation

B.3 Macromolecular coating enables tunable selectivity in a porous PDMS matrix

WILEY-VCH

COPYRIGHT TRANSFER AGREEMENT

Date: 22.11.17 Contributor name: Benjamin Tillmann Käsdorf

Contributor address: Boltzmannstraße 11, 85748 Garching, Germany

Manuscript number: 10.1002/mabi.201700311

Re: Manuscript entitled "Macromolecular coating enables tunable selectivity in a porous PDMS matrix"

for publication in *Macromolecular Bioscience*

published by Wiley-VCH Verlag GmbH & Co. KGaA ("Wiley-VCH")

Dear Contributor(s),

Thank you for submitting your Contribution for publication. In order to expedite the editing and publishing process and enable Wiley-VCH to disseminate your Contribution to the fullest extent, we need to have this Copyright Transfer Agreement executed. If the Contribution is not accepted for publication, or if the Contribution is subsequently rejected, this Agreement will be null and void. **Publication cannot proceed without a signed copy of this Agreement.**

A. RIGHTS GRANTED

1. The Contributor hereby grants to Wiley-VCH for the duration of the statutory term of copyright protection and any extensions or renewals, the full and exclusive rights comprised in the Contribution including but not limited to the right to publish, republish, transmit, sell, distribute, store and process in electronic media of any kind, include in document delivery services and otherwise use the Contribution in whole or in part in electronic and print editions of the Journal and in derivative works throughout the world, in all languages and in all media of expression now known or later developed, and to license or permit others to do so. For the avoidance of doubt, "Contribution" is defined to only include the article submitted by the Contributor for publication in the Journal and does not extend to any supporting information submitted with or referred to in the Contribution ('Supporting Information'). To the extent that any Supporting Information is submitted to the Journal for online hosting, Wiley-VCH is granted a perpetual, non-exclusive license to host and disseminate this Supporting Information for this purpose.

2. Reproduction, posting, transmission or other distribution or use of the final Contribution in whole or in part in any medium by the Contributor as permitted by this Agreement requires a citation to the Journal suitable in form and content as follows: (Title of Article, Contributor, Journal Title and Volume/Issue, Copyright © [year], copyright owner as specified in the Journal, Publisher). Links to the final article on the publisher website are encouraged where appropriate.

3. Please note that Wiley-VCH reserves the right to require changes to the Contribution, including changes to the length of the Contribution, as a condition of acceptance.

4. Please note that Wiley-VCH reserves the right, notwithstanding acceptance, not to publish the Contribution if for any reason such publication would in the reasonable judgement of Wiley-VCH, result in legal liability or violation of journal ethical practices.

B. RETAINED RIGHTS

Notwithstanding the above, the Contributor or, if applicable, the Contributor's employer, retains all proprietary rights other than copyright, such as patent rights, in any process, procedure or article of manufacture described in the Contribution.

C. PERMITTED USES BY CONTRIBUTOR

1. **Submitted Version.** Wiley-VCH licenses back the following rights to the Contributor in the version of the Contribution as originally submitted for publication (the "Submitted Version"):

   a. After publication of the Final Published Version, the right to self-archive the Submitted Version on the Contributor's personal website, place in a not for profit subject-based repository or in a Scholarly Collaboration Network (SCN) which has signed up to the STM article sharing principles [www.stm-assoc.org/stm-consultations/scn-consultation-2015/] ("Compliant SCNs"), or in the Contributor's company/ institutional repository or archive. This right extends to both intranets and the Internet. The Contributor may replace the Submitted Version with the Accepted Version, after any relevant embargo period as set out in paragraph C. 2(a) below has elapsed. The Contributor may wish to add a note about acceptance by the Journal and upon publication it is recommended that Contributors add a Digital Object Identifier (DOI) link back to the Final Published Version.

   b. The right to transmit, print and share copies of the Submitted Version with colleagues, including after publication of the Final Published Version via Compliant SCNs, provided that there is no systematic distribution of the Submitted Version, e.g. posting on a listserve, network (including SCNs which have not signed up to the STM sharing principles) or automated delivery.

2. **Accepted Version.** Wiley-VCH licenses back the following rights to the Contributor in the version of the Contribution that has been peer-reviewed and accepted for publication, but not final (the "Accepted Version"):

   a. The right to self-archive the Accepted Version on the Contributor's personal website, in the Contributor's company/institutional repository or archive, in Compliant SCNs, and in not for profit subject-based repositories such as PubMed Central, subject to an embargo period of 12 months following publication of the Final Published Version. There are separate arrangements with certain funding agencies governing reuse of the Accepted Version as set forth at the following website: www.wiley.com/go/funderstatement. The Contributor may not update the Accepted Version or replace it with the Final Published Version. The Accepted Version posted

must contain a legend as follows: This is the accepted version of the following article: FULL CITE, which has been published in final form at [Link to final article]. This article may be used for non-commercial purposes in accordance with the Wiley Self-Archiving Policy [olabout.wiley.com/WileyCDA/Section/id-820227.html].

b. The right to transmit, print and share copies of the Accepted Version with colleagues, including via Compliant SCNs (in private research groups only before the embargo and publicly after), provided that there is no systematic distribution of the Accepted Version, e.g. posting on a listserve, network (including SCNs which have not signed up to the STM sharing principles) or automated delivery.

3. Final Published Version. Wiley-VCH hereby licenses back to the Contributor the following rights with respect to the final published version of the Contribution (the "Final Published Version"):

a. Copies for colleagues. The personal right of the Contributor only to send or transmit individual copies of the Final Published Version in any format to colleagues upon their specific request, and to share copies in private sharing groups in Compliant SCNs, provided no fee is charged, and further provided that there is no systematic external or public distribution of the Final Published Version, e.g. posting on a listserve, network or automated delivery. Should the Contributor wish to distribute the Contribution in the form of a high-definition PDF file, as purchased re-prints or to a larger group of customers than permitted under this Agreement (e.g. to groups of colleagues or mailing lists), the Contributor shall first directly contact Wiley-VCH.

b. Re-use in other publications. The right to re-use the Final Published Version or parts thereof for any publication authored or edited by the Contributor (excluding journal articles) where such re-used material constitutes less than half of the total material in such publication. In such case, any modifications must be accurately noted.

c. Teaching duties. The right to include the Final Published Version in teaching or training duties at the Contributor's institution/place of employment including in course packs, e-reserves, presentation at professional conferences, in-house training, or distance learning. The Final Published Version may not be used in seminars outside of normal teaching obligations (e.g. commercial seminars). Electronic posting of the Final Published Version in connection with teaching/training at the Contributor's company/institution is permitted subject to the implementation of reasonable access control mechanisms, such as user name and password. Posting the Final Published Version on the open Internet is not permitted.

d. Oral presentations. The right to make oral presentations based on the Final Published Version.

4. Article Abstracts, Figures, Tables, Artwork and Selected Text (up to 250 words).

a. Contributors may re-use unmodified abstracts for any non-commercial purpose. For online uses of the abstracts, Wiley-VCH encourages but does not require linking back to the Final Published Version.

b. Contributors may re-use figures, tables, artwork, and selected text up to 250 words from their Contributions, provided the following conditions are met:

(i) Full and accurate credit must be given to the Final Published Version.
(ii) Modifications to the figures and tables must be noted. Otherwise, no changes may be made.
(iii) The re-use may not be made for direct commercial purposes, or for financial consideration to the Contributor.
(iv) Nothing herein will permit dual publication in violation of journal ethical practices.

D. CONTRIBUTIONS OWNED BY EMPLOYER

1. If the Contribution was written by the Contributor in the course of the Contributor's employment (as a "work-made-for-hire" in the course of employment), the Contribution is owned by the company/institution which must sign this Agreement (in addition to the Contributor's signature). In such case, the company/institution hereby grants to Wiley-VCH the full and exclusive rights comprised in the Contribution as specified in paragraph A above throughout the world for the duration of the statutory term of protection and any extensions and renewals.

2. In addition to the rights specified as retained in paragraph B above and the rights granted back to the Contributor pursuant to paragraph C above, Wiley-VCH hereby grants back, without charge, to such company/institution, its subsidiaries and divisions, the right to make copies of and distribute the Final Published Version internally in print format or electronically on the Company's internal network. Copies so used may not be resold or distributed externally. However, the company/institution may include information and text from the Final Published Version as part of an information package included with software or other products offered for sale or license or included in patent applications. Posting of the Final Published Version by the company/institution on a public access website may only be done with written permission, and payment of any applicable fee(s). Also, upon payment of the applicable reprint fee, the company/institution may distribute print copies of the Final Published Version externally.

E. GOVERNMENT CONTRACTS

In the case of a Contribution prepared under U.S. Government contract or grant, the U.S. Government may reproduce, without charge, all or portions of the Contribution and may authorize others to do so, for official U.S. Government purposes only, if the U.S. Government contract or grant so requires. (U.S. Government, U.K. Government, and other government employees: see notes at end.)

F. COPYRIGHT NOTICE

The Contributor and the company/institution agree that any and all copies of the Final Published Version or any part thereof distributed or posted by them in print or electronic format as permitted herein will include the notice of copyright as stipulated in the Journal and a full citation to the Journal.

G. CONTRIBUTOR'S REPRESENTATIONS

The Contributor represents that the Contribution is the Contributor's original work, all individuals identified as Contributors actually contributed to the Contribution, and all individuals who contributed are included. If the Contribution was prepared jointly, the Contributor has informed the co-Contributors of the terms of this Agreement and has obtained their written permission to sign this Agreement on their behalf. The Contribution is submitted only to this Journal and has not been published before, has not been included in another manuscript, and is not currently under consideration or accepted for publication elsewhere. If excerpts from copyrighted works owned by third parties are included, the Contributor shall obtain written permission from the copyright owners for all uses as set forth in the standard

WILEY-VCH

permissions form or the Journal's Author Guidelines, and show credit to the sources in the Contribution. The Contributor also warrants that the Contribution and any submitted Supporting Information contains no libelous or unlawful statements, does not infringe upon the rights (including without limitation the copyright, patent or trademark rights) or the privacy of others, or contain material or instructions that might cause harm or injury. The Contributor further warrants that there are no conflicts of interest relating to the Contribution, except as disclosed. Accordingly, the Contributor represents that the following information shall be clearly identified on the title page of the Contribution: (1) all financial and material support for the research and work; (2) any financial interests the Contributor or any co-Contributors may have in companies or other entities that have an interest in the information in the Contribution or any submitted Supporting Information (e.g., grants, advisory boards, employment, consultancies, contracts, honoraria, royalties, expert testimony, partnerships, or stock ownership); and (3) indication of no such financial interests if appropriate.

H. USE OF INFORMATION

The Contributor acknowledges that, during the term of this Agreement and thereafter, Wiley-VCH may process the Contributor's personal data, including storing or transferring data outside of the country of the Contributor's residence, in order to process transactions related to this Agreement and to communicate with the Contributor. By entering into this Agreement, the Contributor agrees to the processing of the Contributor's personal data (and, where applicable, confirms that the Contributor has obtained the permission from all other contributors to process their personal data). Wiley-VCH shall comply with all applicable laws, statutes and regulations relating to data protection and privacy and shall process such personal data in accordance with Wiley's Privacy Policy located at: www.wiley.com/go/privacy.

Sharing guidelines for Wiley journal articles

Sharing location	Authors' use of their own article		Authors & other researchers	
	Submitted Version	Accepted Version	Final Article (Version of Record) Subscription articles	Final Article (Version of Record) Gold Open Access articles
Author's personal website, company or institutional repository, and not -for-profit subject-based repositories →	Can post at any time*	Deposit subject to embargo listed on copyright transfer agreement	Private research groups only	Can share at any time as long as Creative Commons license is observed and remains in place
Scholarly Collaboration Networks (SCNs) which have signed up to the STM sharing principles →	Can post at any time*	Private research groups until embargo passes, then can be publicly posted	Private research groups only	
SCNs which have not signed up to the STM sharing principles →	Cannot be shared on these platforms except by agreement with Wiley			
Sharing with individuals upon request for personal use →	Can share at any time			
Use in teaching and training at your institution →	Can be used by faculty as long as reasonable measures taken not to allow open sharing on the internet			
As part of grant application or submission of thesis or doctorate →	Can be used at any time			

For more details, view the full policy online at http://olabout.wiley.com/WileyCDA/Section/id-826716.html

* This is the copyright policy, individual journals may operate different editorial policies and authors should consult the relevant author guidelines .

WILEY

B.4 An optimized purification process for porcine gastric mucin with preservation of its native functional properties

b. You may not exercise any of the rights granted to You in Section 3 above in any manner that is primarily intended for or directed toward commercial advantage or private monetary compensation. The exchange of the Work for other copyrighted works by means of digital file-sharing or otherwise shall not be considered to be intended for or directed toward commercial advantage or private monetary compensation, provided there is no payment of any monetary compensation in connection with the exchange of copyrighted works.

c. If You Distribute, or Publicly Perform the Work or any Adaptations or Collections, You must, unless a request has been made pursuant to Section 4(a), keep intact all copyright notices for the Work and provide, reasonable to the medium or means You are utilizing: (i) the name of the Original Author (or pseudonym, if applicable) if supplied, and/or if the Original Author and/or Licensor designate another party or parties (e.g., a sponsor institute, publishing entity, journal) for attribution ("Attribution Parties") in Licensor's copyright notice, terms of service or by other reasonable means, the name of such party or parties; (ii) the title of the Work if supplied; (iii) to the extent reasonably practicable, the URI, if any, that Licensor specifies to be associated with the Work, unless such URI does not refer to the copyright notice or licensing information for the Work; and, (iv) consistent with Section 3(b), in the case of an Adaptation, a credit identifying the use of the Work in the Adaptation (e.g., "French translation of the Work by Original Author," or "Screenplay based on original Work by Original Author"). The credit required by this Section 4(c) may be implemented in any reasonable manner; provided, however, that in the case of a Adaptation or Collection, at a minimum such credit will appear, if a credit for all contributing authors of the Adaptation or Collection appears, then as part of these credits and in a manner at least as prominent as the credits for the other contributing authors. For the avoidance of doubt, You may only use the credit required by this Section for the purpose of attribution in the manner set out above and, by exercising Your rights under this License, You may not implicitly or explicitly assert or imply any connection with, sponsorship or endorsement by the Original Author, Licensor and/or Attribution Parties, as appropriate, of You or Your use of the Work, without the separate, express prior written permission of the Original Author, Licensor and/or Attribution Parties.

d. For the avoidance of doubt:

   i. **Non-waivable Compulsory License Schemes**. In those jurisdictions in which the right to collect royalties through any statutory or compulsory licensing scheme cannot be waived, the Licensor reserves the exclusive right to collect such royalties for any exercise by You of the rights granted under this License;

   ii. **Waivable Compulsory License Schemes**. In those jurisdictions in which the right to collect royalties through any statutory or compulsory licensing scheme can be waived, the Licensor reserves the exclusive right to collect such royalties for any exercise by You of the rights granted under this License if Your exercise of such rights is for a purpose or use which is otherwise than noncommercial as permitted under Section 4(b) and otherwise waives the right to collect royalties through any statutory or compulsory licensing scheme; and,

   iii. **Voluntary License Schemes**. The Licensor reserves the right to collect royalties, whether individually or, in the event that the Licensor is a member of a collecting society that administers voluntary licensing schemes, via that society, from any exercise by You of the rights granted under this License that is for a purpose or use which is otherwise than noncommercial as permitted under Section 4(c).

e. Except as otherwise agreed in writing by the Licensor or as may be otherwise permitted by applicable law, if You Reproduce, Distribute or Publicly Perform the Work either by itself or as part of any Adaptations or Collections, You must not distort, mutilate, modify or take other derogatory action in relation to the Work which would be prejudicial to the Original Author's honor or reputation. Licensor agrees that in those jurisdictions (e.g. Japan), in which any exercise of the right granted in Section 3(b) of this License (the right to make Adaptations) would be deemed to be a distortion, mutilation, modification or other derogatory action prejudicial to the Original Author's honor and reputation, the Licensor will waive or not assert, as appropriate, this Section, to the fullest extent permitted by the applicable national law, to enable You to reasonably exercise Your right under Section 3(b) of this License (right to make Adaptations) but not otherwise.

5. Representations, Warranties and Disclaimer

UNLESS OTHERWISE MUTUALLY AGREED TO BY THE PARTIES IN WRITING, LICENSOR OFFERS THE WORK AS-IS AND MAKES NO REPRESENTATIONS OR WARRANTIES OF ANY KIND CONCERNING THE WORK, EXPRESS, IMPLIED, STATUTORY OR OTHERWISE, INCLUDING, WITHOUT LIMITATION, WARRANTIES OF TITLE, MERCHANTIBILITY, FITNESS FOR A PARTICULAR PURPOSE, NONINFRINGEMENT, OR THE ABSENCE OF LATENT OR OTHER DEFECTS, ACCURACY, OR THE PRESENCE OF ABSENCE OF ERRORS, WHETHER OR NOT DISCOVERABLE. SOME JURISDICTIONS DO NOT ALLOW THE EXCLUSION OF IMPLIED WARRANTIES, SO SUCH EXCLUSION MAY NOT APPLY TO YOU.

6. Limitation on Liability. EXCEPT TO THE EXTENT REQUIRED BY APPLICABLE LAW, IN NO EVENT WILL LICENSOR BE LIABLE TO YOU ON ANY LEGAL THEORY FOR ANY SPECIAL, INCIDENTAL, CONSEQUENTIAL, PUNITIVE OR EXEMPLARY DAMAGES ARISING OUT OF THIS LICENSE OR THE USE OF THE WORK, EVEN IF LICENSOR HAS BEEN ADVISED OF THE POSSIBILITY OF SUCH DAMAGES.

7. Termination

a. This License and the rights granted hereunder will terminate automatically upon any breach by You of the terms of this License. Individuals or entities who have received Adaptations or Collections from You under this License, however, will not have their licenses terminated provided such individuals or entities remain in full compliance with those licenses. Sections 1, 2, 5, 6, 7, and 8 will survive any termination of this License.

b. Subject to the above terms and conditions, the license granted here is perpetual (for the duration of the applicable copyright in the Work). Notwithstanding the above, Licensor reserves the right to release the Work under different license terms or to stop distributing the Work at any time; provided, however that any such election will not serve to withdraw this License (or any other license that has been, or is required to be, granted under the terms of this License), and this License will continue in full force and effect unless terminated as stated above.

8. Miscellaneous

a. Each time You Distribute or Publicly Perform the Work or a Collection, the Licensor offers to the recipient a license to the Work on the same terms and conditions as the license granted to You under this License.

b. Each time You Distribute or Publicly Perform an Adaptation, Licensor offers to the recipient a license to the original Work on the same terms and conditions as the license granted to You under this License.

c. If any provision of this License is invalid or unenforceable under applicable law, it shall not affect the validity or enforceability of the remainder of the terms of this License, and without further action by the parties to this agreement, such provision shall be reformed to the minimum extent necessary to make such provision valid and enforceable.

d. No term or provision of this License shall be deemed waived and no breach consented to unless such waiver or consent shall be in writing and signed by the party to be charged with such waiver or consent.

e. This License constitutes the entire agreement between the parties with respect to the Work licensed here. There are no understandings, agreements or representations with respect to the Work not specified here. Licensor shall not be bound by any additional provisions that may appear in any communication from You. This License may not be modified without the mutual written agreement of the Licensor and You.

f. The rights granted under, and the subject matter referenced, in this License were drafted utilizing the terminology of the Berne Convention for the Protection of Literary and Artistic Works (as amended on September 28, 1979), the Rome Convention of 1961, the WIPO Copyright Treaty of 1996, the WIPO Performances and Phonograms Treaty of 1996 and the Universal Copyright Convention (as revised on July 24, 1971). These rights and subject matter take effect in the relevant jurisdiction in which the License terms are sought to be enforced according to the corresponding provisions of the implementation of those treaty provisions in the applicable national law. If the standard suite of rights granted under applicable copyright law includes additional rights not granted under this License, such additional rights are deemed to be included in the License; this License is not intended to restrict the license of any rights under applicable law.

B.5 Enzymatically active biomimetic micropropellers for the penetration of mucin gels

C. indicate the Licensed Material is licensed under this Public License, and include the text of, or the URI or hyperlink to, this Public License.

2. You may satisfy the conditions in Section 3(a)(1) in any reasonable manner based on the medium, means, and context in which You Share the Licensed Material. For example, it may be reasonable to satisfy the conditions by providing a URI or hyperlink to a resource that includes the required information.
3. If requested by the Licensor, You must remove any of the information required by Section 3(a)(1)(A) to the extent reasonably practicable.
4. If You Share Adapted Material You produce, the Adapter's License You apply must not prevent recipients of the Adapted Material from complying with this Public License.

Section 4 – Sui Generis Database Rights.

Where the Licensed Rights include Sui Generis Database Rights that apply to Your use of the Licensed Material:

a. for the avoidance of doubt, Section 2(a)(1) grants You the right to extract, reuse, reproduce, and Share all or a substantial portion of the contents of the database for NonCommercial purposes only;
b. if You include all or a substantial portion of the database contents in a database in which You have Sui Generis Database Rights, then the database in which You have Sui Generis Database Rights (but not its individual contents) is Adapted Material; and
c. You must comply with the conditions in Section 3(a) if You Share all or a substantial portion of the contents of the database.

For the avoidance of doubt, this Section 4 supplements and does not replace Your obligations under this Public License where the Licensed Rights include other Copyright and Similar Rights.

Section 5 – Disclaimer of Warranties and Limitation of Liability.

a. Unless otherwise separately undertaken by the Licensor, to the extent possible, the Licensor offers the Licensed Material as-is and as-available, and makes no representations or warranties of any kind concerning the Licensed Material, whether express, implied, statutory, or other. This includes, without limitation, warranties of title, merchantability, fitness for a particular purpose, non-infringement, absence of latent or other defects, accuracy, or the presence or absence of errors, whether or not known or discoverable. Where disclaimers of warranties are not allowed in full or in part, this disclaimer may not apply to You.

b. To the extent possible, in no event will the Licensor be liable to You on any legal theory (including, without limitation, negligence) or otherwise for any direct, special, indirect, incidental, consequential, punitive, exemplary, or other losses, costs, expenses, or damages arising out of this Public License or use of the Licensed Material, even if the Licensor has been advised of the possibility of such losses, costs, expenses, or damages. Where a limitation of liability is not allowed in full or in part, this limitation may not apply to You.

c. The disclaimer of warranties and limitation of liability provided above shall be interpreted in a manner that, to the extent possible, most closely approximates an absolute disclaimer and waiver of all liability.

Section 6 – Term and Termination.

a. This Public License applies for the term of the Copyright and Similar Rights licensed here. However, if You fail to comply with this Public License, then Your rights under this Public License terminate automatically.
b. Where Your right to use the Licensed Material has terminated under Section 6(a), it reinstates:
    1. automatically as of the date the violation is cured, provided it is cured within 30 days of Your discovery of the violation; or
    2. upon express reinstatement by the Licensor.

    For the avoidance of doubt, this Section 6(b) does not affect any right the Licensor may have to seek remedies for Your violations of this Public License.

c. For the avoidance of doubt, the Licensor may also offer the Licensed Material under separate terms or conditions or stop distributing the Licensed Material at any time; however, doing so will not terminate this Public License.
d. Sections 1, 5, 6, 7, and 8 survive termination of this Public License.

Section 7 – Other Terms and Conditions.

a. The Licensor shall not be bound by any additional or different terms or conditions communicated by You unless expressly agreed.
b. Any arrangements, understandings, or agreements regarding the Licensed Material not stated herein are separate from and independent of the terms and conditions of this Public License.

Section 8 – Interpretation.

a. For the avoidance of doubt, this Public License does not, and shall not be interpreted to, reduce, limit, restrict, or impose conditions on any use of the Licensed Material that could lawfully be made without permission under this Public License.
b. To the extent possible, if any provision of this Public License is deemed unenforceable, it shall be automatically reformed to the minimum extent necessary to make it enforceable. If the provision cannot be reformed, it shall be severed from this Public License without affecting the enforceability of the remaining terms and conditions.
c. No term or condition of this Public License will be waived and no failure to comply consented to unless expressly agreed to by the Licensor.
d. Nothing in this Public License constitutes or may be interpreted as a limitation upon, or waiver of, any privileges and immunities that apply to the Licensor or You, including from the legal processes of any jurisdiction or authority.

B.6 Cationic astringents alter the tribological and rheological properties of human saliva and salivary mucin solutions

ELSEVIER LICENSE
TERMS AND CONDITIONS

Sep 13, 2017

This Agreement between Technical University of Munich -- Benjamin Käsdorf ("You") and Elsevier ("Elsevier") consists of your license details and the terms and conditions provided by Elsevier and Copyright Clearance Center.

License Number	4187011357726
License date	Sep 13, 2017
Licensed Content Publisher	Elsevier
Licensed Content Publication	Biotribology
Licensed Content Title	Cationic astringents alter the tribological and rheological properties of human saliva and salivary mucin solutions
Licensed Content Author	Max Biegler,Judith Delius,Benjamin T. Käsdorf,Thomas Hofmann,Oliver Lieleg
Licensed Content Date	Jun 1, 2016
Licensed Content Volume	6
Licensed Content Issue	n/a
Licensed Content Pages	9
Start Page	12
End Page	20
Type of Use	reuse in a thesis/dissertation
Intended publisher of new work	other
Portion	full article
Format	both print and electronic
Are you the author of this Elsevier article?	Yes
Will you be translating?	No
Order reference number	BK17091303
Title of your thesis/dissertation	Structure-function relations of biological hydrogel macromolecules
Expected completion date	Dec 2017
Estimated size (number of pages)	100
Requestor Location	Technical University of Munich Boltzmannstraße 11 Garching, 85748 Germany Attn: Technical University of Munich
Publisher Tax ID	GB 494 6272 12
Total	0.00 EUR
Terms and Conditions	

INTRODUCTION

1. The publisher for this copyrighted material is Elsevier. By clicking "accept" in connection with completing this licensing transaction, you agree that the following terms and conditions apply to this transaction (along with the Billing and Payment terms and conditions established by Copyright Clearance Center, Inc. ("CCC"), at the time that you opened your Rightslink account and that are available at any time at http://myaccount.copyright.com).

GENERAL TERMS

2. Elsevier hereby grants you permission to reproduce the aforementioned material subject to the terms and conditions indicated.
3. Acknowledgement: If any part of the material to be used (for example, figures) has appeared in our publication with credit or acknowledgement to another source, permission must also be sought from that source. If such permission is not obtained then that material may not be included in your publication/copies. Suitable acknowledgement to the source must be made, either as a footnote or in a reference list at the end of your publication, as follows:
"Reprinted from Publication title, Vol /edition number, Author(s), Title of article / title of chapter, Pages No., Copyright (Year), with permission from Elsevier [OR APPLICABLE SOCIETY COPYRIGHT OWNER]." Also Lancet special credit - "Reprinted from The Lancet, Vol. number, Author(s), Title of article, Pages No., Copyright (Year), with permission from Elsevier."
4. Reproduction of this material is confined to the purpose and/or media for which permission is hereby given.
5. Altering/Modifying Material: Not Permitted. However figures and illustrations may be altered/adapted minimally to serve your work. Any other abbreviations, additions, deletions and/or any other alterations shall be made only with prior written authorization of Elsevier Ltd. (Please contact Elsevier at permissions@elsevier.com). No modifications can be made to any Lancet figures/tables and they must be reproduced in full.
6. If the permission fee for the requested use of our material is waived in this instance, please be advised that your future requests for Elsevier materials may attract a fee.
7. Reservation of Rights: Publisher reserves all rights not specifically granted in the combination of (i) the license details provided by you and accepted in the course of this licensing transaction, (ii) these terms and conditions and (iii) CCC's Billing and Payment terms and conditions.
8. License Contingent Upon Payment: While you may exercise the rights licensed immediately upon issuance of the license at the end of the licensing process for the transaction, provided that you have disclosed complete and accurate details of your proposed use, no license is finally effective unless and until full payment is received from you (either by publisher or by CCC) as provided in CCC's Billing and Payment terms and conditions. If full payment is not received on a timely basis, then any license preliminarily granted shall be deemed automatically revoked and shall be void as if never granted. Further, in the event that you breach any of these terms and conditions or any of CCC's Billing and Payment terms and conditions, the license is automatically revoked and shall be void as if never granted. Use of materials as described in a revoked license, as well as any use of the materials beyond the scope of an unrevoked license, may constitute copyright infringement and publisher reserves the right to take any and all action to protect its copyright in the materials.
9. Warranties: Publisher makes no representations or warranties with respect to the licensed material.
10. Indemnity: You hereby indemnify and agree to hold harmless publisher and CCC, and their respective officers, directors, employees and agents, from and against any and all claims arising out of your use of the licensed material other than as specifically authorized pursuant to this license.
11. No Transfer of License: This license is personal to you and may not be sublicensed, assigned, or transferred by you to any other person without publisher's written permission.
12. No Amendment Except in Writing: This license may not be amended except in a writing signed by both parties (or, in the case of publisher, by CCC on publisher's behalf).
13. Objection to Contrary Terms: Publisher hereby objects to any terms contained in any purchase order, acknowledgment, check endorsement or other writing prepared by you, which terms are inconsistent with these terms and conditions or CCC's Billing and Payment terms and conditions. These terms and conditions, together with CCC's Billing and Payment terms and conditions (which are incorporated herein), comprise the entire agreement between you and publisher (and CCC) concerning this licensing transaction. In the event of any conflict between your obligations established by these terms and conditions and those established by CCC's Billing and Payment terms and conditions, these terms and conditions shall control.
14. Revocation: Elsevier or Copyright Clearance Center may deny the permissions described in this License at their sole discretion, for any reason or no reason, with a full refund payable to you. Notice of such denial will be made using the contact information provided by you. Failure to receive such notice will not alter or invalidate the denial. In no event will Elsevier or Copyright Clearance Center be responsible or liable for any costs, expenses or damage incurred by you as a result of a denial of your permission request, other than a refund of the amount(s) paid by you to Elsevier and/or Copyright Clearance Center for denied permissions.

LIMITED LICENSE

The following terms and conditions apply only to specific license types:
15. **Translation**: This permission is granted for non-exclusive world **English** rights only unless your license was granted for translation rights. If you licensed translation rights you may only translate this content into the languages you requested. A professional translator must perform all translations and reproduce the content word for word preserving the integrity of the article.
16. **Posting licensed content on any Website**: The following terms and conditions apply as follows: Licensing material from an Elsevier journal: All content posted to the web site must maintain the copyright information line on the bottom of each image; A hyper-text must be included to the Homepage of the journal from which you are licensing at http://www.sciencedirect.com/science/journal/xxxxx or the Elsevier homepage for books at http://www.elsevier.com; Central Storage: This license does not include permission for a scanned version of the material to be stored in a central repository such as that provided by Heron/XanEdu.
Licensing material from an Elsevier book: A hyper-text link must be included to the Elsevier homepage at http://www.elsevier.com . All content posted to the web site must maintain the copyright information line on the bottom of each image.

Posting licensed content on Electronic reserve: In addition to the above the following clauses are applicable: The web site must be password-protected and made available only to bona fide students registered on a relevant course. This permission is granted for 1 year only. You may obtain a new license for future website posting.
17. **For journal authors:** the following clauses are applicable in addition to the above:
Preprints:
A preprint is an author's own write-up of research results and analysis, it has not been peer-reviewed, nor has it had any other value added to it by a publisher (such as formatting, copyright, technical enhancement etc.).
Authors can share their preprints anywhere at any time. Preprints should not be added to or enhanced in any way in order to appear more like, or to substitute for, the final versions of articles however authors can update their preprints on arXiv or RePEc with their Accepted Author Manuscript (see below).
If accepted for publication, we encourage authors to link from the preprint to their formal publication via its DOI. Millions of researchers have access to the formal publications on ScienceDirect, and so links will help users to find, access, cite and use the best available version. Please note that Cell Press, The Lancet and some society-owned have different preprint policies. Information on these policies is available on the journal homepage.
Accepted Author Manuscripts: An accepted author manuscript is the manuscript of an article that has been accepted for publication and which typically includes author-incorporated changes suggested during submission, peer review and editor-author communications.
Authors can share their accepted author manuscript:

- immediately
  - via their non-commercial person homepage or blog
  - by updating a preprint in arXiv or RePEc with the accepted manuscript
  - via their research institute or institutional repository for internal institutional uses or as part of an invitation-only research collaboration work-group
  - directly by providing copies to their students or to research collaborators for their personal use
  - for private scholarly sharing as part of an invitation-only work group on commercial sites with which Elsevier has an agreement
- After the embargo period
  - via non-commercial hosting platforms such as their institutional repository
  - via commercial sites with which Elsevier has an agreement

In all cases accepted manuscripts should:

- link to the formal publication via its DOI
- bear a CC-BY-NC-ND license - this is easy to do
- if aggregated with other manuscripts, for example in a repository or other site, be shared in alignment with our hosting policy not be added to or enhanced in any way to appear more like, or to substitute for, the published journal article.

Published journal article (JPA): A published journal article (PJA) is the definitive final record of published research that appears or will appear in the journal and embodies all value-adding publishing activities including peer review co-ordination, copy-editing, formatting, (if relevant) pagination and online enrichment.
Policies for sharing publishing journal articles differ for subscription and gold open access articles:
Subscription Articles: If you are an author, please share a link to your article rather than the full-text. Millions of researchers have access to the formal publications on ScienceDirect, and so links will help your users to find, access, cite, and use the best available version.
Theses and dissertations which contain embedded PJAs as part of the formal submission can be posted publicly by the awarding institution with DOI links back to the formal publications on ScienceDirect.
If you are affiliated with a library that subscribes to ScienceDirect you have additional private sharing rights for others' research accessed under that agreement. This includes use for classroom teaching and internal training at the institution (including use in course packs

Appendix B.6 Cationic astringents alter the tribological and rheological properties of human saliva and salivary mucin solutions

B.7 Mucin-inspired lubrication on hydrophobic surfaces

PERMISSION/LICENSE IS GRANTED FOR YOUR ORDER AT NO CHARGE

This type of permission/license, instead of the standard Terms & Conditions, is sent to you because no fee is being charged for your order. Please note the following:

- Permission is granted for your request in both print and electronic formats, and translations.
- If figures and/or tables were requested, they may be adapted or used in part.
- Please print this page for your records and send a copy of it to your publisher/graduate school.
- Appropriate credit for the requested material should be given as follows: "Reprinted (adapted) with permission from (COMPLETE REFERENCE CITATION). Copyright (YEAR) American Chemical Society." Insert appropriate information in place of the capitalized words.
- One-time permission is granted only for the use specified in your request. No additional uses are granted (such as derivative works or other editions). For any other uses, please submit a new request.

C. Full list of publications

1. Walker, D.; **Käsdorf, B. T.**; Jeong, H. H.; Lieleg, O.; Fischer, P., Enzymatically active biomimetic micropropellers for the penetration of mucin gels. Sci Adv 2015, 1, (11), e1500501.

2. **Käsdorf, B. T.**; Arends, F.; Lieleg, O., Diffusion Regulation in the Vitreous Humor. Biophys J 2015, 109, (10), 2171-81.

3. Biegler, M.; Delius, J.; **Käsdorf, B. T.**; Hofmann, T.; Lieleg, O., Cationic astringents alter the tribological and rheological properties of human saliva and salivary mucin solutions. Biotribology 2016, 6, 12-20.

4. Schömig, V. J.; **Käsdorf, B. T.**; Scholz, C.; Bidmon, K.; Lieleg, O.; Berensmeier, S., An optimized purification process for porcine gastric mucin with preservation of its native functional properties. RSC Adv. 2016, 6, (50), 44932-44943.

5. Nowald, C.; **Käsdorf, B. T.**; Lieleg, O., Controlled nanoparticle release from a hydrogel by DNA-mediated particle disaggregation. Journal of controlled release: official journal of the Controlled Release Society 2017, 246, 71-78.

6. Tena-Solsona, M.; Rieß, B.; Grötsch, R. K.; Löhrer, F. C.; Wanzke, C.; **Käsdorf, B. T.**; Bausch, A. R.; Müller-Buschbaum, P.; Lieleg, O.; Boekhoven, J., Non-equilibrium dissipative supramolecular materials with a tunable lifetime. Nat. Commun. 2017, 8, 15895.

7. **Käsdorf, B. T.**; Weber, F.; Petrou, G.; Srivastava, V.; Crouzier, T.; Lieleg, O., Mucin-Inspired Lubrication on Hydrophobic Surfaces. Biomacromolecules 2017, 18, (8), 2454-2462.

8. Winkeljann, B.*; **Käsdorf, B. T.***; Boekhoven, J.; Lieleg, O., Macromolecular coating enables tunable selectivity in a porous PDMS matrix, Macromolecular Bioscience 2018 (accepted) (*both authors contributed equally)

9. Singanayagam, A.; Footitt, J.; **Käsdorf, B. T.**; Finney, J. F.; Trujillo Torralbo, M.; Calderazzo, M.; Aniscenko, J.; Molyneaux, P. L.; Bartlett, N. W.; Moffatt, M.; Cookson, W. O.; Wedzicha, J.; Lieleg, O.; Mallia, P.; Johnston, S. L., MUC5AC Augments Virus-Induced Airway Inflammation and Drives Exacerbation Severity in Chronic Obstructive Pulmonary Disease, The New England Journal of Medicine. (submitted 2017)

D. Supplemental information

D.1 Transient binding promotes molecule penetration into mucin gels

(Draft)

Matthias Marczynski, Benjamin T. Käsdorf*, Andreas Wenzler, Bernhard Altaner, Ulrich Gerland and Oliver Lieleg# (*equal contribution)*

Abstract

Here, we demonstrate a selective accumulation of molecules at the liquid/gel interface of mucin hydrogels which occurs as a function of the molecule charge: for short penetration depths and long contact times, we find that molecular transport into and across the gel is enhanced by transient binding of positively charged molecules to the mucin biopolymers. This observation is supported by a mathematical model which combines increased partitioning of charged, solubilized molecules into the gel with a "sticky diffusion" process of those molecules throughout the gel phase. Our results challenge the prevailing dogma that inert, non-binding molecules were always more efficient in penetrating mucin-based hydrogels such as native mucus than charged molecules. Instead, our results suggest that there is an optimal, intermediate binding affinity between diffusing molecules and the mucin biopolymers which enhances molecular transport across mucin hydrogels.

Introduction

The human gastrointestinal (GI) tract not only regulates the passage of nutrients, growth factors, proteins, hormones, drugs and further beneficial molecules [1], but also serves as a barrier towards the entrance and distribution of pathogens [2]. To achieve those functions, the apical surface of the epithelium of mucosal tissues is lined with a viscoelastic mucus gel (Fig. 1). The macromolecular key components of those gels are mucin glycoproteins. Owing to their high content of sialic acid and sulfate residues, those mucin macromolecules exhibit a strongly polyanionic character [3-5]. Native mucus gels comprise a thin, tightly bound layer adjacent to the epithelial cell surface and a thick, loosely bound layer located at the luminal end of the mucosal tissue [6]. The thickness of those layers (Fig. 1) as well as the expression profiles of the corresponding mucin genes vary between different mucosal tissues.

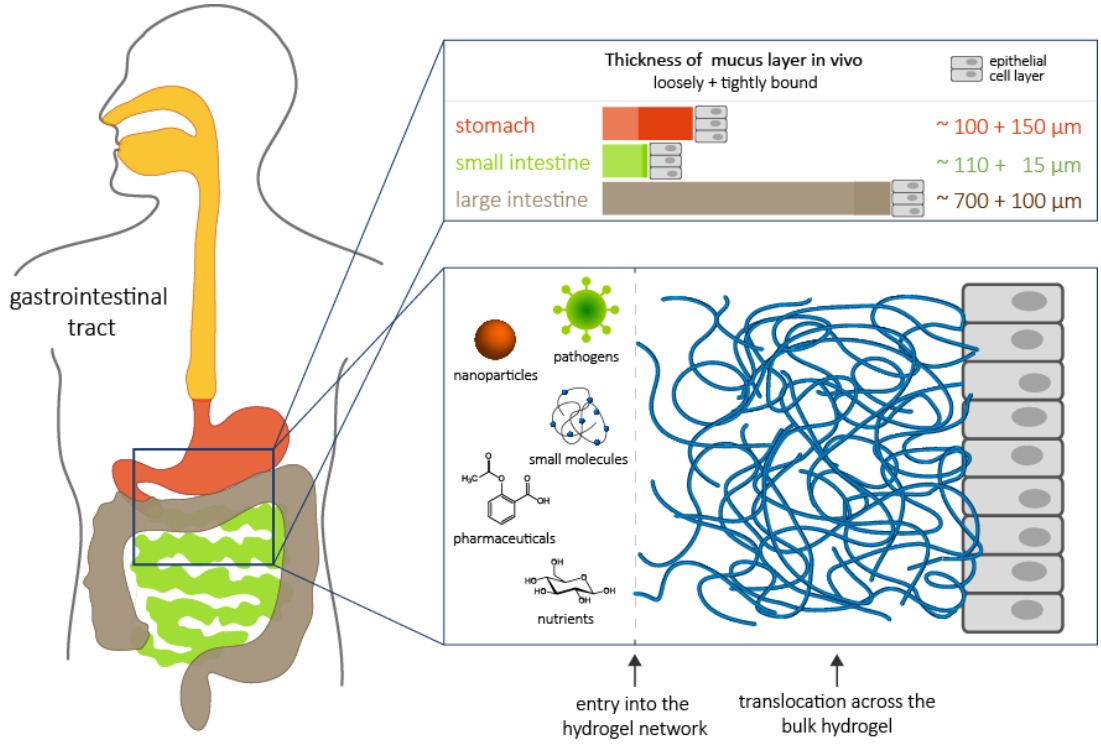

Figure 1: Thickness of different physiological mucin barriers. Mucosal tissues from different compartments in the human body exhibit mucus layers with distinct thicknesses. Those mucosal barriers consist of a thin, tightly bound layer adjacent to the epithelial cell surface (indicated in dark color) and a thick, loosely bound mucus layer located at the luminal end of the mucosal tissue (indicated in lighter color). Mucus serves as a barrier against the intrusion of pathogens into epithelial cells but also regulates the entrance of beneficial molecules.

In the stomach, MUC5AC is the most abundant mucin; here, it forms mucus layers with a total thickness of ~250 µm [7-10]. In contrast, intestinal mucus mainly comprises MUC2 and exhibits a typical thickness of ~100 µm in the small intestine and of ~800 µm in the large intestine, respectively [6, 10-12].

To reach the epithelial surface, pathogens must migrate 'upstream' through the mucus layer [13]. Consequently, the human body continuously secrets and sheds mucus to ensure the removal of trapped pathogens and noxious particles. This mucus renewal mechanism is crucial for maintaining the protective function of this hydrogel barrier but, at the same time, renders the transport of pharmaceuticals across this layer challenging. Mucus renewal times vary considerably between different sites of the GI tract. For instance, in the case of intestinal mucus, this turnover time is estimated to be in the range of one to a few hours [14, 15], and this turnover time sets the time scale at which pharmaceuticals need to achieve diffusive transport across the mucus layer. For drug carriers such as nanoparticles, mucosal transport is even more difficult: according to their larger size compared to molecular drugs, they can be excluded from entering the mucus gel by geometric constraints imposed by the mesh size of the mucus network [16, 17]. Moreover,

even if such nanoparticles are able to enter the mucus gel, their diffusive transport requires more time which is due to the large hydrodynamic radii of those particles. However, nanoparticle delivery to the mucosal epithelium is desirable to achieve spatially and temporally controllable drug release on the one hand and a protection of the enclosed cargo therapeutics from degradation on the other hand [18, 19].

To improve the bioavailability of drugs, mucoadhesive nanoparticles were developed [20]. Both the presence of positive and negative charges on the surface of nanoparticles has been shown to promote mucoadhesion via electrostatic interactions [21]. However, those particles were suggested to be unsuitable for drug delivery, since they adhere too strongly to the mucus network [20, 22]. Instead, it was demonstrated that preventing nanoparticle adhesion to mucus is possible by covalently grafting the nonionic polymer polyethylene glycol (PEG) onto the nanoparticle surface. Moreover, PEG coating of particles enhanced the diffusive mobility of such particles within mucin gels compared to uncoated particles [23-28]. Those findings led to the assumption that inert, non-binding particles and molecules were always more efficient in penetrating mucin-based hydrogels such as native mucus than charged objects. However, to date, most research in the field of mucosal permeability made use of nanoparticles [20, 21, 23, 29-35], and systematic experimental studies analyzing the penetration behavior of molecules are less frequent. Since it is *a priori* not clear if the mucosal transport of such small molecules follows the same physico-chemical principles which govern the transport of nanoparticles, the translocation behavior of such molecules needs to be tested separately.

From a technical perspective, this also calls for a different experimental approach: Whereas single particle tracking is a suitable method for characterizing the diffusion of nanoparticles in hydrogels, this is not feasible with small molecules. Moreover, single particle tracking is typically performed for particles which are artificially embedded into a hydrogel such as mucus [36-39]. Thus, this technique does not take into account partitioning effects, i.e., the entry process of objects into the hydrogel barrier. However, this molecular entry is a crucial first step of the mucus penetration process and might critically influence the translocation efficiency of a molecule ensemble. This limitation can be overcome by using microfluidics as an experimental platform. In such an *in vitro* environment, a stable gel/liquid interface can be generated on-chip [40] which allows for a spatio-temporal analysis of molecular entry into and translocation processes across such a hydrogel barrier [41].

Here, we present a microfluidics approach which allows for quantifying of the diffusive transport of molecules across the interface between a buffer compartment and a reconstituted mucin hydrogel as well as determining the molecular translocation efficiency through the mucin hydrogel barrier. We compare the penetration and translocation

behavior of fluorescent dextrans with different net charges and observe a selective accumulation of positively charged molecules at the buffer/gel interface of both reconstituted gastric and intestinal mucin gels. As a consequence of this increased partitioning of molecules into the mucin gels, we find that the translocation efficiency of positively charged molecules can exceed that of neutral, non-accumulating molecules – at least for thin mucin gel barriers and long penetration times. This experimental observation is reproduced by a mathematical model which accounts for transient binding of molecules to the hydrogel polymers in addition to their diffusive spreading across the hydrogel. Based on predictions from our mathematical model, we suggest that there is an optimal, intermediate binding affinity between molecules and mucins which enhances molecular transport across this hydrogel barrier.

Materials and Methods

Mucin purification and sample preparation

Porcine gastric mucin MUC5AC was purified manually as described previously [42]. In brief, mucus was obtained from gently rinsed pig stomachs by manual scraping the surface of the gastric tissue. The collected mucus was diluted 5-fold in 10 mM sodium phosphate buffer (pH 7.0) containing 170 mM NaCl and stirred at 4 °C overnight. Cellular debris was removed via two centrifugation steps (first at 8300 x g for 30 min at 4 °C, second at 15000 x g for 45 min at 4 °C) and a final ultracentrifugation step (150000 x g for 1 h at 4 °C). Subsequently, the mucins were separated from other macromolecules by size exclusion chromatography using an ÄKTA purifier system (GE Healthcare) and an XK50/100 column packed with Sepharose 6FF. The obtained mucin fractions were pooled, dialyzed against ultrapure water and concentrated by cross-flow filtration. The concentrate was then lyophilized and stored at -80 °C.

For the purification of intestinal mucin MUC2, protease inhibitors (5 mM EDTA, 5 mM benzamidine hydrochloride, 1 mM 2,4'-dibromoacetophenone and 1 mM phenylmethylsulfonyl fluoride) and 0.04 % (w/v) sodium azide were added to the dilution buffer to prevent mucin degradation and bacterial proliferation, respectively. To obtain MUC2 with pH-dependent gel-forming abilities, an additional purification step after size exclusion chromatography had to be performed. Therefore, the purified MUC2 was dissolved again, but this time in high-salt buffer (PBS containing 0.8 M NaCl, pH 7). This mucin solution was then kept on a stirring table at 4 °C overnight to remove non-specifically bound impurities from the mucins. Then, dialysis and protein concentration was performed again by cross-flow filtration. For conducting the microfluidics experiments, the lyophilized mucins were solubilized at a concentration of 1 % (w/v) in ultrapure water before they were injected into the PDMS chips.

Test molecules and particles

Fluorescent dextrans (labelled with fluorescein isothiocyanate = FITC) with an average molecular weight of 4 kDa were purchased from Sigma-Aldrich (St. Louis, MO, USA). We here used three variants of those dextrans: either unmodified (= electrostatically neutral) or modified with carboxymethyl (CM, introducing negative charges to the dextrans) or diethylaminoethyl (DEAE, introducing positive charges to the dextrans) groups. For conducting the molecular penetration experiments, the dextrans were dissolved in 10 mM acetate buffer (pH 4.0) at a concentration of 5 mg mL^{-1} each.

Amine-terminated and carboxyl-terminated polystyrene particles (with a diameter of 100 nm and labelled with a green fluorescing dye with an excitation wavelength of $\lambda_{480\ nm}$ and an emission wavelength of $\lambda_{501\ nm}$) were obtained from Magsphere Inc. (Pasadena, CA, USA) at a stock solution concentration of 2.5 % (w/v). For polyethylene glycol (PEG) coating of amine-modified particles the particles were diluted 1:10 in ultrapure water. A 10-fold excess of α-methoxy-PEG-succinimidyl active ester (Rapp Polymere, Tübingen, Germany) was added to the particle suspension, and the PEGylation reaction was allowed to take place at room temperature overnight. Successful PEGylation was verified by determining the ζ-potential of the modified particles (see supplement). Size and ζ-potential were determined with dynamic light scattering and laser Doppler anemometry, respectively, using a Zetasizer Nano ZS (Malvern Instruments, Herrenberg, Germany). Therefore, the particles were diluted 1:100 in 10 mM acetate buffer (pH 4).

Microfluidics device fabrication

The channel geometry of the microfluidics chips was designed using AutoCAD (Autodesk, Munich, Germany), and the photomask was printed at a resolution of 64000 dpi (Zitzmann, Eching, Germany). The master was fabricated on a 3-inch silicon wafer (Siegert Wafer, Aachen, Germany) using EpoCore (micro resist technology, Berlin, Germany) as a photoresist thus generating elevated structures needed for the following channel molding process. Two spin coating steps using a WS-400B-6NPP/LITE spin coater (Laurell, North Wales, USA) at 300 rpm for 15 s and at 1000 rpm for 35 s, respectively, were used to apply an approximately 100 µm layer of photoresist onto the silicon wafer. Then, two prebaking steps were conducted: first, at 65 °C for 5 min; then, at 95 °C for 10 min. After wafer cooling at room temperature, the photomask was placed onto the photoresist layer and the wafer was exposed to UV light for 10 min to induce photoresist cross-linking. Two post-exposure baking steps were conducted at 65 °C for 5 min and at 95 °C for 20 min, respectively. The wafer was developed by rinsing thoroughly with mr-Dev 600 (micro resist technology, Berlin, Germany) to remove all

remaining uncross-linked photoresist. Finally, the wafer was rinsed with isopropanol to remove any remaining developer.

For the fabrication of microfluidic chips, liquid PDMS prepolymer elastomer was mixed at a 10:1 ratio with curing agent (Dow Corning Sylgard 184, Midland, MI, USA). After degassing for 30 min, the mixture was poured onto the master. The polymer was cured at 70 °C for 1 h. The PDMS layer was peeled off and access holes were punched. Afterwards, the PDMS chips were bonded to glass slides using oxygen plasma at 30 W for 30 s. The bonded devices were stored in an oven at 120 °C overnight so that the PDMS could recover its hydrophobic properties.

Data acquisition and analysis

Fluorescence images of the finger-like structures of each of the three hand-shaped channel systems were taken on a DMi8 Leica microscope (Leica, Wetzlar, Germany) using a 4x objective (Leica). Images were acquired with a digital camera (Orca Flash 4.0 C11440, Hamamatsu, Japan) using the software Leica Application Suite X, and images were taken 5, 10 and 20 min after the fluorescent dextrans were injected into the chip. The exposure time was chosen such that no pixel saturation occurred. Each of the six "fingers" per "hand" was evaluated individually using ImageJ (public domain, version 1.51k, March 2017). A rectangle with a height of 860 pixels and a width of 45 pixels was chosen as region of interest (ROI) and positioned such that the upper 60 pixel lines of this ROI were located in the buffer compartment. This allowed for normalizing the fluorescence intensity data acquired across the mucin gel compartment and converting the measured intensity values into concentration values: the averaged fluorescence intensity obtained from the 60 pixel lines of the rectangle in the "buffer reservoir" was set as reference representing a test molecule concentration of 100 % (i.e. 5 mg/mL). This procedure ensured that the calculated intensity profiles obtained at different time points during the experiments could be compared quantitatively, as photobleaching effects were corrected by this approach.

Further data analysis was conducted using the software Matlab (MathWorks, Natick, MA, USA). For each channel of a chip, the fluorescence intensity within the chosen ROI was averaged per pixel line. In a next step, these average intensity values obtained per line were averaged again, but this time over all "fingers" analyzed for a certain condition. For each experimental condition, at least two different chips (with up to 18 "fingers" each) were analyzed. The normalized intensity values were then plotted against the channel length, and the number of molecules that penetrated into the mucin gel was calculated by integrating over the area under the penetration profiles.

Mathematical modeling

For the theoretical estimation of the diffusion behavior of dextrans through a mucus layer, a simple one-dimensional model was employed. In this model, molecules either diffuse freely through the gel or are transiently bound by the gel matrix (see Fig 2). The spatial coordinate is denoted by x. The binding-diffusion model in the gel $0 \leq x \leq l_G$ is governed by the system of partial differential equations for unbound and bound concentrations $u(x,t)$ and $b(x,t)$

$$u_t = Du_{xx} - R$$
$$b_t = R$$

with the reaction current

$$R(x,t) = k^+(x)u(x,t) - k^-(x)b(x,t)$$

To the left of the gel is a reservoir, which can either be infinite, finite or finite and leaky with rate k^L. To the right is a target region, where the concentration is removed with rate k^T.

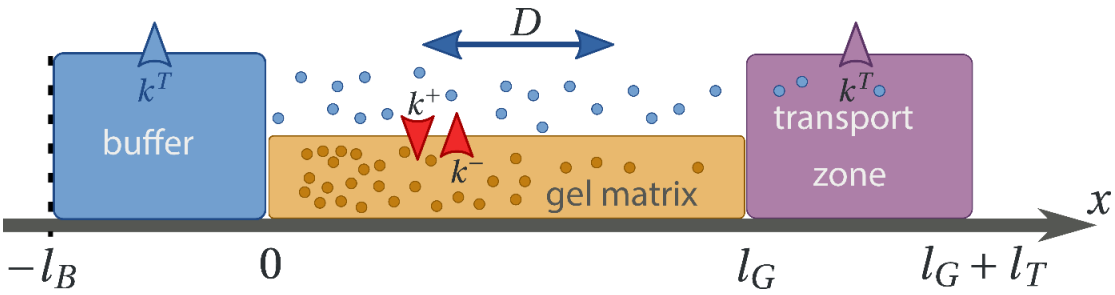

Figure 2: Schematic model of the diffusive transpoert of molecules into a simulated mucin gel. Lateral transport is governed solely by diffusion with diffusion constant *D*. The buffer can be an infinite reservoir, finite or finite and leaky. Molecules can be immobilized by binding to the gel matrix with rates $k^{\pm}$. In the transport, dextran concentration is depleted with rate k^T. For high depletion rates, off-transport can be modeled by fixing zero concentration at $x = l_G$

The diffusion constant can be calculated using the Einstein relation for a Stokes drag particle. For dextrans, $D = 175\ \mu m^2/s$ is obtained, which agrees very well with the data for the non-binding dextrans (see Fig. 4).

Since a passive binding model is assumed here, it is the thermodynamic requirement that

$$ln\frac{k^+}{k^-} = \beta\Delta F$$

where $\beta = (k_B T)^{-1}$ is the inverse thermal energy and ΔF is a (free) energy difference between the bound and unbound dextran state.

As there are sinks in the set-up, the steady state without sources is a depleted concentration everywhere. For an infinite buffer acting as a source, the steady state

solutions are linear profiles from $x = d$ until $x = L$, where the ratio of the concentrations is given by detailed balance (see Fig. 3, left).

Linear profiles $(u(d) = u_d, u(L) = b(L) = 0 \; and \; b(d) = \frac{k^+}{k^-} u_d$ are established on the order of the diffusive time-scale given by

$$\tau_D = \frac{L^2}{D} \approx 10^5 s$$

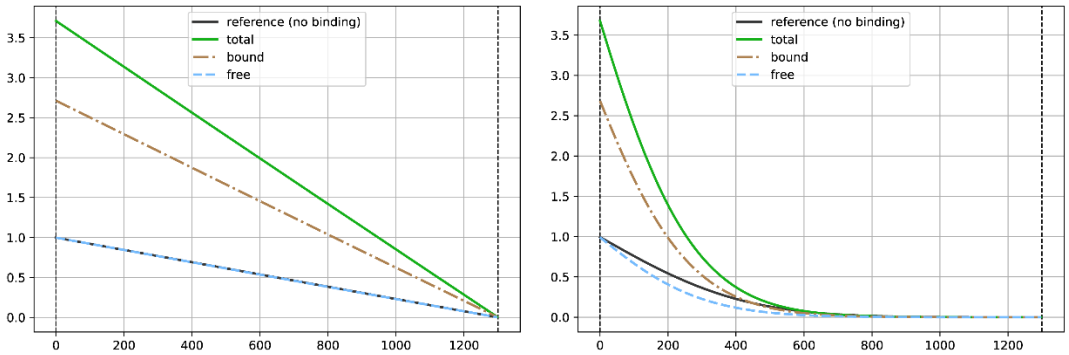

Figure 3: Theoretical diffusion profiles calculated for mucin-binding molecules. Steady state for a infinite reservoir with linear concentration profiles (left). Typical diffusion profile during experimental time-scales. The peak accumulated particles at the gel-interface is already saturated.

However, experiments are observed on shorter time-scales and profiles look more like shown in Fig. 3 (right). We see, that the peak close to the interface has already reached its steady-state value. This typically happens on a faster time-scale, determined by the binding and unbinding rates $k^{\pm}$. The saturation time-scale is governed by the time it takes to reach detailed balance at the interface. It is approximately obtained by solving

$$b_t = -k^- b + k^+ u_d$$

and then demanding that the reative flux R(d) << 1.

From this we find that the saturation time-scale

$$\tau_{sat} = (k^-)^{-1}$$

is governed by the unbinding rate k^{-1}. Before that time-scale is reached, the interface peak is still growing approximately exponentially. From the ratio of the peak concentration to the buffer concentration we can find the ratio of the binding constant (energy difference):

$$\frac{k^+}{k^-} = \frac{c_{peak} - c_{buffer}}{c_{buffer}}$$

For the plots shown in Fig 2. βE has been set to 1, yielding $\frac{k^+}{k^-} = e \approx 2.7$.

Results and Discussion

When studying the diffusive entrance of molecules into a hydrogel, a well-defined interface between the liquid compartment and the hydrogel is required. We achieve such an interface by designing a microfluidics chip with finger-like structures (Fig. 4a) made of the hydrophobic, transparent elastomer PDMS. When a solution containing purified porcine gastric mucin (MUC5AC) or porcine small intestinal mucin (MUC2) is injected into an inlet channel that connects to several of such finger-like structures, the aqueous mucin solution can be gently pushed through the channels separating the fingers. However, when reaching the end of these channels, the mucin solution stops. This is due to the special design of the fingers which slightly expand at their 'tips'. This geometry leads to narrowing of the channels and thus not only induces a slight resistance but also influences the shape of the liquid interface at the finger tips. We observe a relatively flat interface at the PDMS/liquid/air interface which makes the following penetration experiments easier to quantify.

However, this interface is relatively instable and sensitive to erosion by liquid flux. A previous study that investigated molecular mucin penetration made also use of a microfluidics setup but here the experiments were conducted under neutral conditions, i.e., the mucin samples were not analyzed in their gel state [41]. As a consequence, this setup does not provide the possibility to maintain a distinct buffer/gel interface as the mucus solution is washed away consecutively. Thus, before injecting suitable test molecules for the penetration experiments, the interface generated with the novel microfluidic design used here, first needs to be stabilized by inducing gelation of the mucin solution. For mucin solutions, lowering the pH to acidic levels can induce such gelation [43-46], and we achieve this by injecting an acidic buffer solution into the 'reservoir' of the chip and then allow the protons from this buffer to diffuse into the mucin solution (Fig. 4c, d). Successful acidification is verified by two methods: first, the pH sensitive dye Oregon Green is added to the mucin solution before injection. This fluorophore emits light at pH levels of 5 and above but almost completely loses its fluorescent abilities at more acidic levels. Indeed, as expected, we observe rapid elimination of fluorescence inside the mucin compartment as the protons from the buffer enter the mucin solution. As a second control for ensuring efficient gelation of the mucin solution on chip, we track the Brownian motion of 500 nm polystyrene particles embedded into the mucin phase. At neutral pH, where mucin solutions form a liquid with low viscosity, thermal energy is sufficient to induce particle fluctuations with amplitudes large enough so they can be easily detected by single particle tracking microscopy. However, once the mucin solution is acidified, a viscoelastic gel is formed. As a consequence, the embedded polystyrene particles become trapped inside the mesh of the

acidic mucin gel and, consequently, their fluctuation amplitude is drastically reduced (Fig. 4b).

Next, with this stabilized mucin gel/liquid interface, molecular penetration experiments are performed. Therefore, the fluorescently labelled test particles of interest are injected via one of the inlets of the "test reservoir" (Fig. 4e, f). As a molecular platform for these experiments we chose dextrans with molecular weights of ~4 kDa. Our rationale for this choice is as follows: dextrans are relatively inert macromolecules which, by themselves, do not carry any charged or hydrophobic moieties. However, they can be chemically modified so that they become either positively or negatively charged. The former is achieved by grafting diethylaminoethyl (DEAE) groups to the dextrans whereas the latter is realized by grafting carboxymethyl (CM) groups to the macromolecule.

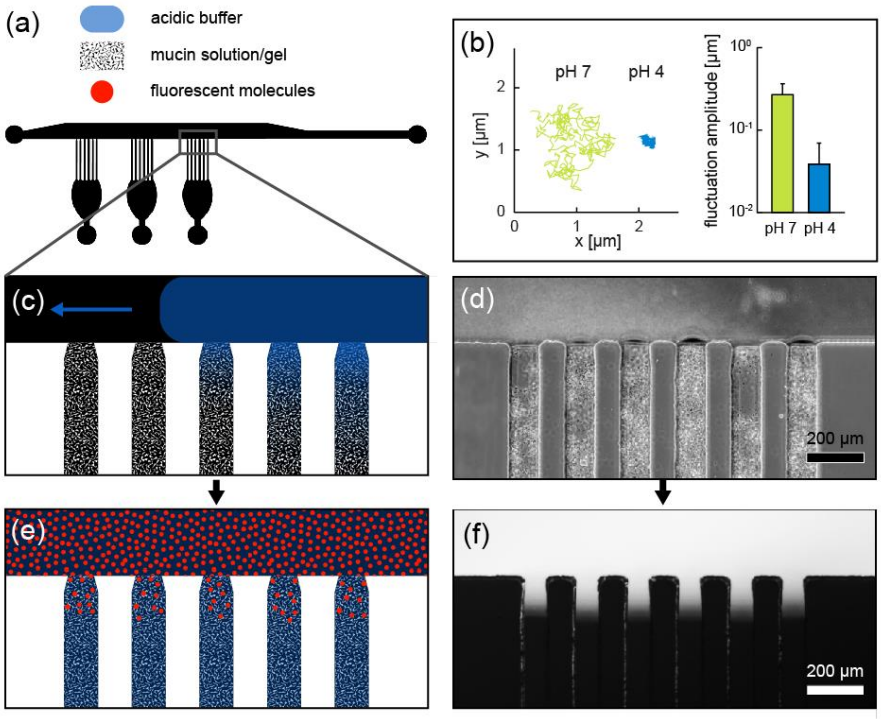

Figure 4: Schematic illustration and microscopic images of the microfluidic setup used for molecular penetration tests into mucin gels. (a) Overview of the microfluidic channel which comprises three hand-like structures which are filled with a mucin solution (b) Thermal fluctuation behavior of polystyrene particles embedded in a mucin solution on chip at pH 7.0 (i.e., before acidification) and in a mucin hydrogel at pH 4.0 (i.e., after acidification on chip). The error bars denote the standard deviation as obtained from three independent measurements in which ~20 particles were analyzed each. (c, d) Gelation of the mucin solution is initiated by injecting acidic buffer into one of the microfluidic channels. (e, f) After gelation has been induced on chip, fluorescently labelled molecules are injected and allowed to penetrate the mucin gel by diffusion.

Moreover, the hydrodynamic radii of those dextrans are all in the range of a few nanometers and thus about two orders of magnitude smaller than the mesh size of mucin gels formulated at the mucin concentrations used here. This ensures that geometric

hindrance effects as responsible for the trapping of polystyrene particles described before can be neglected for the penetration process of dextrans into mucin gels. To allow for their visualization via fluorescence microscopy, all dextran variants carry a fluorophore (FITC).

When determining the penetration profiles of unmodified (= uncharged) dextran molecules, we observe a roughly exponential decay of fluorescence with increasing penetration distance (Fig. 5a, green curves). Such a profile is consistent with unrestricted diffusion of molecules from a reservoir with a high, constant molecule concentration into a compartment with absorbing boundary conditions at its far end, i.e. a "sink" as represented by the relatively large volume of the "hand" structure filled with mucins. A similar behavior is obtained for CM-dextrans (Fig. 5a, blue curves), although we detect a slight "shoulder" in the penetration profiles here. In marked contrast to those rather feature-less penetration profiles, we observe a clear accumulation peak at the liquid/gel interface for positively charged DEAE-dextrans (Fig. 5a, red curves). Within the time frame of the experiments conducted here, i.e. within 20 min after the test molecules were injected, the height of this accumulation peak increases with time. In parallel to this accumulation of molecules at the gel surface, we also observe darker areas in those buffer zones which are located right in front of the buffer/gel interface (Fig. S2). This feature occurs at the beginning of the penetration experiment but is absent for neutral and negatively charged dextrans (which carry the identical fluorophore as the positively charged dextran variants). This underscores that this feature is linked to the charge state of the dextran molecules used for the penetration tests, and it indicates a local depletion of molecules from those areas.

Given those two features, i.e. an accumulation of positively charged molecules at the liquid/gel interface and a local depletion of those molecules in the "atrium" of the gel, it is *a priori* not clear for which dextran species the entry process into the bulk volume of the mucin gel will be most efficient. One could assume that anionic and neutral dextrans, which do not show any detectable interaction with the gel matrix, can enter the gel at higher numbers than cationic dextrans since the former do not experience any entrance barrier. However, when we calculate the number of molecules which are absorbed into the first 50 µm of the gel after different time points, we observe the opposite (Fig. 5c, d): the local concentration of anionic and neutral dextrans is lower in the gel than in the buffer reservoir whereas the concentration of cationic dextrans in the mucin gel exceeds the concentration of those molecules in the buffer compartment. Moreover, this difference becomes more pronounced over time which indicates that an increasing number of cationic dextrans are absorbed into the gel matrix.

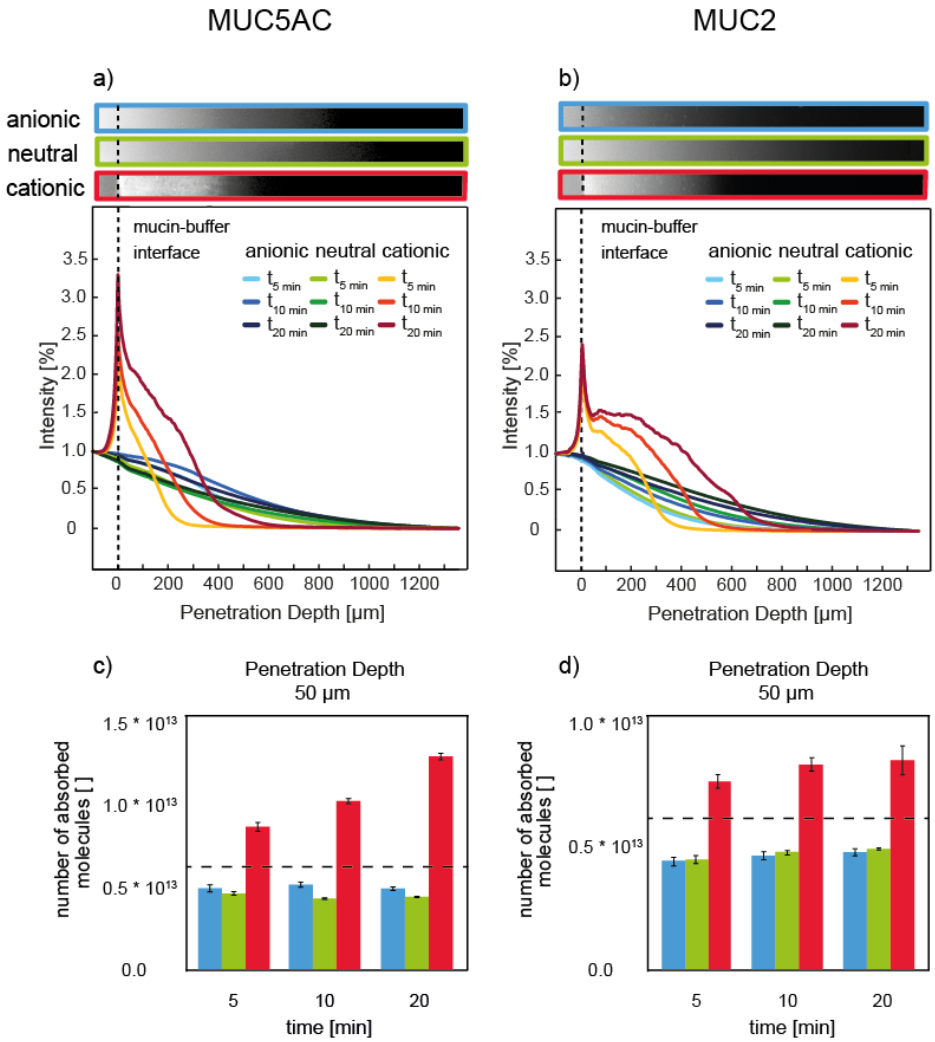

Figure 5: Penetration behavior of different dextran variants into mucin gels. The barrier properties of mucin gels reconstituted from porcine gastric mucin MUC5AC (a, c) are compared to those of gels comprising purified porcine intestinal mucin MUC2 (b, d). The diffusive penetration behavior of cationic dextrans differs strongly from that of either neutral or anionic dextrans. The former accumulate at the buffer/mucin interface whereas the latter two show penetration profiles with local concentrations that continuously decrease with increasing channel depth (a, b). Typical fluorescence images that correspond to the profiles shown in the graph are depicted in the top part of subfigures a) and b), respectively. Even after short penetration times, the number of cationic dextrans which are absorbed into the first 50 µm of the mucin gels exceeds that of neutral or anionic dextrans (c, d). The error bars denote the standard error of the mean as obtained from analyzing at least seven "fingers" each. The dashed line indicates the number of molecules that would be present in the first 50 µm of the mucin gel if the local dextran concentration in the gel would be identical to that in the buffer reservoir.

Of course, for mucus-penetrating molecules to reach the epithelial surface of a mucosal tissue, it is not sufficient to enter the mucus gel but they need to cross the whole mucosal barrier. Since all mucus layers are continuously being replenished by the human body, only those molecules have a chance of arriving at the epithelial surface which travel through the mucus barrier fast enough. Thus, in a next step, we assess this barrier

function of our reconstituted mucin gels by calculating the number of molecules that were successfully able to pass a certain mucin gel thickness d after a given time interval of 20 min. We compare three physiologically relevant mucus thicknesses as they occur throughout the gastrointestinal tract: $d_1 = 100$ µm, $d_2 = 250$ µm and $d_3 = 800$ µm. The first value approximates the thickness of the mucus layer in the small intestine, whereas the larger values are chosen to match the mucosal layers in the stomach and large intestine, respectively.

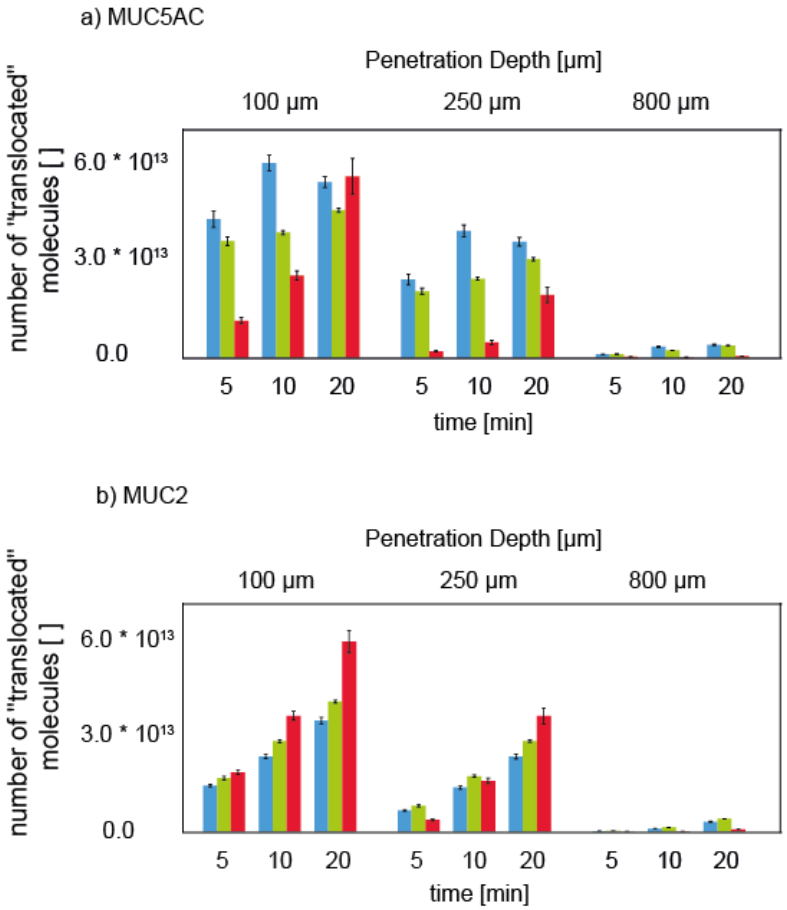

Figure 6: Time dependent translocation efficiency of different dextran variants across mucin gels. From the penetration profiles shown in Fig. 5, the number of molecules which successfully travelled across a mucin gel of thicknesses d ($d_1 = 100$ µm, $d_2 = 250$ µm and $d_3 = 800$ µm) are calculated for porcine gastric mucin gels (a) and porcine small intestinal mucin gels (b). The error bars denote the standard error of the mean as obtained from analyzing at least seven "fingers" each.

For the largest gel thickness, i.e. 800 µm, we find that the number of translocated molecules is very low – and virtually identical for each molecule species (Fig. 6a). Considering the limited diffusion time of 20 min set by our experimental approach, this result is not too surprising since a theoretical estimate of a typical molecular travel distance (see the SI for details) returns a value of similar order. Yet, when calculating the number of molecules which have travelled across a distance of 100 µm of mucin gel,

respectively, we obtain different results for the different dextran variants (Fig. 6a): we find that the number of translocated DEAE-dextran molecules can exceed that of neutral, unmodified dextrans – at least for the longest penetration time. For the larger translocation distance, i.e. 250 µm, the data suggests that the translocation efficiency of positively charged dextrans might also become higher than that of neutral and negatively charged molecules; however, longer diffusion times than studied here are probably necessary to obtain this effect.

For anionic dextrans, we calculate values that exceed both those of neutral and cationic dextrans. Whereas this finding agrees with our observation that the corresponding penetration profiles showed a slight shoulder, i.e. a rather flat regime right after the buffer/gel interface, the reason for this behavior is not obvious. It indicates, however, that also those charged dextran variants somehow interact with the mucin gel matrix – albeit differently and less strongly than the cationic dextrans – and that this interaction somehow promotes the translocation of those dextrans across the mucin gel.

At this point, it is important to recall that the microstructure of mucins is very complex. Due to the high degree of glycosylation, the amino acid sequence constitutes only ~20 % of the total molecular weight of the MUC5AC molecule [47]. Since anionic glycan residues established by sialic acid motifs and sulfated carbohydrate chains are present at high densities in the central, glycosylated region of mucin [45, 47-50] (see SI), the net charge of the MUC5AC macromolecule can be expected to be strongly negative. Thus, this structural feature is likely to be responsible for the strong binding of the cationic DEAE-dextrans observed in Fig. 5. However, at both termini, the mucin molecule is unglycosylated and, as a consequence, its amino acid backbone is exposed. In this region, and at the acidic pH present in our experiments, basic amino acids such as lysine, arginine and histidine will carry positive charges which originate from their side chains. Those positively charged groups could offer binding sites for anionic molecules such as the CM-dextrans used here. However, due to the lower number of positive charges in these terminal domains of the mucin compared to the high density of negative charges in the core region of the glycoprotein, the binding affinities of the mucin macromolecule towards cationic and anionic molecules might be different.

We test this hypothesis by comparing the binding behavior of charged and neutral dextran molecules towards adsorbed mucin layers (see SI). When we test mucin layers from different purification batches, we find that cationic DEAE-dextrans are always bound with a higher affinity than CM-dextrans or unmodified dextrans, respectively. For some MUC5AC batches, we also observe increased binding of anionic dextrans compared to neutral ones (Fig. S3). Thus, the increased penetration efficiency of anionic CM-

dextrans shown in Fig. 6a could reflect low-affinity binding of this polysaccharide to the mucin molecule. Conversely, for a mucin batch where such low-affinity binding of anionic dextrans is not observed, one would expect that both CM-dextrans and unmodified dextrans show similar penetration efficiencies into mucin gels – and indeed this is the case (Fig. S4a, c). However, also the binding affinity of cationic dextrans towards mucin varies a bit for different mucin batches. Consistently, the height of the DEAE-dextran accumulation peak at the buffer/mucin interface can differ for a penetration experiment performed with a different mucin batch (Fig. S4a, c), and higher mucin concentrations are required with such a mucin batch (Fig. S4b, d) to obtain conditions where the transport efficiency of cationic dextrans outperforms that of neutral, non-binding dextrans.

The variations of dextran binding efficiency of different mucin batches can probably in part be attributed to biological variance among the mucin molecules: for instance, differences in the degree of glycosylation might affect the accessibility of charged amino acids on the mucin backbone thus influencing mucin affinity towards charged molecules. In addition, small variations in mucin purity can lead to a similar effect, e.g., when residual ions, protein fragments or other small molecules remain bound to the mucin macromolecule. However, even for a mucin batch with a relatively low affinity towards cationic dextrans, we observed that slightly increasing the mucin concentrations (i.e., from 1 % (w/v) to 3 % (w/v)) was sufficient to also obtain a transport advantage of cationic dextrans. Physiologically, the mucin concentration in gastrointestinal mucus layers can be even higher, i.e. it can reach values of up to 5 % [52]. This suggests, that the effects described here could be even stronger in vivo, especially if native mucus is enriched with other polyanionic molecules such as DNA originating from cellular debris. For nanoparticle transport across mucosal barriers, those slight batch-to-batch variations in mucin affinity are probably less important since nanoparticles – due to their larger size compared to dextran molecules – can form multiple bonds to the mucin network.

So far, we have performed the molecular penetration experiments with mucin gels comprising purified gastric mucin MUC5AC, and such a reconstituted MUC5AC gel is a reasonable model for gastric mucus [51]. In intestinal mucus, however, the dominant mucin type is MUC2, which is why we also tested a hydrogel barrier reconstituted from this particular mucin. When we repeat the penetration experiments with mucin gels comprising purified porcine intestinal mucin MUC2, a similar behavior is observed as we described it for MUC5AC gels above: the positively charged dextrans show a strong accumulation peak at the buffer/gel interface whereas the neutral and negatively charged molecules do not (Fig. 5b). Also the amount of molecules which have successfully entered the first 50 µm of the MUC2 gel is highest for the positively charged DEAE-dextrans and

exceeds the local concentration of those molecules in the buffer reservoir (Fig. 5d). Finally, at longer penetration times, the calculated number of translocated cationic molecules exceeds that of neutral dextrans – this time even for a "barrier width" of 250 µm. Different from the results obtained with gastric mucins, however, anionic dextrans do not outperform the neutral, zwitterionic dextrans in intestinal mucin gels. This observations is, however, consistent with the result obtained from an adsorption-based binding test performed with MUC2 coatings and the three dextran variants we use here (Fig. S3) and indicates that the purified MUC2 mucins only bind cationic dextrans but not the other two polysaccharides.

When extracting the described parameters from the data set of the penetration profiles of porcine intestinal mucin MUC2 and overlaying such simulated profiles with the experimental data we observe that the model and the data of neutral (un-binding) dextrans agree very well (Fig. 7a).

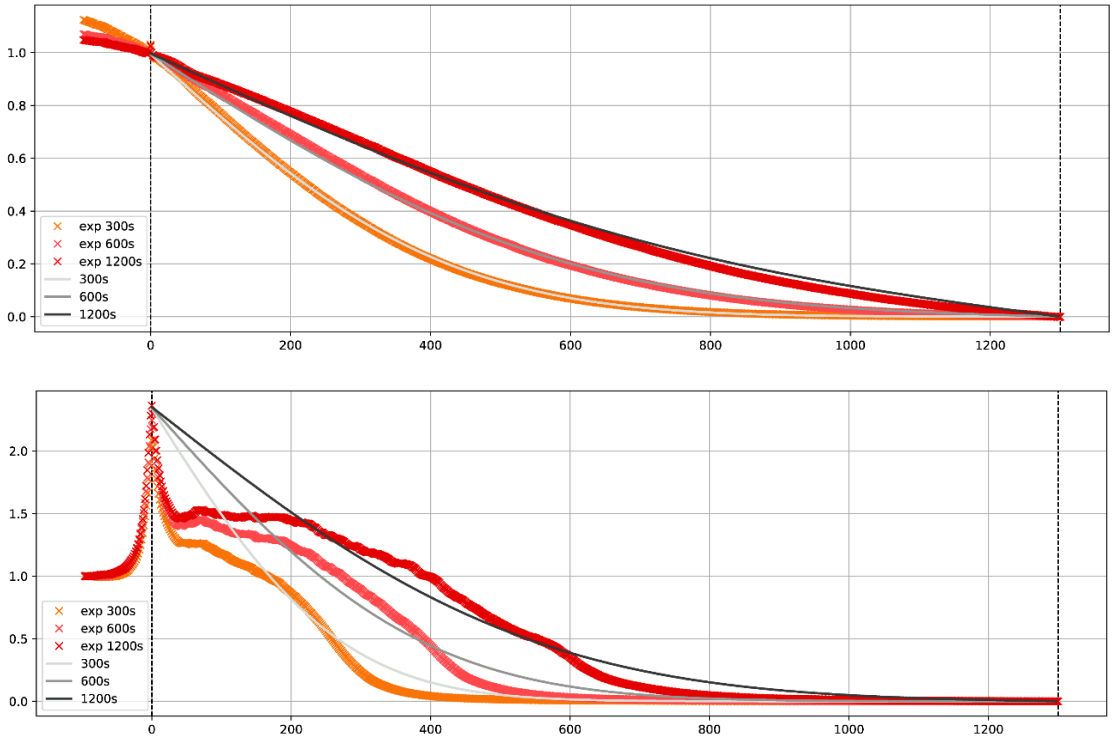

Figure 7: Overlay of experimental diffusing profiles with modelated diffusion curves. The experimental penetration profiles (red curves) of neutral (a) and cationic (b) dextrans into MUC2 gels are compared to calculated theoretical diffusion profiles (grey curves) of non-binding (a) or binding (b) molecules for different penetration time spans. Whereas the experimental diffusion profiles of neutral dextrans into MUC2 gels match the theoretical diffusion profiles quite well, the theoretical diffusion behavior of simple binding molecules is not entirely suited to approximate the *in vitro* behavior.

In contrast, a deviation between the experimental profiles for cationic (binding) molecules and the model exists (Fig. 7b). The overlay indicates that the conditions in the experimental setup cannot be fully approximated by a simple model. However, when integrating the area of the theoretical profiles and determining the theoretical number of molecules and comparing the concentration of penetrated non-binding and binding molecules within distinct depths of the gel (Fig. 8a), the concentration of the mucin-binding molecules exceeds that of non-binding molecules – at every analyzed time point. This data is in strong agreement with the experimental evaluation (Fig. 5c and d).

Furthermore, when the number of molecules is analyzed which have translocated certain theoretical mucin gels with thicknesses of 100 nm, 200 nm or 800 nm (Fig. 8b), again the effect of promoted molecule transport of mucin-binding molecules can be observed. This simulated data also very well reflects the experimental findings. Thus this simple theoretical model of the diffusive transport of binding and non-binding molecules in reconstituted mucin gels is able to approximate the *in vivo* conditions of the experimental microfluidics setup.

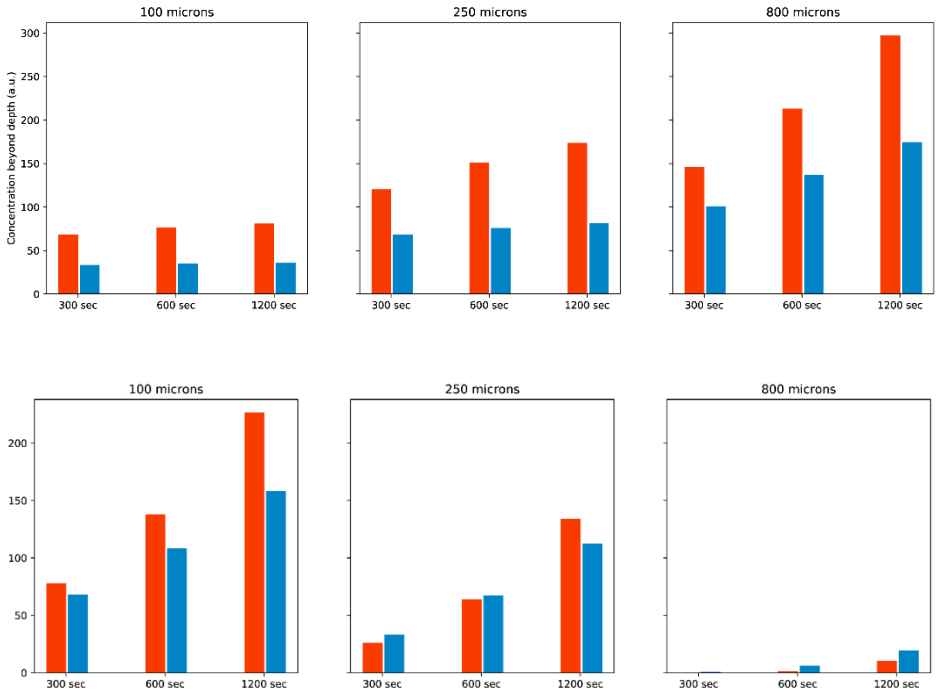

Figure 8: Theoretical time dependent translocation efficiency of molecules across simulated mucin gels. From the penetration profiles shown in Fig. 5, the number of molecules which travelled until (a) or across (b) a simulated mucin gel of thicknesses d (d_1 = 100 µm, d_2 = 250 µm and d_3 = 800 µm) are calculated for non-binding (blue) and mucin-binding (red) molecules.

Conclusion

Both the experimental and theoretical results presented in this study challenge the prevailing dogma, that mucoadhesion prevents the efficient translocation of molecules through mucus hydrogels. The binding affinity of cationic dextran molecules with polyanionic mucin gels results in a strong electrostatic pull of the molecules from the reservoir into the gel and thus entails a strong molecule accumulation at the buffer/gel interface. Now, not *although* but *because* these cationic molecules interact with the mucin hydrogel, the concentration of cationic molecules in the entry area of the mucin gel is far higher compared to the concentration of non-binding molecules. This in turn results further in a promoted diffusive transport of those mucus-binding molecules across the gel: although the overall free diffusion time of cationic molecules is shorter than that of non-binding molecules, the higher initial molecule concentration results in the translocation of a larger number of those molecules across the gel – at least for short distances and long diffusion times.

However, as illustrated by the theoretical modelling as well as the promoted penetration efficiency of anionic CM-dextrans observed in some mucin batches, the binding affinity of objects diffusing through mucin gels appears to be pivotal: if the affinity is low, promoted penetration is observed especially for shorter penetration time (Fig. 6a, CM-dextrans). If the binding affinity is higher (Fig. 6a, DEAE-dextrans) the penetration time must be extended to observe the promoting effect, however the overall effect is more enhanced. Yet, if the binding affinity is too strong, i.e. k_{off} is very small, the accumulation of such objects at the gel interface will be strong but these objects will not be able to penetrate a physiological mucus layer efficiently – which is, e.g., the case for mucoadhesive nanoparticles since they provide numerous of binding sites at once and thus exhibit a considerably smaller koff than smaller molecules that present only few binding sites.

Hence, depending on the thickness and renewal time of the mucus layer that must be overcome, an optimal binding affinity of, e.g., pharmaceutical drugs exists which will provide the highest diffusive transport of such molecules across a mucus barrier. Since an estimation of this binding affinity is possible via the theoretical model presented here, the rational design of drugs might benefit from the insights presented here.

References

1. Lieleg, O. and K. Ribbeck, Biological hydrogels as selective diffusion barriers. Trends Cell Biol, 2011. 21(9): p. 543-51.
2. McGuckin, M.A., et al., Mucin dynamics and enteric pathogens. Nat Rev Microbiol, 2011. 9(4): p. 265-78.
3. Baos, S.C., et al., Distribution of sialic acids on mucins and gels: a defense mechanism. Biophys J, 2012. 102(1): p. 176-84.
4. Gwozdzinski, K., et al., Gastric mucin hydrophobicity: effects of associated and covalently bound lipids, proteolysis, and reduction. Biochemistry international, 1988. 17(5): p. 907-917.
5. Strous, G.J. and J. Dekker, Mucin-type glycoproteins. Crit Rev Biochem Mol Biol, 1992. 27(1-2): p. 57-92.
6. Atuma, C., et al., The adherent gastrointestinal mucus gel layer: thickness and physical state in vivo. American Journal of Physiology - Gastrointestinal and Liver Physiology, 2001. 280(5): p. G922-G929.
7. Jordan, N., et al., A novel method for the visualization of the in situ mucus layer in rat and man. Clin Sci (Lond), 1998. 95(1): p. 97-106.
8. Nordman, H., et al., Gastric MUC5AC and MUC6 are large oligomeric mucins that differ in size, glycosylation and tissue distribution. Biochem J, 2002. 364(Pt 1): p. 191-200.
9. Porchet, N., et al., Human mucin genes: genomic organization and expression of MUC4, MUC5AC and MUC5B. Biochem Soc Trans, 1995. 23(4): p. 800-5.
10. Linden, S.K., et al., Mucins in the mucosal barrier to infection. Mucosal Immunol, 2008. 1(3): p. 183-97.
11. Ogata, S., et al., Mucin gene expression in colonic tissues and cell lines. Cancer Res, 1992. 52(21): p. 5971-8.
12. Strugala, V., et al., Colonic mucin: methods of measuring mucus thickness. Proc Nutr Soc, 2003. 62(1): p. 237-43.
13. Cone, R.A., Barrier properties of mucus. Adv Drug Deliv Rev, 2009. 61(2): p. 75-85.
14. Lehr, C.-M., et al., An estimate of turnover time of intestinal mucus gel layer in the rat in situ loop. International Journal of Pharmaceutics, 1991. 70(3): p. 235-240.
15. Johansson, M.E., Fast renewal of the distal colonic mucus layers by the surface goblet cells as measured by in vivo labeling of mucin glycoproteins. PLoS One, 2012. 7(7): p. e41009.
16. Yildiz, H.M., et al., Size selectivity of intestinal mucus to diffusing particulates is dependent on surface chemistry and exposure to lipids. Journal of Drug Targeting, 2015. 23(7-8): p. 768-774.
17. Kirch, J., et al., Optical tweezers reveal relationship between microstructure and nanoparticle penetration of pulmonary mucus. Proceedings of the National Academy of Sciences, 2012. 109(45): p. 18355-18360.
18. Allen, T.M. and P.R. Cullis, Drug delivery systems: entering the mainstream. Science, 2004. 303(5665): p. 1818-22.
19. Suh, J., M. Dawson, and J. Hanes, Real-time multiple-particle tracking: applications to drug and gene delivery. Adv Drug Deliv Rev, 2005. 57(1): p. 63-78.
20. Lai, S.K., Y.Y. Wang, and J. Hanes, Mucus-penetrating nanoparticles for drug and gene delivery to mucosal tissues. Adv Drug Deliv Rev, 2009. 61(2): p. 158-71.
21. Lieleg, O., I. Vladescu, and K. Ribbeck, Characterization of particle translocation through mucin hydrogels. Biophys J, 2010. 98(9): p. 1782-9.
22. Ensign, L.M., R. Cone, and J. Hanes, Oral drug delivery with polymeric nanoparticles: the gastrointestinal mucus barriers. Adv Drug Deliv Rev, 2012. 64(6): p. 557-70.
23. Lai, S.K., et al., Rapid transport of large polymeric nanoparticles in fresh undiluted human mucus. Proceedings of the National Academy of Sciences, 2007. 104(5): p. 1482-1487.
24. Huckaby, J.T. and S.K. Lai, PEGylation for enhancing nanoparticle diffusion in mucus. Advanced Drug Delivery Reviews, 2017.
25. Suk, J.S., Rapid transport of muco-inert nanoparticles in cystis fibrosis sputum treated with N-acetyl cysteine. Nanomedicine, 2011. 6(2): p. 365-375.
26. Tang, B.C., et al., Biodegradable polymer nanoparticles that rapidly penetrate the human mucus barrier. Proc Natl Acad Sci U S A, 2009. 106(46): p. 19268-73.
27. Wang, Y.Y., et al., Addressing the PEG mucoadhesivity paradox to engineer nanoparticles that "slip" through the human mucus barrier. Angew Chem Int Ed Engl, 2008. 47(50): p. 9726-9.

28. Cu, Y. and W.M. Saltzman, Stealth particles give mucus the slip. Nature materials, 2009. 8(1): p. 11-13.
29. Cu, Y. and W.M. Saltzman, Controlled surface modification with poly(ethylene)glycol enhances diffusion of PLGA nanoparticles in human cervical mucus. Mol Pharm, 2009. 6(1): p. 173-81.
30. Shan, W., et al., Overcoming the Diffusion Barrier of Mucus and Absorption Barrier of Epithelium by Self-Assembled Nanoparticles for Oral Delivery of Insulin. ACS Nano, 2015. 9(3): p. 2345-2356.
31. Dawson, M., et al., Transport of Polymeric Nanoparticle Gene Carriers in Gastric Mucus. Biotechnology Progress, 2004. 20(3): p. 851-857.
32. Desai, M.A., M. Mutlu, and P. Vadgama, A study of macromolecular diffusion through native porcine mucus. Experientia, 1992. 48(1): p. 22-6.
33. Norris, D.A. and P.J. Sinko, Effect of size, surface charge, and hydrophobicity on the translocation of polystyrene microspheres through gastrointestinal mucin. Journal of Applied Polymer Science, 1997. 63(11): p. 1481-1492.
34. Schuster, B.S., et al., Nanoparticle diffusion in respiratory mucus from humans without lung disease. Biomaterials, 2013. 34(13): p. 3439-46.
35. Groo, A.C. and F. Lagarce, Mucus models to evaluate nanomedicines for diffusion. Drug Discovery Today, 2014. 19(8): p. 1097-1108.
36. Crater, J.S. and R.L. Carrier, Barrier Properties of Gastrointestinal Mucus to Nanoparticle Transport. Macromolecular Bioscience, 2010. 10(12): p. 1473-1483.
37. Georgiades, P., et al., Particle tracking microrheology of purified gastrointestinal mucins. Biopolymers, 2014. 101(4): p. 366-77.
38. Murgia, X., et al., Size-Limited Penetration of Nanoparticles into Porcine Respiratory Mucus after Aerosol Deposition. Biomacromolecules, 2016. 17(4): p. 1536-1542.
39. Ensign, L.M., et al., Ex vivo characterization of particle transport in mucus secretions coating freshly excised mucosal tissues. Mol Pharm, 2013. 10(6): p. 2176-82.
40. Arends, F., et al., A microfluidics approach to study the accumulation of molecules at basal lamina interfaces. Lab Chip, 2015. 15(16): p. 3326-34.
41. Li, L.D., et al., Spatial configuration and composition of charge modulates transport into a mucin hydrogel barrier. Biophys J, 2013. 105(6): p. 1357-65.
42. Schomig, V.J., et al., An optimized purification process for porcine gastric mucin with preservation of its native functional properties. RSC Advances, 2016. 6(50): p. 44932-44943.
43. Celli, J.P., et al., Rheology of gastric mucin exhibits a pH-dependent sol-gel transition. Biomacromolecules, 2007. 8(5): p. 1580-6.
44. Cao, X.X., et al., pH-dependent conformational change of gastric mucin leads to sol-gel transition. Biophysical Journal, 1999. 76(3): p. 1250-1258.
45. Bhaskar, K.R., et al., Profound Increase in Viscosity and Aggregation of Pig Gastric Mucin at Low Ph. American Journal of Physiology, 1991. 261(5): p. G827-G833.
46. Lai, S.K., et al., Micro- and macrorheology of mucus. Adv Drug Deliv Rev, 2009. 61(2): p. 86-100.
47. Bansil, R. and B.S. Turner, Mucin structure, aggregation, physiological functions and biomedical applications. Current Opinion in Colloid & Interface Science, 2006. 11(2): p. 164-170.
48. Snary, D. and A. Allen, Studies on gastric mucoproteins. The isolation and characterization of the mucoprotein of the water-soluble mucus from pig cardiac gastric mucosa. Biochem J, 1971. 123(5): p. 845-53.
49. Robinson, C.V., et al., Desulfurization of mucin by Pseudomonas aeruginosa: influence of sulfate in the lungs of cystic fibrosis patients. Journal of Medical Microbiology, 2012. 61(12): p. 1644-1653.
50. Carlstedt, I., et al., Characterization of two different glycosylated domains from the insoluble mucin complex of rat small intestine. J Biol Chem, 1993. 268(25): p. 18771-81.
51. Lock, J.Y., T. Carlson, and R.L. Carrier, Mucus models to evaluate the diffusion of drugs and particles. Advanced Drug Delivery Reviews, 2017.
52. Sellers, L.A., et al., Mechanical characterization and properties of gastrointestinal mucus gel. Biorheology, 1987. 24(6): p. 615-23.

Supplemental information of

Transient binding promotes molecule penetration into mucin gels

(Draft)

Matthias Marczynski*, Benjamin T. Käsdorf*, Andreas Wenzler, Bernhard Altaner, Ulrich Gerland and Oliver Lieleg# (*equal contribution)

Molecular structure of MUC5AC

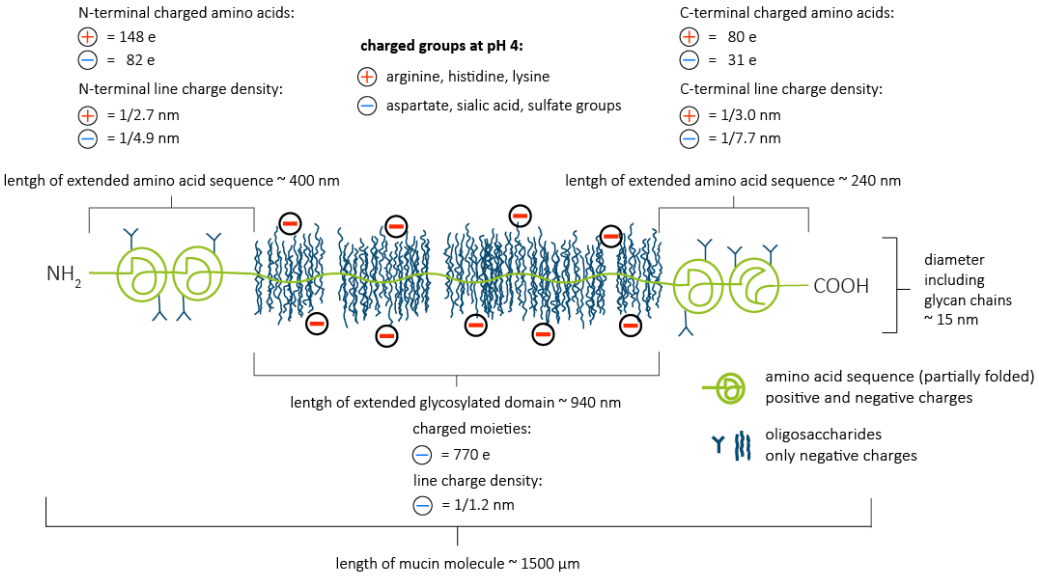

Figure S1: Molecular structure of gastric mucin MUC5AC at acidic pH. Mucin MUC5AC is a highly glycosylated protein consisting of ~80 % carbohydrates. The amino acid backbone contributes the remaining ~20 % of the total molecular weight and can be subdivided into distinct structural regions. A central, glycosylated region (interrupted by short non-glycosylated motifs) carries a high amount of negatively charged sialic acid residues and sulfate groups. Therefore, the glycosylated core regime of the glycoprotein carries – on average – a negative charge every ~1.2 nm. In contrast, the relatively hydrophobic, partially folded termini of the peptide sequence are only sparsely glycosylated and, consequently, the amino acid backbone is exposed. Considering the acidic conditions (pH 4.0) used in our microfluidic experiments, the basic amino acids arginine, histidine and lysine in these regions carry positive charges, whereas solely the acidic amino acid aspartate carries a negative charge. Thus, taking into account those charged amino acid residues, for those terminal domains we estimate a line charge density of one positive charge per ~3.0 nm and one negative charge per ~4.9 – 7.7 nm on the mucin glycoproteins.

Local fluorescence depletion zone in front of the buffer/gel interface

In addition to an accumulation of positively charged DEAE-dextrans at the buffer/gel interface, a depletion of molecules (i.e., a darker area) is observed right in front of the buffer/gel interface (Fig. S2).

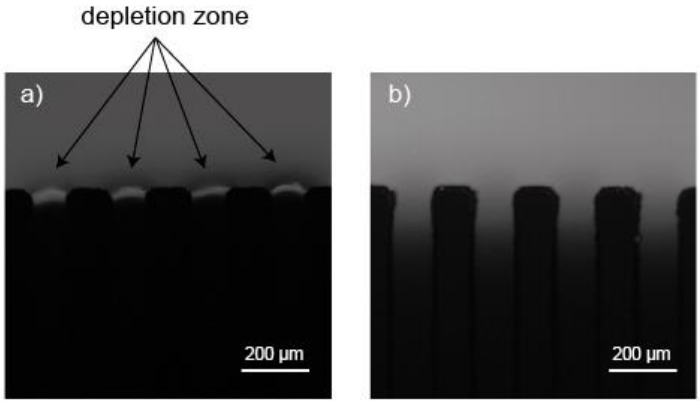

Figure S2: Close-up images of the buffer/gel interface taken immediately after filling of the test reservoir of a microfluidic chip with a solutions of either positively charged (a) or negatively charged dextran molecules (b). In addition to an accumulation of positively charged dextrans at the gel/buffer interface, a local depletion of dextran molecules located in front of the interface (darker areas) was observed (a). For negatively charged dextrans, neither an accumulation nor a depletion of negatively charged molecules could be observed (b). Images were acquired with a 4x objective (HI PLAN 4x/0.10 NA, Leica). The scale bars represent 200 µm.

Theoretical estimation of the maximal molecular penetration distance of dextran molecules into mucin gels

The theoretical travel distance of a molecule in a viscous medium after a given time span (mean squared displacement, $< x^2 >$) is linked to the diffusion coefficient D of that molecules via Equation 1:

$$< x^2 > = 2nDt \tag{1}$$

The diffusion coefficient D is described by the Einstein-Smoluchowski relation (Equation 2):

$$D = \frac{k_B T}{6\pi\eta R} \tag{2}$$

where $k_B T$ denotes the thermal energy, η the viscosity of the medium and R the radius of the diffusing molecule.

When we assume a local water-like viscosity within the mucin gel and a hydrodynamic radius $R = 1.4\,nm$ for the 4 kDa dextran molecules (given by the supplier, Sigma Aldrich), we obtain the following diffusion coefficient at room temperature ($T = 25\,°C$):

$$D = \frac{1.38\times10^{-23}\frac{kg\times m^2}{s^2\times K}\times 298\,K}{6\times\pi\times 0.891\times10^{-3}\frac{kg}{m\times s}\times 1.4\,nm} = 175\,\frac{\mu m^2}{s} \tag{3}$$

Considering a diffusion time of 20 minutes and a one-dimensional diffusion process ($n = 1$), we can calculate the average theoretical travel distance for such a molecule species via Equation 1:

$$x = \sqrt{2 \times 175 \frac{\mu m^2}{s} \times 1200\ s} = 648\ \mu m \tag{4}$$

Evaluation of the binding interaction of dextran molecules with mucins

For testing the binding affinity of the three different dextran variants towards mucin layers, we immobilized mucin MUC5AC from ten different purification batches (or MUC2 from a single purification batch) via physisorption onto the bottom of the wells of 96-well plates. To do so, lyophilized mucin was rehydrated at a concentration of 0.5 % (w/v), and 150 µL of each batch solution were filled into each well, 15 such mucin-coated wells were prepared per mucin batch. After incubation at 4 °C overnight, the mucin solutions were discarded and the wells were washed twice with 10 mM acetate buffer (pH 4.0). Thereafter, the wells were filled with 60 µL of dextran solution (0.02 % (w/v) in 10 mM acetate buffer pH 4.0) each, and five wells were filled per dextran variant. Additionally, for each dextran variant five uncoated wells were filled with dextran solution as reference. After incubation at room temperature for 4 h, 50 µL from each well were transferred to new 96-well plates and the fluorescence intensity at a wavelength of $\lambda_{535\ nm}$ was measured for each well using a VICTOR3 V Multilabel Counter (PerkinElmer, Waltham, MA, USA). The fraction of dextran molecules that were retained in the solution is given by the quotient of the fluorescence intesity of dextran solutions that were incubated in a mucin-coated well and the fluorescence intensity of dextran solutions that were incubated in uncoated reference wells (Fig. S2).

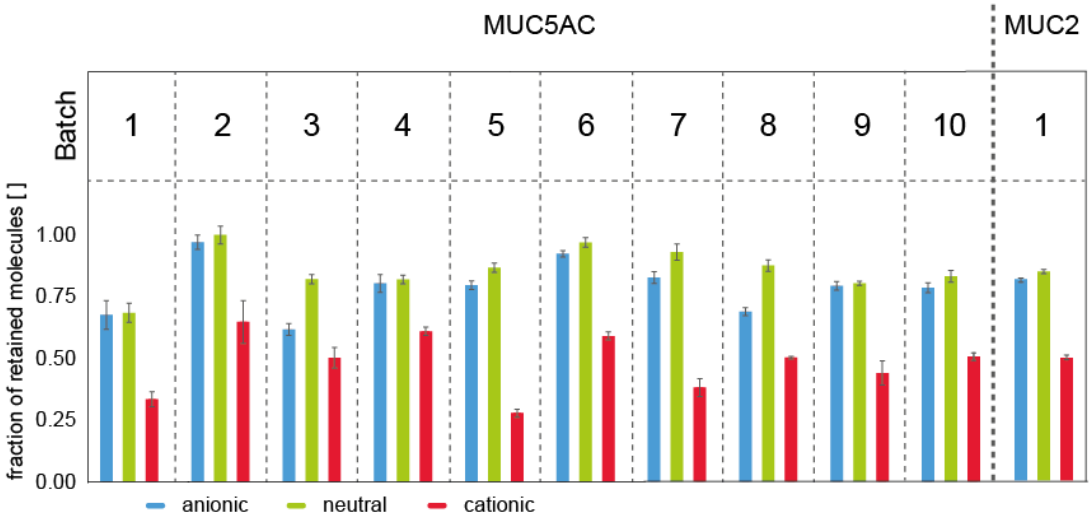

Figure S3: Adsorption efficiency of different dextran variants to surface coatings performed with purified gastric mucin MUC5AC and purified small intestinal mucin MUC2, respectively. The adsorption behavior of three different dextran variants to layers of porcine gastric mucin is compared by a depletion assay (see text above). In all tested mucin batches, cationic dextrans show the highest adsorption efficiency. However, the amount of depleted cationic dextrans varies within the different batches. For at least two batches of gastric mucin (batch 3 and 8), an increased adsorption of anionic dextrans – compared to neutral dextrans – is observed. The error bars denote the standard error of the mean.

1. Penetration behavior of dextrans into a mucin gel reconstituted from a different batch of MUC5AC

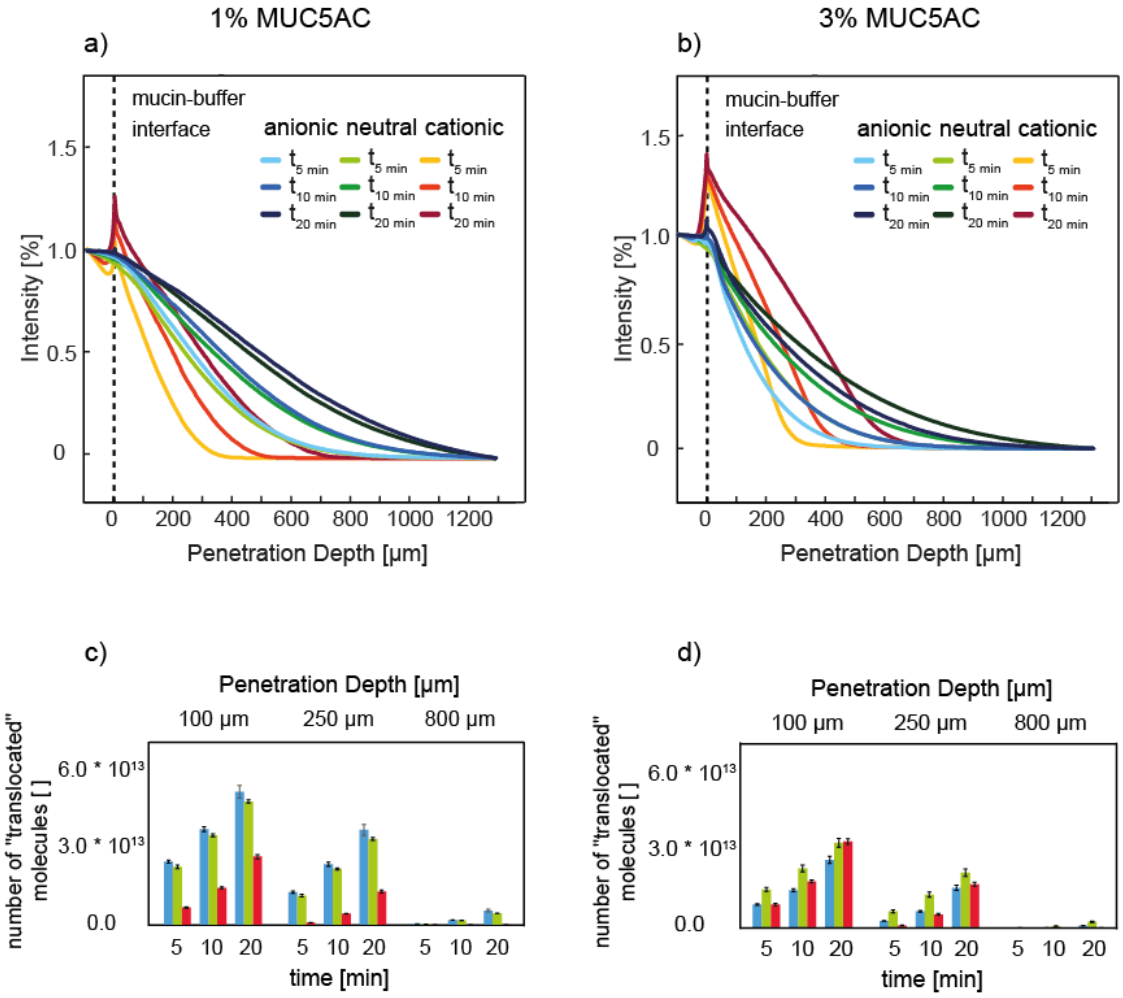

Figure S4: Penetration behavior of different dextran variants into porcine gastric mucin gels reconstituted at mucin concentrations of 1% (a) and 3% (b), respectively. The data shown in this graph was obtained with a different MUC5AC purification batch than that shown in the main paper in Fig. 3a. Also here, the diffusive penetration behavior of cationic dextrans differs from that of either neutral or anionic dextrans. The former accumulate at the buffer/mucin interface whereas the latter two show penetration profiles with local concentrations that continuously

decrease with increasing channel depth (a, b). For this mucin batch, even for thin mucin barrier thicknesses a penetration time of 20 minutes is not sufficient to obtain an enhanced translocation efficiency of cationic dextrans compared to neutral dextrans. At an increased mucin concentration (3 % instead of the initial 1 %) the penetration of cationic molecules is promoted again and already is efficient on short time scales or thicker mucin barriers (c, d). The error bars denote the standard error of the mean as obtained from analyzing at least seven "fingers" each.

D.2 Influence of charged moieties on the lubricating and gel-forming abilities of mucin

Mucin macromolecules possess several charged moieties which confer these glycoproteins a fairly polyanionic character. In addition to charged amino acids, these moieties include a high number of charged glycans. Porcine gastric mucin (MUC5AC), for example, comprises up to 3 wt% sialic acid and sulfated glycans. These numbers are even higher for human salivary mucin (MUC5B) where the anionic glycans make up 13 wt% of the mucin dry weight (**Figure 24**). These numbers illustrate, that mucins carry a high number of negative charges, but the detailed amount of charged residues seems to differ within the diverse mucin family.

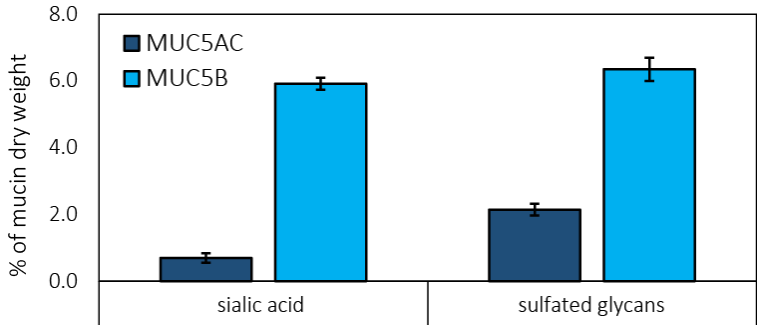

Figure 24: Amount of charged glycans in mucin: Percentage of sialic acid and sulfated glycans in porcine gastric mucin (MUC5AC) and human salivary mucin (MUC5B) as determined by enzymatic digestion of mucin and subsequent measurement of free sialic acid and sulfate.

In Section 4.7 it was demonstrated how important hydrophobic mucin domains are for the adsorption and lubrication of hydrophobic surfaces such as PDMS. Here, the influence of the removal of the charged moieties from mucin was analyzed. This removal was achieved by enzymatic digestion via a neuraminidase or a sulfatase treatment, respectively. When probing the lubricating abilities of MUC5B after removal of those charged glycans, a drastic increase of the coefficient of friction can be observed, especially in the boundary friction regime at low sliding speeds (**Figure 25a**). This behavior was not expected, as the hydrophobic mucin domains are still present as are the numerous uncharged glycans that establish a high hydration of the glycoprotein – thus adsorption to PDMS and hydration lubrication should still be feasible. Surprisingly, this effect does not occur for MUC5AC from gastric mucosa; here, the Stribeck curve obtained with digested MUC5AC is virtually identical to that obtained with native porcine gastric mucin (**Figure 25b**). However, as depicted in **Figure 24**, MUC5AC contains far less charged glycans, therefore their removal could be expected to result in a less pronounced effect. Additionally, the gastric mucosa also contains DNA molecules [122, 202]. It is possible that MUC5AC is, in contrast to MUC5B, physiologically associated with those highly anionic polymers.

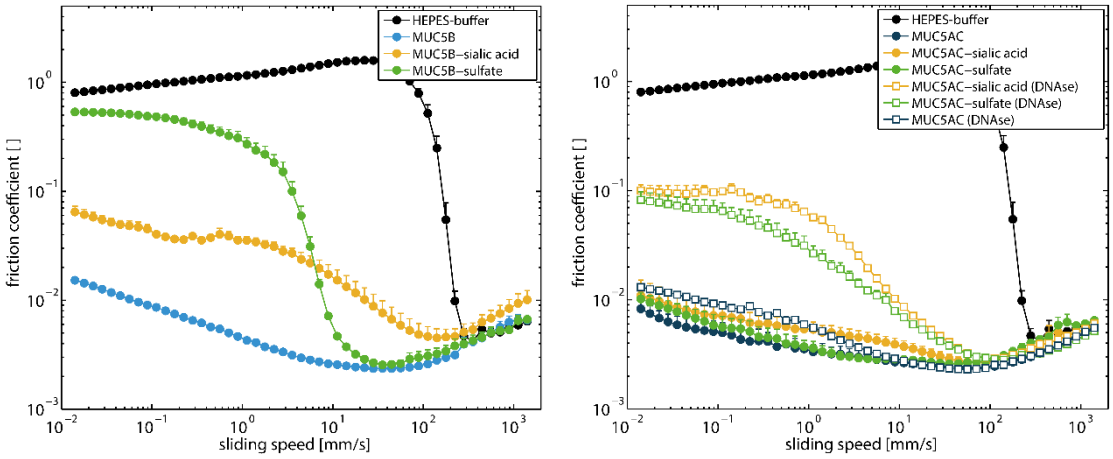

Figure 25: Lubricity of native and enzymatically treated mucins: Tribological measurements were performed with a steel/PDMS pairing using 0.1 mg/mL mucin dissolved in HEPES buffer. The measurements show the lubricating abilities of either native or enzymatically digested MUC5B (a) or MUC5AC (b), respectively. HEPES buffer is included as a reference. The error bars denote the standard deviation as obtained from three independent measurements.

Enzymatic treatment of MUC5AC with DNAse and subsequent sample analysis revealed that DNA is indeed present in purified porcine gastric mucin (**Figure 26**). When now, in addition to charged glycans, DNA is removed from MUC5AC as well and the lubricating qualities of the double-treated mucins are probed again, indeed an increase of the friction coefficient similar to MUC5B can be observed. In contrast, DNA-free MUC5AC with an intact glycosylation pattern does not show reduced lubricity in the tribology setup used here.

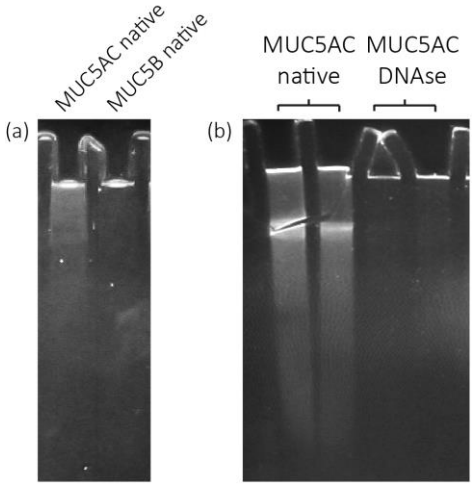

Figure 26: Electrophoretic analysis of native and DNAse digested mucin: Mucin samples were separated chromatographically and subsequently stained with SYBR Green to visualize residual DNA via fluorescence (indicated by the white signal). Analyzed were native porcine gastric MUC5AC and human MUC5B (a) as well as MUC5AC treated with DNAse (b).

To obtain more information about how charged glycans and bound DNA affect the biophysical properties of mucin, another aspect was studied: the formation of mucin gels at acidic conditions. Since both MUC5B and MUC5AC are gel-forming mucins, they are able to build reversible crosslinks at acidic pH and therefore form a viscoelastic gel. Although this gel formation is not yet fully understood, a combination of hydrophobic

and electrostatic interactions is suggested to be responsible [51, 63]. When the viscoelastic properties of the mucin samples were probed by single particle tracking, decreasing the pH from 7 to 4 increased the plateau modulus more than two orders of magnitudes for native MUC5AC as well as MUC5B (**Figure 27**). When the gel-forming abilities of the enzymatically treated mucins are probed, a similar picture compared to the tribological experiments is revealed: only for MUC5B a strong effect of the removal of charged glycans can be observed as the plateau modulus at pH 7 and 4 exhibits similar low values. In contrast, for enzymatically digested MUC5AC, only minor reductions in G_0 occur and the large difference between pH 7 and 4 is still present – indicating successful mucin gelation at acidic pH. However, when DNA is enzymatically removed from the sialic acid- or sulfate-deficient gastric mucins as well, the obtained G_0 values agree with the data from MUC5B: the plateau moduli are similarly low regardless of pH.

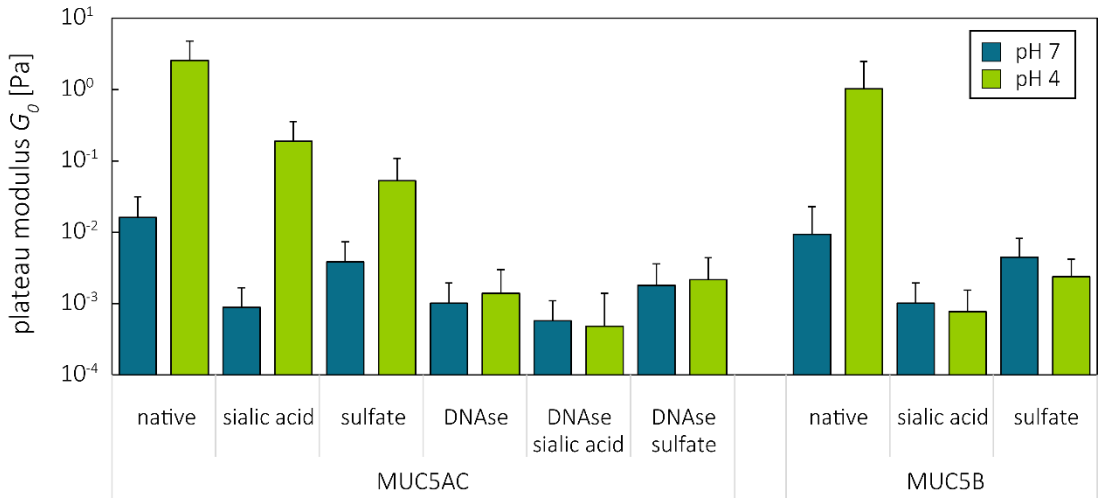

Figure 27: Calculated plateau modulus of native and enzymatically digested mucins: The plateau modulus G_0 was determined by single particle tracking in various MUC5AC and MUC5B samples at neutral or acidic pH. The error bars denote the standard deviation as obtained from three independent measurements.

Similar to the lubricating ability of mucins, the gel formation abilities of this glycoproteins seem to be influenced by the removal of anionic sulfated glycans or sialic acid residues as well as the removal of associated DNA molecules. These results therefore suggest the involvement of the charged glycan chains in the mucin core region in the process of mucin-mucin association as required for the formation of a viscoelastic mucin network. However, if the mucin-associated glycans are directly involved in this gelation process, e.g., by establishing transient intermolecular crosslinks or if they just provide the correct conformation of the mucin molecule to enable intermolecular crosslinks, is still to be revealed.

Bibliography

1. Lieleg, O.; Ribbeck, K., Biological hydrogels as selective diffusion barriers. *Trends in cell biology* 2011, 21, (9), 543-51.

2. Arends, F.; Nowald, C.; Pflieger, K.; Boettcher, K.; Zahler, S.; Lieleg, O., The biophysical properties of Basal lamina gels depend on the biochemical composition of the gel. *Plos One* 2015, 10, (2), e0118090.

3. Hardestam, J.; Petterson, L.; Ahlm, C.; Evander, M.; Lundkvist, A.; Klingstrom, J., Antiviral effect of human saliva against hantavirus. *J Med Virol* 2008, 80, (12), 2122-6.

4. Lai, S. K.; Hida, K.; Shukair, S.; Wang, Y. Y.; Figueiredo, A.; Cone, R.; Hope, T. J.; Hanes, J., Human immunodeficiency virus type 1 is trapped by acidic but not by neutralized human cervicovaginal mucus. *Journal of virology* 2009, 83, (21), 11196-200.

5. Lieleg, O.; Lieleg, C.; Bloom, J.; Buck, C. B.; Ribbeck, K., Mucin biopolymers as broad-spectrum antiviral agents. *Biomacromolecules* 2012, 13, (6), 1724-32.

6. Shibayama, M., Mucin coating on polymeric material surfaces to suppress bacterial adhesion. *Colloids and Surfaces B: Biointerfaces* 2000, 17, 229-239.

7. Witten, J.; Ribbeck, K., The particle in the spider's web: transport through biological hydrogels. *Nanoscale* 2017, 9, (24), 8080-8095.

8. Crockett, R., Boundary Lubrication in Natural Articular Joints. *Tribology Letters* 2009, 35, (2), 77-84.

9. Wang, X.; Du, M.; Han, H.; Song, Y.; Zheng, Q., Boundary lubrication by associative mucin. *Langmuir : the ACS journal of surfaces and colloids* 2015, 31, (16), 4733-40.

10. Lieleg, O.; Baumgartel, R. M.; Bausch, A. R., Selective filtering of particles by the extracellular matrix: an electrostatic bandpass. *Biophysical journal* 2009, 97, (6), 1569-77.

11. Stylianopoulos, T.; Poh, M. Z.; Insin, N.; Bawendi, M. G.; Fukumura, D.; Munn, L. L.; Jain, R. K., Diffusion of particles in the extracellular matrix: the effect of repulsive electrostatic interactions. *Biophys J* 2010, 99, (5), 1342-9.

12. Colwell, L. J.; Brenner, M. P.; Ribbeck, K., Charge as a selection criterion for translocation through the nuclear pore complex. *PLoS Comput Biol* 2010, 6, (4), e1000747.

13. Hansing, J.; Ciemer, C.; Kim, W. K.; Zhang, X.; DeRouchey, J. E.; Netz, R. R., Nanoparticle filtering in charged hydrogels: Effects of particle size, charge asymmetry and salt concentration. *The European physical journal. E, Soft matter* 2016, 39, (5), 53.

14. Ribbeck, K.; Gorlich, D., The permeability barrier of nuclear pore complexes appears to operate via hydrophobic exclusion. *EMBO J* 2002, 21, (11), 2664-71.

15. Zhang, X.; Hansing, J.; Netz, R. R.; DeRouchey, J. E., Particle transport through hydrogels is charge asymmetric. *Biophys J* 2015, 108, (3), 530-9.

16. Crater, J. S.; Carrier, R. L., Barrier Properties of Gastrointestinal Mucus to Nanoparticle Transport. *Macromolecular Bioscience* 2010, 10, (12), 1473-1483.

17. Desai, M. A.; Mutlu, M.; Vadgama, P., A study of macromolecular diffusion through native porcine mucus. *Experientia* 1992, 48, (1), 22-6.

18. Hirota, N.; Kumaki, Y.; Narita, T.; Gong, J. P.; Osada, Y., Effect of Charge on Protein Diffusion in Hydrogels. *The Journal of Physical Chemistry B* 2000, 104, (42), 9898-9903.

19. Resnikoff, S.; Pascolini, D.; Etya'ale, D.; Kocur, I.; Pararajasegaram, R.; Pokharel, G. P.; Mariotti, S. P., Global data on visual impairment in the year 2002. *Bulletin of the World Health Organization* 2004, 82, (11), 844-51.

20. Cunha-Vaz, J. G., The blood-retinal barriers system. Basic concepts and clinical evaluation. *Experimental eye research* 2004, 78, (3), 715-21.

21. Duvvuri, S.; Majumdar, S.; Mitra, A. K., Drug delivery to the retina: challenges and opportunities. *Expert opinion on biological therapy* 2003, 3, (1), 45-56.

22. Macha, S.; Mitra, A. K., Ocular pharmacokinetics in rabbits using a novel dual probe microdialysis technique. *Experimental eye research* 2001, 72, (3), 289-99.

23. Hughes, P. M.; Olejnik, O.; Chang-Lin, J. E.; Wilson, C. G., Topical and systemic drug delivery to the posterior segments. *Advanced drug delivery reviews* 2005, 57, (14), 2010-2032.

24. Diegelmann, R. F.; Evans, M. C., Wound healing: an overview of acute, fibrotic and delayed healing. *Front Biosci* 2004, 9, 283-9.

25. Bao, P.; Kodra, A.; Tomic-Canic, M.; Golinko, M. S.; Ehrlich, H. P.; Brem, H., The role of vascular endothelial growth factor in wound healing. *J Surg Res* 2009, 153, (2), 347-58.

26. Hameedaldeen, A.; Liu, J.; Batres, A.; Graves, G. S.; Graves, D. T., FOXO1, TGF-beta regulation and wound healing. *Int J Mol Sci* 2014, 15, (9), 16257-69.

27. Peer, D.; Karp, J. M.; Hong, S.; Farokhzad, O. C.; Margalit, R.; Langer, R., Nanocarriers as an emerging platform for cancer therapy. *Nat Nano* 2007, 2, (12), 751-760.

28. Huynh, The rise and rise of stealth nanocarriers for cancer Therapy. *Nanomedicine* 2010.

29. Torchilin, V. P., Multifunctional nanocarriers. *Advanced drug delivery reviews* 2006, 58, (14), 1532-55.

30. Allen, T. M.; Cullis, P. R., Liposomal drug delivery systems: From concept to clinical applications. *Advanced drug delivery reviews* 2013, 65, (1), 36-48.

31. Allison, S. D., Liposomal Drug Delivery. *Journal of Infusion Nursing* 2007, 30, (2), 89-95.

32. Florey, H., The Croonian Lecture: Mucin and the Protection of the Body. *Proceedings of the Royal Society of London. Series B, Biological Sciences* 1955, 143, (911), 147-158.

33. Amerongen, A. V. N.; Bolscher, J. G. M.; Veerman, E. C. I., Salivary mucins: protective functions in relation to their diversity. *Glycobiology* 1995, 5, (8), 733-740.

34. Ranc, H.; Elkhyat, A.; Servais, C.; Mac-Mary, S.; Launay, B.; Humbert, P., Friction coefficient and wettability of oral mucosal tissue: Changes induced by a salivary layer. *Colloids and Surfaces A: Physicochemical and Engineering Aspects* 2006, 276, (1-3), 155-161.

35. Girod, Role of the physicochemical properties of mucus in the protection of the respiratory epithelium. *EurRespirJ* 1992.

36. Miyake, K.; Tanaka, T.; McNeil, P. L., Disruption-induced mucus secretion: repair and protection. *PLoS biology* 2006, 4, (9), e276.

37. Coles, J. M.; Chang, D. P.; Zauscher, S., Molecular mechanisms of aqueous boundary lubrication by mucinous glycoproteins. *Current Opinion in Colloid & Interface Science* 2010, 15, (6), 406-416.

38. Linden, S. K.; Florin, T. H.; McGuckin, M. A., Mucin dynamics in intestinal bacterial infection. *Plos One* 2008, 3, (12), e3952.

39. Habte, H. H.; Kotwal, G. J.; Lotz, Z. E.; Tyler, M. G.; Abrahams, M.; Rodriques, J.; Kahn, D.; Mall, A. S., Antiviral activity of purified human breast milk mucin. *Neonatology* 2007, 92, (2), 96-104.

40. Tian, P.; Brandl, M.; Mandrell, R., Porcine gastric mucin binds to recombinant norovirus particles and competitively inhibits their binding to histo-blood group antigens and Caco-2 cells. *Letters in applied microbiology* 2005, 41, (4), 315-20.

41. McGuckin, M. A.; Linden, S. K.; Sutton, P.; Florin, T. H., Mucin dynamics and enteric pathogens. *Nature reviews. Microbiology* 2011, 9, (4), 265-78.

42. Linden, S. K.; Sutton, P.; Karlsson, N. G.; Korolik, V.; McGuckin, M. A., Mucins in the mucosal barrier to infection. *Mucosal immunology* 2008, 1, (3), 183-97.

43. Habte, H. H.; Mall, A. S.; de Beer, C.; Lotz, Z. E.; Kahn, D., The role of crude human saliva and purified salivary MUC5B and MUC7 mucins in the inhibition of Human Immunodeficiency Virus type 1 in an inhibition assay. *Virol J* 2006, 3.

44. Gaunitz, S.; Liu, J. N.; Nilsson, A.; Karlsson, N.; Holgersson, J., Avian influenza H5 hemagglutinin binds with high avidity to sialic acid on different O-linked core structures on mucin-type fusion proteins. *Glycoconjugate J* 2014, 31, (2), 145-159.

45. Co, J. Y.; Crouzier, T.; Ribbeck, K., Probing the Role of Mucin-Bound Glycans in Bacterial Repulsion by Mucin Coatings. *Advanced Materials Interfaces* 2015, 2, (17), 1500179-n/a.

46. Caldara, M.; Friedlander, R. S.; Kavanaugh, N. L.; Aizenberg, J.; Foster, K. R.; Ribbeck, K., Mucin biopolymers prevent bacterial aggregation by retaining cells in the free-swimming state. *Curr Biol* 2012, 22, (24), 2325-30.

47. Boukari, H.; Brichacek, B.; Stratton, P.; Mahoney, S. F.; Lifson, J. D.; Margolis, L.; Nossal, R., Movements of HIV-virions in human cervical mucus. *Biomacromolecules* 2009, 10, (9), 2482-8.

48. Cone, R. A., Barrier properties of mucus. *Advanced drug delivery reviews* 2009, 61, (2), 75-85.

49. Hollingsworth, M. A.; Swanson, B. J., Mucins in cancer: protection and control of the cell surface. *Nature reviews. Cancer* 2004, 4, (1), 45-60.

50. Velcich, A.; Yang, W.; Heyer, J.; Fragale, A.; Nicholas, C.; Viani, S.; Kucherlapati, R.; Lipkin, M.; Yang, K.; Augenlicht, L., Colorectal cancer in mice genetically deficient in the mucin Muc2. *Science* 2002, 295, (5560), 1726-9.

51. Bansil, R.; Turner, B. S., Mucin structure, aggregation, physiological functions and biomedical applications. *Current Opinion in Colloid & Interface Science* 2006, 11, (2-3), 164-170.

52. Kočevar-Nared, J.; Kristl, J.; Šmid-Korbar, J., Comparative rheological investigation of crude gastric mucin and natural gastric mucus. *Biomaterials* 1997, 18, (9), 677-681.

53. Svensson, O.; Arnebrant, T., Mucin layers and multilayers — Physicochemical properties and applications. *Current Opinion in Colloid & Interface Science* 2010, 15, (6), 395-405.

54. Lee, S., Characterization of Lubricity of Mucins at Polymeric Surfaces for Biomedical Applications. *World Academy of Science, Engineering and Technology, International Journal of Medical, Health, Biomedical, Bioengineering and Pharmaceutical Engineering* 2013, 7, (3), 145-150.

55. Lee, S.; Muller, M.; Rezwan, K.; Spencer, N. D., Porcine gastric mucin (PGM) at the water/poly(dimethylsiloxane) (PDMS) interface: influence of pH and ionic strength on its conformation, adsorption, and aqueous lubrication properties. *Langmuir : the ACS journal of surfaces and colloids* 2005, 21, (18), 8344-53.

56. Nikogeorgos, N.; Madsen, J. B.; Lee, S., Influence of impurities and contact scale on the lubricating properties of bovine submaxillary mucin (BSM) films on a hydrophobic surface. *Colloid Surface B* 2014, 122, 760-766.

57. Desai, M. A.; Vadgama, P., Estimation of effective diffusion coefficients of model solutes through gastric mucus: assessment of a diffusion chamber technique based on spectrophotometric analysis. *Analyst* 1991, 116, (11), 1113-6.

58. Schuster, B. S.; Suk, J. S.; Woodworth, G. F.; Hanes, J., Nanoparticle diffusion in respiratory mucus from humans without lung disease. *Biomaterials* 2013, 34, (13), 3439-46.

59. Olmsted, S. S.; Padgett, J. L.; Yudin, A. I.; Whaley, K. J.; Moench, T. R.; Cone, R. A., Diffusion of macromolecules and virus-like particles in human cervical mucus. *Biophysical journal* 2001, 81, (4), 1930-7.

60. Schreiber, S.; Scheid, P., Gastric mucus of the guinea pig: proton carrier and diffusion barrier. *Am J Physiol* 1997, 272, (1 Pt 1), G63-70.

61. Lieleg, O.; Vladescu, I.; Ribbeck, K., Characterization of particle translocation through mucin hydrogels. *Biophysical journal* 2010, 98, (9), 1782-9.

62. Celli, J. P.; Turner, B. S.; Afdhal, N. H.; Ewoldt, R. H.; McKinley, G. H.; Bansil, R.; Erramilli, S., Rheology of gastric mucin exhibits a pH-dependent sol-gel transition. *Biomacromolecules* 2007, 8, (5), 1580-6.

63. Cao, X. X.; Bansil, R.; Bhaskar, K. R.; Turner, B. S.; LaMont, J. T.; Niu, N.; Afdhal, N. H., pH-dependent conformational change of gastric mucin leads to sol-gel transition. *Biophysical journal* 1999, 76, (3), 1250-1258.

64. Celli, J.; Gregor, B.; Turner, B.; Afdhal, N. H.; Bansil, R.; Erramilli, S., Viscoelastic properties and dynamics of porcine gastric mucin. *Biomacromolecules* 2005, 6, (3), 1329-1333.

65. Suh, J.; Dawson, M.; Hanes, J., Real-time multiple-particle tracking: applications to drug and gene delivery. *Advanced drug delivery reviews* 2005, 57, (1), 63-78.

66. Dawson, M.; Krauland, E.; Wirtz, D.; Hanes, J., Transport of Polymeric Nanoparticle Gene Carriers in Gastric Mucus. *Biotechnology Progress* 2004, 20, (3), 851-857.

67. Norris, D. A.; Sinko, P. J., Effect of size, surface charge, and hydrophobicity on the translocation of polystyrene microspheres through gastrointestinal mucin. *Journal of Applied Polymer Science* 1997, 63, (11), 1481-1492.

68. Yoshiyama, H.; Nakazawa, T., Unique mechanism of Helicobacter pylori for colonizing the gastric mucus. *Microbes Infect* 2000, 2, (1), 55-60.

69. Schmitz, J. M.; Durham, C. G.; Ho, S. B.; Lorenz, R. G., Gastric mucus alterations associated with murine Helicobacter infection. *The journal of histochemistry and cytochemistry : official journal of the Histochemistry Society* 2009, 57, (5), 457-67.

70. Celli, J. P.; Turner, B. S.; Afdhal, N. H.; Keates, S.; Ghiran, I.; Kelly, C. P.; Ewoldt, R. H.; McKinley, G. H.; So, P.; Erramilli, S.; Bansil, R., Helicobacter pylori moves through mucus by reducing mucin viscoelasticity. *Proceedings of the National Academy of Sciences of the United States of America* 2009, 106, (34), 14321-6.

71. Bansil, R.; Celli, J. P.; Hardcastle, J. M.; Turner, B. S., The Influence of Mucus Microstructure and Rheology in Helicobacter pylori Infection. *Frontiers in immunology* 2013, 4, 310.

72. Walker, D.; Kasdorf, B. T.; Jeong, H. H.; Lieleg, O.; Fischer, P., Enzymatically active biomimetic micropropellers for the penetration of mucin gels. *Sci Adv* 2015, 1, (11), e1500501.

73. Arends, F.; Sellner, S.; Seifert, P.; Gerland, U.; Rehberg, M.; Lieleg, O., A microfluidics approach to study the accumulation of molecules at basal lamina interfaces. *Lab on a chip* 2015, 15, (16), 3326-3334.

74. Gendler, S. J.; Spicer, A., Epithelial mucin genes. *Annual review of physiology* 1995, 57, (1), 607-634.

75. Tabak, L. A., Structure and function of human salivary mucins. *Crit Rev Oral Biol Med* 1990, 1, (4), 229-34.

76. Yakubov, G. E.; McColl, J.; Bongaerts, J. H.; Ramsden, J. J., Viscous boundary lubrication of hydrophobic surfaces by mucin. *Langmuir : the ACS journal of surfaces and colloids* 2009, 25, (4), 2313-21.

77. Bongaerts, J. H. H.; Rossetti, D.; Stokes, J. R., The Lubricating Properties of Human Whole Saliva. *Tribology Letters* 2007, 27, (3), 277-287.

78. Ma, S.; Lee, H.; Liang, Y.; Zhou, F., Astringent Mouthfeel as a Consequence of Lubrication Failure. *Angewandte Chemie* 2016, 55, (19), 5793-7.

79. Bajec, M. R.; Pickering, G. J., Astringency: mechanisms and perception. *Critical reviews in food science and nutrition* 2008, 48, (9), 858-875.

80. Schwarz, B.; Hofmann, T., Is there a direct relationship between oral astringency and human salivary protein binding? *European Food Research and Technology* 2008, 227, (6), 1693-1698.

81. Hufnagel, J. C.; Hofmann, T., Orosensory-Directed Identification of Astringent Mouthfeel and Bitter-Tasting Compounds in Red Wine. *Journal of Agricultural and Food Chemistry* 2008, 56, (4), 1376-1386.

82. Glabasnia, A.; Hofmann, T., Sensory-Directed Identification of Taste-Active Ellagitannins in American (Quercus alba L.) and European Oak Wood (Quercus robur L.) and Quantitative Analysis in Bourbon Whiskey and Oak-Matured Red Wines. *Journal of Agricultural and Food Chemistry* 2006, 54, (9), 3380-3390.

83. Scharbert, S.; Holzmann, N.; Hofmann, T., Identification of the astringent taste compounds in black tea infusions by combining instrumental analysis and human bioresponse. *J Agric Food Chem* 2004, 52, (11), 3498-508.

84. Davidson, H. J.; Kuonen, V. J., The tear film and ocular mucins. *Vet. Ophthalmol.* 2004, 7, (2), 71-77.

85. Gipson, I. K., Distribution of mucins at the ocular surface. *Experimental eye research* 2004, 78, (3), 379-388.

86. Ablamowicz, A. F.; Nichols, J. J., Ocular Surface Membrane-Associated Mucins. *Ocul. Surf.* 2016, 14, (3), 331-41.

87. Levin, R. J., The ins and outs of vaginal lubrication. *Sexual and Relationship Therapy* 2003, 18, (4), 509-513.

88. Tavares Fde, P.; Fernandes, R. S.; Bernardes, T. F.; Bonfioli, A. A.; Soares, E. J., Dry eye disease. *Semin Ophthalmol* 2010, 25, (3), 84-93.

89. Cassolato, S. F.; Turnbull, R. S., Xerostomia: Clinical Aspects and Treatment. *Gerodontology* 2003, 20, (2), 64-77.

90. Hills, B. A., Boundary lubrication in vivo. *Proc Inst Mech Eng H* 2000, 214, (1), 83-94.

91. Hsu, S. M., Boundary lubrication: current understanding. *Tribol. Lett.* 1997, 3, (1), 1-11.

92. Hsu, S. M.; Gates, R. S., Boundary lubricating films: formation and lubrication mechanism. *Tribol Int* 2005, 38, (3), 305-312.

93. Ma, L.; Gaisinskaya-Kipnis, A.; Kampf, N.; Klein, J., Origins of hydration lubrication. *Nat. Commun.* 2015, 6, 6060.

94. Jahn, S.; Klein, J., Hydration Lubrication: The Macromolecular Domain. *Macromolecules* 2015, 48, (15), 5059-5075.

95. Jahanmir, S.; Beltzer, M., An Adsorption Model for Friction in Boundary Lubrication. *ASLE Trans.* 1986, 29, (3), 423-430.

96. Hamrock, B. J.; Schmid, S. R.; Jacobson, B. O., *Fundamentals of fluid film lubrication*. CRC press: 2004.

97. Chan, S. M. T.; Neu, C. P.; DuRaine, G.; Komvopoulos, K.; Reddi, A. H., Tribological altruism: A sacrificial layer mechanism of synovial joint lubrication in articular cartilage. *J. Biomech.* 2012, 45, (14), 2426-2431.

98. Bishop, P. N., Structural macromolecules and supramolecular organisation of the vitreous gel. *Progress in retinal and eye research* 2000, 19, (3), 323-44.

99. Bishop, P., The biochemical structure of mammalian vitreous. *Eye* 1996, 10 (Pt 6), 664-70.

100. Scott, J. E., The chemical morphology of the vitreous. *Eye* 1992, 6 (Pt 6), 553-5.

101. Nickerson, C. S.; Park, J.; Kornfield, J. A.; Karageozian, H., Rheological properties of the vitreous and the role of hyaluronic acid. *Journal of biomechanics* 2008, 41, (9), 1840-6.

102. Sharif-Kashani, P.; Hubschman, J. P.; Sassoon, D.; Kavehpour, H. P., Rheology of the vitreous gel: effects of macromolecule organization on the viscoelastic properties. *Journal of biomechanics* 2011, 44, (3), 419-23.

103. Le Goff, M. M.; Bishop, P. N., Adult vitreous structure and postnatal changes. *Eye* 2008, 22, (10), 1214-22.

104. Thornton, D. J.; Rousseau, K.; McGuckin, M. A., Structure and function of the polymeric mucins in airways mucus. *Annual review of physiology* 2008, 70, 459-86.

105. Yakubov, G. E.; Papagiannopoulos, A.; Rat, E.; Easton, R. L.; Waigh, T. A., Molecular structure and rheological properties of short-side-chain heavily glycosylated porcine stomach mucin. *Biomacromolecules* 2007, 8, (11), 3467-77.

106. Strous, G. J.; Dekker, J., Mucin-type glycoproteins. *Crit Rev Biochem Mol Biol* 1992, 27, (1-2), 57-92.

107. Jentoft, N., Why Are Proteins O-Glycosylated. *Trends Biochem Sci* 1990, 15, (8), 291-294.

108. Levine, M. J.; Reddy, M. S.; Tabak, L. A.; Loomis, R. E.; Bergey, E. J.; Jones, P. C.; Cohen, R. E.; Stinson, M. W.; Alhashimi, I., Structural Aspects of Salivary Glycoproteins. *J Dent Res* 1987, 66, (2), 436-441.

109. Robinson, C. V.; Elkins, M. R.; Bialkowski, K. M.; Thornton, D. J.; Kertesz, M. A., Desulfurization of mucin by Pseudomonas aeruginosa: influence of sulfate in the lungs of cystic fibrosis patients. *J Med Microbiol* 2012, 61, (12), 1644-1653.

110. Thornton, D. J.; Khan, N.; Mehrotra, R.; Howard, M.; Veerman, E.; Packer, N. H.; Sheehan, J. K., Salivary mucin MG1 is comprised almost entirely of different glycosylated forms of the MUC5B gene product. *Glycobiology* 1999, 9, (3), 293-302.

111. Pearce, E. I. F.; Major, G. N., Colorimetric Analysis of Sialic-Acid in Human Saliva and Bovine Salivary Mucin. *J Dent Res* 1978, 57, (11-1), 995-1002.

112. Thomsson, K. A.; Carlstedt, I.; Karlsson, N. G.; Karlsson, H.; Hansson, G. C., Different O-glycosylation of respiratory mucin glycopeptides from a patient with cystic fibrosis. *Glycoconjugate J* 1998, 15, (8), 823-833.

113. Tram, T. H.; Miller, J. C. B.; McNeil, Y.; McVeagh, P., Sialic acid content of infant saliva: comparison of breast fed with formula fed infants. *Arch Dis Child* 1997, 77, (4), 315-318.

114. Bhaskar, K. R.; Gong, D.; Bansil, R.; Pajevic, S.; Hamilton, J. A.; Turner, B. S.; Lamont, J. T., Profound Increase in Viscosity and Aggregation of Pig Gastric Mucin at Low Ph. *Am J Physiol* 1991, 261, (5), G827-G833.

115. Snary, D.; Allen, A., Studies on gastric mucoproteins. The isolation and characterization of the mucoprotein of the water-soluble mucus from pig cardiac gastric mucosa. *Biochem J* 1971, 123, (5), 845-53.

116. Yakubov, G. E.; Papagiannopoulos, A.; Rat, E.; Waigh, T. A., Charge and interfacial behavior of short side-chain heavily glycosylated porcine stomach mucin. *Biomacromolecules* 2007, 8, (12), 3791-9.

117. Perez-Vilar, J.; Hill, R. L., The structure and assembly of secreted mucins. *J Biol Chem* 1999, 274, (45), 31751-4.

118. Sheehan, J. K.; Kirkham, S.; Howard, M.; Woodman, P.; Kutay, S.; Brazeau, C.; Buckley, J.; Thornton, D. J., Identification of molecular intermediates in the assembly pathway of the MUC5AC mucin. *J Biol Chem* 2004, 279, (15), 15698-705.

119. An, J.; Jin, C.; Dedinaite, A.; Holgersson, J.; Karlsson, N. G.; Claesson, P. M., Influence of Glycosylation on Interfacial Properties of Recombinant Mucins: Adsorption, Surface Forces, and Friction. *Langmuir* 2017, 33, (18), 4386-4395.

120. An, J.; Dedinaite, A.; Nilsson, A.; Holgersson, J.; Claesson, P. M., Comparison of a brush-with-anchor and a train-of-brushes mucin on poly(methyl methacrylate) surfaces: adsorption, surface forces, and friction. *Biomacromolecules* 2014, 15, (4), 1515-25.

121. Zappone, B.; Ruths, M.; Greene, G. W.; Jay, G. D.; Israelachvili, J. N., Adsorption, Lubrication, and Wear of Lubricin on Model Surfaces: Polymer Brush-Like Behavior of a Glycoprotein. *Biophys. J.* 2007, 92, (5), 1693-1708.

122. Lai, S. K.; Wang, Y. Y.; Wirtz, D.; Hanes, J., Micro- and macrorheology of mucus. *Advanced drug delivery reviews* 2009, 61, (2), 86-100.

123. Maleki, A.; Lafitte, G.; Kjoniksen, A. L.; Thuresson, K.; Nystrom, B., Effect of pH on the association behavior in aqueous solutions of pig gastric mucin. *Carbohydr Res* 2008, 343, (2), 328-40.

124. Hong, Z. N.; Chasan, B.; Bansil, R.; Turner, B. S.; Bhaskar, K. R.; Afdhal, N. H., Atomic force microscopy reveals aggregation of gastric mucin at low pH. *Biomacromolecules* 2005, 6, (6), 3458-3466.

125. Bromberg, L. E.; Barr, D. P., Self-Association of Mucin. *Biomacromolecules* 2000, 1, (3), 325-334.

126. McCullagh, C. M.; Gupta, R.; Jamieson, A. M.; Blackwell, J., Gelation of fractionated canine submaxillary mucin in a chaotropic solvent. *International Journal of Biological Macromolecules* 1996, 18, (4), 247-253.

127. Bell, A. E.; Allen, A.; Morris, E. R.; Ross-Murphy, S. B., Functional interactions of gastric mucus glycoprotein. *International Journal of Biological Macromolecules* 1984, 6, (6), 309-315.

128. Allen, A.; Garner, A., Mucus and Bicarbonate Secretion in the Stomach and Their Possible Role in Mucosal Protection. *Gut* 1980, 21, (3), 249-262.

129. Bahari, Demonstration of a pH gradient across the mucus layer on the surface of human gastric mucosa in vitro. *gut.bmj.com* 1982.

130. Li, L.; Lieleg, O.; Jang, S.; Ribbeck, K.; Han, J., A microfluidic in vitro system for the quantitative study of the stomach mucus barrier function. *Lab on a chip* 2012, 12, (20), 4071-9.

131. Lai, S. K.; Wang, Y. Y.; Hida, K.; Cone, R.; Hanes, J., Nanoparticles reveal that human cervicovaginal mucus is riddled with pores larger than viruses. *Proceedings of the National Academy of Sciences of the United States of America* 2010, 107, (2), 598-603.

132. Lai, S. K.; O'Hanlon, D. E.; Harrold, S.; Man, S. T.; Wang, Y. Y.; Cone, R.; Hanes, J., Rapid transport of large polymeric nanoparticles in fresh undiluted human mucus. *Proceedings of the National Academy of Sciences of the United States of America* 2007, 104, (5), 1482-7.

133. Ensign, L. M.; Henning, A.; Schneider, C. S.; Maisel, K.; Wang, Y. Y.; Porosoff, M. D.; Cone, R.; Hanes, J., Ex vivo characterization of particle transport in mucus secretions coating freshly excised mucosal tissues. *Molecular pharmaceutics* 2013, 10, (6), 2176-82.

134. De Gier, J.; Mandersloot, J. G.; Van Deenen, L. L. M., Lipid composition and permeability of liposomes. *Biochimica et Biophysica Acta (BBA) - Biomembranes* 1968, 150, (4), 666-675.

135. Barza, M.; Stuart, M.; Szoka, F., Jr., Effect of size and lipid composition on the pharmacokinetics of intravitreal liposomes. *Investigative ophthalmology & visual science* 1987, 28, (5), 893-900.

136. Li, J.; Wang, X.; Zhang, T.; Wang, C.; Huang, Z.; Luo, X.; Deng, Y., A review on phospholipids and their main applications in drug delivery systems. *Asian Journal of Pharmaceutical Sciences* 2015, 10, (2), 81-98.

137. Mouritsen, O. G.; Jorgensen, K., Micro-, nano- and meso-scale heterogeneity of lipid bilayers and its influence on macroscopic membrane properties. *Molecular membrane biology* 1995, 12, (1), 15-20.

138. Masaharu, U.; Shoshin, Y.; Isamu, H., Characteristics of the Membrane Permeability of Temperature-Sensitive Liposome. *Bulletin of the Chemical Society of Japan* 1991, 64, (5), 1588-1593.

139. Rutherford, R. B.; Jones, D. N.; Bergentz, S. E.; Bergqvist, D.; Karmody, A. M.; Dardik, H.; Moore, W. S.; Goldstone, J.; Flinn, W. R.; Comerota, A. J.; et al., The efficacy of dextran 40 in preventing early postoperative thrombosis following difficult lower extremity bypass. *J Vasc Surg* 1984, 1, (6), 765-73.

140. Bonnar, J.; Walsh, J., Prevention of thrombosis after pelvic surgery by British dextran 70. *Lancet* 1972, 1, (7751), 614-6.

141. Technical data of polystyrene FluoSpheres®, Certificate of analysis. *life technologies, Invitrogen* 2011, https://www.thermofisher.com/order/catalog/product/F8887, (visited on 17/11/06).

142. Technical data of FITC-dextrans (Product information on webpage). *Sigma-Aldrich* 2017, http://www.sigmaaldrich.com/catalog/product/sigma/53557, (visited on 17/11/06).

143. Bodas, D.; Khan-Malek, C., Formation of more stable hydrophilic surfaces of PDMS by plasma and chemical treatments. *Microelectronic Engineering* 2006, 83, (4), 1277-1279.

144. Toepke, M. W.; Beebe, D. J., PDMS absorption of small molecules and consequences in microfluidic applications. *Lab Chip* 2006, 6, (12), 1484-6.

145. Tan, S. H.; Nguyen, N. T.; Chua, Y. C.; Kang, T. G., Oxygen plasma treatment for reducing hydrophobicity of a sealed polydimethylsiloxane microchannel. *Biomicrofluidics* 2010, 4, (3), 32204.

146. Bhattacharya, S.; Datta, A.; Berg, J. M.; Gangopadhyay, S., Studies on surface wettability of poly(dimethyl) siloxane (PDMS) and glass under oxygen-plasma treatment and correlation with bond strength. *Journal of Microelectromechanical Systems* 2005, 14, (3), 590-597.

147. Shi, L.; Caldwell, K. D., Mucin Adsorption to Hydrophobic Surfaces. *J Colloid Interf Sci* 2000, 224, (2), 372-381.

148. Hills, B. A., Lubrication of visceral movement and gastric motility by peritoneal surfactant. *J. Gastroenterol. Hepatol.* 1996, 11, (9), 797-803.

149. Crockett, R.; Grubelnik, A.; Roos, S.; Dora, C.; Born, W.; Troxler, H., Biochemical composition of the superficial layer of articular cartilage. *Journal of Biomedical Materials Research Part A* 2007, 82A, (4), 958-964.

150. von Smoluchowski, M., Zur kinetischen Theorie der Brownschen Molekularbewegung und der Suspensionen. *Annalen der Physik* 1906, 326, (14), 756-780.

151. Einstein, A., Über die von der molekularkinetischen Theorie der Wärme geforderte Bewegung von in ruhenden Flüssigkeiten suspendierten Teilchen. *Annalen der Physik* 1905, 322, (8), 549-560.

152. Kometani, N.; Tanabe, M.; Su, L.; Yang, K.; Nishinari, K., In Situ Observations of Thermoreversible Gelation and Phase Separation of Agarose and Methylcellulose Solutions under High Pressure. *The Journal of Physical Chemistry B* 2015, 119, (22), 6878-6883.

153. Sauerbrey, G., Verwendung von Schwingquarzen zur Wägung dünner Schichten und zur Mikrowägung. *Zeitschrift für Physik* 1959, 155, (2), 206-222.

154. Lucklum, R.; Behling, C.; Hauptmann, P., Role of Mass Accumulation and Viscoelastic Film Properties for the Response of Acoustic-Wave-Based Chemical Sensors. *Analytical Chemistry* 1999, 71, (13), 2488-2496.

155. Kasdorf, B. T.; Arends, F.; Lieleg, O., Diffusion Regulation in the Vitreous Humor. *Biophysical journal* 2015, 109, (10), 2171-81.

156. Nowald, C.; Kasdorf, B. T.; Lieleg, O., Controlled nanoparticle release from a hydrogel by DNA-mediated particle disaggregation. *Journal of controlled release : official journal of the Controlled Release Society* 2017, 246, 71-78.

157. Schömig, V. J.; Käsdorf, B. T.; Scholz, C.; Bidmon, K.; Lieleg, O.; Berensmeier, S., An optimized purification process for porcine gastric mucin with preservation of its native functional properties. *RSC Adv.* 2016, 6, (50), 44932-44943.

158. Biegler, M.; Delius, J.; Käsdorf, B. T.; Hofmann, T.; Lieleg, O., Cationic astringents alter the tribological and rheological properties of human saliva and salivary mucin solutions. *Biotribology* 2016, 6, 12-20.

159. Kasdorf, B. T.; Weber, F.; Petrou, G.; Srivastava, V.; Crouzier, T.; Lieleg, O., Mucin-Inspired Lubrication on Hydrophobic Surfaces. *Biomacromolecules* 2017, 18, (8), 2454-2462.

160. Zhou, D., Understanding physicochemical properties for pharmaceutical product development and manufacturing--dissociation, distribution/partition, and solubility. *Journal of Validation Technology* 2009 Spring, 2009, p 13+.

161. Jabs, D. A.; Newman, C.; De Bustros, S.; Polk, B. F., Treatment of cytomegalovirus retinitis with ganciclovir. *Ophthalmology* 1987, 94, (7), 824-30.

162. Henderly, D. E.; Freeman, W. R.; Causey, D. M.; Rao, N. A., Cytomegalovirus retinitis and response to therapy with ganciclovir. *Ophthalmology* 1987, 94, (4), 425-34.

163. Allen, T. M., Long-circulating (sterically stabilized) liposomes for targeted drug delivery. *Trends in Pharmacological Sciences* 1994, 15, (7), 215-220.

164. Gabizon, A. A., Selective Tumor Localization and Improved Therapeutic Index of Anthracyclines Encapsulated in Long-Circulating Liposomes. *Cancer Research* 1992, 52, (4), 891-896.

165. Li, L. D.; Crouzier, T.; Sarkar, A.; Dunphy, L.; Han, J.; Ribbeck, K., Spatial configuration and composition of charge modulates transport into a mucin hydrogel barrier. *Biophysical journal* 2013, 105, (6), 1357-65.

166. Lehr, C.-M.; Poelma, F. G. J.; Junginger, H. E.; Tukker, J. J., An estimate of turnover time of intestinal mucus gel layer in the rat in situ loop. *Int J Pharm* 1991, 70, (3), 235-240.

167. Johansson, M. E. V., Fast Renewal of the Distal Colonic Mucus Layers by the Surface Goblet Cells as Measured by In Vivo Labeling of Mucin Glycoproteins. *PloS one* 2012, 7, (7), e41009.

168. Atuma, C.; Strugala, V.; Allen, A.; Holm, L., The adherent gastrointestinal mucus gel layer: thickness and physical state in vivo. *Am J Physiol Gastrointest Liver Physiol* 2001, 280, (5), G922-9.

169. Kerss, S.; Allen, A.; Garner, A., A Simple Method for Measuring Thickness of the Mucus Gel Layer Adherent to Rat, Frog and Human Gastric Mucosa: Influence of Feeding, Prostaglandin,N-Acetylcysteine and other Agents. *Clinical Science* 1982, 63, (2), 187-195.

170. Jordan, N.; Newton, J.; Pearson, J.; Allen, A., A novel method for the visualization of the in situ mucus layer in rat and man. *Clin Sci (Lond)* 1998, 95, (1), 97-106.

171. Veronese, F. M.; Pasut, G., PEGylation, successful approach to drug delivery. *Drug Discov Today* 2005, 10, (21), 1451-8.

172. Otsuka, H.; Nagasaki, Y.; Kataoka, K., PEGylated nanoparticles for biological and pharmaceutical applications. *Advanced drug delivery reviews* 2003, 55, (3), 403-419.

173. Allen, T. M.; Cullis, P. R., Drug Delivery Systems: Entering the Mainstream. *Science* 2004, 303, (5665), 1818-1822.

174. Knop, K.; Hoogenboom, R.; Fischer, D.; Schubert, U. S., Poly(ethylene glycol) in Drug Delivery: Pros and Cons as Well as Potential Alternatives. *Angewandte Chemie International Edition* 2010, 49, (36), 6288-6308.

175. Wang, Y. Y.; Lai, S. K.; Suk, J. S.; Pace, A.; Cone, R.; Hanes, J., Addressing the PEG mucoadhesivity paradox to engineer nanoparticles that "slip" through the human mucus barrier. *Angewandte Chemie* 2008, 47, (50), 9726-9.

176. Huckaby, J. T.; Lai, S. K., PEGylation for enhancing nanoparticle diffusion in mucus. *Advanced drug delivery reviews* 2017.

177. Kumari, A.; Yadav, S. K., Cellular interactions of therapeutically delivered nanoparticles. *Expert Opinion on Drug Delivery* 2011, 8, (2), 141-151.

178. Schoemig, V.; Isik, E.; Martin, L.; Berensmeier, S., Solid liquid liquid extraction of porcine gastric mucins from homogenized animal material. *RSC Adv.* 2017, 7, (63), 39708-39717.

179. Peacocke, J.; Lotz, Z.; de Beer, C.; Roux, P.; Mall, A. S., The role of crude saliva and purified salivary mucins in the inhibition of the Human Immunodeficiency Virus type 1. *Virology Journal* 2012, 9, 177-177.

180. Bergey, E. J.; Cho, M.-I.; Blumberg, B. M.; Hammarskjöld, M.-L.; Rekosh, D.; Epstein, L. G.; Levine, M. J., Interaction of HIV-1 and Human Salivary Mucins. *JAIDS Journal of Acquired Immune Deficiency Syndromes* 1994, 7, (10), 995-1002.

181. Keough, E. M.; Mackey, W. C.; Connolly, R.; Foxall, T.; Ramberg-Laskaris, K.; McCullough, J. L.; O'Donnell, T. F.; Callow, A. D., The interaction of blood components with PDMS(polydimethylsiloxane) and LDPE (low-density polyethylene) in a baboon ex vivo arteriovenous shunt model. *Journal of Biomedical Materials Research* 1985, 19, (5), 577-587.

182. Amoako, K. A.; Sundaram, H. S.; Suhaib, A.; Jiang, S.; Cook, K. E., Multimodal, Biomaterial-Focused Anticoagulation via Superlow Fouling Zwitterionic Functional Groups Coupled with Anti-Platelet Nitric Oxide Release. *Advanced Materials Interfaces* 2016, 3, (6), 1500646.

183. Scharbert, S.; Holzmann, N.; Hofmann, T., Identification of the Astringent Taste Compounds in Black Tea Infusions by Combining Instrumental Analysis and Human Bioresponse. *Journal of Agricultural and Food Chemistry* 2004, 52, (11), 3498-3508.

184. Tiffany, J. M., Measurement of wettability of the corneal epithelium. *Acta Ophthalmologica* 1990, 68, (2), 175-181.

185. Holly, F. J.; Lemp, M. A., Wettability and wetting of corneal epithelium. *Experimental Eye Research* 1971, 11, (2), 239-250.

186. Crouzier, T.; Boettcher, K.; Geonnotti, A. R.; Kavanaugh, N. L.; Hirsch, J. B.; Ribbeck, K.; Lieleg, O., Modulating Mucin Hydration and Lubrication by Deglycosylation and Polyethylene Glycol Binding. *Advanced Materials Interfaces* 2015, 2, (18), 1500308-1500315.

187. Tirosh, O.; Barenholz, Y.; Katzhendler, J.; Priev, A., Hydration of Polyethylene Glycol-Grafted Liposomes. *Biophys J* 1998, 74, (3), 1371-1379.

188. Branca, C.; Magazù, S.; Maisano, G.; Migliardo, F.; Migliardo, P.; Romeo, G., Hydration Study of PEG/Water Mixtures by Quasi Elastic Light Scattering, Acoustic and Rheological Measurements. *The Journal of Physical Chemistry B* 2002, 106, (39), 10272-10276.

189. Hermanson, G. T., *Bioconjugate techniques*. 3rd ed.; Academic press: London, 2013.

190. Schmid, J.; Heider, D.; Wendel, N. J.; Sperl, N.; Sieber, V., Bacterial Glycosyltransferases: Challenges and Opportunities of a Highly Diverse Enzyme Class Toward Tailoring Natural Products. *Frontiers in Microbiology* 2016, 7, 182.

191. Tang, S.; Puryear, W. B.; Seifried, B. M.; Dong, X.; Runstadler, J. A.; Ribbeck, K.; Olsen, B. D., Antiviral Agents from Multivalent Presentation of Sialyl Oligosaccharides on Brush Polymers. *ACS Macro Letters* 2016, 5, (3), 413-418.

192. Bielecki, R. M.; Crobu, M.; Spencer, N. D., Polymer-Brush Lubrication in Oil: Sliding Beyond the Stribeck Curve. *Tribology Letters* 2013, 49, (1), 263-272.

193. Bielecki, R. M.; Benetti, E. M.; Kumar, D.; Spencer, N. D., Lubrication with Oil-Compatible Polymer Brushes. *Tribology Letters* 2012, 45, (3), 477-487.

194. Round, A. N.; Berry, M.; McMaster, T. J.; Stoll, S.; Gowers, D.; Corfield, A. P.; Miles, M. J., Heterogeneity and persistence length in human ocular mucins. *Biophys J* 2002, 83, (3), 1661-70.

195. Shogren, R.; Gerken, T. A.; Jentoft, N., Role of glycosylation on the conformation and chain dimensions of O-linked glycoproteins: light-scattering studies of ovine submaxillary mucin. *Biochemistry* 1989, 28, (13), 5525-36.

196. Dawson, M.; Wirtz, D.; Hanes, J., Enhanced viscoelasticity of human cystic fibrotic sputum correlates with increasing microheterogeneity in particle transport. *Journal of Biological Chemistry* 2003, 278, (50), 50393-50401.

197. Russell, D.; Oldham, N. J.; Davis, B. G., Site-selective chemical protein glycosylation protects from autolysis and proteolytic degradation. *Carbohydr Res* 2009, 344, (12), 1508-14.

198. Pearce, O. M. T.; Laubli, H., Sialic acids in cancer biology and immunity. *Glycobiology* 2016, 26, (2), 111-28.

199. Hang, H. C.; Bertozzi, C. R., The chemistry and biology of mucin-type O-linked glycosylation. *Bioorganic & Medicinal Chemistry* 2005, 13, (17), 5021-5034.

200. Taniguchi, T.; Woodward, A. M.; Magnelli, P.; McColgan, N. M.; Lehoux, S.; Jacobo, S. M. P.; Mauris, J.; Argueso, P., N-Glycosylation affects the stability and barrier function of the MUC16 mucin. *J Biol Chem* 2017, 292, (26), 11079-11090.

201. Yildiz, H. M.; Speciner, L.; Ozdemir, C.; Cohen, D. E.; Carrier, R. L., Food-associated stimuli enhance barrier properties of gastrointestinal mucus. *Biomaterials* 2015, 54, 1-8.

202. Sanders, N. N.; De Smedt, S. C.; Demeester, J., The Physical Properties of Biogels and their Permeability for Macromolecular Drugs and Colloidal Drug Carriers. *Journal of Pharmaceutical Sciences* 2000, 89, (7), 835-849.

Acknowledgements

Zu guter Letzt möchte ich mich nun herzlichst bei allen Personen bedanken, die zum Gelingen dieser Arbeit beigetragen haben und mich während meiner Promotionszeit unterstützt haben.

Mein besonderer Dank gilt dabei meinem Doktorvater Prof. Dr. Oliver Lieleg zum einen dafür, dass er sein Vertrauen in einen Biologen wie mich gesetzt hat und mich behutsam an die spannende Welt der Polymerphysik herangeführt hat. Zum anderen möchte ich mich auch für die besondere Betreuung seinerseits danken die so sicherlich nicht in jeder Arbeitsgruppe zu finden ist: Danke Oliver, dass deine Tür jederzeit für sämtliche Fragen offen stand. Ebenso danke für die zahlreichen fachlichen Diskussionen die zu so mancher großen Erleuchtung geführt haben. Großen Dank auch für deine immense Geduld falls in diesen Diskussionen auch mal „komplexere“ Mathematik auftauchte die mich zum Schwitzen brachte. Danke auch für deine tatkräftige Unterstützung so mancher ausgefallenen Tier- und Fabelwesen-Trends die in unserer Arbeitsgruppe des Öfteren mal unvermittelt aufgetaucht sind und ebenfalls danke dafür, mir trotz hartnäckiger Weigerung meinerseits letztendlich das Present Progressive auszutreiben!

Ein weiterer großer Dank geht an alle meine Arbeitskollegen und Studenten: ihr habt unsere gemeinsame Zeit mit viel Spaß und spannenden Kickermatches wie im Flug vergehen lassen. Durch euch hat es sich oft nicht wie Arbeit angefühlt sondern wie ein lustiges Treffen unter Freunden! Vielen Dank an euch alle, besonders auch für die herzliche und entspannte Atmosphäre und dafür, dass jeder von euch jederzeit ohne Zögern seine eigene Arbeit liegengelassen hat um einem Kollegen behilflich zu sein!

Vielen Dank Fabi für deine tatkräftige (mathematische) Unterstützung, deine praktischen Matlab Skripte sowie die teilweise kräftezehrenden Diskussionen bei denen du mir geduldig die alltägliche und wissenschaftliche Physik in meinen Kopf gezwungen hast. Ich hoffe ich konnte mich durch die anschauliche Demonstration kompliziertester Klettertechniken wieder etwas revanchieren. Vielen Dank auch an dich Stefan, für die zahlreichen Lachkrämpfe die meine Bauchmuskulatur bis heute gestärkt haben, Chewie lässt grüßen! Danke auch für deine Unterstützung bei rheologischen Fragestellungen und die Einführung in die Welt der Mechanik. Vielen Dank an dich Tin, du hast mit deinem Surferboy-Lächeln immerzu gute Laune verbreitet und jederzeit die Laborarbeit mit deinen (nicht immer so ganz politisch korrekten) Witzen versüßt. Danke auch für die Unterstützung und Fütterung des Cookie-Monsters falls meine Vorräte mal aufgebraucht waren. Weiterhin geht mein Dank an Kathrin: danke für die unterhaltsamen Kaffeepausen und auch dafür, dass du aus jeder Situation etwas Gutes herausholen konntest und immer einen guten Ratschlagt parat gehabt hast. Ebenfalls vielen Dank für deine Statistik-Nachhilfe und den Beistand bei der Bändigung von so manchem bösen Matlab-Skript welches aus unerklärlichen Gründen seinen Dienst verweigert hatte. Vielen

Dank an dich Ben für all die High-Intesity Kicker Spiele, bei denen der Ball sich öfters mehr außerhalb des Tisches (oder in der Luft) befunden hat als Bodenkontakt zu haben und die der ein oder anderen Figur den Kopf gekostet haben. Vielen Dank auch für die immer wieder unterhaltsamen Schranken-Durchfahrten („Ich und mein Zoo würden gerne zum IMETUM...“) sowie deine Begeisterung für die ganz großen Legenden wie etwa den zeitlosen Pingu, das majestätische Robot-Unicorn, einen gewissen Vogel der gerne Stöcke sammelt oder das mutigste Tier der Welt, den Crazy Nastyass Honey Badger. Thanks for the treat stupid! Danke auch für dein Gespür für relativ „kurze“ Wartezeiten beim begehrten Gourmet-Imbiss um die Ecke und nicht zuletzt auch dafür, dass du mich in die erlesene Welt des Wacholderschnapses eingeführt hast! Vielen Dank auch an dich Caro für deinen einzigartigen trockenen Humor, dein occasional Noot Nooooot! und ganz besonders für die Offenbarung, dass man Tequila aus Salatgurken trinken kann!

Ganz großen Dank auch an alle Studenten die während meiner Promotionszeit in unserer Arbeitsgruppe geforscht haben und immer eine fröhliche Stimmung verbreitet haben. Besonderen Dank geht dabei an Andi „The Honey Badger“ Wenzler und meinen designierten Nachfolger Matthias „Matzl“ Marczynski für die super lustige Zeit und die produktive Zusammenarbeit die nicht nur im Labor stattfand! Es war mir eine Ehre, euch betreuen zu dürfen.

Ebenso möchte ich mich auch für die tatkräftige Unterstützung unserer technischen Assistentinnen Tina und Christine im Labor bedanken wie auch für die Unterstützung bei den zahlreichen Mucin-Aufreinigungen. Weiterhin auch vielen Dank an Iris für die Hilfe bei verwaltungstechnischen Fragen und dem fachlichen Beistand für die komplexen Reisekostenabrechnungen.

Nicht zuletzt noch ein ganz großes Dankeschön an meine Eltern: Vielen Dank für all die Unterstützung die ich schon immer von euch bekommen habe. Ich hoffe ihr könnt nun ruhiger schlafen, nachdem ich meine biologische Ausbildung jetzt doch etwas aufgebessert habe und nun vielleicht gute Chancen auf einen „richtigen“ Job habe.

Last but definitely not least, ein gigantisches Dankeschön an die beste Frau der Welt (meine!!!): Vielen Dank, dass du während meiner Promotionszeit immer für mich da warst und mich auch nach den weniger erfolgreichen Arbeitstagen jederzeit mit einem strahlenden Lächeln wieder glücklich gemacht hast. Ich bin froh dass es dich gibt!